THE UNIVERSITY OF TULSA
THE GRADUATE SCHOOL

INJECTION/FALLOFF TESTING OF VERTICAL AND HORIZONTAL WELLS

by
Amina Boughrara

A dissertation submitted in partial fulfillment of
the requirements for the degree of Doctor of Philosophy
in the Discipline of Petroleum Engineering

The Graduate School
The University of Tulsa

2007

T H E U N I V E R S I T Y O F T U L S A

THE GRADUATE SCHOOL

INJECTION/FALLOFF TESTING OF VERTICAL AND HORIZONTAL WELLS

by
Amina Boughrara

A DISSERTATION

APPROVED FOR THE DISCIPLINE OF

PETROLEUM ENGINEERING

By Dissertation Committee

_____ , Chairperson
Dr. Albert C. Reynolds

_____
Dr. Gaoming Li

_____
Dr. Richard Redner

_____
Dr. Leslie Thompson

COPYRIGHT STATEMENT

ABSTRACT

Amina Boughrara (Doctor of Philosophy in Petroleum Engineering)

Injection/Falloff Testing of Vertical and Horizontal Wells

Directed by Dr. Albert C. Reynolds

454 pp. Chapter 6

(338 words)

Our focus is on replacing production/buildup tests by injection/falloff tests in order to estimate reservoir parameters such as permeability and mechanical skin. These tests are economically attractive because they are associated with waterflooding projects. Moreover, they are also used for the purpose of eliminating emissions during well-testing operations. Typically, the reservoir is flooded with water having a temperature considerably below that of the reservoir fluids. This significantly complicates the problem of well test analysis. Not only is the flow in the reservoir governed by the water and oil relative permeabilities, temperature changes induced by injection of cold water also occur in the system. These effects make the associated initial boundary-value problem non-linear. As a consequence, analytical solutions for the pressure are difficult to obtain and the superposition technique usually applied to generate the pressure solution for variable rate problems cannot be theoretically justified.

The intent of this study is to provide a theoretical understanding of the injection/falloff testing of water injection wells. Models for the movement of water injected via a horizontal or a vertical well are developed to generate new approximate analytical solutions for injection and falloff pressures. When incorporating the thermal effects into the analysis, temperature profiles in the reservoir during injection and falloff periods are also constructed analytically. The accuracy of results from our approximate solutions is checked by comparing them to solutions generated from a black-oil reservoir simulator.

The final objective of this work is to provide a practical analysis technique for injection/falloff testing of water injection wells. We demonstrate that our analytical solutions can be used to estimate reservoir and well properties. Injection/falloff data are analyzed using non-linear regression with our approximate analytical model used to construct the predicted pressure response. This approach allows us to estimate important parameters such as the absolute permeability of the reservoir (isotropic and anisotropic), the mechanical skin factor, the length of the horizontal well and the two-phase relative permeability curves assuming a power law model.

ACKNOWLEDGEMENTS

My deepest gratitude is to my advisor Dr. Albert Reynolds. I have been amazingly fortunate to have an advisor who gave me continuous guidance, encouragement and freedom to explore on my own over the course of this research. Dr. Reynolds, you taught me how to work hard and how to be persistent in solving problems. I will always be indebted to you for believing in me.

I also wish to express my sincere appreciation to my dissertation committee members Dr. Gaoming Li, Dr. Richard Redner and Dr. Leslie Thompson for accepting to review my work on a very short notice and for offering insightful comments. A special "Merci" goes to Dr. Leslie Thompson for always allocating time to answer my endless questions and for the countless discussions which helped me sort out some technical details of my work.

Gratitude is also extended to the members companies of the Tulsa University Petroleum Reservoir Exploitation Projects for their financial support and interest. I am especially indebted to Dr. Alvaro Peres from Petrobras for his invaluable intellectual contributions to this work as well as his support.

I gratefully acknowledge all the faculty members of the Petroleum Engineering Department of the University of Tulsa for their dedication to high quality teaching and research and for making the PE department one of the best place in the world to start a career in petroleum engineering. I have learnt a great deal from them and will never thank them enough.

The Petroleum Engineering Department of the University of Tulsa does not only consist of outstanding professors and researchers, but also exceptional and devoted staff to whom I am deeply grateful: Judy Teal for providing me not only with exceptional administrative help but also with her valuable friendship; Reta Watkins for always having a smile for me and for all the "sweet bars" ordered for the weekly graduate seminars that

I enjoyed and Lori Watts for sweetening my after lunch coffee with all the chocolate and candies that she offered me.

I extend many thanks to my fellow graduate students of the Petroleum Engineering Department for their friendship. Special thanks go to the TUPREP students for being wonderful colleagues and making the long nights of work bearable.

On a more personal note, I shared many tears and laughs over this dissertation with my wonderful sister, Nedjma and long time friends: Sarah Farhi, Madjid Anane and Nacera Hank. Thank you for being there for me. I also want to acknowledge my best friend and soulmate Hayder Salman for his love and encouragement throughout my last year at the University of Tulsa. Nothing in a simple sentence can express the love I have for you Hayder.

This manuscript is dedicated to two very special people in my life: to my Mom, Zoubida and my Dad, Hafid.

TABLE OF CONTENTS

LIST OF TABLES

LIST OF FIGURES

CHAPTER 1

INTRODUCTION

Waterflooding is a method of secondary recovery in which water is injected into a reservoir to displace oil that has been left behind after primary recovery. Waterflooding usually involves the injection of water through wells especially set up for water injection. Once injected, water sweeps the displaced oil to production wells. Most oil reservoirs are subjected to waterflooding at some point in their development. Injectivity and falloff tests are run on water injection wells in order to obtain pressure transient data, crucial for reservoir monitoring and management.

1.1 Literature Review

There exist numerous articles in the literature which provide insight and a general understanding of the injection and falloff pressures at a complete-penetration vertical injection well and theory for the analysis of these pressure data. We cite for example Abbaszadeh and Kamal [4] and Bratvold and Horne [11] who derived an analytical solution for injectivity tests which accounts for the saturation profile behind the front. They relied on the fact that the injection solution for a line source well can be correlated in terms of the Boltzmann transform and an approximation to the saturation profile can be obtained from the radial flow Buckley-Leverett model. Abbaszadeh and Kamal [4] formulated their solution by using a multibank approach where the banks continually move during the injection period resulting in an advance with time of all boundaries between banks. The Bratvold and Horne [11] approach is somewhat simpler in that, they directly solve a moving boundary problem where the boundary corresponds to the location of the front as predicted from Buckley-Leverett frontal advance equation for radial flow. Both papers also presented a solution for the falloff period. Abbaszadeh and Kamal [4] have shown

that the falloff solution can be generated reasonably accurately by superposing two single-phase radially multi-composite solutions where the single-phase multi-composite solutions are based on the reservoir total mobility profile at the instant of shut-in. These authors suggested that falloff data can be analyzed using type curves generated from the analytical solution with relative permeabilities and rock and fluid compressibilities known. From the type curve match, one can then estimate effective water permeability at residual water saturation and therefore the absolute permeability, the skin factor and even the average mobility in the oil bank. In their approach for constructing an analytical solution for falloff, Bratvold and Horne [11] used the fact that the mobility profile does not change during shut-in as suggested by Abbaszadeh and Kamal [4]. Thus, the initial-boundary value problem for the pressure during shut-in can be represented as a single-phase radially multi-composite problem based on the total mobility profile at shut-in with the initial condition obtained from the injection solution evaluated at the instant of shut-in. They solved this problem using the Laplace transform and inverted it numerically to obtain the falloff solution as a function of time. With that said, the solution techniques used by Abbaszadeh and Kamal [4] or Bratvold and Horne [11] cannot be implemented for a horizontal configuration as we do not know the analogous analytical multi-composite solution for a horizontal well.

Thompson and Reynolds [34] and Thompson and Reynolds [33] presented a general theory for the pressure behavior in radially heterogeneous reservoirs under multiphase flow conditions. They found that derivative data reflect a weighted average of permeability-mobility over the reservoir. The averaging process gives large weights to regions where total rate and total mobility change most rapidly with time. The general solution procedure introduced by Thompson and Reynolds relies on the concept of a steady-state zone which propagates into the reservoir when the well is flowing. The theory applies for both production and injection wells and solutions generated with this theory include the single-phase flow solutions as special cases. Banerjee et al. [5] applied the ideas of Thompson and Reynolds to injectivity tests for vertical wells in heterogeneous reservoirs. For the radial flow water injection problem, the steady-state zone corresponds to the region concentric

with the wellbore where the total in-situ flow rate may be treated as constant. Beyond the steady-state zone, the in-situ flow rate decreases and is equal to zero at points far from the injection well. Under single-phase flow conditions, the change in pressure with time is completely determined by the properties at points in the reservoir where the rate is changing with time. For any reasonable values of reservoir properties, this constant rate steady-state zone propagates faster than the water flood front. A schematic illustrating the overall process is shown in Fig. 1.1 for the case where the initial water saturation is equal to irreducible water saturation. The Banerjee et al. [5] solution, based on the steady-state theory, and which was constructed without assuming that variables could be correlated in terms of the Boltzmann variable, differs from the Bratvold and Horne [11] solution which is based on the Boltzmann transform. In their work, Banerjee et al. [5] deleted a term from the solution that is not always negligible. Peres and Reynolds [27] showed that if the neglected term is included, then the Banerjee et al. [5] solution is consistent with the solution provided by Bratvold and Horne [11].

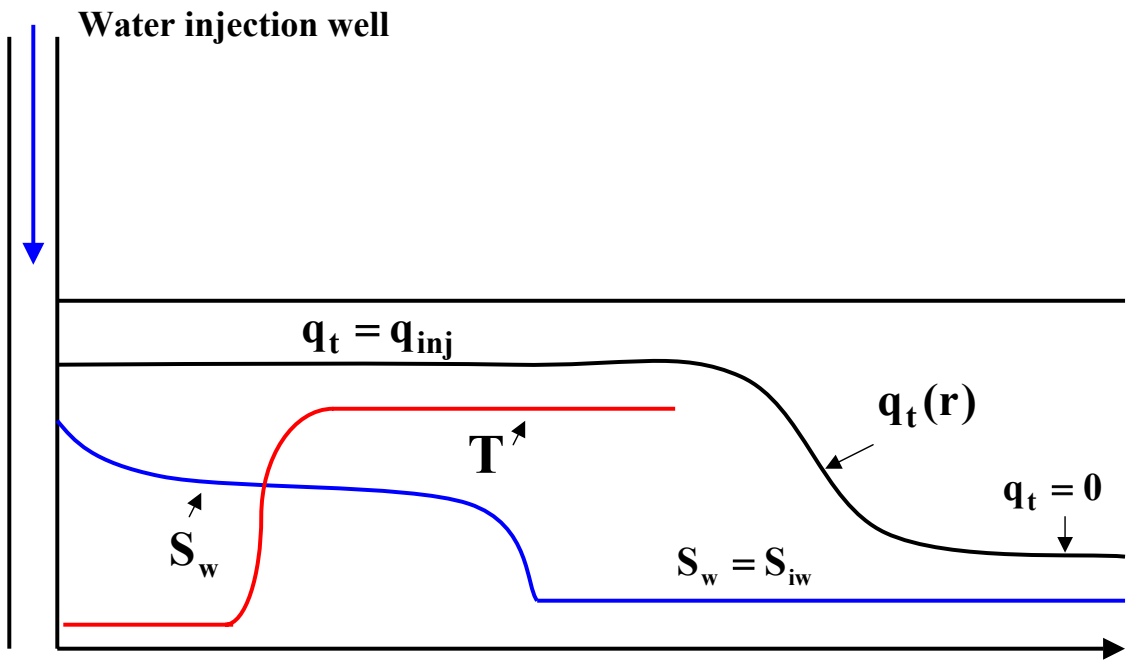

Figure 1.1: Propagation of steady-state zone and flood front for radial geometry.

As mentioned before, the pressure diffusion and the advancement of the flood front occur on different time scales for the vertical well case. For the horizontal well

case, however, not only do the pressure diffusion and the propagation of the flood front occur on different time scales, but also in different planes or directions promoting the appearance of new flow regimes in addition to the standard flow regimes exhibited by horizontal wells under single-phase flow. Because of this, the pressure response due to water injection through a horizontal well is expected to be considerably more complex than in the vertical well case. Peres and Reynolds [27] were the first to develop an accurate approximate analytical solution for the injection response at a horizontal water well and to show the existence of these new flow regimes. Their solution was derived using the steady-state theory of Thompson and Reynolds [33] combined with a technique introduced by Deppe [18] and a combination of Boltzmann transforms for the different flow regimes. However, their solution assumes an isotropic reservoir and that the horizontal well is equidistant from the top and bottom reservoir boundaries. In addition, Peres and Reynolds [27] restricted their analysis to the injection period only, that is, the falloff was not considered.

Levitan [24] presented a new method for the analytical solution of two-phase pressure transient problems. His solution is more general, in that it applies to multirate injection tests including the case where one or more of the rates can be set to zero to simulate a falloff test. The Levitan [24] solution method is based on a special transformation of variables that simplifies the coefficients of the governing pressure equation for radial flow.

Except for the work of Bratvold and Horne [11] and Levitan [24], all the authors cited earlier assumed that the injected fluid is at the same temperature as the in-situ reservoir fluid when constructing solutions for the pressure response during an injection/falloff test on water injection wells. In practice, this is not the case since the injected water is at a lower temperature than the reservoir oil.

When cold water is injected into a hot reservoir, the formation around the water injector will cool down to the temperature of the injected water. This creates a cold water bank around the injector which expands with time into the reservoir. Similar to the saturation front, the temperature front will also propagate in the reservoir as shown

in Fig. 1.1. The nonisothermal two phase problem is therefore described by mass and energy conservation equations. The heat exchange in the reservoir occurs mainly through three processes: convective heat transfer between injected fluid and solid matrix, heat conduction and heat transfer between solid grains by radiation. The last mechanism is not considered to be important in porous media and therefore is usually neglected when the gas phase is not involved. Heat transfer by convection is accounted for by assuming that thermal equilibrium exists at all times between the rock matrix and surrounding fluids. Conductive heat transfer that occurs in the reservoir can be split up in two processes: horizontal conduction occurring in the direction of fluid flow and vertical conduction that happens perpendicular to the overlying and underlying strata.

The early work of Witterholt and Tixier [35] on thermal effects considered the use of mathematical models which describe the exchange of heat between injected water, wellbore, surrounding formation and injection zone in order to study the behavior of the bottom hole temperature during an injection/falloff test. The mathematics involved in the modelling, as pointed out by these authors, is taken from Carslaw and Jaeger [14] and thus, the intent of their simplistic approach used in the computation of temperature profiles was not to provide a quantitative match with field data. Their solution for the temperature during injection takes into account not only the convective heat flux in the radial direction but also the heat that is transferred through vertical conduction. However, Witterholt and Tixier [35] assumed a step function injection zone temperature profile, generally obtained when only convection is considered, when solving for the temperature profile in the wellbore during the shut-in period.

Using the Verigin model which assumes that the injected fluid displaces the formation fluid in a piston-like manner (two-bank system), Woodward and Thambynayagam [36] presented an analytical solution for the pressure response that they generalized to nonisothermal conditions. Their study indicated that the effect of temperature variations during injection are found to behave as skin effects. Despite the fact that their analytical solutions were validated by comparison with results obtained from a numerical simulation, the authors did not provide a formal derivation for the Verigin generalization to

nonisothermal conditions.

Similarly to Woodward and Thambynayagam [36], Barkve [6] considered the displacement to be piston-like. By decoupling the mass and energy equations, the author was able to analytically solve the system for temperature and pressure in the reservoir during injection providing, therefore, a formal derivation of the results presented by Woodward and Thambynayagam [36].

Platenkamp [30] conducted a numerical study in order to show the relative importance of the three heat exchange processes involved when injecting cold water into a hot reservoir, that is convection, vertical and horizontal conduction. He concluded from this study that it is a good approximation to neglect the heat transfer contribution from conduction compared to that from convection during an injection period as long as the duration of the test is not too long and the injection rate is sufficiently high.

As mentioned earlier, Bratvold and Horne [11] incorporated the effects of temperature into their two-phase solution. Based on the study of Platenkamp [30], the temperature distribution was assumed to be completely dominated by convective mechanism of heat transfer during the injection period leading to a quasilinear hyperbolic system for water saturation and temperature that they solved using the method of characteristics (see Temple [32]). In constructing their falloff solution, Bratvold and Horne [11] did not take into account the heat exchange through conduction (specifically vertical conduction) in the wellbore and the reservoir as they used the nonisothermal Buckley-Leverett saturation distribution and the temperature profile generated during the injection period and evaluated at the instant of shut-in. Levitan [24] used the approach of Bratvold and Horne [11] to account for the temperature changes induced by water injection into his solution.

In summary, several studies pertaining to injection and falloff testing of vertical and horizontal wells have been presented. However, some questions remain unanswered. How can we generalize analytical solutions derived previously for configurations other than a complete penetration vertical well case and a horizontal well of equal offset. How can we generate solutions that take into account the fact that the permeability field is anisotropic. Most importantly, how can we incorporate the different mechanisms for heat

exchange into our solutions when cold waterflooding a hot reservoir. These points need to be addressed.

1.2 Objectives and Research Scope

The work of Peres and Reynolds [27] provides a sound starting point for this research. As mentioned previously, these authors derived approximate analytical solutions for the injection pressure change at vertical and horizontal wells which incorporate the water saturation gradient. In the vertical well case, their solution assumed a complete-penetration well; in the horizontal well case, it assumed that the well is equidistant from the top and bottom reservoir boundaries. Moreover, these authors assumed water injection into an isotropic reservoir. The principal objectives of this work are: (i) to remove these assumptions by constructing approximate analytical pressure solutions for the restricted-entry vertical well case and for a horizontal well with an unequal offset configuration in isotropic and anisotropic reservoirs, (ii) to construct analytical solutions for the falloff response, (iii) to extend the solutions for injectivity and falloff tests to include the non-isothermal effects as we invariably inject cold water into hot oil, and (iv) to provide a practical analysis procedure based on non-linear regression which can be used to estimate reservoir and well properties.

There are 6 chapters in this dissertation. In chapter 1, we give a review of relevant literature and state the objectives of the study. Chapter 2 is on injection testing of vertical and horizontal wells under isothermal conditions. It includes a description of models for the movement of water when injected through the different configurations considered here, the derivation of the pressure response based on the steady-state theory of Thompson and Reynolds and the flow regimes observed during an injection test, a discussion of the spatial transformation used to handle the anisotropy and a validation of numerical results generated using our models. Falloff testing of vertical and horizontal wells under isothermal conditions is addressed in chapter 3. Two conceptually different analytical methods to solve for the falloff response are presented and validated using a commercial simulator. Chapter 4 covers the mathematical modeling of the nonisothermal waterflood-

ing. A discussion of the different mechanisms to heat transfer in porous media as well as their effect on the injection and falloff pressure data is provided in this chapter. Chapter 5 presents a practical analysis of injection and falloff data for the estimation of parameters such as absolute permeabilities, mechanical skin factor and relative permeabilities. In chapter 6, we discuss the relevant results and give conclusions.

CHAPTER 2

INJECTION TESTING OF VERTICAL AND HORIZONTAL WELLS

In this chapter, we present some theoretical results relevant to injectivity tests in vertical and horizontal wells completed in an oil reservoir above bubble point pressure. These results include models for the movement of water when injected through restricted-entry vertical wells and horizontal wells with unequal offsets in order to map the water saturation distributions and therefore, the total mobility profiles during the injection period. This is crucial for the generation of approximate analytical solutions for the injection pressure if one wishes to pursue the solution techniques used by Peres and Reynolds [27] and based on the steady-state theory of Thompson and Reynolds [33]. The solutions are first presented for an isotropic reservoir and then generalized to an anisotropic reservoir by introducing a spatial transformation to convert an anisotropic system to an equivalent isotropic system. The analytical results are verified with numerical results obtained from a black oil reservoir simulator. The behavior of the pressure and its derivative observed under steady-state conditions for the different configurations considered in this work is explained.

2.1 Steady-State Theory for Radial Flow

We consider injection of water at a constant rate given by q_{inj} through a vertical well in a homogeneous reservoir of constant porosity. For now, we assume that the reservoir is isotropic. It is also assumed that the initial saturation distribution is uniform and equal to irreducible water saturation, S_{iw}. No wellbore storage is considered. For now, we assume pure radial flow through a completely-penetrating well into a reservoir of constant formation thickness, h. We will show that we can apply the same theoretical approach used by Peres and Reynolds [28] to construct an analytical solution for the injection pres-

sure at a restricted-entry vertical well as well as a horizontal well. The theory is based on an infinite cylindrical reservoir with a restricted-entry vertical well at the center. For the horizontal well case, the well is not necessary equidistant from the top and bottom boundary of the reservoir.

We begin with the case of pure radial flow through a completely-penetrating water injection well at the center of an infinite cylindrical reservoir. The starting point of this analysis is Darcy's law which we can write after rearranging and integrating as

$$\Delta p = \frac{\alpha}{h} \int_{r_w}^{\infty} \frac{q_t(r,t)}{\lambda_t(r,t)} \frac{dr}{rk(r)}, \tag{2.1}$$

where $q_t(r,t)$ represents the total reservoir rate. Eq. 2.1 is general and applies for both production and injection. Since the focus here is on the water injection problem, $q_t(r_w,t) = q_{inj} > 0$ represents the specified injection rate in RB/day and

$$\Delta p = p_{wf}(t) - p_i, \tag{2.2}$$

where p_{wf} is the injection pressure at the wellbore and p_i is the initial reservoir pressure. The total mobility λ_t is defined by

$$\lambda_t = \frac{k_{ro}(S_w)}{\mu_o} + \frac{k_{rw}(S_w)}{\mu_w}. \tag{2.3}$$

We also define the oil mobility at irreducible water saturation by $\hat{\lambda}_o = \frac{k_{ro}(S_{iw})}{\mu_o}$ and the water mobility at residual oil saturation by $\hat{\lambda}_w = \frac{k_{rw}(1-S_{or})}{\mu_w}$. α is a constant which depends on the units system used. In field units, $\alpha = 141.2$. In Eq. 2.1, the permeability $k(r)$ is assumed to be variable in order to account for the change of the permeability near the wellbore region due to the mechanical skin. Therefore, we set it equal to

$$k(r) = \begin{cases} k_s & \text{for } r_w < r < r_s, \\ k & \text{for } r > r_s. \end{cases} \tag{2.4}$$

Eq. 2.4 assumes a reservoir with a thick skin zone concentric with the well with a radius

r_s. The permeability in the damaged zone is k_s. We can rewrite Eq. 2.1 as follows

$$\Delta p = \frac{\alpha}{h}\int_{r_w}^{r_f(t)} \frac{q_t(r,t)}{\lambda_t(r,t)}\frac{dr}{rk(r)} + \frac{\alpha}{h}\int_{r_f(t)}^{\infty} \frac{q_t(r,t)}{\lambda_t(r,t)}\frac{dr}{rk(r)} + \frac{\alpha}{h}\int_{r_w}^{r_f(t)} \frac{q_t(r,t)}{\hat{\lambda}_o}\frac{dr}{rk(r)} - \frac{\alpha}{h}\int_{r_w}^{r_f(t)} \frac{q_t(r,t)}{\hat{\lambda}_o}\frac{dr}{rk(r)}, \quad (2.5)$$

where r_f is the radius of the flood front predicted by Buckley-Leverett theory. Rearranging Eq. 2.5, we obtain

$$\Delta p = \frac{\alpha}{h\hat{\lambda}_o}\int_{r_w}^{r_f(t)} \left(\frac{\hat{\lambda}_o}{\lambda_t(r,t)} - 1\right) q_t(r,t)\frac{dr}{rk(r)} + \frac{\alpha}{h}\int_{r_f(t)}^{\infty} \frac{q_t(r,t)}{\lambda_t(r,t)}\frac{dr}{rk(r)} + \frac{\alpha}{h}\int_{r_w}^{r_f(t)} \frac{q_t(r,t)}{\hat{\lambda}_o}\frac{dr}{rk(r)}. \quad (2.6)$$

Note that ahead of the water front, i.e., for $r > r_f$, we have $\lambda_t(r,t) = \hat{\lambda}_o$. In addition, according to the steady-state theory of Thompson and Reynolds, the total rate $q(r,t)$ is equal to the constant injection rate for $r < r_{ss}$, where $r_{ss} = r_{ss}(t)$ denotes the radius of the steady-state zone of constant total rate at injection time t. For any set of physically reasonable values of reservoir and well data, we have $r_f(t) < r_{ss}(t)$ [28]. Therefore, the equation $q_t(r,t) = q_{inj}$ holds everywhere behind the front, i.e., for $r < r_f$ and Eq. 2.6 becomes

$$\Delta p = \frac{\alpha}{h\hat{\lambda}_o}\int_{r_w}^{\infty} q_t(r,t)\frac{dr}{rk(r)} + \frac{\alpha q_{inj}}{h\hat{\lambda}_o}\int_{r_w}^{r_f(t)} \left(\frac{\hat{\lambda}_o}{\lambda_t(r,t)} - 1\right)\frac{dr}{rk(r)}, \quad (2.7)$$

or simply

$$\Delta p = \Delta p_o + \frac{\alpha q_{inj}}{h\hat{\lambda}_o}\int_{r_w}^{r_f(t)} \left(\frac{\hat{\lambda}_o}{\lambda_t(r,t)} - 1\right)\frac{dr}{rk(r)}, \quad (2.8)$$

where Δp_o is the injectivity single-phase flow pressure change based on oil properties at irreducible water saturation, i.e., the single-phase pressure change that we would obtain

by injecting oil through a vertical well into an oil reservoir of permeability $k(r)$, defined by Eq. 2.4. To evaluate this pressure change, one would use the term $kk_{ro}(S_{iw})/\mu_o$ for k/μ_o and $\hat{c}_{to} = c_o(1 - S_{iw}) + c_w S_{iw} + c_r$ for the total compressibility of the system in the single-phase solution.

At this point of the analysis, we need to consider two distinct cases with respect to the location of the flood front: (i) the flood front is still moving in the skin zone so that the permeability $k(r)$ in Eq. 2.4 is simply replaced by the permeability in the skin zone, k_s. Under this condition, Eq. 2.8 becomes

$$\Delta p = \Delta p_o + \frac{\alpha q_{inj}}{k_s h \hat{\lambda}_o} \int_{r_w}^{r_f(t)} \left(\frac{\hat{\lambda}_o}{\lambda_t(r,t)} - 1 \right) \frac{dr}{r}. \tag{2.9}$$

We let Z be the similarity variable also known as the Boltzmann variable defined by

$$Z = \frac{r^2}{4t}. \tag{2.10}$$

Differentiating Eq. 2.10 with respect to r yields

$$dZ = 2\frac{r}{4t}dr = 2\frac{r^2}{4t}\frac{dr}{r} = 2Z\frac{dr}{r}, \tag{2.11}$$

or

$$\frac{dZ}{Z} = 2\frac{dr}{r}. \tag{2.12}$$

If we also define the Boltzmann variable at the water front by

$$Z_f = \frac{r_f^2}{4t}, \tag{2.13}$$

then Eq. 2.9 becomes

$$\Delta p = \Delta p_o + \frac{\alpha q_{inj}}{2k_s h \hat{\lambda}_o} \int_{r_w^2/4t}^{Z_f} \left(\frac{\hat{\lambda}_o}{\lambda_t(Z)} - 1 \right) \frac{dZ}{Z}. \tag{2.14}$$

Here, we assumed that the saturation profile can be approximated by the one obtained

by injecting water through a line source well. In the Z variable, the location of the water front Z_f is stationary, i.e., it does not vary with time. Moreover, λ_t is a unique function of Z so that $\lambda_t(r,t) = \lambda_t(Z)$. If we take the derivative of Δp with respect to the logarithm of time, we obtain

$$\Delta p' = \frac{d\Delta p}{d\ln t} = \frac{d\Delta p_o}{d\ln t} + \frac{\alpha q_{inj}}{2k_s h\hat{\lambda}_o} t\frac{d}{dt}\int_{r_w^2/4t}^{Z_f}\left(\frac{\hat{\lambda}_o}{\lambda_t(Z)} - 1\right)\frac{dZ}{Z}. \tag{2.15}$$

By applying Leibnitz integral rule, it is easy to show that

$$\begin{aligned}\frac{d}{dt}\int_{r_w^2/4t}^{Z_f}\left(\frac{\hat{\lambda}_o}{\lambda_t(Z)} - 1\right)\frac{dZ}{Z} &= -\left(\frac{\hat{\lambda}_o}{\lambda_t(r_w^2/4t)} - 1\right)\frac{4t}{r_w^2}\left(-\frac{r_w^2}{4t^2}\right)\\ &= \frac{1}{t}\left(\frac{\hat{\lambda}_o}{\lambda_t(r_w,t)} - 1\right).\end{aligned} \tag{2.16}$$

Substituting Eq. 2.16 into Eq. 2.15 and using the result that $\lambda_t = \hat{\lambda}_w$ at r_w give

$$\Delta p' = \Delta p'_o + \frac{\alpha q_{inj}}{2k_s h\hat{\lambda}_o}\left(\frac{\hat{\lambda}_o}{\hat{\lambda}_w} - 1\right). \tag{2.17}$$

Introducing the end-point mobility ratio, $\hat{M} = \frac{\hat{\lambda}_w}{\hat{\lambda}_o}$ and rewriting the preceding equation,

$$\Delta p' = \Delta p'_o + \frac{\alpha q_{inj}}{2k_s h\hat{\lambda}_o}\left(\frac{1}{\hat{M}} - 1\right). \tag{2.18}$$

At sufficiently large values of t, the single-phase solution based on oil mobility at irreducible water saturation is given by

$$\Delta p_o = \frac{\alpha q_{inj}}{kh\hat{\lambda}_o}\left[\frac{1}{2}\ln\left(\frac{\beta k\hat{\lambda}_o t}{\phi\hat{c}_{to}r_w^2}\right) + 0.4045 + s\right], \tag{2.19}$$

and its derivative with respect to the logarithm of time by

$$\Delta p'_o = \frac{\alpha q_{inj}}{2kh\hat{\lambda}_o}. \tag{2.20}$$

In Eq. 2.19, s denotes the mechanical skin factor and β is a constant which depends on the

system of units used. If oil field units with time in hours are used, then $\beta = 2.637 \times 10^{-4}$. Using Eq. 2.20 in Eq. 2.18 yields

$$\Delta p' = \frac{\alpha q_{inj}}{2kh\hat{\lambda}_o}\left[1 + \frac{k}{k_s}\left(\frac{1}{\hat{M}} - 1\right)\right], \tag{2.21}$$

or rearranging the preceding equation

$$\Delta p' = \frac{\alpha q_{inj}}{2k_s h\hat{\lambda}_w}\left[1 - \hat{M}\left(1 - \frac{k_s}{k}\right)\right]. \tag{2.22}$$

Eq. 2.22 clearly indicates that the pressure derivative can be negative at early times provided that

$$\hat{M}\left(1 - \frac{k_s}{k}\right) > 1. \tag{2.23}$$

Note that this condition holds only if the well is damaged ($s > 0$) and the mobility ratio is unfavorable ($\hat{M} > 1$).

(ii) If the water front is beyond the skin zone, that is $r_s \leq r_f$, Eq. 2.8 becomes

$$\Delta p = \Delta p_o + \frac{\alpha q_{inj}}{k_s h\hat{\lambda}_o}\int_{r_w}^{r_s}\left(\frac{\hat{\lambda}_o}{\lambda_t(r,t)} - 1\right)\frac{dr}{r} + \frac{\alpha q_{inj}}{kh\hat{\lambda}_o}\int_{r_s}^{r_f(t)}\left(\frac{\hat{\lambda}_o}{\lambda_t(r,t)} - 1\right)\frac{dr}{r}. \tag{2.24}$$

By adding and subtracting to Eq. 2.24 an integral from r_w to r_s, we have

$$\begin{aligned}\Delta p = \Delta p_o + \frac{\alpha q_{inj}}{k_s h\hat{\lambda}_o}\int_{r_w}^{r_s}\left(\frac{\hat{\lambda}_o}{\lambda_t(r,t)} - 1\right)\frac{dr}{r} + \frac{\alpha q_{inj}}{kh\hat{\lambda}_o}\int_{r_s}^{r_f(t)}\left(\frac{\hat{\lambda}_o}{\lambda_t(r,t)} - 1\right)\frac{dr}{r} \\ + \frac{\alpha q_{inj}}{kh\hat{\lambda}_o}\int_{r_w}^{r_s}\left(\frac{\hat{\lambda}_o}{\lambda_t(r,t)} - 1\right)\frac{dr}{r} - \frac{\alpha q_{inj}}{kh\hat{\lambda}_o}\int_{r_w}^{r_s}\left(\frac{\hat{\lambda}_o}{\lambda_t(r,t)} - 1\right)\frac{dr}{r},\end{aligned} \tag{2.25}$$

or simplifying,

$$\Delta p = \Delta p_o + \frac{\alpha q_{inj}}{kh\hat{\lambda}_o}\left[\left(\frac{k}{k_s} - 1\right)\int_{r_w}^{r_s}\left(\frac{\hat{\lambda}_o}{\lambda_t(r,t)} - 1\right)\frac{dr}{r} + \int_{r_w}^{r_f(t)}\left(\frac{\hat{\lambda}_o}{\lambda_t(r,t)} - 1\right)\frac{dr}{r}\right]. \tag{2.26}$$

Using the Boltzmann variable as defined previously, Eq. 2.26 becomes

$$\Delta p = \Delta p_o + \frac{\alpha q_{inj}}{2kh\hat{\lambda}_o}\left[\left(\frac{k}{k_s}-1\right)\int_{r_w^2/4t}^{r_s^2/4t}\left(\frac{\hat{\lambda}_o}{\lambda_t(Z)}-1\right)\frac{dZ}{Z}+\int_{r_w^2/4t}^{Z_f}\left(\frac{\hat{\lambda}_o}{\lambda_t(Z)}-1\right)\frac{dZ}{Z}\right]. \quad (2.27)$$

Again, if we differentiate Δp with respect to $\ln(t)$ and use Leibnitz rule, we obtain

$$\Delta p' = \Delta p'_o + \frac{\alpha q_{inj}}{2kh\hat{\lambda}_o}\left[\left(\frac{k}{k_s}-1\right)\left[-\left(\frac{\hat{\lambda}_o}{\lambda_t(r_s^2/4t)}-1\right)+\left(\frac{\hat{\lambda}_o}{\lambda_t(r_w^2/4t)}-1\right)\right] + \left(\frac{\hat{\lambda}_o}{\lambda_t(r_w^2/4t)}-1\right)\right]. \quad (2.28)$$

By letting $\lambda_t(r_w^2/4t) = \lambda_t(r_w,t) = \hat{\lambda}_w$ and substituting Eq. 2.20 in Eq. 2.28, we finally obtain

$$\Delta p' = \frac{\alpha q_{inj}}{2kh\hat{\lambda}_w}\left[1-\left(\frac{k}{k_s}-1\right)\left(\frac{\hat{\lambda}_w}{\lambda_t(r_s,t)}-1\right)\right]. \quad (2.29)$$

Note that once the flood front moves outside the skin zone, Eq. 2.29 predicts a negative pressure derivative only if the following condition is satisfied:

$$\left(\frac{k}{k_s}-1\right)\left(\frac{\hat{\lambda}_w}{\lambda_t(r_s,t)}-1\right) > 1, \quad (2.30)$$

or equivalently

$$\lambda_t(r_s,t) < \hat{\lambda}_w\left(1-\frac{k_s}{k}\right). \quad (2.31)$$

Two remarks with respect to Eq. 2.31 are in order. First, this condition is independent of the end-point mobility ratio. Therefore, unlike Eq. 2.23, it can hold even for favorable mobility cases. Second, once the skin zone is completely swept by water, $\lambda_t(r_s,t)$ becomes equal to $\hat{\lambda}_w$ and Eq. 2.29 gives

$$\Delta p' = \frac{\alpha q_{inj}}{2kh\hat{\lambda}_w}, \tag{2.32}$$

reflecting water properties at residual oil saturation at long injection times.

One key observation inherent in the analytical solutions obtained using the steady-state theory of Thompson and Reynolds [33] is that the analytical solution for the injection pressure is written as the sum of the solution based on single-phase oil properties at irreducible (or initial) water saturation and a multiphase flow term which represents the additional pressure change due to the contrast between oil mobility at irreducible saturation and total mobility in the zone invaded by injected water. If one wishes to use the same approach, it is crucial to generate the water distribution in the reservoir for the computation of the total mobility profile during the injection period. So, what is required are models that describe the movement of water when injected through a vertical or horizontal well. In the next section, we will present models for the movement of water based on a combination of Buckley-Leverett equations that allow us to accurately approximate the two-phase flow component of the analytical solution for a restricted-entry vertical well case and a horizontal well with an unequal offset.

2.2 Models for the Movement of Injected Water

2.2.1 Restricted-Entry Vertical Well Case

Even though the Buckley-Leverett theory provides an analytical method for generating the saturation profile, its application requires the knowledge of the flow direction. For the single-phase flow through a restricted-entry vertical well, it is well known that near the well, we may have radial flow adjacent to the open interval, but far from the well, radial flow occurs over the entire thickness of the formation. For our injection problem, we expect that water, when injected, will move radially such that the height of the water bank increases with time until the height is equal to the formation thickness. We can, therefore, evaluate the water saturation distribution and associated total mobility profile from a Buckley-Leverett equation based on radial flow through a system of variable

thickness given by

$$\int_{r_w}^{r(S_w)} rh(r)dr = \frac{\theta q_{inj} t}{2\pi\phi} \frac{df_w(S_w)}{dS_w}, \tag{2.33}$$

where the constant θ depends on the system of units used with $\theta = 5.615/24 = 0.23396$ if oil field units are used with time in hours. Eq. 2.33 gives a relation between $r(S_w)$, the location of the saturation S_w at time t, and other parameters for all values of water saturation between S_{wf} and $1 - S_{or}$. This equation assumes that the injection rate q_{inj} is constant. To apply Eq. 2.33 to compute the saturation profile requires knowledge of $h(r)$.

We start the discussion by presenting two relatively simple models for which the bottom of the perforated interval is adjacent to the bottom of the formation. Later, we will generalize them to an arbitrary configuration with respect to the location of the open interval. Fig. 2.1 gives a schematic of model 1. With this model, it is assumed that injected water moves radially adjacent to the open interval with the height of the water bank equal to h_p, until the water front reaches the radius r_c and then moves radially over the total thickness, h. The true profile could be quite different than this because between the two zones where the flow of water is radial, there must be a significant component of vertical flow. In our model for approximating the saturation profile, we simply ignore the transitional flow between the two radial flow regions. Specifically, we assume that $h(r)$ is given by

$$h(r) = \begin{cases} h_p & \text{if } r < r_c, \\ h & \text{if } r > r_c. \end{cases} \tag{2.34}$$

Model 2 is shown in Fig. 2.2. In this model, the formation thickness varies linearly with the radial distance in the inner region. this model is more realistic in the sense that it approximates the transitional flow between the two radial flow regions. In this case, the height of the water bank is given by

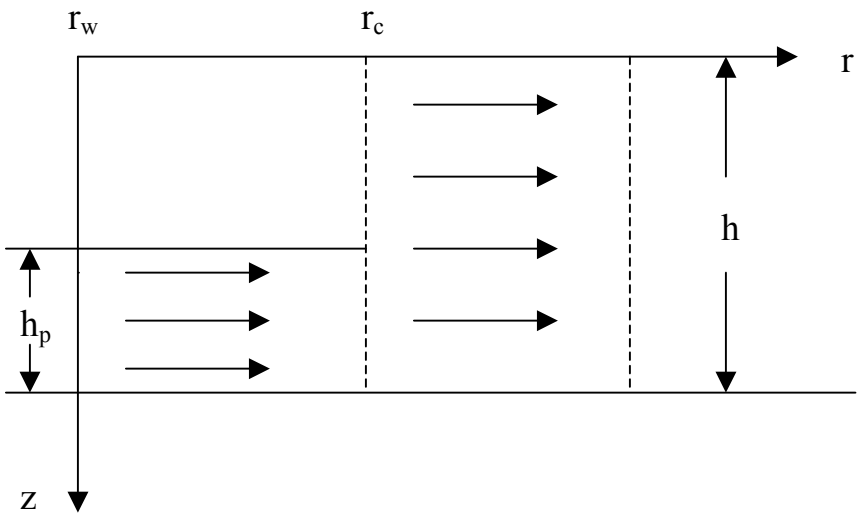

Figure 2.1: Radial flow regime for the restricted entry problem, model 1

$$h(r) = \begin{cases} h + (\frac{h-h_p}{r_c-r_w})(r-r_c) & \text{if } r \le r_c, \\ h & \text{if } r \ge r_c. \end{cases} \tag{2.35}$$

Here, r_c is referred to as the radius of convergence. More specifically, r_c is the radius of convergence of flow lines derived from single-phase theory. For the single-phase restricted-entry case, the flow lines convergence can be approximated by two concentric radial regions. In both regions, the flow lines are assumed to have a perfectly one-dimensional radial symmetry. At the interface of radius r_c, we require the pressure and flow rate to be continuous in order to derive a formula for this transitional point. A more detailed discussion on how to obtain the new transitional point r_c for each model is provided in Appendix A.

For the restricted-entry case based on model 1, the radial location at time t of any saturation S_w with $S_{wf} < S_w < 1 - S_{or}$ is calculated using Eq. 2.34 in Eq. 2.33. Specifically, if $r(S_w) < r_c$, then Eqs. 2.33 and 2.34 imply that

$$r^2(S_w) = r_w^2 + \frac{\theta q_{inj} t}{\pi \phi h_p} \frac{df_w(S_w)}{dS_w}. \tag{2.36}$$

Similarly, if $r(S_w) > r_c$

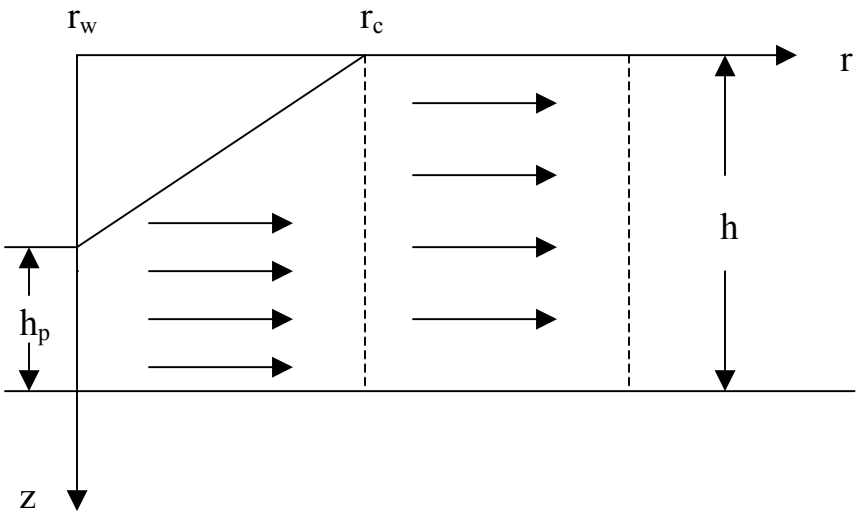

Figure 2.2: Radial flow regime for the restricted entry problem, model 2

$$r^2(S_w) = br_w^2 + (1-b)r_c^2 + \frac{\theta q_{inj} t}{\pi \phi h} \frac{df_w(S_w)}{dS_w}, \tag{2.37}$$

where b denotes the penetration ratio defined by

$$b = \frac{h_p}{h}. \tag{2.38}$$

For model 2, calculation of the saturation distribution is more complex. The appropriate formulas are obtained by replacing Eq. 2.35 into Eq. 2.33. Thus, we have

$$\int_{r_w}^{r(S_w)} r\left[h + (\frac{h-h_p}{r_c - r_w})(r - r_c)\right] dr = \frac{\theta q_{inj} t}{2\pi\phi} \frac{df_w(S_w)}{dS_w}, \tag{2.39}$$

or after integration,

$$\frac{1}{3}(1-b)(r^3(S_w) - r_w^3) + \frac{1}{2}(br_c - r_w)(r^2(S_w) - r_w^2) = \frac{\theta q_w B_w t}{2\pi\phi h} \frac{df_w(S_w)}{dS_w}(r_c - r_w), \tag{2.40}$$

provided the equation results in $r(S_w) < r_c$. Otherwise, the location of S_w is obtained from

$$\int_{r_w}^{r_c} r\left[h + (\frac{h-h_p}{r_c-r_w})(r-r_c)\right]dr + \int_{r_c}^{r(S_w)} rhdr = \frac{\theta q_{inj} t}{2\pi\phi}\frac{df_w(S_w)}{dS_w}, \tag{2.41}$$

if $r(S_w) > r_c$. Integration of Eq. 2.41 yields

$$r^2(S_w) = \frac{\theta q_{inj} t}{\pi\phi h}\frac{df_w(S_w)}{dS_w} + \frac{1}{3}[(1-b)r_c^2 + (1-b)r_c r_w + (1+2b)r_w^2]. \tag{2.42}$$

2.2.2 Horizontal Well Case

Here, the Peres and Reynolds [28] model for the movement of water when injected through a horizontal well in the center of the reservoir formation is extended to the case where the horizontal well has unequal offset, i.e., the distance from the centerline of the well to the top boundary is not equal to the distance to the bottom boundary. The two potential models considered are conceptually equivalent to the models introduced for a restricted-entry vertical well. In the following, it is assumed that the centerline of the well of length L coincides with the y-axis and that z_w represents the distance from the centerline of the well to the closest boundary in the z-direction. Here, the top boundary is closest to the centerline of the well.

The geometry of model 1 is shown in Fig. 2.3. The idea of this model is to assume that at early times, the injected water moves radially in the plane (x, z). Once the flood front reaches the top reservoir boundary, a first linear flow regime develops causing the propagation of water in the x-direction for $x_1 < x < x_2$ with a cross-sectional area to flow equal to $2z_wL$. As long as the well tips are not felt, a second linear flow regime occurs in the x-direction for $x > x_2$ with the cross-sectional area to flow given by hL. Later on, a second radial flow regime which reflects radial pressure diffusion in the (x, y) plane develops when both top and bottom boundaries and flow in the reservoir beyond the well tips significantly affect the pressure response. As shown previously by [28], this situation, illustrated in Fig. 2.4, occurs once the water front reaches the distance

$$x_3 = \frac{\pi}{8}L. \tag{2.43}$$

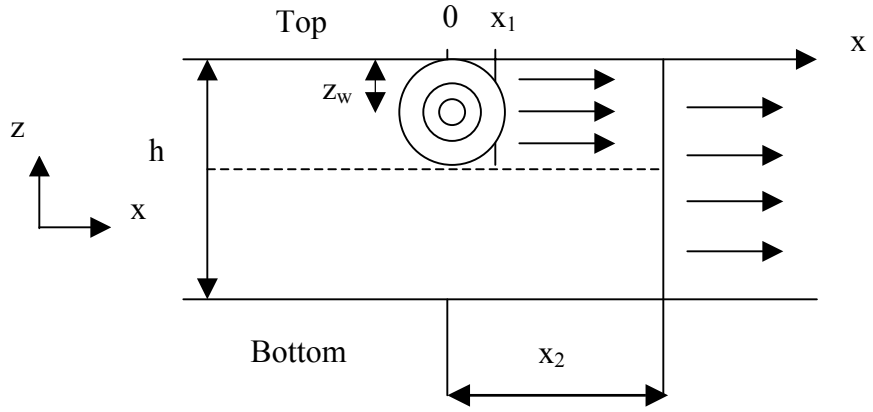

Figure 2.3: Radial and linear flow regimes in the (x-z) plane, model 1

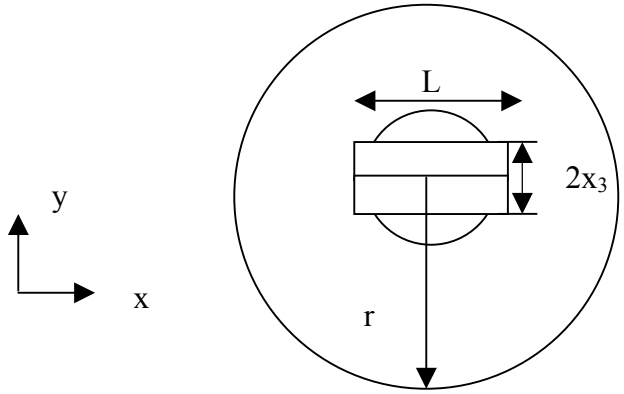

Figure 2.4: Radial flow regime in the (x-y) plane.

The parameter x_1 is obtained by applying Deppe's procedure (see [18]) based on preservation of injected water volume, which translates in terms of area as

$$\frac{\pi}{2} z_w^2 = 2 z_w x_1, \tag{2.44}$$

or equivalently

$$x_1 = \frac{\pi}{4} z_w. \tag{2.45}$$

Fig. 2.5 displays model 2. Here, as for model 1, we assume that the injected water front propagates radially and uniformly along the entire wellbore in the (x, z) plane before it hits the top reservoir boundary. Then, water moves linearly over a variable thickness

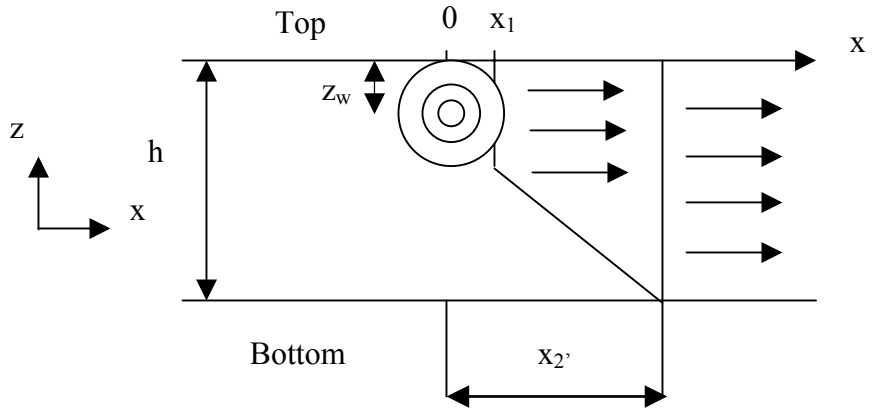

Figure 2.5: Radial and linear flow regimes on the (x-z) plane, model 2

from x_1 to x_2 until the front reaches x_2, and after this time, the movement of water is the same as in model 1. Similar to the radius of convergence r_c in the restricted-entry case, the position x_2 in both models is a parameter that we can obtain based on single-phase flow analysis of the convergence pseudo-skin factor due to convergence of flow lines. Having said that, it is important to realize that the position x_2 defined for model 1 is different from the one defined for model 2 due to a difference in geometry of the two models. A discussion on how to determine this parameter for each model will be given later. For model 1, the variable thickness is given by

$$h(x) = \begin{cases} 2z_w & \text{if } 0 \leq x \leq x_2, \\ h & \text{if } x > x_2, \end{cases} \tag{2.46}$$

whereas, for model 2, it is given by

$$h(x) = \begin{cases} 2z_w & \text{if } 0 \leq x \leq x_1, \\ h + (\frac{h-2z_w}{x_2-x_1})(x - x_2) & \text{if } x_1 \leq x \leq x_2, \\ h & \text{if } x \geq x_2. \end{cases} \tag{2.47}$$

In order to apply these models, we will combine three one-dimensional Buckley-Leverett equations to generate the water saturation and total mobility profiles necessary for the evaluation of the multiphase pressure change. Each of these equations starts at

time $t = 0$ and is applied for all saturations such that $S_{wf} \leq S_w \leq 1 - S_{or}$. For radial flow in the (x, z) plane, the radial distance of any saturation, that we denote by r_{zx}, can be obtained from

$$r_{zx}^2(S_w) = \frac{\theta q_{inj} t}{\pi \phi L} \frac{df_w(S_w)}{dS_w} + r_w^2. \tag{2.48}$$

In particular, the location of the water front $r_{zx}(S_{wf})$, which we simply denote by $r_{zx,f}$ can be obtained by evaluating Eq. 2.48 at the water front saturation S_{wf}.

For the movement of water in the x-direction, the location of a saturation S_w is obtained from a Buckley-Leverett equation based on linear flow through a system of variable thickness. Thus, we have

$$\int_0^{x(S_w)} h(x) L dx = \frac{\theta q_{inj} t}{2\phi} \frac{df_w(S_w)}{dS_w}. \tag{2.49}$$

By using the appropriate formula for $h(x)$, Eq. 2.49 can be applied for both models 1 and 2. For the unequal offset horizontal well case based on model 1, the position x of the water saturation S_w is obtained by replacing Eq. 2.46 into Eq. 2.49 as follows

$$\int_0^{x(S_w)} 2 z_w L dx = \frac{\theta q_{inj} t}{2\phi} \frac{df_w(S_w)}{dS_w}, \tag{2.50}$$

provided the equation results in $x(S_w) \leq x_2$. Integrating Eq. 2.50 yields

$$x(S_w) = \frac{\theta q_{inj} t}{4\phi z_w L} \frac{df_w(S_w)}{dS_w}. \tag{2.51}$$

If $x > x_2$, the saturation profile in obtained as follows

$$\int_0^{x_2} 2 z_w L dx + \int_{x_2}^{x(S_w)} h L dx = \frac{\theta q_{inj} t}{2\phi} \frac{df_w(S_w)}{dS_w}. \tag{2.52}$$

Integrating Eq. 2.52 and rearranging gives

$$x(S_w) = \frac{\theta q_{inj} t}{2\phi h L} \frac{df_w(S_w)}{dS_w} + (1 - \frac{2 z_w}{h}) x_2, \tag{2.53}$$

where the second term of Eq. 2.53 represents the location of the flood front at the position x_2. For model 2, the saturation distribution is generated by substituting Eq. 2.47 into Eq. 2.49. For any $x \leq x_2$, we have

$$\int_0^{x_1} 2z_w L dx + \int_{x_1}^{x(S_w)} \left[h - \frac{(h-2z_w)}{(x_2-x_1)}(x_2-x)\right] L dx = \frac{\theta q_{inj} t}{2\phi L}\frac{df_w(S_w)}{dS_w}. \tag{2.54}$$

If we integrate Eq. 2.54 and rearrange, we obtain the following quadratic equation

$$(h-2z_w)x^2(S_w) + 2(2z_w x_2 - h x_1)x(S_w) - \left[(2z_w - h)x_1^2 + \frac{\theta q_{inj} t}{\phi L}\frac{df_w(S_w)}{dS_w}(x_2 - x_1)\right] = 0. \tag{2.55}$$

The solution for $x(S_w)$ that we retain is

$$x(S_w) = \frac{h x_1 - 2z_w x_2 + \sqrt{\Delta}}{h - 2z_w}, \tag{2.56}$$

where the discriminant Δ is given by

$$\Delta = (x_2 - x_1)\left[4z_w\left(z_w x_2 - (h - z_w)x_1\right) + (h - 2z_w)\frac{\theta q_{inj} t}{\phi L}\frac{df_w(S_w)}{dS_w}\right]. \tag{2.57}$$

Similarly, if $x(S_w) > x_2$, the saturation distribution is derived from

$$\int_0^{x_1} 2z_w L dx + \int_{x_1}^{x_2} L\left[h - \frac{(h-2z_w)}{(x_2-x_1)}(x_2-x)\right] dx + \int_{x_2}^{x(S_w)} L h dx = \frac{\theta q_{inj} t}{2\phi}\frac{df_w(S_w)}{dS_w}, \tag{2.58}$$

which after integration and manipulation yields the expression for $x(S_w)$ given by

$$x(S_w) = \frac{\theta q_{inj} t}{2\phi L h}\frac{df_w(S_w)}{dS_w} + \frac{1}{2}(1 - \frac{2z_w}{h})(x_1 + x_2). \tag{2.59}$$

By evaluating Eq. 2.51 or 2.53 for model 1 and Eq. 2.56 or 2.59 for model 2 at S_{wf}, the location of the water front that we denote by x_f can be found.

Finally, for the radial flow of water in the (x, y) plane, the following Buckley-Leverett formula is applied:

$$r_{xy}^2(S_w) = \frac{\theta q_{inj} t}{\pi \phi h} \frac{df_w(S_w)}{dS_w}. \tag{2.60}$$

The location of the flood front, denoted by $r_{f,xy}$, when propagating in the (x, y) plane is obtained by evaluating Eq. 2.60 at the water front saturation S_{wf}.

It remains to determine the position x_2 for each model. Similar to formulas derived to compute the radius of convergence r_c in the restricted-entry case (see Appendix A), the position x_2 is determined by single-phase flow theory. For both models, we start the analysis by writing the pressure change from r_w to x_2 as the sum of the pressure change from x_1 to x_2 due to linear flow through a cross-sectional area given by $h(x)L$ and the pressure change due to radial flow from r_w to z_w. Therefore, for this steady-state single-phase flow in a homogeneous isotropic reservoir, one gets

$$p_{x_2} - p_{wf} = \frac{\alpha q B \mu}{kL} \int_{r_w}^{z_w} \frac{dr}{r} + \frac{\pi \alpha q B \mu}{kL} \int_{x_1}^{x_2} \frac{dx}{h(x)}. \tag{2.61}$$

The total pressure change due to linear flow from 0 to x_2 is

$$p_{x_2} - p_{wf} = \frac{\pi \alpha q B \mu}{kL} \int_{0}^{x_2} \frac{dx}{h} = \frac{\pi \alpha q B \mu}{khL} x_2. \tag{2.62}$$

It is easy to see that the extra pressure drop due to flow lines convergence (from a linear to a radial geometry) is obtained by subtracting Eq. 2.62 from Eq. 2.61 to obtain

$$\Delta p_{conv} = \frac{\alpha q B \mu}{kL} \left[\ln\left(\frac{z_w}{r_w}\right) + \pi \int_{x_1}^{x_2} \frac{dx}{h(x)} - \frac{\pi}{h} x_2 \right]. \tag{2.63}$$

We let S_{conv} denotes the pseudo-skin factor associated with the convergence pressure change Δp_{conv} so that

$$\Delta p_{conv} = \frac{\alpha q B \mu}{kL} s_{conv}. \tag{2.64}$$

Thus, equating the right sides of Eqs. 2.63 and 2.64 gives

$$s_{conv} = \ln\left(\frac{z_w}{r_w}\right) + \pi \int_{x_1}^{x_2} \frac{dx}{h(x)} - \frac{\pi}{h} x_2. \tag{2.65}$$

To proceed further requires a choice for $h(x)$. For model 1, $h(x)$ is defined by Eq. 2.46. In this case, Eq. 2.65 simplifies to

$$s_{conv} = \ln\left(\frac{z_w}{r_w}\right) + \pi \int_{x_1}^{x_2} \frac{dx}{2z_w} - \frac{\pi}{h} x_2, \tag{2.66}$$

or equivalently

$$s_{conv} = \ln\left(\frac{z_w}{r_w}\right) + \frac{\pi}{2z_w}(x_2 - x_1) - \frac{\pi}{h} x_2. \tag{2.67}$$

Using Eq. 2.45 in Eq. 2.67 and solving for x_2 gives

$$x_2 = \frac{h}{\pi(\frac{h}{2z_w} - 1)} \left[s_{conv} - \ln\left(\frac{z_w}{r_w}\right) + \frac{\pi^2}{8} \right]. \tag{2.68}$$

Odeh and Babu [25] and Kuchuk et al. [23] derived the following analytical expression for the exact convergence pseudo-skin factor for the single phase flow

$$s_{conv} = \ln\left(\frac{h}{2\pi r_w \sin(\pi z_w / h)}\right). \tag{2.69}$$

Finally, replacing Eq. 2.69 in Eq. 2.68 gives

$$x_2 = \frac{h}{\pi(\frac{h}{2z_w} - 1)} \left[\ln\left(\frac{h}{2\pi z_w \sin(\pi z_w / h)}\right) + \frac{\pi^2}{8} \right]. \tag{2.70}$$

For model 2, $h(x)$ is defined by Eq. 2.47. Thus, Eq. 2.65 yields

$$s_{conv} = \ln\left(\frac{z_w}{r_w}\right) + \pi \int_{x_1}^{x_2} \frac{dx}{h + (\frac{h - 2z_w}{x_2 - x_1})(x - x_2)} - \frac{\pi}{h} x_2. \tag{2.71}$$

Integrating Eq. 2.71 and rearranging, we obtain

$$s_{conv} = \ln\left(\frac{z_w}{r_w}\right) + \frac{\pi(x_2 - x_1)}{(h - 2z_w)} \ln\left(\frac{h}{2z_w}\right) - \frac{\pi}{h} x_2. \tag{2.72}$$

Finally, using Eqs. 2.45 and 2.69 in Eq. 2.72 and solving for x_2 gives

$$x_2 = \frac{\frac{\pi^2}{8(h/2z_w - 1)} \ln\left(\frac{h}{2z_w}\right) + \ln\left(\frac{h}{2\pi z_w \sin(\pi z_w/h)}\right)}{\frac{\pi}{h}\left[\frac{h/2z_w}{(h/2z_w - 1)} \ln\left(\frac{h}{2z_w}\right) - 1\right]}. \tag{2.73}$$

2.3 Pressure Response

2.3.1 Injection Through a Restricted-Entry Vertical Well

Previously, we derived an analytical solution for the injection pressure at a completely-penetrating vertical well located at the center of an infinite acting reservoir (see Eq. 2.8). To apply Eq. 2.8 to the restricted-entry case, we simply use the single-phase restricted-entry solution for Δp_o and modify the two-phase flow integral to account for the fact that the injected water moves radially in the region adjacent to the open interval ("height" or thickness given by h_p) and at later times moves radially over the total thickness, h, of the reservoir. In this case, we have

$$\Delta p = \Delta p_o + \frac{\alpha q_{inj}}{\hat{\lambda}_o} \int_{r_w}^{r_f(t)} \left(\frac{\hat{\lambda}_o}{\lambda_t(r,t)} - 1\right) \frac{dr}{rh(r)k(r)}. \tag{2.74}$$

For the single-phase flow restricted-entry case, we may obtain radial flow adjacent to the open interval near the well (length of perforated interval is h_p), whereas far from the well, radial flow occurs over the total formation thickness, h. Thus, as mentioned earlier, it is convenient to visualize the reservoir as two concentric regions in which the flow lines have a perfectly 1D radial symmetry. The interface is characterized by a radius, that we called radius of convergence r_c, see Fig. 2.1 or Fig. 2.2. For a two-phase flow problem, on the other hand, the propagation of the water flood front and the propagation of the pressure diffusion (steady-state zone) occur on different time scales. Due to this, three distinct flow regimes can develop during an injectivity test in a partially-completed

vertical well. These flow regimes are: first radial/first radial, second radial/first radial and second radial/second radial where the first name in each flow regime corresponds to the behavior of the single-phase component and the second term corresponds to the movement of water. For simplicity, we derive specific flow regime equations only for model 1, although it is expected that the equations for model 2 will not be radically different at least at early and late times when water moves radially.

First Radial/First Radial Flow Regime

This flow regime corresponds to the time period when Δp_o is given by the following equation

$$\Delta p_o = \frac{\alpha q_{inj}}{k h_p \hat{\lambda}_o}\left[\frac{1}{2}\ln\left(\frac{4\eta_o t}{e^{\gamma} r_w^2}\right) + s\right], \tag{2.75}$$

and the water front is moving radially in the region $r < r_c$. In Eq. 2.75, γ is Euler's constant ($\gamma = 0.57722$) and η_o is the reservoir diffusivity based on oil properties defined by

$$\eta_o = \frac{\beta k \hat{\lambda}_o}{\phi \mu \hat{c}_{to}}, \tag{2.76}$$

where β is a unit conversion constant already defined. Recall, in oil field units with time in hours, $\beta = 2.637 \times 10^{-4}$. Also, recall that $\hat{c}_{to} = c_o(1 - S_{iw}) + c_w S_{iw} + c_r$. Assuming first that the front is still in the damaged zone and using Eq. 2.75 in Eq. 2.74, we obtain

$$\Delta p = \frac{\alpha q_{inj}}{k h_p \hat{\lambda}_o}\left[\frac{1}{2}\ln\left(\frac{4\eta_o t}{e^{\gamma} r_w^2}\right) + s\right] + \frac{\alpha q_{inj}}{k_s h \hat{\lambda}_o}\int_{r_w}^{r_f(t)}\left(\frac{\hat{\lambda}_o}{\lambda_t(r,t)} - 1\right)\frac{h}{h(r)}\,\frac{dr}{r}. \tag{2.77}$$

For model 1, $h(r) = h_p$ for $r < r_c$ and Eq. 2.77 simplifies to

$$\Delta p = \frac{\alpha q_{inj}}{k h_p \hat{\lambda}_o}\left[\frac{1}{2}\ln\left(\frac{4\eta_o t}{e^{\gamma} r_w^2}\right) + s + \frac{k}{k_s}\int_{r_w}^{r_f(t)}\left(\frac{\hat{\lambda}_o}{\lambda_t(r,t)} - 1\right)\frac{dr}{r}\right]. \tag{2.78}$$

Rewriting Eq. 2.78 in terms of the Boltzmann variable, Z, gives

$$\Delta p = \frac{\alpha q_{inj}}{k h_p \hat{\lambda}_o}\left[\frac{1}{2}\ln\left(\frac{4\eta_o t}{e^{\gamma} r_w^2}\right) + s + \frac{k}{2k_s}\int_{r_w^2/4t}^{Z_f}\left(\frac{\hat{\lambda}_o}{\lambda_t(Z)} - 1\right)\frac{dZ}{Z}\right], \tag{2.79}$$

where Z_f is the Boltzmann variable at the water front defined by Eq. 2.13. Similarly to the pure radial flow case, we assume that the saturation profile can be approximated by the one obtained by injecting water through a line source well such that $S_w = S_w(Z)$. Then, the location of the water front Z_f is stationary. Moreover, λ_t is a unique function of Z so that $\lambda_t(r,t) = \lambda_t(Z)$. If we take the derivative of Δp with respect to the logarithm of time, we obtain

$$\Delta p' = \frac{d\Delta p}{d\ln t} = \frac{\alpha q_{inj}}{2k h_p \hat{\lambda}_o}\left[1 + \frac{k}{k_s} t \frac{d}{dt}\int_{r_w^2/4t}^{Z_f}\left(\frac{\hat{\lambda}_o}{\lambda_t(Z)} - 1\right)\frac{dZ}{Z}\right]. \tag{2.80}$$

By applying Leibnitz integral rule, it is easy to show that

$$\begin{aligned}\frac{d}{dt}\int_{r_w^2/4t}^{Z_f}\left(\frac{\hat{\lambda}_o}{\lambda_t(Z)} - 1\right)\frac{dZ}{Z} &= -\left(\frac{\hat{\lambda}_o}{\lambda_t(r_w^2/4t)} - 1\right)\frac{4t}{r_w^2}\left(-\frac{r_w^2}{4t^2}\right) \\ &= \frac{1}{t}\left(\frac{\hat{\lambda}_o}{\lambda_t(r_w,t)} - 1\right).\end{aligned} \tag{2.81}$$

Substituting Eq. 2.81 into Eq. 2.80 and setting $\lambda_t(r_w,t) = \hat{\lambda}_w$ give

$$\Delta p' = \frac{\alpha q_{inj}}{2k h_p \hat{\lambda}_o}\left[1 + \frac{k}{k_s}\left(\frac{\hat{\lambda}_o}{\hat{\lambda}_w} - 1\right)\right], \tag{2.82}$$

or by introducing the end-point mobility ratio, $\hat{M} = \frac{\hat{\lambda}_w}{\hat{\lambda}_o}$ and rearranging the above equation

$$\Delta p' = \frac{\alpha q_{inj}}{2k_s h_p \hat{\lambda}_w}\left[1 - \hat{M}\left(1 - \frac{k_s}{k}\right)\right]. \tag{2.83}$$

This is the same solution derived for the complete-penetrating vertical well case given by Eq. 2.22 except h has been replaced by h_p. The pressure derivative is negative when $r_f(t) < r_s$ provided that

$$\hat{M}\left(1-\frac{\bar{k}_s}{\bar{k}}\right)>1. \tag{2.84}$$

As mentioned earlier, this condition cannot hold unless $k_s < k$ and the end-point mobility ratio is unfavorable.

Now, let us consider the case where the water front is beyond the damaged zone. Note we are still using model 1 and assuming $r_f < r_c$ so $h(r) = h_p$. In this case, the wellbore pressure drop during the injection period is given by

$$\Delta p=\frac{\alpha q_{inj}}{kh_p\hat{\lambda}_o}\left[\frac{1}{2}\ln\left(\frac{4\eta t}{e^{\gamma}r_w^2}\right)+s\right]+\frac{\alpha q_{inj}}{k_s h_p\hat{\lambda}_o}\int_{r_w}^{r_s}\left(\frac{\hat{\lambda}_o}{\lambda_t(r,t)}-1\right)\frac{dr}{r} + \frac{\alpha q_{inj}}{kh_p\hat{\lambda}_o}\int_{r_s}^{r_f(t)}\left(\frac{\hat{\lambda}_o}{\lambda_t(r,t)}-1\right)\frac{dr}{r}. \tag{2.85}$$

By adding and subtracting an integral from r_w to r_s, Eq. 2.85 becomes

$$\Delta p=\frac{\alpha q_{inj}}{kh_p\hat{\lambda}_o}\left[\frac{1}{2}\ln\left(\frac{4\eta t}{e^{\gamma}r_w^2}\right)+s\right]+\frac{\alpha q_{inj}}{k_s h_p\hat{\lambda}_o}\int_{r_w}^{r_s}\left(\frac{\hat{\lambda}_o}{\lambda_t(r,t)}-1\right)\frac{dr}{r} + \frac{\alpha q_{inj}}{kh_p\hat{\lambda}_o}\int_{r_s}^{r_f(t)}\left(\frac{\hat{\lambda}_o}{\lambda_t(r,t)}-1\right)\frac{dr}{r}+\frac{\alpha q_{inj}}{kh_p\hat{\lambda}_o}\int_{r_w}^{r_s}\left(\frac{\hat{\lambda}_o}{\lambda_t(r,t)}-1\right)\frac{dr}{r} - \frac{\alpha q_{inj}}{kh_p\hat{\lambda}_o}\int_{r_w}^{r_s}\left(\frac{\hat{\lambda}_o}{\lambda_t(r,t)}-1\right)\frac{dr}{r}, \tag{2.86}$$

or simply

$$\Delta p=\frac{\alpha q_{inj}}{kh_p\hat{\lambda}_o}\left[\frac{1}{2}\ln\left(\frac{4\eta t}{e^{\gamma}r_w^2}\right)+s+\left(\frac{k}{k_s}-1\right)\int_{r_w}^{r_s}\left(\frac{\hat{\lambda}_o}{\lambda_t(r,t)}-1\right)\frac{dr}{r}+ \int_{r_w}^{r_f(t)}\left(\frac{\hat{\lambda}_o}{\lambda_t(r,t)}-1\right)\frac{dr}{r}\right]. \tag{2.87}$$

Using the Boltzmann variable as defined previously, Eq. 2.87 becomes

$$\Delta p = \frac{\alpha q_{inj}}{2kh_p\hat{\lambda}_o}\left[\ln\left(\frac{4\eta t}{e^{\gamma}r_w^2}\right) + 2s + \left(\frac{k}{k_s}-1\right)\int_{r_w^2/4t}^{r_s^2/4t}\left(\frac{\hat{\lambda}_o}{\lambda_t(Z)}-1\right)\frac{dZ}{Z} + \int_{r_w^2/4t}^{Z_f}\left(\frac{\hat{\lambda}_o}{\lambda_t(Z)}-1\right)\frac{dZ}{Z}\right]. \quad (2.88)$$

Again, if we differentiate Δp with respect to $\ln(t)$ and use Leibnitz rule, we obtain

$$\Delta p' = \frac{\alpha q_{inj}}{2kh_p\hat{\lambda}_o}\left[1 + \left(\frac{k}{k_s}-1\right)\left[-\left(\frac{\hat{\lambda}_o}{\lambda_t(r_s^2/4t)}-1\right) + \left(\frac{\hat{\lambda}_o}{\lambda_t(r_w^2/4t)}-1\right)\right] + \left(\frac{\hat{\lambda}_o}{\lambda_t(r_w^2/4t)}-1\right)\right], \quad (2.89)$$

or by using $\lambda_t(r_w^2/4t) = \lambda_t(r_w, t) = \hat{\lambda}_w$,

$$\Delta p' = \frac{\alpha q_{inj}}{2kh_p\hat{\lambda}_w}\left[1 - \left(\frac{k}{k_s}-1\right)\left(\frac{\hat{\lambda}_w}{\lambda_t(r_s,t)}-1\right)\right]. \quad (2.90)$$

Eq. 2.90 is similar to Eq. 2.29 obtained for the complete-penetrating vertical well case except that, here, h is also replaced by h_p. Therefore, if the condition given by Eq. 2.31 is satisfied, then the pressure derivative takes negative values as a consequence of the presence of a damaged zone around the well.

Second Radial/First Radial Flow Regime

This flow regime occurs if the water front is still moving radially in the region $r < r_c$ whereas, the single-phase solution Δp_o is given by the following pseudo radial flow equation:

$$\Delta p_o = \frac{\alpha q_{inj}}{kh\hat{\lambda}_o}\left[\frac{1}{2}\ln\left(\frac{4\eta_o t}{e^{\gamma}r_w^2}\right) + \frac{s}{b} + s_b\right], \quad (2.91)$$

where b is the penetration ratio defined by Eq. 2.38 and s_b denotes the pseudo-skin factor due to restricted-entry. In this case, using Eq. 2.91 in Eq. 2.74, we can rewrite the injectivity wellbore pressure change as follows:

$$\Delta p = \frac{\alpha q_{inj}}{kh\hat{\lambda}_o}\left[\frac{1}{2}\ln\left(\frac{4\eta_o t}{e^\gamma r_w^2}\right) + \frac{s}{b} + s_b + \frac{1}{b}\frac{k}{k_s}\int_{r_w}^{r_f(t)}\left(\frac{\hat{\lambda}_o}{\lambda_t(r,t)} - 1\right)\frac{dr}{r}\right]. \tag{2.92}$$

Note that Eq. 2.92 assumes the water front is in the skin region. The integral in Eq. 2.92 can be rewritten as

$$\begin{aligned}\int_{r_w}^{r_f(t)}\left(\frac{\hat{\lambda}_o}{\lambda_t(r,t)} - 1\right)\frac{dr}{r} &= \frac{\hat{\lambda}_o}{\hat{\lambda}_w}\int_{r_w}^{r_f(t)}\left(\frac{\hat{\lambda}_w}{\lambda_t(r,t)} - \frac{\hat{\lambda}_w}{\hat{\lambda}_o}\right)\frac{dr}{r} \\ &= \frac{\hat{\lambda}_o}{\hat{\lambda}_w}\int_{r_w}^{r_f(t)}\left(\frac{\hat{\lambda}_w}{\lambda_t(r,t)} - 1\right)\frac{dr}{r} + \left(\frac{\hat{\lambda}_o}{\hat{\lambda}_w} - 1\right)\int_{r_w}^{r_f(t)}\frac{dr}{r} \\ &= \frac{1}{\hat{M}}\int_{r_w}^{r_f(t)}\left(\frac{\hat{\lambda}_w}{\lambda_t(r,t)} - 1\right)\frac{dr}{r} + \left(\frac{1}{\hat{M}} - 1\right)\ln\left(\frac{r_f(t)}{r_w}\right). \end{aligned}\tag{2.93}$$

If we also assume that the total mobility correlates in terms of the Boltzmann transform, we can rewrite Eq. 2.93 as follows:

$$\int_{r_w}^{r_f(t)}\left(\frac{\hat{\lambda}_o}{\lambda_t(r,t)} - 1\right)\frac{dr}{r} = \frac{1}{2\hat{M}}\left[\int_{r_w^2/4t}^{Z_f}\left(\frac{\hat{\lambda}_w}{\lambda_t(Z)} - 1\right)\frac{dZ}{Z} + (1-\hat{M})\ln\left(\frac{Z_f}{r_w^2/4t}\right)\right], \tag{2.94}$$

or

$$\begin{aligned}\int_{r_w}^{r_f(t)}\left(\frac{\hat{\lambda}_o}{\lambda_t(r,t)} - 1\right)\frac{dr}{r} = \frac{1}{2\hat{M}}\Bigg[&\int_{r_w^2/4t}^{Z_f}\left(\frac{\hat{\lambda}_w}{\lambda_t(Z)} - 1\right)\frac{dZ}{Z} + (1-\hat{M})\ln\left(\frac{Z_f e^\gamma}{\eta_o}\right) \\ &+ (1-\hat{M})\ln\left(\frac{4\eta_o t}{e^\gamma r_w^2}\right)\Bigg]. \end{aligned}\tag{2.95}$$

Defining s_λ by

$$s_\lambda = \frac{1}{2}\left[\int_{r_w^2/4t}^{Z_f}\left(\frac{\hat{\lambda}_w}{\lambda_t(Z)} - 1\right)\frac{dZ}{Z} + (1-\hat{M})\ln\left(\frac{Z_f e^\gamma}{\eta_o}\right)\right], \tag{2.96}$$

then, Eq. 2.95 can be rewritten as

$$\int_{r_w}^{r_f(t)} \left(\frac{\hat{\lambda}_o}{\lambda_t(r,t)} - 1 \right) \frac{dr}{r} = \frac{1}{2\hat{M}} \left[(1-\hat{M}) \ln \left(\frac{4\eta_o t}{e^{\gamma} r_w^2} \right) + 2s_\lambda \right]. \tag{2.97}$$

Because of the assumption that the Boltzmann transform applies, Z_f is a constant. Also, note that if we take the derivative of the integral in Eq. 2.96 with respect to time using Leibnitz's rule, we obtain

$$\frac{d}{dt} \int_{r_w^2/4t}^{Z_f} \left(\frac{\hat{\lambda}_w}{\lambda_t(Z)} - 1 \right) \frac{dZ}{Z} = \frac{1}{t} \left(\frac{\hat{\lambda}_w}{\lambda_t(r_w^2/4t)} - 1 \right) = 0, \tag{2.98}$$

because $\lambda_t(r_w^2/4t) = \hat{\lambda}_w$. Therefore, the term s_λ does not depend on time. Using Eq. 2.97 in Eq. 2.92 and simplifying gives

$$\Delta p = \frac{\alpha q_{inj}}{2kh\hat{\lambda}_o} \left[\left(1 + \frac{k}{bk_s} \frac{1-\hat{M}}{\hat{M}} \right) \ln \left(\frac{4\eta_o t}{e^{\gamma} r_w^2} \right) + 2s_t^{(2,1)} \right], \tag{2.99}$$

where the total skin factor during the second radial/first radial flow regime that we denote by $s_t^{(2,1)}$ is defined by

$$s_t^{(2,1)} = \frac{s}{b} + s_b + \frac{1}{b} \frac{k}{k_s} \frac{s_\lambda}{\hat{M}}. \tag{2.100}$$

Taking the derivative of Eq. 2.99 with respect to $\ln(t)$ gives

$$\begin{aligned} \Delta p' &= \frac{\alpha q_{inj}}{2kh\hat{\lambda}_o} \left[1 + \frac{1}{b} \frac{k}{k_s} \left(\frac{1-\hat{M}}{\hat{M}} \right) \right] \\ &= \frac{\alpha q_{inj}}{2k_s h_p \hat{\lambda}_w} \left[1 - \left(1 - b\frac{k_s}{k} \right) \hat{M} \right]. \end{aligned} \tag{2.101}$$

Note that the pressure derivative is negative if

$$\left(1 - b\frac{k_s}{k} \right) \hat{M} > 1. \tag{2.102}$$

For the zero skin case, i.e., $k_s = k$, Eq. 2.101 simplifies to

$$\Delta p' = \frac{\alpha q_{inj}}{2k_s h_p \hat{\lambda}_w}\left[1-(1-b)\hat{M}\right]. \tag{2.103}$$

Thus, the zero skin case will show a negative derivative whenever

$$(1-b)\hat{M} > 1. \tag{2.104}$$

Next, the case where $r_f > r_s$ is considered. Eq. 2.92 may be rewritten as

$$\Delta p = \frac{\alpha q_{inj}}{kh\hat{\lambda}_o}\left[\frac{1}{2}\ln\left(\frac{4\eta_o t}{e^{\gamma} r_w^2}\right) + \frac{s}{b} + s_b + \frac{1}{b}\left(\frac{k}{k_s}-1\right)\int_{r_w}^{r_s}\left(\frac{\hat{\lambda}_o}{\lambda_t(r,t)}-1\right)\frac{dr}{r} + \frac{1}{b}\int_{r_w}^{r_f(t)}\left(\frac{\hat{\lambda}_o}{\lambda_t(r,t)}-1\right)\frac{dr}{r}\right], \tag{2.105}$$

or in terms of Boltzmann transform and using Eq. 2.97

$$\Delta p = \frac{\alpha q_{inj}}{2kh\hat{\lambda}_o}\left[\left(1+\frac{1-\hat{M}}{b\hat{M}}\right)\ln\left(\frac{4\eta_o t}{e^{\gamma} r_w^2}\right) + 2\left(\frac{s}{b}+s_b+\frac{s_\lambda}{b\hat{M}}\right) + \frac{1}{b}\left(\frac{k}{k_s}-1\right)\int_{r_w^2/4t}^{r_s^2/4t}\left(\frac{\hat{\lambda}_o}{\lambda_t(Z)}-1\right)\frac{dZ}{Z}\right]. \tag{2.106}$$

Similar to Eq. 2.93, it is easy to show that

$$\begin{aligned}\int_{r_w^2/4t}^{r_s^2/4t}\left(\frac{\hat{\lambda}_o}{\lambda_t(Z)}-1\right)\frac{dZ}{Z} &= \frac{\hat{\lambda}_o}{\hat{\lambda}_w}\int_{r_w^2/4t}^{r_s^2/4t}\left(\frac{\hat{\lambda}_w}{\lambda_t(Z)}-1\right)\frac{dZ}{Z} + 2\left(\frac{\hat{\lambda}_o}{\hat{\lambda}_w}-1\right)\ln\left(\frac{r_s}{r_w}\right) \\ &= \frac{1}{\hat{M}}\int_{r_w^2/4t}^{r_s^2/4t}\left(\frac{\hat{\lambda}_w}{\lambda_t(Z)}-1\right)\frac{dZ}{Z} + 2\left(\frac{1}{\hat{M}}-1\right)\ln\left(\frac{r_s}{r_w}\right).\end{aligned} \tag{2.107}$$

Using Eq. 2.107 in Eq. 2.106 yields

$$\Delta p = \frac{\alpha q_{inj}}{2kh\hat{\lambda}_o}\left[\left(1+\frac{1-\hat{M}}{b\hat{M}}\right)\ln\left(\frac{4\eta_o t}{e^{\gamma}r_w^2}\right)+2\left(\frac{s}{b}+s_b+\frac{s_\lambda}{b\hat{M}}\right)\right.$$
$$\left.+\frac{1}{b\hat{M}}\left(\frac{k}{k_s}-1\right)\int_{r_w^2/4t}^{r_s^2/4t}\left(\frac{\hat{\lambda}_w}{\lambda_t(Z)}-1\right)\frac{dZ}{Z}+\frac{2}{b}\left(\frac{k}{k_s}-1\right)\left(\frac{1}{\hat{M}}-1\right)\ln\left(\frac{r_s}{r_w}\right)\right]. \quad (2.108)$$

Hawkin's [21] formula for the mechanical skin factor s is given by

$$s = \left(\frac{k}{k_s}-1\right)\ln\left(\frac{r_s}{r_w}\right). \quad (2.109)$$

If we use this relation, Eq. 2.108 simplifies to

$$\Delta p = \frac{\alpha q_{inj}}{2kh\hat{\lambda}_o}\left[\left(1+\frac{1-\hat{M}}{b\hat{M}}\right)\ln\left(\frac{4\eta_o t}{e^{\gamma}r_w^2}\right)+2\left(s_b+\frac{s+s_\lambda}{b\hat{M}}\right)\right.$$
$$\left.+\frac{1}{b\hat{M}}\left(\frac{k}{k_s}-1\right)\int_{r_w^2/4t}^{r_s^2/4t}\left(\frac{\hat{\lambda}_w}{\lambda_t(Z)}-1\right)\frac{dZ}{Z}\right]. \quad (2.110)$$

Taking the log-derivative using Leibnitz's rule gives

$$\Delta p' = \frac{\alpha q_{inj}}{2kh\hat{\lambda}_o}\left[\left(1+\frac{1-\hat{M}}{b\hat{M}}\right)+\frac{1}{b\hat{M}}\left(\frac{k}{k_s}-1\right)\left(1-\frac{\hat{\lambda}_w}{\lambda_t(r_s,t)}+\frac{\hat{\lambda}_w}{\lambda_t(r_w,t)}-1\right)\right], \quad (2.111)$$

or using $\lambda_t(r_w,t)=\hat{\lambda}_w$ and simplifying the preceding equation,

$$\Delta p' = \frac{\alpha q_{inj}}{2kh_p\hat{\lambda}_w}\left[1-\hat{M}(1-b)+\left(\frac{k}{k_s}-1\right)\left(1-\frac{\hat{\lambda}_w}{\lambda_t(r_s,t)}\right)\right]. \quad (2.112)$$

Thus, the derivative is negative for $r_f > r_s$ provided that

$$\lambda_t(r_s,t)\left[1-\hat{M}(1-b)+\left(\frac{k}{k_s}-1\right)\right] < \left(\frac{k}{k_s}-1\right)\hat{\lambda}_w. \quad (2.113)$$

Once the damaged region is completely flooded, $\lambda_t(r_s,t)=\hat{\lambda}_w$ and Eq. 2.112 becomes

$$\Delta p' = \frac{\alpha q_{inj}}{2kh_p\hat{\lambda}_w}\left[1 - \hat{M}(1-b)\right]. \tag{2.114}$$

Here, the derivative can also be negative as long as $\hat{M}(1-b) > 1$.

Second Radial/Second Radial Flow Regime

This flow regime pertains to the case where the flood front is moving radially beyond the radius of convergence, i.e., $r_f > r_c$ and Δp_o is given by Eq. 2.91. Using Eq. 2.91 in Eq. 2.74, the injection pressure drop is expressed by

$$\Delta p = \frac{\alpha q_{inj}}{kh\hat{\lambda}_o}\left[\frac{1}{2}\ln\left(\frac{4\eta_o t}{e^\gamma r_w^2}\right) + \frac{s}{b} + s_b + \frac{1}{b}\left(\frac{k}{k_s} - 1\right)\int_{r_w}^{r_s}\left(\frac{\hat{\lambda}_o}{\lambda_t(r,t)} - 1\right)\frac{dr}{r} + \frac{1}{b}\int_{r_w}^{r_c}\left(\frac{\hat{\lambda}_o}{\lambda_t(r,t)} - 1\right)\frac{dr}{r} + \int_{r_c}^{r_f(t)}\left(\frac{\hat{\lambda}_o}{\lambda_t(r,t)} - 1\right)\frac{dr}{r}\right]. \tag{2.115}$$

From Eq. 2.107, expressed in terms of r and t variables, we have

$$\int_{r_w}^{r_s}\left(\frac{\hat{\lambda}_o}{\lambda_t(r,t)} - 1\right)\frac{dr}{r} = \frac{1}{\hat{M}}\int_{r_w}^{r_s}\left(\frac{\hat{\lambda}_w}{\lambda_t(r,t)} - 1\right)\frac{dr}{r} + \left(\frac{1}{\hat{M}} - 1\right)\ln\left(\frac{r_s}{r_w}\right). \tag{2.116}$$

Substituting Eq. 2.116 into Eq. 2.115 and using Hawkin's formula gives

$$\Delta p = \frac{\alpha q_{inj}}{kh\hat{\lambda}_o}\left[\frac{1}{2}\ln\left(\frac{4\eta_o t}{e^\gamma r_w^2}\right) + \frac{s}{b} + s_b + \frac{1-\hat{M}}{b\hat{M}}s + \frac{1}{b\hat{M}}\left(\frac{k}{k_s} - 1\right)\int_{r_w}^{r_s}\left(\frac{\hat{\lambda}_w}{\lambda_t(r,t)} - 1\right)\frac{dr}{r} + \frac{1}{b}\int_{r_w}^{r_c}\left(\frac{\hat{\lambda}_o}{\lambda_t(r,t)} - 1\right)\frac{dr}{r} + \int_{r_c}^{r_f(t)}\left(\frac{\hat{\lambda}_o}{\lambda_t(r,t)} - 1\right)\frac{dr}{r}\right]. \tag{2.117}$$

For the second radial/second radial flow regime, it is reasonable to assume that oil saturation has been reduced to residual oil saturation in the skin zone so the first integral on the right-hand side of the above equation is equal to zero. Using this assumption, Eq. 2.117 reduces to

$$\Delta p = \frac{\alpha q_{inj}}{kh\hat{\lambda}_o}\left[\frac{1}{2}\ln\left(\frac{4\eta_o t}{e^{\gamma} r_w^2}\right) + \frac{s}{b\hat{M}} + s_b + \frac{1}{b}\int_{r_w}^{r_c}\left(\frac{\hat{\lambda}_o}{\lambda_t(r,t)} - 1\right)\frac{dr}{r} + \int_{r_c}^{r_f(t)}\left(\frac{\hat{\lambda}_o}{\lambda_t(r,t)} - 1\right)\frac{dr}{r}\right]. \quad (2.118)$$

Adding and subtracting an integral from r_w to r_c yields

$$\Delta p = \frac{\alpha q_{inj}}{kh\hat{\lambda}_o}\left[\frac{1}{2}\ln\left(\frac{4\eta_o t}{e^{\gamma} r_w^2}\right) + \frac{s}{b\hat{M}} + s_b + \frac{1}{b}\int_{r_w}^{r_c}\left(\frac{\hat{\lambda}_o}{\lambda_t(r,t)} - 1\right)\frac{dr}{r} + \int_{r_c}^{r_f(t)}\left(\frac{\hat{\lambda}_o}{\lambda_t(r,t)} - 1\right)\frac{dr}{r} + \int_{r_w}^{r_c}\left(\frac{\hat{\lambda}_o}{\lambda_t(r,t)} - 1\right)\frac{dr}{r} - \int_{r_w}^{r_c}\left(\frac{\hat{\lambda}_o}{\lambda_t(r,t)} - 1\right)\frac{dr}{r}\right], \quad (2.119)$$

or after rearranging,

$$\Delta p = \frac{\alpha q_{inj}}{kh\hat{\lambda}_o}\left[\frac{1}{2}\ln\left(\frac{4\eta_o t}{e^{\gamma} r_w^2}\right) + \frac{s}{b\hat{M}} + s_b + \left(\frac{1-b}{b}\right)\int_{r_w}^{r_c}\left(\frac{\hat{\lambda}_o}{\lambda_t(r,t)} - 1\right)\frac{dr}{r} + \int_{r_w}^{r_f(t)}\left(\frac{\hat{\lambda}_o}{\lambda_t(r,t)} - 1\right)\frac{dr}{r}\right]. \quad (2.120)$$

Similar to Eq. 2.116, it can be shown that

$$\int_{r_w}^{r_c}\left(\frac{\hat{\lambda}_o}{\lambda_t(r,t)} - 1\right)\frac{dr}{r} = \frac{1}{\hat{M}}\int_{r_w}^{r_c}\left(\frac{\hat{\lambda}_w}{\lambda_t(r,t)} - 1\right)\frac{dr}{r} + \left(\frac{1}{\hat{M}} - 1\right)\ln\left(\frac{r_c}{r_w}\right). \quad (2.121)$$

Using this result and Eq. 2.97 in Eq. 2.120 gives

$$\Delta p = \frac{\alpha q_{inj}}{2kh\hat{\lambda}_o}\left[\frac{1}{\hat{M}}\ln\left(\frac{4\eta_o t}{e^{\gamma}r_w^2}\right) + 2\left(\frac{s}{b\hat{M}} + s_b + \frac{s_\lambda}{\hat{M}}\right) + 2\left(\frac{1-b}{b\hat{M}}\right)\int_{r_w}^{r_c}\left(\frac{\hat{\lambda}_w}{\lambda_t(r,t)} - 1\right)\frac{dr}{r} + 2\frac{(1-b)}{b}\frac{(1-\hat{M})}{\hat{M}}\ln\left(\frac{r_c}{r_w}\right)\right]. \quad (2.122)$$

Based on the derivations in Appendix A, the radius of convergence r_c for model 1 is defined by (see Eq. A.14)

$$r_c = r_w \exp\left(\frac{bs_b}{1-b}\right). \quad (2.123)$$

Using this result in Eq. 2.122 and rearranging gives

$$\Delta p = \frac{\alpha q_{inj}}{2kh\hat{\lambda}_w}\left[\ln\left(\frac{4\eta_o t}{e^{\gamma}r_w^2}\right) + 2\left(\frac{s}{b} + s_b + s_\lambda\right) + 2\left(\frac{1-b}{b}\right)\int_{r_w}^{r_c}\left(\frac{\hat{\lambda}_w}{\lambda_t(r,t)} - 1\right)\frac{dr}{r}\right], \quad (2.124)$$

or in terms of Boltzmann transform

$$\Delta p = \frac{\alpha q_{inj}}{2kh\hat{\lambda}_w}\left[\ln\left(\frac{4\eta_o t}{e^{\gamma}r_w^2}\right) + 2\left(\frac{s}{b} + s_b + s_\lambda\right) + \left(\frac{1-b}{b}\right)\int_{r_w^2/4t}^{r_c^2/4t}\left(\frac{\hat{\lambda}_w}{\lambda_t(Z)} - 1\right)\frac{dZ}{Z}\right]. \quad (2.125)$$

Differentiating Eq. 2.125 with respect to $\ln(t)$ gives

$$\Delta p' = \frac{\alpha q_{inj}}{2kh\hat{\lambda}_w}\left[1 + \left(\frac{1-b}{b}\right)\left(1 - \frac{\hat{\lambda}_w}{\lambda_t(r_c,t)}\right)\right], \quad (2.126)$$

or simply

$$\Delta p' = \frac{\alpha q_{inj}}{2kh_p\hat{\lambda}_w}\left[1 - (1-b)\frac{\hat{\lambda}_w}{\lambda_t(r_c,t)}\right]. \quad (2.127)$$

Eq. 2.127 indicates that for the pressure derivative to be negative, one must have

$$\frac{\hat{\lambda}_w}{\lambda_t(r_c,t)}(1-b)>1, \tag{2.128}$$

or equivalently

$$\lambda_t(r_c,t)<(1-b)\hat{\lambda}_w. \tag{2.129}$$

As time increases, $\lambda_t(r_c,t)$ approaches $\hat{\lambda}_w$ and Eqs. 2.124 and 2.127, respectively, simplify to

$$\Delta p=\frac{\alpha q_{inj}}{kh\hat{\lambda}_w}\left[\frac{1}{2}\ln\left(\frac{4\eta_o t}{e^{\gamma}r_w^2}\right)+s_t^{(2,2)}\right], \tag{2.130}$$

$$\Delta p'=\frac{\alpha q_{inj}}{2kh\hat{\lambda}_w}. \tag{2.131}$$

In Eq. 2.130, $s_t^{(2,2)}$ represents the total skin factor for the second radial/second radial flow regime defined by

$$s_t^{(2,2)}=\frac{s}{b}+s_b+s_\lambda. \tag{2.132}$$

Under these circumstances, it is expected that the wellbore pressure change will display a semi-log slope that reflects water properties over the thickness of the reservoir.

2.3.2 Injection Through a Horizontal Well

The pressure transient behavior at a horizontal water injector is completely different from the pressure transient behavior of a vertical injector because of the existence of more than one flow regime (radial, linear,...etc). Moreover, the propagation of the water front and the propagation of the total flow rate in the reservoir occur on different time scales making the problem of horizontal well even more complicated. As the authors of reference [28] pointed out, a total of six different flow regimes may occur during an injection test depending on the position of the steady-state radius and the position of

the water front as well. These flow regimes are classified as first radial/first radial, first linear/first radial, first linear/first linear, second radial/first radial, second radial/first linear and second radial/second radial where the first name in each flow regime corresponds to the behavior of the single-phase component and the second term corresponds to the movement of water.

Throughout this discussion, we will consider water injection at a constant rate given by q_{inj} through a horizontal well of radius r_w and length L that penetrates a reservoir of constant formation thickness, h. As we proceeded for the restricted-entry problem, we first assume an isotropic reservoir. In the next section, we will extend the analysis to the anisotropic case.

First Radial/First Radial Flow Regime

This period pertains to the case when both steady-state zone of constant rate and the flood front are moving radially in the (x, z) plane. The wellbore pressure solution for this case is obtained by rearranging and integrating Darcy's law as follows

$$\Delta p = p_{wf} - p_i = \frac{\alpha}{L} \int_{r_w}^{\infty} \frac{q_t(r,t)}{k(r)\lambda_t(r,t)} \frac{dr}{r}. \tag{2.133}$$

In Eq. 2.133, recall that α is a constant which depends on the units system used. In field units, $\alpha = 141.2$. Note we are able to write ∞ as the upper limit because we assume that the top and bottom reservoir boundaries have no influence on the solution, or more specifically that $q_t(r,t) = 0$ when r is greater than or equal to z_w. Here, we also assume a variable permeability $k(r)$ in order to account for the mechanical skin near the wellbore region of radius r_s. Similarly to the vertical well case, it is given by

$$k(r) = \begin{cases} k_s & \text{for } r_w < r < r_s, \\ k & \text{for } r > r_s. \end{cases} \tag{2.134}$$

In Eq. 2.133, we introduce the flood front $r_{zx,f}$ to obtain

$$\Delta p = \frac{\alpha}{L} \int_{r_w}^{r_{zx,f}(t)} \frac{q_t(r,t)}{k(r)\lambda_t(r,t)} \frac{dr}{r} + \frac{\alpha}{L} \int_{r_{zx,f}(t)}^{\infty} \frac{q_t(r,t)}{k(r)\lambda_t(r,t)} \frac{dr}{r}. \tag{2.135}$$

By adding and subtracting to Eq. 2.135 an integral from r_w to $r_{zx,f}$, we have

$$\Delta p = \frac{\alpha}{L}\int_{r_w}^{r_{zx,f}(t)} \frac{q_t(r,t)}{k(r)\lambda_t(r,t)}\,\frac{dr}{r} + \frac{\alpha}{L}\int_{r_{zx,f}(t)}^{\infty} \frac{q_t(r,t)}{k(r)\lambda_t(r,t)}\,\frac{dr}{r} + \frac{\alpha}{L\hat{\lambda}_o}\int_{r_w}^{r_{zx,f}(t)} \frac{q_t(r,t)}{k(r)}\,\frac{dr}{r} - \frac{\alpha}{L\hat{\lambda}_o}\int_{r_w}^{r_{zx,f}(t)} \frac{q_t(r,t)}{k(r)}\,\frac{dr}{r}. \quad (2.136)$$

Next, we rewrite Eq. 2.136 using the steady-state theory which assumes that the flood front is within the steady-state region so that $q_t(r,t) = q_{inj}$ for $r < r_{zx,f}$ and by noting that $\lambda_t(r,t) = \hat{\lambda}_o$ for $r > r_{zx,f}$. The result is

$$\Delta p = \frac{\alpha}{L\hat{\lambda}_o}\int_{r_w}^{\infty} \frac{q_t(r,t)}{k(r)}\,\frac{dr}{r} + \frac{\alpha q_{inj}}{L\hat{\lambda}_o}\int_{r_w}^{r_{zx,f}(t)} \left(\frac{\hat{\lambda}_o}{\lambda_t(r,t)} - 1\right)\frac{dr}{rk(r)}, \quad (2.137)$$

where the first term on the right hand side of this equation represents the single-phase solution during the first radial flow regime based on end-point oil mobility and total compressibility evaluated at irreducible water saturation. Except at early times [25], it is given by the semi-log equation

$$\Delta p_o = \frac{\alpha q_{inj}}{kL\hat{\lambda}_o}\left[\ln\left(\frac{4\beta k\hat{\lambda}_o t}{e^{\gamma}\phi\mu\hat{c}_{to}r_w^2}\right) + s - \ln\left(\frac{2z_w}{r_w}\right)\right]. \quad (2.138)$$

Eq. 2.138 assumes the horizontal well is not drilled in the center of the formation and therefore, the diffusion may exhibit a semi-radial flow regime due to the effect of the nearest boundary (similar to the behavior of the solution for a vertical well near a fault). If the well is in the center of the formation, Eq. 2.138 is replaced by the following approximation

$$\Delta p_o = \frac{\alpha q_{inj}}{kL\hat{\lambda}_o}\left[\frac{1}{2}\ln\left(\frac{4\beta k\hat{\lambda}_o t}{e^{\gamma}\phi\mu\hat{c}_{to}r_w^2}\right) + s\right]. \quad (2.139)$$

Replacing Eq. 2.138 into Eq. 2.137 gives

$$\Delta p = \frac{\alpha q_{inj}}{kL\hat{\lambda}_o}\left[\ln\left(\frac{4\beta k\hat{\lambda}_o t}{e^{\gamma}\phi\mu\hat{c}_{to}r_w^2}\right)+s-\ln\left(\frac{2z_w}{r_w}\right)\right]+\frac{\alpha q_{inj}}{L\hat{\lambda}_o}\int_{r_w}^{r_{zx,f}(t)}\left(\frac{\hat{\lambda}_o}{\lambda_t(r,t)}-1\right)\frac{dr}{rk(r)}. \tag{2.140}$$

At this point, we distinguish two cases:

(i) If the water front is in the skin zone, i.e., $r_{zx,f} < r_s$, we simply replace $k(r)$ by k_s and Eq. 2.140 becomes

$$\Delta p = \frac{\alpha q_{inj}}{kL\hat{\lambda}_o}\left[\ln\left(\frac{4\beta k\hat{\lambda}_o t}{e^{\gamma}\phi\mu\hat{c}_{to}r_w^2}\right)+s-\ln\left(\frac{2z_w}{r_w}\right)\right]+\frac{\alpha q_{inj}}{k_sL\hat{\lambda}_o}\int_{r_w}^{r_{zx,f}}\left(\frac{\hat{\lambda}_o}{\lambda_t(r,t)}-1\right)\frac{dr}{r}. \tag{2.141}$$

By introducing the Boltzmann variable and by assuming that λ_t is a unique function of Z so that $\lambda_t(r,t) = \lambda_t(Z)$, we can rewrite Eq. 2.141 as

$$\Delta p = \frac{\alpha q_{inj}}{kL\hat{\lambda}_o}\left[\ln\left(\frac{4\beta k\hat{\lambda}_o t}{e^{\gamma}\phi\mu\hat{c}_{to}r_w^2}\right)+s-\ln\left(\frac{2z_w}{r_w}\right)\right]+\frac{\alpha q_{inj}}{2k_sL\hat{\lambda}_o}\int_{r_w^2/4t}^{Z_f}\left(\frac{\hat{\lambda}_o}{\lambda_t(Z)}-1\right)\frac{dZ}{Z}. \tag{2.142}$$

Taking the derivative of Eq. 2.142 with respect to the natural logarithm of time using Leibnitz's rule with Z_f constant gives

$$\Delta p' = \frac{\alpha q_{inj}}{kL\hat{\lambda}_o}+\frac{\alpha q_{inj}t}{2k_sL\hat{\lambda}_o}\left[-\left(\frac{\hat{\lambda}_o}{\lambda_t(r_w^2/4t)}-1\right)\left(\frac{4t}{r_w^2}\right)\left(-\frac{r_w^2}{4t^2}\right)\right], \tag{2.143}$$

which reduces to

$$\Delta p' = \frac{\alpha q_{inj}}{kL\hat{\lambda}_o}\left[1+\frac{k}{2k_s}\left(\frac{\hat{\lambda}_o}{\lambda_t(r_w,t)}-1\right)\right]. \tag{2.144}$$

Note that at r_w, $\lambda_t(r_w,t) = \hat{\lambda}_w$. Using the definition of the end-point mobility ratio, Eq. 2.144 becomes simply

$$\Delta p' = \frac{\alpha q_{inj}}{kL\hat{\lambda}_o}\left[1 + \frac{k}{2k_s}\left(\frac{1}{\hat{M}} - 1\right)\right]. \tag{2.145}$$

Eq. 2.145 clearly shows that the pressure derivative can be negative at early times (times corresponding to where the front is still propagating in the skin zone) provided that

$$1 + \frac{k}{2k_s}\left(\frac{1}{\hat{M}} - 1\right) < 0, \tag{2.146}$$

or equivalently

$$\hat{M}\left(1 - \frac{2k_s}{k}\right) > 1. \tag{2.147}$$

Clearly, this condition holds if the well is damaged and the mobility ratio is unfavorable. An important remark is that we would obtain the same condition given by Eq. 2.23 and derived for the complete-penetration vertical well case if the horizontal well has an equal offset.

(ii) If the water front is beyond the skin zone, i.e., $r_{zx,f} > r_s$, Eq. 2.140 becomes

$$\Delta p = \frac{\alpha q_{inj}}{kL\hat{\lambda}_o}\left[\ln\left(\frac{4\beta k\hat{\lambda}_o t}{e^{\gamma}\phi\mu\hat{c}_{to}r_w^2}\right) + s - \ln\left(\frac{2z_w}{r_w}\right)\right] + \frac{\alpha q_{inj}}{k_s L\hat{\lambda}_o}\int_{r_w}^{r_s}\left(\frac{\hat{\lambda}_o}{\lambda_t(r,t)} - 1\right)\frac{dr}{r} + \frac{\alpha q_{inj}}{kL\hat{\lambda}_o}\int_{r_s}^{r_{zx,f}(t)}\left(\frac{\hat{\lambda}_o}{\lambda_t(r,t)} - 1\right)\frac{dr}{r}. \tag{2.148}$$

By adding and subtracting an integral from r_w to r_s, Eq. 2.148 in rewritten as

$$\Delta p = \frac{\alpha q_{inj}}{kL\hat{\lambda}_o}\left[\ln\left(\frac{4\beta k\hat{\lambda}_o t}{e^{\gamma}\phi\mu\hat{c}_{to}r_w^2}\right) + s - \ln\left(\frac{2z_w}{r_w}\right)\right] + \frac{\alpha q_{inj}}{k_s L\hat{\lambda}_o}\int_{r_w}^{r_s}\left(\frac{\hat{\lambda}_o}{\lambda_t(r,t)} - 1\right)\frac{dr}{r} + \frac{\alpha q_{inj}}{kL\hat{\lambda}_o}\int_{r_s}^{r_{zx,f}(t)}\left(\frac{\hat{\lambda}_o}{\lambda_t(r,t)} - 1\right)\frac{dr}{r} + \frac{\alpha q_{inj}}{kL\hat{\lambda}_o}\int_{r_w}^{r_s}\left(\frac{\hat{\lambda}_o}{\lambda_t(r,t)} - 1\right)\frac{dr}{r} - \frac{\alpha q_{inj}}{kL\hat{\lambda}_o}\int_{r_w}^{r_s}\left(\frac{\hat{\lambda}_o}{\lambda_t(r,t)} - 1\right)\frac{dr}{r}, \tag{2.149}$$

or rearranging,

$$\Delta p = \frac{\alpha q_{inj}}{k\ L\hat{\lambda}_o}\left[\ln\left(\frac{4\beta k\hat{\lambda}_o t}{e^{\gamma}\phi\mu\hat{c}_{to}r_w^2}\right)+s-\ln\left(\frac{2z_w}{r_w}\right)\right]+\frac{\alpha q_{inj}}{kL\hat{\lambda}_o}\left[\left(\frac{k}{k_s}-1\right)\int_{r_w}^{r_s}\left(\frac{\hat{\lambda}_o}{\lambda_t(r,t)}-1\right)\frac{dr}{r} + \int_{r_w}^{r_{zx,f}(t)}\left(\frac{\hat{\lambda}_o}{\lambda_t(r,t)}-1\right)\frac{dr}{r}\right]. \quad (2.150)$$

In terms of Boltzmann variable, Eq. 2.150 can be expressed as

$$\Delta p = \frac{\alpha q_{inj}}{kL\hat{\lambda}_o}\left[\ln\left(\frac{4\beta k\hat{\lambda}_o t}{e^{\gamma}\phi\mu\hat{c}_{to}r_w^2}\right)+s-\ln\left(\frac{2z_w}{r_w}\right)\right]+\frac{\alpha q_{inj}}{2kL\hat{\lambda}_o}\left[\left(\frac{k}{k_s}-1\right)\int_{r_w^2/4t}^{r_s^2/4t}\left(\frac{\hat{\lambda}_o}{\lambda_t(Z)}-1\right)\frac{dZ}{Z} + \int_{r_w^2/4t}^{Z_f}\left(\frac{\hat{\lambda}_o}{\lambda_t(Z)}-1\right)\frac{dZ}{Z}\right]. \quad (2.151)$$

Taking the derivative of Eq. 2.151 with respect to the natural log of t using Leibnitz's rule gives

$$\Delta p' = \frac{\alpha q_{inj}}{kL\hat{\lambda}_o}+\frac{\alpha q_{inj}t}{2kL\hat{\lambda}_o}\left[\left(\frac{k}{k_s}-1\right)\left[\left(\frac{\hat{\lambda}_o}{\lambda_t(r_s^2/4t)}-1\right)\left(\frac{4t}{r_s^2}\right)\left(-\frac{r_s^2}{4t^2}\right) - \left(\frac{\hat{\lambda}_o}{\lambda_t(r_w^2/4t)}-1\right)\left(\frac{4t}{r_w^2}\right)\left(-\frac{r_w^2}{4t^2}\right)\right]-\left(\frac{\hat{\lambda}_o}{\lambda_t(r_w^2/4t)}-1\right)\left(\frac{4t}{r_w^2}\right)\left(-\frac{r_w^2}{4t^2}\right)\right]. \quad (2.152)$$

Using $\lambda_t(r_w,t)=\hat{\lambda}_w$, Eq. 2.152 simplifies to

$$\Delta p' = \frac{\alpha q_{inj}}{2kL\hat{\lambda}_w}\left[1+\hat{M}-\left(\frac{k}{k_s}-1\right)\left(\frac{\hat{\lambda}_w}{\lambda_t(r_s,t)}-1\right)\right]. \quad (2.153)$$

Eq. 2.153 suggests that we might observe a decline in the wellbore pressure, i.e., a negative pressure derivative, during this period of injection if the following equation is satisfied:

$$\left(\frac{k}{k_s}-1\right)\left(\frac{\hat{\lambda}_w}{\lambda_t(r_s,t)}-1\right) > 1+\hat{M}, \quad (2.154)$$

or equivalently,

$$\lambda_t(r_s,t)\left(1+\frac{k_s}{k}\hat{M}\right) < \hat{\lambda}_w\left(1-\frac{k_s}{k}\right). \tag{2.155}$$

Note that we would obtain the same condition given by Eq. 2.31 and derived for the complete-penetration vertical well case if the horizontal well has an equal offset or at time before any boundary affects the pressure solution (for an unequal offset horizontal well).

First Linear/First Radial Flow Regime

This case pertains to the situation when the steady-state region of constant rate is moving linearly in the x-direction while the flood front is still moving radially in the (x,z) plane. With the configuration of the problem (see Figs. 2.3 and 2.5), the wellbore pressure drop is given by

$$\Delta p = \frac{\pi\alpha}{kL}\int_{x_1}^{\infty}\frac{q_t(x,t)}{\lambda_t(x,t)}\frac{dx}{h(x)} + \frac{\alpha}{L}\int_{r_w}^{z_w}\frac{q_t(r,t)}{k(r)\lambda_t(r,t)}\frac{dr}{r}, \tag{2.156}$$

where the position x_1 is defined by Eq. 2.45. Introducing the water front $r_{zx,f}$ and setting $\lambda_t = \hat{\lambda}_o$ in the unevaded region and $q_t = q_{inj}$ in the flooded zone, Eq. 2.156 becomes

$$\begin{aligned}\Delta p = \frac{\pi\alpha}{kL\hat{\lambda}_o}\int_{x=0}^{\infty} q_t(x,t)\frac{dx}{h(x)} - \frac{\pi\alpha q_{inj}}{kL\hat{\lambda}_o}\int_0^{x_1}\frac{dx}{h(x)} \\ + \frac{\alpha q_{inj}}{L\hat{\lambda}_o}\int_{r_w}^{r_{zx,f}(t)}\frac{\hat{\lambda}_o}{k(r)\lambda_t(r,t)}\frac{dr}{r} + \frac{\alpha q_{inj}}{L\hat{\lambda}_o}\int_{r_{zx,f}(t)}^{z_w}\frac{1}{k(r)}\frac{dr}{r}.\end{aligned} \tag{2.157}$$

Using the fact that $h(x) = 2z_w$ for $0 < x < x_1$ and adding and subtracting to Eq. 2.157 an integral from r_w to $r_{zx,f}$, we have

$$\begin{aligned}\Delta p = \frac{\pi\alpha}{kL\hat{\lambda}_o}\int_{x=0}^{\infty} q_t(x,t)\frac{dx}{h(x)} - \frac{\pi\alpha q_{inj}}{2kL\hat{\lambda}_o z_w}x_1 \\ + \frac{\alpha q_{inj}}{L\hat{\lambda}_o}\int_{r_w}^{r_{zx,f}(t)}\frac{\hat{\lambda}_o}{k(r)\lambda_t(r,t)}\frac{dr}{r} + \frac{\alpha q_{inj}}{L\hat{\lambda}_o}\int_{r_{zx,f}(t)}^{z_w}\frac{1}{k(r)}\frac{dr}{r} \\ + \frac{\alpha q_{inj}}{L\hat{\lambda}_o}\int_{r_w}^{r_{zx,f}(t)}\frac{1}{k(r)}\frac{dr}{r} - \frac{\alpha q_{inj}}{L\hat{\lambda}_o}\int_{r_w}^{r_{zx,f}(t)}\frac{1}{k(r)}\frac{dr}{r},\end{aligned} \tag{2.158}$$

or by combining integrals,

$$\Delta p = \frac{\pi\alpha}{kL\hat{\lambda}_o}\int_{x=0}^{\infty} q_t(x,t)\,\frac{dx}{h(x)} - \frac{\pi\alpha q_{inj}}{2kL\hat{\lambda}_o z_w}x_1 + \frac{\alpha q_{inj}}{L\hat{\lambda}_o}\int_{r_w}^{r_{zx,f}(t)}\left(\frac{\hat{\lambda}_o}{\lambda_t(r,t)}-1\right)\frac{dr}{rk(r)} + \frac{\alpha q_{inj}}{L\hat{\lambda}_o}\int_{r_w}^{z_w}\frac{1}{k(r)}\,\frac{dr}{r}. \quad (2.159)$$

The last integral of the above equation can be written by using the appropriate permeability in the domain $r_w < r < z_w$ as

$$\begin{aligned}\int_{r_w}^{z_w}\frac{1}{k(r)}\,\frac{dr}{r} &= \frac{1}{k_s}\int_{r_w}^{r_s}\frac{dr}{r} + \frac{1}{k}\int_{r_s}^{z_w}\frac{dr}{r}\\ &= \frac{1}{k}\left(\frac{k}{k_s}-1\right)\int_{r_w}^{r_s}\frac{dr}{r} + \frac{1}{k}\int_{r_w}^{z_w}\frac{dr}{r}\\ &= \frac{1}{k}\left[\left(\frac{k}{k_s}-1\right)\ln\left(\frac{r_s}{r_w}\right) + \ln\left(\frac{z_w}{r_w}\right)\right]. \end{aligned} \quad (2.160)$$

Hawkin's [21] formula for the mechanical skin factor, s, is given by

$$s = \left(\frac{k}{k_s}-1\right)\ln(\frac{r_s}{r_w}). \quad (2.161)$$

Using Eq. 2.161 in Eq. 2.160 and substituting the resulting equation into Eq. 2.159 yields

$$\Delta p = \frac{\pi\alpha}{kL\hat{\lambda}_o}\int_{x=0}^{\infty} q_t(x,t)\,\frac{dx}{h(x)} + \frac{\alpha q_{inj}}{kL\hat{\lambda}_o}\left[\ln\left(\frac{z_w}{r_w}\right) - \frac{\pi x_1}{2z_w} + s\right] + \frac{\alpha q_{inj}}{L\hat{\lambda}_o}\int_{r_w}^{r_{zx,f}(t)}\left(\frac{\hat{\lambda}_o}{\lambda_t(r,t)}-1\right)\frac{dr}{rk(r)}, \quad (2.162)$$

or

$$\Delta p = \frac{\pi\alpha}{kL\hat{\lambda}_o}\int_{x=0}^{\infty} q_t(x,t)\,\frac{dx}{h(x)} + \frac{\alpha q_{inj}}{kh\hat{\lambda}_o}\left[\frac{h}{L}(s_z+s)\right] + \frac{\alpha q_{inj}}{L\hat{\lambda}_o}\int_{r_w}^{r_{zx,f}(t)}\left(\frac{\hat{\lambda}_o}{\lambda_t(r,t)}-1\right)\frac{dr}{rk(r)}, \quad (2.163)$$

where s_z is the pseudo-skin factor due to the convergence of the flow lines defined according to Eq. 2.162 as

$$s_z = \ln\left(\frac{z_w}{r_w}\right) - \frac{\pi x_1}{2z_w}, \quad (2.164)$$

or by substituting the expression for x_1 provided by Eq. 2.45 into Eq. 2.164,

$$s_z = \ln\left(\frac{z_w}{r_w}\right) - \frac{\pi^2}{8}. \quad (2.165)$$

The sum of the two first terms of the right hand side of the above equation represents the single-phase transient solution for linear flow that we usually denote by Δp_o. The third term is an additional pressure drop due to the multiphase effect. Note that there are two possibilities with respect to the position of the water front: (i) The water front is in the skin zone. In this case, Eq. 2.163 becomes

$$\Delta p = \Delta p_o + \frac{\alpha q_{inj}}{k_s L\hat{\lambda}_o}\int_{r_w}^{r_{zx,f}(t)}\left(\frac{\hat{\lambda}_o}{\lambda_t(r,t)}-1\right)\frac{dr}{r}. \quad (2.166)$$

If we rewrite Eq. 2.166 in terms of Boltzmann variable, we obtain

$$\Delta p = \Delta p_o + \frac{\alpha q_{inj}}{2k_s L\hat{\lambda}_o}\int_{r_w^2/4t}^{Z_f}\left(\frac{\hat{\lambda}_o}{\lambda_t(Z)}-1\right)\frac{dZ}{Z}. \quad (2.167)$$

Differentiating Eq. 2.167 with respect to $\ln(t)$ using Leibnitz's rule with Z_f constant yields

$$\Delta p' = \Delta p'_o + \frac{\alpha q_{inj}}{2k_s L\hat{\lambda}_o}\left(\frac{\hat{\lambda}_o}{\hat{\lambda}_w} - 1\right)$$
$$= \Delta p'_o + \frac{\alpha q_{inj}}{2k_s L\hat{\lambda}_o}\left(\frac{1-\hat{M}}{\hat{M}}\right). \quad (2.168)$$

The analytical solution for the pressure response under single-phase flow during a linear flow regime is well known (see references [23], [20] and [25]). It is defined by the following equation:

$$\Delta p_o = \frac{\alpha q_{inj}}{kh\hat{\lambda}_o}\left[\sqrt{\frac{4\pi\beta k\hat{\lambda}_o t}{\phi\hat{c}_{to}L^2}} + \frac{h}{L}(s_z + s)\right]. \quad (2.169)$$

Its derivative with respect to logarithm of time based on oil properties at irreducible water saturation is given by

$$\Delta p'_o = \frac{\alpha q_{inj}}{2kh\hat{\lambda}_o}\sqrt{\frac{4\pi\beta k\hat{\lambda}_o t}{\phi\hat{c}_{to}L^2}}. \quad (2.170)$$

Then, using Eq. 2.170 in Eq. 2.168 and rearranging gives

$$\Delta p' = \frac{\alpha q_{inj}}{2kh\hat{\lambda}_o}\left[\sqrt{\frac{4\pi\beta k\hat{\lambda}_o t}{\phi\hat{c}_{to}L^2}} + \frac{h}{L}\frac{k}{k_s}\left(\frac{1-\hat{M}}{\hat{M}}\right)\right]. \quad (2.171)$$

Eq. 2.171 shows that during this flow period where the damaged zone is not swept yet by water, the pressure behavior is such that its derivative is shifted from the single-phase oil solution by a constant which depends on the end-point mobility ratio. Moreover, the two-phase solution for the derivative is expected to either fall below or above the single phase flow derivative if $\hat{M} > 1$ or $\hat{M} < 1$ respectively.

(ii) The front is beyond the skin zone. Eq. 2.163 becomes

$$\Delta p = \Delta p_o + \frac{\alpha q_{inj}}{k_s L\hat{\lambda}_o}\int_{r_w}^{r_s}\left(\frac{\hat{\lambda}_o}{\lambda_t(r,t)} - 1\right)\frac{dr}{r} + \frac{\alpha q_{inj}}{kL\hat{\lambda}_o}\int_{r_s}^{r_{zx,f}(t)}\left(\frac{\hat{\lambda}_o}{\lambda_t(r,t)} - 1\right)\frac{dr}{r}, \quad (2.172)$$

which we rewrite as

$$\Delta p = \Delta p_o + \frac{\alpha q_{inj}}{kL\hat{\lambda}_o}\left[\left(\frac{k}{k_s}-1\right)\int_{r_w}^{r_s}\left(\frac{\hat{\lambda}_o}{\lambda_t(r,t)}-1\right)\frac{dr}{r}+\int_{r_w}^{r_{zx,f}(t)}\left(\frac{\hat{\lambda}_o}{\lambda_t(r,t)}-1\right)\frac{dr}{r}\right], \quad (2.173)$$

or by using the Boltzmann variable,

$$\Delta p = \Delta p_o + \frac{\alpha q_{inj}}{2kL\hat{\lambda}_o}\left[\left(\frac{k}{k_s}-1\right)\int_{r_w^2/4t}^{r_s^2/4t}\left(\frac{\hat{\lambda}_o}{\lambda_t(Z)}-1\right)\frac{dZ}{Z}+\int_{r_w^2/4t}^{Z_f}\left(\frac{\hat{\lambda}_o}{\lambda_t(Z)}-1\right)\frac{dZ}{Z}\right]. \quad (2.174)$$

From the above equation, it is easy to find the pressure derivative. We simply need to use Leibnitz's rule when differentiating with respect to $\ln(t)$. The resulting equation is

$$\Delta p' = \frac{\alpha q_{inj}}{2kh\hat{\lambda}_o}\sqrt{\frac{4\pi\beta k\hat{\lambda}_o t}{\phi\hat{c}_{to}L^2}}+\frac{\alpha q_{inj}}{2kL\hat{\lambda}_w}\left[1-\hat{M}-\left(\frac{k}{k_s}-1\right)\left(\frac{\hat{\lambda}_w}{\lambda_t(r_s,t)}-1\right)\right]. \quad (2.175)$$

Once the skin zone is completely swept by water, i.e., $\lambda_t(r_s,t)=\hat{\lambda}_w$, Eq. 2.175 simplifies to

$$\Delta p' = \frac{\alpha q_{inj}}{2kh\hat{\lambda}_o}\left[\sqrt{\frac{4\pi\beta k\hat{\lambda}_o t}{\phi\hat{c}_{to}L^2}}+\frac{h}{L}\left(\frac{1-\hat{M}}{\hat{M}}\right)\right], \quad (2.176)$$

which is identical to Eq. 2.171 obtained for the case where the flood front is within the damaged zone for a zero skin case, i.e., $k_s = k$.

First Linear/First Linear Flow Regime

This flow regime occurs when both the steady-state zone and water front move in the x-direction. Eq. 2.156 for the wellbore pressure drop also holds during this period but if we introduce the water front x_f, this equation becomes

$$\Delta p = \frac{\pi\alpha}{kL}\int_{x_1}^{x_f(t)}\frac{q_t(x,t)}{\lambda_t(x,t)}\frac{dx}{h(x)}+\frac{\pi\alpha}{kL}\int_{x_f(t)}^{\infty}\frac{q_t(x,t)}{\lambda_t(x,t)}\frac{dx}{h(x)} + \frac{\alpha}{L}\int_{r_w}^{z_w}\frac{q_t(r,t)}{\lambda_t(r,t)}\frac{dr}{rk(r)}. \quad (2.177)$$

Since the water front is ahead of the zone $r_w < r < z_w$, the total rate q_t can be replaced by q_{inj} in the last integral so that

$$\frac{\alpha}{L}\int_{r_w}^{z_w}\frac{q_t(r,t)}{\lambda_t(r,t)}\frac{dr}{rk(r)} = \frac{\alpha q_{inj}}{L\hat{\lambda}_o}\int_{r_w}^{z_w}\frac{\hat{\lambda}_o}{\lambda_t(r,t)}\frac{dr}{rk(r)}. \tag{2.178}$$

If we add and subtract to Eq. 2.178 an integral from r_w to z_w, we have

$$\frac{\alpha}{L}\int_{r_w}^{z_w}\frac{q_t(r,t)}{\lambda_t(r,t)}\frac{dr}{rk(r)} = \frac{\alpha q_{inj}}{L\hat{\lambda}_o}\int_{r_w}^{z_w}\frac{\hat{\lambda}_o}{\lambda_t(r,t)}\frac{dr}{rk(r)} + \frac{\alpha q_{inj}}{L\hat{\lambda}_o}\int_{r_w}^{z_w}\frac{dr}{rk(r)} - \frac{\alpha q_{inj}}{L\hat{\lambda}_o}\int_{r_w}^{z_w}\frac{dr}{rk(r)}. \tag{2.179}$$

If we combine integrals, Eq. 2.179 becomes

$$\frac{\alpha}{L}\int_{r_w}^{z_w}\frac{q_t(r,t)}{\lambda_t(r,t)}\frac{dr}{rk(r)} = \frac{\alpha q_{inj}}{L\hat{\lambda}_o}\int_{r_w}^{z_w}\left(\frac{\hat{\lambda}_o}{\lambda_t(r,t)}-1\right)\frac{dr}{rk(r)} + \frac{\alpha q_{inj}}{k_s L\hat{\lambda}_o}\int_{r_w}^{r_s}\frac{dr}{r} + \frac{\alpha q_{inj}}{kL\hat{\lambda}_o}\int_{r_s}^{z_w}\frac{dr}{r}, \tag{2.180}$$

or after some manipulations,

$$\frac{\alpha}{L}\int_{r_w}^{z_w}\frac{q_t(r,t)}{\lambda_t(r,t)}\frac{dr}{rk(r)} = \frac{\alpha q_{inj}}{L\hat{\lambda}_o}\int_{r_w}^{z_w}\left(\frac{\hat{\lambda}_o}{\lambda_t(r,t)}-1\right)\frac{dr}{rk(r)} + \frac{\alpha q_{inj}}{kL\hat{\lambda}_o}\left[\left(\frac{k}{k_s}-1\right)\ln(r_s/r_w)+\ln(z_w/r_w)\right]. \tag{2.181}$$

Introducing Hawkin's formula in Eq. 2.181 yields

$$\frac{\alpha}{L}\int_{r_w}^{z_w}\frac{q_t(r,t)}{\lambda_t(r,t)}\frac{dr}{rk(r)} = \frac{\alpha q_{inj}}{L\hat{\lambda}_o}\int_{r_w}^{z_w}\left(\frac{\hat{\lambda}_o}{\lambda_t(r,t)}-1\right)\frac{dr}{rk(r)} + \frac{\alpha q_{inj}}{kL\hat{\lambda}_o}\left[s+\ln\left(\frac{z_w}{r_w}\right)\right]. \tag{2.182}$$

Substituting Eq. 2.182 into Eq. 2.177 and setting $\lambda_t = \hat{\lambda}_o$ ahead of the front gives

$$\Delta p = \frac{\pi\alpha q_{inj}}{kL\hat{\lambda}_o}\int_{x_1}^{x_f(t)} \frac{\hat{\lambda}_o}{\lambda_t(x,t)}\,\frac{dx}{h(x)} + \frac{\pi\alpha}{kL\hat{\lambda}_o}\int_{x_f(t)}^{\infty} q_t(x,t)\,\frac{dx}{h(x)} + \frac{\alpha q_{inj}}{L\hat{\lambda}_o}\int_{r_w}^{z_w}\left(\frac{\hat{\lambda}_o}{\lambda_t(r,t)}-1\right)\frac{dr}{rk(r)} + \frac{\alpha q_{inj}}{kL\hat{\lambda}_o}\left[s+\ln\left(\frac{z_w}{r_w}\right)\right], \quad (2.183)$$

or

$$\Delta p = \frac{\pi\alpha q_{inj}}{kL\hat{\lambda}_o}\int_{x_1}^{x_f(t)} \frac{\hat{\lambda}_o}{\lambda_t(x,t)}\,\frac{dx}{h(x)} + \frac{\pi\alpha}{kL\hat{\lambda}_o}\int_{0}^{\infty} q_t(x,t)\,\frac{dx}{h(x)} - \frac{\pi\alpha}{kL\hat{\lambda}_o}\int_{0}^{x_1} q_t(x,t)\,\frac{dx}{h(x)} - \frac{\pi\alpha}{kL\hat{\lambda}_o}\int_{x_1}^{x_f(t)} q_t(x,t)\,\frac{dx}{h(x)} + \frac{\alpha q_{inj}}{L\hat{\lambda}_o}\int_{r_w}^{z_w}\left(\frac{\hat{\lambda}_o}{\lambda_t(r,t)}-1\right)\frac{dr}{rk(r)} + \frac{\alpha q_{inj}}{kL\hat{\lambda}_o}\left[s+\ln\left(\frac{z_w}{r_w}\right)\right]. \quad (2.184)$$

We can simplify Eq. 2.184 by noting that $q_t(x,t) = q_{inj}$ for $x < x_f$ and using the fact that according to both model 1 and 2, $h(x) = 2z_w$ for $x < x_1$. The result is

$$\Delta p = \frac{\pi\alpha q_{inj}}{kL\hat{\lambda}_o}\int_{x_1}^{x_f(t)}\left(\frac{\hat{\lambda}_o}{\lambda_t(x,t)}-1\right)\frac{dx}{h(x)} + \frac{\alpha q_{inj}}{L\hat{\lambda}_o}\int_{r_w}^{z_w}\left(\frac{\hat{\lambda}_o}{\lambda_t(r,t)}-1\right)\frac{dr}{rk(r)} + \frac{\pi\alpha}{kL\hat{\lambda}_o}\int_{0}^{\infty} q_t(x,t)\,\frac{dx}{h(x)} + \frac{\alpha q_{inj}}{kL\hat{\lambda}_o}\left[s+\ln\left(\frac{z_w}{r_w}\right)-\frac{\pi x_1}{2z_w}\right]. \quad (2.185)$$

Using Eq. 2.164 in Eq. 2.185 gives

$$\Delta p = \frac{\pi\alpha}{kL\hat{\lambda}_o}\int_{0}^{\infty} q_t(x,t)\,\frac{dx}{h(x)} + \frac{\alpha q_{inj}}{kh\hat{\lambda}_o}\left[\frac{h}{L}(s+s_z)\right] + \frac{\alpha q_{inj}}{L\hat{\lambda}_o}\int_{r_w}^{z_w}\left(\frac{\hat{\lambda}_o}{\lambda_t(r,t)}-1\right)\frac{dr}{rk(r)} + \frac{\pi\alpha q_{inj}}{kL\hat{\lambda}_o}\int_{x_1}^{x_f(t)}\left(\frac{\hat{\lambda}_o}{\lambda_t(x,t)}-1\right)\frac{dx}{h(x)}, \quad (2.186)$$

or noting that the single-phase oil pressure change, Δp_o, is given by

$$\Delta p_o = \frac{\pi\alpha}{kL\hat{\lambda}_o}\int_0^{\infty} q_t(x,t)\,\frac{dx}{h(x)} + \frac{\alpha q_{inj}}{kh\hat{\lambda}_o}\left[\frac{h}{L}(s+s_z)\right], \tag{2.187}$$

Eq. 2.186 is equivalent to

$$\Delta p = \Delta p_o + \frac{\alpha q_{inj}}{L\hat{\lambda}_o}\int_{r_w}^{z_w}\left(\frac{\hat{\lambda}_o}{\lambda_t(r,t)}-1\right)\frac{dr}{rk(r)} + \frac{\pi\alpha q_{inj}}{kL\hat{\lambda}_o}\int_{x_1}^{x_f(t)}\left(\frac{\hat{\lambda}_o}{\lambda_t(x,t)}-1\right)\frac{dx}{h(x)}. \tag{2.188}$$

Eq. 2.188 indicates that the multiphase term has two contributions as the consequence of the radial and the linear movement of water during the injection period. In order to understand the behavior of the wellbore pressure change during this flow regime, we assume that the water front $x_f(t)$ is beyond the point of convergence x_2 so that $h(x)$ reduces to the total thickness of the reservoir, i.e., h for $x > x_2$. Rewriting Eq. 2.188 gives

$$\begin{aligned}\Delta p = \Delta p_o &+ \frac{\alpha q_{inj}}{k_s L\hat{\lambda}_o}\int_{r_w}^{r_s}\left(\frac{\hat{\lambda}_o}{\lambda_t(r,t)}-1\right)\frac{dr}{r} + \frac{\alpha q_{inj}}{kL\hat{\lambda}_o}\int_{r_s}^{z_w}\left(\frac{\hat{\lambda}_o}{\lambda_t(r,t)}-1\right)\frac{dr}{r}\\ &+ \frac{\pi\alpha q_{inj}}{kL\hat{\lambda}_o}\int_{x_1}^{x_2}\left(\frac{\hat{\lambda}_o}{\lambda_t(x,t)}-1\right)\frac{dx}{h(x)} + \frac{\pi\alpha q_{inj}}{kL\hat{\lambda}_o h}\int_{x_2}^{x_f(t)}\left(\frac{\hat{\lambda}_o}{\lambda_t(x,t)}-1\right)dx.\end{aligned} \tag{2.189}$$

In Eq. 2.189, we kept $h(x)$ variable for $x_1 < x < x_2$ in order to have the flexibility of using either model 1, where $h(x)$ is constant according to Eq. 2.46, or model 2 for which $h(x)$ is variable and given by Eq. 2.47. Rearranging Eq. 2.189 yields

$$\begin{aligned}\Delta p = \Delta p_o &+ \frac{\alpha q_{inj}}{kL\hat{\lambda}_o}\left[\left(\frac{k}{k_s}-1\right)\int_{r_w}^{r_s}\left(\frac{\hat{\lambda}_o}{\lambda_t(r,t)}-1\right)\frac{dr}{r} + \int_{r_w}^{z_w}\left(\frac{\hat{\lambda}_o}{\lambda_t(r,t)}-1\right)\frac{dr}{r}\right]\\ &+ \frac{\pi\alpha q_{inj}}{kL\hat{\lambda}_o h}\left[\int_{x_1}^{x_2}\left(\frac{\hat{\lambda}_o}{\lambda_t(x,t)}-1\right)\frac{h}{h(x)}dx + \int_{x_2}^{x_f(t)}\left(\frac{\hat{\lambda}_o}{\lambda_t(x,t)}-1\right)dx\right].\end{aligned} \tag{2.190}$$

Assuming the skin zone is completely swept by water so that the total mobility is equal to the end-point water mobility and by also assuming that for very long injection times, the total mobility will eventually be equal to $\hat{\lambda}_w$ in the region of the reservoir corresponding

to $x < x_2$ as the reservoir in this zone will be swept by water, Eq. 2.190 becomes

$$\Delta p = \Delta p_o + \frac{\alpha q_{inj}}{kL\hat{\lambda}_o}\left(\frac{\hat{\lambda}_o}{\hat{\lambda}_w} - 1\right)\left[\left(\frac{k}{k_s} - 1\right)\ln\left(\frac{r_s}{r_w}\right) + \ln\left(\frac{z_w}{r_w}\right)\right] + \frac{\pi\alpha q_{inj}}{kL\hat{\lambda}_o h}\left[\left(\frac{\hat{\lambda}_o}{\hat{\lambda}_w} - 1\right)\int_{x_1}^{x_2}\frac{h}{h(x)}dx + \int_{x_2}^{x_f(t)}\left(\frac{\hat{\lambda}_o}{\lambda_t(x,t)} - 1\right)dx\right], \quad (2.191)$$

or by using Hawkin's formula and the definition of the end-point mobility ratio $\hat{M}$,

$$\Delta p = \Delta p_o + \frac{\alpha q_{inj}}{kL\hat{\lambda}_w}(1 - \hat{M})\left[s + \ln\left(\frac{z_w}{r_w}\right)\right] + \frac{\pi\alpha q_{inj}}{kL\hat{\lambda}_o h}\left[\left(\frac{1 - \hat{M}}{\hat{M}}\right)\int_{x_1}^{x_2}\frac{h}{h(x)}dx + \int_{x_2}^{x_f(t)}\left(\frac{\hat{\lambda}_o}{\lambda_t(x,t)} - 1\right)dx\right]. \quad (2.192)$$

Let us introduce a Boltzmann variable for the x-direction given by

$$Y = \frac{x}{t}, \quad (2.193)$$

and make a change of variable for the last integral of Eq. 2.192 as follows

$$\Delta p = \Delta p_o + \frac{\alpha q_{inj}}{kL\hat{\lambda}_w}(1 - \hat{M})\left[s + \ln\left(\frac{z_w}{r_w}\right)\right] + \frac{\pi\alpha q_{inj}}{kL\hat{\lambda}_o h}\left[\left(\frac{1 - \hat{M}}{\hat{M}}\right)\int_{x_1}^{x_2}\frac{h}{h(x)}dx + t\int_{x_2/t}^{Y_f}\left(\frac{\hat{\lambda}_o}{\lambda_t(Y)} - 1\right)dY\right], \quad (2.194)$$

where Y_f denotes the Boltzmann variable at the water front defined according to Eq. 2.193 as

$$Y_f = \frac{x_f}{t}. \quad (2.195)$$

We again assume that the total mobility $\lambda_t(x,t)$ is a unique function of the Boltzmann type variable, $Y = \frac{x}{t}$ and that the location of the water front Y_f in the Y variable

is stationary. Thus, Differentiating Eq. 2.194 with respect to logarithm of time using Leibnitz's rule yields

$$\Delta p' = \Delta p'_o + \frac{\alpha\pi q_{inj}}{kL\hat{\lambda}_o h}\left[t\int_{x_2/t}^{Y_f}\left(\frac{\hat{\lambda}_o}{\lambda_t(Y)}-1\right)dY + x_2\left(\frac{\hat{\lambda}_o}{\lambda_t(x_2,t)}-1\right)\right], \tag{2.196}$$

or by setting $\lambda_t(x_2,t)=\hat{\lambda}_w$

$$\Delta p' = \Delta p'_o + \frac{\alpha\pi q_{inj}}{kL\hat{\lambda}_o h}\left[\left(\frac{1-\hat{M}}{\hat{M}}\right)x_2 + t\int_{x_2/t}^{Y_f}\left(\frac{\hat{\lambda}_o}{\lambda_t(Y)}-1\right)dY\right]. \tag{2.197}$$

Since it is difficult to understand the behavior of the pressure derivative during this flow regime directly from Eq. 2.197, we make the following approximation

$$\begin{aligned}\int_{x_2/t}^{Y_f}\left(\frac{\hat{\lambda}_o}{\lambda_t(Y)}-1\right)dY \approx \left(\frac{\hat{\lambda}_o}{\hat{\lambda}_w}-1\right)\int_{x_2/t}^{Y_f}dY &= \left(\frac{\hat{\lambda}_o}{\hat{\lambda}_w}-1\right)(Y_f-\frac{x_2}{t}),\\ &= \frac{1}{t}\left(\frac{1-\hat{M}}{\hat{M}}\right)(x_f(t)-x_2).\end{aligned} \tag{2.198}$$

Then, Eq. 2.197 simplifies to

$$\Delta p' = \Delta p'_o + \frac{\pi\alpha q_{inj}}{kL\hat{\lambda}_w h}(1-\hat{M})x_f(t). \tag{2.199}$$

Here, two remarks deserve mention. First, the pressure derivative will be either below or above the pressure derivative for the single-phase based on oil properties depending on whether the end-point mobility ratio is unfavorable or favorable. Second, this deviation from the single-phase solution increases with time as the front is moving along the x-direction.

Second Radial/First Radial Flow Regime

This flow regime occurs when the steady-state zone of constant rate is moving in the (x,y) plane while the water front is still moving radially in the (x,z) plane. The

equation for the wellbore pressure change during this period is given by

$$\Delta p = \frac{\alpha}{kh}\int_{L/2}^{\infty}\frac{q_t(r,t)}{\lambda_t(r,t)}\frac{dr}{r} + \frac{\pi\alpha}{kL}\int_{x_1}^{x_3}\frac{q_t(x,t)}{\lambda_t(x,t)}\frac{dx}{h(x)} + \frac{\alpha}{L}\int_{r_w}^{z_w}\frac{q_t(r,t)}{\lambda_t(r,t)}\frac{dr}{rk(r)}. \tag{2.200}$$

According to the Thompson and Reynolds theory, the steady zone is propagating at the constant wellbore rate up to x_3. Therefore, we can take the total rate out of the two last integrals of the above equation and replace it by q_{inj}. On another hand, we know that the total mobility ahead of the front is equal to the end-point oil mobility. Using these two remarks leads to

$$\Delta p = \frac{\alpha}{kh\hat{\lambda}_o}\int_{L/2}^{\infty}q_t(r,t)\frac{dr}{r} + \frac{\pi\alpha q_{inj}}{kL\hat{\lambda}_o}\int_{x_1}^{x_3}\frac{dx}{h(x)} + \frac{\alpha q_{inj}}{L\hat{\lambda}_o}\int_{r_w}^{z_w}\frac{\hat{\lambda}_o}{\lambda_t(r,t)}\frac{dr}{rk(r)}. \tag{2.201}$$

Introducing the water front radius $r_{zx,f}$, we obtain

$$\begin{aligned}\Delta p = \frac{\alpha}{kh\hat{\lambda}_o}\int_{L/2}^{\infty}q_t(r,t)\frac{dr}{r} + \frac{\pi\alpha q_{inj}}{kL\hat{\lambda}_o}\int_{x_1}^{x_3}\frac{dx}{h(x)} + \frac{\alpha q_{inj}}{L\hat{\lambda}_o}\int_{r_w}^{r_{zx,f}(t)}\frac{\hat{\lambda}_o}{\lambda_t(r,t)}\frac{dr}{rk(r)} \\ + \frac{\alpha q_{inj}}{L\hat{\lambda}_o}\int_{r_{zx,f}(t)}^{z_w}\frac{dr}{rk(r)}.\end{aligned} \tag{2.202}$$

The last integral of Eq. 2.202 can be written as

$$\begin{aligned}\int_{r_{zx,f}}^{z_w}\frac{dr}{rk(r)} &= \int_{r_w}^{z_w}\frac{dr}{rk(r)} - \int_{r_w}^{r_{zx,f}(t)}\frac{dr}{rk(r)} \\ &= \frac{1}{k_s}\int_{r_w}^{r_s}\frac{dr}{r} + \frac{1}{k}\int_{r_s}^{z_w}\frac{dr}{r} - \int_{r_w}^{r_{zx,f}(t)}\frac{dr}{rk(r)} \\ &= \frac{1}{k}\left[\left(\frac{k}{k_s}-1\right)\ln\left(\frac{r_s}{r_w}\right) + \ln\left(\frac{z_w}{r_w}\right)\right] - \int_{r_w}^{r_{zx,f}(t)}\frac{dr}{rk(r)} \\ &= \frac{1}{k}\left[s + \ln\left(\frac{z_w}{r_w}\right)\right] - \int_{r_w}^{r_{zx,f}(t)}\frac{dr}{rk(r)}.\end{aligned} \tag{2.203}$$

Using the result of Eq. 2.203 in Eq. 2.202 and rearranging gives

$$\Delta p = \frac{\alpha}{kh\hat{\lambda}_o}\int_{L/2}^{\infty} q_t(r,t)\,\frac{dr}{r} + \frac{\pi\alpha q_{inj}}{kL\hat{\lambda}_o}\int_{x_1}^{x_3}\frac{dx}{h(x)} + \frac{\alpha q_{inj}}{kL\hat{\lambda}_o}\left[s + \ln\left(\frac{z_w}{r_w}\right)\right] + \frac{\alpha q_{inj}}{L\hat{\lambda}_o}\int_{r_w}^{r_{zx,f}(t)}\left(\frac{\hat{\lambda}_o}{\lambda_t(r,t)} - 1\right)\frac{dr}{rk(r)}. \quad (2.204)$$

From Eq. 2.164, we have

$$\ln\left(\frac{z_w}{r_w}\right) = s_z + \frac{\pi x_1}{2z_w}. \quad (2.205)$$

If we substitute this result in Eq. 2.204, we obtain

$$\Delta p = \frac{\alpha}{kh\hat{\lambda}_o}\int_{L/2}^{\infty} q_t(r,t)\,\frac{dr}{r} + \frac{\alpha q_{inj}}{kh\hat{\lambda}_o}\left[\frac{h}{L}(s + s_z + \frac{\pi x_1}{2z_w}) + \frac{\pi h}{L}\int_{x_1}^{x_3}\frac{dx}{h(x)}\right] + \frac{\alpha q_{inj}}{L\hat{\lambda}_o}\int_{r_w}^{r_{zx,f}(t)}\left(\frac{\hat{\lambda}_o}{\lambda_t(r,t)} - 1\right)\frac{dr}{rk(r)}. \quad (2.206)$$

By setting

$$s_{xy} = \frac{\pi h}{L}\left[\frac{x_1}{2z_w} + \int_{x_1}^{x_3}\frac{dx}{h(x)}\right] + \frac{1}{2}\ln\left(\frac{16}{e^{\gamma}}\right), \quad (2.207)$$

and using the fact that for sufficiently long times, we can approximate

$$\frac{\alpha}{kh\hat{\lambda}_o}\int_{L/2}^{\infty} q_t(r,t)\,\frac{dr}{r} = \frac{\alpha q_{inj}}{2kh\hat{\lambda}_o}\ln\left(\frac{16\beta k\hat{\lambda}_o t}{e^{\gamma}\phi\hat{c}_{to}L^2}\right), \quad (2.208)$$

Eq. 2.206 simply becomes

$$\Delta p = \frac{\alpha q_{inj}}{kh\hat{\lambda}_o}\left[\frac{1}{2}\ln\left(\frac{\beta k\hat{\lambda}_o t}{\phi\hat{c}_{to}L^2}\right) + \frac{h}{L}(s + s_z) + s_{xy}\right] + \frac{\alpha q_{inj}}{L\hat{\lambda}_o}\int_{r_w}^{r_{zx,f}}\left(\frac{\hat{\lambda}_o}{\lambda_t(r,t)} - 1\right)\frac{dr}{rk(r)}. \quad (2.209)$$

It is clear from this expression (see for instance references [20], [25] and [23]) that the first term represents the single-phase pressure drop based on oil properties at irreducible water saturation whereas the second term is the additional pressure drop caused by the difference of mobility in the (x, z) plane of the reservoir. The factor s_{xy} is the pseudo-skin due to the convergence of the flow lines in the (x, y) plane from radial to linear lines. If we assume that the well is in the center of the formation, it follows that $z_w = h/2$ and $h(x) = h$. Eq. 2.207 simplifies to

$$s_{xy} = \frac{\pi}{L} x_3 + \frac{1}{2} \ln\left(\frac{16}{e^{\gamma}}\right), \tag{2.210}$$

which is exactly the expression that [29] obtained for this particular geometry.

As Eq. 2.209 is somewhat similar to the one derived during the first radial/first radial flow regime (see Eq. 2.137 with Δp_o given by Eq. 2.139 which is the equal offset case or equivalently the complete-penetration vertical well case), we expect the behavior of the multiphase pressure derivative to be the same whether the water front is inside or outside of the skin region. Since the derivative of the single-phase oil solution is given by

$$\Delta p'_o = \frac{\alpha q_{inj}}{2kh\hat{\lambda}_o}, \tag{2.211}$$

the wellbore pressure derivative is therefore obtained by differentiating Eq. 2.209 with respect to logarithm of time using Leibnitz's rule. The result is

$$\Delta p' = \frac{\alpha q_{inj}}{2kh\hat{\lambda}_o}\left[1 + \frac{h}{L}\frac{k}{k_s}\frac{1-\hat{M}}{\hat{M}}\right], \tag{2.212}$$

if the flood front is in the skin zone and

$$\Delta p' = \frac{\alpha q_{inj}}{2kh\hat{\lambda}_w}\left(\hat{M} + \frac{h}{L}\left[\left(\frac{k}{k_s} - 1\right)\left(1 - \frac{\hat{\lambda}_w}{\lambda_t(r_s, t)}\right) + 1 - \hat{M}\right]\right), \tag{2.213}$$

if the front is beyond the damaged region.

Second Radial/First Linear Flow Regime

This is the case where the flood front propagates in the x-direction whereas the steady-state diffuses in the (x, y) plane. Following the same procedure as in the previous subsection, the pressure change at the wellbore is expressed by

$$\Delta p = \frac{\alpha}{kh\hat{\lambda}_o}\int_{L/2}^{\infty} q_t(r,t)\,\frac{dr}{r} + \frac{\pi\alpha q_{inj}}{kL\hat{\lambda}_o}\int_{x_1}^{x_f(t)} \frac{\hat{\lambda}_o}{\lambda_t(x,t)}\,\frac{dx}{h(x)} + \frac{\pi\alpha q_{inj}}{kL\hat{\lambda}_o}\int_{x_f(t)}^{x_3}\frac{dx}{h(x)} + \frac{\alpha q_{inj}}{L\hat{\lambda}_o}\int_{r_w}^{z_w}\frac{\hat{\lambda}_o}{\lambda_t(r,t)}\,\frac{dr}{rk(r)}. \quad (2.214)$$

By manipulating the integrals in Eq. 2.214, we can rewrite

$$\Delta p = \frac{\alpha}{kh\hat{\lambda}_o}\int_{L/2}^{\infty} q_t(r,t)\,\frac{dr}{r} + \frac{\pi\alpha q_{inj}}{kL\hat{\lambda}_o}\int_{x_1}^{x_f(t)} \left(\frac{\hat{\lambda}_o}{\lambda_t(x,t)} - 1\right)\frac{dx}{h(x)} + \frac{\pi\alpha q_{inj}}{kL\hat{\lambda}_o}\int_{x_1}^{x_3}\frac{dx}{h(x)} + \frac{\alpha q_{inj}}{L\hat{\lambda}_o}\int_{r_w}^{z_w}\left(\frac{\hat{\lambda}_o}{\lambda_t(r,t)} - 1\right)\frac{dr}{rk(r)} + \frac{\alpha q_{inj}}{L\hat{\lambda}_o}\int_{r_w}^{z_w}\frac{dr}{rk(r)}. \quad (2.215)$$

From Eq. 2.203, we can show that

$$\frac{\alpha q_{inj}}{L\hat{\lambda}_o}\int_{r_w}^{z_w}\frac{dr}{rk(r)} = \frac{\alpha q_{inj}}{kL\hat{\lambda}_o}\left[s + \ln\left(\frac{z_w}{r_w}\right)\right]. \quad (2.216)$$

Using Eq. 2.216 in Eq. 2.215 yields

$$\Delta p = \frac{\alpha}{kh\hat{\lambda}_o}\int_{L/2}^{\infty} q_t(r,t)\,\frac{dr}{r} + \frac{\alpha q_{inj}}{kL\hat{\lambda}_o}\left[s + \ln\left(\frac{z_w}{r_w}\right) + \pi\int_{x_1}^{x_3}\frac{dx}{h(x)}\right] + \frac{\alpha q_{inj}}{L\hat{\lambda}_o}\int_{r_w}^{z_w}\left(\frac{\hat{\lambda}_o}{\lambda_t(r,t)} - 1\right)\frac{dr}{rk(r)} + \frac{\pi\alpha q_{inj}}{kL\hat{\lambda}_o}\int_{x_1}^{x_f(t)}\left(\frac{\hat{\lambda}_o}{\lambda_t(x,t)} - 1\right)\frac{dx}{h(x)}. \quad (2.217)$$

In order to simplify the above equation, we introduce the pseudo-skin factors s_z and s_{xy} already defined by Eqs. 2.164 and 2.207, respectively, to obtain

$$\Delta p = \frac{\alpha}{kh\hat{\lambda}_o}\int_{L/2}^{\infty} q_t(r,t)\,\frac{dr}{r} + \frac{\pi\alpha q_{inj}}{kh\hat{\lambda}_o}\left[s_{xy} - \frac{1}{2}\ln(16/e^{\gamma}) + \frac{h}{L}(s+s_z)\right] + \frac{\alpha q_{inj}}{L\hat{\lambda}_o}\int_{r_w}^{z_w}\left(\frac{\hat{\lambda}_o}{\lambda_t(r,t)} - 1\right)\frac{dr}{rk(r)} + \frac{\pi\alpha q_{inj}}{kL\hat{\lambda}_o}\int_{x_1}^{x_f}\left(\frac{\hat{\lambda}_o}{\lambda_t(x,t)} - 1\right)\frac{dx}{h(x)}, \quad (2.218)$$

or finally by substituting Eq. 2.208 into this equation

$$\Delta p = \frac{\alpha q_{inj}}{kh\hat{\lambda}_o}\left[\frac{1}{2}\ln\left(\frac{\beta k\hat{\lambda}_o t}{\phi\hat{c}_{to}L^2}\right) + s_{xy} + \frac{h}{L}(s+s_z)\right] + \frac{\alpha q_{inj}}{L\hat{\lambda}_o}\int_{r_w}^{z_w}\left(\frac{\hat{\lambda}_o}{\lambda_t(r,t)} - 1\right)\frac{dr}{rk(r)} + \frac{\pi\alpha q_{inj}}{kL\hat{\lambda}_o}\int_{x_1}^{x_f(t)}\left(\frac{\hat{\lambda}_o}{\lambda_t(x,t)} - 1\right)\frac{dx}{h(x)}. \quad (2.219)$$

If we want to compute the pressure derivative during this period, it is obvious that the result for the multiphase term will be the same as the one derived for the first linear/first linear flow regime assuming that the water front is beyond x_2 and that the region $x < x_2$ is completely invaded by water. It is therefore easy to show that the pressure derivative at the wellbore is provided by

$$\Delta p' = \frac{\pi\alpha q_{inj}}{2kh\hat{\lambda}_o}\left[1 + \frac{2\pi}{L}\frac{(1-\hat{M})}{\hat{M}}x_f(t)\right], \quad (2.220)$$

indicating a derivative that is slightly below the single-phase derivative based on oil properties if the end-point mobility ratio $\hat{M} > 1$ and a slightly higher derivative in the other case, that is for $\hat{M} < 1$.

Second Radial/Second Radial Flow Regime

If the injection time is long enough, the water front will flow radially in the (x, y) plane and a second radial/second radial flow regime will develop as long as the reservoir boundaries are not felt. In this case, we express the pressure drop at the wellbore by

$$\Delta p = \frac{\alpha}{kh\hat{\lambda}_o}\int_{r_{xy,f}(t)}^{\infty} q_t(r,t)\,\frac{dr}{r} + \frac{\alpha q_{inj}}{kh\hat{\lambda}_o}\int_{L/2}^{r_{xy,f}(t)} \frac{\hat{\lambda}_o}{\lambda_t(r,t)}\,\frac{dr}{r} + \frac{\pi\alpha q_{inj}}{kL\hat{\lambda}_o}\int_{x_1}^{x_3} \frac{\hat{\lambda}_o}{\lambda_t(x,t)}\,\frac{dx}{h(x)} + \frac{\alpha q_{inj}}{L\hat{\lambda}_o}\int_{r_w}^{z_w} \frac{\hat{\lambda}_o}{\lambda_t(r,t)}\,\frac{dr}{rk(r)}. \quad (2.221)$$

If we rearrange the integrals of this equation, it is easy to show that

$$\Delta p = \frac{\alpha}{kh\hat{\lambda}_o}\int_{L/2}^{\infty} q_t(r,t)\,\frac{dr}{r} + \frac{\alpha q_{inj}}{kh\hat{\lambda}_o}\int_{L/2}^{r_{xy,f}(t)} \left(\frac{\hat{\lambda}_o}{\lambda_t(r,t)} - 1\right)\frac{dr}{r} + \frac{\pi\alpha q_{inj}}{kL\hat{\lambda}_o}\int_{x_1}^{x_3} \left(\frac{\hat{\lambda}_o}{\lambda_t(x,t)} - 1\right)\frac{dx}{h(x)} + \frac{\pi\alpha q_{inj}}{kL\hat{\lambda}_o}\int_{x_1}^{x_3} \frac{dx}{h(x)} + \frac{\alpha q_{inj}}{L\hat{\lambda}_o}\int_{r_w}^{z_w} \left(\frac{\hat{\lambda}_o}{\lambda_t(r,t)} - 1\right)\frac{dr}{rk(r)} + \frac{\alpha q_{inj}}{L\hat{\lambda}_o}\int_{r_w}^{z_w} \frac{dr}{rk(r)}. \quad (2.222)$$

Substituting Eq. 2.216 into Eq. 2.222 gives

$$\Delta p = \frac{\alpha}{kh\hat{\lambda}_o}\int_{L/2}^{\infty} q_t(r,t)\,\frac{dr}{r} + \frac{\alpha q_{inj}}{kL\hat{\lambda}_o}\left[s + \ln\left(\frac{z_w}{r_w}\right) + \pi\int_{x_1}^{x_3} \frac{dx}{h(x)}\right] + \frac{\alpha q_{inj}}{L\hat{\lambda}_o}\int_{r_w}^{z_w} \left(\frac{\hat{\lambda}_o}{\lambda_t(r,t)} - 1\right)\frac{dr}{rk(r)} + \frac{\pi\alpha q_{inj}}{kL\hat{\lambda}_o}\int_{x_1}^{x_3} \left(\frac{\hat{\lambda}_o}{\lambda_t(x,t)} - 1\right)\frac{dx}{h(x)} + \frac{\alpha q_{inj}}{kh\hat{\lambda}_o}\int_{L/2}^{r_{xy,f}(t)} \left(\frac{\hat{\lambda}_o}{\lambda_t(r,t)} - 1\right)\frac{dr}{r}. \quad (2.223)$$

By introducing the pseudo-skin factors s_z and s_{xy} and using the log approximation given by Eq. 2.208

$$\Delta p = \frac{\alpha q_{inj}}{kh\hat{\lambda}_o}\left[\frac{1}{2}\ln\left(\frac{\beta k\hat{\lambda}_o t}{\phi\hat{c}_{to}L^2}\right) + s_{xy} + \frac{h}{L}(s + s_z)\right] + \frac{\alpha q_{inj}}{L\hat{\lambda}_o}\int_{r_w}^{z_w} \left(\frac{\hat{\lambda}_o}{\lambda_t(r,t)} - 1\right)\frac{dr}{rk(r)} + \frac{\pi\alpha q_{inj}}{kL\hat{\lambda}_o}\int_{x_1}^{x_3} \left(\frac{\hat{\lambda}_o}{\lambda_t(x,t)} - 1\right)\frac{dx}{h(x)} + \frac{\alpha q_{inj}}{kh\hat{\lambda}_o}\int_{L/2}^{r_{xy,f}(t)} \left(\frac{\hat{\lambda}_o}{\lambda_t(r,t)} - 1\right)\frac{dr}{r}. \quad (2.224)$$

In order to have a better understanding of the behavior of the solution during this flow period, we can assume that up to the front radius, the total mobility is equal to the end-point water mobility which is the case of long injection times. In this case, we rewrite Eq. 2.224 as

$$\Delta p = \frac{\alpha q_{inj}}{kh\hat{\lambda}_o}\left[\frac{1}{2}\ln\left(\frac{\beta k\hat{\lambda}_o t}{\phi\hat{c}_{to}L^2}\right) + s_{xy} + \frac{h}{L}(s+s_z)\right] + \frac{\alpha q_{inj}}{L\hat{\lambda}_o}\left(\frac{1}{\hat{M}}-1\right)\int_{r_w}^{z_w}\frac{dr}{rk(r)} + \frac{\pi\alpha q_{inj}}{kL\hat{\lambda}_o}\left(\frac{1}{\hat{M}}-1\right)\int_{x_1}^{x_3}\frac{dx}{h(x)} + \frac{\alpha q_{inj}}{kh\hat{\lambda}_o}\left(\frac{1}{\hat{M}}-1\right)\int_{L/2}^{r_{xy,f}(t)}\frac{dr}{r}. \quad (2.225)$$

Note that two first integrals in the above equation are constant with respect to t. However, the third integral is not because of the front radius $r_{xy,f}$ which depends on t through the relation given by Eq. 2.60 evaluated at the water front saturation S_{wf}. It follows that taking the derivative of Eq. 2.225 with respect to logarithm of time reduces simply to

$$\Delta p' = \frac{\alpha q_{inj}}{2kh\hat{\lambda}_o} + \frac{\alpha q_{inj}}{kh\hat{\lambda}_o}\left(\frac{1}{\hat{M}}-1\right)t\frac{\partial}{\partial t}\ln\left(\frac{r_{xy,f}(t)}{L/2}\right), \quad (2.226)$$

or rearranging,

$$\begin{aligned}\Delta p' &= \frac{\alpha q_{inj}}{2kh\hat{\lambda}_o}\left[1+\left(\frac{1}{\hat{M}}-1\right)t\frac{\partial}{\partial t}\ln(r_{xy,f}^2(t))\right] \\ &= \frac{\alpha q_{inj}}{2kh\hat{\lambda}_o}\left[1+\left(\frac{1}{\hat{M}}-1\right)\frac{t}{r_{xy,f}^2}\frac{\partial r_{xy,f}^2}{\partial t}\right]. \end{aligned} \quad (2.227)$$

From Eq. 2.60, we have

$$r_{xy,f}^2 = \frac{\theta q_{inj} t}{\pi\phi h}\frac{df_w(S_{wf})}{dS_w}. \quad (2.228)$$

Therefore,

$$\frac{\partial r_{xy,f}^2}{\partial t} = \frac{\theta q_{inj}}{\pi \phi h} \frac{df_w(S_{wf})}{dS_w} = \frac{r_{xy,f}^2}{t}, \tag{2.229}$$

and Eq. 2.227 becomes

$$\Delta p' = \frac{\alpha q_{inj}}{2kh\hat{\lambda}_w}, \tag{2.230}$$

meaning that for long injection times, the pressure derivative is supposed to exhibit a slope based on water properties at residual oil saturation.

Generalized Injection Solution

Based on the analysis of the different flow regimes observed during an injection test through a horizontal well, we show that the equations derived for each period can be represented by one expression given by

$$\Delta p = p_{wf}(t) - p_i = \Delta p_o + \Delta\, p_{x-z}(t) + \Delta\, p_x(t) + \Delta\, p_{x-y}(t), \tag{2.231}$$

where Δp_o is the single-phase pressure change obtained by injecting or producing oil through a horizontal well of radius r_w into an oil reservoir of permeability $k(r)$. The terms $\Delta\, p_{x-z}$, $\Delta\, p_x$ and $\Delta\, p_{x-y}$ denote additional pressure change expressed respectively in the (x, z) plane, x-direction and the (x, y) plane caused by the contrast between total mobility behind the water front and oil mobility ahead the front. They are given by

$$\Delta\, p_{x-z}(t) = \frac{\alpha q_{inj}}{L\hat{\lambda}_o} \int_{r_w}^{\min(z_w, r_{zx,f}(t))} \left(\frac{\hat{\lambda}_o}{\lambda_t(r,t)} - 1\right) \frac{dr}{rk(r)}, \tag{2.232}$$

$$\Delta\, p_x(t) = \frac{\pi \alpha q_{inj}}{kL\hat{\lambda}_o} \int_{x_1}^{b} \left(\frac{\hat{\lambda}_o}{\lambda_t(x,t)} - 1\right) \frac{dx}{h(x)}, \tag{2.233}$$

and

$$\Delta\, p_{x-y}(t) = \frac{\alpha q_{inj}}{kh\hat{\lambda}_o} \int_{\frac{L}{2}}^{\max(\frac{L}{2}, r_{xy,f}(t))} \left(\frac{\hat{\lambda}_o}{\lambda_t(r,t)} - 1\right) \frac{dr}{r}. \tag{2.234}$$

In Eq. 2.233, the constant b is defined by

$$b = \min(\max(x_1, x_f(t)), x_3). \tag{2.235}$$

2.4 Transformation from Anisotropic into an Equivalent Isotropic Reservoir

In the previous section, the analytical solutions for the injection wellbore pressure at vertical and horizontal injection wells were generated using the Thompson-Reynolds steady-state theory. However, these solutions assumed the reservoir is isotropic, that is, the permeabilities in the three directions are the same. Here, the procedure is extended to construct an analytical injection pressure solution for a restricted-entry vertical well and for a horizontal well with unequal offsets in an anisotropic reservoir. The main idea is to apply a spatial transformation to the anisotropic system in order to convert it to an equivalent isotropic system with new properties for which the analytical solutions developed previously for an isotropic permeability field can still be used to obtain the injection wellbore pressure in an anisotropic reservoir.

We denote by k_x the permeability in the x-direction, by k_y the permeability in the y-direction and by k_z the permeability in the z-direction. A spatial transformation is defined from the (x, y, z) system into a new Cartesian coordinate system denoted by (x_n, y_n, z_n) such that

$$x_n = \sqrt{\frac{\bar{k}}{k_x}}x, \tag{2.236}$$

$$y_n = \sqrt{\frac{\bar{k}}{k_y}}y, \tag{2.237}$$

and

$$z_n = \sqrt{\frac{\bar{k}}{k_z}}z, \tag{2.238}$$

where $\bar{k}$ is a constant parameter. As suggested by Besson [9], one way to choose $\bar{k}$ is to require that the spatial transformation preserves volumes. That means

$$\sqrt{\frac{\bar{k}}{k_x}}\sqrt{\frac{\bar{k}}{k_y}}\sqrt{\frac{\bar{k}}{k_z}} = 1, \tag{2.239}$$

which simply gives

$$\bar{k} = (k_x k_y k_z)^{1/3}. \tag{2.240}$$

In the following, we consider first a single-phase flow to a vertical and a horizontal well in an anisotropic reservoir for which the transformation given above will be applied. Later, we will give a generalization to our two-phase problem.

2.4.1 Single-Phase Problem for Vertical Well Case

For now, we assume that a vertical well penetrates a reservoir of constant formation thickness, h. We assume also that the well is producing at a constant in situ rate q. Under these conditions, the equation that describes the flow is given in field units by

$$k_x \frac{\partial^2 p}{\partial x^2} + k_y \frac{\partial^2 p}{\partial y^2} + k_z \frac{\partial^2 p}{\partial z^2} = \frac{\phi \mu_o c_t}{\beta} \frac{\partial p}{\partial t}, \tag{2.241}$$

where $\beta = 2.637 \times 10^{-4}$ with time in hours. Eq. 2.241 is subject to an inner boundary condition that will be defined later. First, we apply the spatial transformation to the diffusivity Eq. 2.241. We have

$$\begin{aligned} \overrightarrow{\nabla} &= \left(\frac{\partial}{\partial x}, \frac{\partial}{\partial y}, \frac{\partial}{\partial z} \right)^T \\ &= \left(\frac{\partial}{\partial x_n} \frac{\partial x_n}{\partial x}, \frac{\partial}{\partial y_n} \frac{\partial y_n}{\partial y}, \frac{\partial}{\partial z_n} \frac{\partial z_n}{\partial z} \right)^T \\ &= \left(\sqrt{\frac{\bar{k}}{k_x}} \frac{\partial}{\partial x_n}, \sqrt{\frac{\bar{k}}{k_y}} \frac{\partial}{\partial y_n}, \sqrt{\frac{\bar{k}}{k_z}} \frac{\partial}{\partial z_n} \right)^T, \end{aligned} \tag{2.242}$$

so

$$\begin{aligned} k_x \frac{\partial^2 p}{\partial x^2} + k_y \frac{\partial^2 p}{\partial y^2} + k_z \frac{\partial^2 p}{\partial z^2} &= k_x \frac{\bar{k}}{k_x} \frac{\partial^2 p}{\partial x_n^2} + k_y \frac{\bar{k}}{k_y} \frac{\partial^2 p}{\partial y_n^2} + k_z \frac{\bar{k}}{k_z} \frac{\partial^2 p}{\partial z_n^2} \\ &= \frac{\phi \mu_o c_t}{\beta} \frac{\partial p}{\partial t}, \end{aligned} \tag{2.243}$$

or simply

$$\nabla_n^2 p = \frac{\phi \mu_o c_t}{\beta \bar{k}} \frac{\partial p}{\partial t}. \tag{2.244}$$

Eq. 2.244 represents the diffusivity equation in an isotropic reservoir of permeability $\bar{k}$ given by Eq. 2.240. Here, we assume a vertical uniform flux well of radius r_w fully penetrating a formation of uniform thickness h is producing at a rate q RB/day. Then, assuming a uniform flux well, the inner boundary condition in the original system is given by

$$q = \int_0^{2\pi} h(r \overrightarrow{v}.\overrightarrow{n})_{r=r_w} d\theta, \tag{2.245}$$

where $\overrightarrow{n}$ is the unit outward normal vector to the surface S. Using Darcy's law, the velocity $\overrightarrow{v}$ in the (x, y, z) coordinate system in oil field units is given by

$$\overrightarrow{v} = \begin{pmatrix} v_x \\ v_y \\ v_z \end{pmatrix} = -1.127 \times 10^{-3} \begin{pmatrix} \frac{k_x}{\mu} \frac{\partial p}{\partial x} \\ \frac{k_y}{\mu} \frac{\partial p}{\partial y} \\ \frac{k_z}{\mu} \frac{\partial p}{\partial z} \end{pmatrix}, \tag{2.246}$$

whereas, the normal vector $\overrightarrow{n}$ is in the (x, y) plane. Its components are

$$\overrightarrow{n} = \begin{pmatrix} n_x \\ n_y \\ n_z \end{pmatrix} = \begin{pmatrix} -\cos\theta \\ -\sin\theta \\ 0 \end{pmatrix}. \tag{2.247}$$

It follows from Eqs. 2.246 and 2.247 that the scalar product $\overrightarrow{v}.\overrightarrow{n}$ is

$$\overrightarrow{v}.\overrightarrow{n} = 1.127 \times 10^{-3} \left[\frac{k_x}{\mu} \frac{\partial p}{\partial x} \cos\theta + \frac{k_y}{\mu} \frac{\partial p}{\partial y} \sin\theta \right], \tag{2.248}$$

or in terms of the new coordinates

$$\overrightarrow{v}.\overrightarrow{n} = 1.127 \times 10^{-3} \left[\frac{k_x}{\mu} \frac{\partial p}{\partial x_n} \frac{\partial x_n}{\partial x} \cos\theta + \frac{k_y}{\mu} \frac{\partial p}{\partial y_n} \frac{\partial y_n}{\partial y} \sin\theta \right]. \tag{2.249}$$

From Eqs. 2.236 - 2.238, we have

$$\frac{\partial x_n}{\partial x} = \sqrt{\frac{\bar{k}}{k_x}}, \tag{2.250}$$

and

$$\frac{\partial y_n}{\partial y} = \sqrt{\frac{\bar{k}}{k_y}}. \tag{2.251}$$

Substituting Eqs. 2.250 and 2.251 into Eq. 2.249 yields

$$\overrightarrow{v}.\overrightarrow{n} = 1.127 \times 10^{-3} \frac{\sqrt{\bar{k}}}{\mu} \left[\sqrt{k_x} \frac{\partial p}{\partial x_n} \cos\theta + \sqrt{k_y} \frac{\partial p}{\partial y_n} \sin\theta \right]. \tag{2.252}$$

We let r_n and θ_n denote the radial and angular coordinates in the new system. Thus,

$$r_n = \sqrt{x_n^2 + y_n^2}, \tag{2.253}$$

and

$$\theta_n = \arctan\left(\frac{y_n}{x_n}\right). \tag{2.254}$$

Since x_n and y_n are function of r_n and θ_n, we can rewrite Eq. 2.252 as

$$\overrightarrow{v}.\overrightarrow{n} = 1.127 \times 10^{-3} \frac{\sqrt{\bar{k}}}{\mu} \left[\sqrt{k_x} \left(\frac{\partial p}{\partial r_n} \frac{\partial r_n}{\partial x_n} + \frac{\partial p}{\partial \theta_n} \frac{\partial \theta_n}{\partial x_n} \right) \cos\theta + \sqrt{k_y} \left(\frac{\partial p}{\partial r_n} \frac{\partial r_n}{\partial y_n} + \frac{\partial p}{\partial \theta_n} \frac{\partial \theta_n}{\partial y_n} \right) \sin\theta \right]. \tag{2.255}$$

Here, a crucial point for the rest of the analysis deserves mention. In the new coordinate system, the flow is assumed to be radial. Therefore, the pressure at any point (r_n, θ_n, z_n) in the reservoir where the diffusivity equation given by Eq. 2.244 is applicable, is assumed to be function of only the radial coordinate r_n. Then, Eq. 2.255 simplifies to

$$\overrightarrow{v}.\overrightarrow{n} = 1.127 \times 10^{-3} \frac{\sqrt{\bar{k}}}{\mu} \left[\sqrt{k_x} \frac{\partial p}{\partial r_n} \frac{\partial r_n}{\partial x_n} \cos\theta + \sqrt{k_y} \frac{\partial p}{\partial r_n} \frac{\partial r_n}{\partial y_n} \sin\theta \right]. \tag{2.256}$$

Differentiating Eq. 2.253 with respect to x_n gives

$$\frac{\partial r_n}{\partial x_n} = \frac{x_n}{\sqrt{x_n^2 + y_n^2}}, \tag{2.257}$$

or

$$\frac{\partial r_n}{\partial x_n} = \frac{x_n}{r_n}. \tag{2.258}$$

If we differentiate Eq. 2.253 with respect to y_n, by analogy to Eq. 2.258, we can write

$$\frac{\partial r_n}{\partial y_n} = \frac{y_n}{r_n}. \tag{2.259}$$

Using Eqs. 2.258 and 2.259, Eq. 2.256 becomes

$$\overrightarrow{v}.\overrightarrow{n} = 1.127 \times 10^{-3} \frac{\sqrt{\bar{k}}}{\mu} \frac{1}{r_n} \frac{\partial p}{\partial r_n} \left[\sqrt{k_x} x_n \cos\theta + \sqrt{k_y} y_n \sin\theta \right]. \tag{2.260}$$

From Eqs. 2.236 and 2.237, we have

$$x_n = \sqrt{\frac{\bar{k}}{k_x}} x = \sqrt{\frac{\bar{k}}{k_x}} r \cos\theta, \tag{2.261}$$

and

$$y_n = \sqrt{\frac{\bar{k}}{k_y}} y = \sqrt{\frac{\bar{k}}{k_y}} r \sin\theta. \tag{2.262}$$

Substituting Eqs. 2.261 and 2.262 into Eq. 2.260 gives

$$\overrightarrow{v}.\overrightarrow{n} = 1.127 \times 10^{-3} \frac{\bar{k}}{\mu} \frac{r}{r_n} \frac{\partial p}{\partial r_n}. \tag{2.263}$$

Now, if we use the preceding equation in Eq. 2.245, we simply obtain

$$q = 1.127 \times 10^{-3} \frac{\bar{k}h}{\mu} \int_0^{2\pi} \left(\frac{r^2}{r_n} \frac{\partial p}{\partial r_n} \right)_{r=r_{we}} d\theta. \tag{2.264}$$

Using Eqs. 2.261 and 2.262 in Eq. 2.253 gives

$$r_n^2 = \frac{\bar{k}}{k_x} x^2 + \frac{\bar{k}}{k_y} y^2 = \frac{\bar{k}}{k_x} r^2 \cos^2\theta + \frac{\bar{k}}{k_y} r^2 \sin^2\theta. \tag{2.265}$$

If we rearrange Eq. 2.265, we obtain

$$\frac{r^2}{r_n^2} = \frac{1}{\frac{\bar{k}}{k_x}\cos^2\theta + \frac{\bar{k}}{k_y}\sin^2\theta}. \tag{2.266}$$

Using the preceding expression in Eq. 2.264 yields

$$q = 1.127 \times 10^{-3} \frac{\bar{k}h}{\mu} \int_0^{2\pi} \left(r_n \frac{\partial p}{\partial r_n} \right)_{r=r_{we}} \frac{d\theta}{\left[\frac{\bar{k}}{k_x}\cos^2\theta + \frac{\bar{k}}{k_y}\sin^2\theta \right]}. \tag{2.267}$$

As stated above, the flow is assumed to be radial in the new coordinate system. The solution for our problem can be approximated by the line source solution or at late times by the log approximation given by

$$\Delta p(r_n, t) = p_i - p(r_n, t) = \frac{\alpha q \mu}{2\bar{k}h_n} \ln\left(\frac{4\bar{\eta}t}{e^{\gamma} r_n^2} \right), \tag{2.268}$$

where p_i is the initial reservoir pressure and $\bar{\eta}$ is the equivalent reservoir diffusivity defined by

$$\bar{\eta} = \frac{2.637 \times 10^{-4} \bar{k}}{\phi \mu c_t}, \tag{2.269}$$

for time t in hours. Differentiating Eq. 2.268 with respect to the radial coordinate r_n gives

$$-\frac{\partial p}{\partial r_n} = -\frac{\alpha q \mu}{\bar{k}h_n} \frac{1}{r_n}, \tag{2.270}$$

or simply

$$r_n \frac{\partial p}{\partial r_n} = \frac{\alpha q \mu}{\bar{k} h_n}. \tag{2.271}$$

Eq. 2.271 clearly shows that the term $r_n \frac{\partial p}{\partial r_n}$ is constant when the log approximation holds. In particular, $\left(r_n \frac{\partial p}{\partial r_n} \right)_{r_n = r_{wn}}$ is also equal to the constant given by Eq. 2.271. Thus, we can take it outside the integral of Eq. 2.267 to obtain

$$q = 1.127 \times 10^{-3} \frac{h}{\mu} \left(r_n \frac{\partial p}{\partial r_n} \right)_{r = r_{we}} \int_0^{2\pi} \frac{d\theta}{\frac{\cos^2 \theta}{k_x} + \frac{\sin^2 \theta}{k_y}}. \tag{2.272}$$

From an integral table, we find

$$\int_0^{2\pi} \frac{d\theta}{\frac{\cos^2 \theta}{k_x} + \frac{\sin^2 \theta}{k_y}} = 2\pi \sqrt{k_x k_y}. \tag{2.273}$$

Using the result of Eq. 2.273 in Eq. 2.272, we obtain

$$q = 2\pi \times 1.127 \times 10^{-3} \frac{\sqrt{k_x k_y} h}{\mu} \left(r_n \frac{\partial p}{\partial r_n} \right)_{r = r_{we}}. \tag{2.274}$$

Note that h can be replaced by $\sqrt{\frac{k_z}{k}} h_n$ in Eq. 2.274. We also need to introduce $\bar{k}$ by using the fact that $k_x k_y k_z = \bar{k}^3$. Then, Eq. 2.274 becomes

$$q = 2\pi \times 1.127 \times 10^{-3} \frac{\bar{k} h_n}{\mu} \left(r_n \frac{\partial p}{\partial r_n} \right)_{r = r_{we}}, \tag{2.275}$$

which represents the boundary condition for our equivalent isotropic problem. At this point of the analysis, it is clear that the system described by Eqs. 2.244 and 2.274 is exactly the system that we would write for a case of a constant production rate through a vertical well of an effective radius r_{we} in an isotropic reservoir of permeability $\bar{k}$.

Here, a crucial point deserves mention. In the (x, y, z) coordinate system, the flow lines are elliptical due essentially to the anisotropy. However, because of the spatial transformation, the flow lines are circular in the new system except the circular wellbore is transformed to an elliptical wellbore. To correct for this early time effect, Brigham [13] showed that the wellbore behaves as if its radius is the arithmetic average of the major

and minor axes of the elliptic section as follows

$$r_{we} = \frac{a+b}{2}, \tag{2.276}$$

where a and b are given respectively by

$$a = \sqrt{\frac{\bar{k}}{k_y}} r_w, \tag{2.277}$$

$$b = \sqrt{\frac{\bar{k}}{k_x}} r_w. \tag{2.278}$$

Since the spatial transformation keeps the volumes unchanged, we have

$$\pi r_w^2 h = \pi a b h_n. \tag{2.279}$$

Recall that h_n is the formation thickness in the new coordinate system defined by

$$h_n = \sqrt{\frac{\bar{k}}{k_z}} h. \tag{2.280}$$

From Eq. 2.279, we have

$$ab = r_w^2 \frac{h}{h_n}. \tag{2.281}$$

Using the following algebraic manipulation:

$$a + b = \sqrt{a^2 + b^2 + 2ab}, \tag{2.282}$$

and substituting it together with Eq. 2.281 into Eq. 2.276, we obtain

$$r_{we} = \frac{1}{2}\sqrt{a^2 + b^2 + 2r_w^2\frac{h}{h_n}}$$
$$= \frac{r_w}{2}\sqrt{\left(\frac{a}{r_w}\right)^2 + \left(\frac{b}{r_w}\right)^2 + 2\frac{h}{h_n}}. \tag{2.283}$$

We can express the effective wellbore radius r_{wn} in terms of the permeabilities by using Eqs. 2.277, 2.278 and 2.280 in Eq. 2.283 to obtain

$$r_{we} = \frac{r_w}{2}\sqrt{\frac{\bar{k}}{k_x} + \frac{\bar{k}}{k_y} + 2\sqrt{\frac{k_z}{\bar{k}}}}. \tag{2.284}$$

Another way to obtain an expression for the equivalent wellbore radius is to note that the line source solution, or, more specifically, the log approximation holds in the new coordinate system since the flow is radial. Thus, the pressure drop $\Delta p(r_n, t)$ is given by

$$\frac{\bar{k}h_n}{\alpha q\mu}\Delta p(r_n, t) = \frac{1}{2}\ln\left(\frac{4\bar{\eta}t}{e^{\gamma}r_n^2}\right). \tag{2.285}$$

At the wellbore, $r_n = r_{we}$, the above equation becomes

$$\frac{\bar{k}h_n}{\alpha q\mu}\Delta p(r_{we}, t) = \frac{1}{2}\ln\left(\frac{4\bar{\eta}t}{e^{\gamma}r_{we}^2}\right)$$
$$= \frac{1}{2}\ln\left(\frac{4\bar{\eta}t}{e^{\gamma}r_w^2}\right) - \frac{1}{2}\ln\left(\frac{r_{we}^2}{r_w^2}\right). \tag{2.286}$$

From Eq. 2.265, we have

$$\frac{r_{we}^2}{r_w^2} = \frac{\bar{k}}{k_x}\cos^2\theta + \frac{\bar{k}}{k_y}\sin^2\theta. \tag{2.287}$$

If we substitute Eq. 2.287 into Eq. 2.286, we find that

$$\frac{\bar{k}h_n}{\alpha q\mu}\Delta p(r_{we}, t) = \frac{1}{2}\ln\left(\frac{4\bar{\eta}t}{e^{\gamma}r_w^2}\right) - \frac{1}{2}\ln\left(\frac{\bar{k}}{k_x}\cos^2\theta + \frac{\bar{k}}{k_y}\sin^2\theta\right). \tag{2.288}$$

Eq. 2.288 clearly shows that the wellbore pressure drop $\Delta p(r_{we}, t) = \Delta p(r_w, \theta, t)$ is not uniform in θ . One way to get rid of the θ dependance is to introduce an average wellbore pressure drop defined by

$$\overline{\Delta p}_{wf} = \frac{1}{2\pi} \int_0^{2\pi} \Delta p(r_{we}, t)\, d\theta = \frac{1}{2\pi} \int_0^{2\pi} \Delta p(r_w, \theta, t)\, d\theta. \tag{2.289}$$

If we integrate Eq. 2.288 with respect to the variable θ, we obtain

$$\int_0^{2\pi} \frac{\bar{k} h_n}{\alpha q \mu} \Delta p(r_{we}, t)\, d\theta = \int_0^{2\pi} \frac{1}{2} \ln\left(\frac{4\bar{\eta} t}{e^{\gamma} r_w^2}\right) d\theta - \int_0^{2\pi} \frac{1}{2} \ln\left(\frac{\bar{k}}{k_x} \cos^2\theta + \frac{\bar{k}}{k_y} \sin^2\theta\right) d\theta, \tag{2.290}$$

or using Eq. 2.289,

$$2\pi \frac{\bar{k} h_n}{\alpha q \mu} \overline{\Delta p}_{wf} = \frac{2\pi}{2} \ln\left(\frac{4\bar{\eta} t}{e^{\gamma} r_w^2}\right) - \frac{1}{2} \int_0^{2\pi} \ln\left(\frac{\bar{k}}{k_x} \cos^2\theta + \frac{\bar{k}}{k_y} \sin^2\theta\right) d\theta. \tag{2.291}$$

Let

$$I = \int_0^{2\pi} \ln\left(\frac{\bar{k}}{k_x} \cos^2\theta + \frac{\bar{k}}{k_y} \sin^2\theta\right) d\theta. \tag{2.292}$$

Because $\cos^2\theta$ and $\sin^2\theta$ are π-periodic functions, we have

$$I = 2 \int_0^{\pi} \ln\left(\frac{\bar{k}}{k_x} \cos^2\theta + \frac{\bar{k}}{k_y} \sin^2\theta\right) d\theta. \tag{2.293}$$

To simplify the integrand of Eq. 2.293, we use the following trigonometric relationships:

$$\sin^2\theta = 1 - \cos^2\theta, \tag{2.294}$$

and

$$\cos(2\theta) = 2\cos^2\theta - 1, \tag{2.295}$$

to obtain

$$
\begin{aligned}
I &= 2\int_0^{\pi} \ln\left[\left(\frac{\bar{k}}{k_x}-\frac{\bar{k}}{k_y}\right)\cos^2\theta+\frac{\bar{k}}{k_y}\right]d\theta \\
&= 2\int_0^{\pi} \ln\left[\left(\frac{\bar{k}}{k_x}-\frac{\bar{k}}{k_y}\right)\left(\frac{\cos(2\theta)+1}{2}\right)+\frac{\bar{k}}{k_y}\right]d\theta \\
&= 2\int_0^{\pi} \ln\left[\frac{1}{2}\left(\frac{\bar{k}}{k_x}-\frac{\bar{k}}{k_y}\right)\cos(2\theta)+\frac{1}{2}\left(\frac{\bar{k}}{k_x}+\frac{\bar{k}}{k_y}\right)\right]d\theta, \qquad (2.296)
\end{aligned}
$$

or letting $\omega = 2\theta$,

$$
I = \int_0^{2\pi} \ln\left[\frac{1}{2}\left(\frac{\bar{k}}{k_x}-\frac{\bar{k}}{k_y}\right)\cos\omega+\frac{1}{2}\left(\frac{\bar{k}}{k_x}+\frac{\bar{k}}{k_y}\right)\right]d\omega, \qquad (2.297)
$$

which is also equivalent to

$$
I = 2\int_0^{\pi} \ln\left[\frac{1}{2}\left(\frac{\bar{k}}{k_x}-\frac{\bar{k}}{k_y}\right)\cos\omega+\frac{1}{2}\left(\frac{\bar{k}}{k_x}+\frac{\bar{k}}{k_y}\right)\right]d\omega. \qquad (2.298)
$$

From an integral table, we have

$$
\int_0^{\pi} \ln(a\cos\omega+b)\,d\omega = \pi\ln\left[\frac{\sqrt{b^2-a^2}+b}{2}\right], \qquad (2.299)
$$

so by analogy to Eq. 2.299, Eq. 2.298 becomes

$$
I = 2\pi\ln\left(\frac{1}{2}\left[\frac{1}{2}\left(\frac{\bar{k}}{k_x}+\frac{\bar{k}}{k_y}\right)+\sqrt{\frac{1}{4}\left(\frac{\bar{k}}{k_x}+\frac{\bar{k}}{k_y}\right)^2-\frac{1}{4}\left(\frac{\bar{k}}{k_x}-\frac{\bar{k}}{k_y}\right)^2}\right]\right), \qquad (2.300)
$$

or by simplifying the above expression,

$$
I = 2\pi\ln\left[\frac{1}{4}\left(\frac{\bar{k}}{k_x}+\frac{\bar{k}}{k_y}+2\frac{\bar{k}}{\sqrt{k_xk_y}}\right)\right]. \qquad (2.301)
$$

If we substitute Eq. 2.301 into Eq. 2.291, we obtain

$$
2\pi\frac{\bar{k}h_n}{\alpha q\mu}\overline{\Delta p}_{wf} = \frac{2\pi}{2}\ln\left(\frac{4\bar{\eta}t}{e^{\gamma}r_w^2}\right)-\frac{2\pi}{2}\ln\left[\frac{1}{4}\left(\frac{\bar{k}}{k_x}+\frac{\bar{k}}{k_y}+2\frac{\bar{k}}{\sqrt{k_xk_y}}\right)\right], \qquad (2.302)
$$

or

$$\frac{\bar{k}h_n}{\alpha q\mu}\overline{\Delta p}_{wf} = \frac{1}{2}\ln\left(\frac{4\bar{\eta}t}{e^{\gamma}r_w^2}\right) - \frac{1}{2}\ln\left[\frac{1}{4}\left(\frac{\bar{k}}{k_x}+\frac{\bar{k}}{k_y}+2\frac{\bar{k}}{\sqrt{k_xk_y}}\right)\right]. \tag{2.303}$$

The second term of the left hand side of Eq. 2.303 is an additional dimensionless pressure change due to the anisotropy. We refer to it as a pseudo-skin factor s_a so that

$$s_a = -\frac{1}{2}\ln\left[\frac{1}{4}\left(\frac{\bar{k}}{k_x}+\frac{\bar{k}}{k_y}+2\frac{\bar{k}}{\sqrt{k_xk_y}}\right)\right]. \tag{2.304}$$

On the other hand, Eq. 2.286 is

$$\frac{\bar{k}h_n}{\alpha q\mu}\Delta p(r_{we},t) = \frac{1}{2}\ln\left(\frac{4\bar{\eta}t}{e^{\gamma}r_w^2}\right) - \frac{1}{2}\ln\left(\frac{r_{we}^2}{r_w^2}\right). \tag{2.305}$$

Therefore, the effective wellbore radius r_{we} is given by

$$\frac{r_{we}^2}{r_w^2} = \frac{1}{4}\left(\frac{\bar{k}}{k_x}+\frac{\bar{k}}{k_y}+2\frac{\bar{k}}{\sqrt{k_xk_y}}\right), \tag{2.306}$$

or simply,

$$r_{we} = \frac{r_w}{2}\sqrt{\left(\frac{\bar{k}}{k_x}+\frac{\bar{k}}{k_y}+2\frac{\bar{k}}{\sqrt{k_xk_y}}\right)}. \tag{2.307}$$

Eq. 2.307 is identical to the formula for the effective wellbore radius obtained by arithmetically averaging the minor and the major axes (see Eq. 2.284) because

$$\frac{\bar{k}}{\sqrt{k_xk_y}} = \frac{\bar{k}\sqrt{k_z}}{\sqrt{k_xk_yk_z}} = \frac{\bar{k}\sqrt{k_z}}{\sqrt{\bar{k}^3}} = \sqrt{\frac{k_z}{\bar{k}}}. \tag{2.308}$$

We need to keep in mind that the derivations above for the effective wellbore radius were obtained based on a 3D transformation. In the following, we would like to still be able to find the effective wellbore radius for a 2D problem such as a fully penetrating vertical well where the z transformation is unnecessary. This is a well known problem in the literature (see, for example [31]). To do so, the starting point is Eq. 2.303 which we rewrite, using the fact that $\bar{k}h_n = \sqrt{k_xk_y}h$, and rearrange to obtain

$$\frac{\sqrt{k_x k_y}h}{\alpha q\mu}\overline{\Delta p}_{wf} = \frac{1}{2}\ln\left(\frac{4\beta\sqrt{k_x k_y}t}{e^{\gamma}\phi c_t \mu r_w^2}\right) + \frac{1}{2}\ln\left(\frac{\bar{k}}{\sqrt{k_x k_y}}\right) - \frac{1}{2}\ln\left[\frac{1}{4}\left(\frac{\bar{k}}{k_x} + \frac{\bar{k}}{k_y} + 2\frac{\bar{k}}{\sqrt{k_x k_y}}\right)\right], \tag{2.309}$$

or simplifying,

$$\frac{\sqrt{k_x k_y}h}{\alpha q\mu}\overline{\Delta p}_{wf} = \frac{1}{2}\ln\left(\frac{4\beta\sqrt{k_x k_y}t}{e^{\gamma}\phi c_t \mu r_w^2}\right) - \frac{1}{2}\ln\left[\frac{1}{4}\left(\sqrt{\frac{k_y}{k_x}} + \sqrt{\frac{k_x}{k_y}} + 2\right)\right]. \tag{2.310}$$

Eq. 2.310 indicates that the pseudo-skin factor due to the anisotropy in this case is given by

$$s_a = -\frac{1}{2}\ln\left[\frac{1}{4}\left(\sqrt{\frac{k_y}{k_x}} + \sqrt{\frac{k_x}{k_y}} + 2\right)\right]. \tag{2.311}$$

Similar to Eqs. 2.305- 2.307, we find

$$\frac{r_{we}^2}{r_w^2} = \frac{1}{4}\left(\sqrt{\frac{k_y}{k_x}} + \sqrt{\frac{k_x}{k_y}} + 2\right), \tag{2.312}$$

which we can rewrite as

$$\frac{r_{we}^2}{r_w^2} = \frac{1}{4}\left(\left[\left(\frac{k_x}{k_y}\right)^{1/4}\right]^2 + \left[\left(\frac{k_y}{k_x}\right)^{1/4}\right]^2 + 2\left(\frac{k_x}{k_y}\right)^{1/4}\left(\frac{k_y}{k_x}\right)^{1/4}\right), \tag{2.313}$$

or, using the binomial formula,

$$\frac{r_{we}^2}{r_w^2} = \frac{1}{4}\left[\left(\frac{k_x}{k_y}\right)^{1/4} + \left(\frac{k_y}{k_x}\right)^{1/4}\right]^2. \tag{2.314}$$

Finally, we obtain for the effective wellbore radius the expression

$$r_{we} = \frac{r_w}{2}\left[\left(\frac{k_x}{k_y}\right)^{1/4} + \left(\frac{k_y}{k_x}\right)^{1/4}\right], \tag{2.315}$$

which is exactly the formula given in the literature for a radial flow system in an anisotropic

reservoir.

2.4.2 Single-Phase Problem for Horizontal Well Case

For the horizontal well case, we apply the same transformation used for a vertical well and defined by Eqs. 2.236 to 2.238 to convert from an anisotropic problem to an equivalent isotropic reservoir problem of permeability $\bar{k}$ for which the solution is known. Recall that $\bar{k}$ is given by the following equation

$$\bar{k} = (k_x k_y k_z)^{\frac{1}{3}}, \tag{2.316}$$

In the new coordinate system that we denoted by (x_n, y_n, z_n), the thickness of the reservoir, the distance from the centerline of the well to the top boundary of the reservoir and the length of the horizontal well are given respectively by

$$h_n = \sqrt{\frac{\bar{k}}{k_z}} h, \tag{2.317}$$

$$z_{wn} = \sqrt{\frac{\bar{k}}{k_z}} z_w, \tag{2.318}$$

and

$$L_n = \sqrt{\frac{\bar{k}}{k_y}} L. \tag{2.319}$$

In writing Eq. 2.319, we are assuming that the axis of the well is along the y-direction. As mentioned before, the flow lines are circular in the (x_n, z_n) plane but the wellbore becomes elliptical as a consequence of applying the spatial transformation. Similar to the vertical well case, an effective wellbore radius is introduced in order to correct for this early time effect. According to the literature (see references [13] and [23] for instance), this effective wellbore radius is given by

$$r_{we} = \frac{r_w}{2}\left(\sqrt{\frac{\bar{k}}{k_x}} + \sqrt{\frac{\bar{k}}{k_z}}\right). \tag{2.320}$$

Analytical solutions for the pressure response of horizontal wells under single-phase

flow are well known (see references [23], [20] and [25] for example). They are summarized in reference [26]. In the following, we will first review the analytical solutions for the pressure drop at a horizontal well completely penetrating an anisotropic reservoir then we will apply the transformation to these solutions obtained for the different flow periods for this case. The objective behind this is to establish the equivalence between the real and the converted system. Here, we are mainly concerned by the first radial, the first linear and the second radial flow regimes.

During the semi-radial flow regime (semi-radial flow in the (x, z) plane that may occur if the well is not drilled near the center of the formation), the pressure behavior is given by

$$\Delta p = p_i - p_{wf} = \frac{\alpha q B \mu}{\sqrt{k_x k_z} L}\left[\ln\left(\frac{4\beta\sqrt{k_x k_z}t}{e^{\gamma}\phi\mu c_t r_w^2}\right) + s + s'\right], \tag{2.321}$$

where α and β are unit conversion constants given in oil field units by 141.2 and 2.637×10^{-4} respectively. The term s represents the mechanical skin and s' is the pseudo-skin factor due to anisotropy and defined according to Kuchuk et al. [23] by

$$s' = -\ln\left[\left(1 + \sqrt{\frac{k_x}{k_z}}\right)\frac{z_w}{r_w}\right]. \tag{2.322}$$

We can easily see that if the reservoir were isotropic, that is $k_x = k_y = k_z = k$, the pseudo-skin factor s' would reduce to

$$s' = -\ln\left(\frac{2z_w}{r_w}\right), \tag{2.323}$$

and the pressure change in this case would simplify to Eq. 2.138. Using the relationship between L and L_n given by Eq. 2.319, and using Eq. 2.322 in Eq. 2.321, we obtain

$$\Delta p = \frac{\alpha q B \mu \sqrt{\bar{k}}}{\sqrt{k_y k_z k_x} L_n}\left[\ln\left(\frac{4\beta\sqrt{k_x k_z}t}{e^{\gamma}\phi\mu c_t r_w^2}\right) + s - \ln\left[\left(1 + \sqrt{\frac{k_x}{k_z}}\right)\frac{z_w}{r_w}\right]\right]. \tag{2.324}$$

By introducing $\bar{k}$ and r_{we} in the first log term of Eq. 2.324, we can show that

$$\Delta p = \frac{\alpha q B \mu}{\bar{k} L_n}\left[\ln\left(\frac{4\beta\bar{k}t}{e^{\gamma}\phi\mu c_t r_{we}^2}\frac{\sqrt{k_x k_z}}{\bar{k}}\frac{r_{we}^2}{r_w^2}\right) + s - \ln\left[\left(1+\sqrt{\frac{k_x}{k_z}}\right)\frac{z_w}{r_w}\right]\right], \tag{2.325}$$

or

$$\Delta p = \frac{\alpha q B \mu}{\bar{k} L_n}\left[\ln\left(\frac{4\beta\bar{k}t}{e^{\gamma}\phi\mu c_t r_{we}^2}\right) + s + \ln\left(\frac{\sqrt{k_x k_z}}{\bar{k}}\frac{r_{we}^2}{r_w^2}\right) - \ln\left[\left(1+\sqrt{\frac{k_x}{k_z}}\right)\frac{z_w}{r_w}\right]\right]. \tag{2.326}$$

From Eq. 2.320, we have

$$\sqrt{\frac{\bar{k}}{k_x}} + \sqrt{\frac{\bar{k}}{k_z}} = 2\frac{r_{we}}{r_w}, \tag{2.327}$$

or

$$\sqrt{\frac{\bar{k}}{k_x}}\left(1+\sqrt{\frac{k_x}{k_z}}\right) = 2\frac{r_{we}}{r_w}. \tag{2.328}$$

Thus,

$$\left(1+\sqrt{\frac{k_x}{k_z}}\right) = 2\frac{r_{we}}{r_w}\sqrt{\frac{k_x}{\bar{k}}}, \tag{2.329}$$

which we substitute in Eq. 2.326 to give

$$\Delta p = \frac{\alpha q B \mu}{\bar{k} L_n}\left[\ln\left(\frac{4\beta\bar{k}t}{e^{\gamma}\phi\mu c_t r_{we}^2}\right) + s + \ln\left(\frac{\sqrt{k_x k_z}}{\bar{k}}\frac{r_{we}^2}{r_w^2}\right) - \ln\left(2\frac{r_{we}}{r_w}\sqrt{\frac{k_x}{\bar{k}}}\frac{z_w}{r_w}\right)\right]. \tag{2.330}$$

Using the relationship between z_w and z_{wn} provided by Eq. 2.318 in Eq. 2.330 and rearranging, it is easy to show that

$$\Delta p = \frac{\alpha q B \mu}{\bar{k} L_n}\left[\ln\left(\frac{4\beta\bar{k}t}{e^{\gamma}\phi\mu c_t r_{we}^2}\right) + s + \ln\left(\frac{\sqrt{k_x k_z}}{\bar{k}}\frac{r_{we}^2}{r_w^2}\right) - \ln\left(\frac{\sqrt{k_x k_z}}{\bar{k}}\frac{r_{we}^2}{r_w^2}\frac{2z_{wn}}{r_{we}}\right)\right], \tag{2.331}$$

which simplifies to

$$\Delta p = \frac{\alpha q B \mu}{\bar{k} L_n}\left[\ln\left(\frac{4\beta\bar{k}t}{e^{\gamma}\phi\mu c_t r_{we}^2}\right) + s - \ln\left(\frac{2z_{wn}}{r_{we}}\right)\right]. \tag{2.332}$$

A comparison between Eq. 2.332 and Eq. 2.138 clearly indicates that by making the transformation, we converted the anisotropic problem during the first radial flow regime to a system where the reservoir is isotropic of permeability $\bar{k}$ and where the horizontal well of a centerline distant to the closest reservoir boundary by z_{wn} in the z-direction, is characterized by its length L_n and its radius r_{we}.

Peres and Reynolds [26] also reported the pressure response of a horizontal well during the first linear flow regime as follows:

$$\Delta p = p_i - p_{wf} = \frac{\alpha q B \mu}{k_x h}\left[\sqrt{\frac{4\pi\beta k_x t}{\phi\mu c_t L^2}} + \sqrt{\frac{k_x}{k_z}}\frac{h}{L}(s_z + s)\right]. \tag{2.333}$$

Recall that s_z is a pseudo-skin factor which represents an additional dimensionless pressure drop due to the convergence of flow lines from linear to radial near the wellbore. An expression for s_z in the case of isotropy is given by the following equation

$$s_z = \ln\left(\frac{h}{2\pi r_w \sin(\pi z_w/h)}\right). \tag{2.334}$$

In the anisotropic case, Kuchuk et al. [23] replace r_w by r'_w, where r'_w is given by

$$r'_w = \frac{r_w}{2}\left(1 + \sqrt{\frac{k_z}{k_x}}\right). \tag{2.335}$$

Again, if we assume an isotropic case, $r'_w = r_w$ and Eq. 2.333 simplifies to

$$\Delta p = \frac{\alpha q B \mu}{kh}\left[\sqrt{\frac{4\pi\beta k t}{\phi\mu c_t L^2}} + \frac{h}{L}\ln\left(\frac{h}{2\pi r_w \sin(\pi z_w/h)}\right) + \frac{h}{L}s\right]. \tag{2.336}$$

If we transform Eq. 2.333 into the new coordinate system by using Eqs. 2.317-Eq. 2.319 and introducing $\bar{k}$, we find

$$\Delta p = p_i - p_{wf} = \frac{\alpha q B \mu}{\bar{k} h_n} \frac{\bar{k}}{k_x} \sqrt{\frac{\bar{k}}{k_z}} \left[\sqrt{\frac{4\pi\beta\bar{k}t}{\phi\mu c_t L_n^2}} \sqrt{\frac{\bar{k}}{k_y}} \sqrt{\frac{k_x}{\bar{k}}} + \sqrt{\frac{k_x}{k_z}} \frac{h_n}{L_n} \sqrt{\frac{k_z}{\bar{k}}} \sqrt{\frac{\bar{k}}{k_y}} \left(\ln \left(\frac{h_n \sqrt{\frac{k_z}{\bar{k}}}}{2\pi r'_w \sin(\pi z_{wn}/h_n)} \right) + s \right) \right], \quad (2.337)$$

or by simplifying the above equation

$$\Delta p = p_i - p_{wf} = \frac{\alpha q B \mu}{\bar{k} h_n} \left[\sqrt{\frac{4\pi\beta\bar{k}t}{\phi\mu c_t L_n^2}} + \frac{h_n}{L_n} \ln \left(\frac{h_n \sqrt{\frac{k_z}{\bar{k}}}}{2\pi r'_w \sin(\pi z_{wn}/h_n)} \right) + \frac{h_n}{L_n} s \right]. \quad (2.338)$$

Introducing the effective wellbore radius r_{we}, we can rewrite Eq. 2.338 as

$$\Delta p = p_i - p_{wf} = \frac{\alpha q B \mu}{\bar{k} h_n} \left[\sqrt{\frac{4\pi\beta\bar{k}t}{\phi\mu c_t L_n^2}} + \frac{h_n}{L_n} \ln \left(\frac{h_n}{2\pi r_{we} \sin(\pi z_{wn}/h_n)} \right) + \frac{h_n}{L_n} s + \frac{h_n}{L_n} \ln \left(\sqrt{\frac{k_z}{\bar{k}}} \frac{r_{we}}{r'_w} \right) \right]. \quad (2.339)$$

Finally, using the expressions for r'_w (Eq. 2.335) and r_{we} (Eq. 2.320), it is easy to show that the last term in Eq. 2.339 vanishes leading to

$$\Delta p = p_i - p_{wf} = \frac{\alpha q B \mu}{\bar{k} h_n} \left[\sqrt{\frac{4\pi\beta\bar{k}t}{\phi\mu c_t L_n^2}} + \frac{h_n}{L_n} \ln \left(\frac{h_n}{2\pi r_{wn} \sin(\pi z_{wn}/h_n)} \right) + \frac{h_n}{L_n} s \right], \quad (2.340)$$

which is equivalent to the isotropic-single phase solution for the first linear flow period. The equivalent permeability is also equal to $\bar{k}$ where $\bar{k} = \sqrt[3]{k_x k_y k_z}$.

During the second radial flow regime, the pressure response as derived by Kuchuk et al. [23] is

$$\Delta p = p_i - p_{wf} = \frac{\alpha q B \mu}{\sqrt{k_x k_y} h}\left[\frac{1}{2}\ln\left(\frac{4\beta k_y t}{e^{\gamma}\phi\mu c_t L^2}\right) + C + \sqrt{\frac{k_y}{k_z}}\frac{h}{L}(s_z + s'_z + s)\right], \tag{2.341}$$

where we previously defined s_z (see Eq. 2.334). The expression for s'_z is given by

$$s'_z = -2\sqrt{\frac{k_y}{k_z}}\frac{h}{L}\left[\frac{1}{3} - \frac{z_w}{h} + \left(\frac{z_w}{h}\right)^2\right]. \tag{2.342}$$

In Eq. 2.342, C is a constant whose value depends on how the wellbore boundary condition is represented mathematically. For an infinite conductivity wellbore model, Goode and Thambynayagam [20] give $C = 1.791$ whereas, Odeh and Babu [25] give a value of $C = 2.094$ for a uniform flux wellbore model. The pressure drop for an isotropic reservoir reduces to

$$\Delta p = p_i - p_{wf} = \frac{\alpha q B \mu}{kh}\left[\frac{1}{2}\ln\left(\frac{4\beta k t}{e^{\gamma}\phi\mu c_t L^2}\right) + C + \right.$$
$$\left.\frac{h}{L}\left(\ln\left(\frac{h}{2\pi r_w \sin(\pi z_w/h)}\right) - 2\frac{h}{L}\left[\frac{1}{3} - \frac{z_w}{h} + \left(\frac{z_w}{h}\right)^2\right] + s\right)\right]. \tag{2.343}$$

Similarly to what we did for the first radial and first linear flow periods, we can show that by applying the transformation to Eq. 2.341, we are able to obtain an equation similar to Eq. 2.343. Eq. 2.341 can be rewritten as

$$\Delta p = p_i - p_{wf} = \frac{\alpha q B \mu}{\bar{k} h_n}\frac{\bar{k}}{\sqrt{k_x k_y}}\sqrt{\frac{\bar{k}}{k_z}}\left[\frac{1}{2}\ln\left(\frac{4\beta \bar{k} t}{e^{\gamma}\phi\mu c_t L_n^2}\frac{k_y}{\bar{k}}\frac{\bar{k}}{k_y}\right) + C + \right.$$
$$\left.\sqrt{\frac{k_y}{k_z}}\frac{h_n}{L_n}\sqrt{\frac{\bar{k}}{k_y}}\sqrt{\frac{k_z}{\bar{k}}}\left(\ln\left(\frac{h_n\sqrt{\frac{k_z}{\bar{k}}}}{2\pi r'_w \sin(\pi z_{wn}/h_n)}\right) - 2\frac{h_n}{L_n}\left[\frac{1}{3} - \frac{z_{wn}}{h_n} + \left(\frac{z_{wn}}{h_n}\right)^2\right] + s\right)\right], \tag{2.344}$$

which, using the expressions for r'_w (Eq. 2.335) and r_{we} (Eq. 2.320) and rearranging, can be written as

$$\Delta p = p_i - p_{wf} = \frac{\alpha q B \mu}{\bar{k} h_n}\left[\frac{1}{2}\ln\left(\frac{4\beta\bar{k}t}{e^{\gamma}\phi\mu c_t L_n^2}\right) + C + \right.$$
$$\left.\frac{h_n}{L_n}\left(\ln\left(\frac{h_n}{2\pi r_{we}\sin(\pi z_{wn}/h_n)}\right) + \ln\left(\sqrt{\frac{k_z}{\bar{k}}}\frac{r_{we}}{r'_w}\right) - 2\frac{h_n}{L_n}\left[\frac{1}{3} - \frac{z_{wn}}{h_n} + \left(\frac{z_{wn}}{h_n}\right)^2\right] + s\right)\right], \tag{2.345}$$

which simplifies to

$$\Delta p = p_i - p_{wf} = \frac{\alpha q B \mu}{\bar{k} h_n}\left[\frac{1}{2}\ln\left(\frac{4\beta\bar{k}t}{e^{\gamma}\phi\mu c_t L_n^2}\right) + C + \right.$$
$$\left.\frac{h_n}{L_n}\left(\ln\left(\frac{h_n}{2\pi r_{we}\sin(\pi z_{wn}/h_n)}\right) - 2\frac{h_n}{L_n}\left[\frac{1}{3} - \frac{z_{wn}}{h_n} + \left(\frac{z_{wn}}{h_n}\right)^2\right] + s\right)\right]. \tag{2.346}$$

It is clear that the solutions for the different flow periods described by Eqs. 2.332, 2.340 and 2.346 are exactly the same that we would write for a case of a constant production rate through a horizontal well of an effective radius r_{we} in an isotropic reservoir of permeability $\bar{k}$. Now that we established the equivalence between the solutions in two coordinate systems through the transformation defined in Eqs. 2.236 to 2.238, we will construct analytical solutions for the pressure change during an injection test for a vertical and a horizontal well located in an anisotropic reservoir.

2.4.3 Injection Solution into an Anisotropic Reservoir, Vertical Well Case

In this section, we construct analytical pressure solution for a vertical well located in an anisotropic reservoir. Starting from Darcy's law expressed in the new coordinate system as follows:

$$\Delta p = p_{wf}(t) - p_i = \alpha \int_{r_{we}}^{\infty} \frac{q_t(r_n, t)}{\lambda_t(r_n, t)} \frac{dr_n}{r_n \bar{k}(r_n) h_n(r)}, \tag{2.347}$$

and using the same theoretical approach based on the steady-state theory applied for the isotropic case, it is easy to show that the general solution for the wellbore pressure change

during the injection period is given by

$$\Delta p = \overline{\Delta p}_o + \frac{\alpha q_{inj}}{h_n \hat{\lambda}_o} \int_{r_{we}}^{r_{fn}(t)} \left(\frac{\hat{\lambda}_o}{\lambda_t(r_n, t)} - 1 \right) \frac{h_n}{\bar{k}(r_n) h_n(r_n)} \frac{dr_n}{r_n}, \tag{2.348}$$

where $\overline{\Delta p}_o$ is the single-phase pressure change obtained by injecting oil through a vertical well of radius r_{we} into an oil reservoir of permeability $\bar{k}(r_n)$ and r_{fn} is the water front position in the new coordinate system. Eq. 2.348 applies to the restricted-entry case since it takes into account the fact that in the transformed coordinate system, the injected water moves radially over a variable thickness denoted here by $h_n(r_n)$. For the complete penetrating case, we simply set $h_n(r_n) = h_n$ in Eq. 2.348 to obtain the pressure solution.

In Eq. 2.348, the equivalent isotropic permeability $\bar{k}(r_n)$ is a function of the radial distance in the new system so that the effect of the mechanical skin is accounted for in the analysis. It is given by

$$\bar{k}(r_n) = \begin{cases} \bar{k}_s & \text{for } r_{we} < r_n < r_{sn}, \\ \bar{k} = \sqrt[3]{k_x k_y k_z} & \text{for } r_n > r_{sn}. \end{cases} \tag{2.349}$$

Eq. 2.349 assumes that the skin zone becomes concentric with the well with a radius r_{sn} when applying the spatial transformation to the anisotropic system. In the new coordinate system, the permeability in the damaged zone is $\bar{k}_s = \sqrt[3]{k_{xs} k_{ys} k_{zs}}$ where k_{xs}, k_{ys} and k_{zs} denote the permeabilities of the damaged zone in the x, y and z-directions, respectively, and are assumed to have the same anisotropy ratios as the permeabilities k_x, k_y and k_z.

In the new coordinate system, the location of a saturation S_w is obtained from the following Buckley-Leverett equation

$$\int_{r_{we}}^{r_n(S_w)} r_n h_n(r_n) dr_n = \frac{\theta q_{inj} t}{2\pi\phi} \frac{df_w(S_w)}{dS_w}, \tag{2.350}$$

where θ is a constant which depends on the system of units used with $\theta = 0.23396$ if oil field units are used with time in hours. The variable thickness $h_n(r_n)$ is given by

$$h_n(r_n) = \begin{cases} h_{pn} & \text{if } r_n < r_{cn}, \\ h_n & \text{if } r_n > r_{cn}, \end{cases} \tag{2.351}$$

for model 1 and by

$$h_n(r_n) = \begin{cases} h_n \left[1 + (\frac{1-b}{r_{cn}-r_{wn}})(r_n - r_{cn}) \right] & \text{if } r_n \leq r_{cn}, \\ h_n & \text{if } r_n \geq r_{cn}, \end{cases} \tag{2.352}$$

for model 2. In these expressions, the open interval h_{pn} is defined through the spatial transformation by

$$h_{pn} = \sqrt{\frac{\bar{k}}{k_z}} h_p, \tag{2.353}$$

and r_{cn} is the radius of convergence in the (x_n, y_n, z_n) system.

For model 1, the radial location at time t is obtained by substituting Eq. 2.351 in Eq. 2.350. The result is

$$r_n^2(S_w) = \frac{\theta q_{inj} t}{\pi \phi h_{pn}} \frac{df_w(S_w)}{dS_w} + r_{we}^2. \tag{2.354}$$

If this equation gives $r_n(S_w) > r_{cn}$, then $r_n(S_w)$ is calculated with the following equation:

$$r_n^2(S_w) = \frac{\theta q_{inj} t}{\pi \phi h_n} \frac{df_w(S_w)}{dS_w} + b r_{we}^2 + (1-b) r_{cn}^2, \tag{2.355}$$

where $b = \frac{h_{pn}}{h_n} = \frac{h_p}{h}$. For model 2, similar to the derivations of Eqs. 2.40 and 2.42, we can use Eq. 2.352 in Eq. 2.350 and integrate to obtain

$$\frac{1}{3}(1-b)(r_n^3(S_w) - r_{we}^3) + \frac{1}{2}(b r_{cn} - r_{we})(r_n^2(S_w) - r_{we}^2) = \frac{\theta q_w B_w t}{2\pi \phi h_n} \frac{df_w(S_w)}{dS_w}(r_{cn} - r_{we}), \tag{2.356}$$

if $r_n < r_{cn}$ and

$$r_n^2(S_w) = \frac{\theta q_w B_w t}{\pi \phi h_n} \frac{df_w(S_w)}{dS_w} + \frac{1}{3}\left[(1-b)r_{cn}^2 + (1-b)r_{cn}r_{we} + (1+2b)r_{we}^2\right], \qquad (2.357)$$

if $r_n > r_{cn}$.

One way to determine r_{cn} is by first expressing the single-phase pressure drop in the inner region $r_n < r_{cn}$ as well as in the outer region $r_n > r_{cn}$ using the new coordinate system and then requiring continuity at the interface r_{cn} as was done to determine r_c for the isotropic case (see Appendix A). A simpler way is to compute r_{cn} is to use the fact that the volume of water injected at any time t is conserved regardless of the system used. This translates to

$$\int_{r_{we}}^{r_{cn}} r_n h_n(r_n) dr_n = \int_{r_w}^{r_c} r h(r) dr, \qquad (2.358)$$

where r_c is given by Eq. A.14 for model 1 and Eq. A.22 for model 2. Replacing $h(r)$ and $h_n(r_n)$ by their expressions given, respectively, by Eq. 2.34 and Eq. 2.351 for model 1 and integrating, we get

$$\frac{1}{2}h_{pn}(r_{cn}^2 - r_{we}^2) = \frac{1}{2}h_p(r_c^2 - r_w^2), \qquad (2.359)$$

or simply after rearranging

$$r_{cn} = \sqrt{\frac{h_p}{h_{pn}}(r_c^2 - r_w^2) + r_{we}^2}. \qquad (2.360)$$

In a similar way, we determine the radius of the skin zone r_{sn} by setting $r_n = r_{sn}$ and evaluating Eq. 2.358 as follows

$$\int_{r_{we}}^{r_{sn}} r_n h_n(r_n) dr_n = \int_{r_w}^{r_s} r h(r) dr. \qquad (2.361)$$

For a small damaged region, it is reasonable to assume that $r_s << r_c$ or equivalently $r_{sn} << r_{cn}$. In this case, we also have

$$r_{sn} = \sqrt{\frac{h_p}{h_{pn}}(r_s^2 - r_w^2) + r_{we}^2}. \tag{2.362}$$

The radius of convergence r_{cn} for model 2 is different from the one of model 1. However, it is determined by the same technique as for model 1. Using Eq. 2.358 combined with Eq. 2.352 and its equivalence in the original coordinate system, we have

$$\int_{r_{we}}^{r_{cn}} h_n \left[1 + \left(\frac{1-b}{r_{cn} - r_{we}}\right)(r_n - r_{cn})\right] r_n dr_n = \int_{r_w}^{r_c} h \left[1 + \left(\frac{1-b}{r_c - r_w}\right)(r - r_c)\right] r dr. \tag{2.363}$$

Integrating Eq. 2.363 gives

$$h_n \left[(b+2)r_{cn}^2 + (b-1)r_{cn}r_{we} - (2b+1)r_{we}^2\right] = h\left[(b+2)r_c^2 + (b-1)r_c r_w - (2b+1)r_w^2\right], \tag{2.364}$$

or after rearranging,

$$(b+2)r_{cn}^2 + (b-1)r_{we}r_{cn} - (2b+1)r_{we}^2 - \frac{h}{h_n}\left[(b+2)r_c^2 + (b-1)r_c r_w - (2b+1)r_w^2\right] = 0. \tag{2.365}$$

Eq. 2.365 is a second degree equation of unknown r_{cn}. Its positive root (positive r_{cn}) is given by

$$r_{cn} = \frac{(1-b)r_{we} + \sqrt{\Delta_c}}{2(2+b)}, \tag{2.366}$$

where Δ_c is given by

$$\Delta_c = 9(b+1)^2 r_{we}^2 + 4(b+2)\frac{h}{h_n}\left[(b+2)r_c^2 + (b-1)r_c r_w - (2b+1)r_w^2\right]. \tag{2.367}$$

The radius of the skin zone r_{sn} for this model needs to be determined given r_s in the orig-

inal coordinate system. To do so, we also use Eq. 2.361 established from the conservation of the volume that we combine with the expression of $h_n(r_n)$ in the inner region given by Eq. 2.352 assuming that the damaged zone is small enough such that $r_s << r_c$. It is obvious that the resulting equations are similar to the ones determined for the radius of convergence. We simply need to replace r_c by r_s and r_{cn} by r_{sn} in Eqs. 2.366 and 2.367 to obtain finally

$$r_{sn} = \frac{(1-b)r_{we} + \sqrt{\Delta_s}}{2(2+b)}, \tag{2.368}$$

where

$$\Delta_s = 9(b+1)^2 r_{we}^2 + 4(b+2)\frac{h}{h_n}\left[(b+2)r_s^2 + (b-1)r_s r_w - (2b+1)r_w^2\right]. \tag{2.369}$$

2.4.4 Injection Solution into an Anisotropic Reservoir, Horizontal Well Case

Similarly to the isotropic case, the general solution for the wellbore pressure change during the injection period is given by

$$\Delta p = p_{wf}(t) - p_i = \overline{\Delta p}_o + \Delta\, p_{x_n - z_n}(t) + \Delta\, p_{x_n}(t) + \Delta\, p_{x_n - y_n}(t), \tag{2.370}$$

where $\overline{\Delta p}_o$ is the single-phase pressure change obtained by injecting oil through a horizontal well of radius r_{wn} into an oil reservoir of permeability $\bar{k}(r_n)$ defined by Eq. 2.349 to account for the mechanical skin. The terms $\Delta\, p_{x_n - z_n}$, $\Delta\, p_{x_n}$ and $\Delta\, p_{x_n - y_n}$ denote additional pressure changes expressed in the new coordinate system respectively in the (x_n, z_n) plane, x_n-direction and the (x_n, y_n) plane caused by the contrast between total mobility behind the water front and oil mobility ahead the front. They are given by

$$\Delta\, p_{x_n - z_n}(t) = \frac{\alpha q_{inj}}{\bar{k} L_n \hat{\lambda_o}} \int_{r_{we}}^{\min(z_{wn}, r_{zx,fn}(t))} \left(\frac{\hat{\lambda_o}}{\lambda_t(r_n, t)} - 1\right) \frac{\bar{k}}{\bar{k}(r_n)} \frac{dr_n}{r_n}, \tag{2.371}$$

$$\Delta p_{x_n}(t) = \frac{\pi \alpha q_{inj}}{\bar{k} L_n \hat{\lambda_o}} \int_{x_{n1}}^{b_n} \Big(\frac{\hat{\lambda_o}}{\lambda_t(x_n, t)} - 1 \Big) \frac{dx_n}{h_n(x_n)}, \tag{2.372}$$

and

$$\Delta p_{x_n - y_n}(t) = \frac{\alpha q_{inj}}{\bar{k} h_n \hat{\lambda_o}} \int_{\frac{L_n}{2}}^{\max(\frac{L_n}{2}, r_{xy,fn}(t))} \Big(\frac{\hat{\lambda_o}}{\lambda_t(r_n, t)} - 1 \Big) \frac{dr_n}{r_n}, \tag{2.373}$$

where the constant b_n is defined by

$$b_n = \min(\max(x_{n1}, x_{fn}(t)), x_{n3}). \tag{2.374}$$

In the transformed system, the water distributions and consequently the total mobility profiles are obtained using three one-dimensional Buckley-Leverett equations expressed by equations similar to the isotropic case where r_w and L in Eq. 2.48 are replaced by r_{we} and L_n respectively and the thickness h in Eq. 2.60 by h_n. For the movement of the water in the x_n-direction, the location of a saturation S_w is obtained from

$$\int_0^{x_n(S_w)} h_n(x_n) L_n dx_n = \frac{\theta q_{inj} t}{2\phi} \frac{df_w(S_w)}{dS_w}, \tag{2.375}$$

where the variable thickness $h_n(x_n)$ is given by

$$h_n(x_n) = \begin{cases} 2z_{wn} & \text{for } 0 \leq x_n \leq x_{n2}, \\ h_n & \text{for } x_{n2} < x_n \leq x_{n3}, \end{cases} . \tag{2.376}$$

for model 1 and by

$$h_n(x_n) = \begin{cases} 2z_{wn} & \text{for } 0 \leq x_n \leq x_{n1}, \\ h_n - \frac{(h_n - 2z_{wn})}{(x_{n2} - x_{n1})}(x_{n2} - x_n) & \text{for } x_{n1} \leq x_n \leq x_{n2}, \\ h_n & \text{for } x_{n2} \leq x_n \leq x_{n3}, \end{cases} . \tag{2.377}$$

for model 2. In these expressions, the positions x_{n1}, x_{n2} and x_{n3} are the parameters of the two models that correspond respectively to the positions x_1, x_2 and x_3 in the real system.

Using the derivation of Eqs. 2.45 and 2.43, it is easy to show that by applying Deppe's procedure in the new coordinate system, we obtain

$$x_{n1} = \frac{\pi}{4} z_{wn}, \tag{2.378}$$

and

$$x_{n3} = \frac{\pi}{8} L_n. \tag{2.379}$$

As for the parameter x_{n2}, we can compute it by applying the steady-state single-phase theory for convergence pseudo-skin factor computations as we did for the evaluation of x_2. The result is identical to the one obtained in the real system (Eq. 2.70 for model 1 and Eq. 2.73 for model 2) with h and z_w replaced by h_n and z_{wn}. Thus, we have

$$x_{n2} = \frac{h_n}{\pi(\frac{h_n}{2z_{wn}} - 1)} \left[\ln \left(\frac{h_n}{2\pi z_{wn} \sin(\pi z_{wn}/h_n)} \right) + \frac{\pi^2}{8} \right], \tag{2.380}$$

for model 1 and

$$x_{n2} = \frac{\frac{\pi^2}{8(h_n/2z_{wn}-1)} \ln \left(\frac{h_n}{2z_{wn}} \right) + \ln \left(\frac{h_n}{2\pi z_{wn} \sin(\pi z_{wn}/h_n)} \right)}{\frac{\pi}{h_n} \left[\frac{h_n/2z_{wn}}{(h_n/2z_{wn}-1)} \ln \left(\frac{h_n}{2z_{wn}} \right) - 1 \right]}, \tag{2.381}$$

for model 2.

2.5 Numerical Behavior and Validation

In order to verify and validate the approximate analytical results derived in this chapter, several cases of injection/falloff test through vertical and horizontal wells were simulated using CMG's IMEX black oil simulator (see reference [1]). Water in each case was injected at a constant rate into the well for a certain time denoted by t_p and then the well was shut-in for a falloff test. Here, we only discuss the results that pertain to the injection period. The falloff results for each example will be considered in chapter 3. The relative permeability curves used for all examples presented are shown in Fig. 2.6 and the

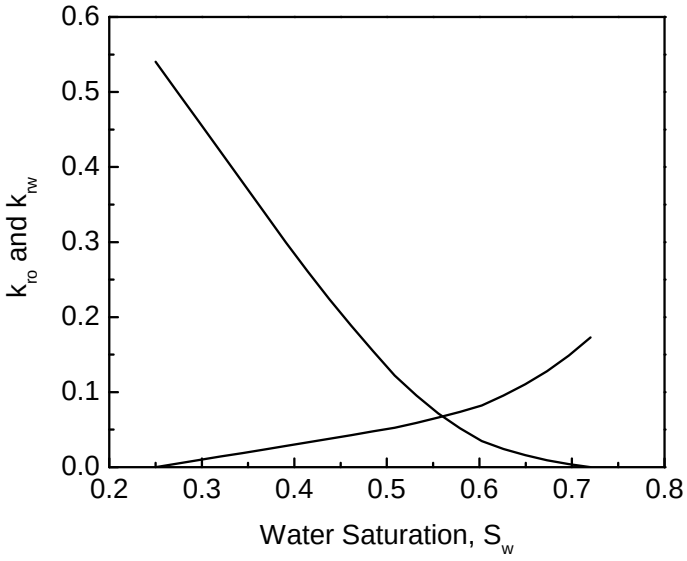

Figure 2.6: Relative permeability curves.

Property	Value
Porosity, ϕ	0.32
Rock compressibility, c_r, psi^{-1}	5.63×10^{-6}
Residual oil saturation, S_{or}	0.28
Irreducible water saturation, S_{iw}	0.25
Oil FVF, B_o, RB/STB	1.318
Oil compressibility, c_o, psi^{-1}	8.0×10^{-6}
Water FVF, B_w, RB/STB	1.008
Water compressibility, c_w, psi^{-1}	2.84×10^{-6}
Water viscosity, μ_w, cp	0.516
Wellbore radius, r_w, ft	0.35

Table 2.1: Reservoir and well data.

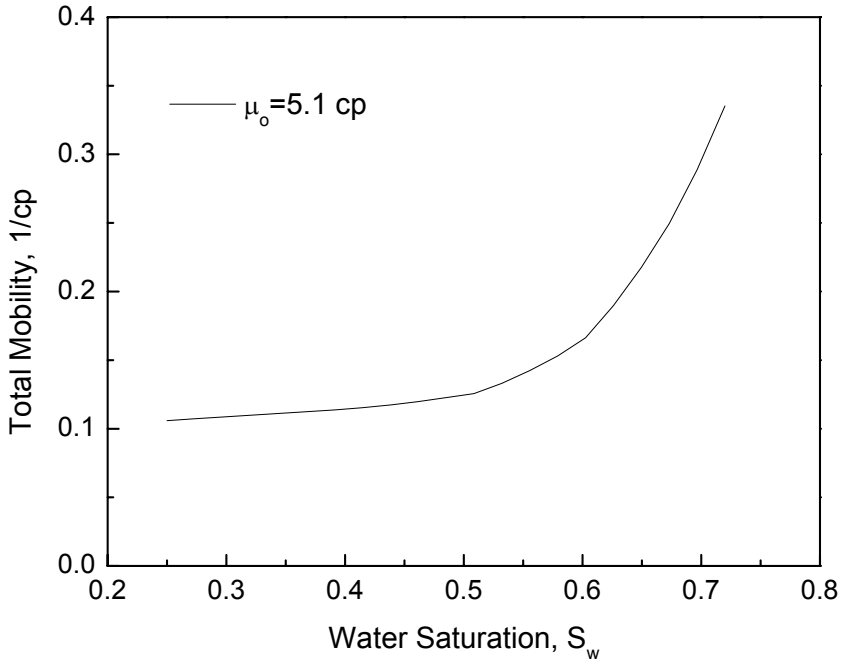

Figure 2.7: Total mobility curve, unfavorable case, $\hat{M} = 3.165$.

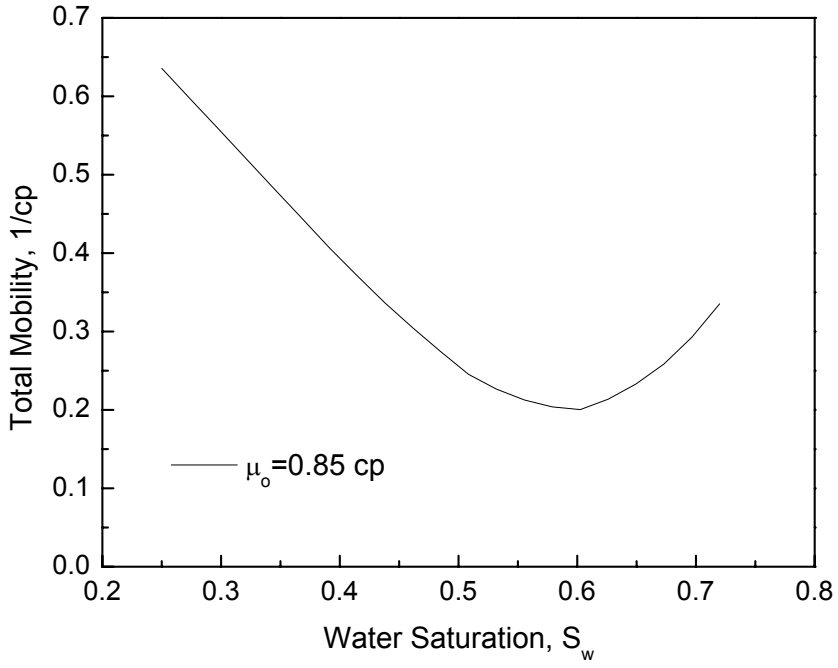

Figure 2.8: Total mobility curve, favorable case, $\hat{M} = 0.527$.

basic data used for the computations are summarized in Table 2.1.

Two cases with respect to the oil viscosity were considered here. For the unfavorable mobility case, $\mu_o = 5.1$ cp and the end-point mobility ratio gives $\hat{M} = 3.165$. The favorable mobility case considered pertains to $\mu_o = 0.85$ cp and $\hat{M} = 0.527$. Total mobility as a function of water saturation is shown in Fig. 2.7 for the unfavorable case and in Fig. 2.8 for the favorable case. Based on the classical fractional flow theory, the saturation of the water front is $S_{wf} = 0.275$ for the unfavorable case and $S_{wf} = 0.627$ for the favorable case.

2.5.1 Example 1: Skin Effect on the Wellbore Pressure Response at a Vertical Well

The objective of this example is to illustrate that the analytical solution for the injection wellbore pressure given by Eq. 2.8 for a pure radial flow is accurate for both the zero and nonzero skin cases. We also want to show the effect of the presence of a damaged zone around the wellbore on the pressure response. To do so, a case of injection of water through a complete-penetration vertical well was simulated where water was injected at a constant rate of $q_{inj} = 18,869$ STB/day for $t_p = 3$ days for the unfavorable case and $t_p = 1$ day for the favorable case. Here, the thickness of the reservoir is $h = 78.74$ ft and the reservoir with an initial pressure of $p_i = 3461.4$ psi, is isotropic of permeability $k = 2700$ mD. In all runs, the mesh consisted of a $110(r)$ by $1(\theta)$ by $1(z)$ cylindrical coordinate system for the unfavorable mobility case. However, a more extensive meshing was needed ($2400(r)$ by $1(\theta)$ by $1(z)$) for the favorable mobility case in order to get rid of the oscillations exhibited by the two-phase solution. For both cases, a variable gridblock size was used in the r-direction.

To ensure the adequacy of the grid, the single-phase case based on oil properties at irreducible water saturation was run and compared to the analytical solution. In Figs. 2.9 and Fig. 2.10, the numerical injection pressure change and its derivative with respect to $\ln(t)$ obtained for the unfavorable and favorable mobility case are shown by solid circles whereas, the analytical solutions for the wellbore pressure change and its derivative are represented by a solid line. As we can see, the two solutions for both cases are in good

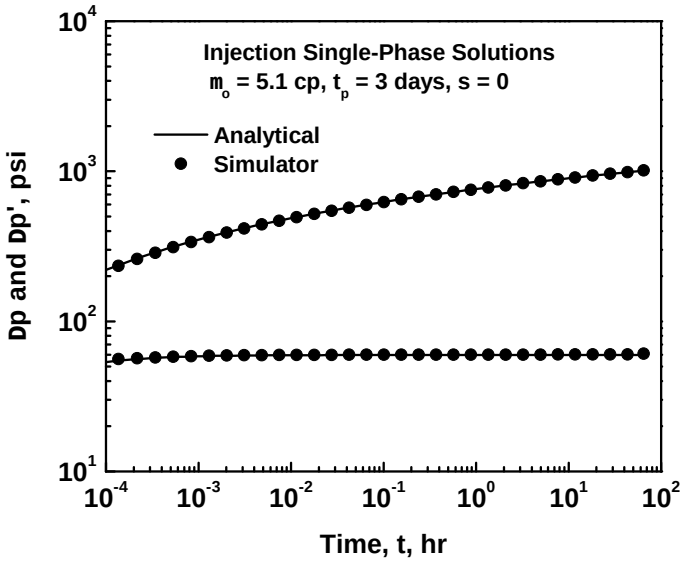

Figure 2.9: Comparison of numerical results to analytical solution for injectivity, single-phase flow.

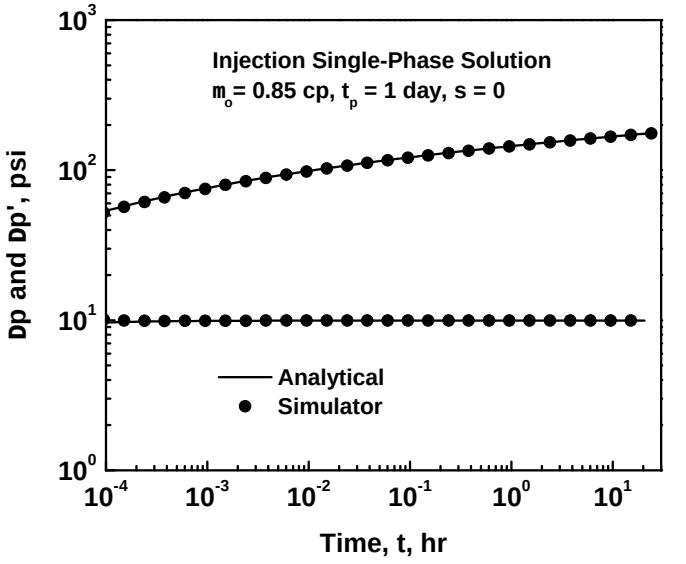

Figure 2.10: Comparison of numerical results to analytical solution for injectivity, single-phase flow.

agreement. Figs. 2.9 and Fig. 2.10 also show the standard behavior for a complete-penetrating vertical well. The semi-log slope exhibited by the pressure derivative is equal to $\Delta p' = \frac{\alpha q_{inj}}{2kh\hat{\lambda}_o} = 59.15$ for the unfavorable mobility case and $\Delta p' = 9.86$ for the favorable case.

The same simulation grid described previously was used to obtain an injection solution for the water-oil phase problem. In order to generate the analytical solutions for the injection period from the model, the integral in Eq. 2.8 which represents the multiphase component was evaluated numerically for different values of time upon the determination of the total mobility profile from Buckley-Leverett theory (Eq. 2.37 with $b = 1$) and the result was added to the single-phase solution based on oil properties. The pressure derivative data were obtained by performing a numerical differentiation on the corresponding pressure change data generated. Fig. 2.11 presents a comparison between the solution for the change in injection pressure and its derivative obtained from the reservoir simulator and the solution generated analytically. This figure which pertains to the unfavorable mobility case with $s = 0$ shows a good agreement between the simulator and the analytical solution. Equally good agreement was obtained between the analytical and numerical solutions for the favorable mobility case with $s = 0$ displayed in Fig. 2.12. Figs. 2.11 and 2.12 also indicate that at late times, the injection solution gives a derivative value which reflects the semi-log slope based on water properties at residual oil saturation as predicted by Eq. 2.32 and given by

$$\Delta p' = \frac{\alpha q_{inj}}{2kh\hat{\lambda}_w} = 18.7. \tag{2.382}$$

Note that this semi-log slope begins at $t \approx 0.8$ hours for the unfavorable case and much earlier ($t \approx 0.1$ hours) for the favorable case.

Next, we considered the same problem but with a positive skin factor, $s = 4.75$ obtained by setting $k_s = 540$ mD in a cylindrical region around the wellbore of radius $r_s = 1.15$ ft. Fig. 2.13 compares the pressure and pressure derivative solution obtained analytically to the corresponding data generated from the simulator with an end-point

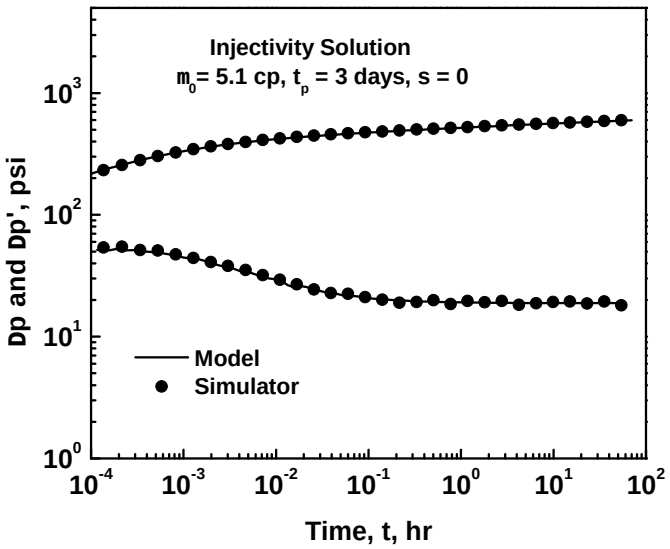

Figure 2.11: Comparison of numerical results to analytical solution for injectivity, zero skin case.

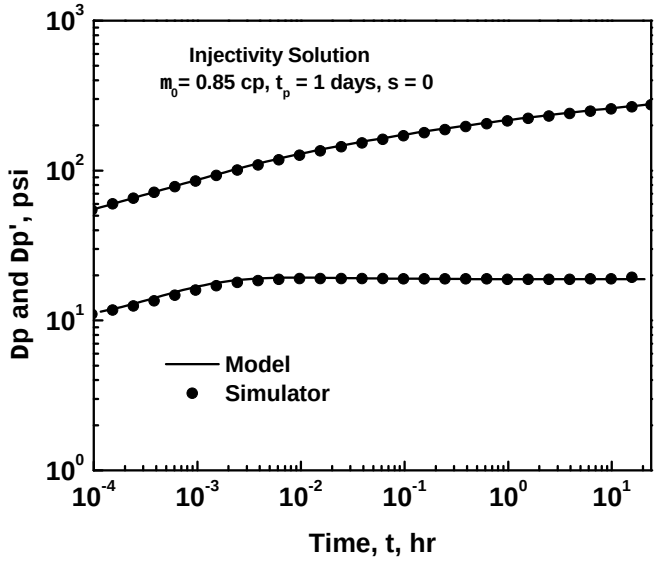

Figure 2.12: Comparison of numerical results to analytical solution for injectivity, zero skin case.

mobility ratio of 3.165. This figure shows a good agreement between the two solutions. It also indicates that the pressure derivative takes negative values from 0.0009 to 0.08 hours. According to the Buckley-Leverett Eq. 2.37, the time corresponding to when the water front reaches the radius r_s is 0.006 hours. As predicted by Eq. 2.22, as long as the flood front is inside the skin zone, the pressure derivative is negative because the condition given by Eq. 2.23 is satisfied for the unfavorable mobility case. Once the water front is outside the skin zone, Eq. 2.29 predicts negative values of the pressure derivative only if Eq. 2.31 holds which is exactly the situation as negative values of the pressure derivative persist for a longer period of time (from 0.006 to 0.08 hours) as shown in Fig. 2.13. As time goes on, the water saturation increases to a level such that $\lambda_t(r_s, t) = \hat{\lambda}_w$ causing the derivative to reach the semi-log slope given by Eq. 2.382 in a way similar to the nonzero skin case.

Fig. 2.14 considers the injectivity solution for the same set of parameters as in Fig. 2.13 but with an end-point mobility ratio equal to 0.527. Again, the match between the numerical and the analytical solutions for the pressure and its derivative with respect to $\ln t$ is quite good for this case. An interesting remark about this case is the apparent discontinuity in the derivative data that we observe at $t \approx 0.008$ hours. This corresponds to the time when the water front reaches the outer radius of the skin zone. Again, this situation occurs because the multiphase component of the pressure change decreases rapidly due to the rapid increase of the total mobility $\lambda_t(r_s, t)$ and the pressure derivative becomes negative as predicted by Eq. 2.29. Another remark is the noticeable increase in the pressure derivative observed right before the discontinuity. This occurs because the water front is still within the skin zone so that the pressure derivative increases to eventually reach a value inversely proportional to $k_s\hat{\lambda}_o$ if the skin zone is large enough. The numerical value of this semi-log slope is given by

$$\Delta p' = \frac{\alpha q_{inj}}{2k_s h\hat{\lambda}_o} = 49.3. \tag{2.383}$$

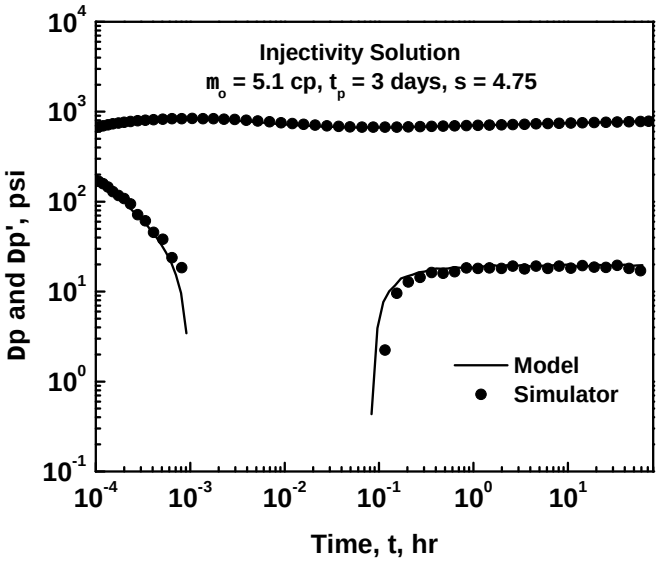

Figure 2.13: Comparison of numerical results to analytical solution for injectivity, nonzero skin case.

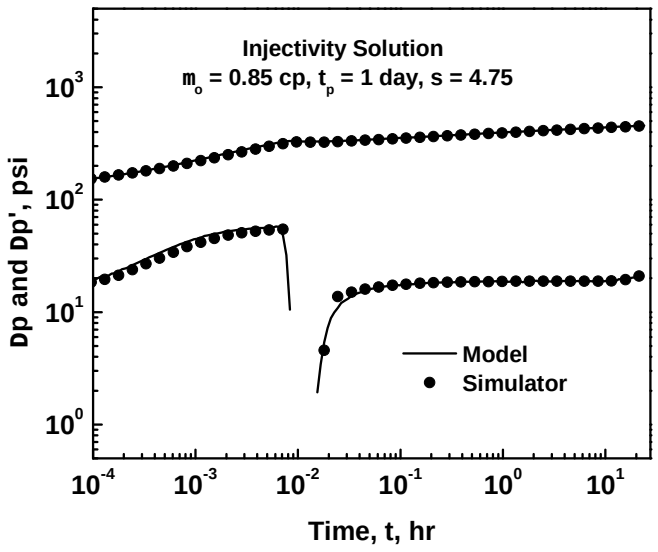

Figure 2.14: Comparison of numerical results to analytical solution for injectivity, nonzero skin case.

2.5.2 Example 2: Wellbore Pressure Response at a Restricted-Entry Vertical Well

For the runs considered in this subsection, the initial reservoir pressure is $p_i = 3941$ psi, the thickness of the reservoir $h = 236.55$ ft and the open interval $h_p = 81.69$ ft from the bottom reservoir boundary. Note that the penetration ratio is given by $b = 0.345$. Water was injected at a constant rate of $q_{inj} = 18869$ STB/day into the well for about 300 days. Both the favorable and unfavorable mobility cases were considered here. The horizontal permeability is given by $k_h = k_x = k_y = 2700$ mD whereas, the vertical permeability $k_v = 300$ mD. The permeability ratio $\frac{k_v}{k_h} = \frac{1}{9}$ falls into the typical range of values for anisotropic reservoirs. Some other relevant data to this example are the isotropic equivalent permeability (Eq. 2.240) $\bar{k} = 1298$ mD, the effective wellbore radius (Eq. 2.284) $r_{we} = 0.243$ ft, the total thickness of the reservoir in the new coordinate system (Eq. 2.280) $h_n = 492$ ft and the open interval $h_{pn} = 170$ ft. Due to this particular case of a radial flow, there was no need to use cartesian grids when simulating the injection test. Instead, the mesh consisted simply of $125(r)$ by $1(\theta)$ by $34(z)$ cylindrical coordinate system. A variable gridblock size was used in both the r and z-directions. First, we set the mechanical skin factor to zero to emphasize that unlike the complete-penetration case (see example 1), the negative pressure derivative is not due to a damaged zone.

Fig. 2.15 illustrates a comparison between the analytical anisotropic single-phase pressure change and its derivative with respect to $\ln(t)$ obtained with the real data of the problem represented by triangles and the equivalent isotropic analytical solution for the pressure drop and its derivative shown by solid lines. Both solutions match very well validating the spatial transformation used.

In order to calibrate the black oil simulator (IMEX), the single-phase case based on oil properties at irreducible water saturation was run and compared to the equivalent isotropic analytical solution. In Fig. 2.16, the numerical injection pressure change and its derivative with respect to $\ln(t)$ are shown by solid circles whereas, we kept the same legend for the analytical solution. This is the unfavorable mobility case. The favorable mobility case is shown in Fig. 2.17. For both cases, the two solutions are in good agreement. Figs. 2.15- 2.17 also show the standard behavior for a partially penetrating well. At early

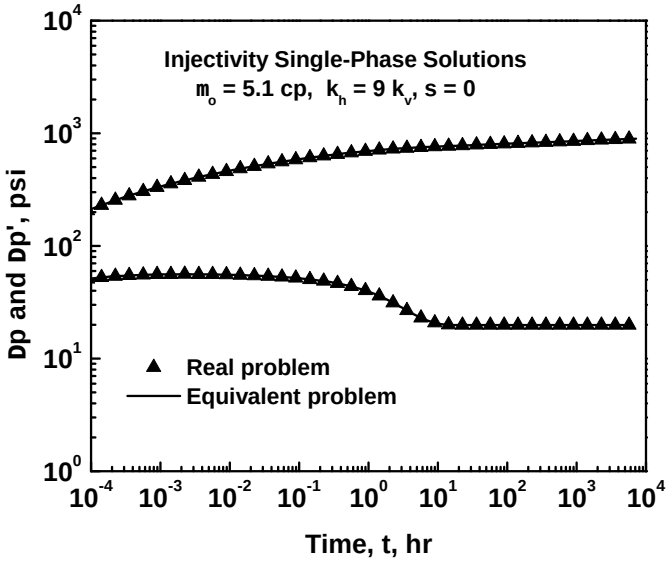

Figure 2.15: Comparison of analytical anisotropic solution for injectivity and its equivalent isotropic solution, single-phase flow.

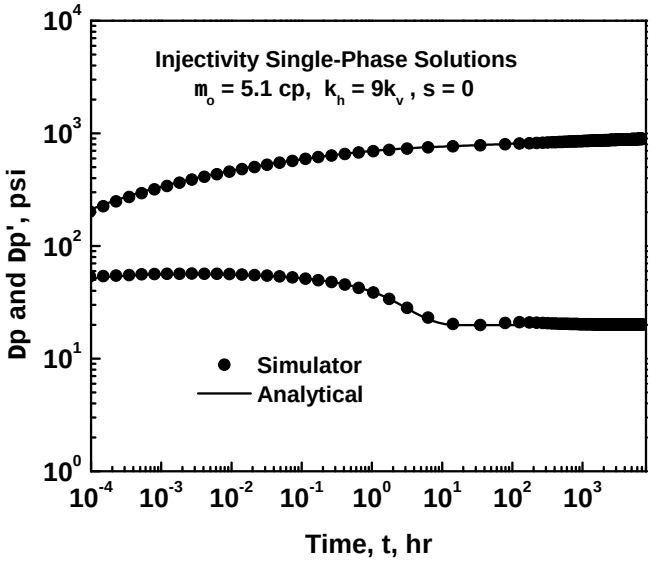

Figure 2.16: Comparison of numerical results to analytical solution for injectivity, single-phase flow, $\hat{M} = 3.165$.

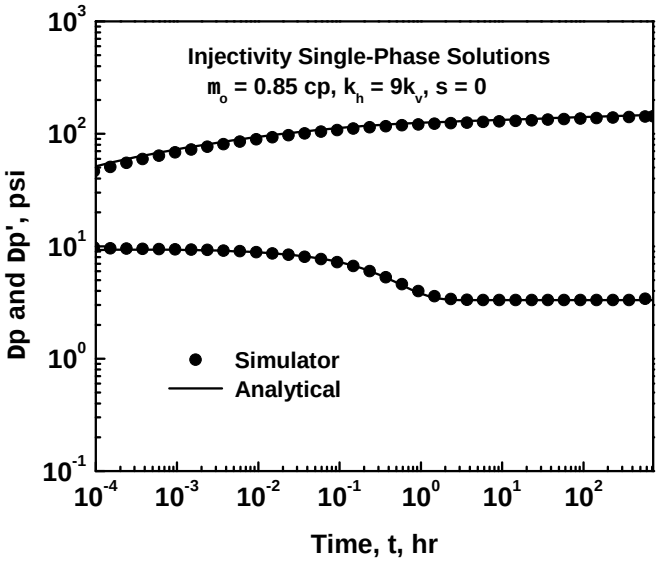

Figure 2.17: Comparison of numerical results to analytical solution for injectivity, single-phase flow, $\hat{M} = 0.527$.

times, the semi-log slope exhibited by the pressure derivative is equal to

$$\Delta p' = \frac{\alpha q_{inj}}{2\bar{k}h_{pn}\hat{\lambda}_o} = \begin{cases} 57.46 & \text{for } \hat{M} = 3.165, \\ 9.5 & \text{for } \hat{M} = 0.527, \end{cases} \tag{2.384}$$

reflecting oil properties over the equivalent opening interval h_{pn}. At late time, the semi-log line reflects oil properties over the entire equivalent thickness of the formation, h_n, i.e.,

$$\Delta p' = \frac{\alpha q_{inj}}{2\bar{k}h_n\hat{\lambda}_o} = \begin{cases} 19.85 & \text{for } \hat{M} = 3.165, \\ 3.281 & \text{for } \hat{M} = 0.527. \end{cases} \tag{2.385}$$

It is important to note that the products $\bar{k}h_{pn}$ and $\bar{k}h_n$ are $\sqrt{k_x k_y}h_p$ and $\sqrt{k_x k_y}h$ respectively.

For the injection test with an unfavorable mobility ratio, the water front r_f went beyond the convergence radius r_c for both models. For model 1, the radius of convergence given by Eq. A.14 is numerically equal to $r_c = 154.66$ ft. Its value in the new coordinate system is $r_{cn} = 107.23$ ft. The water front at the instant of shut-in was located at

$r_{fn}(t_p) = 489.81$ ft. For model 2, solving numerically Eq. A.22 gave a value of $r_c = 777.9$ ft in the real system and $r_{cn} = 539.37$ ft in the new coordinate system while the water front at the instant of shut-in was at $r_{fn}(t_p) = 545$ ft. The same simulation grid described previously was used to generate an injection solution for the water-oil two-phase flow problem. Figs. 2.18 is a log-log plot that illustrates a comparison between model 1 and the simulator for the pressure change and its derivative. Similarly, a comparison between model 2 and the simulator is displayed in Fig. 2.19. Note that Fig. 2.18 shows that the analytical and numerical pressure drop are in good agreement at early times but are noticeably different at late times. However, Fig. 2.19 exhibits a much better match between the data and model 2 for all times. This observation is better illustrated in Fig. 2.20 which represents a semi-log plot of the pressure derivative versus time. While model 2 follows the numerical trend, the derivative obtained using model 1 exhibits an oscillation corresponding to the time period when, according to our Buckley-Leverett model, the movement of water changes from propagation over the thickness h_p for $r < r_c$ to propagation over a thickness h in the region $r > r_c$. This abrupt change in the thickness used in the Buckley-Leverett equation causes the sharp change in the pressure derivative. On the other hand, for model 2, the thickness in the Buckley-Leverett equation increases continuously from h_p to h and the pressure derivative is quite smooth. Another interesting remark concerning Fig. 2.20 is that during a certain period of time corresponding to times $1.5 < t < 1700$ hours, the pressure derivative is negative. For this example, the condition $\hat{M}(1-b) = 2.07 > 1$ (Eq. 2.104) is satisfied. Therefore, the pressure change decreases with time during the second radial/first radial flow regime and the semi-log slope exhibited by the pressure derivative during this time can be approximated by Eq. 2.103 expressed in the new coordinate system by

$$\Delta p' = \frac{\alpha q_{inj}}{2\bar{k}h_{pn}\hat{\lambda}_w}\left[1-(1-b)\hat{M}\right] = -19.44, \tag{2.386}$$

which is represented in Fig. 2.20 by a dotted line. Note the derivation of Eq. 2.386 was based on model 1 and the solution for model 1 approximately exhibits this line for

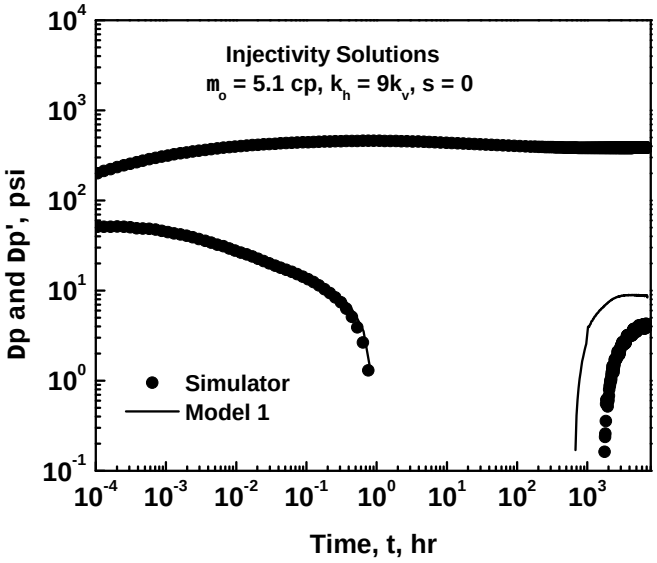

Figure 2.18: Comparison between the results for the injection test from the simulator and the analytical solution from model 1, $\hat{M} = 3.165$, $s = 0$.

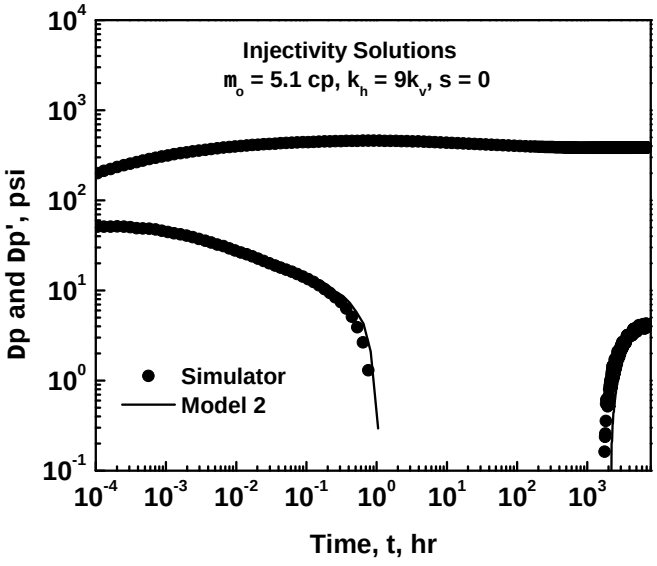

Figure 2.19: Comparison between the results for the injection test from the simulator and the analytical solution from model 2, $\hat{M} = 3.165$, $s = 0$.

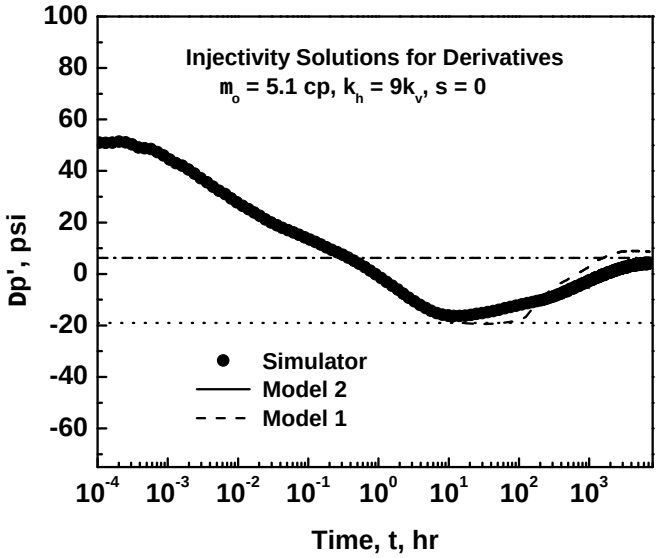

Figure 2.20: Comparison between the results for the derivative for the injection test from the simulator and the analytical solutions, $\hat{M} = 3.165$, $s = 0$.

$10 < t < 100$ hours. The derivative for the model 2 solution approaches the value predicted by Eq. 2.386 but never reaches it. Eq. 2.127 also predicts a negative pressure derivative during the second radial/second radial flow regime until the water saturation at r_c (or equivalently r_{cn}) increases to a level such that the condition given by Eq. 2.129 no longer holds. Both models for the movement of water predict large values of r_c. Thus, for this example, Eq. 2.129 holds for a considerable period of time and it is not surprising that the pressure derivative is negative throughout most of the test and never reaches the late time semi-log line given by Eq. 2.131 and represented in Fig. 2.20 by a dash dotted line.

Next, we consider the favorable mobility case, $\hat{M} = 0.527$. Since the observation from the previous test was that model 2 performed better than model 1, we give in the following only results obtained from model 2. Fig. 2.21 shows the comparison between the analytical results and simulation data in terms of pressure change and pressure derivative with respect to $\ln(t)$. Again, the analytical and numerical solutions are in good agreement. At early times corresponding to $t < 0.03$ hours, the pressure derivative increases to reach

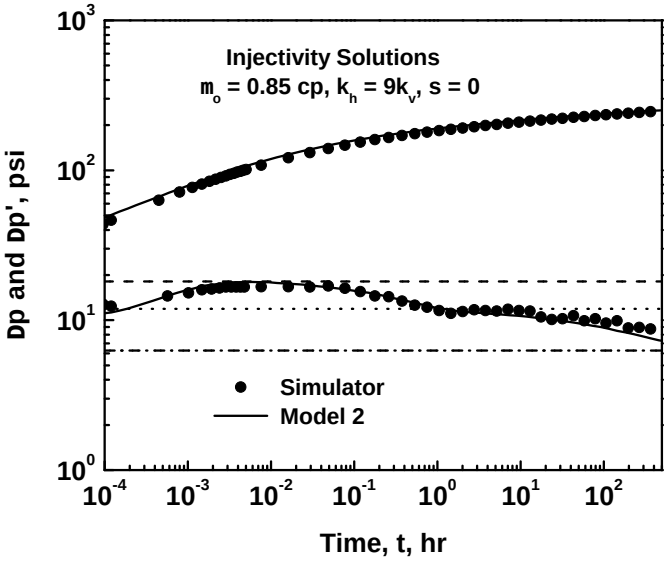

Figure 2.21: Comparison between the results for the injection test from the simulator and the analytical solution from model 2, $\hat{M} = 0.527$, $s = 0$.

the value $\Delta p' = 18.15$ represented by a dashed line in Fig. 2.21. This derivative value coincides with the value given by Eq. 2.83 for a zero skin case expressed in the new coordinate system by

$$\Delta p' = \frac{\alpha q_{inj}}{2\bar{k}h_{pn}\hat{\lambda}_w}, \tag{2.387}$$

representing the signature of the first radial/first radial flow regime. Note that during the second radial/first radial flow regime, the pressure derivative does not take negative values for this case. This is due to the fact that Eq. 2.104 is not satisfied for the favorable mobility cases. The semi-log slope exhibited by the pressure derivative during this time, given by Eq. 2.386 and also represented by a dotted line in Fig. 2.21 takes a numerical value of $\Delta p' = 11.88$. The pressure derivative stays positive throughout the test and eventually will reach the late time semi-log line defined by Eq. 2.131 and represented in the same figure by a dash dotted line with a much longer injection test.

Using the same data, another injection test was simulated where a positive mechanical skin factor was considered by setting the permeabilities to $k_{xs} = k_{ys} = 200$

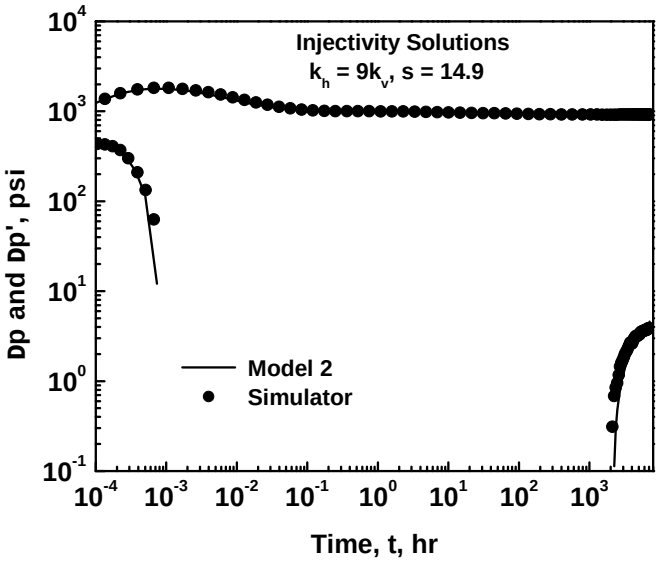

Figure 2.22: Comparison between the results for the injection test from the simulator and the analytical solution from model 2, $\hat{M} = 3.165$, $s = 14.9$.

mD and $k_{zs} = 22.22$ mD in the first twelve radial grid blocks and maintaining the values $k_x = k_y = 2700$ mD and $k_z = 300$ mD everywhere else. Note that the permeabilities of the damaged zone have the same anisotropy ratios as the permeability of the formation. The value of the damaged permeability in the new coordinate system is $\bar{k}_s = \sqrt[3]{k_{xs}k_{ys}k_{zs}} = 96.15$ mD. The corresponding radius of the skin zone r_s is equal to 1.15 ft and its value in the new coordinate system computed using Eq. 2.368 for model 2 is $r_{sn} = 0.8$ ft. With these parameters, the value of the mechanical skin factor computed from Hawkin's formula is

$$s = \left(\frac{\bar{k}}{\bar{k}_s} - 1\right) \ln\left(\frac{r_{sn}}{r_{wn}}\right) = 14.9. \tag{2.388}$$

In Fig. 2.22, we show on a log-log plot a comparison between the injectivity pressure change and its derivative evaluated analytically and the data obtained from the simulator. Again, an excellent match is observed between the two solutions. We also notice that the pressure derivative exhibits negative values throughout most of the test unlike in the zero skin case. This is due to the combined effect of skin at early time and the restricted

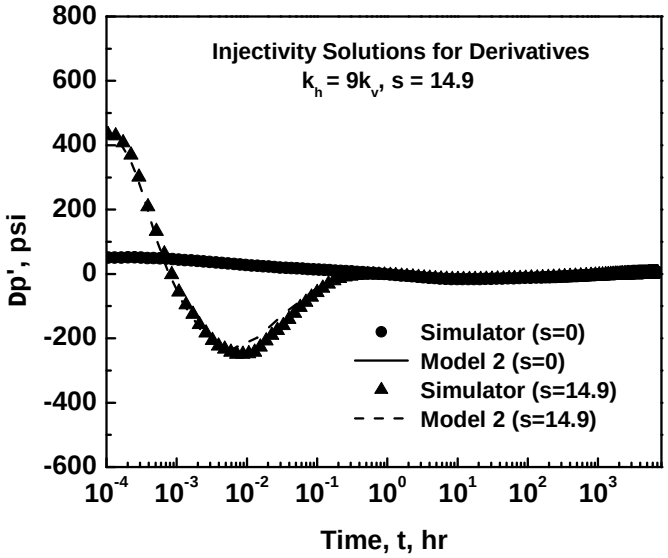

Figure 2.23: Comparison between the results for the derivative for the injection test from the simulator and the analytical solution, $\hat{M} = 3.165$.

entry at later time as illustrated in Fig. 2.23. This graph presents a comparison between the derivative obtained for the zero skin case and the pressure derivative obtained for the same example with a positive skin. The difference between the two corresponding curves resides in the early period of time $t < 0.3$ hrs. In order to identify the flow regime during this period, we note that the only case where the pressure derivative depends on the damaged permeability during the second radial/first radial regime is when the water front is still in the damaged zone. In this case, the semi-log slope that we may see is the one given by Eq. 2.101 expressed in the new coordinate system as

$$\Delta p' = \frac{\alpha q_{inj}}{2\bar{k}_s h_{pn} \hat{\lambda}_w} \left[1 - \left(1 - b \frac{\bar{k}_s}{\bar{k}} \right) \hat{M} \right] = -510.64. \tag{2.389}$$

However, we do not observe this value on the graph which suggests that by the time the diffusion is in the second radial, the flood front is already moving beyond the skin region. We should also note that Eq. 2.389 was derived based on model 1 but our computational results indicate that model 2 is more appropriate. This also means that the effect of the mechanical skin for this example occurs during the first radial/first radial flow regime.

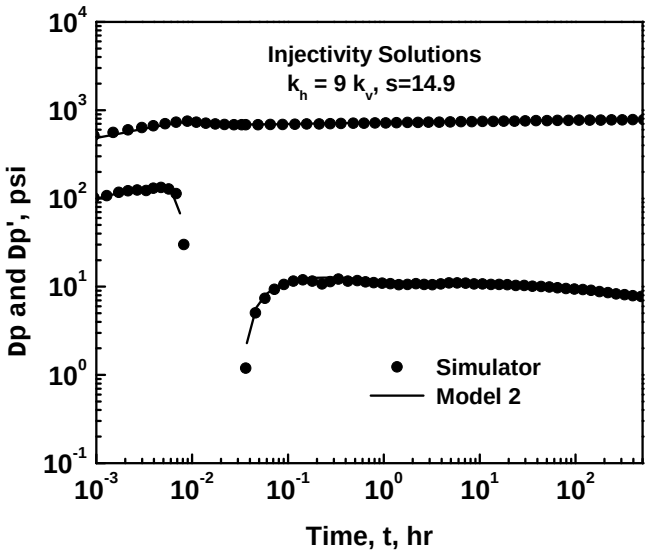

Figure 2.24: Comparison between the results for the injection test from the simulator and the analytical solution from model 2, $\hat{M} = 0.527$, $s = 14.9$.

A comparison between the injectivity pressure change and its derivative evaluated analytically and the data obtained from the simulator for the favorable mobility ratio case is illustrated in Fig. 2.24. Although the numerical solution provided by the simulator exhibits oscillations, the two sets of data are in good agreement. Similar to the completely-penetration vertical well case with a non zero skin (see Fig. 2.14), the early time derivative data exhibit large values followed by a discontinuity at $t \approx 0.01$ hours. This is, as explained for the radial flow case, a mechanical skin factor effect on the wellbore pressure response.

The next case assumes a complete anisotropic reservoir. The permeabilities in the three directions are given by $k_x = 2700$ mD, $k_y = 300$ mD and $k_z = 200$ mD. The gridding consisted of a 69 (x) by 69 (y) by 34 (z) rectangular grid blocks. Adding to that, a 16 (r) by 1 (θ) by 1 (z) was used in all the well blocks as a local hybrid grid refinement in order to capture the early time flow. One important remark about the gridding is that due to the anisotropy, a grid aspect ratio of about $\frac{\Delta x}{\Delta y} = \sqrt{\frac{k_x}{k_y}} = 3$ was necessary when building the grids. Except for the permeability values, all the other reservoir and well data remained the same. Only the unfavorable mobility case was considered here. The relevant data to this case are the isotropic equivalent permeability $\bar{k} = 545.14$ mD, the

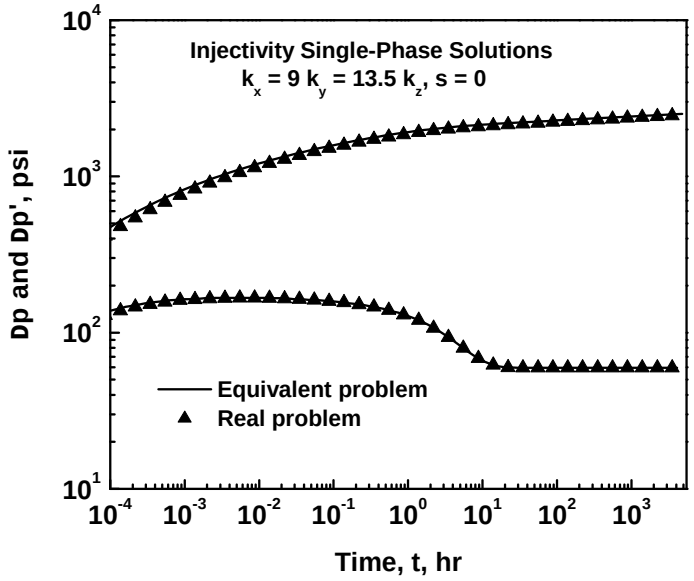

Figure 2.25: Comparison of the analytical anisotropic solution results for injectivity and its equivalent isotropic solution, single-phase flow.

effective wellbore radius $r_{we} = 0.314$ ft, the total thickness of the reservoir in the new coordinate system $h_n = 390.53$ ft and the height of the open interval in the new coordinate system $h_{pn} = 134.87$ ft. Note also that for this test, the water front, r_f went beyond the convergence radius, r_c for both models. As model 2 performed better than model 1, we will show in the following only results obtained using model 2. The radius of convergence $r_c = 548.42$ ft obtained by solving numerically Eq. A.22 is equivalent to $r_{cn} = 426.83$ ft in the new coordinate system. At the instant of shut-in, the flood front in this coordinate system is located at $r_{fn}(t_p) = 482.5$ ft.

As we did previously, the injectivity single-phase flow solution for the pressure change based on oil properties at irreducible water saturation was evaluated analytically using the real data of the problem and compared to the single-phase flow solution that we obtained by considering the equivalent properties of the reservoir and the well. Fig. 2.25 illustrates this comparison. Here also, both solutions are in good agreement validating one more time the spatial transformation used for the conversion from an isotropic to an anisotropic system.

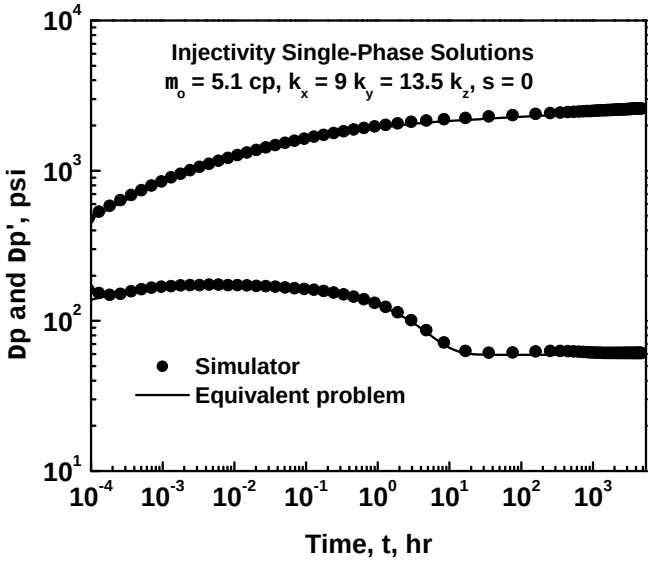

Figure 2.26: Comparison of numerical results to analytical solution for injectivity, single-phase flow.

Fig. 2.26 shows a comparison between the single-phase pressure change and its derivative obtained from the simulator in solid triangles and the analytical solution for the pressure drop and its derivative shown by solid lines obtained using the equivalent isotropic system during the injection period. The purpose of this comparison is to make sure of the adequacy of the gridding used to construct numerical solutions. We need to keep in mind that the validation of our models is done by comparison with simulations; thus, accurate numerical solutions are required. As we can see from Fig. 2.26, both solutions match very well.

In Fig. 2.27, we show on a log-log plot the results for the injectivity pressure drop and its derivative computed using model 2 against the data obtained from the simulator. Again, excellent agreement is observed. Note the behavior of the injection solution for the restricted-entry well as the pressure derivative is negative throughout a specific period of the test. For a better visualization, we also present a semi-log plot of only the pressure derivative function of time obtained using our model as well as the simulator. As we can see from Fig. 2.28, it is easy to identify the flow regimes that occurs during the injection test. At very late time, the pressure derivative approaches the semi-log slope given by

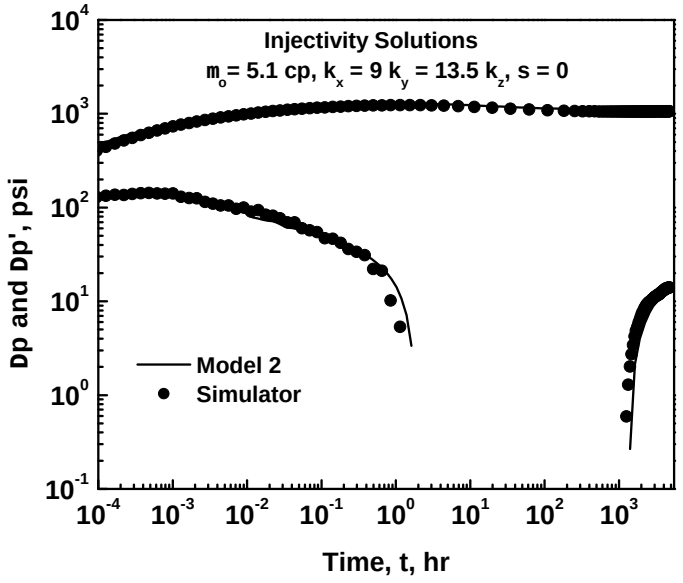

Figure 2.27: Comparison between the results for the injection test from the simulator and the analytical solution from model 2, $\hat{M} = 3.165$, $s = 0$.

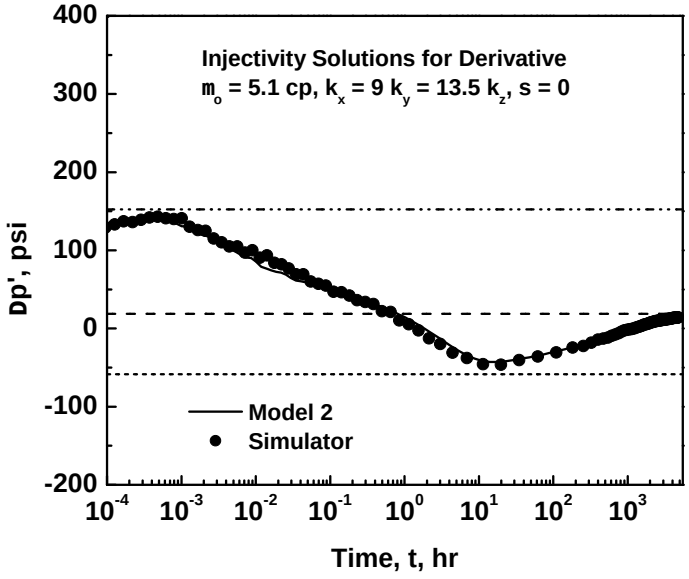

Figure 2.28: Comparison between the results for the pressure derivative for the injection test from the simulator and the analytical solution, $\hat{M} = 3.165$, $s = 0$.

$$\Delta p' = \frac{\alpha q_{inj}}{2\bar{k}h_n\hat{\lambda}_w} = 18.81, \tag{2.390}$$

which is the signature of the second radial/second radial flow regime. On the other hand, during an intermediate period of time corresponding to the second radial/first radial flow period, the derivative takes negative values because the condition $\hat{M}(1-b) > 1$ is satisfied, and flattens out for a very short period of time around the value given by the equation

$$\Delta p' = \frac{\alpha q_{inj}}{2\bar{k}h_{pn}\hat{\lambda}_w}\left[1 - \hat{M}(1-b)\right] = -58.4, \tag{2.391}$$

and represented by a dot line in Fig. 2.28.

2.5.3 Example 3: Wellbore Pressure Response at a Horizontal Well

A case of an injection test through a horizontal well distant from the top reservoir boundary of $z_w = 5$ ft was simulated using CMG's Imex simulator where water was injected at a constant rate of 31450 STB/day for 10 days for the unfavorable mobility case with $\hat{M} = 3.165$ and 4 days for the favorable mobility case of $\hat{M} = 0.527$. Here, the initial reservoir pressure is $p_i = 3922$ psi, the thickness of the formation is $h = 78.74$ ft and the length of the well is $L = 1312.4$ ft. See Table 2.1 for the other well and reservoir data. In both cases, the permeabilities in the three directions are the same given by $k = 5600$ mD. The gridding for this particular case consisted of a $232(x)$ by $89(y)$ by $5(z)$ rectangular grid blocks. Variable grid block sizes were used in all direction to better capture the flood front moving away from the well. Adding to that, the local-hybrid grid refinement option was also used in all well blocks. A $10(r)$ by $4(\theta)$ by $1(z')$ was used where the z'-direction coincides with the y-direction. In this particular case, we did not consider the mechanical skin.

In order to calibrate the simulator, the single-phase case based on oil properties at irreducible water saturation was run and compared to the analytical solution. In Figs. 2.29 and 2.30, the analytical solutions for the pressure change and its derivative with respect to $\ln(t)$ are shown by solid lines whereas, the numerical injection pressure

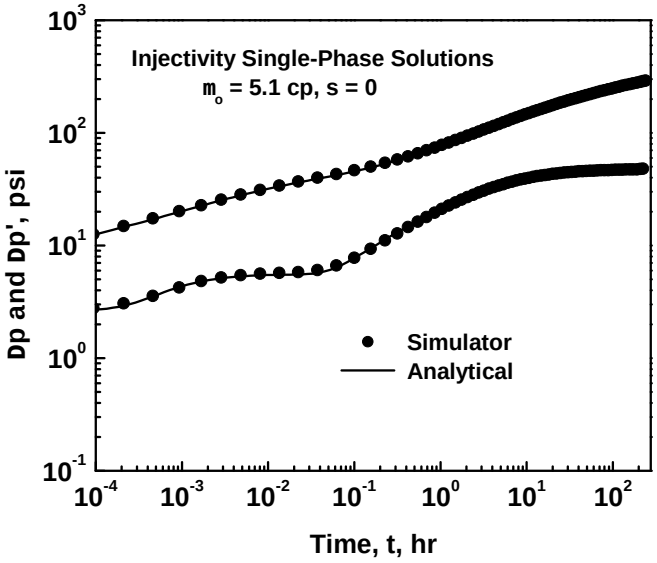

Figure 2.29: Comparison of numerical results to analytical solution for injectivity single-phase flow, $\hat{M} = 3.165$, $s = 0$.

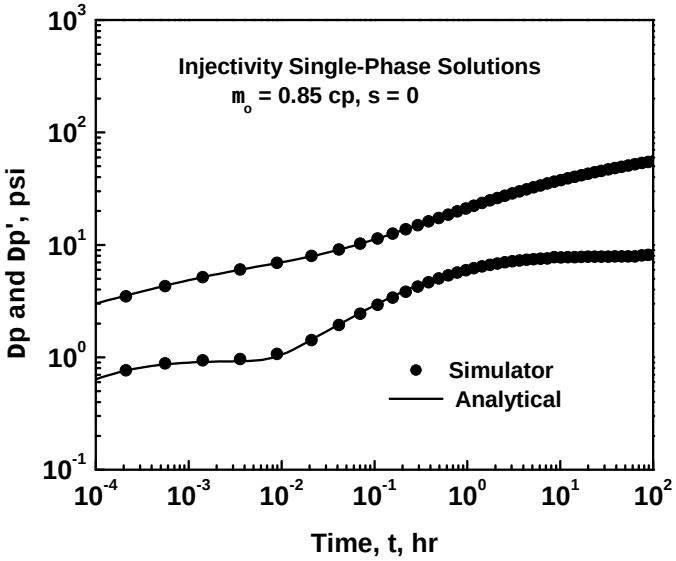

Figure 2.30: Comparison of numerical results to analytical solution for injectivity single-phase flow, $\hat{M} = 0.527$, $s = 0$.

change and its corresponding derivative are represented by solid circles for the unfavorable and favorable mobilities respectively. Note that in both cases, the numerical single-phase solution matches the corresponding solution obtained analytically very well. These figures also show a typical behavior for an offset horizontal well except for the semi-log slope that the pressure derivative should exhibit at very early times due to the first radial flow regime which is equal to

$$\Delta p' = \frac{\alpha q_{inj}}{2kL\hat{\lambda}_o} = \begin{cases} 2.87 & \text{for } \hat{M} = 3.165, \\ 0.48 & \text{for } \hat{M} = 0.527. \end{cases} \tag{2.392}$$

What we observe in both figures is a slope equal to twice the values in Eq. 2.392, which reflect the double slope due to the fact that the well is very close to one reservoir boundary (recall that we considered the extreme case of $z_w = 5$ ft). For intermediate times, the pressure derivative shows a half-slope line which is the signature of the linear flow regime. Finally, for times bigger than 50 hours for the unfavorable case and 10 hours for the favorable case, the derivative is constant and equal to

$$\Delta p' = \frac{\alpha q_{inj}}{2kh\hat{\lambda}_o} = \begin{cases} 47.90 & \text{for } \hat{M} = 3.165, \\ 7.98 & \text{for } \hat{M} = 0.527, \end{cases} \tag{2.393}$$

which corresponds to the second radial flow period.

We used the same simulation grid described previously to obtain an injection solution for the two-phase problem. In order to generate the analytical solutions from the models that we developed, the saturation profiles corresponding to each flow period were first constructed, then the multiphase components given by each model were evaluated numerically for different values of time and the results were added to the single-phase solution based on oil properties obtained previously (from the simulator). Note that for both models, the numerical values of the parameters x_1 and x_3 are equal to 3.93 ft and 515.4 ft respectively. For model 1, the parameter $x_2 = 13.75$ ft and the water front at the instant of shut-in is at 108.6 ft for the unfavorable mobility case and 40.74 ft for the

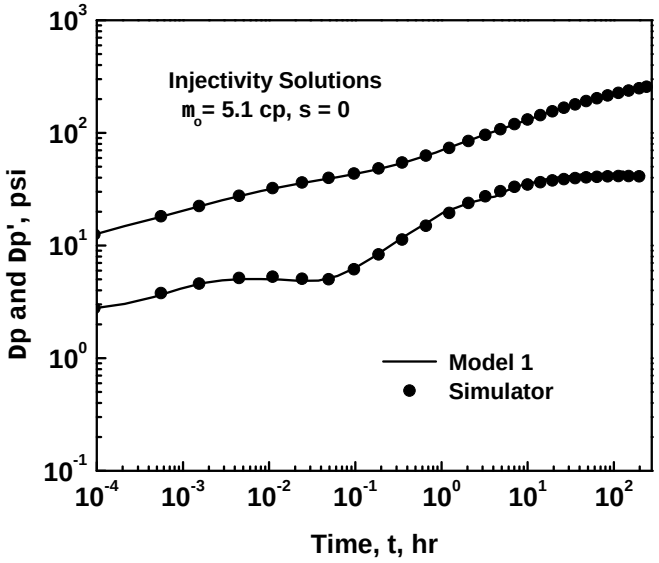

Figure 2.31: Comparison between the results for the injection test from the simulator and the analytical solution from model 1, $\hat{M} = 3.165$, $s = 0$.

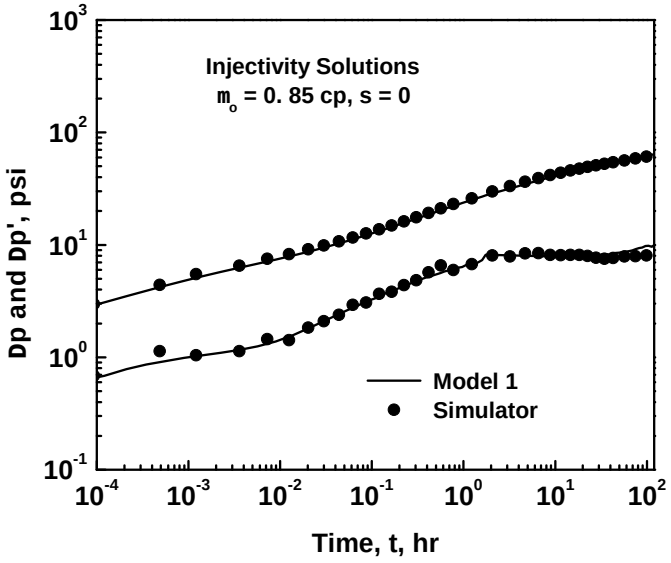

Figure 2.32: Comparison between the results for the injection test from the simulator and the analytical solution from model 1, $\hat{M} = 0.527$, $s = 0$.

favorable case. For model 2, $x_2 = 53.44$ ft whereas the flood front is at 121.6 ft and 54.0 ft for the unfavorable and favorable case respectively. Because $x_f < x_3$ for both models and both cases, the water front did not reach the point when it would begin, according to our model to propagate radially in the (x, y) plane.

Figs. 2.31 and 2.32 compare our analytical solution and its derivative obtained with model 1 with the results generated from the simulator for the unfavorable and favorable mobility case respectively. Similarly, a comparison between the analytical solutions based on model 2 and the simulator are displayed in Figs. 2.33 and 2.34 for both cases. The two sets of results for injection pressure change and its derivative obtained for the unfavorable case are in good agreement for both models although model 2 gives slightly better agreement. As for the favorable mobility case, despite the oscillations exhibited by the numerical pressure derivative data, both the pressure and derivative data obtained from the simulator seem to have the same trend as the solutions obtained by our models.

The single-phase solutions based on oil properties at irreducible water saturation were added to Figs. 2.33 and 2.34 in solid stars. A comparison between the injection solution and the single-phase solution indicates that the two solutions correlate reasonably well as suggested by Peres and Reynolds for an equal offset horizontal well case (see reference [27]). Moreover, these figures show that at intermediate and late times, the injection data are above the single-phase solution for the unfavorable case whereas, they fall below the single-phase solution for the favorable case, behavior that is also consistent with the results obtained by the previous authors.

In the second example, a damaged region around and along the entire length of the horizontal well was simulated by reducing the permeability in the first 5 radial grid blocks from $k = 5600$ mD to $k_s = 200$ mD. The radius of the skin zone is $r_s = 1.06$ ft and the value of the corresponding mechanical skin factor computed from Hawkin's formula is $s = 30$. Fig. 2.35 illustrates a comparison between the simulator results with the analytical solution generated from model 2 with $\hat{M} = 3.165$. Note the agreement between the model and the simulator is very good. Note also that shortly after injection starts, the wellbore pressure change declines causing the pressure derivative to take negative values

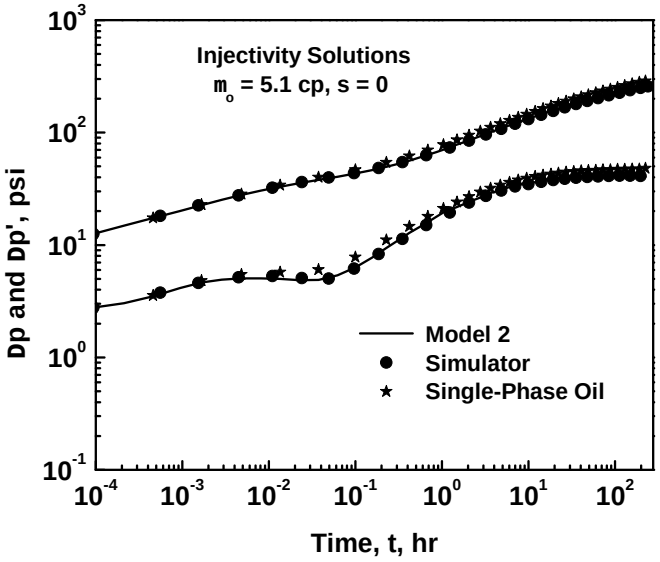

Figure 2.33: Comparison between the results for the injection test from the simulator and the analytical solution from model 2, $\hat{M} = 3.165$, $s = 0$.

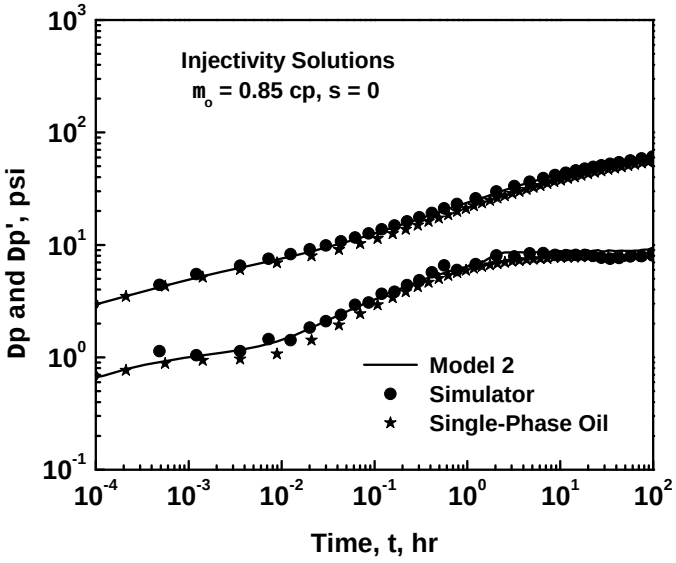

Figure 2.34: Comparison between the results for the injection test from the simulator and the analytical solution from model 2, $\hat{M} = 0.527$, $s = 0$.

from 0.0018 hours to 0.38 hours. Eventually, the pressure derivative data become positive as soon as the pressure change at the wellbore begins to increase. When deriving the equations for the different flow regimes observed during an injection test on a horizontal well, we have shown that the pressure derivative could become negative if the condition given by Eq. 2.147 is satisfied assuming that the water front is moving within the damaged zone or when Eq. 2.155 holds if the water front is beyond the skin zone. For the case considered here, our computations based on the Buckley-Leverett equation indicate that it takes 0.05 hours for the front to reach the location r_s. Since Eq. 2.147 gives

$$\hat{M}\left(1-\frac{2k_s}{k}\right)=3.165\left(1-2\frac{500}{5600}\right)=2.6>1, \tag{2.394}$$

negative values of the pressure derivatives up to 0.05 hours is consistent with what we observe in Fig. 2.35. On another hand, application of Eq. 2.155 yields

$$\lambda_t(r_s,t)\left(1+3.165\frac{500}{5600}\right)<\hat{\lambda}_w\left(1-\frac{500}{5600}\right), \tag{2.395}$$

or simply

$$\lambda_t(r_s,t)<0.71\hat{\lambda}_w. \tag{2.396}$$

This means that the pressure derivative data remain negative until the total mobility at the skin radius becomes greater than $0.71\hat{\lambda}_w$ which occurs according to Fig. 2.35 around 0.38 hours.

In Fig. 2.36, the comparison between the simulator and model 2 for the favorable mobility case ($\hat{M}=0.527$) is illustrated. As can be seen, the agreement is poor at early times. As pointed out by Peres et al. ([26]), this early time behavior exhibited by the simulator is an artifact caused by the first gridblocks for cases where $\hat{M}<1$. However, model 2 reproduces the simulator results for times greater than 0.1 hours. Here, we also observe a decline of the wellbore pressure change leading to negative pressure derivative data from 0.067 hours to 0.24 hours. For this case, the water front hits the radius r_s around 0.067 hours according to the Buckley-Leverett equation. This means that the

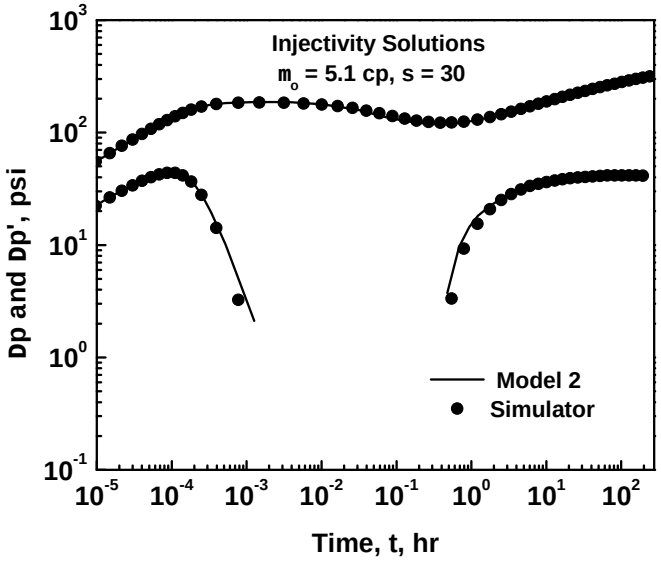

Figure 2.35: Comparison between the results for the injection test from the simulator and the analytical solution from model 2, $\hat{M} = 3.165$, $s = 30$.

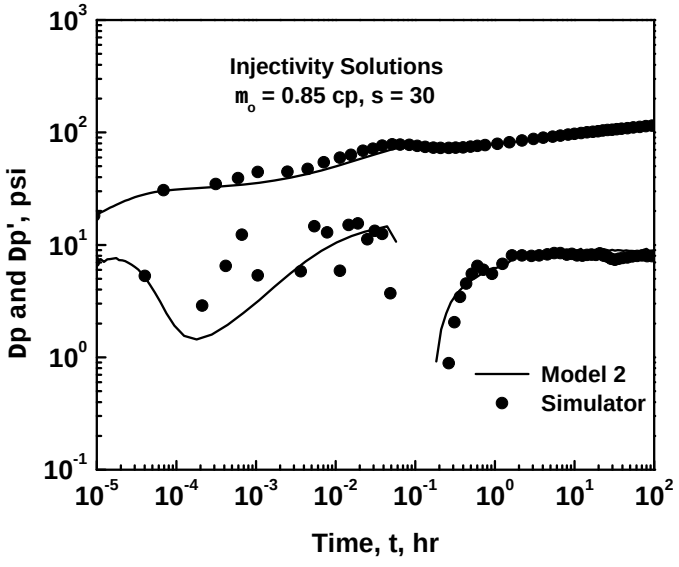

Figure 2.36: Comparison between the results for the injection test from the simulator and the analytical solution from model 2, $\hat{M} = 0.527$, $s = 30$.

decline in the pressure drop does not occur until the water front is beyond the skin region for which the condition given by Eq. 2.155 holds up to 0.24 hours. An interesting remark is that unlike the unfavorable mobility case, Eq. 2.147 is not satisfied and the pressure derivative does not become negative when the water front is in the damaged zone, i.e., for $t < 0.067$ hours.

Next, two cases of injection of water through a horizontal well were simulated where water was injected for a longer period of time (100 days). Subsequent to injection, the well was shut-in for a falloff test for 100 days. The falloff data for this case will be discussed in the next chapter. Except for the reservoir permeability field, all the other data used for the simulations were the same as above. Here, we consider only the unfavorable mobility case. The first case pertains to a well located in the center of the formation, that is $z_w = 39.37$ ft whereas in the second case, the well is closer to the top reservoir boundary with $z_w = 5$ ft. In both cases, the permeabilities in the three directions are given by $k_x = 2700$ mD, $k_y = 4500$ mD and $k_z = 300$ mD. The gridding in the first example consisted of a 104 (x) by 67 (y) by 13 (z) Cartesian grid plus a local hybrid grid refinement of 8 (r) by 1 (θ) by 1 (z') used in all the well blocks where z'-direction coincides with the y-direction. In the offset well case, a combination of a Cartesian gridding of 104 (x) by 63 (y) by 16 (z) and a hybrid grid refinement of 8 (r) by 4 (θ) by 1 (z') applied to all well blocks was used. Due to the anisotropy, a grid aspect ratio of about $\frac{\Delta x}{\Delta z} = \sqrt{\frac{k_x}{k_z}} = 3$ was necessary when building the grids in both cases as the horizontal well is along the y-direction. In the new coordinate system, the isotropic equivalent permeability is $\bar{k} = 1539$ mD and the thickness of the reservoir is $h_n = 178.34$ ft. The well is characterized by an effective length of $L_n = 767.5$ ft and an effective radius of $r_{we} = 0.53$ ft. Other relevant data in the new system are the parameters used to generate the saturation profiles. They are: $x_{n1} = 70.03$ ft and $x_{n3} = 301.395$ ft for the first example and $x_{n1} = 8.89$ ft, $x_{n2} = 121.04$ ft (assuming model 2) and $x_{n3} = 301.395$ ft for the second case. For both runs, the water front at the instant of shut-in is beyond x_{n3} meaning that for some times right before the shut-in, the flood front moves radially in the (x_n, y_n) plane according to our model.

In the following, we give the results obtained using the model described previously,

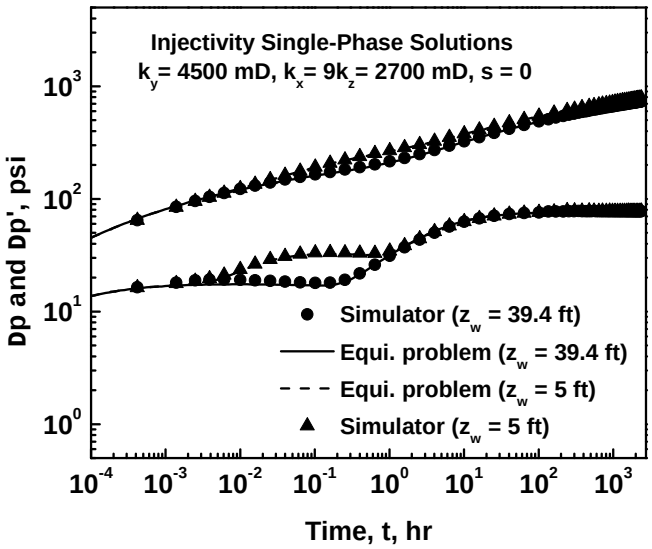

Figure 2.37: Comparison of numerical results to analytical solution for injectivity, single-phase flow, $\mu_o = 5.1$ cp, $s = 0$.

but first, we show a comparison between the results for a single-phase flow simulated using the CMG IMEX's black oil simulator and the corresponding equivalent isotropic analytical solution as a step to validate the spatial transformation applied to the horizontal well case. In Fig. 2.37, the analytical solutions for the injection pressure change and its derivative with respect to the natural log of t are represented by solid lines for the equal offset well and by dashed lines for the unequal offset case. The circle and triangle dots represent numerical solutions for the corresponding cases. As you can see from this figure, very good agreement is observed. Note also the behavior of the single-phase solution for the unequal offset well as its derivative exhibits the doubling of slope at early time due to the top boundary effect.

Solutions under water injection were generated analytically by adding single-phase oil solutions obtained using the simulator for both cases to the corresponding additional pressure changes due to multiphase effects computed analytically from model 2. Fig. 2.38 presents a log-log plot of the injection pressure change and its derivative obtained from our model as well as the solution obtained from the reservoir simulator. We also show on this figure the results obtained from a single-phase solution based on oil properties and

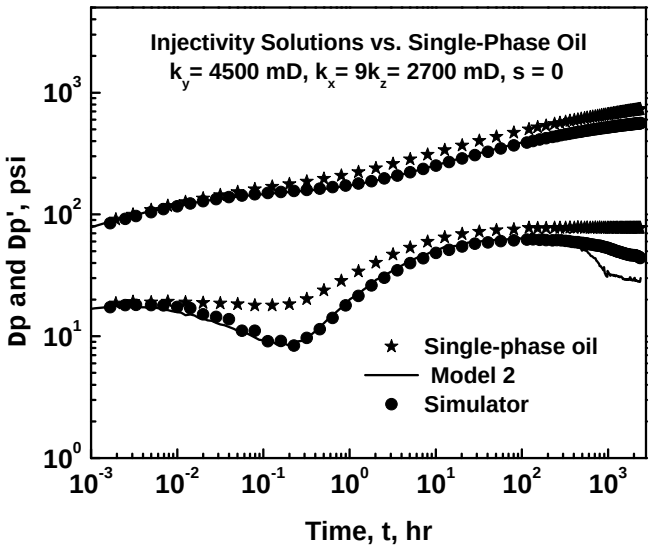

Figure 2.38: Comparison between the results for the injection test and the single-phase oil solution; $z_w = 39.4$ ft, $\hat{M} = 3.165$, $s = 0$.

represented by stars. The well is in the center of the formation in this case. Two remarks are in order here. (i) Except for the very early time period, the multiphase solution is not as close to the single-phase solution based on oil properties as in the isotropic case (see Fig. 2.33 for example). (ii) Excellent agreement between the two set of results for injection pressure change and its derivative is observed up to a time of 500 hours. After that, the derivative obtained from the model deviates from the numerical derivative. We will return to this point later to explain the cause of this behavior in our injectivity solution.

For this example, five flow regimes are identified by the mean of the behavior of the diffusion as well as the times for which the flood front propagates from the (x_n, z_n) plane to the x_n-direction to finally the (x_n, y_n) plane. Recall that for the definition of the flow regimes, the first term refers to the direction of pressure diffusion and the second to the direction of propagation of the water front. We start by the first radial/first radial flow regime that we observe up to times $t < 0.15$ hrs. As expected, the injection wellbore pressure reflects the oil zone as it coincides with the single-phase oil solution ar very early times. As predicted by Eq. 2.22, the pressure derivative during the first radial/first radial

flow regime is also supposed to exhibit a semi-log slope given by

$$\Delta p' = \frac{\alpha q_{inj}}{2\bar{k} L_n \hat{\lambda}_w} = 5.65. \tag{2.397}$$

However, this is not what the injectivity pressure derivative reflects as it approaches this value but never reaches it. Note that Eq. 2.22 is derived for a non zero skin vertical well case. In order to get Eq. 2.397, we simply set $\bar{k}_s = \bar{k}$ and replace h_n by L_n.

The time between $0.15 < t < 10$ hrs corresponds to the first linear/first radial flow regime. As we can see from Fig. 2.38, the two-phase solution for the pressure change and its derivative falls below the single-phase oil solution. This is exactly what Eq. 2.171 predicts as the end-point mobility ratio $\hat{M} > 1$.

An interesting point is that during the second radial/first radial flow regime which we observe for times from around 40 hrs to 230.5 hrs, the pressure derivative reaches a semi-log slope given by Eq. 2.213 that becomes for our case ($\bar{k} = \bar{k}_s$)

$$\Delta p' = \frac{\alpha q_{inj}}{2\bar{k} h_n \hat{\lambda}_w} \left(\hat{M} + \frac{h_n}{L_n} [1 - \hat{M}] \right) = 64.7. \tag{2.398}$$

Again, this flow regime is interesting in a sense that it represents the only period of time where the derivative reflects some type of semi-log slopes that we observe practically.

The second radial/first linear flow regime manifests itself during the time period $230.5 < t < 992$ hrs followed by a second radial/second radial flow regime. Our analytical solution clearly indicates that not only is the derivative below the single-phase oil solution but the shift is also increasing with time during the second radial/first linear period, a result that agrees with Eq. 2.220. During the last flow regime observed in Fig. 2.38, the derivative obtained from the simulator approaches the semi-log slope based on water properties but does not quite reach it as mentioned before.

Fig. 2.39 compares our analytical solution and its derivative obtained from the model proposed with the results generated from the simulator for the case where the well is offset. The single-phase oil solution is also displayed in the same figure. Again, the analytical and simulation results are in good agreement for times corresponding to

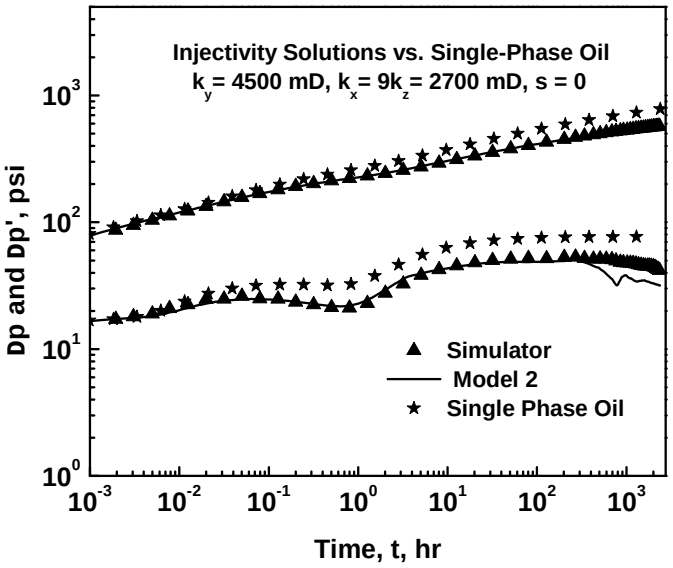

Figure 2.39: Comparison between the results for the injection test and the single-phase oil solution; $z_w = 5$ ft, $\hat{M} = 3.165$, $s = 0$.

$t < 450$ hrs. However, for longer injection times, similar to the equal offset case, our pressure derivative obtained using the model exhibits a deviation from the derivative computed from the simulation solution. As mentioned before, this point will be discussed later.

Five different flow regimes occur for this particular case but only one is observable. Note that because the water front hits the top boundary earlier as it is closer to it, the movement of the water in the (x_n, z_n) plane is supposed to last for a shorter period of time promoting the appearance of flow regimes that do not exist for the case of a well located in the center of the formation considered here (for instance the first linear/first linear flow regime). These flow regimes are :(i) first radial/first radial for $t < 0.7$ hrs, (ii) first linear/first radial for $0.7 < t < 3.7$ hrs, (iii) first linear/first linear for $3.7 < t < 20$ hrs, (iv) second radial/first linear for $20 < t < 805$ hrs and finally (v) second radial/second radial flow regime for $t > 805$ hrs. Similarly to the equal offset well, oil mobility is reflected at very early times. We also need to mention that the only additional semi-log slope observed in Fig. 2.39 is the one exhibited by the pressure derivative at the end of

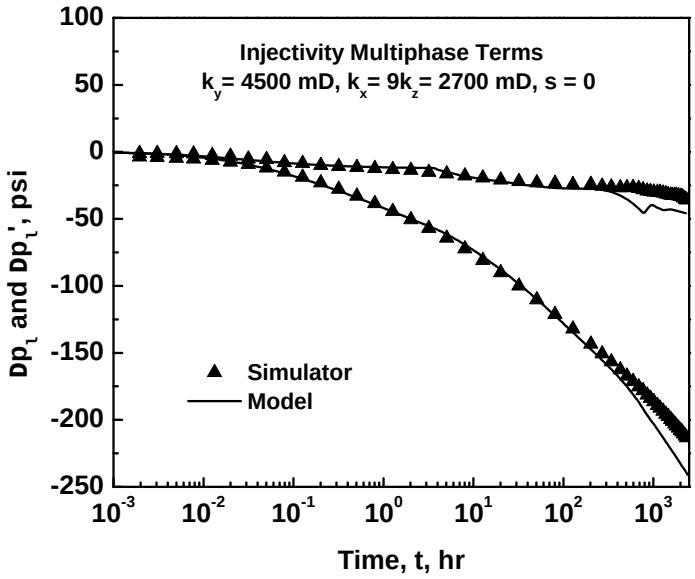

Figure 2.40: Comparison of numerical results to analytical solution for injectivity multiphase terms, $z_w = 5$ ft.

the first radial/first radial period, which according to Eq. 2.153 is given by

$$\Delta p' = \frac{\alpha q_{inj}}{2\bar{k}L_n\hat{\lambda}_w}(1+\hat{M}) = 23.5. \tag{2.399}$$

As we pointed out earlier, for very long injection times, our model predicts smaller values of the pressure and its derivative compared to the ones obtained from the simulator. This behavior as can be seen from Figs. 2.38 and 2.39, occurs when the single-phase based on oil properties is diffusing radially in the (x_n, y_n) plane and the flood front is propagating linearly in the x_n-direction a short time before our model predicts it will begin to propagate radially in the (x_n, y_n) plane. To better illustrate this discrepancy, the single-phase oil solution was eliminated by considering only our analytical additional pressure change terms due to the difference of mobilities which we compare to the corresponding numerical term obtained by simply subtracting the numerical single-phase solution from the two-phase solution obtained using the simulator. The result is shown in Fig. 2.40 for the unequal offset case. Similar results were obtained for the equal offset well.

To have a better idea of why this behavior happens, we considered only radial then

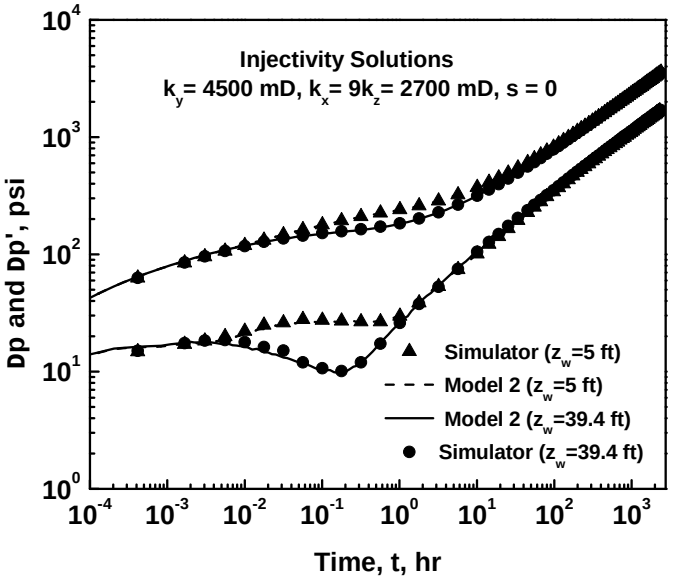

Figure 2.41: Comparison of numerical results to analytical solution for injectivity, linear flow.

linear flow of the injected water. To generate this case, the numerical pressure change and its derivative were obtained using the same simulation runs but with the boundaries of the reservoir in the y-direction coinciding with the length of the horizontal well. The analytical solutions were generated following our model by adding to the single-phase oil solution only the pressure drop due to the radial movement of water in the (x_n, z_n) plane and the pressure change due to the linear propagation of the injected water. Fig. 2.41 compares the two sets of data for both equal and unequal offset wells. As you can see, the agreement between the simulator and our solutions is excellent. Moreover, this result suggests that the problem of mismatch for long injection times encountered above is due to the way the model parameter x_{n3} or equivalently x_3 is obtained. Recall that this parameter given by Eq. 2.379 is obtained by applying a Deppe's construction that assumes a radial flow for any radial distance $r_n > L_n/2$. However, this may be an erroneous assumption as the flow around the horizontal well is ellipsoidal. We expect it to be radial only for much longer injection times specially if the length of the well is very large.

CHAPTER 3

FALLOFF TESTING OF VERTICAL AND HORIZONTAL WELLS

In this chapter, our focus is on the pressure falloff behavior subsequent to injection of water at a constant rate q_{inj} into an oil reservoir operating above bubble-point condition. For now, we consider only radial flow of fluids. Oil, water and rock compressibilities, denoted respectively by c_o, c_w and c_r, are assumed to be constant as well as are fluid viscosities, μ_o and μ_w. The total compressibility of the system, denoted by c_t, is a unique function of water saturation and thus is considered to be a function of position and time as shown by the following equation

$$c_t(r,t) = c_r + c_o S_o(r,t) + c_w S_w(r,t) = c_r + c_o + (c_w - c_o) S_w(r,t). \tag{3.1}$$

The system is also described by a total mobility given at any distance r from the center of the vertical well at a time t by Eq. 2.3. The saturation distribution, and consequently mobility and compressibility profiles, are constructed from the Buckley-Leverett equation, given for a radial flow by

$$r^2(S_w) = \frac{\theta q_{inj} t}{\pi \phi h} \frac{df_w(S_w)}{dS_w} + r_w^2. \tag{3.2}$$

In Eq. 3.1, the constant θ depends on the system of units used with $\theta = 5.615/24 = 0.23396$ if oil field units are used with time in hours. The well is shut-in after injecting water for a time t_p. At this point, we make an important assumption: immediately upon shut-in and during the falloff period, the radius of the water front and consequently the water saturation distribution remain stationary. This assumption is strictly true only if the fluids are incompressible (see reference [4]). Under this condition, the governing differential equation that describes the physical system during a falloff test is given in field units by

$$\frac{\beta}{r}\frac{\partial}{\partial r}\left[k(r)\lambda_t(r,t_p)r\frac{\partial p(r,\Delta t)}{\partial r}\right]=\phi c_t(r,t_p)\frac{\partial p(r,\Delta t)}{\partial \Delta t}, \tag{3.3}$$

where the shut-in time is defined by $\Delta t = t - t_p$ such that Eq. 3.3 is valid for any $\Delta t > 0$. Eq. 3.3 is subject to the two following boundary conditions

$$r\frac{\partial p(r,\Delta t)}{\partial r}\mid_{r=r_w}=0, \tag{3.4}$$

and

$$\lim_{r\to\infty} p(r,\Delta t)=p_i. \tag{3.5}$$

The initial pressure distribution of the system is given by the injection solution at the instant of shut-in, i.e., $p_{inj}(r,t_p)$. This translates into

$$p(r,\Delta t=0)=p_{inj}(r,t_p). \tag{3.6}$$

At the instant of shut-in and throughout the entire falloff test, the reservoir is assumed to be divided into two distinct regions. The first zone consists of a mixture of oil and water. The second region is the oil zone. Water in the oil zone is immobile. It is clear that the properties of the fluids in the two banks (total mobility and total compressibility) are different. In the water bank, they vary with r due to the variation of the water saturation whereas, in the oil zone, they are constant. Due to this, the pressure equation Eq. 3.3 is difficult to solve analytically. The difficulty of this problem also lies on the fact that the initial pressure distribution is non-uniform. In this work, we present two methods for constructing analytical solutions for the falloff response. The first one is based on the steady-state theory of Thompson and Reynolds combined with rate superposition. The second procedure is based on perturbation theory to solve the initial boundary value problem. For now, we proceed with the first approach.

For the completely penetrating well case, we can apply Eq. 2.1 at the shut-in time Δt to obtain the falloff solution subsequent to injection at the constant rate q_{inj} for a

time t_p. Replacing t by Δt in Eq. 2.1 gives

$$\Delta p_{ws} = p_{ws}(\Delta t) - p_i = \frac{\alpha}{h} \int_{r_w}^{\infty} \frac{q_s(r, \Delta t)}{\lambda_t(r, \Delta t)} \frac{dr}{rk(r)}, \tag{3.7}$$

where $q_s(r, \Delta t)$ gives the rate profile at shut-in time Δt, and $p_{ws}(\Delta t)$ is the wellbore pressure during shut-in, i.e., the wellbore pressure during falloff. α is a constant which depends on the units system used. In field units, $\alpha = 141.2$. Under the assumption that the mobility profile does not change during falloff, Eq. 3.7 is rewritten as

$$\Delta p_{ws} = \frac{\alpha}{h} \int_{r_w}^{r_f(t_p)} \frac{q_s(r, \Delta t)}{rk(r)\lambda_t(r, t_p)}\, dr + \frac{\alpha}{h} \int_{r_f(t_p)}^{\infty} \frac{q_s(r, \Delta t)}{rk(r)\lambda_t(r, t_p)}\, dr, \tag{3.8}$$

where $r_f(t_p)$ is the radius of the flood front at the instant of shut-in. In the region of the reservoir uninvaded by injected water, the total rate is equal to the oil rate denoted by $\hat{q}_{os}$. An important assumption that we make is that this oil rate profile during shut-in is identical to the oil rate profile that would be obtained in the uninvaded region for a shut-in period obtained subject to injecting oil at a rate numerically equal to q_{inj}. As we will see later, the approximate validity of this assumption has been verified numerically using a reservoir simulator. Adding and subtracting the term

$$\frac{\alpha}{h} \int_{r_w}^{r_f(t_p)} \frac{\hat{q}_{os}(r, \Delta t)}{k(r)\hat{\lambda}_o} \frac{dr}{r},$$

to Eq. 3.8, we obtain

$$\Delta p_{ws} = \frac{\alpha}{h} \int_{r_w}^{r_f(t_p)} \frac{q_s(r, \Delta t)}{rk(r)\lambda_t(r, t_p)}\, dr + \frac{\alpha}{h} \int_{r_f(t_p)}^{\infty} \frac{q_s(r, \Delta t)}{rk(r)\lambda_t(r, t_p)}\, dr + \frac{\alpha}{h} \int_{r_w}^{r_f(t_p)} \frac{\hat{q}_{os}(r, \Delta t)}{k(r)\hat{\lambda}_o} \frac{dr}{r} - \frac{\alpha}{h} \int_{r_w}^{r_f(t_p)} \frac{\hat{q}_{os}(r, \Delta t)}{k(r)\hat{\lambda}_o} \frac{dr}{r}. \tag{3.9}$$

Note that for $r > r_f(t_p)$, $q_s(r, \Delta t) = \hat{q}_{os}(r, \Delta t)$ and $\lambda_t(r, t_p) = \hat{\lambda}_o$. It is then easy to show that

$$\Delta p_{ws} = \frac{\alpha}{h\hat{\lambda}_o}\int_{r_w}^{\infty}\frac{\hat{q}_{os}(r,\Delta t)}{k(r)}\frac{dr}{r} + \frac{\alpha}{h}\int_{r_w}^{r_f(t_p)}\left(\frac{q_s(r,\Delta t)}{\lambda_t(r,t_p)} - \frac{\hat{q}_{os}(r,\Delta t)}{\hat{\lambda}_o}\right)\frac{dr}{rk(r)}. \tag{3.10}$$

Under our assumption, the first integral on the right side of Eq. 3.10 simply represents the single-phase falloff solution that would be obtained by injecting oil into an oil reservoir and is denoted by $\Delta\hat{p}_{os}$. The second integral represents the pressure change due to the contrast between initial total mobility $\hat{\lambda}_o$ and the total mobility in the invaded zone. We rewrite Eq. 3.10 as

$$\Delta p_{ws} = \Delta\hat{p}_{os} + \frac{\alpha}{h\hat{\lambda}_o}\int_{r_w}^{r_f(t_p)}\left(\frac{\hat{\lambda}_o}{\lambda_t(r,t_p)}q_s(r,\Delta t) - \hat{q}_{os}(r,\Delta t)\right)\frac{dr}{rk(r)}. \tag{3.11}$$

The evaluation of the multiphase component in Eq. 3.11 requires the knowledge of the total mobility profile at the instant of shut-in. As discussed in chapter 2, models for the movement of water based on a combination of the Buckley-Leverett equations can be used to generate the water distribution in the reservoir at any time during the injection period and specifically at the instant of shut-in t_p. For a complete-penetration vertical well case, the water saturation distribution is generated using Eq. 3.2 evaluated at the instant of shut-in t_p. The knowledge of the flow rate distributions q_t and $\hat{q}_{os}$ during the shut-in time is also crucial in the evaluation of the falloff pressure change given by Eq. 3.11. For a linear problem, Duhamel's principle, also called superposition in time, applies and is usually used to construct single-phase flow rate profiles during buildup periods. However, the use of superposition for a two-phase problem cannot be justified theoretically. In the following, we will show that we can use this concept in a reasonable but ad-hoc way to estimate the rate profiles needed to compute the multiphase component.

3.1 Rate Superposition for Single-Phase Flow

We first consider a single-phase flow problem for an oil reservoir produced at a constant insitu oil rate equal to q_{inj} with water saturation fixed at irreducible water saturation

and total compressibility equal to $\hat{c}_{to} = c_o(1 - S_{iw}) + c_w S_{iw} + c_r$. The production/buildup pressure drop solution for this problem is the same as the solution for the pressure increase that would be obtained by injecting oil at the rate q_{inj} into an oil reservoir with irreducible water saturation as initial saturation assuming water is immobile. Thus, it is convenient to define all dimensionless variables in terms of oil properties at irreducible water saturation. We will denote dimensionless pressure change, dimensionless flow rate, dimensionless radial distance, dimensionless injection (flowing) time and dimensionless shut-in time, respectively, by p_D, q_D, r_D, t_{pD}, and Δt_D where dimensionless time is based on wellbore radius squared. Because we are interested in an injection/falloff as opposed to a drawdown/buildup test, we define

$$p_D(r_D, t_D) = \frac{kh\hat{\lambda}_o(p(r,t) - p_i)}{\alpha q_{inj}}. \tag{3.12}$$

At the wellbore, Eq. 3.12 becomes

$$p_{wD}(t_D) = \frac{kh\hat{\lambda}_o \Delta p}{\alpha q_{inj}}, \tag{3.13}$$

where

$$\Delta p = p_{wf}(t) - p_i. \tag{3.14}$$

Dimensionless time is defined by

$$t_D = \frac{\beta k\hat{\lambda}_o t}{\phi \hat{c}_{to} r_w^2}, \tag{3.15}$$

where β is a constant which depends on the system of units used. If oil field units with time in hours are used, then $\beta = 2.637 \times 10^{-4}$. Evaluation of Eq. 3.15 at t_p gives the dimensionless injection time, t_{pD}. Evaluation at shut-in time Δt gives the dimensionless shut-in time, Δt_D. For the falloff period, we denote the dimensionless pressure change by $p_{sD}(r_D, \Delta t_D)$, where similar to Eq. 3.12 we have

$$p_{sD}(r_D, \Delta t_D) = \frac{kh\hat{\lambda}_o(p(r,\Delta t) - p_i)}{\alpha q_{inj}}. \tag{3.16}$$

At the wellbore, we use the notation

$$p_{wsD}(\Delta t_D) = \frac{kh\hat{\lambda}_o \Delta p_{ws}}{\alpha q_{inj}}, \tag{3.17}$$

for the dimensionless pressure change. Here,

$$\Delta p_{ws} = p_{ws} - p_i, \tag{3.18}$$

where $p_{ws} = p_{ws}(\Delta t)$ denotes the wellbore pressure during shut-in. The dimensionless radial distance and dimensionless rate are defined respectively by

$$r_D = \frac{r}{r_w}, \tag{3.19}$$

and

$$q_D(r_D, t_D) = \frac{q(r,t)}{q_{inj}}. \tag{3.20}$$

Note at the sandface, $r_D = 1$, and $q_D(1, t_D) = 1$ during injection and $q_D(1, t_D) = 0$ during falloff. In general, $q_D(r_D, t_D)$ denotes the dimensional flow rate through a cylinder of radius r concentric with the wellbore. For the analogous dimensionless flow rate during shut-in, we will use the notation $q_{sD}(r_D, \Delta t_D)$ where

$$q_{sD}(r_D, \Delta t_D) = \frac{q_s(r, \Delta t)}{q_{inj}}. \tag{3.21}$$

3.1.1 Rate Superposition for Radial Flow

For a radial flow case, application of Duhamel's principle gives

$$p_{sD}(r_D, \Delta t_D) = p_{cD}(r_D, t_{pD} + \Delta t_D) - p_{cD}(r_D, \Delta t_D), \tag{3.22}$$

where p_{cD} represents the single-phase liquid solution for injection at a constant sandface rate q_{inj} and $q_{cD}(r_D, t_D)$ denotes the associated dimensionless rate at (r_D, t_D) (the subscript c refers to constant rate injection at the wellbore). Because

$$q_{cD}(r_D, t_D) = -r_D \frac{\partial}{\partial r_D} p_{cD}(r_D, t_D), \tag{3.23}$$

we can differentiate Eq. 3.22 with respect to r_D and multiply by $-r_D$, to obtain

$$q_{sD}(r_D, \Delta t_D) = q_{cD}(r_D, t_{pD} + \Delta t_D) - q_{cD}(r_D, \Delta t_D). \tag{3.24}$$

Note $q_{cD}(r_D, t_D + \Delta t_D)$ represents the dimensionless rate that would exist at r_D if we injected at the constant rate q_{inj} for a total time of $t_{pD} + \Delta t_D$.

If the line source solution applies, then

$$p_D(r_D, t_D) = \frac{1}{2} E_1\left(\frac{r_D^2}{4t_D}\right), \tag{3.25}$$

where

$$E_1(x) = \int_x^\infty \frac{\exp(-u)}{u} du. \tag{3.26}$$

Using Eq. 3.25 in Eq. 3.23, it is easy to show that

$$q_{cD}(r_D, t_D) = -r_D \frac{\partial}{\partial r_D} p_{cD}(r_D, t_D) = \exp\Big(-\frac{r_D^2}{4t_D}\Big). \tag{3.27}$$

Using this result in Eq. 3.24 gives

$$q_{sD}(r_D, \Delta t_D) = \exp\Big(-\frac{r_D^2}{4(t_{pD} + \Delta t_D)}\Big) - \exp\Big(-\frac{r_D^2}{4\Delta t_D}\Big), \tag{3.28}$$

or equivalently

$$q_s(r, \Delta t) = q_{inj}\left[\exp\Big(-\frac{r_D^2}{4(t_{pD} + \Delta t_D)}\Big) - \exp\Big(-\frac{r_D^2}{4\Delta t_D}\Big)\right]. \tag{3.29}$$

3.1.2 Rate Superposition for Linear Flow

For one-dimensional linear flow in the x-direction through a uniform cross sectional area, superposition of rates still applies such that

$$q_s(x, \Delta t) = q_c(x, t_p + \Delta t) - q_c(x, \Delta t). \tag{3.30}$$

For an infinite-acting linear flow problem where fluid is injected at $x = 0$ and flows in both the positive and negative x-direction through a cross sectional area A, one can show that [14]

$$q_c(x, t) = -q_{inj} \frac{\alpha k \hat{\lambda}_o A}{2\pi \mu_o} \frac{\partial p_c(x, t)}{\partial x} = q_{inj} \text{erfc}\left(\frac{x_D}{2\sqrt{t_D}}\right), \tag{3.31}$$

where erfc denotes the complementary error function defined by

$$\text{erfc}(x) = \frac{2}{\sqrt{\pi}} \int_x^\infty \exp(-u^2) du. \tag{3.32}$$

For a single-phase case based on oil properties at irreducible water saturation, the argument of the complementary error function is given by

$$\frac{x_D}{2\sqrt{t_D}} = \frac{x\sqrt{\phi \hat{c}_{to} \mu_o}}{2\sqrt{\beta k \hat{\lambda}_o t}}. \tag{3.33}$$

Thus, the analogue of Eq. 3.29 for a one dimensional linear flow in the x-direction through a uniform cross sectional area is given by

$$q_s(x, \Delta t) = q_{inj} \left[\text{erfc}\left(\frac{x_D}{2\sqrt{t_{pD} + \Delta t_D}}\right) - \text{erfc}\left(\frac{x_D}{2\sqrt{\Delta t_D}}\right) \right]. \tag{3.34}$$

3.2 Pressure Response

For the completely-penetrating well case, the falloff pressure change can be obtained from Eq. 3.11 provided we can obtain an expression for the flow rates $q_s(r, \Delta t)$ and $\hat{q}_{os}(r, \Delta t)$. For any realistic case, the location of the water front at the instant of shut-in is beyond the radius of the damaged zone, i.e., $r_f(t_p) > r_s$. Using Eq. 2.4 in Eq. 3.11 and rearranging, we obtain the following expression:

$$\Delta p_{ws} = \Delta \hat{p}_{os} + \frac{\alpha}{kh\hat{\lambda}_o}\left[\left(\frac{k}{k_s}-1\right)\int_{r_w}^{r_s}\left(\frac{\hat{\lambda}_o}{\lambda_t(r,t_p)}q_s(r,\Delta t)-\hat{q}_{os}(r,\Delta t)\right)\frac{dr}{r} + \int_{r_w}^{r_f(t_p)}\left(\frac{\hat{\lambda}_o}{\lambda_t(r,t_p)}q_s(r,\Delta t)-\hat{q}_{os}(r,\Delta t)\right)\frac{dr}{r}. \quad (3.35)$$

Since $\hat{q}_{os}(r,\Delta t)$ is a single-phase flow rate, we can use the rate superposition equation Eq. 3.29 to obtain

$$\hat{q}_{os}(r,\Delta t) = q_{inj}\left[\exp\Big(-\frac{r_D^2}{4(t_{pD}+\Delta t_D)}\Big)-\exp\Big(-\frac{r_D^2}{4\Delta t_D}\Big)\right]. \quad (3.36)$$

Converting the dimensional variables using Eqs. 3.15 and 3.19, we can rewrite Eq. 3.36 as

$$\hat{q}_{os}(r,\Delta t) = q_{inj}\left[\exp\Big(-\frac{\phi\hat{c}_{to}r^2}{4\beta k\hat{\lambda}_o(t_p+\Delta t)}\Big)-\exp\Big(-\frac{\phi\hat{c}_{to}r^2}{4\beta k\hat{\lambda}_o\Delta t}\Big)\right]. \quad (3.37)$$

As there is no theoretical procedure for evaluating the total rate $q_s(r,\Delta t)$ in the two-phase flow region, we will apply the single-phase rate superposition equation, i.e., we will use

$$q_s(r,\Delta t) = q_c(r,t_p+\Delta t) - q_c(r,\Delta t), \quad (3.38)$$

and formally use Eqs. 3.29 and 3.38 to obtain

$$q_s(r,\Delta t) = q_{inj}\left[\exp\Big(-\frac{r_D^2}{4(t_{pD}+\Delta t_D)}\Big)-\exp\Big(-\frac{r_D^2}{4\Delta t_D}\Big)\right]. \quad (3.39)$$

In order to apply this for two-phase flow, we have to decide what to use for mobility and total compressibility when evaluating the dimensionless times in Eq. 3.39. We have found that we obtain a more accurate solution if we use values of these properties that exist at the instant of shut-in and change with r. Therefore, the definition of dimensionless times used is actually a function of r. Specifically, we set

$$\frac{t_{pD}+\Delta t_D}{r_D^2}=\frac{\beta k\lambda_t(r,t_p)(t_p+\Delta t)}{\phi c_t(r,t_p)r^2}, \tag{3.40}$$

and

$$\frac{\Delta t_D}{r_D^2}=\frac{\beta k\lambda_t(r,t_p)\Delta t}{\phi c_t(r,t_p)r^2}, \tag{3.41}$$

in Eq. 3.39 to obtain

$$q_s(r,\Delta t)=q_{inj}\left[\exp\Big(-\frac{\phi c_t(r,t_p)r^2}{4\beta k\lambda_t(r,t_p)(t_p+\Delta t)}\Big)-\exp\Big(-\frac{\phi c_t(r,t_p)r^2}{4\beta k\lambda_t(r,t_p)\Delta t}\Big)\right]. \tag{3.42}$$

While Eq. 3.42 is an obvious guess for extending rate superposition to the multiphase flow case, it is clearly ad hoc. With $q_s(r,\Delta t)$ evaluated using Eq. 3.42, $\hat{q}_{os}(r,\Delta t)$ evaluated by Eq. 3.37, we can generate an approximation to the falloff solution from Eq. 3.35.

When comparing falloff solutions for radial flow problems, we will usually plot Δp_s and its log-derivative $\Delta p_s'$ with respect to Agarwal's equivalent time $t_e=\frac{t_p\Delta t}{t_p+\Delta t}$, defined respectively by

$$\Delta p_s(\Delta t)=p_{wf,s}-p_{ws}(\Delta t), \tag{3.43}$$

and

$$\Delta p_s'=\frac{d\Delta p_{ws}}{d\ln(t_e)}, \tag{3.44}$$

where $p_{wf,s}$ is the injection solution at the instant of shut-in given by

$$p_{wf,s}-p_i=\Delta p_o(t_p)+\frac{\alpha q_{inj}}{kh\hat{\lambda}_o}\left[\Big(\frac{k}{k_s}-1\Big)\int_{r_w}^{r_s}\left(\frac{\hat{\lambda}_o}{\lambda_t(r,t_p)}-1\right)\frac{dr}{r}+\int_{r_w}^{r_f(t_p)}\left(\frac{\hat{\lambda}_o}{\lambda_t(r,t_p)}-1\right)\frac{dr}{r}\right]. \tag{3.45}$$

Note that Eq. 3.45 is obtained by simply considering $t=t_p$ in Eq. 2.26. Note also that Eq. 3.45 assumes the water front is beyond the damaged zone at the instant of shut-in

which is generally true in practice.

It has been shown from previous work (see for instance references [4] and [11]) that the falloff solution behavior is similar to a single-phase heterogenous reservoir. At early shut-in times, the pressure derivative reflects water mobility in the flooded zone, then, it reflects a weighted average between mobilities. At later times, the rates q_s and $\hat{q}_{os}$ predicted by rate superposition are for all practical purposes equal to zero for $r_w < r < r_f(t_p)$ so that the multiphase contribution to the solution is zero and the falloff pressure change reduces to $\Delta\hat{p}_{os}$ reflecting oil mobility in the uninvaded zone. For a completely penetrating vertical well at very late times, the single-phase oil solution or equivalently the falloff solution is given by

$$p_{ws}(\Delta t) - p_i = \Delta\hat{p}_{os}(\Delta t) = \frac{\alpha q_{inj}}{2kh\hat{\lambda}_o} \ln\Big(\frac{t_{pD} + \Delta t_D}{\Delta t_D}\Big). \tag{3.46}$$

Subtracting Eq. 3.46 from Eq. 3.45 yields

$$\begin{aligned} p_{wf,s} - p_{ws}(\Delta t) = \Delta p_o(t_p) - \frac{\alpha q_{inj}}{2kh\hat{\lambda}_o} \ln\Big(\frac{t_{pD} + \Delta t_D}{\Delta t_D}\Big) \\ + \frac{\alpha q_{inj}}{kh\hat{\lambda}_o}\left[\Big(\frac{k}{k_s} - 1\Big)\int_{r_w}^{r_s}\left(\frac{\hat{\lambda}_o}{\lambda_t(r,t_p)} - 1\right)\frac{dr}{r} + \int_{r_w}^{r_f(t_p)}\left(\frac{\hat{\lambda}_o}{\lambda_t(r,t_p)} - 1\right)\frac{dr}{r}\right]. \end{aligned} \tag{3.47}$$

For the problem under consideration, the single-phase oil solution $\Delta p_o(t)$ is given by Eq. 2.19. Specifically, at the instant of shut-in, Eq. 2.19 is written as

$$\Delta p_o(t_p) = \frac{\alpha q_{inj}}{kh\hat{\lambda}_o}\left[\frac{1}{2}\ln\left(\frac{4t_{pD}}{e^\gamma}\right) + s\right]. \tag{3.48}$$

Using Eq. 3.48 in Eq. 3.47, it is easy to show that at late shut-in times

$$\begin{aligned} p_{wf,s} - p_{ws}(\Delta t) = \frac{\alpha q_{inj}}{kh\hat{\lambda}_o}\left[\frac{1}{2}\ln\Big(\frac{4t_{pD}\Delta t_D}{e^\gamma(t_{pD} + \Delta t_D)}\Big) + s + \Big(\frac{k}{k_s} - 1\Big)\int_{r_w}^{r_s}\left(\frac{\hat{\lambda}_o}{\lambda_t(r,t_p)} - 1\right)\frac{dr}{r}\right. \\ \left. + \int_{r_w}^{r_f(t_p)}\left(\frac{\hat{\lambda}_o}{\lambda_t(r,t_p)} - 1\right)\frac{dr}{r}\right], \end{aligned} \tag{3.49}$$

or simply

$$p_{wf,s} - p_{ws}(\Delta t) = \frac{\alpha q_{inj}}{kh\hat{\lambda}_o}\left[\frac{1}{2}\ln\left(\frac{4t_{eD}}{e^{\gamma}}\right) + s_t\right], \tag{3.50}$$

where t_{eD} is dimensionless equivalent time and the total skin factor is given by

$$s_t = s + \left(\frac{k}{k_s} - 1\right)\int_{r_w}^{r_s}\left(\frac{\hat{\lambda}_o}{\lambda_t(r,t_p)} - 1\right)\frac{dr}{r} + \int_{r_w}^{r_f(t_p)}\left(\frac{\hat{\lambda}_o}{\lambda_t(r,t_p)} - 1\right)\frac{dr}{r}. \tag{3.51}$$

It is reasonable to expect that oil saturation in the skin zone will be essentially reduced to residual oil saturation during the injection period. We therefore assume that $\lambda_t(r,t_p) = \hat{\lambda}_w$ for $r_w < r \leq r_s$. It follows

$$s_t = s + \left(\frac{\hat{\lambda}_o}{\hat{\lambda}_w} - 1\right)\left(\frac{k}{k_s} - 1\right)\ln\left(\frac{r_s}{r_w}\right) + \int_{r_w}^{r_f(t_p)}\left(\frac{\hat{\lambda}_o}{\lambda_t(r,t_p)} - 1\right)\frac{dr}{r}, \tag{3.52}$$

or by using Hawkin's formula for the mechanical skin and simplifying

$$s_t = \frac{\hat{\lambda}_o}{\hat{\lambda}_w}s + \int_{r_w}^{r_f(t_p)}\left(\frac{\hat{\lambda}_o}{\lambda_t(r,t_p)} - 1\right)\frac{dr}{r}. \tag{3.53}$$

Eq. 3.53 represents the combination of the mechanical skin and the pseudo-skin due to the difference of mobilities in the reservoir. It is clear that an estimate of the mechanical skin from a semilog analysis relies entirely on the knowledge of the multiphase term.

3.2.1 Falloff Solution, Restricted-Entry vertical Well

In this section, we assume that the vertical injection well partially penetrates the reservoir and that the open interval to flow is h_p. We also assume that the well is shut-in after injecting water at a constant rate given by q_{inj} during t_p. As in the complete-penetration case, the falloff solution should be given by the single-phase solution based on oil properties plus a multiphase pressure change term due to the contrast between the total mobility and the end-point oil mobility in the region invaded by water. To

compute the multiphase component of the solution requires that we are able to generate the saturation/total mobility profile in the flooded region. For this purpose, two models for generating saturation distributions have been proposed and provided in chapter 2. Recall that in these models, the reservoir is pictured as two concentric regions with an interface characterized by a radius, that we referred to as the radius of convergence, r_c (see Appendix A). For $r < r_c$, the saturation distribution is generated by a radial flow Buckley-Leverett solution with variable thickness, $h(r)$ where at the wellbore, $h(r_w)$ is equal to the height of the perforated interval and for $r > r_c$, $h(r) = h$. In this case, the pressure change due to water injection (the integral in Eq. 3.11) must be modified by putting h inside the integral sign and replacing it by $h(r)$. The approximate falloff solution for the restricted-entry problem is given by the following modification to Eq. 3.11:

$$\Delta p_{ws} = \Delta \hat{p}_{os} + \frac{\alpha}{\hat{\lambda}_o} \int_{r_w}^{r_f(t_p)} \left(\frac{\hat{\lambda}_o}{\lambda_t(r, t_p)} q_s(r, \Delta t) - \hat{q}_{os}(r, \Delta t) \right) \frac{dr}{rk(r)h(r)}. \tag{3.54}$$

It is reasonable to assume that the water front is beyond the damaged zone at the instant of shut-in. Therefore, we can write

$$\begin{aligned} \Delta p_{ws} = \Delta \hat{p}_{os} + \frac{\alpha}{k_s \hat{\lambda}_o} \int_{r_w}^{r_s} \left(\frac{\hat{\lambda}_o}{\lambda_t(r, t_p)} q_s(r, \Delta t) - \hat{q}_{os}(r, \Delta t) \right) \frac{dr}{rh(r)} \\ + \frac{\alpha}{k\hat{\lambda}_o} \int_{r_s}^{r_f(t_p)} \left(\frac{\hat{\lambda}_o}{\lambda_t(r, t_p)} q_s(r, \Delta t) - \hat{q}_{os}(r, \Delta t) \right) \frac{dr}{rh(r)}. \end{aligned} \tag{3.55}$$

By adding and subtracting to the above equation an integral from r_w to r_s, we have

$$\Delta p_{ws} = \Delta \hat{p}_{os} + \frac{\alpha}{k_s \hat{\lambda}_o} \int_{r_w}^{r_s} \left(\frac{\hat{\lambda}_o}{\lambda_t(r,t_p)} q_s(r,\Delta t) - \hat{q}_{os}(r,\Delta t) \right) \frac{dr}{rh(r)} + \frac{\alpha}{k \hat{\lambda}_o} \int_{r_s}^{r_f(t_p)} \left(\frac{\hat{\lambda}_o}{\lambda_t(r,t_p)} q_s(r,\Delta t) - \hat{q}_{os}(r,\Delta t) \right) \frac{dr}{rh(r)} + \frac{\alpha}{k \hat{\lambda}_o} \int_{r_w}^{r_s} \left(\frac{\hat{\lambda}_o}{\lambda_t(r,t_p)} q_s(r,\Delta t) - \hat{q}_{os}(r,\Delta t) \right) \frac{dr}{rh(r)} - \frac{\alpha}{k \hat{\lambda}_o} \int_{r_w}^{r_s} \left(\frac{\hat{\lambda}_o}{\lambda_t(r,t_p)} q_s(r,\Delta t) - \hat{q}_{os}(r,\Delta t) \right) \frac{dr}{rh(r)}. \quad (3.56)$$

or simply

$$\Delta p_{ws} = \Delta \hat{p}_{os} + \frac{\alpha}{k \hat{\lambda}_o} \left[\left(\frac{k}{k_s} - 1 \right) \int_{r_w}^{r_s} \left(\frac{\hat{\lambda}_o}{\lambda_t(r,t_p)} q_s(r,\Delta t) - \hat{q}_{os}(r,\Delta t) \right) \frac{dr}{rh(r)} + \int_{r_w}^{r_f(t_p)} \left(\frac{\hat{\lambda}_o}{\lambda_t(r,t_p)} q_s(r,\Delta t) - \hat{q}_{os}(r,\Delta t) \right) \frac{dr}{rh(r)} \right]. \quad (3.57)$$

As mentioned earlier, in computing the multiphase flow component of the falloff solution, the saturation and mobility profiles are generated from the Buckley-Leverett equation for radial flow over a variable thickness evaluated at the instant of shut-in using either model 1 or 2 as described in chapter 2. Since this involves only one dimension, it is reasonable to apply one-dimensionless single-phase radial flow with a variable thickness $h(r)$ in order to obtain a method for approximating the flow rate profiles that appear in Eq. 3.57. One way to proceed is to approximate $h(r)$ by the piecewise constant function as follows

$$\tilde{h}(r) = \begin{cases} h_i \equiv h(\tilde{r}_i) \text{ for } r_{i-1} < r < r_i, \text{ for } i = 1, 2, \cdots n \\ h, \text{ for } r_n < r < \infty \end{cases} \quad (3.58)$$

where $r_0 = r_w < r_1 < \cdots < r_n = r_c$ and $\tilde{r}_i$ is the midpoint of the interval $[r_{i-1}, r_i]$. It follows that we can write the single-phase oil injection problem as a radially composite reservoir problem where except for the thickness, all zones have identical properties. If we assume a line source well, the inner boundary condition becomes

$$\lim_{r_w \to 0} \Big(- \frac{r k h_1 \hat{\lambda}_o}{\alpha q_{inj}} \frac{\partial (p(r,t) - p_i)}{\partial r} \Big)_{r_w} = 1. \tag{3.59}$$

Note this equation also gives $q_D(r_D = 1, t_D) = q(r_w, t)/q_{inj} = 1$. Writing the partial differential equation describing flow in each zone and applying the condition that the flow rates from the left and the right at each r_i are equal (continuity of flow rates), it can be shown that for $r_{i-1} < r < r_i$,

$$\begin{aligned} -r \frac{h_i}{h} \frac{k h \hat{\lambda}_o}{\alpha q_{inj}} \frac{\partial (p(r,t) - p_i)}{\partial r} &= -r_D \frac{h_i}{h} \frac{\partial p_{cD}(r_D, t_D)}{\partial r_D} \\ &= q_{cD}(r_D, t_D) \qquad (3.60) \\ &= \exp\Big(- \frac{r_D^2}{4 t_D} \Big). \qquad (3.61) \end{aligned}$$

Eq. 3.61 provides motivation for using Eqs. 3.37 and 3.42 to compute the rate profiles involved in Eq. 3.57 for the restricted-entry vertical well case.

Because the behavior of the falloff solution is similar to a single-phase heterogenous reservoir with the heterogeneity characterized by the values of the total mobility, the pressure derivative is expected to reflect end-point water mobility adjacent to the perforated interval at very early times, that is

$$\frac{d\big(p_{wf,s} - p_{ws}(\Delta t)\big)}{d \ln(t_e)} = \frac{\alpha q_{inj}}{2 k h_p \hat{\lambda}_w}, \tag{3.62}$$

and the end-point oil mobility over the thickness of the formation at late times, that is

$$\frac{d\big(p_{wf,s} - p_{ws}(\Delta t)\big)}{d \ln(t_e)} = \frac{\alpha q_{inj}}{2 k h \hat{\lambda}_o}. \tag{3.63}$$

When the well is shut-in, the total rate propagates out a zero rate from the wellbore. At later times, the rate is also equal to zero throughout the flooded region $r_w < r < r_f(t_p)$ and the falloff solution given by Eq. 3.57 reduces to the single-phase oil solution as follows

$$p_{ws}(\Delta t) - p_i = \Delta\hat{p}_{os}(\Delta t) = \frac{\alpha q_{inj}}{2kh\hat{\lambda}_o} \ln\left(\frac{t_{pD} + \Delta t_D}{\Delta t_D}\right). \tag{3.64}$$

The injection solution for the restricted-entry vertical well is provided by Eq. 2.74. Specifically, at the instant of shut-in, we have

$$p_{wf,s} - p_i = \Delta p_o(t_p) + \frac{\alpha q_{inj}}{\hat{\lambda}_o} \int_{r_w}^{r_f(t_p)} \left(\frac{\hat{\lambda}_o}{\lambda_t(r, t_p)} - 1\right) \frac{dr}{rh(r)k(r)}, \tag{3.65}$$

that we can rewrite, assuming the water front at the instant of shut-in t_p is beyond the skin zone, as

$$p_{wf,s} - p_i = \Delta p_o(t_p) + \frac{\alpha q_{inj}}{k\hat{\lambda}_o}\left[\left(\frac{k}{k_s} - 1\right) \int_{r_w}^{r_s} \left(\frac{\hat{\lambda}_o}{\lambda_t(r, t_p)} - 1\right) \frac{dr}{rh(r)} + \int_{r_w}^{r_f(t_p)} \left(\frac{\hat{\lambda}_o}{\lambda_t(r, t_p)} - 1\right) \frac{dr}{rh(r)}\right]. \tag{3.66}$$

Assuming that the oil saturation within the skin zone is reduced to residual oil saturation by the end of the injection period and using the Hawkin's formula, it is easy to show that Eq. 3.66 simplifies to

$$p_{wf,s} - p_i = \Delta p_o(t_p) + \frac{\alpha q_{inj}}{kh\hat{\lambda}_o}\left[\left(\frac{\hat{\lambda}_o}{\hat{\lambda}_w} - 1\right)\frac{s}{b} + \int_{r_w}^{r_f(t_p)} \left(\frac{\hat{\lambda}_o}{\lambda_t(r, t_p)} - 1\right) \frac{h}{h(r)}\frac{dr}{r}\right]. \tag{3.67}$$

Note that in deriving the preceding expression, we assumed that $h(r) = h_p$ in the region $r_w < r < r_s$ which is what model 1 predicts. If t_p is sufficiently large, then the single-phase oil solution $\Delta p_o(t)$ is given by the pseudo-radial flow Eq. 2.91. At the instant of shut-in, this equation becomes

$$\Delta p_o(t_p) = \frac{\alpha q_{inj}}{kh\hat{\lambda}_o}\left[\frac{1}{2}\ln\left(\frac{4t_{pD}}{e^\gamma}\right) + \frac{s}{b} + s_b\right]. \tag{3.68}$$

subtracting Eq. 3.64 from Eq. 3.67 and substituting Eq. 3.68 in the resulting equation yields

$$p_{wf,s} - p_{ws}(\Delta t) = \frac{\alpha q_{inj}}{kh\hat{\lambda}_o}\left[\frac{1}{2}\ln\left(\frac{4t_{pD}\Delta t_D}{e^{\gamma}(t_{pD}+\Delta t_D)}\right) + \frac{s}{b} + s_b + \left(\frac{\hat{\lambda}_o}{\hat{\lambda}_w} - 1\right)\frac{s}{b} + \int_{r_w}^{r_f(t_p)}\left(\frac{\hat{\lambda}_o}{\lambda_t(r,t_p)} - 1\right)\frac{h}{h(r)}\frac{dr}{r}\right], \quad (3.69)$$

or equivalently

$$p_{wf,s} - p_{ws}(\Delta t) = \frac{\alpha q_{inj}}{kh\hat{\lambda}_o}\left[\frac{1}{2}\ln\left(\frac{4t_{pD}\Delta t_{eD}}{e^{\gamma}}\right) + s_t\right], \quad (3.70)$$

such that

$$s_t = \frac{\hat{\lambda}_o}{\hat{\lambda}_w}\frac{s}{b} + s_b + \int_{r_w}^{r_f(t_p)}\left(\frac{\hat{\lambda}_o}{\lambda_t(r,t_p)} - 1\right)\frac{h}{h(r)}\frac{dr}{r}. \quad (3.71)$$

A comparison between Eq. 3.61 and Eq. 3.53 indicates that for the restricted-entry case, not only does the total skin depends on the mechanical skin and the pseudo-skin due to the multiphase component, but also on the pseudo-skin due to the convergence of the flow lines. The two equations are exactly the same if we set $b = 1$, $h(r) = h$ and $s_b = 0$ (which is the pure radial flow case).

3.2.2 Falloff Solution, Horizontal Well

Here, we construct approximate analytical solutions for the pressure falloff response subsequent to water injection at a horizontal well. Similar to the vertical well case, the horizontal falloff solutions can be written as the sum of the falloff single-phase oil solution and a multiphase component which represents the additional pressure change due to contrast between λ_t and $\hat{\lambda}_o$ in regions of the reservoir invaded by injected water. Depending on the location of the water front at the instant of shut-in, the multiphase term is presented as a sum of one to three integrals. Our computations are based on stationary profiles for the total mobility throughout the falloff period. In other words, the saturations profiles, or equivalently the total mobility profiles in the reservoir, are assumed to be equal to the ones existing at the instant of shut-in. Evaluation of each

integral in the multiphase component also requires the construction of rate profiles. Next, we consider the falloff solutions for specific flow regimes observed in the horizontal well case.

First Radial/First Radial Flow Regime

The analytical pressure change during falloff for this period can be obtained from the one given for a completely-penetrating vertical well where flow occurs only in the radial direction (the $(x-z)$ plane). Therefore, by analogy to Eq. 3.11, we have

$$\Delta p_{ws} = \Delta \hat{p}_{os} + \frac{\alpha}{L\hat{\lambda}_o} \int_{r_w}^{r_{zx,f}(t_p)} \left(\frac{\hat{\lambda}_o}{\lambda_t(r,t_p)} q_s(r,\Delta t) - \hat{q}_{os}(r,\Delta t) \right) \frac{dr}{rk(r)}, \tag{3.72}$$

where rate superposition (Eqs. 3.37 and 3.42) is applied to compute $\hat{q}_{os}(r,\Delta t)$ and $q_s(r,\Delta t)$ and the radial Buckley-Leverett Eq. 2.48 evaluated at the instant of shut-in is used to generate the total mobility profile $\lambda_t(r,t_p)$.

First Linear/First Radial and First Linear/First Linear Flow Regimes

Similar to the injection solution (Eq. 2.156), we write

$$\Delta p_{ws} = p_{ws}(\Delta t) - p_i = \frac{\pi\alpha}{kL} \int_{x_1}^{\infty} \frac{q_s(x,\Delta t)}{\lambda_t(x,t_p)} \frac{dx}{h(x)} + \frac{\alpha}{L} \int_{r_w}^{z_w} \frac{q_s(r,\Delta t)}{\lambda_t(r,t_p)} \frac{dr}{rk(r)}, \tag{3.73}$$

where $p_{ws}(\Delta t)$ is the falloff pressure as a function of shut-in time Δt. This equation applies for both the first linear/first radial and first linear/first linear flow regimes. For the first linear/first radial flow, however, $\lambda_t(x,t_p) = \hat{\lambda}_o$ for $x \geq x_1$. For now, we derive the equations in a general way and then address the first linear/first radial flow regime as a particular case. By expanding the first integral in Eq. 3.73, we obtain

$$\Delta p_{ws} = \frac{\pi\alpha}{kL} \int_{x_1}^{x_f(t_p)} \frac{q_s(x,\Delta t)}{\lambda_t(x,t_p)} \frac{dx}{h(x)} + \frac{\pi\alpha}{kL} \int_{x_f(t_p)}^{\infty} \frac{q_s(x,\Delta t)}{\lambda_t(x,t_p)} \frac{dx}{h(x)} + \frac{\alpha}{L} \int_{r_w}^{z_w} \frac{q_s(r,\Delta t)}{\lambda_t(r,t_p)} \frac{dr}{rk(r)}, \tag{3.74}$$

where $x_f(t_p)$ is the location of the water front at the instant of shut-in t_p. If $x_f(t_p) \leq x_1$, we can simply recombine the first two integrals in Eq. 3.74 and set $\lambda_t(x,t_p) = \hat{\lambda}_o$ for $x \geq x_1$. If we add and subtract appropriate terms in this equation, we obtain

$$\Delta p_{ws} = \frac{\pi\alpha}{kL}\int_{x_1}^{x_f(t_p)} \frac{q_s(x,\Delta t)}{\lambda_t(x,t_p)}\frac{dx}{h(x)} + \frac{\pi\alpha}{kL}\int_{x_f(t_p)}^{\infty} \frac{q_s(x,\Delta t)}{\lambda_t(x,t_p)}\frac{dx}{h(x)} + \frac{\pi\alpha}{kL\hat{\lambda}_o}\int_{x_1}^{x_f(t_p)} \hat{q}_{os}(x,\Delta t)\frac{dx}{h(x)} - \frac{\pi\alpha}{kL\hat{\lambda}_o}\int_{x_1}^{x_f(t_p)} \hat{q}_{os}(x,\Delta t)\frac{dx}{h(x)} + \frac{\alpha}{L}\int_{r_w}^{z_w} \frac{q_s(r,\Delta t)}{\lambda_t(r,t_p)}\frac{dr}{rk(r)} + \frac{\alpha}{L\hat{\lambda}_o}\int_{r_w}^{z_w} \hat{q}_{os}(r,\Delta t)\frac{dr}{rk(r)} - \frac{\alpha}{L\hat{\lambda}_o}\int_{r_w}^{z_w} \hat{q}_{os}(r,\Delta t)\frac{dr}{rk(r)}. \quad (3.75)$$

In Eq. 3.75, $\hat{q}_{os}(r,\Delta t)$ denotes the oil rate distribution under single-phase flow conditions, i.e., if we injected oil at a rate q_{inj} RB/D. For $x \geq x_f(t_p)$, we assume $q_s(x,\Delta t) = \hat{q}_{os}(x,\Delta t)$ and we know that $\lambda_t(x,t_p) = \hat{\lambda}_o$. Thus, Eq. 3.75 becomes

$$\Delta p_{ws} = \frac{\alpha}{L\hat{\lambda}_o}\int_{r_w}^{z_w} \hat{q}_{os}(r,\Delta t)\frac{dr}{rk(r)} + \frac{\pi\alpha}{kL\hat{\lambda}_o}\int_{x_1}^{\infty} \hat{q}_{os}(x,\Delta t)\frac{dx}{h(x)} + \frac{\alpha}{L\hat{\lambda}_o}\int_{r_w}^{z_w} \left[\frac{\hat{\lambda}_o}{\lambda_t(r,t_p)}q_s(r,\Delta t) - \hat{q}_{os}(r,\Delta t)\right]\frac{dr}{rk(r)} + \frac{\pi\alpha}{kL\hat{\lambda}_o}\int_{x_1}^{x_f(t_p)} \left[\frac{\hat{\lambda}_o}{\lambda_t(x,t_p)}q_s(x,\Delta t) - \hat{q}_{os}(x,\Delta t)\right]\frac{dx}{h(x)}. \quad (3.76)$$

Since the sum of the first two integrals in this equation represents the falloff single-phase solution based on oil properties, which is denoted by $\Delta\hat{p}_{os}$, we can rewrite Eq. 3.76 as

$$\Delta p_{ws} = \Delta\hat{p}_{os} + \frac{\alpha}{L\hat{\lambda}_o}\int_{r_w}^{z_w} \left[\frac{\hat{\lambda}_o}{\lambda_t(r,t_p)}q_s(r,\Delta t) - \hat{q}_{os}(r,\Delta t)\right]\frac{dr}{rk(r)} + \frac{\pi\alpha}{kL\hat{\lambda}_o}\int_{x_1}^{x_f(t_p)} \left[\frac{\hat{\lambda}_o}{\lambda_t(x,t_p)}q_s(x,\Delta t) - \hat{q}_{os}(x,\Delta t)\right]\frac{dx}{h(x)}. \quad (3.77)$$

Note that for the first linear/first radial flow regime, the second integral vanishes since the water is moving only radially in the (x,z) plane and Eq. 3.77 reduces to

$$\Delta p_{ws} = \Delta \hat{p}_{os} + \frac{\alpha}{L\hat{\lambda}_o} \int_{r_w}^{\min(z_w, r_{zx,f}(t_p))} \left[\frac{\hat{\lambda}_o}{\lambda_t(r,t_p)} q_s(r,\Delta t) - \hat{q}_{os}(r,\Delta t) \right] \frac{dr}{rk(r)}. \tag{3.78}$$

Now, the question is how to generate the flow rate during shut-in. We apply rate superposition to compute $\hat{q}_{os}(r,\Delta t)$ and $\hat{q}_{os}(x,\Delta t)$ according to Eqs. 3.37 and 3.34 respectively. For the term $q_s(r,\Delta t)$ which occurs in the first integral of Eq. 3.77 or Eq. 3.78, we simply use the procedure given for the vertical well (see Eq. 3.42). For the linear flow in the x-direction, we will apply the single-phase rate superposition equation given by

$$q_s(x,\Delta t) = q_{inj} \left[\text{erfc}\left(\frac{x_D}{2\sqrt{t_{pD} + \Delta t_D}} \right) - \text{erfc}\left(\frac{x_D}{2\sqrt{\Delta t_D}} \right) \right], \tag{3.79}$$

and use local values of total mobility $\lambda_t(x,t_p)$ and total compressibility $c_t(x,t_p)$ based on the saturation distributions computed from the Buckley-Leverett theory when evaluating the dimensionless times. With the approach, Eq. 3.79 can be rewritten as

$$q_s(x,\Delta t) = q_{inj} \left[\text{erfc}\Big(\frac{x\sqrt{\phi c_t(x,t_p)}}{2\sqrt{\beta k \lambda_t(x,t_p)(t_p + \Delta t)}} \Big) - \text{erfc}\Big(\frac{x\sqrt{\phi c_t(x,t_p)}}{2\sqrt{\beta k \lambda_t(x,t_p)\Delta t}} \Big) \right]. \tag{3.80}$$

Second Radial/First Radial, Second Radial/First Linear and Second Radial/Second Radial Flow Regimes

The equation for the falloff wellbore pressure change is given by

$$\Delta p_{ws} = p_{ws}(\Delta t) - p_i = \frac{\alpha}{kh} \int_{L/2}^{\infty} \frac{q_s(r,\Delta t)}{\lambda_t(r,t_p)} \frac{dr}{r} + \frac{\pi\alpha}{kL} \int_{x_1}^{x_3} \frac{q_s(x,\Delta t)}{\lambda_t(x,t_p)} \frac{dx}{h(x)} + \frac{\alpha}{L} \int_{r_w}^{z_w} \frac{q_s(r,\Delta t)}{\lambda_t(r,t_p)} \frac{dr}{rk(r)}. \tag{3.81}$$

This expression applies when the steady-state zone of constant rate is in the (x,y) plane while the water front at the instant of shut-in is in the plane (x,y) (second radial/second radial flow). For the second radial/first linear flow regime, we simply set $\lambda_t(r,t_p) = \hat{\lambda}_o$

for $r \geq L/2$. If in addition, $\lambda_t(x, t_p) = \hat{\lambda}_o$ for $x \geq x_1$, then Eq. 3.81 will apply for the case where the water front at the instant of shut-in is in the (x, z) plane (second radial/first radial flow). Here, we derive the equation in a general way and then address each flow regime specifically. By introducing the radius of water front at the instant of shut-in $r_{xy,f}(t_p)$, we can rewrite Eq. 3.81 as

$$\Delta p_{ws} = \frac{\alpha}{kh}\int_{L/2}^{r_{xy,f}(t_p)} \frac{q_s(r,\Delta t)}{\lambda_t(r,t_p)}\frac{dr}{r} + \frac{\alpha}{kh}\int_{r_{xy,f}(t_p)}^{\infty} \frac{q_s(r,\Delta t)}{\lambda_t(r,t_p)}\frac{dr}{r} + \frac{\pi\alpha}{kL}\int_{x_1}^{x_3} \frac{q_s(x,\Delta t)}{\lambda_t(x,t_p)}\frac{dx}{h(x)} + \frac{\alpha}{L}\int_{r_w}^{z_w} \frac{q_s(r,\Delta t)}{\lambda_t(r,t_p)}\frac{dr}{rk(r)}. \quad (3.82)$$

If we add and subtract the same terms in this equation, we obtain

$$\begin{aligned}\Delta p_{ws} = {} & \frac{\alpha}{kh}\int_{L/2}^{r_{xy,f}(t_p)} \frac{q_s(r,\Delta t)}{\lambda_t(r,t_p)}\frac{dr}{r} + \frac{\alpha}{kh}\int_{r_{xy,f}(t_p)}^{\infty} \frac{q_s(r,\Delta t)}{\lambda_t(r,t_p)}\frac{dr}{r} \\ & + \frac{\alpha}{kh\hat{\lambda}_o}\int_{L/2}^{r_{xy,f}(t_p)} \hat{q}_{os}(r,\Delta t)\frac{dr}{r} - \frac{\alpha}{kh\hat{\lambda}_o}\int_{L/2}^{r_{xy,f}(t_p)} \hat{q}_{os}(r,\Delta t)\frac{dr}{r} \\ & + \frac{\pi\alpha}{kL}\int_{x_1}^{x_3} \frac{q_s(x,\Delta t)}{\lambda_t(x,t_p)}\frac{dx}{h(x)} + \frac{\pi\alpha}{kL\hat{\lambda}_o}\int_{x_1}^{x_3} \hat{q}_{os}(x,\Delta t)\frac{dx}{h(x)} \\ & - \frac{\pi\alpha}{kL\hat{\lambda}_o}\int_{x_1}^{x_3} \hat{q}_{os}(x,\Delta t)\frac{dx}{h(x)} + \frac{\alpha}{L}\int_{r_w}^{z_w} \frac{q_s(r,\Delta t)}{\lambda_t(r,t_p)}\frac{dr}{rk(r)} \\ & + \frac{\alpha}{L\hat{\lambda}_o}\int_{r_w}^{z_w} \hat{q}_{os}(r,\Delta t)\frac{dr}{rk(r)} - \frac{\alpha}{L\hat{\lambda}_o}\int_{r_w}^{z_w} \hat{q}_{os}(r,\Delta t)\frac{dr}{rk(r)}. \quad (3.83)\end{aligned}$$

For $r \geq L/2$, $q_s(r, \Delta t) = \hat{q}_{os}(r, \Delta t)$ and $\lambda_t(r, t_p) = \hat{\lambda}_o$. Thus, Eq. 3.83 becomes

$$\Delta p_{ws} = \frac{\alpha}{L\hat{\lambda}_o}\int_{r_w}^{z_w}\hat{q}_{os}(r,\Delta t)\,\frac{dr}{rk(r)} + \frac{\pi\alpha}{kL\hat{\lambda}_o}\int_{x_1}^{x_3}\hat{q}_{os}(x,\Delta t)\,\frac{dx}{h(x)} + \frac{\alpha}{kh\hat{\lambda}_o}\int_{L/2}^{\infty}\hat{q}_{os}(r,\Delta t)\,\frac{dr}{r}$$
$$+ \frac{\alpha}{L\hat{\lambda}_o}\int_{r_w}^{z_w}\left[\frac{\hat{\lambda}_o}{\lambda_t(r,t_p)}q_s(r,\Delta t) - \hat{q}_{os}(r,\Delta t)\right]\frac{dr}{rk(r)}$$
$$+ \frac{\pi\alpha}{kL\hat{\lambda}_o}\int_{x_1}^{x_3}\left[\frac{\hat{\lambda}_o}{\lambda_t(x,t_p)}q_s(x,\Delta t) - \hat{q}_{os}(x,\Delta t)\right]\frac{dx}{h(x)}$$
$$+ \frac{\alpha}{kh\hat{\lambda}_o}\int_{L/2}^{r_{xy,f}(t_p)}\left[\frac{\hat{\lambda}_o}{\lambda_t(r,t_p)}q_s(r,\Delta t) - \hat{q}_{os}(r,\Delta t)\right]\frac{dr}{r}. \quad (3.84)$$

The sum of the three first integrals in this equation represents the falloff-single-phase solution based on oil properties at irreducible water saturation. Therefore, we can rewrite Eq. 3.84 as

$$\Delta p_{ws} = \Delta\hat{p}_{os} + \frac{\alpha}{L\hat{\lambda}_o}\int_{r_w}^{z_w}\left[\frac{\hat{\lambda}_o}{\lambda_t(r,t_p)}q_s(r,\Delta t) - \hat{q}_{os}(r,\Delta t)\right]\frac{dr}{rk(r)}$$
$$+ \frac{\pi\alpha}{kL\hat{\lambda}_o}\int_{x_1}^{x_3}\left[\frac{\hat{\lambda}_o}{\lambda_t(x,t_p)}q_s(x,\Delta t) - \hat{q}_{os}(x,\Delta t)\right]\frac{dx}{h(x)}$$
$$+ \frac{\alpha}{kh\hat{\lambda}_o}\int_{L/2}^{r_{xy,f}(t_p)}\left[\frac{\hat{\lambda}_o}{\lambda_t(r,t_p)}q_s(r,\Delta t) - \hat{q}_{os}(r,\Delta t)\right]\frac{dr}{r}. \quad (3.85)$$

For the second radial/first linear flow regime, the last integral of Eq. 3.86 vanishes and the wellbore pressure change in this case reduces to

$$\Delta p_{ws} = \Delta\hat{p}_{os} + \frac{\alpha}{L\hat{\lambda}_o}\int_{r_w}^{z_w}\left[\frac{\hat{\lambda}_o}{\lambda_t(r,t_p)}q_s(r,\Delta t) - \hat{q}_{os}(r,\Delta t)\right]\frac{dr}{rk(r)}$$
$$+ \frac{\pi\alpha}{kL\hat{\lambda}_o}\int_{x_1}^{x_f(t_p)}\left[\frac{\hat{\lambda}_o}{\lambda_t(x,t_p)}q_s(x,\Delta t) - \hat{q}_{os}(x,\Delta t)\right]\frac{dx}{h(x)}. \quad (3.86)$$

For the second radial/first radial flow regime, both last integrals are zero since the water at the instant of shut-in is in the (x,z) plane and Eq. 3.86 reduces to

$$\Delta p_{ws} = \Delta \hat{p}_{os} + \frac{\alpha}{L\hat{\lambda}_o} \int_{r_w}^{r_{zx,f}(t_p)} \left[\frac{\hat{\lambda}_o}{\lambda_t(r,t_p)} q_s(r,t) - \hat{q}_{os}(r,t) \right] \frac{dr}{rk(r)}. \tag{3.87}$$

Generalized Falloff Solution

Combining the previous results for the falloff solutions, we can show that the generalized equation for the falloff pressure solution for an offset horizontal well in an isotropic reservoir is given by

$$\begin{aligned} \Delta p_{ws} = p_{ws} - p_i = \Delta \hat{p}_{os} &+ \frac{\alpha}{L\hat{\lambda}_o} \int_{r_w}^{\min(z_w, r_{zx,f}(t_p))} \left[\frac{\hat{\lambda}_o}{\lambda_t(r,t_p)} q_s(r,\Delta t) - \hat{q}_{os}(r,\Delta t) \right] \frac{dr}{rk(r)} \\ &+ \frac{\pi\alpha}{kL\hat{\lambda}_o} \int_{x_1}^{b} \left[\frac{\hat{\lambda}_o}{\lambda_t(x,t_p)} q_s(x,\Delta t) - \hat{q}_{os}(x,\Delta t) \right] \frac{dx}{h(x))} \\ &+ \frac{\alpha}{kh\hat{\lambda}_o} \int_{L/2}^{\max(\frac{L}{2}, r_{xy,f}(t_p))} \left[\frac{\hat{\lambda}_o}{\lambda_t(r,t_p)} q_s(r,\Delta t) - \hat{q}_{os}(r,\Delta t) \right] \frac{dr}{r}, \end{aligned} \tag{3.88}$$

where b was defined by Eq. 2.235 in chapter 2.

At late times, the rates q_s and $\hat{q}_{os}$ in Eq. 3.88 go to zero. Thus, the multiphase contribution to the falloff pressure change is zero which reduces the solution to

$$\Delta p_{ws} = \Delta \hat{p}_{os} = \frac{\alpha q_{inj}}{2kh\hat{\lambda}_o} \ln\left(\frac{t_{pD} + \Delta t_D}{\Delta t_D} \right), \tag{3.89}$$

where the dimensionless shut-in time Δt_D is defined by

$$\Delta t_D = \frac{4\beta k\hat{\lambda}_o \Delta t}{\phi \hat{c}_{to} L^2}. \tag{3.90}$$

At the end of injection, the wellbore pressure change is given according to Eqs. 2.231 to 2.234 by

$$\begin{aligned} \Delta p(t_p) = p_{wf,s} - p_i = \Delta p_o(t_p) &+ \frac{\alpha q_{inj}}{L\hat{\lambda}_o} \int_{r_w}^{\min(z_w, r_{zx,f}(t_p))} \left(\frac{\hat{\lambda}_o}{\lambda_t(r,t_p)} - 1 \right) \frac{dr}{rk(r)} + \\ &\frac{\pi\alpha q_{inj}}{kL\hat{\lambda}_o} \int_{x_1}^{b} \left(\frac{\hat{\lambda}_o}{\lambda_t(x,t_p)} - 1 \right) \frac{dx}{h(x)} + \frac{\alpha q_{inj}}{kh\hat{\lambda}_o} \int_{\frac{L}{2}}^{\max(\frac{L}{2}, r_{xy,f}(t_p))} \left(\frac{\hat{\lambda}_o}{\lambda_t(r,t_p)} - 1 \right) \frac{dr}{r}, \end{aligned} \tag{3.91}$$

where $\Delta p_o(t_p)$ for very long times is given according to Eq. 2.341 for an isotropic case by

$$\Delta p_o(t_p) = \frac{\alpha q_{inj}}{kh\hat{\lambda}_o}\left[\frac{1}{2}\ln\left(\frac{4t_{pD}}{e^{\gamma}}\right) + C + \frac{h}{L}(s_z + s'_z + s)\right]. \tag{3.92}$$

Subtracting Eq. 3.89 from Eq. 3.91 and using Eq. 3.92 in the resulting equation gives

$$\begin{aligned} p_{wf,s} - p_{ws}(\Delta t) = {} & \frac{\alpha q_{inj}}{kh\hat{\lambda}_o}\left[\frac{1}{2}\ln\left(\frac{4t_{pD}}{e^{\gamma}}\right) + C + \frac{h}{L}(s_z + s'_z + s)\right] + \\ & \frac{\alpha q_{inj}}{L\hat{\lambda}_o}\int_{r_w}^{\min(z_w, r_{zx,f}(t_p))}\left(\frac{\hat{\lambda}_o}{\lambda_t(r,t_p)} - 1\right)\frac{dr}{rk(r)} + \frac{\pi\alpha q_{inj}}{kL\hat{\lambda}_o}\int_{x_1}^{b}\left(\frac{\hat{\lambda}_o}{\lambda_t(x,t_p)} - 1\right)\frac{dx}{h(x)} + \\ & \frac{\alpha q_{inj}}{kh\hat{\lambda}_o}\int_{\frac{L}{2}}^{\max(\frac{L}{2}, r_{xy,f}(t_p))}\left(\frac{\hat{\lambda}_o}{\lambda_t(r,t_p)} - 1\right)\frac{dr}{r} - \frac{\alpha q_{inj}}{2kh\hat{\lambda}_o}\ln\left(\frac{t_{pD} + \Delta t_D}{\Delta t_D}\right), \end{aligned} \tag{3.93}$$

or

$$\begin{aligned} p_{wf,s} - p_{ws}(\Delta t) = {} & \frac{\alpha q_{inj}}{kh\hat{\lambda}_o}\left[\frac{1}{2}\ln\left(\frac{4t_{pD}\Delta t_D}{e^{\gamma}(t_{pD} + \Delta t_D)}\right) + C + \frac{h}{L}(s_z + s'_z + s) + \right. \\ & \frac{h}{L}\int_{r_w}^{\min(z_w, r_{zx,f}(t_p))}\left(\frac{\hat{\lambda}_o}{\lambda_t(r,t_p)} - 1\right)\frac{k}{k(r)}\frac{dr}{r} + \frac{\pi h}{L}\int_{x_1}^{b}\left(\frac{\hat{\lambda}_o}{\lambda_t(x,t_p)} - 1\right)\frac{dx}{h(x)} + \\ & \left.\int_{\frac{L}{2}}^{\max(\frac{L}{2}, r_{xy,f}(t_p))}\left(\frac{\hat{\lambda}_o}{\lambda_t(r,t_p)} - 1\right)\frac{dr}{r}\right]. \end{aligned} \tag{3.94}$$

If we assume that the skin zone is completely swept by water such that $\lambda_t(r,t_p) = \hat{\lambda}_w$ for $r_w < r < r_s$, it can be shown that

$$\begin{aligned} \int_{r_w}^{\min(z_w, r_{zx,f}(t_p))}\left(\frac{\hat{\lambda}_o}{\lambda_t(r,t_p)} - 1\right)\frac{dr}{rk(r)} = {} & \frac{1}{k}\left(\frac{k}{k_s} - 1\right)\left(\frac{\hat{\lambda}_o}{\hat{\lambda}_w} - 1\right)\ln\left(\frac{r_s}{r_w}\right) + \\ & \frac{1}{k}\int_{r_w}^{\min(z_w, r_{zx,f}(t_p))}\left(\frac{\hat{\lambda}_o}{\lambda_t(r,t_p)} - 1\right)\frac{dr}{r}, \end{aligned} \tag{3.95}$$

or by using Hawkin's formula for the mechanical skin

$$\int_{r_w}^{\min(z_w,r_{zx,f}(t_p))}\left(\frac{\hat{\lambda}_o}{\lambda_t(r,t_p)}-1\right)\frac{dr}{rk(r)}=\left(\frac{\hat{\lambda}_o}{\hat{\lambda}_w}-1\right)\frac{s}{k}+\frac{1}{k}\int_{r_w}^{\min(z_w,r_{zx,f}(t_p))}\left(\frac{\hat{\lambda}_o}{\lambda_t(r,t_p)}-1\right)\frac{dr}{r}. \tag{3.96}$$

Finally, substituting Eq. 3.96 in Eq. 3.94 gives

$$p_{wf,s}-p_{ws}(\Delta t)=\frac{\alpha q_{inj}}{kh\hat{\lambda}_o}\left[\frac{1}{2}\ln\left(\frac{4t_{eD}}{e^{\gamma}}\right)+C+\frac{h}{L}\left(s_z+s'_z+\frac{s}{\hat{M}}+\right.\right.$$
$$\int_{r_w}^{\min(z_w,r_{zx,f}(t_p))}\left(\frac{\hat{\lambda}_o}{\lambda_t(r,t_p)}-1\right)\frac{dr}{r}+\pi\int_{x_1}^{b}\left(\frac{\hat{\lambda}_o}{\lambda_t(x,t_p)}-1\right)\frac{dx}{h(x)}+$$
$$\left.\left.\frac{L}{h}\int_{\frac{L}{2}}^{\max(\frac{L}{2},r_{xy,f}(t_p))}\left(\frac{\hat{\lambda}_o}{\lambda_t(r,t_p)}-1\right)\frac{dr}{r}\right)\right]. \tag{3.97}$$

Note that the total skin denoted by s_t for the case of a horizontal well is given by the following expression:

$$s_t=s_z+s'_z+\frac{s}{\hat{M}}+\int_{r_w}^{\min(z_w,r_{zx,f}(t_p))}\left(\frac{\hat{\lambda}_o}{\lambda_t(r,t_p)}-1\right)\frac{dr}{r}+$$
$$\pi\int_{x_1}^{b}\left(\frac{\hat{\lambda}_o}{\lambda_t(x,t_p)}-1\right)\frac{dx}{h(x)}+\frac{L}{h}\int_{\frac{L}{2}}^{\max(\frac{L}{2},r_{xy,f}(t_p))}\left(\frac{\hat{\lambda}_o}{\lambda_t(r,t_p)}-1\right)\frac{dr}{r}. \tag{3.98}$$

It represents a combination of the mechanical skin s, the pseudo-skins s_z and s'_z due to the convergence of flow lines and the pseudo skin that combines the three integrals in Eq. 3.98 due to the contrast of mobilities in the reservoir. An accurate estimation of s from a semilog analysis depends therefore on the knowledge of these additional skins.

3.3 Falloff Solutions for an Anisotropic Reservoir

Up to now, all the falloff solutions that we wrote for the different geometrical configurations considered in this work assumed an isotropic reservoir. In this section, we construct accurate analytical solutions during a falloff test for cases where the condition of isotropy does not hold. Based on the single-phase flow analysis developed in the fourth

section of chapter 2, we were able to establish an equivalence between the real anisotropic system of permeability field $\overrightarrow{k}$ defined by

$$\overrightarrow{k} = \begin{pmatrix} k_x & 0 & 0 \\ 0 & k_y & 0 \\ 0 & 0 & k_z \end{pmatrix}, \tag{3.99}$$

and the isotropic problem of permeability $\bar{k}$ given by

$$\bar{k}(r_n) = \begin{cases} \bar{k}_s = \sqrt[3]{k_{xs}k_{ys}k_{zs}} & \text{for } r_{wn} < r_n < r_{sn}, \\ \bar{k} = \sqrt[3]{k_x k_y k_z} & \text{for } r_n > r_{sn}. \end{cases} \tag{3.100}$$

The spatial coordinate transformation which allowed us to perform this conversion is defined through Eqs. 2.236 to 2.238.

Using the same theoretical approach based on the steady-state theory combined with rate superposition applied for the isotropic case, it is easy to show that the general solution for the wellbore pressure change during the falloff period for a vertical well is given by

$$\Delta p_{ws} = \Delta \hat{p}_{os} + \frac{\alpha}{\hat{\lambda}_o} \int_{r_{wn}}^{r_{fn}(t_p)} \left(\frac{\hat{\lambda}_o}{\lambda_t(r_n, t_p)} q_s(r_n, \Delta t) - \hat{q}_{os}(r_n, \Delta t) \right) \frac{dr_n}{r_n \bar{k}(r_n) h_n(r_n)}, \tag{3.101}$$

where $\Delta \hat{p}_{os}$ here, is the falloff single-phase flow pressure change based on oil properties at irreducible water saturation assuming oil is injected through a vertical well of radius r_{wn} (given by Eq. 2.284) into an oil reservoir of permeability $\bar{k}(r_n)$ at an injection rate of q_{inj}. The location of the water front at the instant of shut-in in the new coordinate system, denoted by $r_{fn}(t_p)$, is determined either by Eqs. 2.354 or 2.355 if model 1 is used or by Eqs. 2.356 to 2.357 if model 2 is applied. For a complete-penetration vertical well case, we simply set $h_n(r_n) = h_n$ in Eq. 3.101 and use Eq. 2.355 with $b = 1$ to compute the location $r_{fn}(t_p)$. As seen before, the knowledge of the flow rate distributions in Eq. 3.101 is crucial in the evaluation of the multiphase component. Similar to the

isotropic case, $\hat{q}_{os}(r_n, \Delta)$ and $q_s(r_n, \Delta t)$ are computed using rate superposition applied in the new coordinate system. Thus, we have

$$\hat{q}_{os}(r_n, \Delta t) = q_{inj}\left[\exp\Big(-\frac{\phi\hat{c}_{to}r_n^2}{4\beta\bar{k}(r_n)\hat{\lambda}_o(t_p+\Delta t)}\Big) - \exp\Big(-\frac{\phi\hat{c}_{to}r_n^2}{4\beta\bar{k}(r_n)\hat{\lambda}_o\Delta t}\Big)\right], \quad (3.102)$$

and

$$q_s(r_n, \Delta t) = q_{inj}\left[\exp\Big(-\frac{\phi c_t(r_n,t_p)r_n^2}{4\beta\bar{k}(r_n)\lambda_t(r_n,t_p)(t_p+\Delta t)}\Big) - \exp\Big(-\frac{\phi c_t(r_n,t_p)r_n^2}{4\beta\bar{k}(r_n)\lambda_t(r_n,t_p)\Delta t}\Big)\right]. \quad (3.103)$$

For the horizontal well case, the equivalent isotropic system is also characterized by the permeability of Eq. 3.100. However, the effective wellbore radius in this case is defined by Eq. 2.320 and the distance from the centerline of the well to the top boundary of the reservoir and the length of the horizontal well are given respectively by Eqs. 2.318 and 2.319. Here, we are assuming that the axis of the well is along the y_n-direction.

Similar to the isotropic case, we simply add the multiphase component to the single-phase solution based on oil properties at irreducible water saturation expressed in the new coordinate system. The total pressure change due to multiphase flow is now given by the sum of the following terms:

$$\Delta p_{ws}^{x_n-z_n}(\Delta t) = \frac{\alpha}{L_n\hat{\lambda}_o}\int_{r_{wn}}^{\min(z_{wn},r_{zx,fn}(t_p))}\left[\frac{\hat{\lambda}_o}{\lambda_t(r_n,t_p)}q_s(r_n,\Delta t) - \hat{q}_{os}(r_n,\Delta t)\right]\frac{dr_n}{r_n\bar{k}(r_n)}, \quad (3.104)$$

$$\Delta p_{ws}^{x_n}(\Delta t) = \frac{\pi\alpha}{\bar{k}L_n\hat{\lambda}_o}\int_{x_{n1}}^{b_n}\left[\frac{\hat{\lambda}_o}{\lambda_t(x_n,t_p)}q_s(x_n,\Delta t) - \hat{q}_{os}(x_n,\Delta t)\right]\frac{dx_n}{h_n(x_n)}, \quad (3.105)$$

and

$$\Delta p_{ws}^{x_n-y_n}(\Delta t) = \frac{\alpha}{\bar{k}h_n\hat{\lambda}_o}\int_{L_n/2}^{\max(\frac{L_n}{2},r_{xy,fn}(t_p))}\left[\frac{\hat{\lambda}_o}{\lambda_t(r_n,t_p)}q_s(r_n,\Delta t) - \hat{q}_{os}(r_n,\Delta t)\right]\frac{dr_n}{r_n}. \quad (3.106)$$

In these equations, rate superposition (Eqs. 3.102 and 3.103) is applied to compute $\hat{q}_{os}(r_n, \Delta t)$ and $q_s(r_n, \Delta t)$. As for the flow rate distributions $\hat{q}_{os}(x_n, \Delta t)$ and $q_s(x_n, \Delta t)$ in the x_n-direction, they are computed for the same formulas as in the isotropic case, that is Eqs. 3.34 and 3.80 that we express in the transformed system respectively as

$$\hat{q}_{os}(x_n, \Delta t) = q_{inj}\left[\operatorname{erfc}\Big(\frac{x_n\sqrt{\phi\hat{c}_{to}}}{2\sqrt{\beta\bar{k}\hat{\lambda}_o(t_p+\Delta t)}}\Big) - \operatorname{erfc}\Big(\frac{x_n\sqrt{\phi\hat{c}_{to}}}{2\sqrt{\beta\bar{k}\hat{\lambda}_o\Delta t}}\Big)\right], \tag{3.107}$$

and

$$q_s(x_n, \Delta t) = q_{inj}\left[\operatorname{erfc}\Big(\frac{x_n\sqrt{\phi c_t(x_n,t_p)}}{2\sqrt{\beta\bar{k}\lambda_t(x_n,t_p)(t_p+\Delta t)}}\Big) - \operatorname{erfc}\Big(\frac{x_n\sqrt{\phi c_t(x_n,t_p)}}{2\sqrt{\beta\bar{k}\lambda_t(x_n,t_p)\Delta t}}\Big)\right]. \tag{3.108}$$

3.4 Application of Perturbation Theory

In this chapter, approximate solutions for the falloff response subsequent to water injection at a vertical and horizontal wells were constructed by using the steady-state theory combined with rate superposition. However, as mentioned earlier, there is no rigorous theoretical justification for using rate superposition in a non-linear problem (two-phase flow of water and oil). In this section, we present a new procedure based on perturbation theory to solve the initial boundary value problem given by Eqs. 3.3 to 3.6. The idea behind the perturbation method is to identify a small parameter such that when this parameter is set to zero, the problem becomes solvable. In our case, we will see that the use of perturbation theory is justified if one assumes a small variation of the water saturation in the region invaded by water. Note that the derivation presented here are only for radial flow of fluids.

3.4.1 Model Description

Assuming incompressible fluids, the water saturation distribution will remain stationary immediately upon well shut-in and throughout the entire falloff test. Thus, the reservoir consists of two regions with distinct fluid properties. The inner region that we also refer to as the water bank is characterized by a total compressibility and a total mo-

bility which gradually change due to the variation of the water saturation. In the outer region, referred to as the oil bank, the total compressibility and the total mobility are constant and equal to $\hat{c}_{to}$ and $\hat{\lambda}_o$ respectively. Assuming that the pressure distribution is given by $p_{in}(r, \Delta t)$ in the inner region and by $p_{ou}(r, \Delta t)$ in the outer zone, we can rewrite the system described by Eqs. 3.3 to 3.6 as

$$\frac{\beta}{r}\frac{\partial}{\partial r}\left[k(r)\lambda_t(r)r\frac{\partial p_{in}(r,\Delta t)}{\partial r}\right] = \phi c_t(r)\frac{\partial p_{in}(r,\Delta t)}{\partial \Delta t},\ \text{for } r_w < r < r_f(t_p)\ ,\ \Delta t > 0 \quad (3.109)$$

$$r\frac{\partial p_{in}(r,\Delta t)}{\partial r}\ |_{r=r_w} = 0, \forall \Delta t \geq 0 \quad (3.110)$$

$$p_{in}(r, \Delta t = 0) = p_{inj,in}(r, t_p),\ \text{for } r_w \leq r \leq r_f(t_p) \quad (3.111)$$

$$\frac{\beta k}{r}\hat{\lambda}_o\frac{\partial}{\partial r}\left[r\frac{\partial p_{ou}(r,\Delta t)}{\partial r}\right] = \phi\hat{c}_{to}\frac{\partial p_{ou}(r,\Delta t)}{\partial \Delta t},\ \text{for } r_f(t_p) < r\ ,\ \Delta t > 0 \quad (3.112)$$

$$\lim_{r\to\infty} p_{ou}(r, \Delta t) = p_i, \forall \Delta t \geq 0 \quad (3.113)$$

and

$$p_{ou}(r, \Delta t = 0) = p_{inj,ou}(r, t_p),\ \text{for } r_f(t_p) \leq r. \quad (3.114)$$

Two additional equations are needed to solve the above system. These are the continuity of the pressure and the flux equations given respectively by

$$p_{in}(r_f(t_p), \Delta t) = p_{ou}(r_f(t_p), \Delta t), \forall \Delta t \geq 0 \quad (3.115)$$

and

$$\lambda_t(r) r \frac{\partial p_{in}}{\partial r} \mid_{r=r_f(t_p)} = \hat{\lambda}_o r \frac{\partial p_{ou}}{\partial r} \mid_{r=r_f(t_p)}, \forall \Delta t \geq 0. \tag{3.116}$$

Note that Eq. 3.109 assumes a variable absolute permeability in order to account for the change of the permeability near the wellbore region due to the mechanical skin. Note also that in Eq. 3.112, the water front is beyond the damaged zone at the instant of shut-in which is a reasonable assumption in practice.

For practical purposes, the dimensionless variables introduced in this section will be defined in terms of water properties at residual oil saturation, S_{or}. In the following, we will denote dimensionless radial distance, dimensionless shut-in time, dimensionless pressure change, dimensionless total mobility, dimensionless total compressibility, respectively, by r_D, Δt_D, p_D, λ_{tD} and c_{tD} such that

$$r_D = \frac{r}{r_w}, \tag{3.117}$$

$$\Delta t_D = \frac{\beta k \hat{\lambda}_w}{\phi \hat{c}_{tw} r_w^2} \Delta t, \tag{3.118}$$

$$p_D = \frac{k \hat{\lambda}_w h}{\alpha q} (p - p_i), \tag{3.119}$$

$$\lambda_{tD} = \frac{\lambda_t}{\hat{\lambda}_w}, \tag{3.120}$$

and

$$c_{tD} = \frac{c_t}{\hat{c}_{tw}}, \tag{3.121}$$

where $\hat{c}_{tw}$ is obtained by evaluating Eq. 3.1 at $S_w = 1 - S_{or}$. With these definitions, the governing differential equations and associated conditions can be rewritten in dimensionless form as

$$\frac{1}{r_D}\frac{\partial}{\partial r_D}\left[\frac{k(r_D)}{k}\lambda_{tD}(r_D)r_D\frac{\partial p_{D,in}(r_D,\Delta t_D)}{\partial r_D}\right]=c_{tD}(r_D)\frac{\partial p_{D,in}(r_D,\Delta t_D)}{\partial \Delta t_D},$$

$$\text{for } 1<r_D<r_{fD}\ ,\ \Delta t_D>0 \tag{3.122}$$

$$r_D\frac{\partial p_{D,in}(r_D,\Delta t_D)}{\partial r_D}\ |_{r_D=1}=0,\forall \Delta t_D\geq 0 \tag{3.123}$$

$$p_{D,in}(r_D,\Delta t_D=0)=p_{Dinj,in}(r_D,t_{pD})=f_1(r_D),\ \text{for } 1\leq r_D\leq r_{fD} \tag{3.124}$$

$$\frac{1}{r_D}\frac{\partial}{\partial r_D}\left[r_D\frac{\partial p_{D,ou}(r_D,\Delta t_D)}{\partial r_D}\right]=\eta\frac{\partial p_{D,ou}(r_D,\Delta t_D)}{\partial \Delta t_D},\ \text{for } r_{fD}<r_D\ ,\ \Delta t_D>0 \tag{3.125}$$

$$\lim_{r_D\to\infty}p_{D,ou}(r_D,\Delta t_D)=0,\forall \Delta t_D\geq 0 \tag{3.126}$$

$$p_{D,ou}(r_D,\Delta t_D=0)=p_{Dinj,ou}(r_D,t_{pD})=f_2(r_D),\ \text{for } r_{fD}\leq r_D \tag{3.127}$$

$$p_{D,in}(r_{fD},\Delta t_D)=p_{D,ou}(r_{fD},\Delta t_D),\forall \Delta t_D\geq 0 \tag{3.128}$$

and

$$\hat{M}\lambda_{tD}(r_D)r_D\frac{\partial p_{D,in}}{\partial r_D}\ |_{r_D=r_{fD}}=r_D\frac{\partial p_{D,ou}}{\partial r_D}\ |_{r_D=r_{fD}}\ \forall \Delta t_D\geq 0. \tag{3.129}$$

In Eq. 3.125, the parameter η is defined by

$$\eta = \hat{M}\frac{\hat{c}_{to}}{\hat{c}_{tw}}, \tag{3.130}$$

where $\hat{M}$ is the end point mobility ratio given by $\hat{M} = \frac{\hat{\lambda}_w}{\hat{\lambda}_o}$.

Next, we transform the above IBVP by taking the Laplace transform with respect to Δt_D. Throughout, u denotes the Laplace variable and a bar over a dimensionless pressure function is used to denote its Laplace transform. After transformation, the system given by Eqs. 3.122 to 3.129 becomes

$$\frac{1}{r_D}\frac{\partial}{\partial r_D}\left[\frac{k(r_D)}{k}\lambda_{tD}(r_D)r_D\frac{\partial \bar{p}_{D,in}(r_D,u)}{\partial r_D}\right] = c_{tD}(r_D)\Big(u\bar{p}_{D,in}(r_D,u) - f_1(r_D)\Big), \text{ for } 1 < r_D < r_{fD} \tag{3.131}$$

$$r_D\frac{\partial \bar{p}_{D,in}(r_D,u)}{\partial r_D}\mid_{r_D=1} = 0, \tag{3.132}$$

$$\frac{1}{r_D}\frac{\partial}{\partial r_D}\left[r_D\frac{\partial \bar{p}_{D,ou}(r_D,u)}{\partial r_D}\right] = \eta\Big(u\bar{p}_{D,ou}(r_D,u) - f_2(r_D)\Big), \text{ for } r_{fD} < r_D \tag{3.133}$$

$$\lim_{r_D\to\infty}\bar{p}_{D,ou}(r_D,u) = 0, \tag{3.134}$$

$$\bar{p}_{D,in}(r_{fD},u) = \bar{p}_{D,ou}(r_{fD},u), \tag{3.135}$$

and

$$\hat{M}\lambda_{tD}(r_D)r_D\frac{\partial \bar{p}_{D,in}}{\partial r_D}\mid_{r_D=r_{fD}} = r_D\frac{\partial \bar{p}_{D,ou}}{\partial r_D}\mid_{r_D=r_{fD}}. \tag{3.136}$$

3.4.2 Pressure Profile at the End of Injection-Initial Condition for Falloff

It is obvious that the knowledge of the initial pressure distribution is crucial in order to solve the initial boundary value problem described above. In our previous derivations

(see chapter 2), we showed we were able to construct an accurate semi-analytical solution for the pressure during an injection test using the concept of the steady-state theory. However, the derivation was given for only the wellbore pressure. Here, we would like to extend the derivation to any radial distance in order to obtain the profile of the injection pressure in particular at the instant of shut-in. We begin by writing Darcy's law as

$$q_t(r,t) = -\frac{k(r)h}{\alpha}\lambda_t(r,t)r\frac{\partial p}{\partial r}, \tag{3.137}$$

where $q_t(r,t)$, $\lambda_t(r,t)$ and $p(r,t)$ represent respectively the total rate profile, the total mobility distribution and the injection pressure in the reservoir during the injection test. In Eq. 3.137, α is a conversion constant previously defined ($\alpha = 141.2$ if oil field units are used with time in hours). Eq. 3.137 can be rewritten as

$$\frac{\partial p}{\partial r} = -\frac{\alpha}{k(r)h}\frac{q_t(r,t)}{r\lambda_t(r,t)}. \tag{3.138}$$

Integrating Eq. 3.138 from any radial distance r to ∞ yields

$$\int_r^\infty \frac{\partial p}{\partial r}dr = -\int_r^\infty \frac{\alpha}{h}\frac{q_t(r,t)}{\lambda_t(r,t)}\frac{dr}{rk(r)}. \tag{3.139}$$

Using the fact that the pressure when $r \longrightarrow \infty$ is equal to the initial pressure p_i, Eq. 3.139 becomes

$$\Delta p(r,t) = p(r,t) - p_i = \frac{\alpha}{h}\int_r^\infty \frac{q_t(r,t)}{\lambda_t(r,t)}\frac{dr}{rk(r)}. \tag{3.140}$$

At this point of the analysis, we distinguish two cases:

(i) For $r \leq r_f$, that is, in the inner region, we are able to write that

$$\Delta p_{in}(r,t) = \frac{\alpha}{h}\int_r^{r_f} \frac{q_t(r,t)}{\lambda_t(r,t)}\frac{dr}{rk(r)} + \frac{\alpha}{h}\int_{r_f}^\infty \frac{q_t(r,t)}{\lambda_t(r,t)}\frac{dr}{rk(r)}. \tag{3.141}$$

By adding and subtracting the same term to Eq. 3.141, we obtain

$$\Delta p_{in}(r,t) = \frac{\alpha}{h}\int_{r}^{r_f} \frac{q_t(r,t)}{\lambda_t(r,t)}\frac{dr}{rk(r)} + \frac{\alpha}{h}\int_{r_f}^{\infty} \frac{q_t(r,t)}{\lambda_t(r,t)}\frac{dr}{rk(r)} + \frac{\alpha}{h}\int_{r_w}^{r_f} \frac{q_t(r,t)}{\hat{\lambda}_o}\frac{dr}{rk(r)} - \frac{\alpha}{h}\int_{r_w}^{r_f} \frac{q_t(r,t)}{\hat{\lambda}_o}\frac{dr}{rk(r)}. \quad (3.142)$$

Note that ahead of the water front, we have $\lambda_t(r,t) = \hat{\lambda}_o$. Thus, Eq. 3.142 becomes

$$\Delta p_{in}(r,t) = \frac{\alpha}{h}\int_{r}^{r_f} \frac{q_t(r,t)}{\lambda_t(r,t)}\frac{dr}{rk(r)} + \frac{\alpha}{h\hat{\lambda}_o}\int_{r_f}^{\infty} q_t(r,t)\frac{dr}{rk(r)} + \frac{\alpha}{h\hat{\lambda}_o}\int_{r_w}^{r_f} q_t(r,t)\frac{dr}{rk(r)} - \frac{\alpha}{h\hat{\lambda}_o}\int_{r_w}^{r_f} q_t(r,t)\frac{dr}{rk(r)}, \quad (3.143)$$

that we rearrange as follows:

$$\Delta p_{in}(r,t) = \frac{\alpha}{h\hat{\lambda}_o}\int_{r_w}^{\infty} q_t(r,t)\frac{dr}{rk(r)} + \frac{\alpha}{h}\int_{r}^{r_f} \frac{q_t(r,t)}{\lambda_t(r,t)}\frac{dr}{rk(r)} - \frac{\alpha}{h\hat{\lambda}_o}\int_{r_w}^{r_f} q_t(r,t)\frac{dr}{rk(r)}. \quad (3.144)$$

The first term of the above equation represents the single-phase pressure change at the wellbore that we would obtain by injecting oil into an oil reservoir assuming the same injection rate. We will denote this term by $\Delta p_o(r_w,t)$. In addition, according to the steady-state theory of Thompson and Reynolds, the equation $q_t(r,t) = q_{inj}$ holds everywhere behind the front so that Eq. 3.144 becomes

$$\Delta p_{in}(r,t) = \Delta p_o(r_w,t) + \frac{\alpha q_{inj}}{h}\int_{r}^{r_f} \frac{1}{\lambda_t(r,t)}\frac{dr}{rk(r)} - \frac{\alpha q_{inj}}{h\hat{\lambda}_o}\int_{r_w}^{r_f} \frac{dr}{rk(r)}. \quad (3.145)$$

Here, we also add and subtract to Eq. 3.145 another term as follows:

$$\Delta p_{in}(r,t) = \Delta p_o(r_w,t) + \frac{\alpha q_{inj}}{h}\int_r^{r_f}\frac{1}{\lambda_t(r,t)}\frac{dr}{rk(r)} - \frac{\alpha q_{inj}}{h\hat{\lambda}_o}\int_{r_w}^{r_f}\frac{dr}{rk(r)} + \frac{\alpha q_{inj}}{h}\int_{r_w}^{r}\frac{1}{\lambda_t(r,t)}\frac{dr}{rk(r)} - \frac{\alpha q_{inj}}{h}\int_{r_w}^{r}\frac{1}{\lambda_t(r,t)}\frac{dr}{rk(r)}, \quad (3.146)$$

which becomes after rearranging

$$\Delta p_{in}(r,t) = \Delta p_o(r_w,t) + \frac{\alpha q_{inj}}{h\hat{\lambda}_o}\int_{r_w}^{r_f}\left(\frac{\hat{\lambda}_o}{\lambda_t(r,t)} - 1\right)\frac{dr}{rk(r)} - \frac{\alpha q_{inj}}{h\hat{\lambda}_o}\int_{r_w}^{r}\frac{\hat{\lambda}_o}{\lambda_t(r,t)}\frac{dr}{rk(r)}. \quad (3.147)$$

The first two terms of Eq. 3.147 is the well known injection solution for the pressure drop evaluated at the wellbore (see Eq. 2.8) and written as

$$\Delta p(r_w,t) = \Delta p_o(r_w,t) + \frac{\alpha q_{inj}}{h\hat{\lambda}_o}\int_{r_w}^{r_f}\left(\frac{\hat{\lambda}_o}{\lambda_t(r,t)} - 1\right)\frac{dr}{rk(r)}. \quad (3.148)$$

Therefore, the pressure distribution during injection is given by

$$\Delta p_{in}(r,t) = \Delta p(r_w,t) - \frac{\alpha q_{inj}}{h\hat{\lambda}_o}\int_{r_w}^{r}\frac{\hat{\lambda}_o}{\lambda_t(r,t)}\frac{dr}{rk(r)}. \quad (3.149)$$

It is desirable to write Eq. 3.149 in a dimensionless form. To do so, we multiply both sides of the equation by the term $\frac{kh\hat{\lambda}_w}{\alpha q_{inj}}$ in order to introduce the dimensionless pressure p_D as follows

$$\frac{kh\hat{\lambda}_w}{\alpha q_{inj}}\Delta p_{in}(r,t) = \frac{kh\hat{\lambda}_w}{\alpha q_{inj}}\Delta p(r_w,t) - \frac{kh\hat{\lambda}_w}{\alpha q_{inj}}\frac{\alpha q_{inj}}{h\hat{\lambda}_o}\int_{r_w}^{r}\frac{\hat{\lambda}_o}{\lambda_t(r,t)}\frac{dr}{rk(r)}, \quad (3.150)$$

or after simplifying and using the definition of the dimensionless mobility, $\lambda_{tD} = \frac{\lambda_t}{\hat{\lambda}_w}$,

$$p_{D,in}(r_D,t_D) = p_D(1,t_D) - \int_1^{r_D} \frac{\hat{\lambda}_w}{\lambda_t}\frac{k}{k(r_D)}\frac{dr_D}{r_D}$$
$$= p_D(1,t_D) - \int_1^{r_D} \frac{1}{\lambda_{tD}(r_D,t_D)}\frac{k}{k(r_D)}\frac{dr_D}{r_D}. \quad (3.151)$$

At the instant of shut-in t_{pD} or equivalently at $\Delta t_D = 0$, we have

$$p_{D,in}(r_D,\Delta t_D = 0) = p_D(1,t_{pD}) - \int_1^{r_D} \frac{1}{\lambda_{tD}(r_D,t_{pD})}\frac{k}{k(r_D)}\frac{dr_D}{r_D}, \quad (3.152)$$

or since we previously set $p_{D,in}(r_D,\Delta t_D = 0) = f_1(r_D)$

$$f_1(r_D) = p_D(1,t_{pD}) - \int_1^{r_D} \frac{1}{\lambda_{tD}(r_D,t_{pD})}\frac{k}{k(r_D)}\frac{dr_D}{r_D}, \quad (3.153)$$

which represents the initial condition in the invaded zone.

(ii) For $r \geq r_f$, that is if we consider the outer region, we write that

$$\Delta p_{ou}(r,t) = \frac{\alpha}{kh}\int_r^{\infty} \frac{q_t(r,t)}{\lambda_t(r,t)}\frac{dr}{r} = \frac{\alpha}{kh\hat{\lambda}_o}\int_r^{\infty} q_t(r,t)\frac{dr}{r}, \quad (3.154)$$

where again, we are using the fact that ahead of the water front, the total mobility is equal to the end-point oil mobility. We are also assuming that the water front is beyond the damaged zone. It is interesting to note from the above equation that the pressure drop during the injection in the univaded region of the reservoir is equivalent to the single-phase pressure drop based on the properties of this zone, that is oil for which an analytical expression is available in the literature (the line source solution). Therefore, Eq. 3.154 becomes

$$\Delta p_{ou}(r,t) = \omega E_i\left(-\frac{\phi\hat{c}_{to}r^2}{4\beta k\hat{\lambda}_o t}\right), \quad (3.155)$$

where ω is a constant that is determined using the continuity of the pressures at the interface r_f. Let us multiply Eq. 3.155 by $\frac{kh\hat{\lambda}_w}{\alpha q_{inj}}$. Let us also use the fact that

$$r = r_w r_D, \tag{3.156}$$

and

$$t = \frac{\phi \hat{c}_{tw} r_w^2}{\beta k \hat{\lambda}_w} t_D, \tag{3.157}$$

so that Eq. 3.155 becomes

$$\frac{kh\hat{\lambda}_w}{\alpha q_{inj}} \triangle p_{ou}(r,t) = \omega \frac{kh\hat{\lambda}_w}{\alpha q_{inj}} E_i\bigg(- \frac{\phi \hat{c}_{to} r_w^2 r_D^2 \beta k \hat{\lambda}_w}{4\beta k \hat{\lambda}_o \phi \hat{c}_{tw} r_w^2 t_D}\bigg), \tag{3.158}$$

or after simplifying,

$$p_{D,ou}(r_D, t_D) = \omega \frac{kh\hat{\lambda}_w}{\alpha q_{inj}} E_i\bigg(- \hat{M} \frac{\hat{c}_{to}}{\hat{c}_{tw}} \frac{r_D^2}{4t_D}\bigg). \tag{3.159}$$

Finally, using Eq. 3.130 in Eq. 3.159 and introducing a new constant ω_D given by

$$\omega_D = \omega \frac{kh\hat{\lambda}_w}{\alpha q_{inj}}, \tag{3.160}$$

we get

$$p_{D,ou}(r_D, t_D) = \omega_D E_i\bigg(- \eta \frac{r_D^2}{4t_D}\bigg). \tag{3.161}$$

Evaluating Eq. 3.161 at the instant of shut-in gives

$$f_2(r_D) = p_{D,ou}(r_D, \Delta t_D = 0) = \omega_D E_i\bigg(- \eta \frac{r_D^2}{4t_{pD}}\bigg). \tag{3.162}$$

As mentioned before, we use the continuity of the dimensionless pressure at the point r_{fD} in order to determine the constant ω_D. The pressure continuity is valid for any dimensionless time t_D, in particular for $t_D = t_{pD}$. For $r_D = r_{fD}$, Eqs. 3.153 and 3.162 give respectively

$$f_1(r_{fD}) = p_D(1, t_{pD}) - \int_1^{r_{fD}} \frac{1}{\lambda_{tD}(r_D, t_{pD})} \frac{k}{k(r_D)} \frac{dr_D}{r_D}, \tag{3.163}$$

and

$$f_2(r_{fD}) = \omega_D E_i\bigg(- \eta\frac{r_{fD}^2}{4t_{pD}}\bigg). \tag{3.164}$$

Continuity of pressure at the interface implies $f_1(r_{fD}) = f_2(r_{fD})$. Thus, we have

$$p_D(1, t_{pD}) - \int_1^{r_{fD}} \frac{1}{\lambda_{tD}(r_D, t_{pD})}\frac{k}{k(r_D)}\frac{dr_D}{r_D} = \omega_D E_i\bigg(- \eta\frac{r_{fD}^2}{4t_{pD}}\bigg), \tag{3.165}$$

or

$$\omega_D = \frac{1}{E_i\bigg(- \eta\frac{r_{fD}^2}{4t_{pD}}\bigg)}\bigg[p_D(1, t_{pD}) - \int_1^{r_{fD}} \frac{1}{\lambda_{tD}(r_D, t_{pD})}\frac{k}{k(r_D)}\frac{dr_D}{r_D}\bigg]. \tag{3.166}$$

Substituting Eq. 3.166 into Eq. 3.162 yields

$$f_2(r_D) = \frac{1}{E_i\bigg(- \eta\frac{r_{fD}^2}{4t_{pD}}\bigg)}\bigg[p_D(1, t_{pD}) - \int_1^{r_{fD}} \frac{1}{\lambda_{tD}(r_D, t_{pD})}\frac{k}{k(r_D)}\frac{dr_D}{r_D}\bigg] E_i\bigg(- \eta\frac{r_D^2}{4t_{pD}}\bigg), \tag{3.167}$$

which represents the dimensionless pressure profile in the outer region of the reservoir at the instant of shut-in.

3.4.3 Perturbation Method

One way to solve the IBVP described by Eqs. 3.122 to 3.129 in real time or by Eqs. 3.131 to 3.136 in Laplace space is to divide the invaded zone into several regions where the saturation is approximated by its average value within each region. By doing so, the problem is transformed into a linear, nonhomogeneous problem in Laplace space (due to the nonzero initial condition) that can be solved analytically (see [11]). Another way is to assume that the variation of the water saturation in the inner zone is small enough such that perturbation theory can be used to solve the initial boundary value problem described above. This is the method we are presenting here.

We start the analysis by writing the following equations:

$$\lambda_t = \lambda_t + \hat{\lambda}_w - \hat{\lambda}_w, \tag{3.168}$$

and

$$c_t = c_t + \hat{c}_{tw} - \hat{c}_{tw}. \tag{3.169}$$

Dividing Eq. 3.168 by $\hat{\lambda}_w$ and Eq. 3.169 by $\hat{c}_{tw}$, using Eqs. 3.120 and 3.121 and rearranging, we obtain

$$\lambda_{tD} = 1 - \frac{\hat{\lambda}_w - \lambda_t}{\hat{\lambda}_w}, \tag{3.170}$$

and

$$c_{tD} = 1 - \frac{\hat{c}_{tw} - c_t}{\hat{c}_{tw}}. \tag{3.171}$$

At this point, we define the following spatial functions

$$f_\lambda(r_D) = \frac{\hat{\lambda}_w - \lambda_t}{\hat{\lambda}_w}, \tag{3.172}$$

and

$$g_c(r_D) = \frac{\hat{c}_{tw} - c_t}{\hat{c}_{tw}}, \tag{3.173}$$

so that Eqs. 3.170 and 3.171, respectively, become

$$\lambda_{tD} = 1 - f_\lambda(r_D), \tag{3.174}$$

and

$$c_{tD} = 1 - g_c(r_D). \tag{3.175}$$

It is important to note that in absolute value, the functions f_λ and g_c do not exceed the value of 1 in the water invaded zone. We can therefore introduce the two perturbation variables ϵ and δ that we choose to define by

$$\epsilon = \max \mid f_\lambda(r_D) \mid, \tag{3.176}$$

and

$$\delta = \max \mid g_c(r_D) \mid . \tag{3.177}$$

By rescaling the functions f_λ and g_c as

$$f(r_D) = \frac{f_\lambda(r_D)}{\epsilon}, \tag{3.178}$$

and

$$g(r_D) = \frac{g_c(r_D)}{\delta}, \tag{3.179}$$

it follows that

$$\lambda_{tD} = 1 - \epsilon f(r_D), \tag{3.180}$$

and

$$c_{tD} = 1 - \delta g(r_D). \tag{3.181}$$

Since the variation of the total mobility and the total compressibility in the invaded zone are assumed to be small (see Eqs. 3.180 and 3.181), their effect on the pressure can be described by a perturbation expansion in powers of ϵ and δ given in terms of dimensionless variables in Laplace space by

$$\bar{p}_D(r_D, u) = \bar{p}_{D0}(r_D, u) + \epsilon \bar{p}_{D1}(r_D, u) + \delta \bar{p}_{D2}(r_D, u) + \epsilon\delta \bar{p}_{D3}(r_D, u) + \ldots . \tag{3.182}$$

This expression is general, that is it applies for both invaded and uninvaded regions. In the following, we assume that an adequate description of the falloff solution for the pressure can be obtained from the first three terms in the above series. Based on perturbation method, the solution of the initial value boundary problem described by Eqs. 3.131 to 3.136 is presented in Appendix B. This solution, in terms of falloff pressure in Laplace space, assumes a homogeneous reservoir with no skin effect around the well. It is given by

$$\bar{p}_{D,in}(r_D,u) = \bar{p}_{D0,in} + \epsilon\bar{p}_{D1,in} + \delta\bar{p}_{D2,in}, \tag{3.183}$$

valid for $1 \leq r_D \leq r_{fD}$ with a leading term defined by

$$\begin{aligned}\bar{p}_{D0,in} = \frac{A_1}{K_1(\sqrt{u})}\Big[K_1(\sqrt{u})I_0(\sqrt{u}r_D) + I_1(\sqrt{u})K_0(\sqrt{u}r_D)\Big] + \\ \frac{I_1(\sqrt{u})}{K_1(\sqrt{u})}K_0(\sqrt{u}r_D)\int_1^{r_{fD}}\xi_D f_1(\xi_D)K_0(\sqrt{u}\xi_D)d\xi_D + \\ K_0(\sqrt{u}r_D)\int_1^{r_D}\xi_D f_1(\xi_D)I_0(\sqrt{u}\xi_D)d\xi_D + I_0(\sqrt{u}r_D)\int_{r_D}^{r_{fD}}\xi_D f_1(\xi_D)K_0(\sqrt{u}\xi_D)d\xi_D,\end{aligned} \tag{3.184}$$

and the two terms of first order given by

$$\begin{aligned}\bar{p}_{D1,in} = \frac{A_3}{K_1(\sqrt{u})}\Big[K_1(\sqrt{u})I_0(\sqrt{u}r_D) + I_1(\sqrt{u})K_0(\sqrt{u}r_D)\Big] \\ - r_{fD}f(r_{fD})\frac{\partial\bar{p}_{D0,in}}{\partial r_D}\Big|_{r_{fD}}\frac{K_0(\sqrt{u}r_{fD})}{K_1(\sqrt{u})}\Big[K_1(\sqrt{u})I_0(\sqrt{u}r_D) + I_1(\sqrt{u})K_0(\sqrt{u}r_D)\Big] \\ - \sqrt{u}\frac{I_1(\sqrt{u})}{K_1(\sqrt{u})}K_0(\sqrt{u}r_D)\int_1^{r_{fD}}\xi_D f(\xi_D)\frac{\partial\bar{p}_{D0,in}}{\partial\xi_D}K_1(\sqrt{u}\xi_D)d\xi_D \\ + \sqrt{u}K_0(\sqrt{u}r_D)\int_1^{r_D}\xi_D f(\xi_D)\frac{\partial\bar{p}_{D0,in}}{\partial\xi_D}I_1(\sqrt{u}\xi_D)d\xi_D \\ - \sqrt{u}I_0(\sqrt{u}r_D)\int_{r_D}^{r_{fD}}\xi_D f(\xi_D)\frac{\partial\bar{p}_{D0,in}}{\partial\xi_D}K_1(\sqrt{u}\xi_D)d\xi_D,\end{aligned} \tag{3.185}$$

and

$$\bar{p}_{D2,in} = \frac{A_5}{K_1(\sqrt{u})}\Big[K_1(\sqrt{u})I_0(\sqrt{u}r_D) + I_1(\sqrt{u})K_0(\sqrt{u}r_D)\Big] + \frac{I_1(\sqrt{u})}{K_1(\sqrt{u})}K_0(\sqrt{u}r_D)\int_1^{r_{fD}} \xi_D g(\xi_D)\Big(u\bar{p}_{D0,in} - f_1(\xi_D)\Big)K_0(\sqrt{u}\xi_D)d\xi_D + I_0(\sqrt{u}r_D)\int_{r_D}^{r_{fD}} \xi_D g(\xi_D)\Big(u\bar{p}_{D0,in} - f_1(\xi_D)\Big)K_0(\sqrt{u}\xi_D)d\xi_D + K_0(\sqrt{u}r_D)\int_1^{r_D} \xi_D g(\xi_D)\Big(u\bar{p}_{D0,in} - f_1(\xi_D)\Big)I_0(\sqrt{u}\xi_D)d\xi_D. \quad (3.186)$$

In Eqs. 3.184, 3.185 and 3.186, the parameters A_1, A_3 and A_5 are functions of only the Laplace variable u. They are obtained using the continuity equations at the interface r_{fD} and are given in Appendix B by Eqs. B.120, B.133 and B.148 respectively.

For $r_D \geq r_{fD}$, the solution is written as

$$\bar{p}_{D,ou}(r_D, u) = \bar{p}_{D0,ou} + \epsilon\bar{p}_{D1,ou} + \delta\bar{p}_{D2,ou}, \quad (3.187)$$

where the terms of this expansion $\bar{p}_{D0,ou}$, $\bar{p}_{D1,ou}$ and $\bar{p}_{D2,ou}$, obtained in Appendix B, are given respectively by the following equations

$$\bar{p}_{D0,ou} = B_2K_0(\sqrt{\eta u}r_D) + \eta I_0(\sqrt{\eta u}r_D)\int_{r_D}^{\infty} \xi_D f_2(\xi_D)K_0(\sqrt{\eta u}\xi_D)d\xi_D + \eta K_0(\sqrt{\eta u}r_D)\int_{r_{fD}}^{r_D} \xi_D f_2(\xi_D)I_0(\sqrt{\eta u}\xi_D)d\xi_D, \quad (3.188)$$

$$\bar{p}_{D1,ou} = B_4K_0(\sqrt{\eta u}r_D), \quad (3.189)$$

and

$$\bar{p}_{D2,ou} = B_6K_0(\sqrt{\eta u}r_D). \quad (3.190)$$

The parameters B_2, B_4 and B_6 are also functions of u and defined by Eqs. B.121, B.134

and B.149 respectively.

3.4.4 Falloff Wellbore Pressure

The dimensionless wellbore pressure during the falloff period is evaluated by setting $r_D = 1$ in the expression for the dimensionless falloff pressure given by Eq. 3.183. Thus, we have in Laplace space

$$\bar{p}_{D,in}(1,u) = \bar{p}_{D0,in}(1,u) + \epsilon\bar{p}_{D1,in}(1,u) + \delta\bar{p}_{D2,in}(1,u), \tag{3.191}$$

where $\bar{p}_{D0,in}(1,u)$, $\bar{p}_{D1,in}(1,u)$ and $\bar{p}_{D2,in}(1,u)$ are given respectively by Eqs. 3.184, 3.185 and 3.186 and evaluated at $r_D = 1$, i.e.,

$$\begin{aligned}\bar{p}_{D0,in}(1,u) = \frac{A_1}{K_1(\sqrt{u})}\Big[K_1(\sqrt{u})I_0(\sqrt{u}) + I_1(\sqrt{u})K_0(\sqrt{u})\Big] \\ + \frac{I_1(\sqrt{u})}{K_1(\sqrt{u})}K_0(\sqrt{u})\int_1^{r_{fD}} \xi_D f_1(\xi_D)K_0(\sqrt{u}\xi_D)d\xi_D \\ + I_0(\sqrt{u})\int_1^{r_{fD}} \xi_D f_1(\xi_D)K_0(\sqrt{u}\xi_D)d\xi_D,\end{aligned} \tag{3.192}$$

$$\begin{aligned}\bar{p}_{D1,in}(1,u) = \frac{A_3}{K_1(\sqrt{u})}\Big[K_1(\sqrt{u})I_0(\sqrt{u}) + I_1(\sqrt{u})K_0(\sqrt{u})\Big] \\ - r_{fD}f(r_{fD})\frac{\partial\bar{p}_{D0,in}}{\partial r_D}\bigg|_{r_{fD}}\frac{K_0(\sqrt{u}r_{fD})}{K_1(\sqrt{u})}\Big[K_1(\sqrt{u})I_0(\sqrt{u}) + I_1(\sqrt{u})K_0(\sqrt{u})\Big] \\ - \sqrt{u}\frac{I_1(\sqrt{u})}{K_1(\sqrt{u})}K_0(\sqrt{u})\int_1^{r_{fD}} \xi_D f(\xi_D)\frac{\partial\bar{p}_{D0,in}}{\partial\xi_D}K_1(\sqrt{u}\xi_D)d\xi_D \\ - \sqrt{u}I_0(\sqrt{u})\int_1^{r_{fD}} \xi_D f(\xi_D)\frac{\partial\bar{p}_{D0,in}}{\partial\xi_D}K_1(\sqrt{u}\xi_D)d\xi_D,\end{aligned} \tag{3.193}$$

and

$$\bar{p}_{D2,in}(1,u) = \frac{A_5}{K_1(\sqrt{u})}\Big[K_1(\sqrt{u})I_0(\sqrt{u}) + I_1(\sqrt{u})K_0(\sqrt{u})\Big] + \frac{I_1(\sqrt{u})}{K_1(\sqrt{u})}K_0(\sqrt{u})\int_1^{r_{fD}} \xi_D g(\xi_D)\Big(u\bar{p}_{D0,in} - f_1(\xi_D)\Big)K_0(\sqrt{u}\xi_D)d\xi_D + I_0(\sqrt{u})\int_1^{r_{fD}} \xi_D g(\xi_D)\Big(u\bar{p}_{D0,in} - f_1(\xi_D)\Big)K_0(\sqrt{u}\xi_D)d\xi_D. \quad (3.194)$$

Using the fact that $K_1(\sqrt{u})I_0(\sqrt{u}) + I_1(\sqrt{u})K_0(\sqrt{u}) = \frac{1}{\sqrt{u}}$, these equations simplify to

$$\bar{p}_{D0,in}(1,u) = \frac{1}{\sqrt{u}K_1(\sqrt{u})}\Big[A_1 + \int_1^{r_{fD}} \xi_D f_1(\xi_D)K_0(\sqrt{u}\xi_D)d\xi_D\Big], \quad (3.195)$$

$$\bar{p}_{D1,in}(1,u) = \frac{1}{\sqrt{u}K_1(\sqrt{u})}\Big[A_3 - r_{fD}f(r_{fD})\frac{\partial \bar{p}_{D0,in}}{\partial r_D}\Big|_{r_{fD}} K_0(\sqrt{u}r_{fD}) - \sqrt{u}\int_1^{r_{fD}} \xi_D f(\xi_D)\frac{\partial \bar{p}_{D0,in}}{\partial \xi_D}K_1(\sqrt{u}\xi_D)d\xi_D\Big], \quad (3.196)$$

and

$$\bar{p}_{D2,in}(1,u) = \frac{1}{\sqrt{u}K_1(\sqrt{u})}\Big[A_5 + \int_1^{r_{fD}} \xi_D g(\xi_D)\Big(u\bar{p}_{D0,in} - f_1(\xi_D)\Big)K_0(\sqrt{u}\xi_D)d\xi_D\Big]. \quad (3.197)$$

Since the dimensionless falloff wellbore pressure is in Laplace space, the Stehfest algorithm will be used to convert it to real time space.

3.4.5 Falloff Solution for Rate Profiles

In this section, we generate an approximate analytical solution for the total rate at any point in the reservoir during the shut-in period using the perturbation method. The total flow rate through a cylinder of radius r concentric with the wellbore during the shut-in is described by the well known Darcy's law given by

$$q_s(r,\Delta t) = -\frac{kh}{\alpha}\lambda_t(r,t_p)r\frac{\partial p}{\partial r}, \tag{3.198}$$

where $\lambda_t(r,t_p)$ represents the total mobility distribution that exists in the reservoir at the instant of shut-in t_p. Introducing the dimensionless shut-in rate q_{sD} defined by the following expression

$$q_{sD}(r_D,\Delta t_D) = \frac{q_s(r,\Delta t)}{q_{inj}}, \tag{3.199}$$

and using Eqs. 3.117, 3.119 and 3.120, we obtain

$$q_{sD}(r_D,\Delta t_D) = -\frac{kh}{\alpha q_{inj}}\lambda_t(r,t_p)\frac{\alpha q_{inj}}{kh\hat{\lambda}_w}r_D\frac{\partial p_D}{\partial r_D}, \tag{3.200}$$

or simply

$$q_{sD}(r_D,\Delta t_D) = -\lambda_{tD}(r_D)r_D\frac{\partial p_D}{\partial r_D}. \tag{3.201}$$

Taking the laplace transform of Eq. 3.201 gives

$$\bar{q}_{sD}(r_D,u) = -\lambda_{tD}(r_D)r_D\frac{\partial \bar{p}_D}{\partial r_D}. \tag{3.202}$$

Previously, we solved for the dimensionless pressure profile in Laplace space. Therefore, Eq. 3.202 is useful for the determination of the dimensionless shut-in flow rate. Recall that the pressure solution has two expressions depending on the value of the radial distance and how far it is with respect to the position of the flood front (see Appendix B). Based on this, we will also consider the two regions when deriving solutions for the rate profiles.

Inner Region Rate Profile

Recall that in this region, the dimensionless falloff pressure solution is expressed by

$$\bar{p}_{D,in}(r_D,u) = \bar{p}_{D0,in} + \epsilon\bar{p}_{D1,in} + \delta\bar{p}_{D2,in}, \tag{3.203}$$

such that $\bar{p}_{D0,in}$, $\bar{p}_{D1,in}$ and $\bar{p}_{D2,in}$ are given by Eqs. 3.184, 3.185 and 3.186 respectively. Using Eq. 3.203 for the dimensionless pressure and Eq. 3.180 for the dimensionless total mobility in Eq. 3.202 gives

$$\bar{q}_{sD}(r_D,u) = -\Big(1-\epsilon f(r_D)\Big)\left[r_D\frac{\partial \bar{p}_{D0,in}}{\partial r_D} + \epsilon r_D\frac{\partial \bar{p}_{D1,in}}{\partial r_D} + \delta r_D\frac{\partial \bar{p}_{D2,in}}{\partial r_D}\right]. \tag{3.204}$$

If we rearrange Eq. 3.204, we obtain

$$\bar{q}_{sD}(r_D,u) = -r_D\frac{\partial \bar{p}_{D0,in}}{\partial r_D} - \epsilon r_D\left[\frac{\bar{p}_{D1,in}}{\partial r_D} - f(r_D)\frac{\partial \bar{p}_{D0,in}}{\partial r_D}\right] - \delta r_D\frac{\partial \bar{p}_{D2,in}}{\partial r_D} + ..., \tag{3.205}$$

that we can rewrite as

$$\bar{q}_{sD}(r_D,u) = q_{D0,in}(r_D,u) + \epsilon q_{D1,in}(r_D,u) + \delta q_{D2,in}(r_D,u) + ..., \tag{3.206}$$

where

$$q_{D0,in}(r_D,u) = -r_D\frac{\partial \bar{p}_{D0,in}}{\partial r_D}, \tag{3.207}$$

$$q_{D1,in}(r_D,u) = -r_D\left[\frac{\partial \bar{p}_{D1,in}}{\partial r_D} - f(r_D)\frac{\partial \bar{p}_{D0,in}}{\partial r_D}\right], \tag{3.208}$$

and

$$q_{D2,in}(r_D,u) = -r_D\frac{\partial \bar{p}_{D2,in}}{\partial r_D}. \tag{3.209}$$

Replacing Eq. B.106 in Eq. 3.207 gives

$$q_{D0,in}(r_D,u) = -\frac{\sqrt{u}r_D}{K_1(\sqrt{u})}\Bigg[A_1\Bigg(K_1(\sqrt{u})I_1(\sqrt{u}r_D) - I_1(\sqrt{u})K_1(\sqrt{u}r_D)\Bigg) + K_1(\sqrt{u})I_1(\sqrt{u}r_D)\int_{r_D}^{r_{fD}} \xi_D f_1(\xi_D)K_0(\sqrt{u}\xi_D)d\xi_D - K_1(\sqrt{u})K_1(\sqrt{u}r_D)\int_1^{r_D} \xi_D f_1(\xi_D)I_0(\sqrt{u}\xi_D)d\xi_D - I_1(\sqrt{u})K_1(\sqrt{u}r_D)\int_1^{r_{fD}} \xi_D f_1(\xi_D)K_0(\sqrt{u}\xi_D)d\xi_D\Bigg]. \quad (3.210)$$

By writing the last integral of Eq. 3.210 as the sum of two integrals, one from 1 to r_D and a second from r_D to r_{fD} and rearranging, we obtain

$$q_{D0,in}(r_D,u) = -\frac{\sqrt{u}r_D}{K_1(\sqrt{u})}\Bigg[A_1\Bigg(K_1(\sqrt{u})I_1(\sqrt{u}r_D) - I_1(\sqrt{u})K_1(\sqrt{u}r_D)\Bigg) + \Bigg(K_1(\sqrt{u})I_1(\sqrt{u}r_D) - I_1(\sqrt{u})K_1(\sqrt{u}r_D)\Bigg)\int_{r_D}^{r_{fD}} \xi_D f_1(\xi_D)K_0(\sqrt{u}\xi_D)d\xi_D - K_1(\sqrt{u}r_D)\int_1^{r_D} \xi_D f_1(\xi_D)\Bigg(K_1(\sqrt{u})I_0(\sqrt{u}\xi_D) + I_1(\sqrt{u})K_0(\sqrt{u}\xi_D)\Bigg)d\xi_D\Bigg]. \quad (3.211)$$

The above expression can be simplified by using the definition of H_0 and G_1 functions given respectively by Eqs. B.112 and B.113. The result is

$$q_{D0,in}(r_D,u) = -\frac{\sqrt{u}r_D}{K_1(\sqrt{u})}\Bigg[A_1G_1(\sqrt{u}r_D,\sqrt{u}) + G_1(\sqrt{u}r_D,\sqrt{u})\int_{r_D}^{r_{fD}} \xi_D f_1(\xi_D)K_0(\sqrt{u}\xi_D)d\xi_D - K_1(\sqrt{u}r_D)\int_1^{r_D} \xi_D f_1(\xi_D)H_0(\sqrt{u}\xi_D,\sqrt{u})d\xi_D\Bigg]. \quad (3.212)$$

From Eq. B.125, we have

$$\frac{\partial \bar{p}_{D1,in}}{\partial r_D} - f(r_D)\frac{\partial \bar{p}_{D0,in}}{\partial r_D} = \frac{A_3\sqrt{u}}{K_1(\sqrt{u})}\Big[K_1(\sqrt{u})I_1(\sqrt{u}r_D) - I_1(\sqrt{u})K_1(\sqrt{u}r_D)\Big]$$
$$- \sqrt{u}r_{fD}f(r_{fD})\frac{\partial \bar{p}_{D0,in}}{\partial r_D}\bigg|_{r_{fD}}\frac{K_0(\sqrt{u}r_{fD})}{K_1(\sqrt{u})}\Big[K_1(\sqrt{u})I_1(\sqrt{u}r_D) - I_1(\sqrt{u})K_1(\sqrt{u}r_D)\Big]$$
$$+ u\frac{I_1(\sqrt{u})}{K_1(\sqrt{u})}K_1(\sqrt{u}r_D)\int_1^{r_{fD}}\xi_D f(\xi_D)\frac{\partial \bar{p}_{D0,in}}{\partial \xi_D}K_1(\sqrt{u}\xi_D)d\xi_D$$
$$- uK_1(\sqrt{u}r_D)\int_1^{r_D}\xi_D f(\xi_D)\frac{\partial \bar{p}_{D0,in}}{\partial \xi_D}I_1(\sqrt{u}\xi_D)d\xi_D$$
$$- uI_1(\sqrt{u}r_D)\int_{r_D}^{r_{fD}}\xi_D f(\xi_D)\frac{\partial \bar{p}_{D0,in}}{\partial \xi_D}K_1(\sqrt{u}\xi_D)d\xi_D. \quad (3.213)$$

Here also, by writing the integral from 1 to r_{fD} as the sum of two integrals, one from 1 to r_D and a second from r_D to r_{fD} and rearranging, we obtain

$$\frac{\partial \bar{p}_{D1,in}}{\partial r_D} - f(r_D)\frac{\partial \bar{p}_{D0,in}}{\partial r_D} = \frac{\sqrt{u}}{K_1(\sqrt{u})}\Bigg[A_3\bigg(K_1(\sqrt{u})I_1(\sqrt{u}r_D) - I_1(\sqrt{u})K_1(\sqrt{u}r_D)\bigg)$$
$$- r_{fD}f(r_{fD})\frac{\partial \bar{p}_{D0,in}}{\partial r_D}\bigg|_{r_{fD}}K_0(\sqrt{u}r_{fD})\bigg(K_1(\sqrt{u})I_1(\sqrt{u}r_D) - I_1(\sqrt{u})K_1(\sqrt{u}r_D)\bigg)$$
$$- \sqrt{u}K_1(\sqrt{u}r_D)\int_1^{r_D}\xi_D f(\xi_D)\frac{\partial \bar{p}_{D0,in}}{\partial \xi_D}\bigg(K_1(\sqrt{u})I_1(\sqrt{u}\xi_D) - I_1(\sqrt{u})K_1(\sqrt{u}\xi_D)\bigg)d\xi_D$$
$$- \sqrt{u}\bigg(K_1(\sqrt{u})I_1(\sqrt{u}r_D) - I_1(\sqrt{u})K_1(\sqrt{u}r_D)\bigg)\int_{r_D}^{r_{fD}}\xi_D f(\xi_D)\frac{\partial \bar{p}_{D0,in}}{\partial \xi_D}K_1(\sqrt{u}\xi_D)d\xi_D\Bigg], \quad (3.214)$$

or by using the definition of G_1

$$\frac{\partial \bar{p}_{D1,in}}{\partial r_D} - f(r_D)\frac{\partial \bar{p}_{D0,in}}{\partial r_D} = \frac{\sqrt{u}}{K_1(\sqrt{u})}\Big[A_3G_1(\sqrt{u}r_D,\sqrt{u})$$
$$- r_{fD}f(r_{fD})\frac{\partial \bar{p}_{D0,in}}{\partial r_D}\bigg|_{r_{fD}}K_0(\sqrt{u}r_{fD})G_1(\sqrt{u}r_D,\sqrt{u})$$
$$- \sqrt{u}K_1(\sqrt{u}r_D)\int_1^{r_D}\xi_D f(\xi_D)\frac{\partial \bar{p}_{D0,in}}{\partial \xi_D}G_1(\sqrt{u}\xi_D,\sqrt{u})d\xi_D$$
$$- \sqrt{u}G_1(\sqrt{u}r_D,\sqrt{u})\int_{r_D}^{r_{fD}}\xi_D f(\xi_D)\frac{\partial \bar{p}_{D0,in}}{\partial \xi_D}K_1(\sqrt{u}\xi_D)d\xi_D\Big]. \quad (3.215)$$

Finally, replacing Eq. 3.215 into Eq. 3.208 yields

$$q_{D1,in}(r_D,u) = -\frac{\sqrt{u}r_D}{K_1(\sqrt{u})}\Bigg[A_3 G_1(\sqrt{u}r_D,\sqrt{u}) - r_{fD}f(r_{fD})\frac{\partial \bar{p}_{D0,in}}{\partial r_D}\bigg|_{r_{fD}} K_0(\sqrt{u}r_{fD})G_1(\sqrt{u}r_D,\sqrt{u}) - \sqrt{u}K_1(\sqrt{u}r_D)\int_1^{r_D}\xi_D f(\xi_D)\frac{\partial \bar{p}_{D0,in}}{\partial \xi_D}G_1(\sqrt{u}\xi_D,\sqrt{u})d\xi_D - \sqrt{u}G_1(\sqrt{u}r_D,\sqrt{u})\int_{r_D}^{r_{fD}}\xi_D f(\xi_D)\frac{\partial \bar{p}_{D0,in}}{\partial \xi_D}K_1(\sqrt{u}\xi_D)d\xi_D\Bigg]. \quad (3.216)$$

The derivative of the dimensionless pressure in the inner region (the $O(\delta)$ term) with respect to the dimensional distance r_D is given by Eq. B.139. Using this equation in Eq. 3.209 gives

$$q_{D2,in}(r_D,u) = -\frac{\sqrt{u}r_D}{K_1(\sqrt{u})}\Bigg[A_5\Big(K_1(\sqrt{u})I_1(\sqrt{u}r_D) - I_1(\sqrt{u})K_1(\sqrt{u}r_D)\Big) - I_1(\sqrt{u})K_1(\sqrt{u}r_D)\int_1^{r_{fD}}\xi_D g(\xi_D)\Big(u\bar{p}_{D0,in} - f_1(\xi_D)\Big)K_0(\sqrt{u}\xi_D)d\xi_D - K_1(\sqrt{u})K_1(\sqrt{u}r_D)\int_1^{r_D}\xi_D g(\xi_D)\Big(u\bar{p}_{D0,in} - f_1(\xi_D)\Big)I_0(\sqrt{u}\xi_D)d\xi_D + K_1(\sqrt{u})I_1(\sqrt{u}r_D)\int_{r_D}^{r_{fD}}\xi_D g(\xi_D)\Big(u\bar{p}_{D0,in} - f_1(\xi_D)\Big)K_0(\sqrt{u}\xi_D)d\xi_D\Bigg], \quad (3.217)$$

or

$$q_{D2,in}(r_D,u) = -\frac{\sqrt{u}r_D}{K_1(\sqrt{u})}\Bigg[A_5\Big(K_1(\sqrt{u})I_1(\sqrt{u}r_D) - I_1(\sqrt{u})K_1(\sqrt{u}r_D)\Big) - K_1(\sqrt{u}r_D)\int_1^{r_D}\xi_D g(\xi_D)\Big(u\bar{p}_{D0,in} - f_1(\xi_D)\Big)\Big(K_1(\sqrt{u})I_0(\sqrt{u}\xi_D) + I_1(\sqrt{u})K_0(\sqrt{u}\xi_D)\Big)d\xi_D + \Big(K_1(\sqrt{u})I_1(\sqrt{u}r_D) - I_1(\sqrt{u})K_1(\sqrt{u}r_D)\Big)\int_{r_D}^{r_{fD}}\xi_D g(\xi_D)\Big(u\bar{p}_{D0,in} - f_1(\xi_D)\Big)K_0(\sqrt{u}\xi_D)d\xi_D\Bigg]. \quad (3.218)$$

Finally, using the definition of H_0 and G_1 functions, Eq. 3.218 becomes simply

$$q_{D2,in}(r_D,u) = -\frac{\sqrt{u}r_D}{K_1(\sqrt{u})}\Bigg[A_5 G_1(\sqrt{u}r_D,\sqrt{u}) - K_1(\sqrt{u}r_D)\int_1^{r_D}\xi_D g(\xi_D)\Big(u\bar{p}_{D0,in} - f_1(\xi_D)\Big)H_0(\sqrt{u}\xi_D,\sqrt{u})d\xi_D + G_1(\sqrt{u}r_D,\sqrt{u})\int_{r_D}^{r_{fD}}\xi_D g(\xi_D)\Big(u\bar{p}_{D0,in} - f_1(\xi_D)\Big)K_0(\sqrt{u}\xi_D)d\xi_D\Bigg]. \quad (3.219)$$

Outer Region Rate Profile

In the outer region, that is $r_D \geq r_{fD}$, the total mobility is equal to the end-point oil mobility. The dimensionless mobility is then given by

$$\lambda_{tD}(r_D) = \frac{\hat{\lambda}_o}{\hat{\lambda}_w} = \frac{1}{\hat{M}}, \quad (3.220)$$

and Eq. 3.202 becomes

$$\bar{q}_{sD}(r_D,u) = -\frac{1}{\hat{M}}r_D\frac{\partial\bar{p}_{D,ou}}{\partial r_D}. \quad (3.221)$$

Since the pressure solution in the outer region is provided by

$$\bar{p}_{D,ou}(r_D,u) = \bar{p}_{D0,ou} + \epsilon\bar{p}_{D1,ou} + \delta\bar{p}_{D2,ou}, \quad (3.222)$$

such that $\bar{p}_{D0,ou}$, $\bar{p}_{D1,ou}$ and $\bar{p}_{D2,ou}$ are given by Eqs. 3.188, 3.189 and 3.190 respectively, then Eq. 3.221 for the dimensionless rate in the outer region becomes

$$\bar{q}_{sD}(r_D,u) = -\frac{1}{\hat{M}}\left[r_D\frac{\partial\bar{p}_{D0,ou}}{\partial r_D} + \epsilon r_D\frac{\partial\bar{p}_{D1,ou}}{\partial r_D} + \delta r_D\frac{\partial\bar{p}_{D2,ou}}{\partial r_D}\right]. \quad (3.223)$$

We rewrite Eq. 3.223 as

$$\bar{q}_{sD}(r_D,u) = q_{D0,ou}(r_D,u) + \epsilon q_{D1,ou}(r_D,u) + \delta q_{D2,ou}(r_D,u), \quad (3.224)$$

with

$$q_{D0,ou}(r_D,u) = -\frac{1}{\hat{M}} r_D \frac{\partial \bar{p}_{D0,ou}}{\partial r_D}, \tag{3.225}$$

$$q_{D1,ou}(r_D,u) = -\frac{1}{\hat{M}} r_D \frac{\partial \bar{p}_{D1,ou}}{\partial r_D}, \tag{3.226}$$

and

$$q_{D2,ou}(r_D,u) = -\frac{1}{\hat{M}} r_D \frac{\partial \bar{p}_{D2,ou}}{\partial r_D}. \tag{3.227}$$

Using Eq. B.107 in Eq. 3.225 gives

$$q_{D0,ou}(r_D,u) = \frac{\sqrt{\eta u} r_D}{\hat{M}} \Bigg[B_2 K_1(\sqrt{\eta u} r_D) - \eta I_1(\sqrt{\eta u} r_D) \int_{r_D}^{\infty} \xi_D f_2(\xi_D) K_0(\sqrt{\eta u}\xi_D) d\xi_D + \eta K_1(\sqrt{\eta u} r_D) \int_{r_{fD}}^{r_D} \xi_D f_2(\xi_D) I_0(\sqrt{\eta u}\xi_D) d\xi_D \Bigg]. \tag{3.228}$$

Similarly, if we replace Eqs. B.128 and B.142 in Eqs. 3.226 and 3.227 respectively, we obtain

$$q_{D1,ou}(r_D,u) = \frac{\sqrt{\eta u} r_D}{\hat{M}} B_4 K_1(\sqrt{\eta u} r_D), \tag{3.229}$$

and

$$q_{D2,ou}(r_D,u) = \frac{\sqrt{\eta u} r_D}{\hat{M}} B_6 K_1(\sqrt{\eta u} r_D). \tag{3.230}$$

3.5 Numerical Results and Validation

In this section, the numerical falloff test data for vertical and horizontal wells are investigated. For this purpose, the same data as in chapter 2 were used (see Table 2.1 and Fig. 2.6 for the relative permeability curves). The examples cited here also pertain to an unfavorable mobility case with the end-point mobility ratio given by $\hat{M} = 3.165$ and a favorable mobility case with $\hat{M} = 0.527$ (see Fig. 2.7 and Fig. 2.8 for the total

mobility as a function of water saturation for the unfavorable and favorable mobility ratio respectively). In most cases, we will present the falloff solution in terms of $\Delta p_s(\Delta t)$ defined by

$$\Delta p_s(\Delta t) = p_{wf,s} - p_{ws}(\Delta t), \tag{3.231}$$

where $p_{wf,s}$ is the pressure at the instant of shut-in. From the reservoir simulator used (see [1]), this equation is simply evaluated by subtracting the pressures $p_{ws}(\Delta t)$ obtained directly from the simulator during the falloff from the pressure $p_{wf,s} = p_{wf}(t_p)$, also taken from the simulator at the end of the injection, i.e., at t_p. The log-derivative of $\Delta p_s(\Delta t)$, defined by

$$\Delta p'_s(\Delta t) = \frac{d\Delta p_s(\Delta t)}{d\ln(t_e)}, \tag{3.232}$$

is with respect to Agarwal's equivalent time $t_e = \frac{t_p \Delta t}{t_p + \Delta t}$. These derivative data are obtained by performing a numerical differentiation on the corresponding pressure data $\Delta p_s(\Delta t)$.

3.5.1 Example 1: Skin Effect on the Wellbore Pressure Response at a Vertical Well

Recall from chapter 2 that in this example, all runs assumed an injection of water at a constant rate of $q_{inj} = 18,869$ STB/day for $t_p = 3$ days for the unfavorable case and $t_p = 1$ day for the favorable case through a complete-penetration vertical well. The reservoir, initially at a pressure $p_i = 3461$ psi, is isotropic of permeability $k = 2700$ mD and has a thickness of $h = 78.74$ ft. Subsequent to the injection period, the well was shut-in for a falloff test. The adequacy of the grid used (see a description in chapter 2) was also verified by comparing the single-phase solution based on oil properties at irreducible water saturation obtained during falloff from the simulator to the corresponding analytical solution. This comparison is illustrated in Fig. 3.1 for the unfavorable mobility case and in Fig. 3.2 for the favorable case. As we can see, we also get a good match between the two solutions. Note also the standard behavior for a pure radial flow during falloff which is similar to the injection period (see Figs. 2.9 and Fig. 2.10).

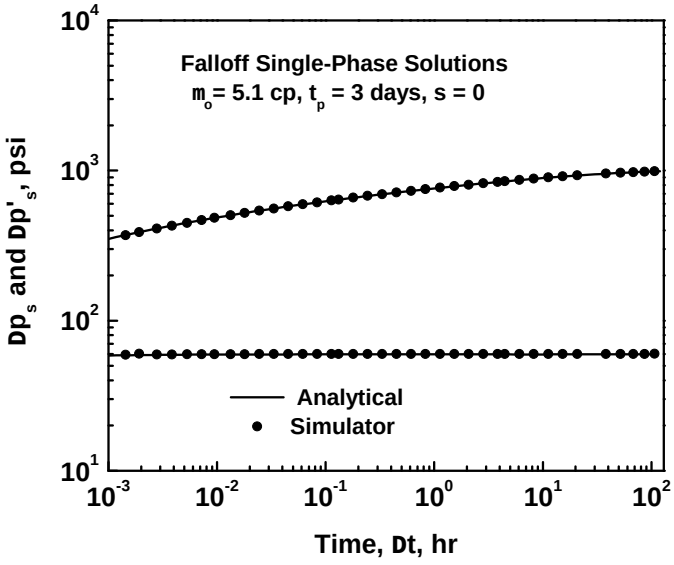

Figure 3.1: Comparison of numerical results to analytical solution for falloff, single-phase flow.

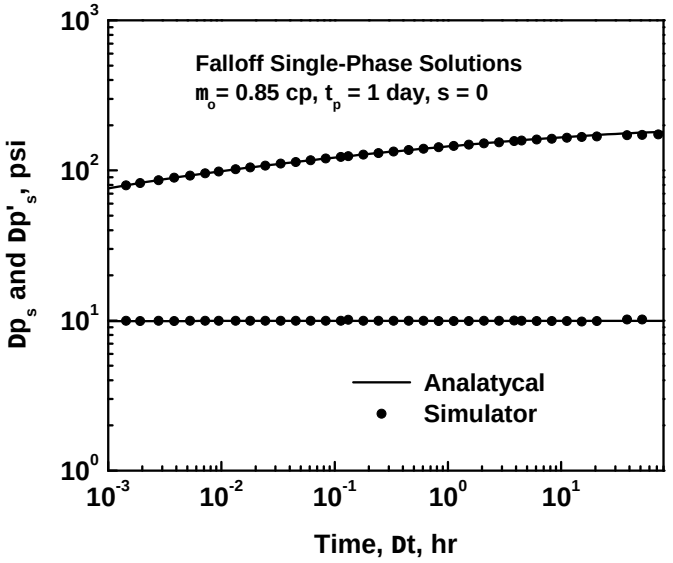

Figure 3.2: Comparison of numerical results to analytical solution for falloff, single-phase flow.

For this specific example, analytical solutions for the falloff response subsequent to water injection were constructed using two different approaches. In the first one, based on the steady-state theory, the falloff solution for the wellbore pressure change is written as the sum of the single-phase oil solution and a multiphase component. To evaluate the multiphase term, the total mobility profile at the instant of shut-in is generated using a radial Buckley-Leverett solution and total rate distributions are obtained in an ad hoc way from rate superposition. In the second approach, the perturbation method is used and the solutions for the pressure change as well as the total rate in the reservoir are presented as perturbation expansions. Solutions for rate profiles and wellbore pressure change were also generated numerically from the simulator and compared to the analytical solutions. Fig. 3.3 shows the total rate profile at five different shut-in times. The open data points curves represent results from the simulator and solid curves represent results predicted from rate superposition (Eq. 3.42). We also show in this graph in solid points results obtained when perturbation method is used (Eqs. 3.212, 3.216 and 3.219 for the invaded zone and Eqs. 3.228 to 3.230 for the uninvaded zone). Since this latter solution is given in Laplace domain, the Stefhest algorithm was used to do the inversion to the time domain. The results of Fig. 3.3 pertain to the unfavorable case. The flood front at the end of the injection for this case is located at $r_f(t_p = 3 \text{ days}) = 120.5$ ft from the wellbore according to the Buckley-Leverett theory. Fig. 3.4 shows similar results for the favorable mobility case for which the water front is at $r_f(t_p = 1 \text{ day}) = 60$ ft. Although the profiles obtained using the perturbation method exhibit oscillations (due to the numerical inversion), both methods for generating rate distributions in the reservoir during falloff match well the corresponding rate profiles extracted from the numerical simulator.

The derivation of the falloff solution assumed that the oil rate profile during the shut-in is identical to the one that would be obtained during shut-in after injection of oil at the same rate as the water injection rate. The approximate validity of this assumption is verified numerically by comparing the falloff oil rate profiles for the two situations. In Fig. 3.5, the oil rate profile and the total rate profile for the two-phase case are compared with the falloff oil rate profile for the single-phase case. This is the favorable mobility

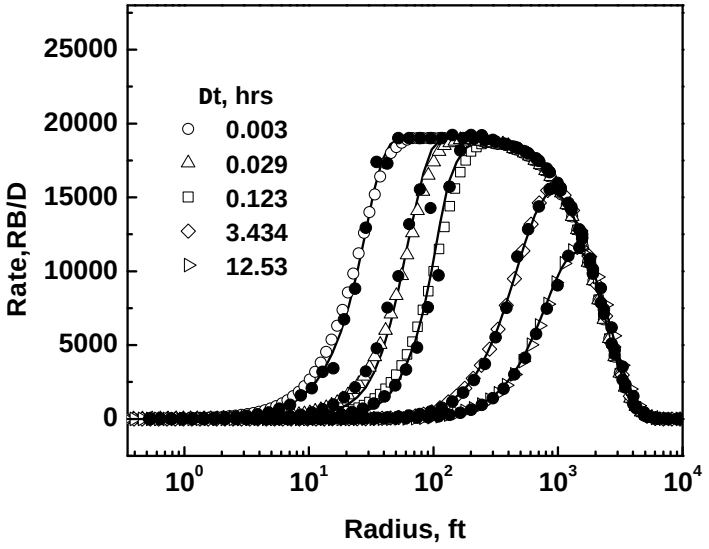

Figure 3.3: Rate profiles from the simulator, rate superposition and perturbation method, $\hat{M} = 3.165$, $t_p = 3$ days.

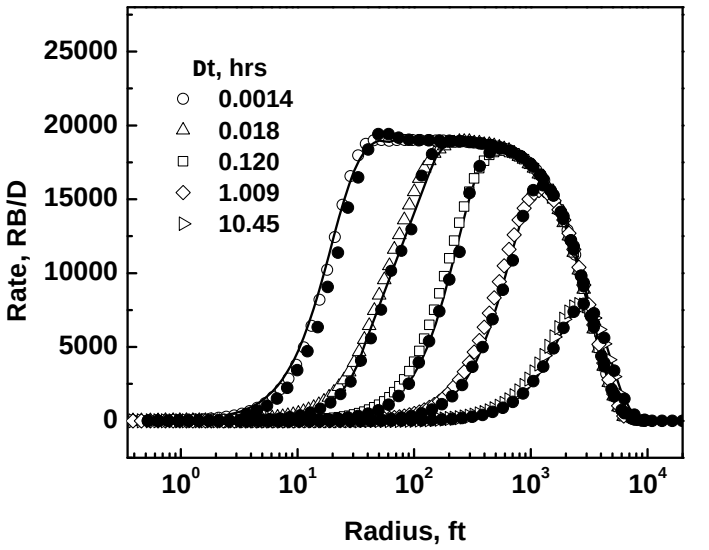

Figure 3.4: Rate profiles from the simulator, rate superposition and perturbation method, $\hat{M} = 0.527$, $t_p = 1$ day.

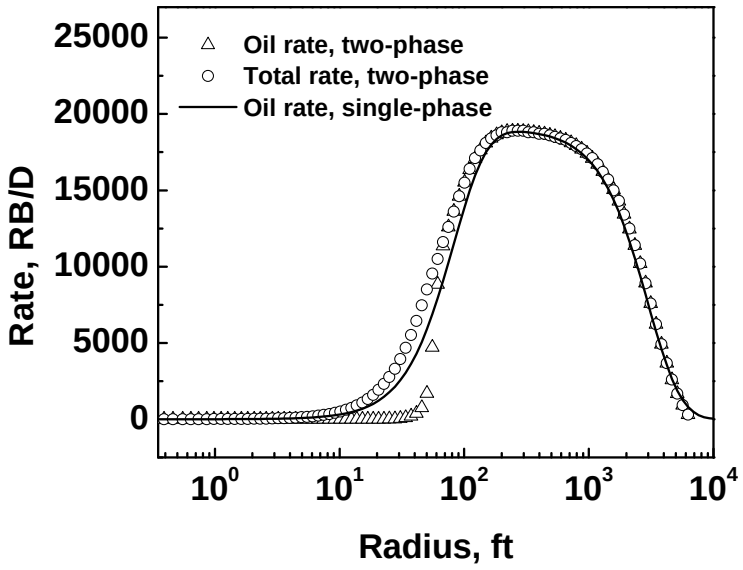

Figure 3.5: Comparison between single- and two-phase oil rate profiles during falloff, $\hat{M} = 0.527$, $\Delta t_p = 0.018$ hours.

ratio case. Note at distances farther from the well, the oil rate profiles for the single-phase and two-phase problems are similar. Therefore, we expect the assumption about the oil rate profile will not have a significant effect on the approximate falloff solution.

The falloff solution for the wellbore pressure change was generated analytically using Eq. 3.10. The integral in Eq. 3.10, which represents the multiphase pressure drop was evaluated numerically for different values of shut-in times upon the determination of the total mobility profile at the instant of shut-in from Buckley-Leverett theory and the flow rate distributions using superposition principle and the result was added to the single-phase solution based on oil properties. Fig. 3.6 presents a comparison between the analytical solution and the data from the simulator for the pressure change and its derivative with respect to equivalent time. The pressure change and its derivative are plotted versus the shut-in time Δt. Note the two sets of results match well. Fig. 3.7 presents similar results for the favorable mobility case. Again, the analytical falloff solution and its derivative are in good agreement with results obtained from the simulator. In Figs. 3.6 and 3.7, the dashed line is the semi-log slope based on oil properties at irreducible water

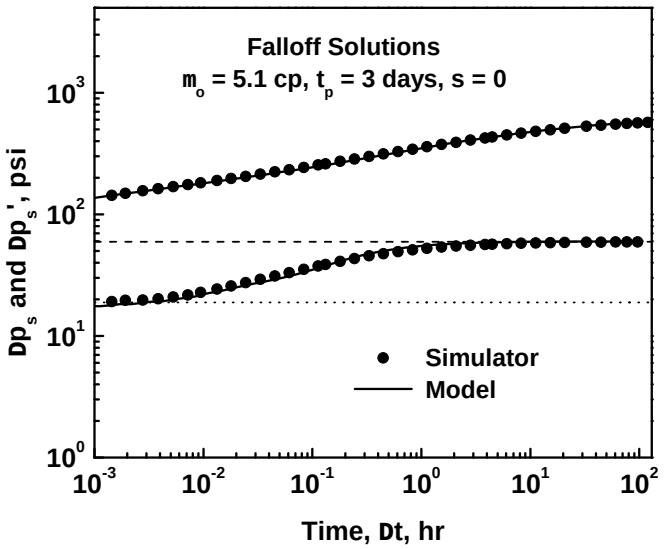

Figure 3.6: Comparison of numerical results to analytical solution (rate superposition) for falloff, zero skin case.

saturation and the dotted line represents the semi-log slope based on water properties at residual oil saturation. Note for both favorable and unfavorable cases, the derivatives reflect water properties at early times and oil properties at later times. This occurs because at early times, the rate transient due to shutting-in the well is entirely in the water bank, reflecting therefore a weighted average of mobility in the invaded zone, whereas, at later shut-in times, the rate profile becomes zero in the region behind the water front, reflecting end-point oil mobility (see Figs. 3.3 and 3.4). The duration of the transition data is about 3 log cycles (from 5×10^{-3} to 3 hours) for the unfavorable mobility case and only 1 log cycle for the favorable case (from 10^{-2} to 10^{-1} hours). Recall that for this particular case, the well was shut-in after one day of water injection (compared to 3 days of injection for the unfavorable mobility case) so the flood did not advance as far into the reservoir allowing therefore the observation of the oil bank.

When performing a Horner analysis of data (derivatives) which reflect oil properties, the falloff pressure change at the wellbore is usually represented by a straight line on a semi-log plot given by

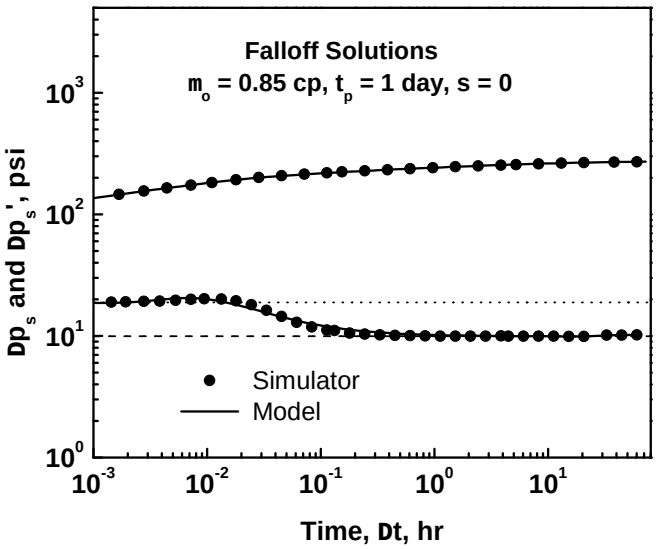

Figure 3.7: Comparison of numerical results to analytical solution (rate superposition) for falloff, zero skin case.

$$\Delta p_{ws}(\Delta t) = p_{ws} - p_i = m \log\left(\frac{t_p + \Delta t}{\Delta t}\right), \tag{3.233}$$

where m is the slope defined in terms of the reservoir properties as

$$m = \frac{162.6 q_{inj}}{kh\hat{\lambda}_o}. \tag{3.234}$$

Horner analysis also provides a total skin in the system given by the following equation

$$s_t = 1.1513\left[\frac{\Delta p_{wf}(\Delta t = 0) - \Delta p_{ws}(\Delta t = 1hour)}{m} + \log\left(\frac{t_p + 1}{t_p}\right) + 3.2275 - \log\left(\frac{k\hat{\lambda}_o}{\phi \hat{c}_{to} r_w^2}\right)\right]. \tag{3.235}$$

In Eq. 3.235, the term $\Delta p_{wf}(\Delta t = 0)$ is the wellbore pressure change at the instant of shut-in, whereas, $\Delta p_{ws}(\Delta t = 1$ hour) represents the wellbore pressure change obtained by evaluating Eq. 3.233 at $\Delta t = 1$ hour. So, by performing a Horner analysis of data

corresponding to $\Delta t > 10$ hours for the unfavorable mobility case and $\Delta t > 1$ hour for the favorable case, Eqs. 3.234 and 3.235 give $k\hat{\lambda}_o = 282.6$ mD/cp (the true value is 286 md/cp) and $s_t = -3.55$ for the unfavorable case and $k\hat{\lambda}_o = 1693$ mD/cp (the true value is 1716.2 md/cp) and $s_t = 4.75$ for the favorable case. Computation of the mechanical skin from Eq. 3.53 gives $s = -0.185$ and $s = -0.36$ for the unfavorable and favorable mobility cases, respectively, whereas the true skin factor is $s = 0$.

Next, we show the results obtained using the perturbation method. Note that this method was applied with the perturbation variables $\epsilon = 0.684$ and $\delta = 0.243$ for the unfavorable mobility case and $\epsilon = 0.34$ and $\delta = 0.044$ for the favorable case. These parameters were computed from Eq. 3.176 for ϵ and Eq. 3.177 for δ.

One important key for the use of this method to solve for the pressure drop in the reservoir during the shut-in period is to determine the pressure distribution in the reservoir at the end of the injection period which constitutes the initial condition for the problem. Based on the steady-state theory, this profile was generated in terms of the dimensionless pressure p_D using Eq. 3.153 in the invaded zone and Eq. 3.167 in the outer region of the reservoir. The resulting distribution was compared to the one obtain numerically from the simulator. This comparison is illustrated in Fig. 3.8 for the case $\hat{M} = 3.165$ and in Fig. 3.9 for the case $\hat{M} = 0.527$. Clearly, these figures indicate an excellent match between the analytical and numerical pressure profile at the instant of shut-in.

In Fig. 3.10, the analytical solution for the wellbore pressure change and its derivative with respect to the natural logarithm of equivalent time obtained from the perturbation method for the unfavorable mobility case is represented by solid triangles. The corresponding solution obtained using the reservoir simulator is shown by solid circles. The solid line in this figure is the approximate analytical solution derived using rate superposition. Excellent agreement between the pressure change curve is observed. However, except for the early and late time periods where the pressure derivative data from perturbation method match the one from the simulator and from rate superposition, a deviation between the data is noticeable in the transition zone. We believe this is due to the fact

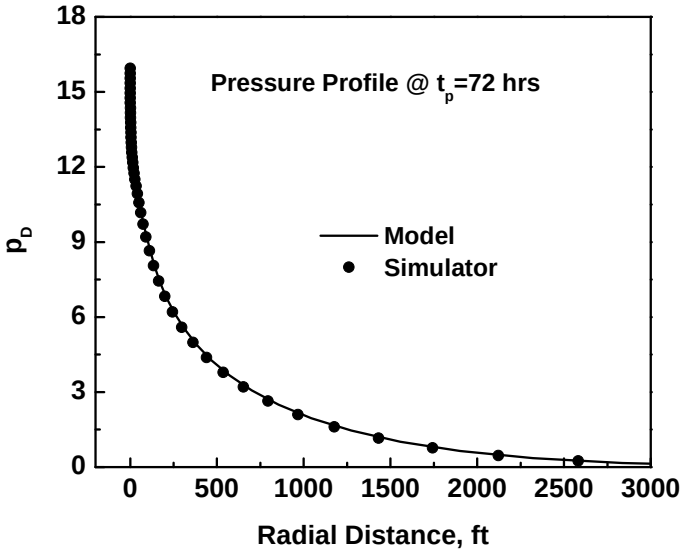

Figure 3.8: Comparison between the results for the injection pressure at the instant of shut-in $t_p = 3$ days from the simulator and the analytical solution, $\hat{M} = 3.165$.

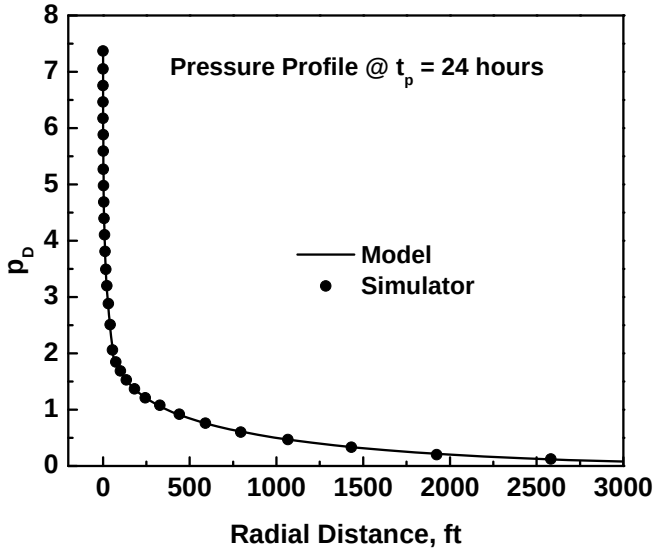

Figure 3.9: Comparison between the results for the injection pressure at the instant of shut-in $t_p = 1$ day from the simulator and the analytical solution, $\hat{M} = 0.527$.

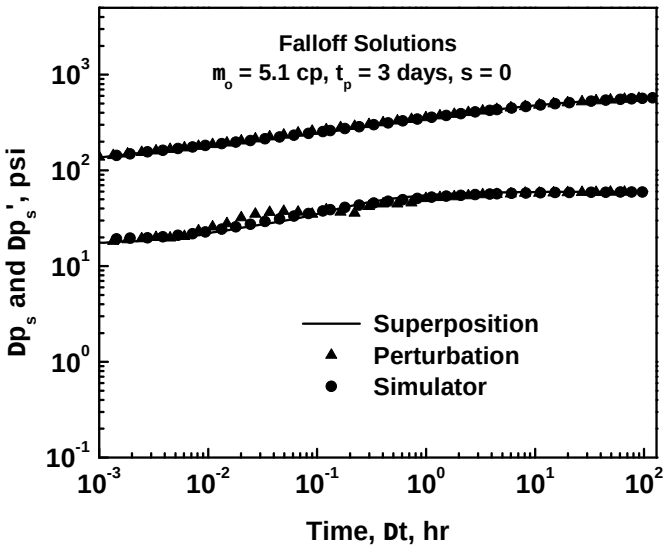

Figure 3.10: Comparison of numerical results to analytical solutions (rate superposition and perturbation) for falloff, zero skin case.

that for the unfavorable mobility case, the water saturation distribution behind the flood front is more diffused with a much smaller value of water front saturation ($S_{wf} = 0.275$) causing the mobility profile as well as the total compressibility distribution at the instant of shut-in to vary over a wider range of water saturation leading to a less accurate solution when using the perturbation method. Fig. 3.11 presents similar results for the favorable mobility case. As we can see, the match between the three solutions is quite good but the derivative of the rate superposition solution is in better agreement with the simulator results than is the perturbation solution.

Since the analytical solution is written as a perturbation expansion in powers of ϵ and δ, it is desirable to see the contribution of each term of the series to the general falloff solution. As mentioned before, the $O(\epsilon)$ term takes into account the variation of the total mobility with the water saturation in the reservoir whereas the $O(\delta)$ term deals with the variation of the total compressibility with water saturation. Fig. 3.12 displays these terms, i.e., $p_{wD,0} = p_{D0,in}(1, \Delta t)$, $p_{wD,1} = p_{D1,in}(1, \Delta t)$ and $p_{wD,2} = p_{D2,in}(1, \Delta t)$ as a function of shut-in time Δt, whereas, in Fig. 3.13, their derivatives with respect to the logarithm of equivalent time are shown. These two figures pertain to the unfavorable mobility case.

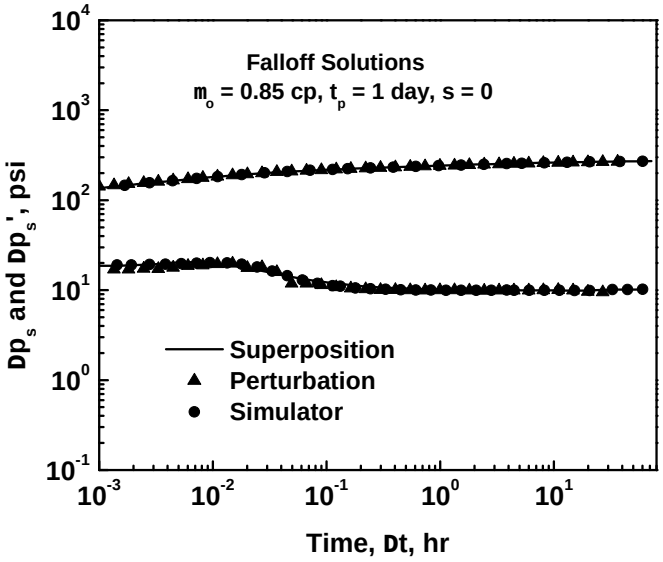

Figure 3.11: Comparison of numerical results to analytical solutions (rate superposition and perturbation) for falloff, zero skin case.

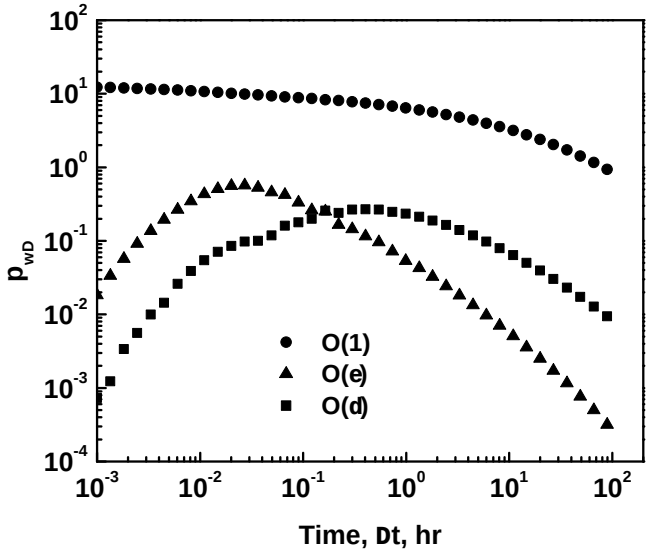

Figure 3.12: Contribution of each order to the total solution; $r_D = 1$, $\hat{M} = 3.165$.

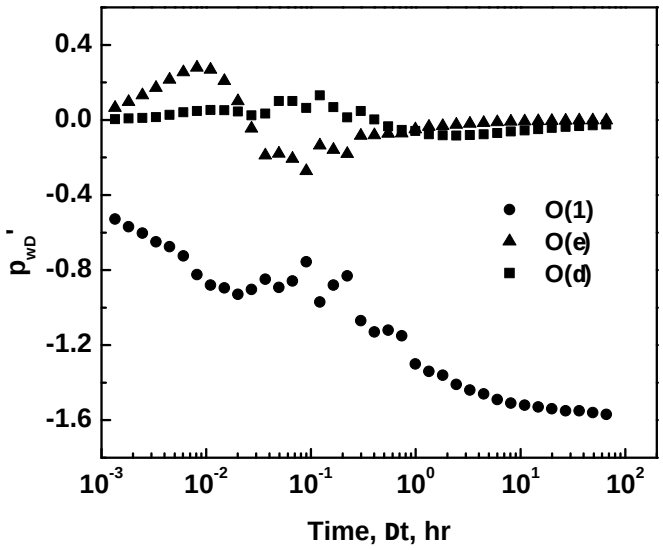

Figure 3.13: Contribution of the derivative of each order to the total solution; $r_D = 1$, $\hat{M} = 3.165$.

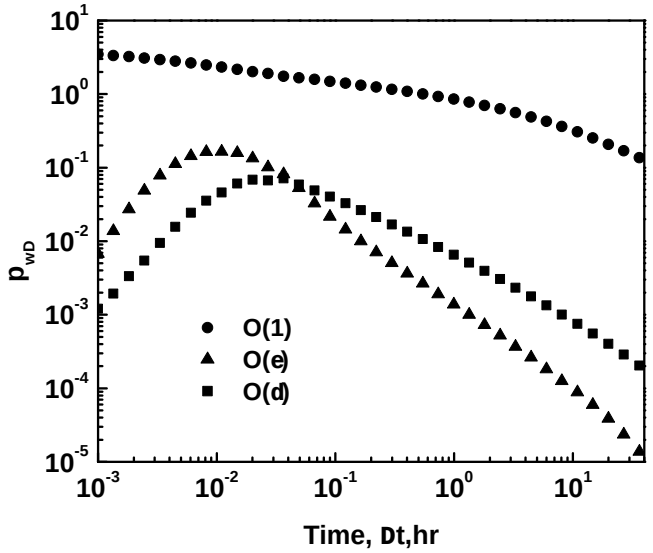

Figure 3.14: Contribution of each order to the total solution; $r_D = 1$, $\hat{M} = 0.527$.

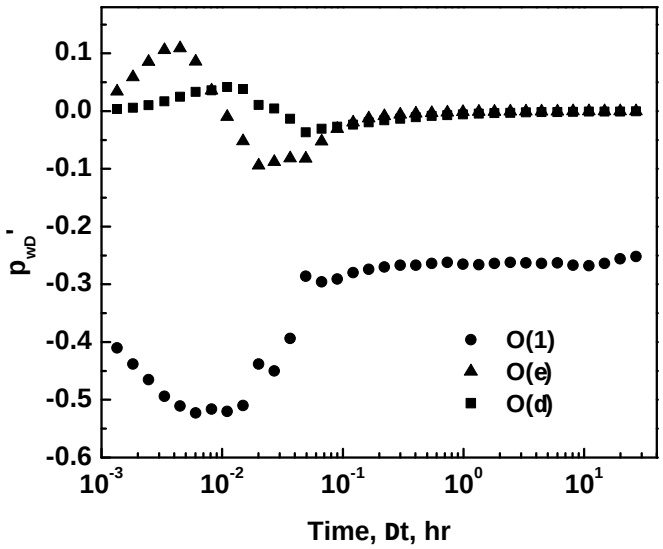

Figure 3.15: Contribution of the derivative of each order to the total solution; $r_D = 1$, $\hat{M} = 0.527$.

Note that first order terms in ϵ and δ do not contribute to the solution at very early and very late time. This is due to the fact that all the information on end-point mobilities in the water and oil banks are contained in the $O(1)$ term that behaves similarly to a piston displacement system. Note also that the contribution of the $O(\delta)$ term to the solution is very small compared to the $O(\epsilon)$ term. This result is expected since fluid and formation compressibility values were chosen small enough so that the assumption of a stationary front during the falloff holds (see Table 2.1). Finally, the variation of the $O(\epsilon)$ term in the transition zone reflects the change in the mobility with water saturation between the two banks. For the favorable mobility case, Fig. 3.14 shows the contribution of each term of the series to the total solution, that is $p_{wD,0}$, $p_{wD,1}$ and $p_{wD,2}$ as a function of shut-in time Δt, and in Fig. 3.15, their derivatives with respect to the logarithm of equivalent time are displayed. We observe a behavior similar to the unfavorable mobility case, that is a negligible contribution of the $O(\delta)$ term and the effect of the $O(\epsilon)$ term in the transition zone except that in this example, this transition zone is much smaller since it's duration is about 1 log cycle as mentioned before. Another remark is the oscillatory behavior of the pressure derivative also observed in Fig. 3.13 for the unfavorable mobility case which

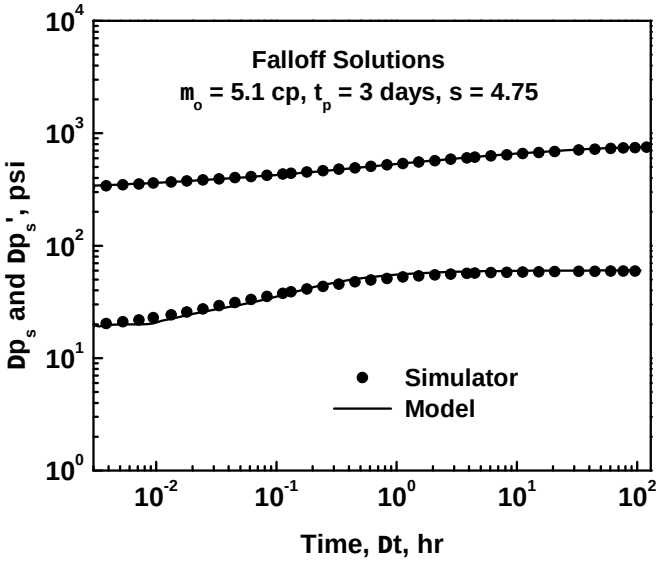

Figure 3.16: Comparison of numerical results to analytical solution (rate superposition) for falloff, nonzero skin case.

is due to the use of Stefhest algorithm as a tool to perform the numerical inversion of the solution.

Next, we redid the same problem including a positive skin factor, $s = 4.75$. Recall from chapter 2 that this value was obtained by setting $k_s = 540$ mD in a cylindrical region around the wellbore of radius $r_s = 1.15$ ft. Fig. 3.16 compares the pressure and pressure derivative solution obtained analytically using rate superposition to the corresponding data obtained from the simulator with an end-point mobility ratio of 3.165. A similar comparison presented in Fig. 3.17 is obtained with an end-point mobility ratio of 0.527. In both cases, the two sets of data agree well. These figures also show that the falloff pressure response is quite different from the injection response as the pressure derivatives do not take negative values at early times due to the skin effect.

Similarly to the zero skin case, a Horner analysis of the data corresponding to $\Delta t > 10$ hours for the unfavorable mobility case and $\Delta t > 1$ hour for the favorable case gave $k\hat{\lambda}_o = 286$ mD/cp and $s_t = -1.97$ for the unfavorable case and $k\hat{\lambda}_o = 1650$ mD/cp and $s_t = 13.3$ for the favorable case. Computation of the mechanical skin from Eq. 3.53 gives $s = 4.84$ and $s = 4.35$ for the unfavorable and favorable mobility cases respectively,

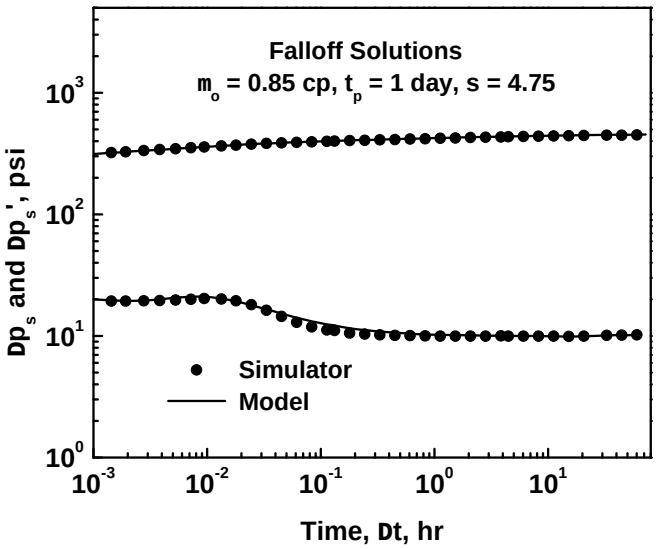

Figure 3.17: Comparison of numerical results to analytical solution (rate superposition) for falloff, nonzero skin case.

compared to the true value $s = 4.75$.

3.5.2 Example 2: Wellbore Pressure Response at a Restricted-Entry Vertical Well

Recall that in this example, water was injected through a restricted-entry vertical well of a penetration ratio $b = 0.345$ at a constant rate of $q_{inj} = 18869$ STB/day. Both the favorable and unfavorable mobility cases were considered. The test consisted of 30 days of injection followed by 20 days of shut-in. For the first run, the horizontal permeability is $k_h = k_x = k_y = 2700$ mD and the vertical permeability $k_v = 300$ mD. The isotropic equivalent permeability computed from (Eq. 2.240) is $\bar{k} = 1298$ mD. For more data pertaining to this example or for a description of the gridding used when simulating the tests, see the last section of chapter 2.

Here, we also compared the falloff single-phase solution for the wellbore pressure change and its derivative with respect to logarithm of equivalent time obtained using the simulator to the equivalent isotropic solution generated analytically using the spatial transformation. The result of the comparison is illustrated in Fig. 3.18 for the unfavorable case and in Fig. 3.19 for the favorable case. As we can see, we also obtain a good match

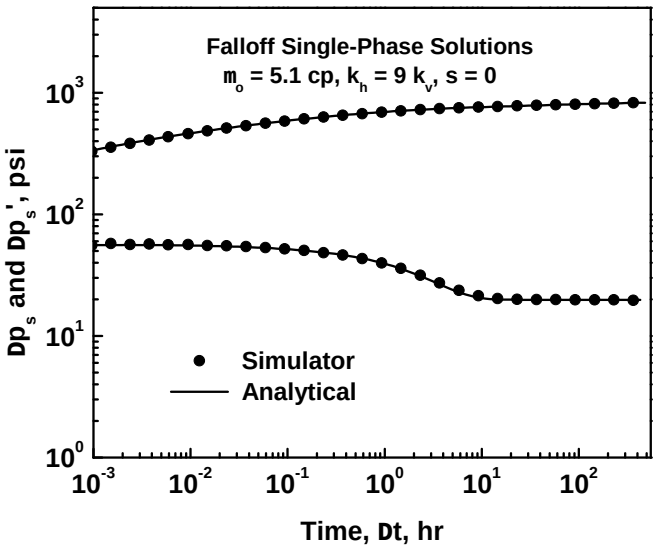

Figure 3.18: Comparison of numerical results to analytical solution for falloff, single-phase flow, $\hat{M} = 3.165$.

between the two solutions. Note also the standard behavior for a partially penetrating well during falloff which is similar to the injection period.

Fig. 3.20 compares the analytical falloff solution and its derivative with corresponding results obtained from the simulator for the case $\hat{M} = 3.165$. Model 1 was used to describe the flow of injected water when generating the total mobility profile (evaluated at the instant of shut-in). Although the analytical solution for the pressure change at the wellbore gives a reasonable match to the simulator solution, its derivative exhibits an oscillatory behavior from 0.02 to around 1 hour. Fig. 3.21 presents similar results for the case where the water saturation and total mobility distributions in the reservoir were generated using model 2. A much better agreement between the data is obtained. Note that at early times, the derivative reflects the mobility in the water bank. In particular, for $\Delta t < 0.01$ hours, the multiphase falloff solution gives a derivative value which approximately reflects the semi-log slope based on water properties at residual oil saturation over the opening interval h_p represented by a dotted line in Fig. 3.21 and given by

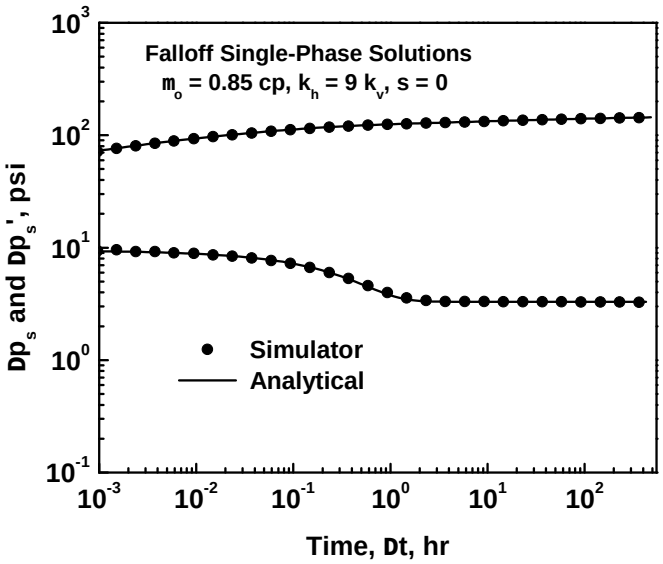

Figure 3.19: Comparison of numerical results to analytical solution for falloff, single-phase flow, $\hat{M} = 0.527$.

$$\Delta p'_s = \frac{\alpha q_{inj}}{2\bar{k}h_{pn}\hat{\lambda}_w} = \frac{\alpha q_{inj}}{2\sqrt{k_x k_y}h_p\hat{\lambda}_w} = 18.15, \tag{3.236}$$

whereas, for times greater than 10 hours, the derivative reflects the semi-log line based on oil properties at irreducible water saturation over the entire thickness of the reservoir h represented by the dashed line in the same figure and defined by

$$\Delta p'_s = \frac{\alpha q_{inj}}{2\bar{k}h_n\hat{\lambda}_o} = \frac{\alpha q_{inj}}{2\sqrt{k_x k_y}h\hat{\lambda}_o} = 19.85. \tag{3.237}$$

See also Eq. 2.385. For this case, $\hat{\lambda}_o h$ is reasonable close to $\hat{\lambda}_w h_p$ and if the data were noisy, one might interpret the model as exhibiting a single radial flow period.

Next, we consider the favorable mobility case. Since model 2 performed better than model 1, we give in the following only results obtained from model 2. In Fig. 3.22, a comparison between the analytical solution and numerical data from the simulator is illustrated. Again, a good match between the two sets of results is observed. We also note that the falloff solution reflects the end-point water mobility over the open interval (Eq. 3.236) for times $\Delta t < 0.04$ hours but eventually joins the single-phase oil solution

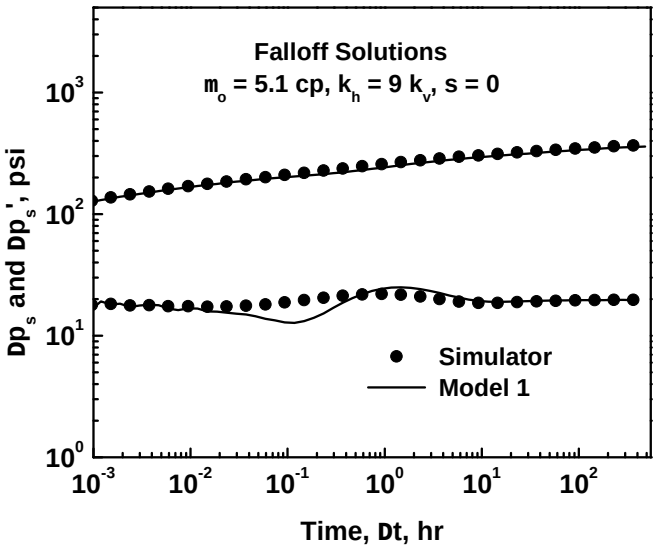

Figure 3.20: Comparison between the results for the falloff test from the simulator and the analytical solution from model 1, $\hat{M} = 3.165$, $s = 0$.

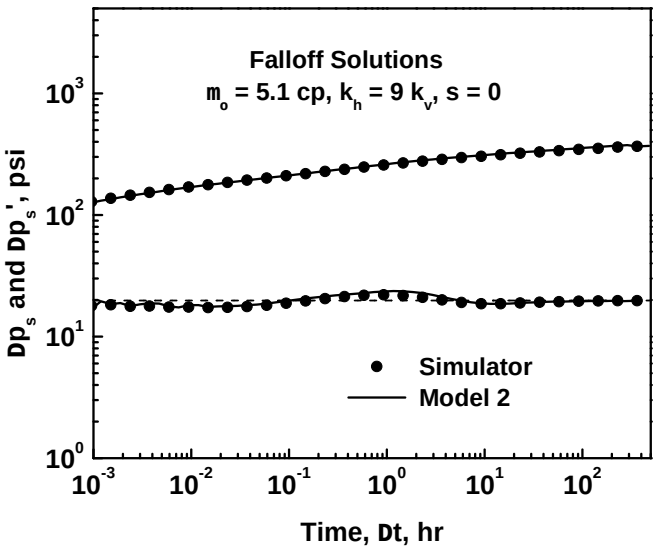

Figure 3.21: Comparison between the results for the falloff test from the simulator and the analytical solution from model 2, $\hat{M} = 3.165$, $s = 0$.

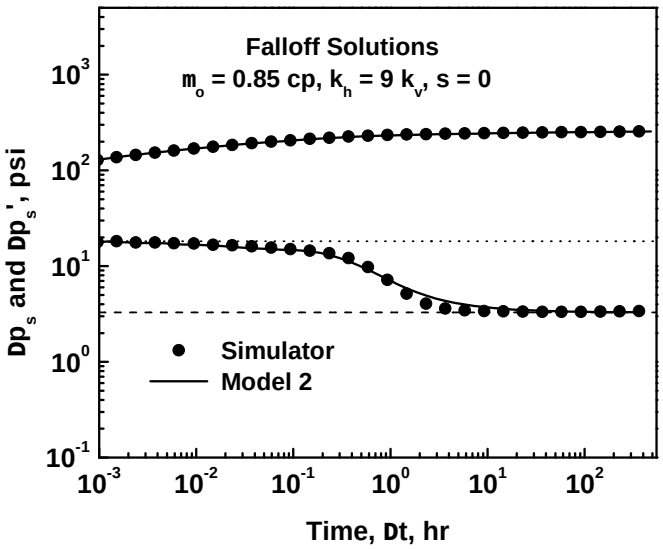

Figure 3.22: Comparison between the results for the falloff test from the simulator and the analytical solution from model 2, $\hat{M} = 0.527$, $s = 0$.

(Eq. 2.385) once a zero rate has propagated throughout the invaded region, which occurs for this case at around 10 hours.

Using the same data, a falloff solution was generated considering a mechanical skin factor of 14.9. Recall that to do so, we set the permeabilities to $k_{xs} = k_{ys} = 200$ mD and $k_{zs} = 22.22$ mD in a cylindrical region of radius $r_s = 1.15$ ft and maintained the values $k_x = k_y = 2700$ mD and $k_z = 300$ mD everywhere else. In the new coordinate system, the value of the damaged permeability is $\bar{k}_s = \sqrt[3]{k_{xs}k_{ys}k_{zs}} = 96.15$ mD and the corresponding radius of the skin zone computed using Eq. 2.368 for model 2 is $r_{sn} = 0.8$ ft. The falloff solution for the wellbore pressure change and its derivative with respect to the natural logarithm of Agarwal's equivalent time generated with model 2 was also compared against the data obtained from the simulator. Fig. 3.23 illustrates this comparison for the case $\hat{M} = 3.165$, whereas, the case $\hat{M} = 0.527$ is shown in Fig. 3.24. A good match is observed in both plots. Similarly to the zero skin factor (see Figs. 3.21 and 3.22), the pressure derivatives in both cases reflect the properties of the invaded zone over the open interval of the well at early times and the properties of the uninvaded zone over the thickness of

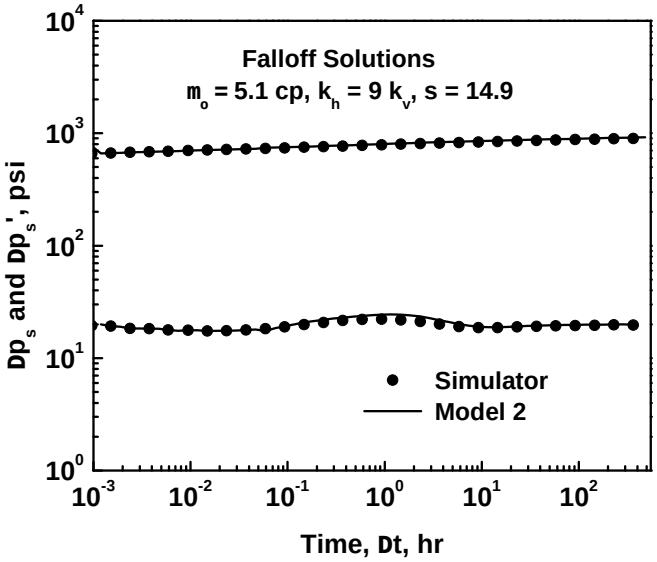

Figure 3.23: Comparison between the results for the falloff test from the simulator and the analytical solution from model 2, $\hat{M} = 3.165$, $s = 14.9$.

the reservoir at late times. However, the pressure change data are much higher than the ones obtained for the zero skin case. Clearly, this is the mechanical skin factor effect.

Based on the behavior of the pressure derivative, a Horner analysis was performed on data which reflect oil mobility. These data correspond to times $\Delta t > 20$ hours. From the semilog straight line slope displayed by the plot Δp_{ws} versus $(t_p + \Delta t)/\Delta t$, we obtained a value of $\bar{k}\hat{\lambda}_o = 139.98$ mD/cp compared to the true value of $\bar{k}\hat{\lambda}_o = 137.51$ mD/cp used in the computation for the unfavorable mobility case and a total skin of $s_t = 14.0$. Computation of the mechanical skin factor from Eq. 3.71 gave $s = 15.17$ compared to its true value of $s = 14.9$. For the favorable mobility case, a Horner analysis also performed on data corresponding to times $\Delta t > 20$ hours gave $\bar{k}\hat{\lambda}_o = 821.0$ mD/cp (the true value for this case is $\bar{k}\hat{\lambda}_o = 825.1$ mD/cp) and a total skin and a mechanical skin factor of $s_t = 107.2$ and $s = 14.3$ respectively.

The last run for the restricted-entry case assumes a completely anisotropic reservoir. An injection test of 30 days followed by a 20 days of shut-in was run using IMEX black oil simulator. The injectivity solution was discussed in the last section of chapter 2.

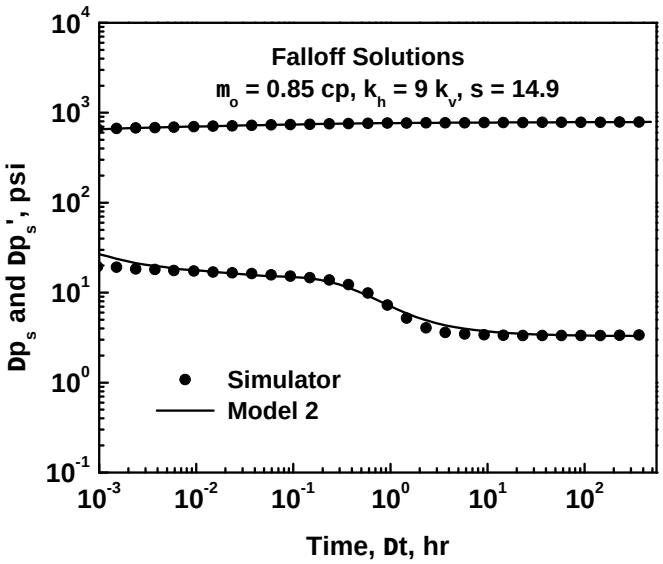

Figure 3.24: Comparison between the results for the falloff test from the simulator and the analytical solution from model 2, $\hat{M} = 0.527$, $s = 14.9$.

Here, we focus on the falloff test. We recall that the permeabilities in the three directions are given by $k_x = 2700$ mD, $k_y = 300$ mD and $k_z = 200$ mD with an isotropic equivalent permeability of $\bar{k} = 545.14$ mD and an equivalent wellbore radius $r_{we} = 0.314$ ft. All other relevant data to this run can be found in chapter 2. Here, we considered only the unfavorable mobility case. As we did previously, the solution for the pressure change and its derivative with respect to the logarithm of equivalent time under single-phase flow (based on oil properties) was obtained from the simulator and compared to the analytical solution obtained using the equivalent isotropic system during the falloff period. Fig. 3.25 is a log-log plot which illustrates this comparison. As we can see, both solutions match reasonably well. However, the numerical solution for the pressure derivative exhibits oscillations around the analytical solution at early time. Due to this early time mismatch, the analytical single-phase solution obtained for the equivalent problem was used instead in order to generate the analytical falloff pressure change.

Fig. 3.26 presents a comparison on a log-log scale between model 2 and the simulator for the pressure change and its derivative during the falloff period. Although the

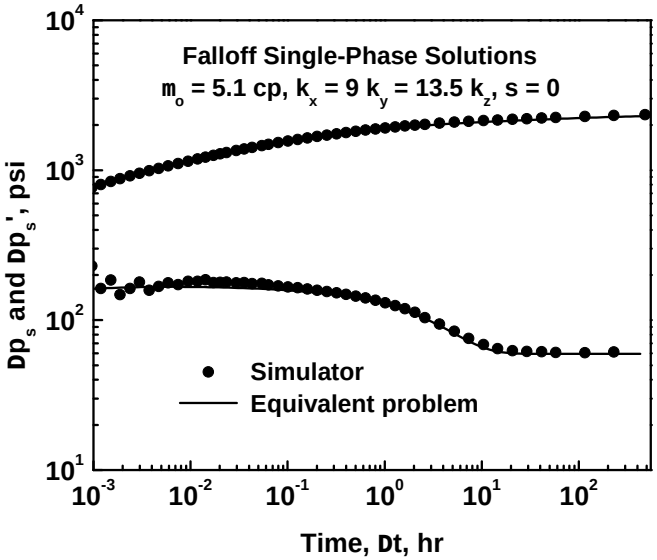

Figure 3.25: Comparison of numerical results to analytical solution for falloff, single-phase flow.

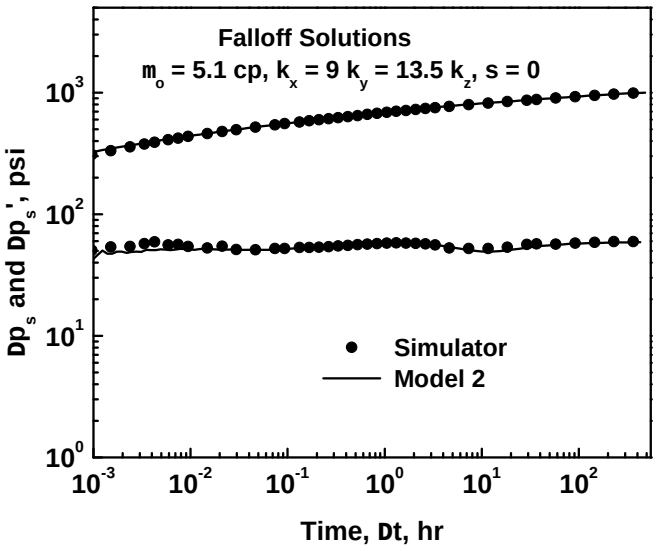

Figure 3.26: Comparison between the results for the falloff test from the simulator and the analytical solution from model 2, $\hat{M} = 3.165$, $s = 0$.

pressure derivative data generated from the simulator exhibit oscillations at early times, the analytical solution matches fairly well the numerical data for the pressure and pressure derivative. As expected, falloff data reflect mobility in the water bank at early times ($\Delta t < 0.1$ hours) corresponding to a semi-log slope given by

$$\Delta p'_s = \frac{\alpha q_{inj}}{2\bar{k}h_{pn}\hat{\lambda}_w} = \frac{\alpha q_{inj}}{2\sqrt{k_x k_y}h_p\hat{\lambda}_w} = 54.5, \tag{3.238}$$

and oil mobility at irreducible water saturation at late times (for $\Delta t > 100$ hours) corresponding to the following semi-log slope

$$\Delta p'_s = \frac{\alpha q_{inj}}{2\bar{k}h_n\hat{\lambda}_o} = \frac{\alpha q_{inj}}{2\sqrt{k_x k_y}h\hat{\lambda}_o} = 59.5. \tag{3.239}$$

Similarly to Fig. 3.20, the pressure derivative is almost constant throughout the entire falloff. Again, this is due to the fact that the product $\hat{\lambda}_w h_p$ is approximately equal to $\hat{\lambda}_o h$. Keep in mind that the only change we made for this run was the values of the permeabilities in the three directions.

3.5.3 Example 3: Wellbore Pressure Response at a Horizontal Well

This example pertains to a horizontal well distant from the top reservoir boundary of $z_w = 5$ feet. Subsequent to injection of water at a rate $q_{inj} = 31450$ STB/day for 10 days for the case $\hat{M} = 3.165$ and 4 days for the case $\hat{M} = 0.527$, the well was shut-in for a falloff test. A discussion of results obtained during the injection period is given in chapter 2. Here, we focus on the falloff period. Also given in chapter 2 is a description of the gridding (Cartesian grids combined to a local-hybrid grid refinement option) used when simulating the different cases. Recall that the first run pertains to an isotropic reservoir with $k_x = k_y = k_z = 5600$ mD with a non damaged wellbore region.

One of the steps taken to ensure the adequacy of the grid was to also compare the numerical results for single-phase flow obtained from the simulator with the analytical horizontal solution. The results, obtained for both end-point mobility ratio values are shown in Figs. 3.27 and 3.28. As we can see on these log-log plots, the numerical single-

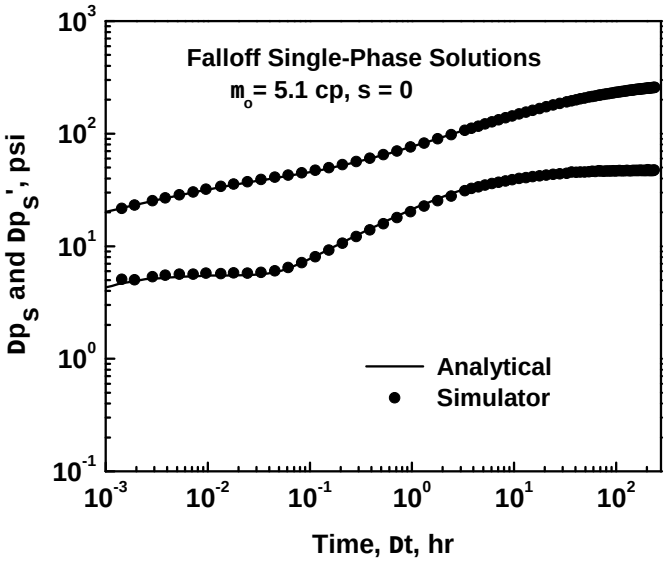

Figure 3.27: Comparison of numerical results to analytical solution for falloff single-phase flow, $\hat{M} = 3.165$, $s = 0$.

phase solutions match the analytical single-phase solutions very well. In addition, the behavior of the single-phase solution during falloff is similar to the one obtained during injection (see Figs. 2.29 and 2.30).

The generalized equation for the falloff solution in terms of the wellbore pressure change for an offset horizontal well is given by Eq. 3.88. Not only does the evaluation of this equation require the knowledge of the total mobility profiles at the instant of shut-in but also the knowledge of rate distributions in the reservoir during the shut-in period. We constructed the total mobility profiles from the water saturation distributions using a series of 1D Buckley-Leverett solutions (one for each integral in the multiphase component) evaluated at the instant of shut-in ($t_p = 10$ days for the unfavorable case and $t_p = 4$ days for the favorable case). As for the rate distributions, we computed them using the rate superposition equations (Eq. 3.42 when water is moving radially in the (x, z) plane and Eq. 3.80 for linear flow of water along the x-direction). Recall from chapter 2 that for both cases, the water front is propagating in the x-direction when the well is put to shut-in. Specifically, for model 1, the water front at the instant of shut-in is at 108.6 ft for the

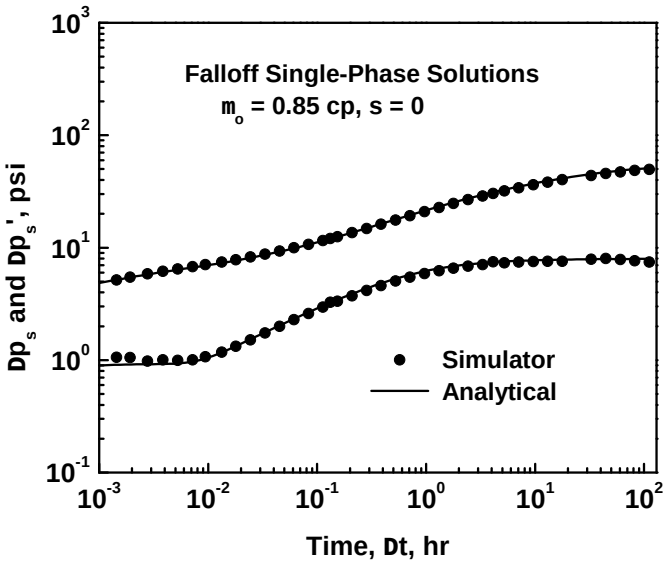

Figure 3.28: Comparison of numerical results to analytical solution for falloff single-phase flow, $\hat{M} = 0.527$, $s = 0$.

unfavorable mobility case and 40.74 ft for the favorable case. For model 2, the flood front is at 121.6 ft and 54.0 ft for the unfavorable and favorable case respectively. The falloff solution for the two-phase problem was also generated using the reservoir simulator. In Fig. 3.29, the solid circles are the numerical falloff pressure change $\Delta p_s = p_{wf,s} - p_{ws}(\Delta t)$ and its logarithmic derivative with respect to equivalent time and the solid lines represent the analytical solution for Δp_s and its derivative obtained using model 1. This figure pertains to the unfavorable mobility ratio case. Fig. 3.30 presents similar results for the favorable mobility ratio case. In both figures, the dotted line represents the semi-log line based on water properties at residual oil saturation defined by the following equation

$$\Delta p_s' = \frac{\alpha q_{inj}}{kL\hat{\lambda}_w} = 1.82, \tag{3.240}$$

and expected to be observed at early times. This slope is equal to twice the value that would be observed in the early radial flow period due to the fact that the well is offset only 5 feet from the top of the formation. The early behavior of the solution is therefore like that of a vertical well near a fault. The dashed line is the semi-log slope based on oil

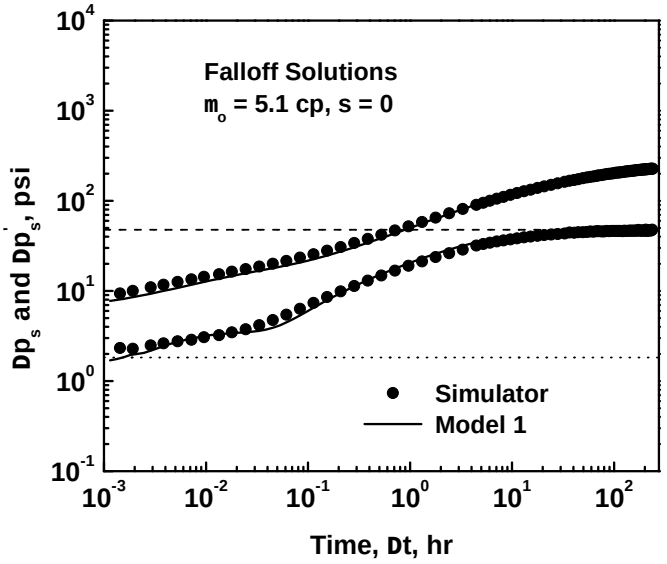

Figure 3.29: Comparison between the results for the falloff test from the simulator and the analytical solution from model 1, $\hat{M} = 3.165$, $s = 0$.

properties at irreducible water saturation given by

$$\Delta p'_s = \frac{\alpha q_{inj}}{2kh\hat{\lambda}_o} = \begin{cases} 47.90 & \text{for } \hat{M} = 3.165, \\ 7.98 & \text{for } \hat{M} = 0.527, \end{cases} \tag{3.241}$$

and observed at late times. Despite the fact that the analytical solutions generated with model 1 give a reasonable match to the simulator solutions, the derivative of the solution based on model 1 falls below the semi-log slope of Eq. 3.240 at early times specifically for the favorable mobility case (see Fig. 3.30). This behavior is not observed in the unfavorable case because the reflection of the properties of the invaded zone occurs at a much earlier time ($\Delta t < 10^{-3}$ hours). Figs. 3.31 and 3.32 compare the analytical solution for falloff and its derivative based on model 2 with the results obtained from the reservoir simulator for both cases $\hat{M} = 3.165$ and $\hat{M} = 0.527$ respectively. Better agreement is obtained when model 2 is used in terms of reflecting the semi-log slope based on water properties at early times for the favorable mobility case (see Fig. 3.32). However, the derivative of the solution generated with model 2 falls slightly below (Fig. 3.31) or slightly above (Fig. 3.32) the

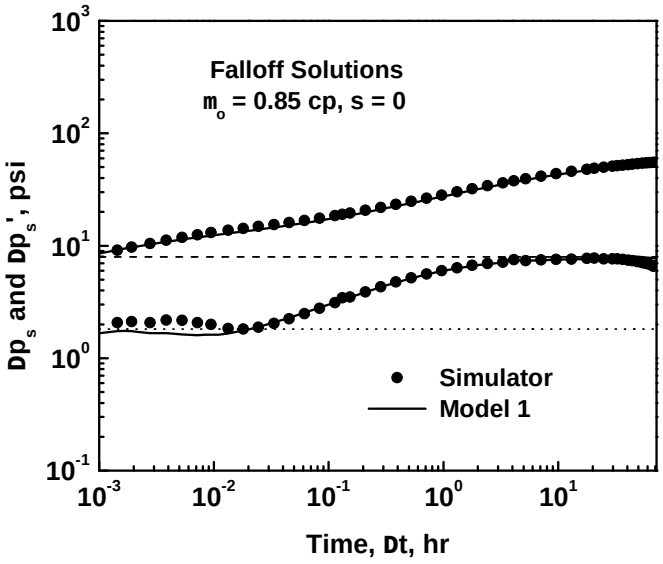

Figure 3.30: Comparison between the results for the falloff test from the simulator and the analytical solution from model 1, $\hat{M} = 0.527$, $s = 0$.

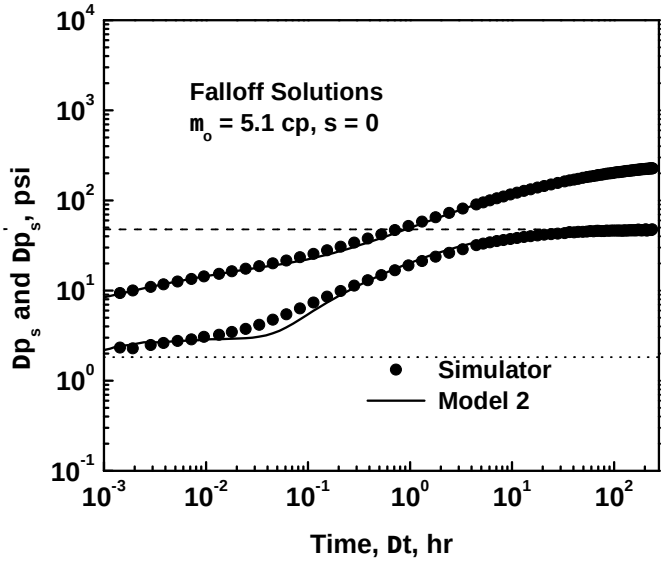

Figure 3.31: Comparison between the results for the falloff test from the simulator and the analytical solution from model 2, $\hat{M} = 3.165$, $s = 0$.

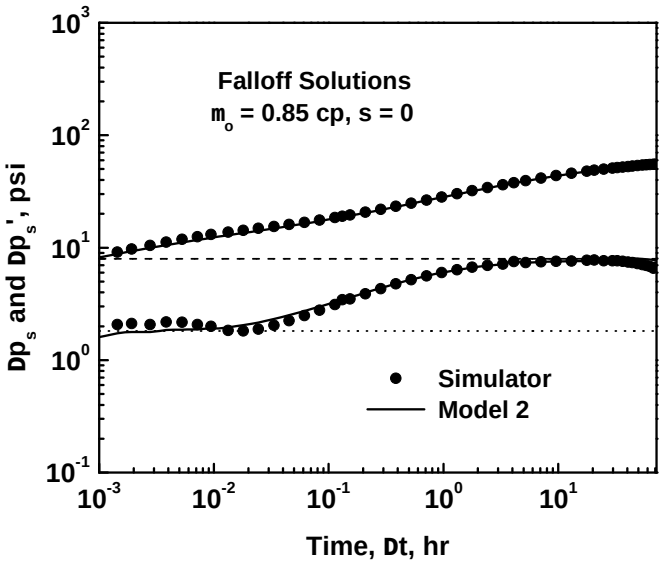

Figure 3.32: Comparison between the results for the falloff test from the simulator and the analytical solution from model 2, $\hat{M} = 0.527$, $s = 0$.

derivative from the simulator during a short time period around $0.02 < \Delta t < 0.1$ hours depending on the value of the end-point mobility ratio $\hat{M}$. Finally, we need to point out that the early time pressure derivative data from the simulator in the case of a favorable mobility ratio exhibit an oscillatory behavior in addition to the fact that they fall slightly above the dotted semi-log line based on water properties.

Next, we considered a damaged region of a radius $r_s = 1.06$ ft around and along the entire length of the horizontal well. The permeability in this region is $k_s = 200$ mD. All other parameters were kept the same as previously. The mechanical skin factor evaluated using Hawkin's formula is $s = 30$. Applying the rate superposition equations, solutions for the pressure change at the wellbore and its derivative for this case were generated analytically using model 2 and compared to results obtained numerically from the reservoir simulator. Fig. 3.33 illustrates this comparison for $\hat{M} = 3.165$ whereas, the results for the case $\hat{M} = 0.527$ are shown in Fig. 3.34. In both cases, the two sets of data agree fairly well.

Next, anisotropy was considered. The permeabilities in the three directions are

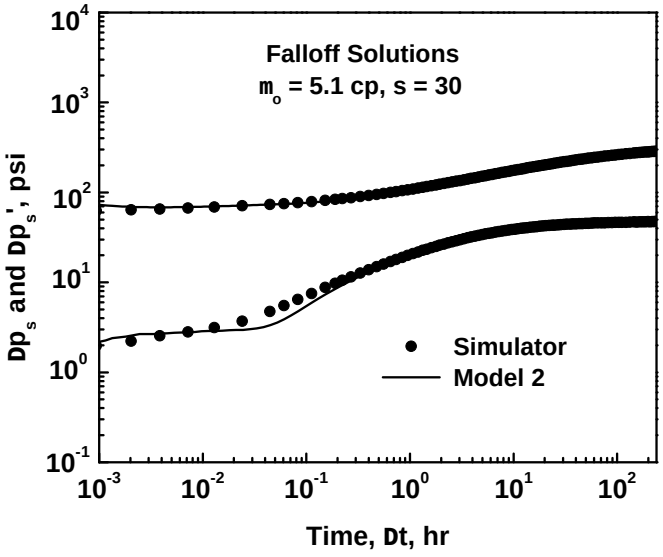

Figure 3.33: Comparison between the results for the falloff test from the simulator and the analytical solution from model 2, $\hat{M} = 3.165$, $s = 30$.

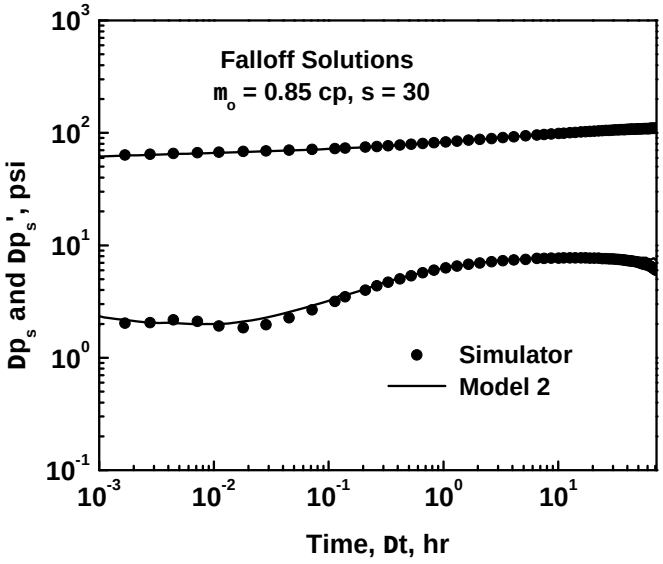

Figure 3.34: Comparison between the results for the falloff test from the simulator and the analytical solution from model 2, $\hat{M} = 0.527$, $s = 30$.

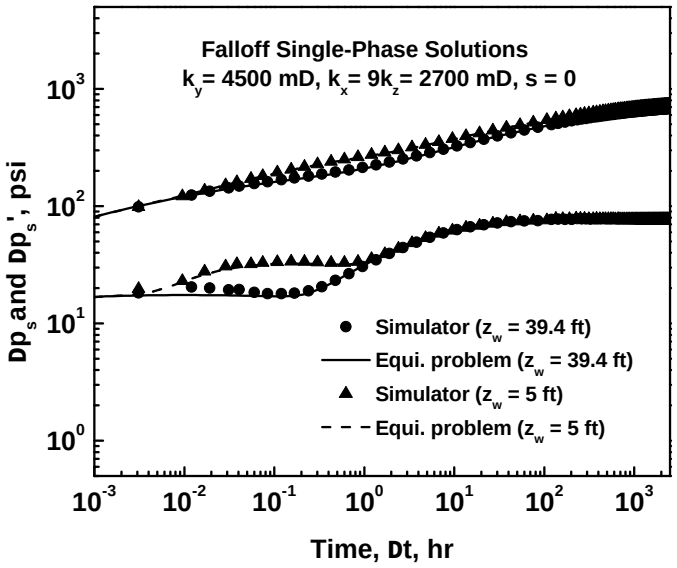

Figure 3.35: Comparison of numerical results to analytical solution for falloff, single-phase flow.

$k_x = 2700$ mD, $k_y = 4500$ mD and $k_z = 300$ mD. All other rock and fluid properties were kept the same. Here, two tests were simulated where water was injected at the same rate as previously for a period of 100 days. The well was then shut-in for a falloff test for also 100 days. Results obtained during the injection period are summarized in chapter 2. Here, we give only the results obtained during the shut-in period. Recall that in the first test, the well is located in the center of the formation, whereas in the second test, the well is closer to the top boundary with $z_w = 5$ ft. We only considered the unfavorable mobility ratio. Due to the fact that the duration of the injection is long, the water front at the instant of shut-in, according to our model, is beyond the parameter x_3. This means that the flood front reached the point where it began to move radially in the (x, y) plane.

The comparison between the falloff single-phase solution obtained analytically from the transformation and the corresponding results from the simulator are summarized for both cases in Fig. 3.35. The agreement, as we can see, is good.

In Fig. 3.36, we show the results for the falloff pressure change and its derivative generated using model 2 compared with the falloff solution obtained for the reservoir solution. Except for the slight deviation of the pressure derivative obtained from the model

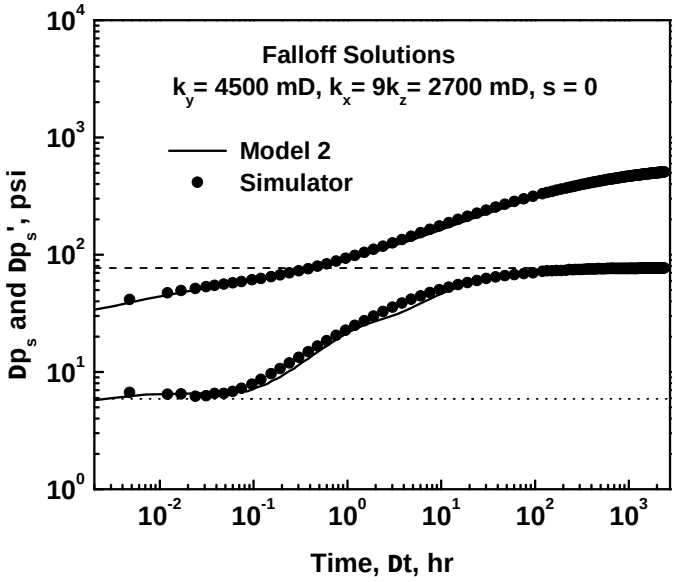

Figure 3.36: Comparison of numerical results to analytical solution for falloff, $z_w = 39.4$ ft.

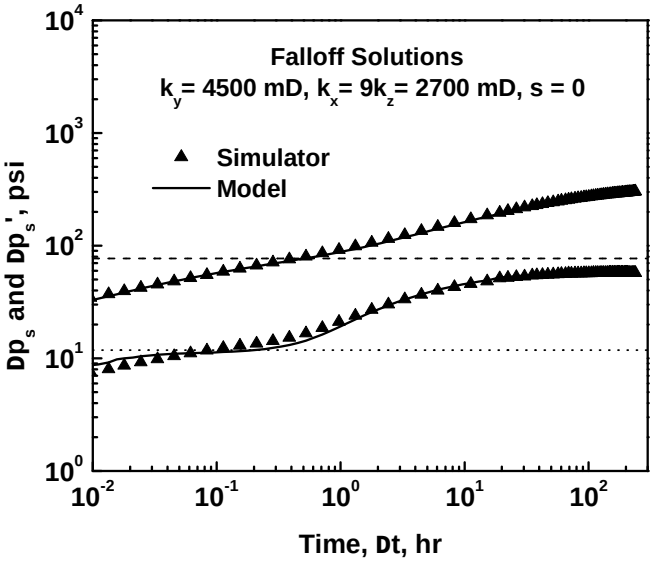

Figure 3.37: Comparison of numerical results to analytical solution for falloff, $z_w = 5$ ft.

during the intermediate times, the agreement between the sets of data seems reasonable. This figure pertains to the equal offset case. As expected, the pressure derivative reflects water mobility at early times, shown by the dotted line and oil mobility at late times represented by the dashed line. Fig. 3.37 shows the same comparison for the unequal offset case. Here also, model 2 matches fairly well the simulator solution although not as well as in the equal offset case.

3.5.4 Sensitivity Analysis on Gravity Effect

The approximate injection and falloff solutions constructed in chapter 2 and 3 assume negligible gravitational effects. However, gravity could have a significant effect on the pressure response if oil and water phases segregate. The segregation of the phases is expected to occur after some time during the falloff period. Therefore, a sensitivity study appears necessary in order to understand the role of gravity during an injection/falloff test.

To investigate the effect of gravity, a few synthetic injectivity/falloff tests through a horizontal well were generated using CMG IMEX's simulator. Two cases with respect to the location of the well were considered. The distance measured from the well axis to the top boundary of the reservoir is equal to 5 ft in one case and 73.74 ft in the other one. The total reservoir thickness and all other properties were kept the same as in the horizontal well example in an isotropic reservoir presented previously ($k = 5600$ mD and $s = 0$ case). Two injection rates were considered in this analysis. The high rate case corresponds to a value of 31450 STB/day whereas, the low rate case is one tenth of the high injection rate, that is 3145 STB/day. In all cases, a combination of a Cartesian gridding of 74(x) by 67(y) by 5(z) and a local hybrid grid of 10(r) by 4(θ) by 1(z') applied to all well blocks was used. The location of the well close to the top was simulated in layer 1 whereas, the location of the well close from the bottom boundary was in layer 5.

Fig. 3.38 compares the injection solutions obtained from the two configurations when water was injected at the high rate for a total time of 60 days. This figure indicates an excellent match between the data throughout the entire test suggesting that gravity has

no effect for this case. In Fig. 3.39, the outcome is different as a slight deviation between the data for the pressure change and its derivative is observed for times $25 < t < 130$ hours. This case pertains to the low injection rate. According to our model (model 2), this period of time coincides with times where the water front propagates linearly in the x-direction with a variable cross sectional area. The higher values of the wellbore pressure change and its derivative obtained during this time period when injecting water from the bottom are explained by the fact that in order to compete against gravitational forces, higher viscous forces (or equivalently higher pressure change since the injection rate is smaller) are required to move the flood from the bottom to the top over the variable thickness when propagating linearly. For the configuration where water is injected from the top, the direction of the flow when propagating linearly is along the direction of gravity which explains the lower values of the wellbore pressure change and its associated derivative. Another observation from Fig. 3.39 is that for a longer injection period (when $t > 130$ hours), the simulator predicts the same pressure drop for the two configurations. This period of time corresponds to the situation where water begins to propagate linearly in the x-direction but over the entire thickness of the reservoir ($x_f(t) > x_2$). The location of the well in this case, does not have any impact on the wellbore pressure response.

In Fig. 3.40, The falloff pressure change and its derivative with respect to logarithm of equivalent time for each offset are displayed on a log-log scale. These data were generated numerically considering a shut-in of 60 days subsequent to an injection of water at a rate of 31450 STB/day for a total time of 60 days. As we see, the difference between the solutions is negligible. However, when the injection rate is cut by a factor of ten, the effect of gravity is clearly observable in Fig. 3.41 manifesting through a shift between the two sets of data, particularly for the pressure derivative, for approximately $\Delta t > 60$ hours, the pressure derivative data obtained when injecting from the top being smaller than the ones obtained when injection from the bottom.

Next, we set the length of the injection to 1 day and considered the lowest injection rate. At the instant of shut-in, The water front according to model 2 is located at $x_f(t_p) = 7$ ft compared to $x_f(t_p) = 77.75$ ft obtained for $t_p = 60$ days. Fig. 3.42 shows

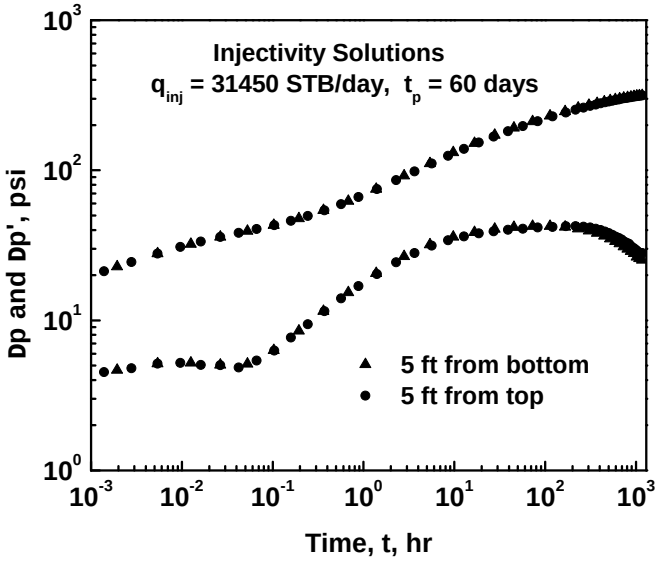

Figure 3.38: Comparison between the results for the injectivity test from the simulator; high rate case.

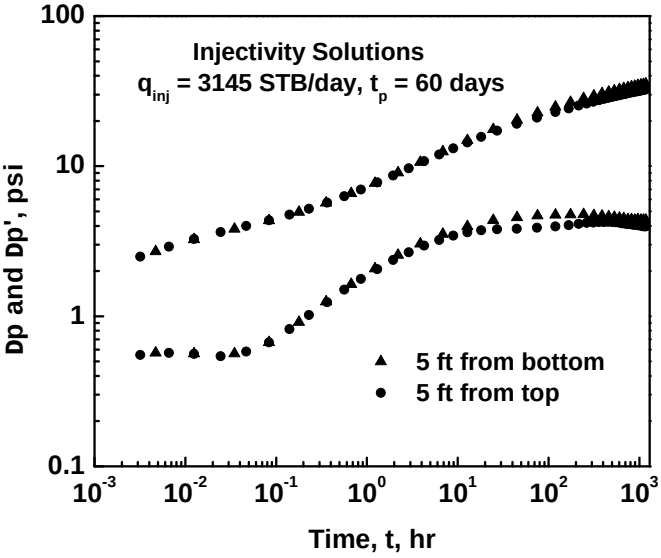

Figure 3.39: Comparison between the results for the injectivity test from the simulator; low rate case.

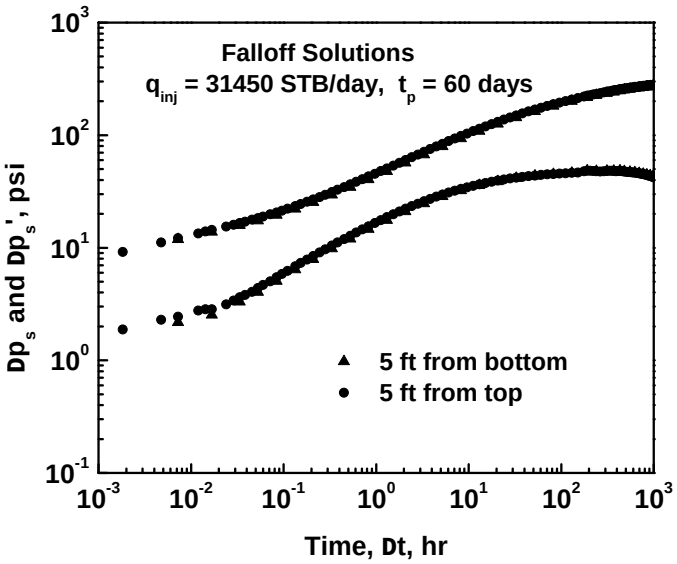

Figure 3.40: Comparison between the results for the falloff test from the simulator; high rate case.

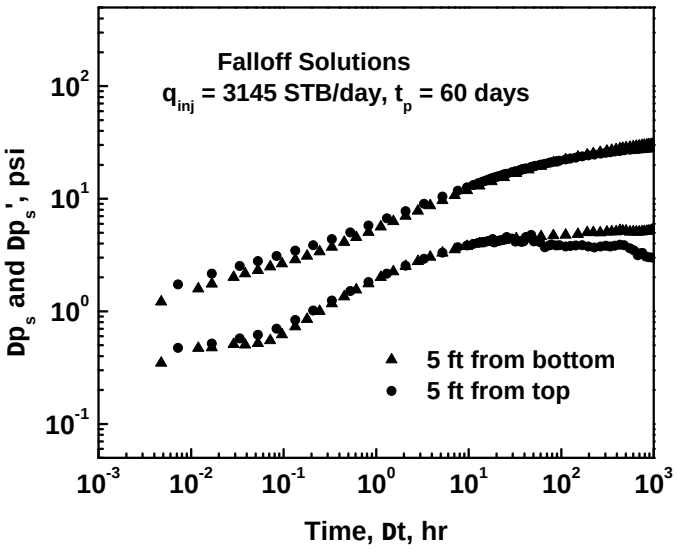

Figure 3.41: Comparison between the results for the falloff test from the simulator; low rate case.

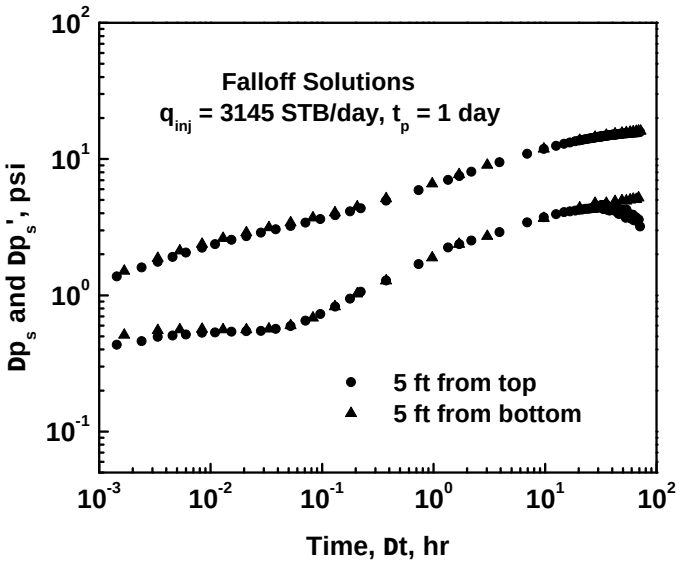

Figure 3.42: Comparison between the results for the falloff test from the simulator; low rate case.

the results when comparing the simulator data for the pressure change and its derivative obtained during the falloff period for both configurations. A mismatch between the pressure derivative data is also observed but at an earlier time ($\Delta t > 30$ hours) compared to 60 hours for the case of 60 days of injection. This is due to the fact that in the case of the long injection test, the saturation distribution of water from top to bottom is reasonably uniform with oil saturation close to residual. Thus, it is expected that it would take longer for the effect of gravity segregation to affect the wellbore pressure unlike the short injection test case.

CHAPTER 4

COLD WATERFLOODING A HOT RESERVOIR

In the previous chapters, when constructing analytical solutions for the pressure response during an injection/falloff test on water injection wells, we made an assumption that the injected fluid is at the same temperature as the in situ reservoir fluid. In practice, this is not the case since the injected water is at a lower temperature than the reservoir oil. Due to this, an expanding cold region develops around the wellbore during the injection and because the fluid viscosities are temperature dependant, this will affect the pressure response during the test. This chapter considers thermal effects that arise when flooding a reservoir with water having a temperature considerably below that of the reservoir.

4.1 Heat Transfer in Porous Media

Heat transfer must occur whenever there exists a temperature difference in a medium or between media. When cold water is injected into a hot reservoir, the formation around the water injector will cool down to the temperature of the injected water. This creates a cold water bank around the injector which expands with time into the reservoir. Both the solid and fluid phases contribute to the heat transfer. The heat exchange in the reservoir occurs mainly through three processes: heat conduction, convective heat transfer and heat transfer by radiation. From an atomistic point of view, conduction is pictured as the transfer of energy from the more energetic to the less energetic molecules in materials due to interactions between them without any displacement. Macroscopically, conduction is the transfer of heat through materials without net mass motion of the material. The mathematical description of heat conduction is based on Fourier's law given by

$$\vec{q_c} = -\bar{\bar{K}}.\vec{\nabla}T, \tag{4.1}$$

where $\vec{q_c}$ represents the rate of heat transfer per unit area or the heat flux and $\vec{\nabla}T$ is the temperature gradient. The tensor $\bar{\bar{K}}$ is referred to as the thermal conductivity tensor. Eq. 4.1 assumes an anisotropic medium. For an isotropic case, the thermal conductivity is a scalar. In a porous medium, conduction manifests itself not only through heat transfer in the solid phase (rock) but also in the fluids contained in the void space of the porous medium. Moreover, conductive heat transfer that occurs in the reservoir can be split up into two processes: horizontal conduction occurring in the direction of fluid flow and vertical conduction that happens perpendicular to the overlying and underlying strata.

Convection is a mechanism of thermal energy transferred by a collective motion of a large number of molecules in fluids in the presence of a temperature gradient. For a porous medium, convection also occurs between a fluid in motion and a solid bounding surface (rock) when the two are at different temperature. The fundamental equation for this type of heat exchange is called "Newton's cooling law" and is expressed in terms of a heat flux as

$$q_v = h(T_r - T_f), \tag{4.2}$$

where T_r and T_f are the temperature of the solid phase and the temperature of the fluid flowing past it. The coefficient h is referred to as heat transfer coefficient.

Thermal radiation is energy emitted by matter when changes in the electron configurations of the constituent atoms or molecules occur. This thermal energy is transferred by photons (electromagnetic waves) which propagate at the speed of light without attenuation (and therefore efficiently) if the medium is a vacuum. All substances emit and receive radiation continuously. The heat flux at which radiation is emitted from a material of absolute temperature T obeys to the Stefan-Boltzmann law given by

$$q_r = \epsilon\sigma T^4, \tag{4.3}$$

where σ is the Stefan-Botzmann constant of numerical value $\sigma = 1.714\times10^{-9} BTU.ft^{-2}.h^{-1}.R^{-4}$ and ϵ is a radiative property of the surface called the emissivity. Its value which lies between 0 and 1 indicates how efficiently the substance emits compared to a black body characterized by $\epsilon = 1$.

For a porous media, thermal radiation usually manifests itself through heat transfer between solid grains of the formation. In order for this process to play an important role in heat exchange, the fluid occupying the pores has to be gas. Clearly, this work is limited to the study of oil and water flow and therefore, heat transfer by thermal radiation will be neglected.

In the following, we write the mass and energy conservation equations that describe the nonisothermal two-phase problem as dictated by the laws of physics. We start by considering a small element of a porous medium of volume $\Delta V = r\Delta r\Delta\theta\Delta z$. The law of conservation of mass for each phase m flowing through this differential element is given in terms of rates by

$$\begin{aligned} r\Delta\theta\Delta z\rho_m u_{mr}|_r\Delta t - r\Delta\theta\Delta z\rho_m u_{mr}|_{(r+\Delta r)}\Delta t + \Delta r\Delta z\rho_m u_{m\theta}|_\theta\Delta t \\ - \Delta r\Delta z\rho_m u_{m\theta}|_{(\theta+\Delta\theta)}\Delta t + r\Delta r\Delta\theta\rho_m u_{mz}|_z\Delta t - r\Delta r\Delta\theta\rho_m u_{mz}|_{(z+\Delta z)}\Delta t = \\ r\Delta r\Delta\theta\Delta z\rho_m S_m\phi|_{(t+\Delta t)} - r\Delta r\Delta\theta\Delta z\rho_m S_m\phi|_t, \quad (4.4) \end{aligned}$$

where the first term of the left hand side of this equation represents the mass of the phase m entering the elementary volume ΔV during the time Δt along the r-direction whereas the second quantity of the same side is the mass of the phase m leaving the differential volume at the same time increment Δt along the same direction. Similarly, the remaining terms of the left hand side represent the net mass transported along the θ and the z-direction respectively. The right hand side of Eq. 4.4 is the mass of the phase m that accumulated within the differential volume during the time Δt. The subscript "m" would be "o" for oil or "w" for water and $\vec{u}_m$ is the vector velocity of the phase m given by Darcy's law as follows

$$\vec{u}_m = -\frac{kk_{rm}}{\mu_m}\left(\vec{\nabla}p_m - \rho_m\vec{g}\right). \tag{4.5}$$

Dividing Eq. 4.4 by $r\Delta r\Delta\theta\Delta z\Delta t$ and rearranging yields

$$-\frac{1}{r\Delta r}\left(r\rho_m u_{mr}|_{(r+\Delta r)} - r\rho_m u_{mr}|_r\right) - \frac{1}{r\Delta\theta}\left(\rho_m u_{m\theta}|_{(\theta+\Delta\theta)} - \rho_m u_{m\theta}|_\theta\right)$$
$$-\frac{1}{\Delta z}\left(\rho_m u_{mz}|_{(z+\Delta z)} - \rho_m u_{mz}|_z\right) = \frac{1}{\Delta t}\left(\rho_m S_m\phi|_{(t+\Delta t)} - \rho_m S_m\phi|_t\right). \tag{4.6}$$

In the limit, as $\Delta r \longrightarrow 0$, $\Delta\theta \longrightarrow 0$, $\Delta z \longrightarrow 0$ and $\Delta t \longrightarrow 0$, the mass equation reduces to

$$-\frac{1}{r}\frac{\partial}{\partial r}\left(r\rho_m u_{mr}\right) - \frac{1}{r}\frac{\partial}{\partial\theta}\left(\rho_m u_{m\theta}\right) - \frac{\partial}{\partial z}\left(r\rho_m u_{mz}\right) = \frac{\partial}{\partial t}\left(\rho_m S_m\phi\right), \tag{4.7}$$

or simply

$$\frac{\partial}{\partial t}\left(\rho_m S_m\phi\right) + \vec{\nabla}.(\rho_m\vec{u}_m) = 0, \tag{4.8}$$

which represents the general mass conservation equation. If fluids are considered incompressible, then ρ_m with $m = w, o$ is constant and Eq. 4.8 simplifies to

$$\frac{\partial}{\partial t}\left(S_m\phi\right) + \vec{\nabla}.(\vec{u}_m) = 0. \tag{4.9}$$

For simplicity, if only one dimensional radial flow is considered and if in addition, we assume the reservoir porosity to be constant, Eq. 4.9 becomes

$$\phi\frac{\partial S_w}{\partial t} + \frac{1}{r}\frac{\partial}{\partial r}\left(ru_w\right) = 0, \tag{4.10}$$

for water and

$$\phi\frac{\partial S_o}{\partial t}+\frac{1}{r}\frac{\partial}{\partial r}\Big(ru_o\Big)=0, \tag{4.11}$$

for oil. The sum of Eqs. 4.10 and 4.11 is

$$\phi\frac{\partial}{\partial t}(S_o+S_w)+\frac{1}{r}\frac{\partial}{\partial r}\Big(r(u_o+u_w)\Big)=0, \tag{4.12}$$

but because $S_o+S_w=1$, then

$$\frac{1}{r}\frac{\partial}{\partial r}\Big(r(u_o+u_w)\Big)=0, \tag{4.13}$$

which indicates that the product $r(u_o+u_w)$ is constant. By introducing the water fractional flow defined by

$$f_w=\frac{u_w}{u_o+u_w}, \tag{4.14}$$

it is easy to show that we can rewrite Eq. 4.10 as

$$\phi\frac{\partial S_w}{\partial t}+\frac{1}{r}\frac{\partial}{\partial r}\Big(r(u_w+u_o)f_w\Big)=0, \tag{4.15}$$

or simply

$$\phi\frac{\partial S_w}{\partial t}+u\frac{\partial f_w}{\partial r}=0, \tag{4.16}$$

with $u=u_w+u_o$ representing the total fluid velocity. As we saw previously, the water fractional flow is given by Eq. 4.14 which we can rewrite using Darcy's law with gravity and capillary effects neglected as

$$f_w=\frac{1}{1+u_o/u_w}=\frac{1}{1+\frac{k_{ro}(S_w)}{k_{rw}(S_w)}\frac{\mu_w(T)}{\mu_o(T)}}. \tag{4.17}$$

Eq. 4.17 clearly shows that not only is the water fractional flow a function of water saturation, but also a function of temperature, that is $f_w=f_w(S_w,T)$. Thus, we can expand the Buckley-Leverett Eq. 4.16 to finally obtain

$$\frac{\partial S_w}{\partial t} + \frac{u}{\phi}\left[\frac{\partial f_w}{\partial S_w}\frac{\partial S_w}{\partial r} + \frac{\partial f_w}{\partial T}\frac{\partial T}{\partial r}\right] = 0. \tag{4.18}$$

Now, let us express the law of conservation of energy for each phase flowing through the differential element ΔV during the time Δt. Again, the system considered here is cylindrical of thickness Δr and length Δz. The equation of change for internal energy given usually in textbooks (see for example [10]) is expressed as

$$\begin{pmatrix}\text{rate of increase}\\ \text{in internal energy}\\ \text{in } \Delta V \text{ during } \Delta t\end{pmatrix} = \begin{pmatrix}\text{net rate of addition}\\ \text{of internal energy}\\ \text{by convective transport}\end{pmatrix} + \begin{pmatrix}\text{net rate of addition}\\ \text{of internal energy}\\ \text{by heat conduction}\end{pmatrix} + \begin{pmatrix}\text{rate of internal}\\ \text{energy increase by thermal}\\ \text{expansion or compression}\end{pmatrix} + \begin{pmatrix}\text{rate of internal}\\ \text{energy increase by}\\ \text{viscous dissipation}\end{pmatrix}. \tag{4.19}$$

Note that Eq. 4.19 does not include radiative, nuclear or chemical forms of energy. Note also that the right hand side of this equation contains two additional terms that contribute to heat transfer. They represent the work done on the moving fluids by pressure forces (thermal expansion or contraction) and by viscous forces respectively. According to the literature ([8] and [22]), the thermal expansion or compression effects in porous media are very small compared to the two main modes for heat transfer and therefore is regarded as negligible when writing the equation of conservation of energy. Moreover, Bear [8] also claims that it is reasonable to neglect the viscous dissipation term in the heat equation. In the following, we let T_w, T_o and T_r, respectively, represent the water, oil and rock temperatures and we assume that convection and conduction are the only mechanisms by which heat is transferred in the reservoir when cold water is injected into a hot reservoir as the work done on the moving fluids by pressure and viscous forces is left out in this analysis. Under these assumptions, the energy balance equation for water is described by

$$
\begin{aligned}
&r\Delta\theta\Delta z\rho_w\varepsilon_w u_{wr}|_r\Delta t - r\Delta\theta\Delta z\rho_w\varepsilon_w u_{wr}|_{(r+\Delta r)}\Delta t + \Delta r\Delta z\rho_w\varepsilon_w u_{w\theta}|_\theta\Delta t \\
&\quad - \Delta r\Delta z\rho_w\varepsilon_w u_{w\theta}|_{(\theta+\Delta\theta)}\Delta t + r\Delta r\Delta\theta\rho_w\varepsilon_w u_{wz}|_z\Delta t - r\Delta r\Delta\theta\rho_w\varepsilon_w u_{wz}|_{(z+\Delta z)}\Delta t \\
&\quad + r\Delta\theta\Delta z\bar{q}_{cw,r}|_r\Delta t - r\Delta\theta\Delta z\bar{q}_{cw,r}|_{(r+\Delta r)}\Delta t + \Delta r\Delta z\bar{q}_{cw,\theta}|_\theta\Delta t \\
&\quad - \Delta r\Delta z\bar{q}_{cw,\theta}|_{(\theta+\Delta\theta)}\Delta t + r\Delta r\Delta\theta\bar{q}_{cw,z}|_z\Delta t - r\Delta r\Delta\theta\bar{q}_{cw,z}|_{(z+\Delta z)}\Delta t = \\
&\quad r\Delta r\Delta\theta\Delta z\rho_w\varepsilon_w S_w\phi|_{(t+\Delta t)} - r\Delta r\Delta\theta\Delta z\rho_w\varepsilon_w S_w\phi|_t \\
&\quad + r\Delta r\Delta\theta\Delta z\Delta t h_{wr}(T_w - T_r) + r\Delta r\Delta\theta\Delta z\Delta t h_{wo}(T_w - T_o), \quad (4.20)
\end{aligned}
$$

where ε_w is the internal energy of the water per unit mass defined by $\varepsilon_w = C_w T_w$ with C_w representing the specific heat capacity of water. The six first terms of the left hand side of Eq. 4.20 represent the net energy transferred by convective transport along the r, θ and z-direction respectively. The remaining terms represent the net energy by conduction along the three directions. The vector $\vec{\bar{q}}_{cw}$, which has components $\bar{q}_{cw,r}$ in the r-direction, $\bar{q}_{cw,\theta}$ in the θ-direction and $\bar{q}_{cw,z}$ in the z-direction, is the rate of heat transfer per unit area in water by conduction defined by Fourier's law (see Eq. 4.1). The bar added over the symbol q_{cw} is to emphasize that this heat flux is with respect to a unit cross-sectional area of the porous medium. We need to keep in mind that it is necessary to average this term for the fluids and solid matrix when deriving the equations of energy for porous media (see [8]). Thus, we write

$$
\vec{\bar{q}}_{cw} = \begin{pmatrix} \bar{q}_{cw,r} \\ \bar{q}_{cw,\theta} \\ \bar{q}_{cw,z} \end{pmatrix} = -\phi S_w K_w \begin{pmatrix} \frac{\partial T_w}{\partial r} \\ \frac{1}{r}\frac{\partial T_w}{\partial \theta} \\ \frac{\partial T_w}{\partial z} \end{pmatrix}, \quad (4.21)
$$

with the water thermal conductivity K_w assumed to be constant. In the right hand side, the first two terms are the energy accumulated within the differential volume during the time Δt. The third quantity describes the energy transfer between the water and the solid matrix. Here, we assume that the system is water-wet. The last term is also an energy transfer but between the two fluids. If we use Eq. 4.21 in Eq. 4.20, express the

internal energy in terms of the water temperature and divide the resulting expression by $r\Delta r\Delta\theta\Delta z\Delta t$, we obtain

$$
\begin{aligned}
&-\frac{1}{r\Delta r}\left(r\rho_w C_w T_w u_{wr}|_{(r+\Delta r)} - r\rho_w C_w T_w u_{wr}|_r\right) - \frac{1}{r\Delta\theta}\left(\rho_w C_w T_w u_{w\theta}|_{(\theta+\Delta\theta)} - \rho_w C_w T_w u_{w\theta}|_\theta\right) \\
&-\frac{1}{\Delta z}\left(\rho_w C_w T_w u_{wz}|_{(z+\Delta z)} - \rho_w C_w T_w u_{wz}|_z\right) + \frac{1}{r\Delta r}\left(\phi S_w K_w r\frac{\partial T_w}{\partial r}|_{(r+\Delta r)} - \phi S_w K_w r\frac{\partial T_w}{\partial r}|_r\right) \\
&+\frac{1}{r^2\Delta\theta}\left(\phi S_w K_w \frac{\partial T_w}{\partial \theta}|_{(\theta+\Delta\theta)} - \phi S_w K_w \frac{\partial T_w}{\partial \theta}|_\theta\right) + \frac{1}{\Delta z}\left(\phi S_w K_w \frac{\partial T_w}{\partial z}|_{(z+\Delta z)} - \phi S_w K_w \frac{\partial T_w}{\partial z}|_z\right) = \\
&\qquad \frac{1}{\Delta t}\left(\rho_w C_w T_w S_w \phi|_{(t+\Delta t)} - \rho_w C_w T_w S_w \phi|_t\right) + h_{wr}(T_w - T_r) + h_{wo}(T_w - T_o), \quad (4.22)
\end{aligned}
$$

or by taking the limit as Δr, $\Delta\theta$, Δz and Δt go to zero and rearranging

$$
\begin{aligned}
&\frac{\partial}{\partial t}\left(\rho_w C_w T_w S_w \phi\right) + \frac{1}{r}\frac{\partial}{\partial r}\left(r\rho_w C_w T_w u_{wr}\right) + \frac{1}{r}\frac{\partial}{\partial \theta}\left(\rho_w C_w T_w u_{w\theta}\right) \\
&+\frac{\partial}{\partial z}\left(\rho_w C_w T_w u_{wz}\right) - \frac{1}{r}\frac{\partial}{\partial r}\left(\phi S_w K_w r\frac{\partial T_w}{\partial r}\right) - \frac{1}{r^2}\frac{\partial}{\partial \theta}\left(\phi S_w K_w \frac{\partial T_w}{\partial \theta}\right) - \frac{\partial}{\partial z}\left(\phi S_w K_w \frac{\partial T_w}{\partial z}\right) = \\
&\qquad - h_{wr}(T_w - T_r) - h_{wo}(T_w - T_o). \quad (4.23)
\end{aligned}
$$

Eq. 4.23 can be rewritten using a vectorial notation as

$$
\frac{\partial}{\partial t}\left(\rho_w C_w T_w S_w \phi\right) + \vec{\nabla}.(\rho_w C_w T_w \vec{u}_w) - \vec{\nabla}.(\phi S_w K_w \vec{\nabla} T_w) = -h_{wr}(T_w - T_r) - h_{wo}(T_w - T_o). \quad (4.24)
$$

Again, the thermal properties of water (the thermal conductivity K_w and the specific heat capacity C_w) are assumed to be constant in Eqs. 4.22, 4.23 and 4.24. We will also assume that the oil and rock thermal properties are constant when deriving the energy equations for the corresponding phases. If we use the fact that

$$
\vec{\nabla}.(\rho_w C_w T_w \vec{u}_w) = \rho_w C_w \vec{\nabla}.(T_w \vec{u}_w) = \rho_w C_w \left(\vec{u}_w.\vec{\nabla} T_w + T_w \vec{\nabla}.\vec{u}_w\right), \quad (4.25)
$$

we can rewrite Eq. 4.24 as

$$\rho_w C_w T_w \frac{\partial}{\partial t}\left(S_w\phi\right) + \rho_w C_w S_w \phi \frac{\partial T_w}{\partial t} + \rho_w C_w \left(\vec{u}_w.\vec{\nabla}T_w + T_w\vec{\nabla}.\vec{u}_w\right) - \vec{\nabla}.(\phi S_w K_w \vec{\nabla}T_w) = - h_{wr}(T_w - T_r) - h_{wo}(T_w - T_o), \quad (4.26)$$

or

$$\rho_w C_w T_w \left[\frac{\partial}{\partial t}\left(S_w\phi\right) + \vec{\nabla}.\vec{u}_w\right] + \rho_w C_w S_w \phi \frac{\partial T_w}{\partial t} + \rho_w C_w \vec{u}_w.\vec{\nabla}T_w - \vec{\nabla}.(\phi S_w K_w \vec{\nabla}T_w) = - h_{wr}(T_w - T_r) - h_{wo}(T_w - T_o). \quad (4.27)$$

According to Eq. 4.9, we have

$$\frac{\partial}{\partial t}\left(S_w\phi\right) + \vec{\nabla}.(\vec{u}_w) = 0. \quad (4.28)$$

Thus, using this result in Eq. 4.27 gives

$$\phi\rho_w C_w S_w \frac{\partial T_w}{\partial t} + \rho_w C_w \vec{u}_w.\vec{\nabla}T_w - \vec{\nabla}.(\phi S_w K_w \vec{\nabla}T_w) = -h_{wr}(T_w - T_r) - h_{wo}(T_w - T_o). \quad (4.29)$$

The energy balance equation for oil is given by

$$\begin{aligned} & r\Delta\theta\Delta z\rho_o\varepsilon_o u_{or}|_r\Delta t - r\Delta\theta\Delta z\rho_o\varepsilon_o u_{or}|_{(r+\Delta r)}\Delta t + \Delta r\Delta z\rho_o\varepsilon_o u_{o\theta}|_\theta\Delta t \\ & - \Delta r\Delta z\rho_o\varepsilon_o u_{o\theta}|_{(\theta+\Delta\theta)}\Delta t + r\Delta r\Delta\theta\rho_o\varepsilon_o u_{oz}|_z\Delta t - r\Delta r\Delta\theta\rho_o\varepsilon_o u_{oz}|_{(z+\Delta z)}\Delta t \\ & - r\Delta\theta\Delta z\phi S_o K_o\frac{\partial T_o}{\partial r}|_r\Delta t + r\Delta\theta\Delta z\phi S_o K_o\frac{\partial T_o}{\partial r}|_{(r+\Delta r)}\Delta t - \Delta r\Delta z\phi S_o K_o\frac{1}{r}\frac{\partial T_o}{\partial\theta}|_\theta\Delta t \\ & + \Delta r\Delta z\phi S_o K_o\frac{1}{r}\frac{\partial T_o}{\partial\theta}|_{(\theta+\Delta\theta)}\Delta t - r\Delta r\Delta\theta\phi S_o K_o\frac{\partial T_o}{\partial z}|_z\Delta t + r\Delta r\Delta\theta\phi S_o K_o\frac{\partial T_o}{\partial z}|_{(z+\Delta z)}\Delta t = \\ & r\Delta r\Delta\theta\Delta z\rho_o\varepsilon_o S_o\phi|_{(t+\Delta t)} - r\Delta r\Delta\theta\Delta z\rho_o\varepsilon_o S_o\phi|_t + r\Delta r\Delta\theta\Delta z\Delta t h_{ow}(T_o - T_w). \quad (4.30) \end{aligned}$$

The internal energy of oil per mass unit, denoted by ε_o is also assumed to be function of temperature only and is given by $\varepsilon_o = C_o T_o$. Similarly to the energy balance equation for water Eq. 4.29, it is easy to show that Eq. 4.30 becomes

$$\phi \rho_o C_o S_o \frac{\partial T_o}{\partial t} + \rho_o C_o \vec{u}_o . \vec{\nabla} T_o - \vec{\nabla} . (\phi S_o K_o \vec{\nabla} T_o) = -h_{ow}(T_o - T_w). \tag{4.31}$$

As for the solid matrix, it is obvious that the net energy transferred by convective transport is zero. Therefore, the energy balance equation for the solid phase is simply given by

$$(1-\phi)\rho_r C_r \frac{\partial T_r}{\partial t} - \vec{\nabla} . ((1-\phi) K_r \vec{\nabla} T_r) = -h_{rw}(T_r - T_w). \tag{4.32}$$

By assuming a local thermal equilibrium (which occurs at low Reynolds number flows), meaning that $T_w = T_o = T_r = T$ and by adding Eqs. 4.29, 4.31 and 4.32, we obtain

$$\begin{aligned} \left[\phi(\rho_w C_w S_w + \rho_o C_o S_o) + (1-\phi)\rho_r C_r\right] \frac{\partial T}{\partial t} + \left[\rho_w C_w \vec{u}_w + \rho_o C_o \vec{u}_o\right] . \vec{\nabla} T \\ - \vec{\nabla} . \left(\left[\phi(S_w K_w + S_o K_o) + (1-\phi) K_r \right] \vec{\nabla} T \right) = 0, \end{aligned} \tag{4.33}$$

or simply

$$(\rho C)_e \frac{\partial T}{\partial t} + (\rho C \vec{u})_e . \vec{\nabla} T - \vec{\nabla} . (K_e \vec{\nabla} T) = 0, \tag{4.34}$$

with

$$(\rho C)_e = \phi(\rho_w C_w S_w + \rho_o C_o S_o) + (1-\phi)\rho_r C_r, \tag{4.35}$$

$$K_e = \phi(S_w K_w + S_o K_o) + (1-\phi) K_r, \tag{4.36}$$

and

$$(\rho C\vec{u})_e = \rho_w C_w \vec{u}_w + \rho_o C_o \vec{u}_o. \tag{4.37}$$

Using the fact that

$$\vec{\nabla}.(K_e \vec{\nabla} T) = K_e \nabla^2 T + \vec{\nabla} T.\vec{\nabla} K_e, \tag{4.38}$$

Eq. 4.34 becomes

$$(\rho C)_e \frac{\partial T}{\partial t} + (\rho C\vec{u})_e.\vec{\nabla} T - K_e \nabla^2 T - \vec{\nabla} T.\vec{\nabla} K_e = 0, \tag{4.39}$$

that we can approximate to

$$(\rho C)_e \frac{\partial T}{\partial t} + (\rho C\vec{u})_e.\vec{\nabla} T - K_e \nabla^2 T = 0, \tag{4.40}$$

since the product $\vec{\nabla} T.\vec{\nabla} K_e$ is usually small. If we consider only the radial dimension, Eq. 4.33 simplifies to

$$(\rho C)_e \frac{\partial T}{\partial t} + (\rho C u)_e \frac{\partial T}{\partial r} - \frac{K_e}{r} \frac{\partial}{\partial r}\left(r \frac{\partial T}{\partial r} \right) = 0. \tag{4.41}$$

The coupled equations Eqs. 4.9 and 4.40 along with the appropriate auxiliary conditions define our nonisothermal two-phase problem. One difficulty of solving the problem analytically resides in the fact that Eq. 4.40 is a second order differential equation due to conductive heat transport. Thus, it is imperative to know the order of magnitude between the convective and the conductive term in Eq. 4.40 and how to incorporate them into the solution. Luckily, convection and conduction do not have an equal importance in flow through porous media during the injection and the falloff period. A numerical study conducted by Platenkamp [30] shows the relative importance of the heat exchange processes considered here, that is convection, vertical and horizontal conduction after 100 days of injection. Fig. 4.1 illustrates the different temperature distributions obtained when considering the different heat transfer mechanisms. The profile represented by dots is the one obtained when considering convection only. It is a unit step function profile

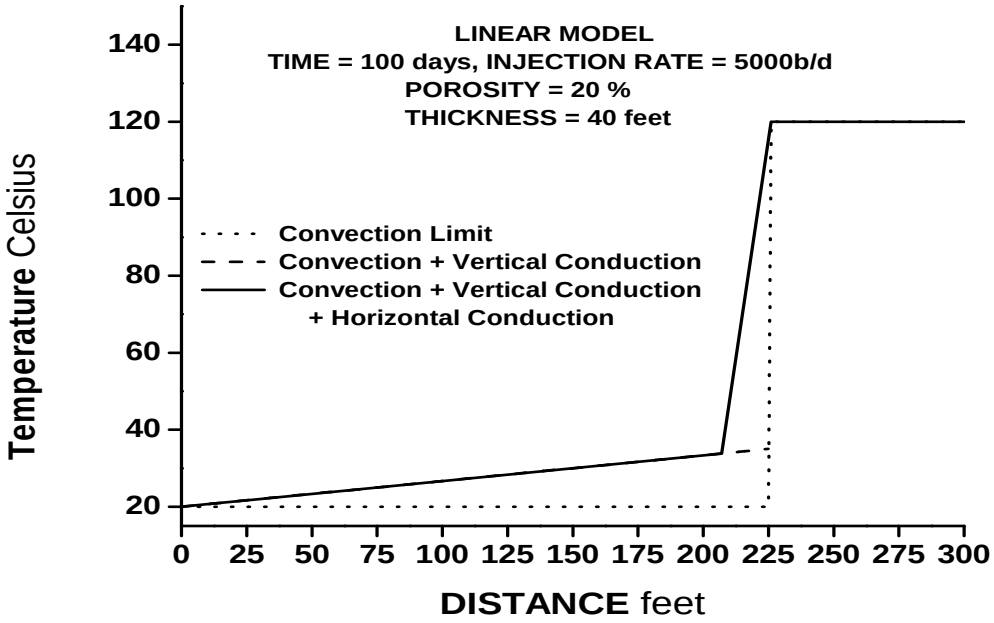

Figure 4.1: Effect of the three heat-exchange processes on the temperature profile (SPE 13746).

with a temperature equal to the injected fluid temperature up to a certain location defined as the temperature front location and a temperature equal to the initial formation temperature away from the temperature front. The curve illustrated by the dashed lines is the one obtained when both convection and vertical conduction were considered. As the author of the paper pointed out, the effect of vertical conduction is to increase the temperature in the cold region without changing the location of the front. Including horizontal conduction leads to a diffused temperature distribution represented in Fig. 4.1 by the solid line. This numerical study shows that it is a good approximation to neglect the heat transfer contribution from conduction compared to that from convection during an injection period as long as the duration of the test is not too long and the injection rate is sufficiently high. However, this is not the case during a shut-in period as conduction is expected to be the dominant process by which heat is exchanged in the reservoir and cannot therefore be neglected in the analysis.

4.2 Injection Solution Under Nonisothermal Conditions

In this study, we consider injection of cold water of temperature T_{wi} at a constant rate given by q_{inj} through a vertical well in the center of a homogeneous reservoir with an

initial temperature T_{oi}. For now, we assume that the reservoir is isotropic and that the well fully penetrates the reservoir of constant formation thickness, h. It is also assumed that the initial saturation distribution is uniform and equal to irreducible water saturation S_{iw} and fluid viscosities are a function of the temperature only. Note also only radial flow of fluids is considered.

As mentioned earlier, it has been shown (see [30]) that temperature changes are primarily due to convective heat transfer when cold waterflooding a hot reservoir and that the effect of conduction on the temperature distribution is negligible. In this case, the temperature distribution can be approximated by the following Heaviside function

$$T(r,t) = \begin{cases} T_{wi} & r \leq r_T(t), \\ T_{oi} & r \geq r_T(t), \end{cases} \tag{4.42}$$

where $r_T(t)$ is the radial position of the temperature front. An estimate of this parameter is determined using a heat balance between the injected water and the formation. To do so, we recall that water, oil and rock specific heat capacities denoted respectively by C_w, C_o and C_r are assumed to be constant. We also denote the volume of the flooded region after an injection time of t by V_f such that $V_f = 2\pi h r_f^2(t)$ where r_f is the position of the water front. The volume of the cooled region during the same injection time is denoted by V_c such that $V_c = 2\pi h r_T^2(t)$. Applying a heat balance on the system gives

$$\int_{r_T}^{r_f} \phi\rho_w C_w S_w (T_{oi} - T_{wi}) 2\pi h r dr = \int_{r_w}^{r_T} (1-\phi)\rho_r C_r (T_{oi} - T_{wi}) 2\pi h r dr + \int_{r_w}^{r_T} \phi\rho_o C_o S_o (T_{oi} - T_{wi}) 2\pi h r dr, \tag{4.43}$$

where the left hand side of Eq. 4.43 expresses the amount of heat gained by the water injected in the zone of volume equal to $V_f - V_c$ while the right hand side is the amount of heat lost by the formation and the oil in the cold zone. By adding and subtracting an integral from r_w to r_T, we can rewrite Eq. 4.43 as

$$\int_{r_T}^{r_f} \phi\rho_w C_w S_w(T_{oi} - T_{wi})2\pi hrdr + \int_{r_w}^{r_T} \phi\rho_w C_w S_w(T_{oi} - T_{wi})2\pi hrdr$$
$$- \int_{r_w}^{r_T} \phi\rho_w C_w S_w(T_{oi} - T_{wi})2\pi hrdr =$$
$$\int_{r_w}^{r_T} (1-\phi)\rho_r C_r(T_{oi} - T_{wi})2\pi hrdr + \int_{r_w}^{r_T} \phi\rho_o C_o S_o(T_{oi} - T_{wi})2\pi hrdr. \quad (4.44)$$

Simplifying and rearranging Eq. 4.44 yields

$$\int_{r_w}^{r_f} \phi\rho_w C_w S_w rdr = \int_{r_w}^{r_T} [\phi(\rho_w C_w S_w + \rho_o C_o S_o) + (1-\phi)\rho_r C_r]rdr. \quad (4.45)$$

By introducing the effective density averaged specific heat capacity for the porous system defined by Eq. 4.35, Eq. 4.45 becomes

$$\int_{r_w}^{r_f} \phi\rho_w C_w S_w rdr = \int_{r_w}^{r_T} (\rho C)_e rdr. \quad (4.46)$$

Since $(\rho C)_e$ is bigger than $\phi\rho_w C_w S_w$, for Eq. 4.46 to hold, the temperature front, r_T, must always be within the flooded region of radius r_f during the injection period. In the following, we will construct the injection analytical pressure solution for a cold waterflooding case. We will show that we are still able to apply the same theoretical approach based on the Thompson-Reynolds steady-state theory used in previous chapters to construct this solution.

4.2.1 Steady-State Theory for Radial Flow

We begin the analysis by assuming that the total rate distribution in the reservoir during the injection test is given by $q_t(r,t)$ and by expressing Darcy's law in term of pressure change at the wellbore as follows

$$\Delta p = p_{wf}(t) - p_i = \frac{\alpha}{h} \int_{r_w}^{\infty} \frac{q_t(r,t)}{\lambda_t(r,t)} \frac{dr}{rk(r)}, \quad (4.47)$$

where p_{wf} is the injection pressure at the wellbore and p_i is the initial reservoir pressure. Here, the permeability k is set to be a function of the spatial coordinate r in order to take into account the change of this parameter near the wellbore region due to the mechanical skin. The way the skin is input into the system is by assuming a reservoir with a thick skin zone concentric with the well with a radius r_s. The total mobility of the system λ_t is defined as

$$\lambda_t = \frac{k_{ro}(S_w)}{\mu_o(T)} + \frac{k_{rw}(S_w)}{\mu_w(T)}. \tag{4.48}$$

At this point, it is important to note that due the the fact that the system has two temperatures (see Eq. 4.42), we introduce a total mobility computed at the temperature T_{wi}, denoted by λ_{tc} and defined by

$$\lambda_{tc} = \frac{k_{ro}(S_w)}{\mu_o(T_{wi})} + \frac{k_{rw}(S_w)}{\mu_w(T_{wi})}, \tag{4.49}$$

which is valid for $r < r_T$. We also define a total mobility determined at the initial formation temperature T_{oi} that we denote by λ_{th} such that

$$\lambda_{th} = \frac{k_{ro}(S_w)}{\mu_o(T_{oi})} + \frac{k_{rw}(S_w)}{\mu_w(T_{oi})}, \tag{4.50}$$

valid for $r > r_T$. By introducing the radius of the temperature front r_T and the radius of the water front r_f and also by adding and subtracting the same term, we can rewrite Eq. 4.47 as

$$\begin{aligned}\Delta p = \frac{\alpha}{h}\int_{r_w}^{r_T(t)} \frac{q_t(r,t)}{\lambda_{tc}(r,t)}\frac{dr}{rk(r)} + \frac{\alpha}{h}\int_{r_T(t)}^{r_f(t)} \frac{q_t(r,t)}{\lambda_{th}(r,t)}\frac{dr}{rk(r)} + \frac{\alpha}{h}\int_{r_f(t)}^{\infty} \frac{q_t(r,t)}{\lambda_{th}(r,t)}\frac{dr}{rk(r)} + \\ \frac{\alpha}{h}\int_{r_w}^{r_f(t)} \frac{q_t(r,t)}{\hat{\lambda}_{oh}}\frac{dr}{rk(r)} - \frac{\alpha}{h}\int_{r_w}^{r_f(t)} \frac{q_t(r,t)}{\hat{\lambda}_{oh}}\frac{dr}{rk(r)},\end{aligned} \tag{4.51}$$

where $\hat{\lambda}_{oh}$ is the oil mobility evaluated at irreducible water saturation and at the initial reservoir temperature given by

$$\hat{\lambda}_{oh} = \frac{k_{ro}(S_{iw})}{\mu_o(T_{oi})}. \tag{4.52}$$

Based on the steady-state theory [34], the equation $q(r,t) = q_{inj}$ holds everywhere behind the flood front, i.e., for $r < r_f$. Note also that ahead of the water front, i.e., for $r > r_f$, we have $\lambda_{th}(r,t) = \hat{\lambda}_{oh}$. Thus, Eq. 4.51 becomes

$$\Delta p = \frac{\alpha q_{inj}}{h} \int_{r_w}^{r_T(t)} \frac{1}{\lambda_{tc}(r,t)} \frac{dr}{rk(r)} + \frac{\alpha q_{inj}}{h} \int_{r_T(t)}^{r_f(t)} \frac{1}{\lambda_{th}(r,t)} \frac{dr}{rk(r)} + \frac{\alpha}{h\hat{\lambda}_{oh}} \int_{r_f(t)}^{\infty} q_t(r,t) \frac{dr}{rk(r)} + \frac{\alpha}{h\hat{\lambda}_{oh}} \int_{r_w}^{r_f(t)} q_t(r,t) \frac{dr}{rk(r)} - \frac{\alpha q_{inj}}{h} \int_{r_w}^{r_f(t)} \frac{1}{\hat{\lambda}_{oh}} \frac{dr}{rk(r)}, \tag{4.53}$$

or simply,

$$\Delta p = \frac{\alpha q_{inj}}{h} \int_{r_w}^{r_T(t)} \frac{1}{\lambda_{tc}(r,t)} \frac{dr}{rk(r)} + \frac{\alpha q_{inj}}{h} \int_{r_T(t)}^{r_f(t)} \frac{1}{\lambda_{th}(r,t)} \frac{dr}{rk(r)} + \frac{\alpha}{h\hat{\lambda}_{oh}} \int_{r_w}^{\infty} q_t(r,t) \frac{dr}{rk(r)} - \frac{\alpha q_{inj}}{h} \int_{r_w}^{r_f(t)} \frac{1}{\hat{\lambda}_{oh}} \frac{dr}{rk(r)}. \tag{4.54}$$

If we add and subtract the term $\frac{\alpha q_{inj}}{h} \int_{r_w}^{r_T(t)} \frac{1}{\lambda_{th}(r,t)} \frac{dr}{rk(r)}$ to the above equation and rearrange the resulting equation, we obtain

$$\Delta p = \frac{\alpha}{h\hat{\lambda}_{oh}} \int_{r_w}^{\infty} q_t(r,t) \frac{dr}{rk(r)} + \frac{\alpha q_{inj}}{h\hat{\lambda}_{oh}} \int_{r_w}^{r_f(t)} \left(\frac{\hat{\lambda}_{oh}}{\lambda_{th}(r,t)} - 1 \right) \frac{dr}{rk(r)} + \frac{\alpha q_{inj}}{h} \int_{r_w}^{r_T(t)} \left(\frac{1}{\lambda_{tc}(r,t)} - \frac{1}{\lambda_{th}(r,t)} \right) \frac{dr}{rk(r)}. \tag{4.55}$$

Note that the first integral of Eq. 4.55 represents the single-phase pressure change that we would obtain by injecting oil through a vertical well into a hot oil reservoir of constant temperature T_{oi}. Let us for simplicity denote this term by Δp_o as we did before. The second integral represents an additional pressure change due to the contrast between oil mobility at irreducible water saturation and total mobility in the zone invaded by injected

water also evaluated at the initial temperature of the reservoir. The sum of the first two terms is the isothermal solution for the injection pressure that we denote by $\Delta p_{(T=Toi)}$. Therefore, it becomes clear that the nonisothermal injection solution for the wellbore pressure change can be written as the sum of the isothermal injection solution based on the initial temperature of the reservoir and an additional pressure change that takes into account the difference of mobilities due to the temperature in the cold region of the reservoir. Thus, we rewrite Eq. 4.55 as

$$\Delta p = \Delta p_{(T=Toi)} + \frac{\alpha q_{inj}}{h} \int_{r_w}^{r_T(t)} \left(\frac{1}{\lambda_{tc}(r,t)} - \frac{1}{\lambda_{th}(r,t)} \right) \frac{dr}{rk(r)}, \tag{4.56}$$

with

$$\Delta p_{(T=Toi)} = \Delta p_o + \frac{\alpha q_{inj}}{h\hat{\lambda}_{oh}} \int_{r_w}^{r_f(t)} \left(\frac{\hat{\lambda}_{oh}}{\lambda_{th}(r,t)} - 1 \right) \frac{dr}{rk(r)}. \tag{4.57}$$

At this point of the analysis, we have to consider three distinct cases:(i) the flood front is still moving in the skin zone of permeability k_s. The solution for the pressure change in this case is obtained by simply replacing the permeability $k(r)$ in Eq. 4.55 by k_s for $r < r_s$ where r_s is the radius of the skin zone. If we do so, we have

$$\Delta p = \Delta p_o + \frac{\alpha q_{inj}}{k_s h\hat{\lambda}_{oh}} \int_{r_w}^{r_f(t)} \left(\frac{\hat{\lambda}_{oh}}{\lambda_{th}(r,t)} - 1 \right) \frac{dr}{r} + \frac{\alpha q_{inj}}{k_s h} \int_{r_w}^{r_T(t)} \left(\frac{1}{\lambda_{tc}(r,t)} - \frac{1}{\lambda_{th}(r,t)} \right) \frac{dr}{r}. \tag{4.58}$$

Recall that Z is the radial Boltzmann variable defined according to Eq. 2.10 by

$$Z = \frac{r^2}{4t}, \tag{4.59}$$

and that for any fixed t, we also have

$$\frac{dZ}{Z} = 2\frac{dr}{r}. \tag{4.60}$$

We also define the Boltzmann variable at the temperature front by $Z_T = \frac{r_T^2}{4t}$ and the Boltzmann variable at the water front by $Z_f = \frac{r_f^2}{4t}$. Then, by making this change of variable in Eq. 4.58, we obtain

$$\Delta p = \Delta p_o + \frac{\alpha q_{inj}}{2k_s h \hat{\lambda}_{oh}} \int_{r_w^2/4t}^{Z_f} \left(\frac{\hat{\lambda}_{oh}}{\lambda_{th}(Z)} - 1 \right) \frac{dZ}{Z} + \frac{\alpha q_{inj}}{2k_s h} \int_{r_w^2/4t}^{Z_T} \left(\frac{1}{\lambda_{tc}(Z)} - \frac{1}{\lambda_{th}(Z)} \right) \frac{dZ}{Z}. \quad (4.61)$$

Two remarks are of order. First, in terms of the Boltzmann transform, the location of the temperature and the flood fronts are stationary, i.e., they do not vary with time. Secondly, as noted in the above equation, the total mobilities λ_{th} and λ_{tc} are unique functions of Z and so $\lambda_{th}(r,t) = \lambda_{th}(Z)$ and $\lambda_{tc}(r,t) = \lambda_{tc}(Z)$. This of course assumes injection through a line source well. Taking the derivative of Eq. 4.61 with respect to the logarithm of time gives

$$\Delta p' = \frac{d\Delta p}{d \ln t} = \Delta p_o' + \frac{\alpha q_{inj}}{2k_s h \hat{\lambda}_{oh}} t \frac{d}{dt} \int_{r_w^2/4t}^{Z_f} \left(\frac{\hat{\lambda}_{oh}}{\lambda_{th}(Z)} - 1 \right) \frac{dZ}{Z} + \frac{\alpha q_{inj}}{2k_s h} t \frac{d}{dt} \int_{r_w^2/4t}^{Z_T} \left(\frac{1}{\lambda_{tc}(Z)} - \frac{1}{\lambda_{th}(Z)} \right) \frac{dZ}{Z}. \quad (4.62)$$

Using Leibnitz integral rule, it is easy to show that

$$\frac{d}{dt} \int_{r_w^2/4t}^{Z_f} \left(\frac{\hat{\lambda}_{oh}}{\lambda_{th}(Z)} - 1 \right) \frac{dZ}{Z} = -\left(\frac{\hat{\lambda}_{oh}}{\lambda_{th}(r_w^2/4t)} - 1 \right) \frac{4t}{r_w^2} \left(-\frac{r_w^2}{4t^2} \right) = \frac{1}{t} \left(\frac{\hat{\lambda}_{oh}}{\lambda_{th}(r_w^2/4t)} - 1 \right). \quad (4.63)$$

Similarly, we have

$$\frac{d}{dt}\int_{r_w^2/4t}^{Z_T}\left(\frac{1}{\lambda_{tc}(Z)}-\frac{1}{\lambda_{th}(Z)}\right)\frac{dZ}{Z}=-\left(\frac{1}{\lambda_{tc}(r_w^2/4t)}-\frac{1}{\lambda_{th}(r_w^2/4t)}\right)\frac{4t}{r_w^2}\left(-\frac{r_w^2}{4t^2}\right)$$
$$=\frac{1}{t}\left(\frac{1}{\lambda_{tc}(r_w^2/4t)}-\frac{1}{\lambda_{th}(r_w^2/4t)}\right). \quad (4.64)$$

Substituting Eqs. 4.63 and 4.64 into Eq. 4.62 gives

$$\Delta p'=\Delta p'_o+\frac{\alpha q_{inj}}{2k_s h\hat{\lambda}_{oh}}\left(\frac{\hat{\lambda}_{oh}}{\lambda_{th}(r_w^2/4t)}-1\right)+\frac{\alpha q_{inj}}{2k_s h\hat{\lambda}_{oh}}\left(\frac{\hat{\lambda}_{oh}}{\lambda_{tc}(r_w^2/4t)}-\frac{\hat{\lambda}_{oh}}{\lambda_{th}(r_w^2/4t)}\right), \quad (4.65)$$

or simply

$$\Delta p'=\Delta p'_o+\frac{\alpha q_{inj}}{2k_s h\hat{\lambda}_{oh}}\left(\frac{\hat{\lambda}_{oh}}{\lambda_{tc}(r_w^2/4t)}-1\right). \quad (4.66)$$

Using the fact that at r_w, $\lambda_{tc}(r_w^2/4t)=\hat{\lambda}_{wc}$ where $\hat{\lambda}_{wc}$ is the water mobility evaluated at residual oil saturation and at the injected water temperature given by $\hat{\lambda}_{wc}=\frac{k_{rw}(1-S_{or})}{\mu_w(T_{wi})}$ and assuming that the steady-state region of constant total rate has propagated beyond the skin zone such that the single-phase flow solution Δp_o based on oil properties at the initial reservoir temperature is given by the following semilog straight line

$$\Delta p_o=\frac{\alpha q_{inj}}{kh\hat{\lambda}_{oh}}\left[\frac{1}{2}\ln\left(\frac{4\eta_o t}{e^{\gamma}r_w^2}\right)+s\right], \quad (4.67)$$

therefore,

$$\Delta p'_o=\frac{\alpha q_{inj}}{2kh\hat{\lambda}_{oh}}, \quad (4.68)$$

and replacing Eq. 4.68 into Eq. 4.66 gives

$$\Delta p'=\frac{\alpha q_{inj}}{2kh\hat{\lambda}_{oh}}\left[1+\frac{k}{k_s}\left(\frac{\hat{\lambda}_{oh}}{\hat{\lambda}_{wc}}-1\right)\right]. \quad (4.69)$$

By introducing oil mobility evaluated at irreducible water saturation at the injected water

temperature given by $\hat{\lambda}_{oc} = \frac{k_{ro}(S_{iw})}{\mu_o(T_{wi})}$, we can write Eq. 4.69 as

$$\Delta p' = \frac{\alpha q_{inj}}{2kh\hat{\lambda}_{oh}}\left[1 - \frac{k}{k_s}\left(1 - \frac{1}{\hat{M}_c}\frac{\hat{\lambda}_{oh}}{\hat{\lambda}_{oc}}\right)\right]. \tag{4.70}$$

In this equation, $\hat{M}_c$ represents the end-point mobility ratio evaluated at the injected water temperature and defined by

$$\hat{M}_c = \frac{\hat{\lambda}_{wc}}{\hat{\lambda}_{oc}}. \tag{4.71}$$

It is interesting to see that Eq. 4.70 indicates a negative pressure derivative at early times provided that

$$1 - \frac{k}{k_s}\left(1 - \frac{1}{\hat{M}_c}\frac{\hat{\lambda}_{oh}}{\hat{\lambda}_{oc}}\right) < 0, \tag{4.72}$$

or equivalently

$$\hat{M}_c(1 - \frac{k_s}{k}) > \frac{\hat{\lambda}_{oh}}{\hat{\lambda}_{oc}} = \frac{\mu_{oc}}{\mu_{oh}}. \tag{4.73}$$

When $\mu_{oc} = \mu_{oh}$ and $\hat{M}_c = \hat{M}$, Eq. 4.73 simplifies to

$$\hat{M}(1 - \frac{k_s}{k}) > 1, \tag{4.74}$$

which is exactly the same condition given by Eq. 2.23 and obtained for an isothermal injection.

(ii) If the water front is beyond the skin zone but not the temperature front, Eq. 4.55 becomes

$$\Delta p = \Delta p_o + \frac{\alpha q_{inj}}{k_s h\hat{\lambda}_{oh}}\int_{r_w}^{r_s}\left(\frac{\hat{\lambda}_{oh}}{\lambda_{th}(r,t)} - 1\right)\frac{dr}{r} + \frac{\alpha q_{inj}}{kh\hat{\lambda}_{oh}}\int_{r_s}^{r_f(t)}\left(\frac{\hat{\lambda}_{oh}}{\lambda_{th}(r,t)} - 1\right)\frac{dr}{r} + \frac{\alpha q_{inj}}{k_s h}\int_{r_w}^{r_T(t)}\left(\frac{1}{\lambda_{tc}(r,t)} - \frac{1}{\lambda_{th}(r,t)}\right)\frac{dr}{r}. \tag{4.75}$$

By adding and subtracting to Eq. 4.75 an integral from r_w to r_s, we have

$$\Delta p = \Delta p_o + \frac{\alpha q_{inj}}{k_s h \hat{\lambda}_{oh}} \int_{r_w}^{r_s} \left(\frac{\hat{\lambda}_{oh}}{\lambda_{th}(r,t)} - 1 \right) \frac{dr}{r} + \frac{\alpha q_{inj}}{k h \hat{\lambda}_{oh}} \int_{r_s}^{r_f(t)} \left(\frac{\hat{\lambda}_{oh}}{\lambda_{th}(r,t)} - 1 \right) \frac{dr}{r} + \frac{\alpha q_{inj}}{k_s h} \int_{r_w}^{r_T(t)} \left(\frac{1}{\lambda_{tc}(r,t)} - \frac{1}{\lambda_{th}(r,t)} \right) \frac{dr}{r} + \frac{\alpha q_{inj}}{k h \hat{\lambda}_{oh}} \int_{r_w}^{r_s} \left(\frac{\hat{\lambda}_{oh}}{\lambda_{th}(r,t)} - 1 \right) \frac{dr}{r} - \frac{\alpha q_{inj}}{k h \hat{\lambda}_{oh}} \int_{r_w}^{r_s} \left(\frac{\hat{\lambda}_{oh}}{\lambda_{th}(r,t)} - 1 \right) \frac{dr}{r}, \quad (4.76)$$

or simplifying,

$$\Delta p = \Delta p_o + \frac{\alpha q_{inj}}{k h \hat{\lambda}_{oh}} \left[\left(\frac{k}{k_s} - 1 \right) \int_{r_w}^{r_s} \left(\frac{\hat{\lambda}_{oh}}{\lambda_{th}(r,t)} - 1 \right) \frac{dr}{r} + \int_{r_w}^{r_f(t)} \left(\frac{\hat{\lambda}_{oh}}{\lambda_{th}(r,t)} - 1 \right) \frac{dr}{r} \right] + \frac{\alpha q_{inj}}{k_s h} \int_{r_w}^{r_T(t)} \left(\frac{1}{\lambda_{tc}(r,t)} - \frac{1}{\lambda_{th}(r,t)} \right) \frac{dr}{r}. \quad (4.77)$$

By making the same change of variable given by Eq. 4.59 and using the same arguments as before, Eq. 4.77 becomes

$$\Delta p = \Delta p_o + \frac{\alpha q_{inj}}{2 k h \hat{\lambda}_{oh}} \left[\left(\frac{k}{k_s} - 1 \right) \int_{r_w^2/4t}^{r_s^2/4t} \left(\frac{\hat{\lambda}_{oh}}{\lambda_{th}(Z)} - 1 \right) \frac{dZ}{Z} + \int_{r_w^2/4t}^{Z_f} \left(\frac{\hat{\lambda}_{oh}}{\lambda_{th}(Z)} - 1 \right) \frac{dZ}{Z} \right] + \frac{\alpha q_{inj}}{2 k_s h} \int_{r_w^2/4t}^{Z_T} \left(\frac{1}{\lambda_{tc}(Z)} - \frac{1}{\lambda_{th}(Z)} \right) \frac{dZ}{Z}. \quad (4.78)$$

By taking the derivative of Eq. 4.78 with respect to $\ln t$, we obtain

$$\Delta p' = \Delta p'_o + \frac{\alpha q_{inj} t}{2 k h \hat{\lambda}_{oh}} \left[\left(\frac{k}{k_s} - 1 \right) \left(\left(\frac{\hat{\lambda}_{oh}}{\lambda_{th}(r_s,t)} - 1 \right) \frac{4t}{r_s^2} \left(- \frac{r_s^2}{4t^2} \right) - \left(\frac{\hat{\lambda}_{oh}}{\lambda_{th}(r_w,t)} - 1 \right) \frac{4t}{r_w^2} \left(- \frac{r_w^2}{4t^2} \right) \right) - \left(\frac{\hat{\lambda}_{oh}}{\lambda_{th}(r_w,t)} - 1 \right) \frac{4t}{r_w^2} \left(- \frac{r_w^2}{4t^2} \right) \right] - \frac{\alpha q_{inj} t}{2 k_s h} \left(\frac{1}{\lambda_{tc}(r_w,t)} - \frac{1}{\lambda_{th}(r_w,t)} \right) \frac{4t}{r_w^2} \left(- \frac{r_w^2}{4t^2} \right), \quad (4.79)$$

which simplifies to

$$\Delta p' = \Delta p'_o + \frac{\alpha q_{inj}}{2kh\hat{\lambda}_{oh}}\left[\frac{k}{k_s}\frac{\hat{\lambda}_{oh}}{\lambda_{tc}(r_w,t)} - \left(\frac{k}{k_s}-1\right)\frac{\hat{\lambda}_{oh}}{\lambda_{th}(r_s,t)} - 1\right]. \tag{4.80}$$

Substituting Eq. 4.68 for $\Delta p'_o$ into Eq. 4.80 and noting that $\lambda_{tc}(r_w,t) = \hat{\lambda}_{wc}$, we obtain

$$\Delta p' = \frac{\alpha q_{inj}}{2kh\hat{\lambda}_{wc}}\left[\frac{k}{k_s} - \left(\frac{k}{k_s}-1\right)\frac{\hat{\lambda}_{wc}}{\lambda_{th}(r_s,t)}\right]. \tag{4.81}$$

Note here that Eq. 4.81 might take negative values for the pressure derivative when

$$\frac{k}{k_s} - \left(\frac{k}{k_s}-1\right)\frac{\hat{\lambda}_{wc}}{\lambda_{th}(r_s,t)} < 0, \tag{4.82}$$

or equivalently

$$\lambda_{th}(r_s,t) < \hat{\lambda}_{wc}\left(1-\frac{k_s}{k}\right). \tag{4.83}$$

(iii) If the temperature front is beyond the skin zone, Eq. 4.77 needs to be extended to

$$\begin{aligned}\Delta p = \Delta p_o &+ \frac{\alpha q_{inj}}{kh\hat{\lambda}_{oh}}\left[\left(\frac{k}{k_s}-1\right)\int_{r_w}^{r_s}\left(\frac{\hat{\lambda}_{oh}}{\lambda_{th}(r,t)}-1\right)\frac{dr}{r} + \int_{r_w}^{r_f(t)}\left(\frac{\hat{\lambda}_{oh}}{\lambda_{th}(r,t)}-1\right)\frac{dr}{r}\right] \\ &+ \frac{\alpha q_{inj}}{k_s h}\int_{r_w}^{r_s}\left(\frac{1}{\lambda_{tc}(r,t)}-\frac{1}{\lambda_{th}(r,t)}\right)\frac{dr}{r} + \frac{\alpha q_{inj}}{kh}\int_{r_s}^{r_T(t)}\left(\frac{1}{\lambda_{tc}(r,t)}-\frac{1}{\lambda_{th}(r,t)}\right)\frac{dr}{r}.\end{aligned} \tag{4.84}$$

Similarly to case (ii), by adding and subtracting an integral from r_w to r_s, we obtain

$$\begin{aligned}\Delta p = \Delta p_o &+ \frac{\alpha q_{inj}}{kh\hat{\lambda}_{oh}}\left[\left(\frac{k}{k_s}-1\right)\int_{r_w}^{r_s}\left(\frac{\hat{\lambda}_{oh}}{\lambda_{th}(r,t)}-1\right)\frac{dr}{r} + \int_{r_w}^{r_f(t)}\left(\frac{\hat{\lambda}_{oh}}{\lambda_{th}(r,t)}-1\right)\frac{dr}{r}\right] \\ &+ \frac{\alpha q_{inj}}{k_s h}\int_{r_w}^{r_s}\left(\frac{1}{\lambda_{tc}(r,t)}-\frac{1}{\lambda_{th}(r,t)}\right)\frac{dr}{r} + \frac{\alpha q_{inj}}{kh}\int_{r_s}^{r_T(t)}\left(\frac{1}{\lambda_{tc}(r,t)}-\frac{1}{\lambda_{th}(r,t)}\right)\frac{dr}{r} \\ &+ \frac{\alpha q_{inj}}{kh}\int_{r_w}^{r_s}\left(\frac{1}{\lambda_{tc}(r,t)}-\frac{1}{\lambda_{th}(r,t)}\right)\frac{dr}{r} - \frac{\alpha q_{inj}}{kh}\int_{r_w}^{r_s}\left(\frac{1}{\lambda_{tc}(r,t)}-\frac{1}{\lambda_{th}(r,t)}\right)\frac{dr}{r},\end{aligned} \tag{4.85}$$

or by rearranging the above equation

$$\Delta p = \Delta p_o + \frac{\alpha q_{inj}}{kh\hat{\lambda}_{oh}}\left[\left(\frac{k}{k_s}-1\right)\int_{r_w}^{r_s}\left(\frac{\hat{\lambda}_{oh}}{\lambda_{th}(r,t)}-1\right)\frac{dr}{r}+\int_{r_w}^{r_f(t)}\left(\frac{\hat{\lambda}_{oh}}{\lambda_{th}(r,t)}-1\right)\frac{dr}{r}\right]$$
$$+\frac{\alpha q_{inj}}{kh}\left[\left(\frac{k}{k_s}-1\right)\int_{r_w}^{r_s}\left(\frac{1}{\lambda_{tc}(r,t)}-\frac{1}{\lambda_{th}(r,t)}\right)\frac{dr}{r}+\int_{r_w}^{r_T(t)}\left(\frac{1}{\lambda_{tc}(r,t)}-\frac{1}{\lambda_{th}(r,t)}\right)\frac{dr}{r}\right]. \tag{4.86}$$

Assuming that the total mobility correlates in terms of the Boltzmann transform, we can rewrite Eq. 4.86 as follows

$$\Delta p = \Delta p_o + \frac{\alpha q_{inj}}{2kh\hat{\lambda}_{oh}}\left[\left(\frac{k}{k_s}-1\right)\int_{r_w^2/4t}^{r_s^2/4t}\left(\frac{\hat{\lambda}_{oh}}{\lambda_{th}(Z)}-1\right)\frac{dZ}{Z}+\int_{r_w^2/4t}^{Z_f}\left(\frac{\hat{\lambda}_{oh}}{\lambda_{th}(Z)}-1\right)\frac{dZ}{Z}\right]$$
$$+\frac{\alpha q_{inj}}{2kh}\left[\left(\frac{k}{k_s}-1\right)\int_{r_w^2/4t}^{r_s^2/4t}\left(\frac{1}{\lambda_{tc}(Z)}-\frac{1}{\lambda_{th}(Z)}\right)\frac{dZ}{Z}+\int_{r_w^2/4t}^{Z_T}\left(\frac{1}{\lambda_{tc}(Z)}-\frac{1}{\lambda_{th}(Z)}\right)\frac{dZ}{Z}\right]. \tag{4.87}$$

Taking the derivative of Eq. 4.87 with respect to $\ln t$ gives

$$\Delta p' = \Delta p'_o + \frac{\alpha q_{inj}}{2kh\hat{\lambda}_{oh}}\left[\left(\frac{k}{k_s}-1\right)\left(\frac{\hat{\lambda}_{oh}}{\lambda_{th}(r_w,t)}-\frac{\hat{\lambda}_{oh}}{\lambda_{th}(r_s,t)}\right)+\frac{\hat{\lambda}_{oh}}{\lambda_{th}(r_w,t)}-1\right]$$
$$+\frac{\alpha q_{inj}}{2kh}\left[\left(\frac{k}{k_s}-1\right)\left(\frac{1}{\lambda_{tc}(r_w,t)}-\frac{1}{\lambda_{th}(r_w,t)}-\frac{1}{\lambda_{tc}(r_s,t)}+\frac{1}{\lambda_{th}(r_s,t)}\right)+\frac{1}{\lambda_{tc}(r_w,t)}-\frac{1}{\lambda_{th}(r_w,t)}\right]$$
$$=\Delta p'_o+\frac{\alpha q_{inj}}{2kh\hat{\lambda}_{oh}}\left[\frac{k}{k_s}\left(\frac{\hat{\lambda}_{oh}}{\lambda_{tc}(r_w,t)}-\frac{\hat{\lambda}_{oh}}{\lambda_{tc}(r_s,t)}\right)+\frac{\hat{\lambda}_{oh}}{\lambda_{tc}(r_s,t)}-1\right]. \tag{4.88}$$

Using Eq. 4.68 into the above equation and simplifying gives

$$\Delta p' = \frac{\alpha q_{inj}}{2kh\hat{\lambda}_{wc}}\left[\frac{k}{k_s}-\left(\frac{k}{k_s}-1\right)\frac{\hat{\lambda}_{wc}}{\lambda_{tc}(r_s,t)}\right]. \tag{4.89}$$

As seen from the above equation, once the damaged region is completely flooded, $\lambda_{tc}(r_s,t) = \hat{\lambda}_{wc}$ and Eq. 4.89 simplifies to

$$\Delta p' = \frac{\alpha q_{inj}}{2kh\hat{\lambda}_{wc}}. \tag{4.90}$$

So, as time increases, we expect to see a semilog slope that reflects water properties evaluated at the injection temperature T_{wi}.

In order to compute the two additional pressure changes due to the multiphase and temperature effects, it is necessary to construct the profiles for the total mobility λ_t via the saturation distributions. Previously (see chapter 2), we were able to obtain these profiles using the Buckley-Leverett theory assuming isothermal flow of incompressible fluids in the reservoir. The situation here is somewhat different as the flow is nonisothermal. In the following section, we will show that we can still use the same theoretical approach of method of characteristics to generate saturation distributions during a cold waterflooding assuming that convection is the only heat exchange mechanism in the system. This has been previously established by Bratvold and Horne [11].

4.2.2 Nonisothermal Buckley-Leverett Saturation Profile for Radial Flow

As mentioned earlier, we will assume that convection is the only heat exchange mechanism in the system during the injection period. In this case, the heat equation given for a pure radial flow by Eq. 4.41 simplifies to

$$(\rho C)_e \frac{\partial T}{\partial t} + (\rho C u)_e \frac{\partial T}{\partial r} = 0. \tag{4.91}$$

Using the definitions of $(\rho C)_e$ and $(\rho C u)_e$ given respectively by Eqs. 4.35 and 4.37 in Eq. 4.91 yields

$$\Big[\phi(\rho_w C_w S_w + \rho_o C_o S_o) + (1-\phi)\rho_r C_r\Big]\frac{\partial T}{\partial t} + \Big[\rho_w C_w u_w + \rho_o C_o u_o\Big]\frac{\partial T}{\partial r} = 0. \tag{4.92}$$

Using the fact that $S_w + S_o = 1$ and introducing the water fractional flow f_w through the velocities u_w and u_o as follows: $u_w = f_w u$ and $u_o = f_o u = (1 - f_w)u$, Eq. 4.92 becomes

$$\phi\left[(\rho_w C_w - \rho_o C_o)S_w + \rho_o C_o + \frac{(1-\phi)}{\phi}\rho_r C_r\right]\frac{\partial T}{\partial t} + u\left[(\rho_w C_w - \rho_o C_o)f_w + \rho_o C_o\right]\frac{\partial T}{\partial r} = 0, \quad (4.93)$$

or equivalently

$$\frac{\partial T}{\partial t} + \frac{u}{\phi}\frac{\left[(\rho_w C_w - \rho_o C_o)f_w + \rho_o C_o\right]}{\left[(\rho_w C_w - \rho_o C_o)S_w + \rho_o C_o + \frac{(1-\phi)}{\phi}\rho_r C_r\right]}\frac{\partial T}{\partial r} = 0. \quad (4.94)$$

For simplicity, we set

$$\lambda = \frac{\rho_o C_o}{\rho_w C_w - \rho_o C_o}, \quad (4.95)$$

and

$$\tau = \frac{\rho_o C_o + \frac{(1-\phi)}{\phi}\rho_r C_r}{\rho_w C_w - \rho_o C_o}, \quad (4.96)$$

so that Eq. 4.94 becomes

$$\frac{\partial T}{\partial t} + \frac{u}{\phi}\left(\frac{f_w + \lambda}{S_w + \tau}\right)\frac{\partial T}{\partial r} = 0. \quad (4.97)$$

The rearranged Eqs. 4.97 and 4.18 can be expressed by a vectorial equation as follows

$$\frac{\partial}{\partial t}\begin{pmatrix} T \\ S_w \end{pmatrix} + A\frac{\partial}{\partial r}\begin{pmatrix} T \\ S_w \end{pmatrix} = \vec{0}, \quad (4.98)$$

where A is a 2×2 matrix given by

$$A = \begin{pmatrix} \frac{u}{\phi}\left(\frac{f_w+\lambda}{S_w+\tau}\right) & 0 \\ \frac{u}{\phi}\frac{\partial f_w}{\partial T} & \frac{u}{\phi}\frac{\partial f_w}{\partial S_w} \end{pmatrix}. \quad (4.99)$$

In order to solve this system, we need auxiliary conditions. The following boundary and initial conditions are used:

$$T(r,t) = T_{wi} \quad \text{for } r = r_w \text{ and } t > 0, \tag{4.100}$$

$$S_w(r,t) = 1 - S_{or} \quad \text{for } r = r_w \text{ and } t > 0, \tag{4.101}$$

$$T(r, t=0) = T_{oi} \quad \text{for } r > r_w, \tag{4.102}$$

and

$$S_w(r, t=0) = S_{wi} \quad \text{for } r > r_w. \tag{4.103}$$

Note that the system described above is a generalization of the Buckley-Leverett equation which is obtained when T is constant. The eigenvalues of the matrix A are obtained by computing the determinant of the matrix $(A - \psi I)$ and finding the roots of the resulting second degree polynomial equation. But since A is a lower triangular matrix, its eigenvalues are the diagonal elements and therefore readily obtained. Thus, its eigenvalues are

$$\psi_1 = \frac{u}{\phi}\left(\frac{f_w + \lambda}{S_w + \tau}\right) = \frac{q_{inj}}{2\pi h \phi r}\left(\frac{f_w + \lambda}{S_w + \tau}\right), \tag{4.104}$$

and

$$\psi_2 = \frac{u}{\phi}\frac{\partial f_w}{\partial S_w} = \frac{q_{inj}}{2\pi h \phi r}\frac{\partial f_w}{\partial S_w}. \tag{4.105}$$

An important result is that the two eigenvalues of the system are real and are functions of the variables T and S_w. The system described by Eq. 4.98 along with the associated boundary and initial conditions Eqs. 4.100 to 4.103 constitutes a quasilinear hyperbolic system that can be solved by the method of characteristics. This method consists in finding a family of characteristic curves in the (r,t) plane such that

$$\frac{dr}{dt} = \psi_i, \tag{4.106}$$

with $i = 1$ or 2. However, the integration of Eq. 4.106 is not a straightforward process as the eigenvalues are functions of the variables T and S_w. We will solve the problem differently (see [7]) by considering the left eigenvectors of the matrix A that we denote by $\vec{r}_i$ with $i = 1$ or 2 and defined by the following equation:

$$(\vec{r}_i)^T(A - \psi_i I) = (0, 0). \tag{4.107}$$

The left eigenvector $\vec{r}_1$ of the matrix A with the associated eigenvalue ψ_1 is therefore given by

$$(\vec{r}_1)^T(A - \psi_1 I) = (r_1^{(1)}, r_1^{(2)}) \begin{pmatrix} 0 & 0 \\ \frac{u}{\phi}\frac{\partial f_w}{\partial T} & \psi_2 - \psi_1 \end{pmatrix} = (0, 0), \tag{4.108}$$

which gives

$$\frac{u}{\phi}\frac{\partial f_w}{\partial T} r_1^{(2)} = 0, \tag{4.109}$$

and

$$(\psi_2 - \psi_1) r_1^{(2)} = 0. \tag{4.110}$$

Thus, $r_1^{(2)} = 0$ and the left eigenvector $\vec{r}_1$ is

$$\vec{r}_1 = \begin{pmatrix} r_1^{(1)} \\ 0 \end{pmatrix}, \tag{4.111}$$

where $r_1^{(1)}$ is any nonzero real number. Similarly, the left eigenvector $\vec{r}_2$ of the matrix A with the associated eigenvalue ψ_2 is given by

$$(\vec{r}_2)^T(A-\psi_2 I) = (r_2^{(1)}, r_2^{(2)}) \begin{pmatrix} \psi_1-\psi_2 & 0 \\ \frac{u}{\phi}\frac{\partial f_w}{\partial T} & 0 \end{pmatrix} = (0,0), \tag{4.112}$$

leading to the following equation

$$(\psi_1-\psi_2)r_2^{(1)} + \frac{u}{\phi}\frac{\partial f_w}{\partial T} r_2^{(2)} = 0. \tag{4.113}$$

Thus, the left eigenvector $\vec{r}_2$ can be chosen such that

$$\vec{r}_2 = \begin{pmatrix} \frac{u}{\phi}\frac{\partial f_w}{\partial T} \\ \psi_2-\psi_1 \end{pmatrix}. \tag{4.114}$$

Let us multiply Eq. 4.98 by the left eigenvector $\vec{r}_2$. We have

$$(\vec{r}_2)^T \frac{\partial}{\partial t}\begin{pmatrix} T \\ S_w \end{pmatrix} + (\vec{r}_2)^T A \frac{\partial}{\partial r}\begin{pmatrix} T \\ S_w \end{pmatrix} = 0. \tag{4.115}$$

From the definition of a left eigenvector given by Eq. 4.107, we can write $(\vec{r}_2)^T A = \psi_2(\vec{r}_2)^T$. Using this result in Eq. 4.115 yields

$$\left(\frac{u}{\phi}\frac{\partial f_w}{\partial T}, \psi_2-\psi_1\right)\frac{\partial}{\partial t}\begin{pmatrix} T \\ S_w \end{pmatrix} + \psi_2\left(\frac{u}{\phi}\frac{\partial f_w}{\partial T}, \psi_2-\psi_1\right)\frac{\partial}{\partial r}\begin{pmatrix} T \\ S_w \end{pmatrix} = 0, \tag{4.116}$$

or simply,

$$\frac{u}{\phi}\frac{\partial f_w}{\partial T}\frac{\partial T}{\partial t} + (\psi_2-\psi_1)\frac{\partial S_w}{\partial t} + \psi_2\left[\frac{u}{\phi}\frac{\partial f_w}{\partial T}\frac{\partial T}{\partial r} + (\psi_2-\psi_1)\frac{\partial S_w}{\partial r}\right] = 0. \tag{4.117}$$

From Eq. 4.104, we have

$$\frac{\partial \psi_1}{\partial T} = \frac{u}{\phi}\frac{1}{S_w+\tau}\frac{\partial f_w}{\partial T}, \tag{4.118}$$

or

$$\frac{u}{\phi}\frac{\partial f_w}{\partial T} = (S_w + \tau)\frac{\partial \psi_1}{\partial T}. \tag{4.119}$$

If we also take the partial derivative of Eq. 4.104 with respect to S_w, we obtain

$$\frac{\partial \psi_1}{\partial S_w} = \frac{u}{\phi}\frac{1}{S_w + \tau}\left[\frac{\partial f_w}{\partial S_w} - \frac{f_w + \lambda}{S_w + \tau}\right], \tag{4.120}$$

or using Eqs. 4.104 and 4.105

$$\frac{\partial \psi_1}{\partial S_w} = \frac{1}{S_w + \tau}(\psi_2 - \psi_1), \tag{4.121}$$

which we rewrite as

$$\psi_2 - \psi_1 = (S_w + \tau)\frac{\partial \psi_1}{\partial S_w}. \tag{4.122}$$

Substituting Eqs. 4.119 and 4.122 in Eq. 4.117 and simplifying gives

$$\frac{\partial \psi_1}{\partial T}\frac{\partial T}{\partial t} + \frac{\partial \psi_1}{\partial S_w}\frac{\partial S_w}{\partial t} + \psi_2\left[\frac{\partial \psi_1}{\partial T}\frac{\partial T}{\partial r} + \frac{\partial \psi_1}{\partial S_w}\frac{\partial S_w}{\partial r}\right] = 0. \tag{4.123}$$

Since $\psi_1 = \psi_1(T, S_w)$ is a function of only the temperature T and the water saturation S_w, we can rewrite Eq. 4.123 as

$$\frac{\partial \psi_1}{\partial t} + \psi_2\frac{\partial \psi_1}{\partial r} = 0. \tag{4.124}$$

Therefore, Eq. 4.97 and 4.124 can be expressed by the following vectorial equation

$$\frac{\partial}{\partial t}\begin{pmatrix} T \\ \psi_1 \end{pmatrix} + B\frac{\partial}{\partial r}\begin{pmatrix} T \\ \psi_1 \end{pmatrix} = \vec{0}, \tag{4.125}$$

where B is a 2×2 matrix given by

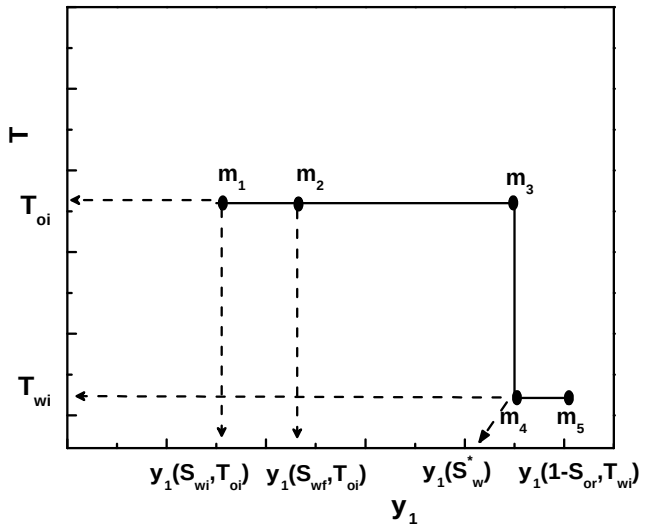

Figure 4.2: Solution in (T, ψ_1) space.

$$B = \begin{pmatrix} \psi_1 & 0 \\ 0 & \psi_2 \end{pmatrix}. \tag{4.126}$$

An important remark about the diagonal matrix B is that it has the same eigenvalues as the matrix A. Note also that by using the new formulation of the problem given by Eq. 4.125, the derivative of the fractional flow with respect to the temperature is not needed anymore as in the case of Eq. 4.98. Moreover, Eq. 4.125 suggests that T and ψ_1 must be constant along the characteristic curves $\frac{dr}{dt} = \psi_1$ and $\frac{dr}{dt} = \psi_2$ respectively. The variables T and ψ_1 constitute the Riemann invariants. For a detailed discussion on the Riemann problem, see references [32] and [7]. The structure of the solution consists of a combination of shocks, where T is constant and the shock speeds are ψ_1 or ψ_2, and a contact discontinuity, where ψ_1 is constant across the discontinuity and the speed of the discontinuity equals to ψ_1.

Fig. 4.2 shows the solution in the (T, ψ_1) plane. Fig. 4.3 is the fractional flow diagram where the fractional flow curve represented by the solid triangles corresponds to the temperature of injected water. We refer to it as the cold fractional flow whereas, the

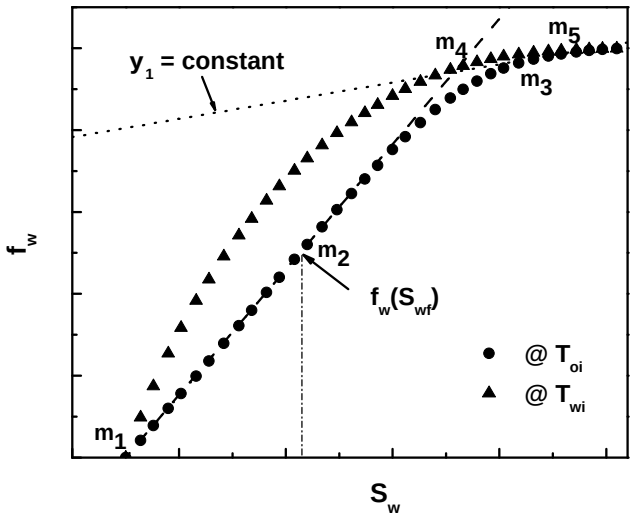

Figure 4.3: Solution on the fractional flow curves.

curve plotted in solid circles corresponds to the initial reservoir temperature. It will be referred to as the hot fractional flow. The dashed line, tangent to the hot fractional flow curve, represents the characteristic curve with slope ψ_2. The dotted line, also tangent to the hot fractional flow curve, is the characteristic curve with slope ψ_1. The point m_1 on both figures corresponds to the initial condition provided by Eq. 4.102 for the temperature and Eq. 4.103 for the water saturation. Thus, starting from the initial condition m_1, we follow the hot fractional flow curve until the point m_2 is reached. This tangent point to the hot fractional flow curve is the first discontinuity point in the profile representing the flood front saturation S_{wf}. In the (T, ψ_1) plane (see Fig. 4.2), this point corresponds to ψ_1 evaluated at S_{wf} and T_{oi}. We continue from the discontinuity point m_2 along the zone of constant temperature $T = T_{oi}$ to the point m_3 which represents the tangent point of the characteristic curve with slope ψ_1 to the hot fractional flow curve. The corresponding water saturation, called temperature front saturation and denoted by S_{wT} is obtained by equating the functions $\psi_1(S_w, T_{oi})$ and $\psi_2(S_w, T_{oi})$. Due to the temperature change, the solution jumps from the discontinuity point m_3 to the landing point m_4 on the cold fractional flow curve. The location of this point in terms of water saturation is obtained

from the equation $\psi_1(S_w^*, T_{wi}) = \psi_1(S_{wT}, T_{oi})$ where the only unknown is S_w^*. Finally, the remaining segment of the solution is obtained by going from the point m_4 on the cold fractional flow curve to the injection point m_5 characterized by a water saturation of $1 - S_{or}$ and a zero speed. This is how the water saturation profile is constructed when cold water is injected in a hot reservoir assuming only convection is the main mechanism to heat transfer. Later, we will proceed to determine some profiles using numerical data.

4.2.3 Generalization to Horizontal Well Case

In this section, we consider injection of cold water of temperature T_{wi} at a constant rate given by q_{inj} through a horizontal well of radius r_w and length L that penetrates a hot reservoir of temperature T_{oi} and of constant formation thickness h. As we proceeded for the vertical well case, we use the Thompson-Reynolds steady-state theory to construct the injection analytical pressure solution for a cold waterflooding case through a horizontal well. We will also show that this nonisothermal injection solution for the wellbore pressure change can be written as the sum of the isothermal injection solution based on the initial temperature of the reservoir and an additional pressure change component that takes into account the thermal effects. Similarly to the isothermal case, several flow regimes can develop during an injectivity test in a horizontal well due to the fact that the propagation of the pressure diffusion and the propagation of the water front occur on different planes. But unlike the isothermal case, the propagation of the temperature front needs to be included into the analysis. Therefore, there will be a third name in each flow regime which is associated with the propagation of the temperature front in the system. In the following, we consider the injection solutions for the specific flow regimes that can be observed in the horizontal well case.

First Radial/First Radial/First Radial Flow Regime

This is the case when the steady-state zone, the flood front and the temperature front are all moving radially in the (x, z) plane. The wellbore pressure change for this particular case is expressed by

$$\Delta p = \frac{\alpha}{L}\int_{r_w}^{\infty} \frac{q_t(r,t)}{k(r)\lambda_t(r,t)}\,\frac{dr}{r}. \tag{4.127}$$

By introducing the flood front $r_{zx,f}$ and the temperature front $r_{zx,T}$ in Eq. 4.127, we obtain

$$\Delta p = \frac{\alpha}{L}\int_{r_w}^{r_{zx,T}(t)} \frac{q_t(r,t)}{k(r)\lambda_{tc}(r,t)}\,\frac{dr}{r} + \frac{\alpha}{L}\int_{r_{zx,T}(t)}^{r_{zx,f}(t)} \frac{q_t(r,t)}{k(r)\lambda_{th}(r,t)}\,\frac{dr}{r} + \frac{\alpha}{L}\int_{r_{zx,f}(t)}^{\infty} \frac{q_t(r,t)}{k(r)\lambda_{th}(r,t)}\,\frac{dr}{r}. \tag{4.128}$$

By adding and subtracting to Eq. 4.128 an integral from r_w to $r_{zx,T}$, we have

$$\begin{aligned}\Delta p = \frac{\alpha}{L}\int_{r_w}^{r_{zx,T}(t)} \frac{q_t(r,t)}{k(r)\lambda_{tc}(r,t)}\,\frac{dr}{r} + \frac{\alpha}{L}\int_{r_{zx,T}(t)}^{r_{zx,f}(t)} \frac{q_t(r,t)}{k(r)\lambda_{th}(r,t)}\,\frac{dr}{r} + \frac{\alpha}{L}\int_{r_{zx,f}(t)}^{\infty} \frac{q_t(r,t)}{k(r)\lambda_{th}(r,t)}\,\frac{dr}{r} \\ + \frac{\alpha}{L}\int_{r_w}^{r_{zx,T}(t)} \frac{q_t(r,t)}{k(r)\lambda_{th}(r,t)}\,\frac{dr}{r} - \frac{\alpha}{L}\int_{r_w}^{r_{zx,T}(t)} \frac{q_t(r,t)}{k(r)\lambda_{th}(r,t)}\,\frac{dr}{r},\end{aligned} \tag{4.129}$$

which reduces to

$$\begin{aligned}\Delta p = \frac{\alpha}{L}\int_{r_w}^{r_{zx,f}(t)} \frac{q_t(r,t)}{k(r)\lambda_{th}(r,t)}\,\frac{dr}{r} + \frac{\alpha}{L}\int_{r_{zx,f}(t)}^{\infty} \frac{q_t(r,t)}{k(r)\lambda_{th}(r,t)}\,\frac{dr}{r} \\ + \frac{\alpha}{L}\int_{r_w}^{r_{zx,T}(t)} \left(\frac{1}{\lambda_{tc}(r,t)} - \frac{1}{\lambda_{th}(r,t)}\right)\frac{q_t(r,t)}{k(r)}\,\frac{dr}{r}.\end{aligned} \tag{4.130}$$

According to Eq. 2.135, the sum of the two first terms in Eq. 4.130 represents the isothermal injection solution for the wellbore pressure change based on the initial temperature of the reservoir that we denote by $\Delta p(T = T_{oi})$. Another expression for this isothermal solution is derived in chapter 2 and given by Eq. 2.137 which we rewrite here as

$$\Delta p(T = T_{oi}) = \Delta p_o(T = T_{oi}) + \frac{\alpha q_{inj}}{L\hat{\lambda}_{oh}}\int_{r_w}^{r_{zx,f}(t)} \left(\frac{\hat{\lambda}_{oh}}{\lambda_{th}(r,t)} - 1\right)\frac{dr}{rk(r)}, \tag{4.131}$$

where $\Delta p_o(T = T_{oi})$ represents the single-phase solution based on oil properties at irreducible water saturation evaluated at the initial temperature of the reservoir and defined by Eq. 2.138 for an offset well and by Eq. 2.139 for a well in the center of the formation. Based on this and using the fact that the temperature front is within the steady-state region such that $q_t(r,t) = q_{inj}$ for $r < r_{zx,T}$, Eq. 4.130 becomes

$$\Delta p = \Delta p(T = T_{oi}) + \frac{\alpha q_{inj}}{L} \int_{r_w}^{r_{zx,T}(t)} \left(\frac{1}{\lambda_{tc}(r,t)} - \frac{1}{\lambda_{th}(r,t)} \right) \frac{dr}{rk(r)}. \tag{4.132}$$

Here, we distinguish three situations with respect to the positions of the water front and the temperature front. These are:

(i) The case for which the water front is in the skin zone. This also means that the temperature front $r_{zx,T} < r_s$. Therefore, Eq. 4.132 becomes

$$\Delta p = \Delta p(T = T_{oi}) + \frac{\alpha q_{inj}}{k_s L} \int_{r_w}^{r_{zx,T}(t)} \left(\frac{1}{\lambda_{tc}(r,t)} - \frac{1}{\lambda_{th}(r,t)} \right) \frac{dr}{r}, \tag{4.133}$$

with $\Delta p(T = T_{oi})$ provided by Eq. 2.141. By introducing the Boltzmann variable and by assuming that λ_{th} and λ_{tc} are unique functions of Z so that $\lambda_{th}(r,t) = \lambda_{th}(Z)$ and $\lambda_{tc}(r,t) = \lambda_{tc}(Z)$, we can rewrite Eq. 4.133 as

$$\Delta p = \Delta p(T = T_{oi}) + \frac{\alpha q_{inj}}{2k_s L \hat{\lambda}_{oh}} \int_{r_w^2/4t}^{Z_T} \left(\frac{\hat{\lambda}_{oh}}{\lambda_{tc}(Z)} - \frac{\hat{\lambda}_{oh}}{\lambda_{th}(Z)} \right) \frac{dZ}{Z}. \tag{4.134}$$

If we first take the derivative of Eq. 4.134 with respect to the natural logarithm of time (using Leibnitz's rule) and then use Eq. 2.144 in the result, we obtain

$$\Delta p' = \frac{\alpha q_{inj}}{kL\hat{\lambda}_{oh}} \left[1 + \frac{k}{2k_s} \left(\frac{\hat{\lambda}_{oh}}{\lambda_{th}(r_w,t)} - 1 \right) \right] + \frac{\alpha q_{inj}}{2k_s L \hat{\lambda}_{oh}} \left(\frac{\hat{\lambda}_{oh}}{\lambda_{tc}(r_w,t)} - \frac{\hat{\lambda}_{oh}}{\lambda_{th}(r_w,t)} \right), \tag{4.135}$$

or simply

$$\Delta p' = \frac{\alpha q_{inj}}{kL\hat{\lambda}_{oh}}\left[1 + \frac{k}{2k_s}\left(\frac{\hat{\lambda}_{oh}}{\lambda_{tc}(r_w,t)} - 1\right)\right]. \tag{4.136}$$

At the wellbore, $\lambda_{tc}(r_w,t) = \hat{\lambda}_{wc}$. If we use the definition of the end-point mobility ratio evaluated at T_{wi} denoted by $\hat{M}_c$, Eq. 4.136 simplifies to

$$\Delta p' = \frac{\alpha q_{inj}}{kL\hat{\lambda}_{oh}}\left[1 + \frac{k}{2k_s}\left(\frac{1}{\hat{M}_c}\frac{\hat{\lambda}_{oh}}{\hat{\lambda}_{oc}} - 1\right)\right], \tag{4.137}$$

or equivalently

$$\Delta p' = \frac{\alpha q_{inj}}{kL\hat{\lambda}_{oh}}\left[1 + \frac{k}{2k_s}\left(\frac{1}{\hat{M}_c}\frac{\mu_{oc}}{\mu_{oh}} - 1\right)\right]. \tag{4.138}$$

This equation indicates that the pressure derivative can be negative at early times if

$$1 + \frac{k}{2k_s}\left(\frac{1}{\hat{M}_c}\frac{\mu_{oc}}{\mu_{oh}} - 1\right) < 0, \tag{4.139}$$

or after rearranging

$$\hat{M}_c\left(1 - \frac{2k_s}{k}\right) > \frac{\mu_{oc}}{\mu_{oh}}. \tag{4.140}$$

(ii) The case for which the water front is beyond the skin zone but the temperature front is still in the damaged region. In this case, the injection wellbore pressure change is also given by Eq. 4.133 but with an isothermal component provided by Eq. 2.150. We rewrite the nonisothermal solution as

$$\begin{aligned}\Delta p = \Delta p_o(T = T_{oi}) + \frac{\alpha q_{inj}}{kL\hat{\lambda}_{oh}}\left[\left(\frac{k}{k_s} - 1\right)\int_{r_w}^{r_s}\left(\frac{\hat{\lambda}_{oh}}{\lambda_{th}(r,t)} - 1\right)\frac{dr}{r}\right.\\ \left. + \int_{r_w}^{r_{zx,f}(t)}\left(\frac{\hat{\lambda}_{oh}}{\lambda_{th}(r,t)} - 1\right)\frac{dr}{r}\right] + \frac{\alpha q_{inj}}{k_s L\hat{\lambda}_{oh}}\int_{r_w}^{r_{zx,T}(t)}\left(\frac{\hat{\lambda}_{oh}}{\lambda_{tc}(r,t)} - \frac{\hat{\lambda}_{oh}}{\lambda_{th}(r,t)}\right)\frac{dr}{r}.\end{aligned} \tag{4.141}$$

In terms of Boltzmann variable, Eq. 4.141 can be expressed as

$$\Delta p = \Delta p_o(T = T_{oi}) + \frac{\alpha q_{inj}}{2kL\hat{\lambda}_{oh}}\left[\left(\frac{k}{k_s}-1\right)\int_{r_w^2/4t}^{r_s^2/4t}\left(\frac{\hat{\lambda}_{oh}}{\lambda_{th}(Z)}-1\right)\frac{dZ}{Z} + \int_{r_w^2/4t}^{Z_f}\left(\frac{\hat{\lambda}_{oh}}{\lambda_{th}(Z)}-1\right)\frac{dZ}{Z}\right] + \frac{\alpha q_{inj}}{2k_sL\hat{\lambda}_{oh}}\int_{r_w^2/4t}^{Z_T}\left(\frac{\hat{\lambda}_{oh}}{\lambda_{tc}(Z)}-\frac{\hat{\lambda}_{oh}}{\lambda_{th}(Z)}\right)\frac{dZ}{Z}. \quad (4.142)$$

From Eq. 2.138, we have

$$\Delta p_o'(T = T_{oi}) = \frac{\alpha q_{inj}}{kL\hat{\lambda}_{oh}}. \quad (4.143)$$

So taking the derivative of Eq. 4.142 with respect to the natural logarithm of time and using the result from Eq. 4.143 gives

$$\Delta p' = \frac{\alpha q_{inj}}{kL\hat{\lambda}_{oh}} + \frac{\alpha q_{inj}}{2kL\hat{\lambda}_{oh}}\left[\left(\frac{k}{k_s}-1\right)\left(\frac{\hat{\lambda}_{oh}}{\lambda_t(r_w^2/4t)}-\frac{\hat{\lambda}_{oh}}{\lambda_{th}(r_s^2/4t)}\right)+\left(\frac{\hat{\lambda}_{oh}}{\lambda_{th}(r_w^2/4t)}-1\right)\right] + \frac{\alpha q_{inj}}{2k_sL\hat{\lambda}_{oh}}\left(\frac{\hat{\lambda}_{oh}}{\lambda_{tc}(r_w^2/4t)}-\frac{\hat{\lambda}_{oh}}{\lambda_{th}(r_w^2/4t)}\right). \quad (4.144)$$

Simplifying more the above expression leads to

$$\Delta p' = \frac{\alpha q_{inj}}{2kL\hat{\lambda}_{oh}}\left[1-\left(\frac{k}{k_s}-1\right)\frac{\hat{\lambda}_{oh}}{\lambda_{th}(r_s,t)}+\frac{k}{k_s}\frac{\hat{\lambda}_{oh}}{\lambda_{tc}(r_w,t)}\right], \quad (4.145)$$

or by noting that $\lambda_{tc}(r_w,t) = \hat{\lambda}_{wc}$ and introducing the end-point mobility ratio evaluated at the initial temperature of the reservoir T_{oi} and denoted by $\hat{M}_h$

$$\Delta p' = \frac{\alpha q_{inj}}{2kL\hat{\lambda}_{wh}}\left[1+\hat{M}_h-\left(\frac{k}{k_s}-1\right)\left(\frac{\hat{\lambda}_{wh}}{\lambda_{th}(r_s,t)}-1\right)+\frac{k}{k_s}\left(\frac{\hat{\lambda}_{wh}}{\hat{\lambda}_{wc}}-1\right)\right]. \quad (4.146)$$

Eq. 4.146 shows that the pressure derivative can take negative values during this period of injection if the following condition is satisfied:

$$1+\hat{M}_h-\left(\frac{k}{k_s}-1\right)\left(\frac{\hat{\lambda}_{wh}}{\lambda_{th}(r_s,t)}-1\right)+\frac{k}{k_s}\left(\frac{\hat{\lambda}_{wh}}{\hat{\lambda}_{wc}}-1\right)<0, \quad (4.147)$$

or equivalently

$$\lambda_{th}(r_s,t)\left(\frac{\mu_{wc}}{\mu_{wh}}+\frac{k_s}{k}\hat{M}_h\right)<\hat{\lambda}_{wh}\left(1-\frac{k_s}{k}\right). \tag{4.148}$$

(iii) The case for which both the water front and the temperature front are beyond the damaged region. In this case, the injection wellbore pressure change is given

$$\Delta p=\Delta p(T=T_{oi})+\frac{\alpha q_{inj}}{k_s L}\int_{r_w}^{r_s}\left(\frac{1}{\lambda_{tc}(r,t)}-\frac{1}{\lambda_{th}(r,t)}\right)\frac{dr}{r} + \frac{\alpha q_{inj}}{kL}\int_{r_s}^{r_{zx,T}(t)}\left(\frac{1}{\lambda_{tc}(r,t)}-\frac{1}{\lambda_{th}(r,t)}\right)\frac{dr}{r}, \tag{4.149}$$

where $\Delta p(T=T_{oi})$ is given by Eq. 2.150. We rewrite Eq. 4.149 as

$$\Delta p=\Delta p(T=T_{oi})+\frac{\alpha q_{inj}}{kL\hat{\lambda}_{oh}}\left[\left(\frac{k}{k_s}-1\right)\int_{r_w}^{r_s}\left(\frac{\hat{\lambda}_{oh}}{\lambda_{tc}(r,t)}-\frac{\hat{\lambda}_{oh}}{\lambda_{th}(r,t)}\right)\frac{dr}{r} + \int_{r_w}^{r_{zx,T}(t)}\left(\frac{\hat{\lambda}_{oh}}{\lambda_{tc}(r,t)}-\frac{\hat{\lambda}_{oh}}{\lambda_{th}(r,t)}\right)\frac{dr}{r}, \tag{4.150}$$

or in terms of the Boltzmann variable as

$$\Delta p=\Delta p(T=T_{oi})+\frac{\alpha q_{inj}}{2kL\hat{\lambda}_{oh}}\left[\left(\frac{k}{k_s}-1\right)\int_{r_w^2/4t}^{r_s^2/4t}\left(\frac{\hat{\lambda}_{oh}}{\lambda_{tc}(Z)}-\frac{\hat{\lambda}_{oh}}{\lambda_{th}(Z)}\right)\frac{dZ}{Z} + \int_{r_w^2/4t}^{Z_T}\left(\frac{\hat{\lambda}_{oh}}{\lambda_{tc}(Z)}-\frac{\hat{\lambda}_{oh}}{\lambda_{th}(Z)}\right)\frac{dZ}{Z}\right], \tag{4.151}$$

where again $\Delta p(T=T_{oi})$ is given by Eq. 4.131 and Eq. 4.143 applies. Taking the derivative of Eq. 4.151 with respect to $\ln(t)$ yields

$$\Delta p' = \frac{\alpha q_{inj}}{kL\hat{\lambda}_{oh}} + \frac{\alpha q_{inj}}{2kL\hat{\lambda}_{oh}}\left[\left(\frac{k}{k_s}-1\right)\left(\frac{\hat{\lambda}_{oh}}{\lambda_{th}(r_w^2/4t)} - \frac{\hat{\lambda}_{oh}}{\lambda_{th}(r_s^2/4t)}\right) + \left(\frac{\hat{\lambda}_{oh}}{\lambda_{th}(r_w^2/4t)}-1\right)\right]$$
$$+ \frac{\alpha q_{inj}}{2kL\hat{\lambda}_{oh}}\left[\left(\frac{k}{k_s}-1\right)\left(\frac{\hat{\lambda}_{oh}}{\lambda_{th}(r_s^2/4t)} - \frac{\hat{\lambda}_{oh}}{\lambda_{tc}(r_s^2/4t)} + \frac{\hat{\lambda}_{oh}}{\lambda_{tc}(r_w^2/4t)} - \frac{\hat{\lambda}_{oh}}{\lambda_{th}(r_w^2/4t)}\right)\right.$$
$$\left. + \frac{\hat{\lambda}_{oh}}{\lambda_{tc}(r_w^2/4t)} - \frac{\hat{\lambda}_{oh}}{\lambda_{th}(r_w^2/4t)}\right]. \quad (4.152)$$

If we simplify and rearrange Eq. 4.152, we obtain

$$\Delta p' = \frac{\alpha q_{inj}}{2kL\hat{\lambda}_{oh}}\left[1 + \left(\frac{k}{k_s}-1\right)\left(\frac{\hat{\lambda}_{oh}}{\lambda_{tc}(r_w,t)} - \frac{\hat{\lambda}_{oh}}{\lambda_{tc}(r_s,t)}\right) + \frac{\hat{\lambda}_{oh}}{\lambda_{tc}(r_w,t)}\right], \quad (4.153)$$

which we can rewrite as

$$\Delta p' = \frac{\alpha q_{inj}}{2kL\hat{\lambda}_{oh}}\left[1 + \left(\frac{k}{k_s}-1\right)\left(\frac{\hat{\lambda}_{oh}}{\hat{\lambda}_{wc}} - \frac{\hat{\lambda}_{oh}}{\lambda_{tc}(r_s,t)}\right) + \frac{\hat{\lambda}_{oh}}{\hat{\lambda}_{wc}}\right], \quad (4.154)$$

or

$$\Delta p' = \frac{\alpha q_{inj}}{2kL\hat{\lambda}_{wc}}\left[1 + \frac{\mu_{oh}}{\mu_{oc}}\hat{M}_c + \left(\frac{k}{k_s}-1\right)\left(1 - \frac{\hat{\lambda}_{wc}}{\lambda_{tc}(r_s,t)}\right)\right]. \quad (4.155)$$

Once the damaged zone is completely flooded, $\lambda_{tc}(r_s,t) = \hat{\lambda}_{wc}$ and Eq. 4.155 becomes

$$\Delta p' = \frac{\alpha q_{inj}}{2kL\hat{\lambda}_{wc}}\left[1 + \frac{\mu_{oh}}{\mu_{oc}}\hat{M}_c\right]. \quad (4.156)$$

First Linear/First Radial/First Radial Flow Regime

This flow regime corresponds to the case when the steady-state zone of constant rate is moving linearly in the x-direction while the flood front and the temperature front are still propagating radially in the (x,z) plane. Recall that the horizontal well is assumed to be along the y-direction. Similarly to the isothermal solution (see Eq. 2.156), the wellbore pressure change for this case is given by

$$\Delta p = \frac{\pi\alpha}{kL}\int_{x_1}^{\infty}\frac{q_t(x,t)}{\lambda_t(x,t)}\frac{dx}{h(x)} + \frac{\alpha}{L}\int_{r_w}^{z_w}\frac{q_t(r,t)}{k(r)\lambda_t(r,t)}\frac{dr}{r}. \tag{4.157}$$

If we introduce the the water front location $r_{zx,f}$ and the temperature front $r_{zx,T}$, we can rewrite Eq. 4.157 as

$$\Delta p = \frac{\pi\alpha}{kL\hat{\lambda}_{oh}}\int_{x=0}^{\infty} q_t(x,t)\frac{dx}{h(x)} - \frac{\pi\alpha q_{inj}}{kL\hat{\lambda}_{oh}}\int_0^{x_1}\frac{dx}{h(x)} + \frac{\alpha q_{inj}}{L}\int_{r_w}^{r_{zx,T}(t)}\frac{1}{\lambda_{tc}(r,t)}\frac{dr}{rk(r)} + \frac{\alpha q_{inj}}{L}\int_{r_{zx,T}(t)}^{r_{zx,f}(t)}\frac{1}{\lambda_{th}(r,t)}\frac{dr}{rk(r)} + \frac{\alpha q_{inj}}{L\hat{\lambda}_{oh}}\int_{r_{zx,f}(t)}^{z_w}\frac{dr}{rk(r)}. \tag{4.158}$$

By adding and subtracting an integral from r_w to $r_{zx,T}$, Eq. 4.158 becomes

$$\Delta p = \frac{\pi\alpha}{kL\hat{\lambda}_{oh}}\int_{x=0}^{\infty} q_t(x,t)\frac{dx}{h(x)} - \frac{\pi\alpha q_{inj}}{kL\hat{\lambda}_{oh}}\int_0^{x_1}\frac{dx}{h(x)} + \frac{\alpha q_{inj}}{L}\int_{r_w}^{r_{zx,T}(t)}\frac{1}{\lambda_{tc}(r,t)}\frac{dr}{rk(r)} + \frac{\alpha q_{inj}}{L}\int_{r_{zx,T}(t)}^{r_{zx,f}(t)}\frac{1}{\lambda_{th}(r,t)}\frac{dr}{rk(r)} + \frac{\alpha q_{inj}}{L\hat{\lambda}_{oh}}\int_{r_{zx,f}(t)}^{z_w}\frac{dr}{rk(r)} + \frac{\alpha q_{inj}}{L}\int_{r_w}^{r_{zx,T}(t)}\frac{1}{\lambda_{th}(r,t)}\frac{dr}{rk(r)} - \frac{\alpha q_{inj}}{L}\int_{r_w}^{r_{zx,T}(t)}\frac{1}{\lambda_{th}(r,t)}\frac{dr}{rk(r)}, \tag{4.159}$$

or after rearranging,

$$\Delta p = \frac{\pi\alpha}{kL\hat{\lambda}_{oh}}\int_{x=0}^{\infty} q_t(x,t)\frac{dx}{h(x)} - \frac{\pi\alpha q_{inj}}{kL\hat{\lambda}_{oh}}\int_0^{x_1}\frac{dx}{h(x)} + \frac{\alpha q_{inj}}{L\hat{\lambda}_{oh}}\int_{r_w}^{r_{zx,f}(t)}\frac{\hat{\lambda}_{oh}}{\lambda_{th}(r,t)}\frac{dr}{rk(r)} + \frac{\alpha q_{inj}}{L\hat{\lambda}_{oh}}\int_{r_{zx,f}(t)}^{z_w}\frac{dr}{rk(r)} + \frac{\alpha q_{inj}}{L\hat{\lambda}_{oh}}\int_{r_w}^{r_{zx,T}(t)}\left(\frac{\hat{\lambda}_{oh}}{\lambda_{tc}(r,t)} - \frac{\hat{\lambda}_{oh}}{\lambda_{th}(r,t)}\right)\frac{dr}{rk(r)}. \tag{4.160}$$

A comparison between this equation and Eq. 2.157 indicates that the nonisothermal solution for the wellbore pressure change is expressed as the sum of the corresponding isothermal solution (Eq. 2.157) and a component that takes into account the difference of mobilities in the flooded bank. Thus, we have

$$\Delta p = \Delta p(T = T_{oi}) + \frac{\alpha q_{inj}}{L\hat{\lambda}_{oh}} \int_{r_w}^{r_{zx,T}(t)} \left(\frac{\hat{\lambda}_{oh}}{\lambda_{tc}(r,t)} - \frac{\hat{\lambda}_{oh}}{\lambda_{th}(r,t)} \right) \frac{dr}{rk(r)}, \tag{4.161}$$

with $\Delta p(T = T_{oi})$ given according to Eq. 2.163 by

$$\begin{aligned} \Delta p(T = T_{oi}) &= \frac{\pi\alpha}{kL\hat{\lambda}_{oh}} \int_{x=0}^{\infty} q_t(x,t) \frac{dx}{h(x)} + \frac{\alpha q_{inj}}{kh\hat{\lambda}_{oh}} \left[\frac{h}{L}(s_z + s) \right] \\ &+ \frac{\alpha q_{inj}}{L\hat{\lambda}_{oh}} \int_{r_w}^{r_{zx,f}(t)} \left(\frac{\hat{\lambda}_{oh}}{\lambda_{th}(r,t)} - 1 \right) \frac{dr}{rk(r)} \\ &= \Delta p_o(T = T_{oi}) + \frac{\alpha q_{inj}}{L\hat{\lambda}_{oh}} \int_{r_w}^{r_{zx,f}(t)} \left(\frac{\hat{\lambda}_{oh}}{\lambda_{th}(r,t)} - 1 \right) \frac{dr}{rk(r)}. \end{aligned} \tag{4.162}$$

Similarly to the first flow regime, we observe three different situations:

(i) The water front and the temperature front are in the skin zone. Eq. 4.161 becomes

$$\begin{aligned} \Delta p = \Delta p_o(T = T_{oi}) &+ \frac{\alpha q_{inj}}{k_s L\hat{\lambda}_{oh}} \int_{r_w}^{r_{zx,f}(t)} \left(\frac{\hat{\lambda}_{oh}}{\lambda_{th}(r,t)} - 1 \right) \frac{dr}{r} \\ &+ \frac{\alpha q_{inj}}{k_s L\hat{\lambda}_{oh}} \int_{r_w}^{r_{zx,T}(t)} \left(\frac{\hat{\lambda}_{oh}}{\lambda_{tc}(r,t)} - \frac{\hat{\lambda}_{oh}}{\lambda_{th}(r,t)} \right) \frac{dr}{r}, \end{aligned} \tag{4.163}$$

that we rewrite in terms of the similarity variable Z as

$$\begin{aligned} \Delta p = \Delta p_o(T = T_{oi}) &+ \frac{\alpha q_{inj}}{2k_s L\hat{\lambda}_{oh}} \int_{r_w^2/4t}^{Z_f} \left(\frac{\hat{\lambda}_{oh}}{\lambda_{th}(Z)} - 1 \right) \frac{dZ}{Z} \\ &+ \frac{\alpha q_{inj}}{2k_s L\hat{\lambda}_{oh}} \int_{r_w^2/4t}^{Z_T} \left(\frac{\hat{\lambda}_{oh}}{\lambda_{tc}(Z)} - \frac{\hat{\lambda}_{oh}}{\lambda_{th}(Z)} \right) \frac{dZ}{Z}. \end{aligned} \tag{4.164}$$

Differentiating Eq. 4.164 with respect to $\ln(t)$ yields

$$\Delta p' = \Delta p'_o(T = T_{oi}) + \frac{\alpha q_{inj}}{2k_s L\hat{\lambda}_{oh}}\left(\frac{\hat{\lambda}_{oh}}{\lambda_{th}(r_w^2/4t)} - 1\right) + \frac{\alpha q_{inj}}{2k_s L\hat{\lambda}_{oh}}\left(\frac{\hat{\lambda}_{oh}}{\lambda_{tc}(r_w^2/4t)} - \frac{\hat{\lambda}_{oh}}{\lambda_{th}(r_w^2/4t)}\right), \quad (4.165)$$

or simply

$$\Delta p' = \Delta p'_o(T = T_{oi}) + \frac{\alpha q_{inj}}{2k_s L\hat{\lambda}_{oh}}\left(\frac{\hat{\lambda}_{oh}}{\lambda_{tc}(r_w, t)} - 1\right). \quad (4.166)$$

The pressure derivative of the single-phase oil solution is defined by Eq. 2.170. Therefore, using this equation along with the fact that $\lambda_{tc}(r_w, t) = \hat{\lambda}_{wc}$ in Eq. 4.166 gives

$$\Delta p'_o = \frac{\alpha q_{inj}}{2kh\hat{\lambda}_{oh}}\left[\sqrt{\frac{4\pi\beta k\hat{\lambda}_{oh}t}{\phi\hat{c}_{to}L^2}} + \frac{h}{L}\frac{k}{k_s}\left(\frac{\hat{\lambda}_{oh}}{\hat{\lambda}_{wc}} - 1\right)\right], \quad (4.167)$$

or finally

$$\Delta p'_o = \frac{\alpha q_{inj}}{2kh\hat{\lambda}_{oh}}\left[\sqrt{\frac{4\pi\beta k\hat{\lambda}_{oh}t}{\phi\hat{c}_{to}L^2}} + \frac{h}{L}\frac{k}{k_s}\left(\frac{\mu_{oc}}{\mu_{oh}}\frac{1}{\hat{M}_c} - 1\right)\right]. \quad (4.168)$$

(ii) The case for which the water front is beyond the skin zone but not the temperature front, is also described by a wellbore pressure drop given by Eq. 4.161 with the isothermal component $\Delta p(T = T_{oi})$ provided by Eq. 2.173. In this case, we have

$$\Delta p = \Delta p_o(T = T_{oi}) + \frac{\alpha q_{inj}}{kL\hat{\lambda}_{oh}}\left[\left(\frac{k}{k_s} - 1\right)\int_{r_w}^{r_s}\left(\frac{\hat{\lambda}_{oh}}{\lambda_{th}(r,t)} - 1\right)\frac{dr}{r} + \int_{r_w}^{r_{zx,f}(t)}\left(\frac{\hat{\lambda}_{oh}}{\lambda_{th}(r,t)} - 1\right)\frac{dr}{r}\right] + \frac{\alpha q_{inj}}{k_s L\hat{\lambda}_{oh}}\int_{r_w}^{r_{zx,T}(t)}\left(\frac{\hat{\lambda}_{oh}}{\lambda_{tc}(r,t)} - \frac{\hat{\lambda}_{oh}}{\lambda_{th}(r,t)}\right)\frac{dr}{r}. \quad (4.169)$$

In terms of Boltzmann variable, Eq. 4.169 is rewritten as

$$\Delta p = \Delta p_o(T=T_{oi}) + \frac{\alpha q_{inj}}{2kL\hat{\lambda}_{oh}}\left[\left(\frac{k}{k_s}-1\right)\int_{r_w^2/4t}^{r_s^2/4t}\left(\frac{\hat{\lambda}_{oh}}{\lambda_{th}(Z)}-1\right)\frac{dZ}{Z}+\int_{r_w^2/4t}^{Z_f}\left(\frac{\hat{\lambda}_{oh}}{\lambda_{th}(Z)}-1\right)\frac{dZ}{Z}\right] + \frac{\alpha q_{inj}}{2k_sL\hat{\lambda}_{oh}}\int_{r_w^2/4t}^{Z_T}\left(\frac{\hat{\lambda}_{oh}}{\lambda_{tc}(Z)}-\frac{\hat{\lambda}_{oh}}{\lambda_{th}(Z)}\right)\frac{dZ}{Z}. \quad (4.170)$$

By using Leibnitz's rule when differentiating Eq. 4.170 with respect to $\ln(t)$, we get the following expression for the pressure derivative

$$\Delta p' = \Delta p'_o(T=T_{oi}) + \frac{\alpha q_{inj}}{2kL\hat{\lambda}_{oh}}\left[\left(\frac{k}{k_s}-1\right)\left(\frac{\hat{\lambda}_{oh}}{\lambda_{th}(r_w^2/4t)}-\frac{\hat{\lambda}_{oh}}{\lambda_{th}(r_s^2/4t)}\right)+\frac{\hat{\lambda}_{oh}}{\lambda_{th}(r_w^2/4t)}-1\right] + \frac{\alpha q_{inj}}{2k_sL\hat{\lambda}_{oh}}\left(\frac{\hat{\lambda}_{oh}}{\lambda_{tc}(r_w^2/4t)}-\frac{\hat{\lambda}_{oh}}{\lambda_{th}(r_w^2/4t)}\right), \quad (4.171)$$

that we simplify to

$$\Delta p' = \Delta p'_o(T=T_{oi}) + \frac{\alpha q_{inj}}{2kL\hat{\lambda}_{oh}}\left[\frac{k}{k_s}\frac{\hat{\lambda}_{oh}}{\hat{\lambda}_{wc}}-1-\left(\frac{k}{k_s}-1\right)\frac{\hat{\lambda}_{oh}}{\lambda_{th}(r_s,t)}\right]. \quad (4.172)$$

Introducing the end-point mobility ratio evaluated at T_{oi}, it is easy to show that Eq. 4.172 can be written as

$$\Delta p' = \Delta p'_o(T=T_{oi}) + \frac{\alpha q_{inj}}{2kL\hat{\lambda}_{wh}}\left[1-\hat{M}_h+\frac{k}{k_s}\left(\frac{\mu_{wc}}{\mu_{wh}}-1\right)-\left(\frac{k}{k_s}-1\right)\left(\frac{\hat{\lambda}_{wh}}{\lambda_{th}(r_s,t)}-1\right)\right], \quad (4.173)$$

or,

$$\Delta p' = \frac{\alpha q_{inj}}{2kh\hat{\lambda}_{oh}}\sqrt{\frac{4\pi\beta k\hat{\lambda}_{oh}t}{\phi\hat{c}_{to}L^2}}+\frac{\alpha q_{inj}}{2kL\hat{\lambda}_{wh}}\left[1-\hat{M}_h+\frac{k}{k_s}\left(\frac{\mu_{wc}}{\mu_{wh}}-1\right)-\left(\frac{k}{k_s}-1\right)\left(\frac{\hat{\lambda}_{wh}}{\lambda_{th}(r_s,t)}-1\right)\right], \quad (4.174)$$

if we use the expression of $\Delta p'_o(T=T_{oi})$ provided by Eq. 2.170.

(iii) This is the case where both fronts are beyond the skin zone. The wellbore pressure change is expressed in terms of (r,t) variables and the Boltzmann variable respectively by

$$\Delta p = \Delta p_o(T=T_{oi}) + \frac{\alpha q_{inj}}{kL\hat{\lambda}_{oh}}\left[\left(\frac{k}{k_s}-1\right)\int_{r_w}^{r_s}\left(\frac{\hat{\lambda}_{oh}}{\lambda_{th}(r,t)}-1\right)\frac{dr}{r} + \int_{r_w}^{r_{zx,f}(t)}\left(\frac{\hat{\lambda}_{oh}}{\lambda_{th}(r,t)}-1\right)\frac{dr}{r}\right] + \frac{\alpha q_{inj}}{kL\hat{\lambda}_{oh}}\left[\left(\frac{k}{k_s}-1\right)\int_{r_w}^{r_s}\left(\frac{\hat{\lambda}_{oh}}{\lambda_{tc}(r,t)}-\frac{\hat{\lambda}_{oh}}{\lambda_{th}(r,t)}\right)\frac{dr}{r} + \int_{r_w}^{r_{zx,T}(t)}\left(\frac{\hat{\lambda}_{oh}}{\lambda_{tc}(r,t)}-\frac{\hat{\lambda}_{oh}}{\lambda_{th}(r,t)}\right)\frac{dr}{r}\right], \tag{4.175}$$

and

$$\Delta p = \Delta p_o(T=T_{oi}) + \frac{\alpha q_{inj}}{2kL\hat{\lambda}_{oh}}\left[\left(\frac{k}{k_s}-1\right)\int_{r_w^2/4t}^{r_s^2/4t}\left(\frac{\hat{\lambda}_{oh}}{\lambda_{th}(Z)}-1\right)\frac{dZ}{Z} + \int_{r_w^2/4t}^{Z_f}\left(\frac{\hat{\lambda}_{oh}}{\lambda_{th}(Z)}-1\right)\frac{dZ}{Z}\right] + \frac{\alpha q_{inj}}{2kL\hat{\lambda}_{oh}}\left[\left(\frac{k}{k_s}-1\right)\int_{r_w^2/4t}^{r_s^2/4t}\left(\frac{\hat{\lambda}_{oh}}{\lambda_{tc}(Z)}-\frac{\hat{\lambda}_{oh}}{\lambda_{th}(Z)}\right)\frac{dZ}{Z} + \int_{r_w^2/4t}^{Z_T}\left(\frac{\hat{\lambda}_{oh}}{\lambda_{tc}(Z)}-\frac{\hat{\lambda}_{oh}}{\lambda_{th}(Z)}\right)\frac{dZ}{Z}\right]. \tag{4.176}$$

Differentiating Eq. 4.176 with respect to $\ln(t)$ gives

$$\begin{aligned}\Delta p' = \Delta p'_o(T=T_{oi}) &+ \frac{\alpha q_{inj}}{2kL\hat{\lambda}_{oh}}\left[\left(\frac{k}{k_s}-1\right)\left(\frac{\hat{\lambda}_{oh}}{\lambda_{th}(r_w^2/4t)}-\frac{\hat{\lambda}_{oh}}{\lambda_{th}(r_s^2/4t)}\right)+\frac{\hat{\lambda}_{oh}}{\lambda_{th}(r_w^2/4t)}-1\right] \\ &+ \frac{\alpha q_{inj}}{2kL\hat{\lambda}_{oh}}\left[\left(\frac{k}{k_s}-1\right)\left(\frac{\hat{\lambda}_{oh}}{\lambda_{th}(r_s^2/4t)}-\frac{\hat{\lambda}_{oh}}{\lambda_{tc}(r_s^2/4t)}+\frac{\hat{\lambda}_{oh}}{\lambda_{tc}(r_w^2/4t)}-\frac{\hat{\lambda}_{oh}}{\lambda_{th}(r_w^2/4t)}\right)\right. \\ &\left.+\frac{\hat{\lambda}_{oh}}{\lambda_{tc}(r_w^2/4t)}-\frac{\hat{\lambda}_{oh}}{\lambda_{th}(r_w^2/4t)}\right].\end{aligned} \tag{4.177}$$

If we simplify and rearrange the above equation, we obtain

$$\Delta p' = \Delta p'_o(T=T_{oi}) + \frac{\alpha q_{inj}}{2kL\hat{\lambda}_{oh}}\left[\frac{\hat{\lambda}_{oh}}{\hat{\lambda}_{wc}}-1+\left(\frac{k}{k_s}-1\right)\left(\frac{\hat{\lambda}_{oh}}{\hat{\lambda}_{wc}}-\frac{\hat{\lambda}_{oh}}{\lambda_{tc}(r_s,t)}\right)\right], \tag{4.178}$$

or equivalently,

$$\Delta p' = \frac{\alpha q_{inj}}{2kh\hat{\lambda}_{oh}}\sqrt{\frac{4\pi\beta k\hat{\lambda}_{oh}t}{\phi\hat{c}_{to}L^2}} + \frac{\alpha q_{inj}}{2kL\hat{\lambda}_{wc}}\left[1 - \frac{\mu_{oh}}{\mu_{oc}}\hat{M}_c + \left(\frac{k}{k_s} - 1\right)\left(1 - \frac{\hat{\lambda}_{wc}}{\lambda_{tc}(r_s,t)}\right)\right], \quad (4.179)$$

where the derivative of the single-phase oil solution, $\Delta p'_o(T = T_{oi})$, was replaced by its expression given by Eq. 2.170. As time goes on, the water saturation increases leading to an increase in the total mobility in the damaged zone. Eventually, $\lambda_{tc}(r_s,t) = \hat{\lambda}_{wc}$ and the pressure derivative becomes simply

$$\Delta p' = \frac{\alpha q_{inj}}{2kh\hat{\lambda}_{oh}}\sqrt{\frac{4\pi\beta k\hat{\lambda}_{oh}t}{\phi\hat{c}_{to}L^2}} + \frac{\alpha q_{inj}}{2kL\hat{\lambda}_{wc}}\left[1 - \frac{\mu_{oh}}{\mu_{oc}}\hat{M}_c\right]. \quad (4.180)$$

First Linear/First Linear/First Radial Flow Regime

This flow regime occurs when both the pressure diffusion and the water front move linearly in the x-direction whereas, the temperature front is still propagating radially in the (x,z) plane. In this case, the wellbore pressure drop is described by the following expression

$$\Delta p = \frac{\pi\alpha}{kL}\int_{x_1}^{x_f(t)} \frac{q_t(x,t)}{\lambda_{th}(x,t)}\frac{dx}{h(x)} + \frac{\pi\alpha}{kL}\int_{x_f(t)}^{\infty} \frac{q_t(x,t)}{\lambda_{th}(x,t)}\frac{dx}{h(x)} + \frac{\alpha}{L}\int_{r_w}^{r_{zx,T}(t)} \frac{q_t(r,t)}{\lambda_{tc}(r,t)}\frac{dr}{rk(r)} + \frac{\alpha}{L}\int_{r_{zx,T}(t)}^{z_w} \frac{q_t(r,t)}{\lambda_{th}(r,t)}\frac{dr}{rk(r)}. \quad (4.181)$$

By adding and subtracting to Eq. 4.181 an integral from r_w to $r_{zx,T}$, we obtain

$$\Delta p = \frac{\pi\alpha}{kL}\int_{x_1}^{x_f(t)} \frac{q_t(x,t)}{\lambda_{th}(x,t)}\frac{dx}{h(x)} + \frac{\pi\alpha}{kL}\int_{x_f(t)}^{\infty} \frac{q_t(x,t)}{\lambda_{th}(x,t)}\frac{dx}{h(x)} + \frac{\alpha}{L}\int_{r_w}^{r_{zx,T}(t)} \frac{q_t(r,t)}{\lambda_{tc}(r,t)}\frac{dr}{rk(r)} + \frac{\alpha}{L}\int_{r_{zx,T}(t)}^{z_w} \frac{q_t(r,t)}{\lambda_{th}(r,t)}\frac{dr}{rk(r)} + \frac{\alpha}{L}\int_{r_w}^{r_{zx,T}(t)} \frac{q_t(r,t)}{\lambda_{th}(r,t)}\frac{dr}{rk(r)} - \frac{\alpha}{L}\int_{r_w}^{r_{zx,T}(t)} \frac{q_t(r,t)}{\lambda_{th}(r,t)}\frac{dr}{rk(r)}, \quad (4.182)$$

or after manipulating

$$\Delta p = \frac{\pi\alpha}{kL}\int_{x_1}^{x_f(t)} \frac{q_t(x,t)}{\lambda_{th}(x,t)}\frac{dx}{h(x)} + \frac{\pi\alpha}{kL}\int_{x_f(t)}^{\infty} \frac{q_t(x,t)}{\lambda_{th}(x,t)}\frac{dx}{h(x)} + \frac{\alpha}{L}\int_{r_w}^{z_w} \frac{q_t(r,t)}{\lambda_{th}(r,t)}\frac{dr}{rk(r)} + \frac{\alpha}{L}\int_{r_w}^{r_{zx,T}(t)} \left[\frac{q_t(r,t)}{\lambda_{tc}(r,t)} - \frac{q_t(r,t)}{\lambda_{th}(r,t)}\right]\frac{dr}{rk(r)}. \quad (4.183)$$

From Eq. 2.182, we have

$$\frac{\alpha}{L}\int_{r_w}^{z_w} \frac{q_t(r,t)}{\lambda_{th}(r,t)}\frac{dr}{rk(r)} = \frac{\alpha q_{inj}}{L\hat{\lambda}_{oh}}\int_{r_w}^{z_w}\left(\frac{\hat{\lambda}_{oh}}{\lambda_{th}(r,t)} - 1\right)\frac{dr}{rk(r)} + \frac{\alpha q_{inj}}{kL\hat{\lambda}_{oh}}\left[s + \ln\left(\frac{z_w}{r_w}\right)\right]. \quad (4.184)$$

Substituting this result into Eq. 4.183 and setting $\lambda_{th} = \hat{\lambda}_{oh}$ ahead the front and $q_t = q_{inj}$ behind the front gives

$$\Delta p = \frac{\pi\alpha q_{inj}}{kL\hat{\lambda}_{oh}}\int_{x_1}^{x_f(t)} \frac{\hat{\lambda}_{oh}}{\lambda_{th}(x,t)}\frac{dx}{h(x)} + \frac{\pi\alpha}{kL\hat{\lambda}_{oh}}\int_{x_f(t)}^{\infty} q_t(x,t)\frac{dx}{h(x)} + \frac{\alpha q_{inj}}{L\hat{\lambda}_{oh}}\int_{r_w}^{z_w}\left(\frac{\hat{\lambda}_{oh}}{\lambda_{th}(r,t)} - 1\right)\frac{dr}{rk(r)} + \frac{\alpha q_{inj}}{kL\hat{\lambda}_{oh}}\left[s + \ln\left(\frac{z_w}{r_w}\right)\right] + \frac{\alpha q_{inj}}{L\hat{\lambda}_{oh}}\int_{r_w}^{r_{zx,T}(t)}\left[\frac{\hat{\lambda}_{oh}}{\lambda_{tc}(r,t)} - \frac{\hat{\lambda}_{oh}}{\lambda_{th}(r,t)}\right]\frac{dr}{rk(r)}. \quad (4.185)$$

Except for the last component, the sum of all the other terms in Eq. 4.185 represents the isothermal pressure change according to Eq. 2.183. Thus, based on this and using Eq. 2.188 which gives a simplified form of the isothermal solution, our nonisothermal pressure change is rewritten as

$$\Delta p = \Delta p_o(T = T_{oi}) + \frac{\alpha q_{inj}}{L\hat{\lambda}_{oh}} \int_{r_w}^{z_w} \left(\frac{\hat{\lambda}_{oh}}{\lambda_{th}(r,t)} - 1 \right) \frac{dr}{rk(r)} + \frac{\pi\alpha q_{inj}}{kL\hat{\lambda}_{oh}} \int_{x_1}^{x_f(t)} \left(\frac{\hat{\lambda}_{oh}}{\lambda_{th}(x,t)} - 1 \right) \frac{dx}{h(x)} + \frac{\alpha q_{inj}}{L\hat{\lambda}_{oh}} \int_{r_w}^{r_{zx,T}(t)} \left[\frac{\hat{\lambda}_{oh}}{\lambda_{tc}(r,t)} - \frac{\hat{\lambda}_{oh}}{\lambda_{th}(r,t)} \right] \frac{dr}{rk(r)}. \quad (4.186)$$

First Linear/First Linear/First Linear Flow Regime

This situation pertains to the case when the steady-state zone and both fronts are propagating linearly along the x-direction. The wellbore pressure change in this case is expressed by

$$\Delta p = \frac{\pi\alpha}{kL} \int_{x_1}^{x_T(t)} \frac{q_t(x,t)}{\lambda_{tc}(x,t)} \frac{dx}{h(x)} + \frac{\pi\alpha}{kL} \int_{x_T(t)}^{x_f(t)} \frac{q_t(x,t)}{\lambda_{th}(x,t)} \frac{dx}{h(x)} + \frac{\pi\alpha}{kL} \int_{x_f(t)}^{\infty} \frac{q_t(x,t)}{\lambda_{th}(x,t)} \frac{dx}{h(x)} + \frac{\alpha}{L} \int_{r_w}^{z_w} \frac{q_t(r,t)}{\lambda_{tc}(r,t)} \frac{dr}{rk(r)}. \quad (4.187)$$

Here, we add and subtract an integral from x_1 to x_T and another one from r_w to z_w to obtain

$$\Delta p = \frac{\pi\alpha}{kL} \int_{x_1}^{x_T(t)} \frac{q_t(x,t)}{\lambda_{tc}(x,t)} \frac{dx}{h(x)} + \frac{\pi\alpha}{kL} \int_{x_T(t)}^{x_f(t)} \frac{q_t(x,t)}{\lambda_{th}(x,t)} \frac{dx}{h(x)} + \frac{\pi\alpha}{kL} \int_{x_f(t)}^{\infty} \frac{q_t(x,t)}{\lambda_{th}(x,t)} \frac{dx}{h(x)} + \frac{\alpha}{L} \int_{r_w}^{z_w} \frac{q_t(r,t)}{\lambda_{tc}(r,t)} \frac{dr}{rk(r)} + \frac{\pi\alpha}{kL} \int_{x_1}^{x_T(t)} \frac{q_t(x,t)}{\lambda_{th}(x,t)} \frac{dx}{h(x)} - \frac{\pi\alpha}{kL} \int_{x_1}^{x_T(t)} \frac{q_t(x,t)}{\lambda_{th}(x,t)} \frac{dx}{h(x)} + \frac{\alpha}{L} \int_{r_w}^{z_w} \frac{q_t(r,t)}{\lambda_{th}(r,t)} \frac{dr}{rk(r)} - \frac{\alpha}{L} \int_{r_w}^{z_w} \frac{q_t(r,t)}{\lambda_{th}(r,t)} \frac{dr}{rk(r)}, \quad (4.188)$$

or

$$\Delta p = \frac{\pi\alpha}{kL}\int_{x_1}^{x_f(t)} \frac{q_t(x,t)}{\lambda_{th}(x,t)}\frac{dx}{h(x)} + \frac{\pi\alpha}{kL}\int_{x_f(t)}^{\infty} \frac{q_t(x,t)}{\lambda_{th}(x,t)}\frac{dx}{h(x)} + \frac{\alpha}{L}\int_{r_w}^{z_w} \frac{q_t(r,t)}{\lambda_{th}(r,t)}\frac{dr}{rk(r)} + \frac{\alpha}{L}\int_{r_w}^{z_w}\left[\frac{q_t(r,t)}{\lambda_{tc}(r,t)} - \frac{q_t(r,t)}{\lambda_{th}(r,t)}\right]\frac{dr}{rk(r)} + \frac{\pi\alpha}{kL}\int_{x_1}^{x_T(t)}\left[\frac{q_t(x,t)}{\lambda_{tc}(x,t)} - \frac{q_t(x,t)}{\lambda_{th}(x,t)}\right]\frac{dx}{h(x)}. \quad (4.189)$$

According to Eq. 2.177, the sum of the three first terms in the above equation represents the injection pressure change evaluated at the initial temperature of the reservoir. This solution as mentioned in our discussion about the first linear/first linear/first radial flow regime is provided by Eq. 2.188. Therefore, if we substitute Eq. 2.188 in Eq. 4.189, we obtain

$$\Delta p = \Delta p_o(T = T_{oi}) + \frac{\alpha q_{inj}}{L\hat{\lambda}_{oh}}\int_{r_w}^{z_w}\left(\frac{\hat{\lambda}_{oh}}{\lambda_{th}(r,t)} - 1\right)\frac{dr}{rk(r)} + \frac{\pi\alpha q_{inj}}{kL\hat{\lambda}_{oh}}\int_{x_1}^{x_f(t)}\left(\frac{\hat{\lambda}_{oh}}{\lambda_{th}(x,t)} - 1\right)\frac{dx}{h(x)} + \frac{\alpha q_{inj}}{L\hat{\lambda}_{oh}}\int_{r_w}^{z_w}\left[\frac{\hat{\lambda}_{oh}}{\lambda_{tc}(r,t)} - \frac{\hat{\lambda}_{oh}}{\lambda_{th}(r,t)}\right]\frac{dr}{rk(r)} + \frac{\pi\alpha q_{inj}}{kL\hat{\lambda}_{oh}}\int_{x_1}^{x_T(t)}\left[\frac{\hat{\lambda}_{oh}}{\lambda_{tc}(x,t)} - \frac{\hat{\lambda}_{oh}}{\lambda_{th}(x,t)}\right]\frac{dx}{h(x)}. \quad (4.190)$$

Generalized Injection Solution

In the above subsections, we discussed the main flow regimes that can be observed when injecting cold water through a horizontal well. However, we did not derive equations associated with the flow regimes corresponding to times when the steady-state region of constant rate propagates radially in the (x, y) plane. These are: second radial/first radial/first radial, second radial/first linear/first radial, second radial/first linear/first linear, second radial/second radial/first radial, second radial/second radial/first linear and second radial/second radial/second radial flow regimes. This is due to the fact that the procedure to do so is similar to the one used in chapter 2 for an isothermal injection. So, based on the analysis of the different flow regime observed during a cold injection

test through a horizontal well, we show that the equations derived for each period can be represented by one general expression given by

$$\Delta p = p_{wf}(t) - p_i = \Delta p(T = T_{oi}) + \Delta\, p_{x-z,T}(t) + \Delta\, p_{x,T}(t) + \Delta\, p_{x-y,T}(t), \tag{4.191}$$

where $\Delta p(T = T_{oi})$ is the wellbore pressure change obtained by injecting water through a horizontal well of radius r_w into an oil reservoir of permeability $k(r)$ at the initial temperature T_{oi}. The general expression of this solution is provided by Eq. 2.231 along with Eqs. 2.232- 2.234. The terms $\Delta\, p_{x-z,T}$, $\Delta\, p_{x,T}$ and $\Delta\, p_{x-y,T}$ denote additional pressure change expressed respectively in the (x, z) plane, x-direction and the (x, y) plane caused by the contrast between total mobility in the cold water bank and total mobility in the hot water bank. They are given by

$$\Delta\, p_{x-z,T}(t) = \frac{\alpha q_{inj}}{L\hat{\lambda_{oh}}} \int_{r_w}^{\min(z_w, r_{zx,f}(t))} \left(\frac{\hat{\lambda_{oh}}}{\lambda_{tc}(r,t)} - \frac{\hat{\lambda_{oh}}}{\lambda_{th}(r,t)}\right) \frac{dr}{rk(r)}, \tag{4.192}$$

$$\Delta\, p_{x,T}(t) = \frac{\pi\alpha q_{inj}}{kL\hat{\lambda_{oh}}} \int_{x_1}^{b} \left(\frac{\hat{\lambda_{oh}}}{\lambda_{tc}(x,t)} - \frac{\hat{\lambda_{oh}}}{\lambda_{th}(x,t)}\right) \frac{dx}{h(x)}, \tag{4.193}$$

and

$$\Delta\, p_{x-y,T}(t) = \frac{\alpha q_{inj}}{kh\hat{\lambda_{oh}}} \int_{\frac{L}{2}}^{\max(\frac{L}{2}, r_{xy,f}(t))} \left(\frac{\hat{\lambda_{oh}}}{\lambda_{tc}(r,t)} - \frac{\hat{\lambda_{oh}}}{\lambda_{th}(r,t)}\right) \frac{dr}{r}. \tag{4.194}$$

In Eq. 4.193, the constant of integration b is defined by Eq. 2.235.

4.3 Falloff Solution under Nonisothermal Conditions for Radial Flow

During falloff, it is expected that heat conduction will be the dominant cause of temperature changes and that the transfer of heat through convection will be small. So, by assuming only conduction, the temperature distributions will spread out as a consequence of an increase of temperature with time behind the temperature front. Eventually, the

temperature front will disappear when the system recovers its original reservoir temperature. On the other hand, the water saturation distribution will remain stationary when the well is shut-in and throughout the entire falloff test since the fluids are considered to be incompressible. The problem consists of finding the temperature of the system during a falloff test in the reservoir which initially has a spatial distribution established within it at the end of the injection test. The falloff pressure solution can then be constructed once the temperature profile is known. These two points are addressed in this section.

4.3.1 Model Description for the Temperature

Throughout, water, oil and rock thermal conductivities, denoted respectively by K_w, K_o and K_r and water, oil and rock specific heat capacities denoted by C_w, C_o and C_r are assumed to be constant. The thermal conductivity of a porous media, denoted by K_e, is defined by Eq. 4.36. Recall that this expression is giving by

$$K_e = \phi(K_w S_w + K_o S_o) + (1-\phi)K_r, \tag{4.195}$$

or simply using the fact that $S_w + S_o = 1$,

$$K_e = \phi[(K_w - K_o)S_w + K_o] + (1-\phi)K_r. \tag{4.196}$$

We also introduced a total specific heat capacity of a porous media defined by Eq. 4.35 and given by

$$(\rho C)_e = \phi(\rho_w C_w S_w + \rho_o C_o S_o) + (1-\phi)\rho_r C_r, \tag{4.197}$$

or

$$(\rho C)_e = \phi[(\rho_w C_w - \rho_o C_o)S_w + \rho_o C_o] + (1-\phi)\rho_r C_r. \tag{4.198}$$

Eq. 4.196 and Eq. 4.198 indicate that K_e and $(\rho C)_e$ are unique functions of water saturation. For simplicity, we let $\hat{K}_{ew}$ and $(\hat{\rho C})_{ew}$ be respectively the thermal conductivity and

the total specific heat capacity of the porous media evaluated at residual oil saturation. They are respectively given according to Eq. 4.196 and Eq. 4.198 by

$$\hat{K}_{ew} = \phi[(K_w - K_o)(1 - S_{or}) + K_o] + (1 - \phi)K_r, \tag{4.199}$$

and

$$(\rho\hat{C})_{ew} = \phi[(\rho_w C_w - \rho_o C_o)(1 - S_{or}) + \rho_o C_o] + (1 - \phi)\rho_r C_r. \tag{4.200}$$

The initial spatial distribution of temperature in the reservoir is given by the following step function

$$T(t = t_p) = \begin{cases} T_{wi} & r \leq r_T(t_p), \\ T_{oi} & r \geq r_T(t_p), \end{cases} \tag{4.201}$$

where T_{wi} is the temperature of the injected fluid and T_{oi} is the initial temperature of the reservoir. The details of the model proposed here are shown in Fig. 4.4. As we can see, the system considered is represented by three distinct regions: the wellbore region, i.e, $0 < r < r_w$, the water bank, i.e, $r_w < r < r_f$ and the oil zone such that $r > r_f$, where $r_f = r_f(t_p)$ represents the water front evaluated at the instant of shut-in t_p. Based on the results of Witterholt and Tixier [35], we may assume that in the uninvaded zone, the temperature distribution is uniform and equal to T_{oi}. Moreover, the boundary $r = r_f$ should be maintained equal to the temperature $T = T_{oi}$ so that the system recovers to the geothermal temperature that exists initially in the reservoir.

Next, we write the conservation of energy equation in the region $r_w < r < r_f$. Fig. 4.4 also shows the energy terms to be considered here. It is a system of length Δr in the r direction with a cross sectional area A_r normal to the r-direction and a length Δz in the z-direction with cross sectional area A_z normal to the vertical direction z. The system has an elementary volume of $\Delta V = 2\pi r \Delta r \Delta z$. The θ-direction is not considered here. The important energy terms during a shut-in are the horizontal and vertical conduction into and out of the system during an interval of time Δt and the energy stored in the

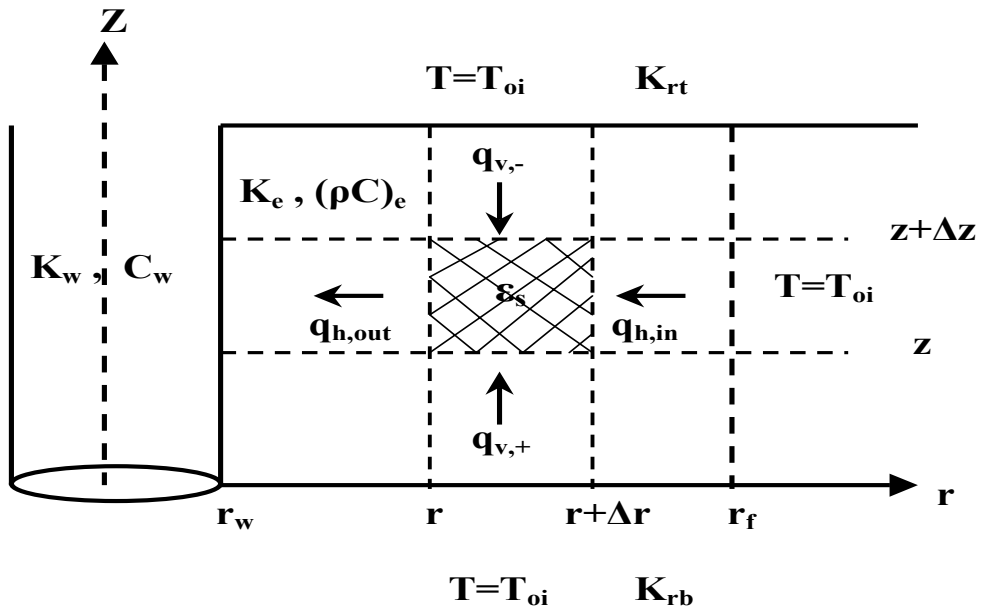

Figure 4.4: Well and reservoir model with important energy terms indicated.

volume ΔV during the same time interval. The energy balance is written directly from Fig. 4.4 as

$$q_{h,in} + q_{v,+} + q_{v,-} = q_{h,out} + \varepsilon_s, \tag{4.202}$$

where the symbol $q_{h,in}$ denotes the rate of energy flow by conduction at the radial position $r + \Delta r$, while $q_{h,out}$ denotes the rate of energy flow by conduction at the radial position r. Similarly, the rate of energy flow by vertical conduction at the position z is denoted by the symbol $q_{v,-}$, whereas $q_{v,+}$ is the rate of energy flow by vertical conduction at the position $z + \Delta z$. These rates are given by the well know Fourier law. As for the rate of energy stored in the system, it is described by the following equation:

$$\varepsilon_s = (\rho C)_e \Delta V (T|_{t+\Delta t} - T|_t). \tag{4.203}$$

In Eq. 4.203, the term $(T|_{t+\Delta t} - T|_t)$ represents the increase of temperature within the volume ΔV during the shut-in time $\Delta t = t - t_p$, with t_p representing the instant of shut-in. Expressing the rates of energy due to conduction by Fourier law and using Eq. 4.203 into Eq. 4.202, we have

$$K_e A_r \frac{\partial T}{\partial r}\bigg|_{r+\Delta r} \Delta t + K_e A_z \frac{\partial T}{\partial z}\bigg|_{z+\Delta z} \Delta t - K_e A_z \frac{\partial T}{\partial z}\bigg|_{z} \Delta t = K_e A_r \frac{\partial T}{\partial r}\bigg|_{r} \Delta t + (\rho C)_e \Delta V (T|_{t+\Delta t} - T|_t). \quad (4.204)$$

Introducing the definition of the cross sectional areas and rearranging Eq. 4.204 give

$$K_e 2\pi r \Delta z \frac{\partial T}{\partial r}\bigg|_{r+\Delta r} \Delta t - K_e 2\pi r \Delta z \frac{\partial T}{\partial r}\bigg|_{r} \Delta t + K_e 2\pi r \Delta r \frac{\partial T}{\partial z}\bigg|_{z+\Delta z} \Delta t - K_e 2\pi r \Delta r \frac{\partial T}{\partial z}\bigg|_{z} \Delta t = (\rho C)_e 2\pi r \Delta r \Delta z (T|_{t+\Delta t} - T|_t), \quad (4.205)$$

or dividing by $2\pi r \Delta r \Delta z \Delta t$

$$\frac{1}{r\Delta r}\left[K_e r \frac{\partial T}{\partial r}\bigg|_{r+\Delta r} - K_e r \frac{\partial T}{\partial r}\bigg|_{r}\right] + \frac{1}{\Delta z}\left[K_e \frac{\partial T}{\partial z}\bigg|_{z+\Delta z} - K_e \frac{\partial T}{\partial z}\bigg|_{z}\right] = (\rho C)_e \left(\frac{T|_{t+\Delta t} - T|_t}{\Delta t}\right). \quad (4.206)$$

In the limit, as $\Delta r \longrightarrow 0$, $\Delta z \longrightarrow 0$ and $\Delta t \longrightarrow 0$, the heat equation reduces to

$$\frac{1}{r}\frac{\partial}{\partial r}\left(K_e r \frac{\partial T}{\partial r}\right) + \frac{\partial}{\partial z}\left(K_e \frac{\partial T}{\partial z}\right) = (\rho C)_e \frac{\partial T}{\partial \Delta t}. \quad (4.207)$$

To give a more simplified representation to the model, we will eliminate the dependence of the temperature in the reservoir on the depth z. We need to keep in mind that water saturation distributions derived from the Buckley-Leverett theory are 1D profiles (pure radial) and there has to be a certain consistency between the variables involved in the system when it comes to dimensions. The other reason for a simple theoretical model is to better understand the basic physical processes involved with the ability to establish a reasonable quantitative analysis of the system. In order to do that, we consider only one grid block in the z-direction of thickness $\Delta z = h$ and we assume that the cap and base

rock of constant thermal conductivity coefficients K_{rt} and K_{rb} respectively to be infinite heat sources at the constant temperature T_{oi} such that the amount of heat $q_{v,-}$ transferred from the cap rock to the reservoir during the time Δt is giving by

$$q_{v,-} = K_{rt} A_z \frac{\partial T}{\partial z}\bigg|_{z+\Delta z} \Delta t = K_{rt} A_z \frac{T_{oi} - T}{h/2} \Delta t, \tag{4.208}$$

and the amount of heat $q_{v,+}$ transferred from the base rock to the reservoir during the same time Δt is provided by

$$q_{v,+} = K_{rb} A_z \frac{\partial T}{\partial z}\bigg|_{z} \Delta t = K_{rb} A_z \frac{T - T_{oi}}{h/2} \Delta t. \tag{4.209}$$

Replacing Eqs. 4.208 and 4.209 into Eq. 4.205 gives after rearranging and simplifying

$$\frac{1}{r\Delta r}\left[K_e r \frac{\partial T}{\partial r}\bigg|_{r+\Delta r} - K_e r \frac{\partial T}{\partial r}\bigg|_{r}\right] + \frac{2}{h^2}(K_{rt} + K_{rb})(T_{oi} - T) = (\rho C)_e \left(\frac{T|_{t+\Delta t} - T|_t}{\Delta t}\right), \tag{4.210}$$

or when $\Delta r \longrightarrow 0$ and $\Delta t \longrightarrow 0$

$$\frac{1}{r}\frac{\partial}{\partial r}\left(K_e r \frac{\partial T_{ou}}{\partial r}\right) + \frac{2}{h^2}(K_{rt} + K_{rb})(T_{oi} - T_{ou}) = (\rho C)_e \frac{\partial T_{ou}}{\partial \Delta t}, \tag{4.211}$$

where the notation T_{ou} is introduced to indicate that the solution is valid in the water bank, that is for $r_w < r < r_f$. Eq. 4.211 is associated with the boundary condition

$$T_{ou}(r = r_f, t) = T_{oi}, \tag{4.212}$$

valid at any time Δt and with an initial condition given by Eq. 4.201.

In the wellbore, i.e., $0 < r < r_w$, the system is characterized by the thermal conductivity K_w and the specific heat capacity C_w (the wellbore is filled with water). If we assume that conduction is the main mechanism for heat transfer in this region, and by performing a similar energy balance on an elementary cylindrical element in the wellbore, it is easy to show that we obtain a similar 2D heat equation Eq. 4.207 with K_e and $(\rho C)_e$

replaced respectively by the constants K_w and $\rho_w C_w$ as follows

$$K_w \frac{1}{r}\frac{\partial}{\partial r}\left(r\frac{\partial T_{in}}{\partial r}\right) + K_w \frac{\partial}{\partial z}\left(\frac{\partial T_{in}}{\partial z}\right) = \rho_w C_w \frac{\partial T_{in}}{\partial \Delta t}. \tag{4.213}$$

One of the boundary conditions associated with this partial differential equation is of an adiabatic type to ensure symmetry. It is given at any time Δt by

$$r\frac{\partial T_{in}}{\partial r}\bigg|_{r=0} = 0. \tag{4.214}$$

The two other boundary conditions are provided by

$$T_{in}(r, z = 0, \Delta t) = T_{oi}, \tag{4.215}$$

and

$$\frac{\partial T_{in}}{\partial z}\bigg|_{z=z_t} = 0. \tag{4.216}$$

In these equations, the z-axis is chosen such that $z = 0$ represents the bottom of the reservoir and $z = z_t$ is assumed to be the surface. As for the initial condition, according to Eq. 4.201, we have $T_{in}(r, z, \Delta t = 0) = T_{wi}$ for any $0 < r < r_w$ and $0 < z < z_t$.

Two additional equations are required to solve the system above. These are the continuity of the temperature and the rate equations at the interface $r = r_w$ for any z between 0 and h and given respectively by

$$T_{in}(r = r_w, z, \Delta t) = T_{ou}(r = r_w, \Delta t), \forall \Delta t \geq 0 \tag{4.217}$$

and

$$K_w \frac{\partial T_{in}}{\partial r}\bigg|_{r=r_w} = K_e \frac{\partial T_{ou}}{\partial r}\bigg|_{r=r_w} \forall \Delta t \geq 0. \tag{4.218}$$

In the following, we define the dimensionless variables in terms of water properties at residual oil saturation, S_{or}. We will denote dimensionless radial distance, dimensionless

vertical distance, dimensionless shut-in time, dimensionless temperature, dimensionless thermal conductivity, dimensionless density averaged specific heat capacity, respectively, by r_D, z_D, Δt_D, T_D, K_{eD} and $(\rho C)_{eD}$ and define these variables by

$$r_D = \frac{r}{r_w}, \tag{4.219}$$

$$z_D = \frac{z}{h}, \tag{4.220}$$

$$\Delta t_D = \frac{\hat{K}_{ew}}{(\hat{\rho C})_{ew} h^2} \Delta t, \tag{4.221}$$

$$T_D = \frac{T_{oi} - T(r, z, \Delta t)}{T_{oi} - T_{wi}}, \tag{4.222}$$

$$K_{eD} = \frac{K_e}{\hat{K}_{ew}}, \tag{4.223}$$

and

$$(\rho C)_{eD} = \frac{(\rho C)_e}{(\hat{\rho C})_{ew}}. \tag{4.224}$$

For simplicity purposes, we also define the following quantities

$$r_{fD} = \frac{r_f}{r_w}, \tag{4.225}$$

$$r_{TD} = \frac{r_T}{r_w}, \tag{4.226}$$

$$z_{tD} = \frac{z_t}{h}, \tag{4.227}$$

$$K_{wD} = \frac{K_w}{\hat{K}_{ew}}, \tag{4.228}$$

and

$$(\rho C)_{wD} = \frac{\rho_w C_w}{(\hat{\rho C})_{ew}}. \tag{4.229}$$

With these definitions, the governing differential equations and associated conditions can be rewritten in dimensionless form as

$$\frac{\partial^2 T_{D,in}(r_D, z_D, \Delta t_D)}{\partial z_D^2} + \frac{h^2}{r_w^2}\frac{1}{r_D}\frac{\partial}{\partial r_D}\left[r_D \frac{\partial T_{D,in}(r_D, z_D, \Delta t_D)}{\partial r_D}\right] = \frac{(\rho c)_{wD}}{K_{wD}}\frac{\partial T_{D,in}(r_D, z_D, \Delta t_D)}{\partial \Delta t_D}, \text{ for } 0 < r_D < 1 \text{ , } 0 < z_D < z_{tD} \text{ and } \Delta t_D > 0 \text{ ,} \tag{4.230}$$

$$r_D \frac{\partial T_{D,in}(r_D, z_D, \Delta t_D)}{\partial r_D}\bigg|_{r_D=0} = 0, \text{ for } 0 < z_D < z_{tD} \text{ and } \Delta t_D \geq 0, \tag{4.231}$$

$$T_{D,in}(r_D, z_D = 0, \Delta t_D) = 0, \text{ for } 0 < r_D < 1 \text{ and } \Delta t_D \geq 0, \tag{4.232}$$

$$\frac{\partial T_{D,in}(r_D, z_D, \Delta t_D)}{\partial z_D}\bigg|_{z_D=z_{tD}} = 0, \text{ for } 0 < r_D < 1 \text{ and } \Delta t_D \geq 0, \tag{4.233}$$

$$T_{D,in}(r_D, z_D, \Delta t_D = 0) = 1, \text{ for } 0 < r_D < 1 \text{ and } 0 < z_D < z_{tD}, \tag{4.234}$$

$$\frac{1}{r_D}\frac{\partial}{\partial r_D}\left[K_{eD}(r_D) r_D \frac{\partial T_{D,ou}(r_D, \Delta t_D)}{\partial r_D}\right] - \frac{2r_w^2}{h^2}\left(\frac{K_{rt} + K_{rb}}{\hat{K}_{ew}}\right) T_{D,ou}(r_D, \Delta t_D) = \frac{r_w^2}{h^2}(\rho c)_{eD}\frac{\partial T_{D,ou}(r_D, \Delta t_D)}{\partial \Delta t_D}, \text{ for } 1 < r_D < r_{fD} \text{ and } \Delta t_D > 0 \text{ ,} \tag{4.235}$$

$$T_{D,ou}(r_{fD}, \Delta t_D) = 0, \text{ for } \Delta t_D \geq 0, \tag{4.236}$$

$$T_{D,ou}(r_D, \Delta t_D = 0) = 1 - H(r_D - r_{TD}) = f_1(r_D), \text{ for } 1 < r_D < r_{fD}, \tag{4.237}$$

$$T_{D,in}(r_D = 1, z_D, \Delta t_D) = T_{D,ou}(r_D = 1, \Delta t_D), \text{ for } 0 < z_D < 1 \text{ and } \Delta t_D \geq 0, \tag{4.238}$$

and

$$K_{wD} \frac{\partial T_{D,in}(r_D, z_D, \Delta t_D)}{\partial r_D}\bigg|_{r_D=1} = K_{eD}(r_D) \frac{\partial T_{D,ou}(r_D, \Delta t_D)}{\partial r_D}\bigg|_{r_D=1}, \quad \text{for } 0 < z_D < 1 \text{ and } \Delta t_D \geq 0. \tag{4.239}$$

Note that in Eq. 4.237, the function denoted by H is the heaviside function. Here, we need to point out that the thermal conductivity K_e and the density averaged specific heat capacity $(\rho c)_e$, or equivalently K_{eD} and $(\rho c)_{eD}$ are independent of time during shut-in. They depend only on the radial position r via the water saturation distribution $S_w(r, t_p)$. Another remark is that we expect the variation of the temperature in the wellbore along the r-direction to be insignificant. Therefore, we introduce an average temperature that we denote by $\hat{T}_{in} = \hat{T}_{in}(z, \Delta t)$ and define by

$$\hat{T}_{in}(z, \Delta t) = \frac{1}{\int_0^{r_w} 2\pi r dr} \int_0^{r_w} T_{in}(r, z, \Delta t) 2\pi r dr, \tag{4.240}$$

or simply

$$\hat{T}_{in}(z, \Delta t) = \frac{2}{{r_w}^2} \int_0^{r_w} T_{in}(r, z, \Delta t) r dr. \tag{4.241}$$

In terms of dimensionless variables, Eq. 4.241 becomes

$$\hat{T}_{D,in}(z_D, \Delta t_D) = 2\int_0^1 T_{D,in}(r_D, z_D, \Delta t_D) r_D dr_D. \tag{4.242}$$

Applying this averaging procedure to Eq. 4.230 gives

$$2\int_0^1 \frac{\partial^2 T_{D,in}(r_D, z_D, \Delta t_D)}{\partial z_D^2} r_D dr_D + 2\frac{h^2}{r_w^2}\int_0^1 \frac{\partial}{\partial r_D}\left(r_D \frac{\partial T_{D,in}(r_D, z_D, \Delta t_D)}{\partial r_D}\right) dr_D = 2\frac{(\rho c)_{wD}}{K_{wD}}\int_0^1 \frac{\partial T_{D,in}(r_D, z_D, \Delta t_D)}{\partial \Delta t_D} r_D dr_D, \tag{4.243}$$

or simply

$$\frac{\partial^2 \hat{T}_{D,in}(z_D, \Delta t_D)}{\partial z_D^2} + 2\frac{h^2}{r_w^2} r_D \frac{\partial T_{D,in}(r_D, z_D, \Delta t_D)}{\partial r_D}\Bigg]_{r_D=0}^{r_D=1} = \frac{(\rho c)_{wD}}{K_{wD}} \frac{\partial \hat{T}_{D,in}(z_D, \Delta t_D)}{\partial \Delta t_D}. \tag{4.244}$$

If we use the adiabatic boundary condition given by Eq. 4.231 in Eq. 4.244, we obtain

$$\frac{\partial^2 \hat{T}_{D,in}}{\partial z_D^2} + 2\frac{h^2}{r_w^2} r_D \frac{\partial T_{D,in}}{\partial r_D}\bigg|_{r_D=1} = \frac{(\rho c)_{wD}}{K_{wD}} \frac{\partial \hat{T}_{D,in}}{\partial \Delta t_D}. \tag{4.245}$$

Note that from the continuity of the fluxes represented by Eq. 4.239, we have

$$r_D \frac{\partial T_{D,in}(r_D, z_D, \Delta t_D)}{\partial r_D}\bigg|_{r_D=1} = \frac{K_{eD}}{K_{wD}} r_D \frac{\partial T_{D,ou}(r_D, \Delta t_D)}{\partial r_D}\bigg|_{r_D=1}. \tag{4.246}$$

Using this result in Eq. 4.245 leads to

$$\frac{\partial^2 \hat{T}_{D,in}}{\partial z_D^2} + 2\frac{h^2}{r_w^2}\frac{K_{eD}}{K_{wD}} r_D \frac{\partial T_{D,ou}}{\partial r_D}\bigg|_{r_D=1} = \frac{(\rho c)_{wD}}{K_{wD}} \frac{\partial \hat{T}_{D,in}}{\partial \Delta t_D}. \tag{4.247}$$

Similarly, if we apply the averaging procedure to Eqs. 4.232, 4.233 and 4.234, we obtain

$$2\int_{r_D=0}^{r_D=1} T_{D,in}(r_D, z_D = 0, \Delta t_D) r_D dr_D = 0, \tag{4.248}$$

which leads to

$$\hat{T}_{D,in}(z_D = 0, \Delta t_D) = 0, \tag{4.249}$$

and

$$2\int_{r_D=0}^{r_D=1} \frac{\partial T_{D,in}(r_D, z_D, \Delta t_D)}{\partial z_D}\bigg|_{z_D=z_{tD}} r_D dr_D = 0, \tag{4.250}$$

or

$$\frac{\partial \hat{T}_{D,in}}{\partial z_D}\bigg|_{z_D=z_{tD}} = 0, \tag{4.251}$$

and

$$2\int_{r_D=0}^{r_D=1} T_{D,in}(r_D, z_D, \Delta t_D = 0) r_D dr_D = 2\int_{r_D=0}^{r_D=1} r_D dr_D = 1, \tag{4.252}$$

giving

$$\hat{T}_{D,in}(z_D, \Delta t_D = 0) = 1. \tag{4.253}$$

By noting that the term $r_D \frac{\partial T_{D,ou}}{\partial r_D}\Big|_{r_D=1}$ in Eq. 4.247 is non zero only in the region $0 \leq z_D \leq 1$, we can rewrite the dimensionless governing differential equations and associated conditions as

$$\frac{\partial^2 \hat{T}_{D,inu}}{\partial z_D^2} = \frac{(\rho c)_{wD}}{K_{wD}} \frac{\partial \hat{T}_{D,inu}}{\partial \Delta t_D}, \text{ for } 1 < z_D < z_{tD} \text{ and } \Delta t_D \geq 0, \tag{4.254}$$

$$\frac{\partial \hat{T}_{D,inu}}{\partial z_D}\bigg|_{z_D=z_{tD}} = 0, \text{ for } \Delta t_D \geq 0, \tag{4.255}$$

$$\hat{T}_{D,inu}(z_D, \Delta t_D = 0) = 1, \text{ for } 1 < z_D < z_{tD}, \tag{4.256}$$

$$\frac{\partial^2 \hat{T}_{D,inl}}{\partial z_D^2} + 2\frac{h^2}{r_w^2}\frac{K_{eD}}{K_{wD}} r_D \frac{\partial T_{D,ou}}{\partial r_D}\bigg|_{r_D=1} = \frac{(\rho c)_{wD}}{K_{wD}} \frac{\partial \hat{T}_{D,inl}}{\partial \Delta t_D}, \text{ for } 0 < z_D < 1 \text{ and } \Delta t_D \geq 0, \tag{4.257}$$

$$\hat{T}_{D,inl}(z_D = 0, \Delta t_D) = 0, \text{ for } \Delta t_D \geq 0, \tag{4.258}$$

$$\hat{T}_{D,inl}(z_D, \Delta t_D = 0) = 1, \text{ for } 0 < z_D < 1, \tag{4.259}$$

$$\hat{T}_{D,inu}(z_D = 1, \Delta t_D) = \hat{T}_{D,inl}(z_D = 1, \Delta t_D), \text{ for } \Delta t_D \geq 0, \tag{4.260}$$

$$\frac{\partial \hat{T}_{D,inu}}{\partial z_D}\bigg|_{z_D=1} = \frac{\partial \hat{T}_{D,inl}}{\partial z_D}\bigg|_{z_D=1}, \text{ for } \Delta t_D \geq 0, \tag{4.261}$$

$$\frac{1}{r_D}\frac{\partial}{\partial r_D}\left[K_{eD}(r_D) r_D \frac{\partial T_{D,ou}(r_D, \Delta t_D)}{\partial r_D}\right] - \frac{2r_w^2}{h^2}\left(\frac{K_{rt} + K_{rb}}{\hat{K}_{ew}}\right) T_{D,ou}(r_D, \Delta t_D) = \frac{r_w^2}{h^2}(\rho c)_{eD} \frac{\partial T_{D,ou}(r_D, \Delta t_D)}{\partial \Delta t_D}, \text{ for } 1 < r_D < r_{fD} \text{ and } \Delta t_D > 0\ , \tag{4.262}$$

$$T_{D,ou}(r_{fD}, \Delta t_D) = 0, \text{ for } \Delta t_D \geq 0, \tag{4.263}$$

$$T_{D,ou}(r_D, \Delta t_D = 0) = 1 - H(r_D - r_{TD}) = f_1(r_D), \text{ for } 1 < r_D < r_{fD}, \tag{4.264}$$

and

$$\hat{T}_{D,inl}(z_D, \Delta t_D) = T_{D,ou}(r_D = 1, \Delta t_D), \text{ for } 0 < z_D < 1 \text{ and } \Delta t_D \geq 0. \tag{4.265}$$

The notations $\hat{T}_{D,inu}$ and $\hat{T}_{D,inl}$ were introduced to differentiate between the solution in the upper part of the wellbore, i.e., for $1 < z_D < z_{tD}$ and the solution in the lower part of the wellbore, i.e., for $0 < z_D < 1$. Having said that, we can apply the Laplace transform to the above IBVP. Throughout, u denotes the Laplace variable and a bar over a dimensionless temperature function is used to denote its Laplace transform. For simplicity, three constants denoted by a, b and c are introduced. They are defined by the following equations:

$$a = 2r_w/h, \tag{4.266}$$

$$b = (\rho c)_{wD}/K_{wD}, \tag{4.267}$$

and

$$c = \frac{K_{rt} + K_{rb}}{2\hat{K}_{ew}}. \tag{4.268}$$

Thus, the system of Eqs. 4.254 to 4.265 becomes

$$\frac{\partial^2 \bar{\hat{T}}_{D,inu}}{\partial z_D^2} - bu\bar{\hat{T}}_{D,inu} = -b, \text{ for } 1 < z_D < z_{tD} \tag{4.269}$$

$$\left.\frac{\partial \bar{\hat{T}}_{D,inu}}{\partial z_D}\right|_{z_D = z_{tD}} = 0, \tag{4.270}$$

$$\frac{\partial^2 \bar{\hat{T}}_{D,inl}}{\partial z_D^2} - bu\bar{\hat{T}}_{D,inl} + \frac{8}{a^2}\frac{K_{eD}}{K_{wD}} r_D \left.\frac{\partial \bar{T}_{D,ou}}{\partial r_D}\right|_{r_D=1} = -b, \text{ for } 0 < z_D < 1 \tag{4.271}$$

$$\bar{\hat{T}}_{D,inl}(z_D = 0, u) = 0, \tag{4.272}$$

$$\bar{\hat{T}}_{D,inu}(z_D = 1, u) = \bar{\hat{T}}_{D,inl}(z_D = 1, u), \tag{4.273}$$

$$\left.\frac{\partial \bar{\hat{T}}_{D,inu}}{\partial z_D}\right|_{z_D=1} = \left.\frac{\partial \bar{\hat{T}}_{D,inl}}{\partial z_D}\right|_{z_D=1}, \tag{4.274}$$

$$\frac{1}{r_D}\frac{\partial}{\partial r_D}\left[K_{eD}(r_D) r_D \frac{\partial \bar{T}_{D,ou}}{\partial r_D}\right] - a^2\left(c + \frac{(\rho c)_{eD}}{4}u\right)\bar{T}_{D,ou} = -\frac{a^2}{4}(\rho c)_{eD} f_1(r_D), \quad \text{for } 1 < r_D < r_{fD} \tag{4.275}$$

$$\bar{T}_{D,ou}(r_{fD}, u) = 0, \tag{4.276}$$

and

$$\bar{\hat{T}}_{D,inl}(z_D, u) = \bar{T}_{D,ou}(r_D = 1, u), \text{ for } 0 < z_D < 1\ . \tag{4.277}$$

4.3.2 Temperature Profiles from Perturbation Theory

Here, we present a method that we applied when solving the pressure equation during a falloff test under isothermal conditions. This procedure, as seen in chapter 3 and appendix B, is based on perturbation theory and its justification lies on the fact that the variation of water saturation in the water bank is small enough so that it can be used to solve the initial boundary value problem described above. We start the analysis by writing that

$$K_e = K_e + \hat{K}_{ew} - \hat{K}_{ew}, \tag{4.278}$$

and

$$(\rho C)_e = (\rho C)_e + (\hat{\rho C})_{ew} - (\hat{\rho C})_{ew}. \tag{4.279}$$

If we divide Eq. 4.278 by $\hat{K}_{ew}$ and Eq. 4.279 by $(\hat{\rho C})_{ew}$, we obtain

$$K_{eD} = 1 - \frac{\hat{K}_{ew} - K_e}{\hat{K}_{ew}} = 1 - f_K(r_D), \tag{4.280}$$

and

$$(\rho C)_{eD} = 1 - \frac{(\hat{\rho C})_{ew} - (\rho C)_e}{(\hat{\rho C})_{ew}} = 1 - g_{\rho C}(r_D), \tag{4.281}$$

where the two spatial functions introduced in Eqs. 4.280 and 4.281 and defined by

$$f_K(r_D) = \frac{\hat{K}_{ew} - K_e}{\hat{K}_{ew}}, \tag{4.282}$$

and

$$g_{\rho C}(r_D) = \frac{(\hat{\rho C})_{ew} - (\rho C)_e}{(\hat{\rho C})_{ew}}, \tag{4.283}$$

do not exceed the value of 1. By introducing the two perturbation variables ϵ and δ defined by

$$\epsilon = \max \mid f_K(r_D) \mid, \tag{4.284}$$

$$\delta = \max \mid g_{\rho C}(r_D) \mid, \tag{4.285}$$

and by rescaling the functions f_K and $g_{\rho C}$ by ϵ and δ as follows

$$f(r_D) = \frac{f_K(r_D)}{\epsilon}, \tag{4.286}$$

$$g(r_D) = \frac{g_{\rho C}(r_D)}{\delta}, \tag{4.287}$$

Eqs. 4.280 and 4.281 become

$$K_{eD} = 1 - \epsilon f(r_D), \tag{4.288}$$

and

$$(\rho C)_{eD} = 1 - \delta g(r_D). \tag{4.289}$$

Thus, the temperature function is described by a perturbation expansion in powers of ϵ and δ given in terms of dimensionless variables in Laplace domain by

$$\bar{T}_D(r_D, u) = \bar{T}_{D0}(r_D, u) + \epsilon\bar{T}_{D1}(r_D, u) + \delta\bar{T}_{D2}(r_D, u) + \epsilon\delta\bar{T}_{D3}(r_D, u) + \ldots. \tag{4.290}$$

This expression is general, that is it applies for both the wellbore and the invaded regions. In the following, we assume that an adequate description of the falloff solution for the temperature can be obtained from the first three terms in the above series.

Water Bank Region Solution

In this zone, the temperature distribution is described by the dimensionless differential equation Eq. 4.275 and its associated boundary condition Eq. 4.276 and continuity condition Eq. 4.277. Based on the perturbation method, we write our solution in this region as

$$\bar{T}_{D,ou}(r_D, u) = \bar{T}_{D0,ou} + \epsilon\bar{T}_{D1,ou} + \delta\bar{T}_{D2,ou}. \tag{4.291}$$

Substituting this equation along with Eqs. 4.288 and 4.289 into Eqs. 4.275, 4.276 and 4.277 gives

$$\begin{aligned}\frac{1}{r_D}\frac{\partial}{\partial r_D}\left[(1-\epsilon f(r_D))r_D\frac{\partial}{\partial r_D}(\bar{T}_{D0,ou} + \epsilon\bar{T}_{D1,ou} + \delta\bar{T}_{D2,ou})\right] \\ - \frac{a^2}{4}[4c + (1-\delta g(r_D))u](\bar{T}_{D0,ou} + \epsilon\bar{T}_{D1,ou} + \delta\bar{T}_{D2,ou}) = \\ - \frac{a^2}{4}(1-\delta g(r_D))f_1(r_D),\end{aligned} \tag{4.292}$$

$$\bar{T}_{D0,ou}(r_{fD},u)+\epsilon\bar{T}_{D1,ou}(r_{fD},u)+\delta\bar{T}_{D2,ou}(r_{fD},u)=0, \tag{4.293}$$

and

$$\bar{T}_{D0,ou}(1,u)+\epsilon\bar{T}_{D1,ou}(1,u)+\delta\bar{T}_{D2,ou}(1,u)=\bar{\hat{T}}_{D0,inl}(z_D,u)+\epsilon\bar{\hat{T}}_{D1,inl}(z_D,u) + \delta\bar{\hat{T}}_{D2,inl}(z_D,u). \tag{4.294}$$

Expanding Eq. 4.292 and dropping higher orders of ϵ and δ yields

$$\frac{1}{r_D}\frac{\partial}{\partial r_D}\left(r_D\frac{\partial\bar{T}_{D0,ou}}{\partial r_D}\right)-\frac{a^2}{4}(4c+u)\bar{T}_{D0,ou}+\epsilon\left[\frac{1}{r_D}\frac{\partial}{\partial r_D}\left(r_D\frac{\partial\bar{T}_{D1,ou}}{\partial r_D}-r_Df(r_D)\frac{\partial\bar{T}_{D0,ou}}{\partial r_D}\right)-\frac{a^2}{4}(4c+u)\bar{T}_{D1,ou}\right]+\delta\left[\frac{1}{r_D}\frac{\partial}{\partial r_D}\left(r_D\frac{\partial\bar{T}_{D2,ou}}{\partial r_D}\right)-\frac{a^2}{4}(4c+u)\bar{T}_{D2,ou}+\frac{a^2}{4}ug(r_D)\bar{T}_{D0,ou}\right] = -\frac{a^2}{4}f_1(r_D)+\delta\frac{a^2}{4}f_1(r_D)g(r_D). \tag{4.295}$$

If we compare both sides of Eqs. 4.295, 4.293 and 4.294, we obtain the following three system of equations

The $O(1)$ system:

$$\frac{1}{r_D}\frac{\partial}{\partial r_D}\left(r_D\frac{\partial\bar{T}_{D0,ou}}{\partial r_D}\right)-\frac{a^2}{4}(4c+u)\bar{T}_{D0,ou}=-\frac{a^2}{4}f_1(r_D), \tag{4.296}$$

$$\bar{T}_{D0,ou}(r_{fD},u)=0, \tag{4.297}$$

$$\bar{T}_{D0,ou}(1,u)=\bar{\hat{T}}_{D0,inl}(z_D,u). \tag{4.298}$$

The $O(\epsilon)$ system:

$$\frac{1}{r_D}\frac{\partial}{\partial r_D}\left(r_D\frac{\partial \bar{T}_{D1,ou}}{\partial r_D}\right)-\frac{a^2}{4}(4c+u)\bar{T}_{D1,ou}=\frac{1}{r_D}\frac{\partial}{\partial r_D}\left(r_D f(r_D)\frac{\partial \bar{T}_{D0,ou}}{\partial r_D}\right), \tag{4.299}$$

$$\bar{T}_{D1,ou}(r_{fD},u)=0, \tag{4.300}$$

$$\bar{T}_{D1,ou}(1,u)=\bar{\hat{T}}_{D1,inl}(z_D,u). \tag{4.301}$$

The $O(\delta)$ system:

$$\frac{1}{r_D}\frac{\partial}{\partial r_D}\left(r_D\frac{\partial \bar{T}_{D2,ou}}{\partial r_D}\right)-\frac{a^2}{4}(4c+u)\bar{T}_{D2,ou}=-\frac{a^2}{4}g(r_D)\left(u\bar{T}_{D0,ou}-f_1(r_D)\right), \tag{4.302}$$

$$\bar{T}_{D2,ou}(r_{fD},u)=0, \tag{4.303}$$

$$\bar{T}_{D2,ou}(1,u)=\bar{\hat{T}}_{D2,inl}(z_D,u). \tag{4.304}$$

The leading system is a non-homogeneous second order differential equation whose solution is the sum of any particular solution $\bar{T}^{p}_{D0,ou}$ and a corresponding homogeneous solution $\bar{T}^{h}_{D0,iou}$ obtained by setting $f_1(r_D)=0$. In appendix B, a similar system given by Eq. B.6 was already solved using the variation of parameters technique. Its solution is provided by Eq. B.30. However, this solution has to be modified accordingly in order to be able to apply it for our case (Eq. 4.296). That means that the argument $\sqrt{u}r_D$ of the Bessel functions and the function $f_1(r_D)$ in Eq. B.30 need to be replaced by $\frac{a}{2}\sqrt{(4c+u)}r_D$ and $\frac{a^2}{4}f_1(r_D)$ respectively. By analogy to Eq. B.30, the solution of Eq. 4.296 is given by

$$\bar{T}_{D0,ou} = B_1 I_0(\frac{a}{2}\sqrt{(4c+u)}r_D) + B_2 K_0(\frac{a}{2}\sqrt{(4c+u)}r_D) + \frac{a^2}{4} I_0(\frac{a}{2}\sqrt{(4c+u)}r_D) \int_{r_D}^{r_{fD}} \xi_D f_1(\xi_D) K_0(\frac{a}{2}\sqrt{(4c+u)}\xi_D) d\xi_D + \frac{a^2}{4} K_0(\frac{a}{2}\sqrt{(4c+u)}r_D) \int_1^{r_D} \xi_D f_1(\xi_D) I_0(\frac{a}{2}\sqrt{(4c+u)}\xi_D) d\xi_D, \quad (4.305)$$

where B_1 and B_2 are two constants to be determined using the boundary conditions Eqs. 4.297 and 4.298. If we replace r_D by r_{fD} in Eq. 4.305 and we set the solution to zero, we obtain

$$B_1 I_0(\frac{a}{2}\sqrt{(4c+u)}r_{fD}) + B_2 K_0(\frac{a}{2}\sqrt{(4c+u)}r_{fD}) + \frac{a^2}{4} K_0(\frac{a}{2}\sqrt{(4c+u)}r_{fD}) \int_1^{r_{fD}} \xi_D f_1(\xi_D) I_0(\frac{a}{2}\sqrt{(4c+u)}\xi_D) d\xi_D = 0, \quad (4.306)$$

or simply,

$$B_2 = -B_1 \frac{I_0(\frac{a}{2}\sqrt{(4c+u)}r_{fD})}{K_0(\frac{a}{2}\sqrt{(4c+u)}r_{fD})} - \frac{a^2}{4} \int_1^{r_{fD}} \xi_D f_1(\xi_D) I_0(\frac{a}{2}\sqrt{(4c+u)}\xi_D) d\xi_D. \quad (4.307)$$

Replacing Eq. 4.307 into the general solution of the leading system Eq. 4.305 and rearranging yields

$$\bar{T}_{D0,ou} = \frac{B_1}{K_0(\frac{a}{2}\sqrt{(4c+u)}r_{fD})} \Big[K_0(\frac{a}{2}\sqrt{(4c+u)}r_{fD}) I_0(\frac{a}{2}\sqrt{(4c+u)}r_D) - I_0(\frac{a}{2}\sqrt{(4c+u)}r_{fD}) \times K_0(\frac{a}{2}\sqrt{(4c+u)}r_D) \Big] - \frac{a^2}{4} K_0(\frac{a}{2}\sqrt{(4c+u)}r_D) \int_1^{r_{fD}} \xi_D f_1(\xi_D) I_0(\frac{a}{2}\sqrt{(4c+u)}\xi_D) d\xi_D + \frac{a^2}{4} K_0(\frac{a}{2}\sqrt{(4c+u)}r_D) \int_1^{r_D} \xi_D f_1(\xi_D) I_0(\frac{a}{2}\sqrt{(4c+u)}\xi_D) d\xi_D + \frac{a^2}{4} I_0(\frac{a}{2}\sqrt{(4c+u)}r_D) \int_{r_D}^{r_{fD}} \xi_D f_1(\xi_D) K_0(\frac{a}{2}\sqrt{(4c+u)}\xi_D) d\xi_D. \quad (4.308)$$

For simplification purposes, we use the definition of the new function $G\nu(\alpha x, \alpha y)$ introduced in appendix B and given by Eq. B.111. In particular, for $\nu = 0$, we can write

$$G_0(\frac{a}{2}\sqrt{(4c+u)}r_D, \frac{a}{2}\sqrt{(4c+u)}r_{fD}) = K_0(\frac{a}{2}\sqrt{(4c+u)}r_{fD})I_0(\frac{a}{2}\sqrt{(4c+u)}r_D) - I_0(\frac{a}{2}\sqrt{(4c+u)}r_{fD})K_0(\frac{a}{2}\sqrt{(4c+u)}r_D). \quad (4.309)$$

Using this result in Eq. 4.308 yields

$$\begin{aligned}\bar{T}_{D0,ou} = &\frac{B_1}{K_0(\frac{a}{2}\sqrt{(4c+u)}r_{fD})}G_0(\frac{a}{2}\sqrt{(4c+u)}r_D, \frac{a}{2}\sqrt{(4c+u)}r_{fD}) \\ &- \frac{a^2}{4}K_0(\frac{a}{2}\sqrt{(4c+u)}r_D)\int_1^{r_{fD}} \xi_D f_1(\xi_D)I_0(\frac{a}{2}\sqrt{(4c+u)}\xi_D)d\xi_D \\ &+ \frac{a^2}{4}K_0(\frac{a}{2}\sqrt{(4c+u)}r_D)\int_1^{r_D} \xi_D f_1(\xi_D)I_0(\frac{a}{2}\sqrt{(4c+u)}\xi_D)d\xi_D \\ &+ \frac{a^2}{4}I_0(\frac{a}{2}\sqrt{(4c+u)}r_D)\int_{r_D}^{r_{fD}} \xi_D f_1(\xi_D)K_0(\frac{a}{2}\sqrt{(4c+u)}\xi_D)d\xi_D. \quad (4.310)\end{aligned}$$

If we replace r_D by 1 in Eq. 4.310 and we set the solution to $\bar{\bar{T}}_{D0,inl}(z_D, u)$ according to the condition Eq. 4.298, we obtain

$$\begin{aligned}\bar{\bar{T}}_{D0,inl}(z_D, u) = &\frac{B_1}{K_0(\frac{a}{2}\sqrt{(4c+u)}r_{fD})}G_0(\frac{a}{2}\sqrt{(4c+u)}, \frac{a}{2}\sqrt{(4c+u)}r_{fD}) \\ &- \frac{a^2}{4}K_0(\frac{a}{2}\sqrt{(4c+u)})\int_1^{r_{fD}} \xi_D f_1(\xi_D)I_0(\frac{a}{2}\sqrt{(4c+u)}\xi_D)d\xi_D \\ &+ \frac{a^2}{4}I_0(\frac{a}{2}\sqrt{(4c+u)})\int_1^{r_{fD}} \xi_D f_1(\xi_D)K_0(\frac{a}{2}\sqrt{(4c+u)}\xi_D)d\xi_D, \quad (4.311)\end{aligned}$$

or using the definition of the function G_0

$$\bar{\hat{T}}_{D0,inl}(z_D,u)=\frac{B_1}{K_0(\frac{a}{2}\sqrt{(4c+u)}r_{fD})}G_0(\frac{a}{2}\sqrt{(4c+u)},\frac{a}{2}\sqrt{(4c+u)}r_{fD})$$
$$-\frac{a^2}{4}\int_1^{r_{fD}}\xi_D f_1(\xi_D)G_0(\frac{a}{2}\sqrt{(4c+u)}\xi_D,\frac{a}{2}\sqrt{(4c+u)})d\xi_D. \quad (4.312)$$

Thus, we can write

$$\frac{B_1}{K_0(\frac{a}{2}\sqrt{(4c+u)}r_{fD})}=\frac{1}{G_0(\frac{a}{2}\sqrt{(4c+u)},\frac{a}{2}\sqrt{(4c+u)}r_{fD})}\Bigg[\bar{\hat{T}}_{D0,inl}(z_D,u)$$
$$+\frac{a^2}{4}\int_1^{r_{fD}}\xi_D f_1(\xi_D)G_0(\frac{a}{2}\sqrt{(4c+u)}\xi_D,\frac{a}{2}\sqrt{(4c+u)})d\xi_D\Bigg], \quad (4.313)$$

and Eq. 4.310 becomes

$$\bar{T}_{D0,ou}=\frac{G_0(\frac{a}{2}\sqrt{(4c+u)}r_D,\frac{a}{2}\sqrt{(4c+u)}r_{fD})}{G_0(\frac{a}{2}\sqrt{(4c+u)},\frac{a}{2}\sqrt{(4c+u)}r_{fD})}\Bigg[\bar{\hat{T}}_{D0,inl}(z_D,u)$$
$$+\frac{a^2}{4}\int_1^{r_{fD}}\xi_D f_1(\xi_D)G_0(\frac{a}{2}\sqrt{(4c+u)}\xi_D,\frac{a}{2}\sqrt{(4c+u)})d\xi_D\Bigg]$$
$$-\frac{a^2}{4}K_0(\frac{a}{2}\sqrt{(4c+u)}r_D)\int_1^{r_{fD}}\xi_D f_1(\xi_D)I_0(\frac{a}{2}\sqrt{(4c+u)}\xi_D)d\xi_D$$
$$+\frac{a^2}{4}K_0(\frac{a}{2}\sqrt{(4c+u)}r_D)\int_1^{r_D}\xi_D f_1(\xi_D)I_0(\frac{a}{2}\sqrt{(4c+u)}\xi_D)d\xi_D$$
$$+\frac{a^2}{4}I_0(\frac{a}{2}\sqrt{(4c+u)}r_D)\int_{r_D}^{r_{fD}}\xi_D f_1(\xi_D)K_0(\frac{a}{2}\sqrt{(4c+u)}\xi_D)d\xi_D. \quad (4.314)$$

The term $r_D\frac{\partial\bar{T}_{D0,ou}}{\partial r_D}\Big|_{r_D=1}$ is needed to obtain a solution in the wellbore region according to Eq. 4.271. But first, note that

$$\frac{\partial}{\partial r_D}G_0(\frac{a}{2}\sqrt{(4c+u)}r_D,\frac{a}{2}\sqrt{(4c+u)}r_{fD})=\frac{\partial}{\partial r_D}\Bigg[K_0(\frac{a}{2}\sqrt{(4c+u)}r_{fD})I_0(\frac{a}{2}\sqrt{(4c+u)}r_D)$$
$$-I_0(\frac{a}{2}\sqrt{(4c+u)}r_{fD})K_0(\frac{a}{2}\sqrt{(4c+u)}r_D)\Bigg]. \quad (4.315)$$

Taking the derivative of the right side of Eq. 4.315 gives

$$\frac{\partial}{\partial r_D}G_0(\frac{a}{2}\sqrt{(4c+u)}r_D,\frac{a}{2}\sqrt{(4c+u)}r_{fD}) = \frac{a}{2}\sqrt{(4c+u)}\Big[K_0(\frac{a}{2}\sqrt{(4c+u)}r_{fD}) \times I_1(\frac{a}{2}\sqrt{(4c+u)}r_D) + I_0(\frac{a}{2}\sqrt{(4c+u)}r_{fD})K_1(\frac{a}{2}\sqrt{(4c+u)}r_D)\Big]. \quad (4.316)$$

According to Eq. B.110, we have

$$H_0(\frac{a}{2}\sqrt{(4c+u)}r_{fD},\frac{a}{2}\sqrt{(4c+u)}r_D) = K_1(\frac{a}{2}\sqrt{(4c+u)}r_D)I_0(\frac{a}{2}\sqrt{(4c+u)}r_{fD}) + I_1(\frac{a}{2}\sqrt{(4c+u)}r_D)K_0(\frac{a}{2}\sqrt{(4c+u)}r_{fD}). \quad (4.317)$$

Using Eq. 4.317, Eq. 4.316 becomes

$$\frac{\partial}{\partial r_D}G_0(\frac{a}{2}\sqrt{(4c+u)}r_D,\frac{a}{2}\sqrt{(4c+u)}r_{fD}) = \frac{a}{2}\sqrt{(4c+u)}H_0(\frac{a}{2}\sqrt{(4c+u)}r_{fD},\frac{a}{2}\sqrt{(4c+u)}r_D). \quad (4.318)$$

Taking the derivative of Eq. 4.314 with respect to r_D gives

$$\begin{aligned}\frac{\partial \bar{T}_{D0,ou}}{\partial r_D} = \frac{a}{2}\sqrt{(4c+u)}\Bigg(&\frac{H_0(\frac{a}{2}\sqrt{(4c+u)}r_{fD},\frac{a}{2}\sqrt{(4c+u)}r_D)}{G_0(\frac{a}{2}\sqrt{(4c+u)},\frac{a}{2}\sqrt{(4c+u)}r_{fD})}\Big[\bar{\hat{T}}_{D0,inl}(z_D,u) \\ &+ \frac{a^2}{4}\int_1^{r_{fD}}\xi_D f_1(\xi_D)G_0(\frac{a}{2}\sqrt{(4c+u)}\xi_D,\frac{a}{2}\sqrt{(4c+u)})d\xi_D\Big] \\ &+ \frac{a^2}{4}K_1(\frac{a}{2}\sqrt{(4c+u)}r_D)\int_1^{r_{fD}}\xi_D f_1(\xi_D)I_0(\frac{a}{2}\sqrt{(4c+u)}\xi_D)d\xi_D \\ &- \frac{a^2}{4}K_1(\frac{a}{2}\sqrt{(4c+u)}r_D)\int_1^{r_D}\xi_D f_1(\xi_D)I_0(\frac{a}{2}\sqrt{(4c+u)}\xi_D)d\xi_D \\ &+ \frac{a^2}{4}I_1(\frac{a}{2}\sqrt{(4c+u)}r_D)\int_{r_D}^{r_{fD}}\xi_D f_1(\xi_D)K_0(\frac{a}{2}\sqrt{(4c+u)}\xi_D)d\xi_D\Bigg). \quad (4.319)\end{aligned}$$

Evaluating the above term at $r_D = 1$ yields

$$r_D\frac{\partial \bar{T}_{D0,ou}}{\partial r_D}\mid_{r_D=1}=\frac{a}{2}\sqrt{(4c+u)}\Bigg(\frac{H_0(\frac{a}{2}\sqrt{(4c+u)}r_{fD},\frac{a}{2}\sqrt{(4c+u)})}{G_0(\frac{a}{2}\sqrt{(4c+u)},\frac{a}{2}\sqrt{(4c+u)}r_{fD})}\Bigg[\bar{\hat{T}}_{D0,inl}(z_D,u)$$
$$+\frac{a^2}{4}\int_1^{r_{fD}}\xi_D f_1(\xi_D)G_0(\frac{a}{2}\sqrt{(4c+u)}\xi_D,\frac{a}{2}\sqrt{(4c+u)})d\xi_D\Bigg]$$
$$+\frac{a^2}{4}K_1(\frac{a}{2}\sqrt{(4c+u)})\int_1^{r_{fD}}\xi_D f_1(\xi_D)I_0(\frac{a}{2}\sqrt{(4c+u)}\xi_D)d\xi_D$$
$$+\frac{a^2}{4}I_1(\frac{a}{2}\sqrt{(4c+u)})\int_1^{r_{fD}}\xi_D f_1(\xi_D)K_0(\frac{a}{2}\sqrt{(4c+u)}\xi_D)d\xi_D\Bigg), \quad (4.320)$$

which is also equal to

$$r_D\frac{\partial \bar{T}_{D0,ou}}{\partial r_D}\mid_{r_D=1}=\frac{a}{2}\sqrt{(4c+u)}\Bigg(\frac{H_0(\frac{a}{2}\sqrt{(4c+u)}r_{fD},\frac{a}{2}\sqrt{(4c+u)})}{G_0(\frac{a}{2}\sqrt{(4c+u)},\frac{a}{2}\sqrt{(4c+u)}r_{fD})}\Bigg[\bar{\hat{T}}_{D0,inl}(z_D,u)$$
$$+\frac{a^2}{4}\int_1^{r_{fD}}\xi_D f_1(\xi_D)G_0(\frac{a}{2}\sqrt{(4c+u)}\xi_D,\frac{a}{2}\sqrt{(4c+u)})d\xi_D\Bigg]$$
$$+\frac{a^2}{4}\int_1^{r_{fD}}\xi_D f_1(\xi_D)H_0(\frac{a}{2}\sqrt{(4c+u)}\xi_D,\frac{a}{2}\sqrt{(4c+u)})d\xi_D\Bigg). \quad (4.321)$$

For simplicity, we introduce the functions $M_1(u)$ and $M_2(u)$ defined respectively by

$$M_1(u)=\frac{a}{2}\sqrt{(4c+u)}\frac{H_0(\frac{a}{2}\sqrt{(4c+u)}r_{fD},\frac{a}{2}\sqrt{(4c+u)})}{G_0(\frac{a}{2}\sqrt{(4c+u)},\frac{a}{2}\sqrt{(4c+u)}r_{fD})}, \quad (4.322)$$

and

$$M_2(u)=\frac{a^2}{4}M_1(u)\int_1^{r_{fD}}\xi_D f_1(\xi_D)G_0(\frac{a}{2}\sqrt{(4c+u)}\xi_D,\frac{a}{2}\sqrt{(4c+u)})d\xi_D$$
$$+\frac{a^3}{8}\sqrt{(4c+u)}\int_1^{r_{fD}}\xi_D f_1(\xi_D)H_0(\frac{a}{2}\sqrt{(4c+u)}\xi_D,\frac{a}{2}\sqrt{(4c+u)})d\xi_D, \quad (4.323)$$

such that Eq. 4.321 becomes simply

$$r_D\frac{\partial \bar{T}_{D0,ou}}{\partial r_D}\Bigg|_{r_D=1}=M_1(u)\bar{\hat{T}}_{D0,inl}(z_D,u)+M_2(u). \quad (4.324)$$

Next, we move to the $O(\epsilon)$ system. Recall that the ODE and the associated boundary conditions that describe this system are given respectively by the following equations

$$\frac{1}{r_D}\frac{\partial}{\partial r_D}\left(r_D\frac{\partial \bar{T}_{D1,ou}}{\partial r_D}\right)-\frac{a^2}{4}(4c+u)\bar{T}_{D1,ou}=\frac{1}{r_D}\frac{\partial}{\partial r_D}\left(r_D f(r_D)\frac{\partial \bar{T}_{D0,ou}}{\partial r_D}\right), \tag{4.325}$$

$$\bar{T}_{D1,ou}(r_{fD},u)=0, \tag{4.326}$$

and

$$\bar{T}_{D1,ou}(1,u)=\bar{\tilde{T}}_{D1,inl}(z_D,u). \tag{4.327}$$

The right hand side of the above ODE is function of only the dimensionless radial distance r_D. Thus, we set

$$Q(r_D)=-\frac{1}{r_D}\frac{\partial}{\partial r_D}\left(f(r_D)r_D\frac{\partial \bar{T}_{D0,ou}}{\partial r_D}\right), \tag{4.328}$$

and Eq. 4.325 becomes

$$\frac{1}{r_D}\frac{\partial}{\partial r_D}\left(r_D\frac{\partial \bar{T}_{D1,ou}}{\partial r_D}\right)-\frac{a^2}{4}(4c+u)\bar{T}_{D1,ou}=-Q(r_D). \tag{4.329}$$

Note that Eq. 4.329 is similar to Eq. 4.296. Therefore, they have the same solution with $\frac{a^2}{4}f_1(r_D)$ replaced by the function that we defined as $Q(r_D)$. So, by analogy to Eq. 4.305, we have

$$\begin{aligned}\bar{T}_{D1,ou}=&B_3I_0(\frac{a}{2}\sqrt{(4c+u)}r_D)+B_4K_0(\frac{a}{2}\sqrt{(4c+u)}r_D)\\&+I_0(\frac{a}{2}\sqrt{(4c+u)}r_D)\int_{r_D}^{r_{fD}}\xi_D Q(\xi_D)K_0(\frac{a}{2}\sqrt{(4c+u)}\xi_D)d\xi_D\\&+K_0(\frac{a}{2}\sqrt{(4c+u)}r_D)\int_1^{r_D}\xi_D Q(\xi_D)I_0(\frac{a}{2}\sqrt{(4c+u)}\xi_D)d\xi_D,\end{aligned} \tag{4.330}$$

where B_3 and B_4 are the new constants of integration. If we use the expression of $Q(r_D)$ given by Eq. 4.328, we have

$$\int_1^{r_D} \xi_D Q(\xi_D) I_0(\frac{a}{2}\sqrt{(4c+u)}\xi_D) d\xi_D = -\int_1^{r_D} \frac{\partial}{\partial \xi_D}\left(f(\xi_D)\xi_D \frac{\partial \bar{T}_{D0,ou}}{\partial \xi_D}\right) I_0(\frac{a}{2}\sqrt{(4c+u)}\xi_D) d\xi_D, \tag{4.331}$$

that we integrate by parts to obtain

$$\begin{aligned}\int_1^{r_D} \xi_D Q(\xi_D) I_0(\frac{a}{2}\sqrt{(4c+u)}\xi_D) d\xi_D = &-\xi_D f(\xi_D) \frac{\partial \bar{T}_{D0,ou}}{\partial \xi_D} I_0(\frac{a}{2}\sqrt{(4c+u)}\xi_D)\Big]_1^{r_D} \\ &+ \frac{a}{2}\sqrt{(4c+u)} \int_1^{r_D} \xi_D f(\xi_D) \frac{\partial \bar{T}_{D0,ou}}{\partial \xi_D} I_1(\frac{a}{2}\sqrt{(4c+u)}\xi_D) d\xi_D, \end{aligned} \tag{4.332}$$

or simplifying using the fact that $f(r_D = 1) = 0$ (see Eqs. 4.286 and 4.282),

$$\begin{aligned}\int_1^{r_D} \xi_D Q(\xi_D) I_0(\frac{a}{2}\sqrt{(4c+u)}\xi_D) d\xi_D = &-r_D f(r_D) \frac{\partial \bar{T}_{D0,ou}}{\partial r_D} I_0(\frac{a}{2}\sqrt{(4c+u)}r_D) \\ &+ \frac{a}{2}\sqrt{(4c+u)} \int_1^{r_D} \xi_D f(\xi_D) \frac{\partial \bar{T}_{D0,ou}}{\partial \xi_D} I_1(\frac{a}{2}\sqrt{(4c+u)}\xi_D) d\xi_D. \end{aligned} \tag{4.333}$$

Similarly, we have

$$\begin{aligned}\int_{r_D}^{r_{fD}} \xi_D Q(\xi_D) K_0(\frac{a}{2}\sqrt{(4c+u)}\xi_D) d\xi_D = \\ -\int_{r_D}^{r_{fD}} \frac{\partial}{\partial \xi_D}\left(f(\xi_D)\xi_D \frac{\partial \bar{T}_{D0,ou}}{\partial \xi_D}\right) K_0(\frac{a}{2}\sqrt{(4c+u)}\xi_D) d\xi_D. \end{aligned} \tag{4.334}$$

Integrating the above equation by parts yields

$$\int_{r_D}^{r_{fD}} \xi_D Q(\xi_D) K_0(\frac{a}{2}\sqrt{(4c+u)}\xi_D) d\xi_D = -\xi_D f(\xi_D) \frac{\partial \bar{T}_{D0,ou}}{\partial \xi_D} K_0(\frac{a}{2}\sqrt{(4c+u)}\xi_D)\Big]_{r_D}^{r_{fD}}$$
$$- \frac{a}{2}\sqrt{(4c+u)} \int_{r_D}^{r_{fD}} \xi_D f(\xi_D) \frac{\partial \bar{T}_{D0,ou}}{\partial \xi_D} K_1(\frac{a}{2}\sqrt{(4c+u)}\xi_D) d\xi_D, \quad (4.335)$$

or

$$\int_{r_D}^{r_{fD}} \xi_D Q(\xi_D) K_0(\frac{a}{2}\sqrt{(4c+u)}\xi_D) d\xi_D = r_D f(r_D) \frac{\partial \bar{T}_{D0,ou}}{\partial r_D} K_0(\frac{a}{2}\sqrt{(4c+u)}r_D)$$
$$- r_{fD} f(r_{fD}) \frac{\partial \bar{T}_{D0,ou}}{\partial r_D}\Big|_{r_{fD}} K_0(\frac{a}{2}\sqrt{(4c+u)}r_{fD}) - \frac{a}{2}\sqrt{(4c+u)}$$
$$\times \int_{r_D}^{r_{fD}} \xi_D f(\xi_D) \frac{\partial \bar{T}_{D0,ou}}{\partial \xi_D} K_1(\frac{a}{2}\sqrt{(4c+u)}\xi_D) d\xi_D. \quad (4.336)$$

Replacing Eqs. 4.333 and 4.336 into Eq. 4.330, rearranging and simplifying gives

$$\bar{T}_{D1,ou} = B_3 I_0(\frac{a}{2}\sqrt{(4c+u)}r_D) + B_4 K_0(\frac{a}{2}\sqrt{(4c+u)}r_D)$$
$$- r_{fD} f(r_{fD}) \frac{\partial \bar{T}_{D0,ou}}{\partial r_D}\Big|_{r_{fD}} K_0(\frac{a}{2}\sqrt{(4c+u)}r_{fD}) I_0(\frac{a}{2}\sqrt{(4c+u)}r_D)$$
$$+ \frac{a}{2}\sqrt{(4c+u)} K_0(\frac{a}{2}\sqrt{(4c+u)}r_D) \int_1^{r_D} \xi_D f(\xi_D) \frac{\partial \bar{T}_{D0,ou}}{\partial \xi_D} I_1(\frac{a}{2}\sqrt{(4c+u)}\xi_D) d\xi_D$$
$$- \frac{a}{2}\sqrt{(4c+u)} I_0(\frac{a}{2}\sqrt{(4c+u)}r_D) \int_{r_D}^{r_{fD}} \xi_D f(\xi_D) \frac{\partial \bar{T}_{D0,ou}}{\partial \xi_D} K_1(\frac{a}{2}\sqrt{(4c+u)}\xi_D) d\xi_D, \quad (4.337)$$

which constitutes the general solution to the $O(\epsilon)$ system. The expression above contains two constants. In order to eliminate one constant, B_4 for instance, we need to apply the outer boundary condition given by Eq. 4.326 as follows

$$\bar{T}_{D1,ou}(r_{fD},u) = B_3 I_0(\frac{a}{2}\sqrt{(4c+u)}r_{fD}) + B_4 K_0(\frac{a}{2}\sqrt{(4c+u)}r_{fD}) \\ - r_{fD}f(r_{fD})\frac{\partial \bar{T}_{D0,ou}}{\partial r_D}\bigg|_{r_{fD}} K_0(\frac{a}{2}\sqrt{(4c+u)}r_{fD})I_0(\frac{a}{2}\sqrt{(4c+u)}r_{fD}) \\ + \frac{a}{2}\sqrt{(4c+u)}K_0(\frac{a}{2}\sqrt{(4c+u)}r_{fD})\int_1^{r_{fD}} \xi_D f(\xi_D)\frac{\partial \bar{T}_{D0,ou}}{\partial \xi_D} I_1(\frac{a}{2}\sqrt{(4c+u)}\xi_D)d\xi_D = 0, \tag{4.338}$$

or

$$B_4 = -B_3\frac{I_0(\frac{a}{2}\sqrt{(4c+u)}r_{fD})}{K_0(\frac{a}{2}\sqrt{(4c+u)}r_{fD})} + r_{fD}f(r_{fD})\frac{\partial \bar{T}_{D0,ou}}{\partial r_D}\bigg|_{r_{fD}} I_0(\frac{a}{2}\sqrt{(4c+u)}r_{fD}) \\ - \frac{a}{2}\sqrt{(4c+u)}\int_1^{r_{fD}} \xi_D f(\xi_D)\frac{\partial \bar{T}_{D0,ou}}{\partial \xi_D} I_1(\frac{a}{2}\sqrt{(4c+u)}\xi_D)d\xi_D. \tag{4.339}$$

If we replace B_4 in Eq. 4.337 by its expression provided above and rearrange, we obtain

$$\bar{T}_{D1,ou} = \left(\frac{B_3}{K_0(\frac{a}{2}\sqrt{(4c+u)}r_{fD})} - r_{fD}f(r_{fD})\frac{\partial \bar{T}_{D0,ou}}{\partial r_D}\bigg|_{r_{fD}}\right)\Big[K_0(\frac{a}{2}\sqrt{(4c+u)}r_{fD}) \\ \times I_0(\frac{a}{2}\sqrt{(4c+u)}r_D) - I_0(\frac{a}{2}\sqrt{(4c+u)}r_{fD})K_0(\frac{a}{2}\sqrt{(4c+u)}r_D)\Big] \\ - \frac{a}{2}\sqrt{(4c+u)}K_0(\frac{a}{2}\sqrt{(4c+u)}r_D)\int_1^{r_{fD}} \xi_D f(\xi_D)\frac{\partial \bar{T}_{D0,ou}}{\partial \xi_D} I_1(\frac{a}{2}\sqrt{(4c+u)}\xi_D)d\xi_D \\ + \frac{a}{2}\sqrt{(4c+u)}K_0(\frac{a}{2}\sqrt{(4c+u)}r_D)\int_1^{r_D} \xi_D f(\xi_D)\frac{\partial \bar{T}_{D0,ou}}{\partial \xi_D} I_1(\frac{a}{2}\sqrt{(4c+u)}\xi_D)d\xi_D \\ - \frac{a}{2}\sqrt{(4c+u)}I_0(\frac{a}{2}\sqrt{(4c+u)}r_D)\int_{r_D}^{r_{fD}} \xi_D f(\xi_D)\frac{\partial \bar{T}_{D0,ou}}{\partial \xi_D} K_1(\frac{a}{2}\sqrt{(4c+u)}\xi_D)d\xi_D, \tag{4.340}$$

or using the definition of the function G_0,

$$\bar{T}_{D1,ou} = \left(\frac{B_3}{K_0(\frac{a}{2}\sqrt{(4c+u)}r_{fD})} - r_{fD}f(r_{fD})\frac{\partial \bar{T}_{D0,ou}}{\partial r_D}\bigg|_{r_{fD}} \right)$$
$$\times G_0(\frac{a}{2}\sqrt{(4c+u)}r_D, \frac{a}{2}\sqrt{(4c+u)}r_{fD})$$
$$- \frac{a}{2}\sqrt{(4c+u)}K_0(\frac{a}{2}\sqrt{(4c+u)}r_D)\int_1^{r_{fD}} \xi_D f(\xi_D)\frac{\partial \bar{T}_{D0,ou}}{\partial \xi_D} I_1(\frac{a}{2}\sqrt{(4c+u)}\xi_D)d\xi_D$$
$$+ \frac{a}{2}\sqrt{(4c+u)}K_0(\frac{a}{2}\sqrt{(4c+u)}r_D)\int_1^{r_D} \xi_D f(\xi_D)\frac{\partial \bar{T}_{D0,ou}}{\partial \xi_D} I_1(\frac{a}{2}\sqrt{(4c+u)}\xi_D)d\xi_D$$
$$- \frac{a}{2}\sqrt{(4c+u)}I_0(\frac{a}{2}\sqrt{(4c+u)}r_D)\int_{r_D}^{r_{fD}} \xi_D f(\xi_D)\frac{\partial \bar{T}_{D0,ou}}{\partial \xi_D} K_1(\frac{a}{2}\sqrt{(4c+u)}\xi_D)d\xi_D. \quad (4.341)$$

In order to obtain the constant B_3, we use Eq. 4.327 in Eq. 4.341 as follows

$$\bar{\hat{T}}_{D1,inl}(z_D,u) = \left(\frac{B_3}{K_0(\frac{a}{2}\sqrt{(4c+u)}r_{fD})} - r_{fD}f(r_{fD})\frac{\partial \bar{T}_{D0,ou}}{\partial r_D}\bigg|_{r_{fD}} \right)$$
$$\times G_0(\frac{a}{2}\sqrt{(4c+u)}, \frac{a}{2}\sqrt{(4c+u)}r_{fD})$$
$$- \frac{a}{2}\sqrt{(4c+u)}K_0(\frac{a}{2}\sqrt{(4c+u)})\int_1^{r_{fD}} \xi_D f(\xi_D)\frac{\partial \bar{T}_{D0,ou}}{\partial \xi_D} I_1(\frac{a}{2}\sqrt{(4c+u)}\xi_D)d\xi_D$$
$$- \frac{a}{2}\sqrt{(4c+u)}I_0(\frac{a}{2}\sqrt{(4c+u)})\int_1^{r_{fD}} \xi_D f(\xi_D)\frac{\partial \bar{T}_{D0,ou}}{\partial \xi_D} K_1(\frac{a}{2}\sqrt{(4c+u)}\xi_D)d\xi_D. \quad (4.342)$$

We can simplify further this expression by using the definition of the function H_0 to combine the two integrals. The result is

$$\bar{\hat{T}}_{D1,inl}(z_D,u) = \left(\frac{B_3}{K_0(\frac{a}{2}\sqrt{(4c+u)}r_{fD})} - r_{fD}f(r_{fD})\frac{\partial \bar{T}_{D0,ou}}{\partial r_D}\bigg|_{r_{fD}} \right)$$
$$\times G_0(\frac{a}{2}\sqrt{(4c+u)}, \frac{a}{2}\sqrt{(4c+u)}r_{fD})$$
$$- \frac{a}{2}\sqrt{(4c+u)}\int_1^{r_{fD}} \xi_D f(\xi_D)\frac{\partial \bar{T}_{D0,ou}}{\partial \xi_D} H_0(\frac{a}{2}\sqrt{(4c+u)}, \frac{a}{2}\sqrt{(4c+u)}\xi_D)d\xi_D. \quad (4.343)$$

From Eq. 4.343, we have

$$\left(\frac{B_3}{K_0(\frac{a}{2}\sqrt{(4c+u)}r_{fD})} - r_{fD}f(r_{fD})\frac{\partial \bar{T}_{D0,ou}}{\partial r_D}\bigg|_{r_{fD}}\right) = \frac{1}{G_0(\frac{a}{2}\sqrt{(4c+u)}, \frac{a}{2}\sqrt{(4c+u)}r_{fD})}$$
$$\times\left[\bar{\hat{T}}_{D1,inl}(z_D,u) + \frac{a}{2}\sqrt{(4c+u)}\int_1^{r_{fD}} \xi_D f(\xi_D)\frac{\partial \bar{T}_{D0,ou}}{\partial \xi_D} H_0(\frac{a}{2}\sqrt{(4c+u)}, \frac{a}{2}\sqrt{(4c+u)}\xi_D)d\xi_D\right]. \tag{4.344}$$

Finally, we replace Eq. 4.344 in Eq. 4.341 to obtain

$$\begin{aligned}
\bar{T}_{D1,ou} = {} & \frac{G_0(\frac{a}{2}\sqrt{(4c+u)}r_D, \frac{a}{2}\sqrt{(4c+u)}r_{fD})}{G_0(\frac{a}{2}\sqrt{(4c+u)}, \frac{a}{2}\sqrt{(4c+u)}r_{fD})}\left[\bar{\hat{T}}_{D1,inl}(z_D,u)\right. \\
& \left. + \frac{a}{2}\sqrt{(4c+u)}\int_1^{r_{fD}} \xi_D f(\xi_D)\frac{\partial \bar{T}_{D0,ou}}{\partial \xi_D} H_0(\frac{a}{2}\sqrt{(4c+u)}, \frac{a}{2}\sqrt{(4c+u)}\xi_D)d\xi_D\right] \\
& - \frac{a}{2}\sqrt{(4c+u)}K_0(\frac{a}{2}\sqrt{(4c+u)}r_D)\int_1^{r_{fD}} \xi_D f(\xi_D)\frac{\partial \bar{T}_{D0,ou}}{\partial \xi_D} I_1(\frac{a}{2}\sqrt{(4c+u)}\xi_D)d\xi_D \\
& + \frac{a}{2}\sqrt{(4c+u)}K_0(\frac{a}{2}\sqrt{(4c+u)}r_D)\int_1^{r_D} \xi_D f(\xi_D)\frac{\partial \bar{T}_{D0,ou}}{\partial \xi_D} I_1(\frac{a}{2}\sqrt{(4c+u)}\xi_D)d\xi_D \\
& - \frac{a}{2}\sqrt{(4c+u)}I_0(\frac{a}{2}\sqrt{(4c+u)}r_D)\int_{r_D}^{r_{fD}} \xi_D f(\xi_D)\frac{\partial \bar{T}_{D0,ou}}{\partial \xi_D} K_1(\frac{a}{2}\sqrt{(4c+u)}\xi_D)d\xi_D.
\end{aligned} \tag{4.345}$$

If we take the derivative of Eq. 4.345 with respect to r_D and use the result of Eq. 4.318, we obtain

$$\frac{\partial \bar{T}_{D1,ou}}{\partial r_D} = \frac{a}{2}\sqrt{(4c+u)}\frac{H_0(\frac{a}{2}\sqrt{(4c+u)}r_{fD}, \frac{a}{2}\sqrt{(4c+u)}r_D)}{G_0(\frac{a}{2}\sqrt{(4c+u)}, \frac{a}{2}\sqrt{(4c+u)}r_{fD})}\left[\bar{\hat{T}}_{D1,inl}(z_D,u)\right.$$
$$\left. + \frac{a}{2}\sqrt{(4c+u)}\int_1^{r_{fD}} \xi_D f(\xi_D)\frac{\partial \bar{T}_{D0,ou}}{\partial \xi_D}H_0(\frac{a}{2}\sqrt{(4c+u)}, \frac{a}{2}\sqrt{(4c+u)}\xi_D)d\xi_D\right]$$
$$+ \frac{a^2}{4}(4c+u)K_1(\frac{a}{2}\sqrt{(4c+u)}r_D)\int_1^{r_{fD}} \xi_D f(\xi_D)\frac{\partial \bar{T}_{D0,ou}}{\partial \xi_D}I_1(\frac{a}{2}\sqrt{(4c+u)}\xi_D)d\xi_D$$
$$- \frac{a^2}{4}(4c+u)K_1(\frac{a}{2}\sqrt{(4c+u)}r_D)\int_1^{r_D} \xi_D f(\xi_D)\frac{\partial \bar{T}_{D0,ou}}{\partial \xi_D}I_1(\frac{a}{2}\sqrt{(4c+u)}\xi_D)d\xi_D$$
$$- \frac{a^2}{4}(4c+u)I_1(\frac{a}{2}\sqrt{(4c+u)}r_D)\int_{r_D}^{r_{fD}} \xi_D f(\xi_D)\frac{\partial \bar{T}_{D0,ou}}{\partial \xi_D}K_1(\frac{a}{2}\sqrt{(4c+u)}\xi_D)d\xi_D$$
$$+ \frac{a}{2}\sqrt{(4c+u)}r_D f(r_D)\frac{\partial \bar{T}_{D0,ou}}{\partial r_D}K_0(\frac{a}{2}\sqrt{(4c+u)}r_D)I_1(\frac{a}{2}\sqrt{(4c+u)}r_D)$$
$$+ \frac{a}{2}\sqrt{(4c+u)}r_D f(r_D)\frac{\partial \bar{T}_{D0,ou}}{\partial r_D}I_0(\frac{a}{2}\sqrt{(4c+u)}r_D)K_1(\frac{a}{2}\sqrt{(4c+u)}r_D), \quad (4.346)$$

or using the fact that

$$I_0(\frac{a}{2}\sqrt{(4c+u)}r_D)K_1(\frac{a}{2}\sqrt{(4c+u)}r_D) + K_0(\frac{a}{2}\sqrt{(4c+u)}r_D)I_1(\frac{a}{2}\sqrt{(4c+u)}r_D)$$
$$= \frac{1}{\frac{a}{2}\sqrt{(4c+u)}r_D}, \quad (4.347)$$

$$\frac{\partial \bar{T}_{D1,ou}}{\partial r_D} = \frac{a}{2}\sqrt{(4c+u)}\frac{H_0(\frac{a}{2}\sqrt{(4c+u)}r_{fD}, \frac{a}{2}\sqrt{(4c+u)}r_D)}{G_0(\frac{a}{2}\sqrt{(4c+u)}, \frac{a}{2}\sqrt{(4c+u)}r_{fD})}\left[\bar{\hat{T}}_{D1,inl}(z_D,u)\right.$$
$$\left. + \frac{a}{2}\sqrt{(4c+u)}\int_1^{r_{fD}} \xi_D f(\xi_D)\frac{\partial \bar{T}_{D0,ou}}{\partial \xi_D}H_0(\frac{a}{2}\sqrt{(4c+u)}, \frac{a}{2}\sqrt{(4c+u)}\xi_D)d\xi_D\right]$$
$$+ \frac{a^2}{4}(4c+u)K_1(\frac{a}{2}\sqrt{(4c+u)}r_D)\int_1^{r_{fD}} \xi_D f(\xi_D)\frac{\partial \bar{T}_{D0,ou}}{\partial \xi_D}I_1(\frac{a}{2}\sqrt{(4c+u)}\xi_D)d\xi_D$$
$$- \frac{a^2}{4}(4c+u)K_1(\frac{a}{2}\sqrt{(4c+u)}r_D)\int_1^{r_D} \xi_D f(\xi_D)\frac{\partial \bar{T}_{D0,ou}}{\partial \xi_D}I_1(\frac{a}{2}\sqrt{(4c+u)}\xi_D)d\xi_D$$
$$- \frac{a^2}{4}(4c+u)I_1(\frac{a}{2}\sqrt{(4c+u)}r_D)\int_{r_D}^{r_{fD}} \xi_D f(\xi_D)\frac{\partial \bar{T}_{D0,ou}}{\partial \xi_D}K_1(\frac{a}{2}\sqrt{(4c+u)}\xi_D)d\xi_D$$
$$+ f(r_D)\frac{\partial \bar{T}_{D0,ou}}{\partial r_D}. \quad (4.348)$$

At $r_D = 1$, Eq. 4.348 becomes

$$r_D \frac{\partial \bar{T}_{D1,ou}}{\partial r_D}\bigg|_{r_D=1} = \frac{a}{2}\sqrt{(4c+u)}\frac{H_0(\frac{a}{2}\sqrt{(4c+u)}r_{fD}, \frac{a}{2}\sqrt{(4c+u)})}{G_0(\frac{a}{2}\sqrt{(4c+u)}, \frac{a}{2}\sqrt{(4c+u)}r_{fD})}\Bigg[\bar{\hat{T}}_{D1,inl}(z_D,u) + \frac{a}{2}\sqrt{(4c+u)}\int_1^{r_{fD}} \xi_D f(\xi_D)\frac{\partial \bar{T}_{D0,ou}}{\partial \xi_D} H_0(\frac{a}{2}\sqrt{(4c+u)}, \frac{a}{2}\sqrt{(4c+u)}\xi_D)d\xi_D\Bigg] + \frac{a^2}{4}(4c+u)K_1(\frac{a}{2}\sqrt{(4c+u)})\int_1^{r_{fD}} \xi_D f(\xi_D)\frac{\partial \bar{T}_{D0,ou}}{\partial \xi_D} I_1(\frac{a}{2}\sqrt{(4c+u)}\xi_D)d\xi_D - \frac{a^2}{4}(4c+u)I_1(\frac{a}{2}\sqrt{(4c+u)})\int_1^{r_{fD}} \xi_D f(\xi_D)\frac{\partial \bar{T}_{D0,ou}}{\partial \xi_D} K_1(\frac{a}{2}\sqrt{(4c+u)}\xi_D)d\xi_D, \quad (4.349)$$

or equivalently,

$$r_D \frac{\partial \bar{T}_{D1,ou}}{\partial r_D}\bigg|_{r_D=1} = \frac{a}{2}\sqrt{(4c+u)}\frac{H_0(\frac{a}{2}\sqrt{(4c+u)}r_{fD}, \frac{a}{2}\sqrt{(4c+u)})}{G_0(\frac{a}{2}\sqrt{(4c+u)}, \frac{a}{2}\sqrt{(4c+u)}r_{fD})}\Bigg[\bar{\hat{T}}_{D1,inl}(z_D,u) + \frac{a}{2}\sqrt{(4c+u)}\int_1^{r_{fD}} \xi_D f(\xi_D)\frac{\partial \bar{T}_{D0,ou}}{\partial \xi_D} H_0(\frac{a}{2}\sqrt{(4c+u)}, \frac{a}{2}\sqrt{(4c+u)}\xi_D)d\xi_D\Bigg] + \frac{a^2}{4}(4c+u)\int_1^{r_{fD}} \xi_D f(\xi_D)\frac{\partial \bar{T}_{D0,ou}}{\partial \xi_D} G_1(\frac{a}{2}\sqrt{(4c+u)}\xi_D, \frac{a}{2}\sqrt{(4c+u)})d\xi_D, \quad (4.350)$$

with

$$G_1(\frac{a}{2}\sqrt{(4c+u)}\xi_D, \frac{a}{2}\sqrt{(4c+u)}) = K_1(\frac{a}{2}\sqrt{(4c+u)})I_1(\frac{a}{2}\sqrt{(4c+u)}\xi_D) - I_1(\frac{a}{2}\sqrt{(4c+u)}) \times K_1(\frac{a}{2}\sqrt{(4c+u)}\xi_D), \quad (4.351)$$

according to the definition of G_ν (Eq. B.111) with $\nu = 1$. By introducing the function

$$M_3(z_D,u) = \frac{a}{2}\sqrt{(4c+u)}\Bigg[M_1(u)\int_1^{r_{fD}} \xi_D f(\xi_D)\frac{\partial \bar{T}_{D0,ou}}{\partial \xi_D} H_0(\frac{a}{2}\sqrt{(4c+u)}, \frac{a}{2}\sqrt{(4c+u)}\xi_D)d\xi_D + \frac{a}{2}\sqrt{(4c+u)}\int_1^{r_{fD}} \xi_D f(\xi_D)\frac{\partial \bar{T}_{D0,ou}}{\partial \xi_D} G_1(\frac{a}{2}\sqrt{(4c+u)}\xi_D, \frac{a^2}{4}(4c+u))d\xi_D\Bigg], \quad (4.352)$$

Eq. 4.350 can be rewritten as

$$r_D \frac{\partial \bar{T}_{D1,ou}}{\partial r_D}\bigg|_{r_D=1} = M_1(u)\bar{\hat{T}}_{D1,inl}(z_D,u) + M_3(z_D,u), \tag{4.353}$$

where $M_1(u)$ was previously defined (see Eq. 4.322). Note that the dependance of M_3 with the variable z_D is through the function $\frac{\partial \bar{T}_{D0,ou}}{\partial r_D}$ as the solution $\bar{T}_{D0,ou}$ implicitly depends on the vertical distance.

Finally, we solve the $O(\delta)$ system. Recall that ODE and the associated boundary conditions that describe the system are given respectively by

$$\frac{1}{r_D}\frac{\partial}{\partial r_D}\left(r_D \frac{\partial \bar{T}_{D2,ou}}{\partial r_D}\right) - \frac{a^2}{4}(4c+u)\bar{T}_{D2,ou} = -\frac{a^2}{4}g(r_D)\left(u\bar{T}_{D0,ou} - f_1(r_D)\right), \tag{4.354}$$

$$\bar{T}_{D2,ou}(r_{fD},u) = 0, \tag{4.355}$$

and

$$\bar{T}_{D2,ou}(1,u) = \bar{\hat{T}}_{D2,inl}(z_D,u). \tag{4.356}$$

We set

$$P(r_D) = \frac{a^2}{4}g(r_D)\left(u\bar{T}_{D0,ou} - f_1(r_D)\right). \tag{4.357}$$

Eq. 4.354 becomes

$$\frac{1}{r_D}\frac{\partial}{\partial r_D}\left(r_D \frac{\partial \bar{T}_{D2,ou}}{\partial r_D}\right) - \frac{a^2}{4}(4c+u)\bar{T}_{D2,ou} = -P(r_D), \tag{4.358}$$

which is again similar to Eq. 4.296. Based on the previous results for the leading problem, we can write our general solution for the $O(\delta)$ system as

$$\bar{T}_{D2,ou} = B_5 I_0(\frac{a}{2}\sqrt{(4c+u)}r_D) + B_6 K_0(\frac{a}{2}\sqrt{(4c+u)}r_D) + I_0(\frac{a}{2}\sqrt{(4c+u)}r_D)\int_{r_D}^{r_{fD}} \xi_D P(\xi_D) K_0(\frac{a}{2}\sqrt{(4c+u)}\xi_D)d\xi_D + K_0(\frac{a}{2}\sqrt{(4c+u)}r_D)\int_1^{r_D} \xi_D P(\xi_D) I_0(\frac{a}{2}\sqrt{(4c+u)}\xi_D)d\xi_D, \quad (4.359)$$

where B_5 and B_6 are the new constants of integration. Using the expression of $P(r_D)$ given by Eq. 4.357, we have

$$\bar{T}_{D2,ou} = B_5 I_0(\frac{a}{2}\sqrt{(4c+u)}r_D) + B_6 K_0(\frac{a}{2}\sqrt{(4c+u)}r_D) + \frac{a^2}{4} I_0(\frac{a}{2}\sqrt{(4c+u)}r_D)\int_{r_D}^{r_{fD}} \xi_D g(\xi_D)\left(u\bar{T}_{D0,ou} - f_1(\xi_D)\right) K_0(\frac{a}{2}\sqrt{(4c+u)}\xi_D)d\xi_D + \frac{a^2}{4} K_0(\frac{a}{2}\sqrt{(4c+u)}r_D)\int_1^{r_D} \xi_D g(\xi_D)\left(u\bar{T}_{D0,ou} - f_1(\xi_D)\right) I_0(\frac{a}{2}\sqrt{(4c+u)}\xi_D)d\xi_D. \quad (4.360)$$

Applying the outer boundary condition given by Eq. 4.355 yields

$$B_5 I_0(\frac{a}{2}\sqrt{(4c+u)}r_{fD}) + B_6 K_0(\frac{a}{2}\sqrt{(4c+u)}r_{fD}) + \frac{a^2}{4} K_0(\frac{a}{2}\sqrt{(4c+u)}r_{fD})\int_1^{r_{fD}} \xi_D g(\xi_D)\left(u\bar{T}_{D0,ou} - f_1(\xi_D)\right) I_0(\frac{a}{2}\sqrt{(4c+u)}\xi_D)d\xi_D = 0, \quad (4.361)$$

or

$$B_6 = -B_5\frac{I_0(\frac{a}{2}\sqrt{(4c+u)}r_{fD})}{K_0(\frac{a}{2}\sqrt{(4c+u)}r_{fD})} - \frac{a^2}{4}\int_1^{r_{fD}} \xi_D g(\xi_D)\left(u\bar{T}_{D0,ou} - f_1(\xi_D)\right) I_0(\frac{a}{2}\sqrt{(4c+u)}\xi_D)d\xi_D. \quad (4.362)$$

Substituting Eq. 4.362 into Eq. 4.360 gives

$$\bar{T}_{D2,ou} = \frac{B_5}{K_0(\frac{a}{2}\sqrt{(4c+u)}r_{fD})}\Bigg[K_0(\frac{a}{2}\sqrt{(4c+u)}r_{fD})I_0(\frac{a}{2}\sqrt{(4c+u)}r_D) - I_0(\frac{a}{2}\sqrt{(4c+u)}r_{fD}) \times K_0(\frac{a}{2}\sqrt{(4c+u)}r_D)\Bigg] - \frac{a^2}{4}K_0(\frac{a}{2}\sqrt{(4c+u)}r_D)\int_1^{r_{fD}} \xi_D g(\xi_D)\Big(u\bar{T}_{D0,ou} - f_1(\xi_D)\Big)I_0(\frac{a}{2}\sqrt{(4c+u)}\xi_D)d\xi_D + \frac{a^2}{4}I_0(\frac{a}{2}\sqrt{(4c+u)}r_D)\int_{r_D}^{r_{fD}} \xi_D g(\xi_D)\Big(u\bar{T}_{D0,ou} - f_1(\xi_D)\Big)K_0(\frac{a}{2}\sqrt{(4c+u)}\xi_D)d\xi_D + \frac{a^2}{4}K_0(\frac{a}{2}\sqrt{(4c+u)}r_D)\int_1^{r_D} \xi_D g(\xi_D)\Big(u\bar{T}_{D0,ou} - f_1(\xi_D)\Big)I_0(\frac{a}{2}\sqrt{(4c+u)}\xi_D)d\xi_D, \tag{4.363}$$

or simply,

$$\bar{T}_{D2,ou} = \frac{B_5}{K_0(\frac{a}{2}\sqrt{(4c+u)}r_{fD})}G_0(\frac{a}{2}\sqrt{(4c+u)}r_D, \frac{a}{2}\sqrt{(4c+u)}r_{fD}) - \frac{a^2}{4}K_0(\frac{a}{2}\sqrt{(4c+u)}r_D)\int_1^{r_{fD}} \xi_D g(\xi_D)\Big(u\bar{T}_{D0,ou} - f_1(\xi_D)\Big)I_0(\frac{a}{2}\sqrt{(4c+u)}\xi_D)d\xi_D + \frac{a^2}{4}I_0(\frac{a}{2}\sqrt{(4c+u)}r_D)\int_{r_D}^{r_{fD}} \xi_D g(\xi_D)\Big(u\bar{T}_{D0,ou} - f_1(\xi_D)\Big)K_0(\frac{a}{2}\sqrt{(4c+u)}\xi_D)d\xi_D + \frac{a^2}{4}K_0(\frac{a}{2}\sqrt{(4c+u)}r_D)\int_1^{r_D} \xi_D g(\xi_D)\Big(u\bar{T}_{D0,ou} - f_1(\xi_D)\Big)I_0(\frac{a}{2}\sqrt{(4c+u)}\xi_D)d\xi_D. \tag{4.364}$$

To evaluate B_5, we use Eq. 4.356 in Eq. 4.364 as follows

$$\bar{\hat{T}}_{D2,inl}(z_D,u) = \frac{B_5}{K_0(\frac{a}{2}\sqrt{(4c+u)}r_{fD})}G_0(\frac{a}{2}\sqrt{(4c+u)}, \frac{a}{2}\sqrt{(4c+u)}r_{fD}) - \frac{a^2}{4}K_0(\frac{a}{2}\sqrt{(4c+u)})\int_1^{r_{fD}} \xi_D g(\xi_D)\Big(u\bar{T}_{D0,ou} - f_1(\xi_D)\Big)I_0(\frac{a}{2}\sqrt{(4c+u)}\xi_D)d\xi_D + \frac{a^2}{4}I_0(\frac{a}{2}\sqrt{(4c+u)})\int_1^{r_{fD}} \xi_D g(\xi_D)\Big(u\bar{T}_{D0,ou} - f_1(\xi_D)\Big)K_0(\frac{a}{2}\sqrt{(4c+u)}\xi_D)d\xi_D, \tag{4.365}$$

that we can rearrange to obtain

$$\bar{\hat{T}}_{D2,inl}(z_D,u)=\frac{B_5}{K_0(\frac{a}{2}\sqrt{(4c+u)}r_{fD})}G_0(\frac{a}{2}\sqrt{(4c+u)},\frac{a}{2}\sqrt{(4c+u)}r_{fD})$$
$$-\frac{a^2}{4}\int_1^{r_{fD}}\xi_D g(\xi_D)\Big(u\bar{T}_{D0,ou}-f_1(\xi_D)\Big)G_0(\frac{a}{2}\sqrt{(4c+u)}\xi_D,\frac{a}{2}\sqrt{(4c+u)})d\xi_D, \quad (4.366)$$

or equivalently,

$$\frac{B_5}{K_0(\frac{a}{2}\sqrt{(4c+u)}r_{fD})}=\frac{1}{G_0(\frac{a}{2}\sqrt{(4c+u)},\frac{a}{2}\sqrt{(4c+u)}r_{fD})}\Bigg[\bar{\hat{T}}_{D2,inl}(z_D,u)+\frac{a^2}{4}$$
$$\times\int_1^{r_{fD}}\xi_D g(\xi_D)\Big(u\bar{T}_{D0,ou}-f_1(\xi_D)\Big)G_0(\frac{a}{2}\sqrt{(4c+u)}\xi_D,\frac{a}{2}\sqrt{(4c+u)})d\xi_D\Bigg]. \quad (4.367)$$

Substituting Eq. 4.367 in Eq. 4.364 yields

$$\bar{T}_{D2,ou}=\frac{G_0(\frac{a}{2}\sqrt{(4c+u)}r_D,\frac{a}{2}\sqrt{(4c+u)}r_{fD})}{G_0(\frac{a}{2}\sqrt{(4c+u)},\frac{a}{2}\sqrt{(4c+u)}r_{fD})}\Bigg[\bar{\hat{T}}_{D2,inl}(z_D,u)+\frac{a^2}{4}$$
$$\times\int_1^{r_{fD}}\xi_D g(\xi_D)\Big(u\bar{T}_{D0,ou}-f_1(\xi_D)\Big)G_0(\frac{a}{2}\sqrt{(4c+u)}\xi_D,\frac{a}{2}\sqrt{(4c+u)})d\xi_D\Bigg]$$
$$-\frac{a^2}{4}K_0(\frac{a}{2}\sqrt{(4c+u)}r_D)\int_1^{r_{fD}}\xi_D g(\xi_D)\Big(u\bar{T}_{D0,ou}-f_1(\xi_D)\Big)I_0(\frac{a}{2}\sqrt{(4c+u)}\xi_D)d\xi_D$$
$$+\frac{a^2}{4}I_0(\frac{a}{2}\sqrt{(4c+u)}r_D)\int_{r_D}^{r_{fD}}\xi_D g(\xi_D)\Big(u\bar{T}_{D0,ou}-f_1(\xi_D)\Big)K_0(\frac{a}{2}\sqrt{(4c+u)}\xi_D)d\xi_D$$
$$+\frac{a^2}{4}K_0(\frac{a}{2}\sqrt{(4c+u)}r_D)\int_1^{r_D}\xi_D g(\xi_D)\Big(u\bar{T}_{D0,ou}-f_1(\xi_D)\Big)I_0(\frac{a}{2}\sqrt{(4c+u)}\xi_D)d\xi_D, \quad (4.368)$$

which represents the dimensionless temperature solution for the $O(\delta)$ system. Taking the derivative of Eq. 4.368 with respect to r_D gives

$$\frac{\partial \bar{T}_{D2,ou}}{\partial r_D} = \frac{a}{2}\sqrt{(4c+u)}\frac{H_0(\frac{a}{2}\sqrt{(4c+u)}r_{fD},\frac{a}{2}\sqrt{(4c+u)}r_D)}{G_0(\frac{a}{2}\sqrt{(4c+u)},\frac{a}{2}\sqrt{(4c+u)}r_{fD})}\Bigg[\bar{\hat{T}}_{D2,inl}(z_D,u)+\frac{a^2}{4}$$
$$\times\int_1^{r_{fD}}\xi_D g(\xi_D)\Big(u\bar{T}_{D0,ou}-f_1(\xi_D)\Big)G_0(\frac{a}{2}\sqrt{(4c+u)}\xi_D,\frac{a}{2}\sqrt{(4c+u)})d\xi_D\Bigg]$$
$$+\frac{a^2}{4}\frac{a}{2}\sqrt{(4c+u)}K_1(\frac{a}{2}\sqrt{(4c+u)}r_D)\int_1^{r_{fD}}\xi_D g(\xi_D)\Big(u\bar{T}_{D0,ou}-f_1(\xi_D)\Big)I_0(\frac{a}{2}\sqrt{(4c+u)}\xi_D)d\xi_D$$
$$+\frac{a^2}{4}\frac{a}{2}\sqrt{(4c+u)}I_1(\frac{a}{2}\sqrt{(4c+u)}r_D)\int_{r_D}^{r_{fD}}\xi_D g(\xi_D)\Big(u\bar{T}_{D0,ou}-f_1(\xi_D)\Big)K_0(\frac{a}{2}\sqrt{(4c+u)}\xi_D)d\xi_D$$
$$-\frac{a^2}{4}\frac{a}{2}\sqrt{(4c+u)}K_1(\frac{a}{2}\sqrt{(4c+u)}r_D)\int_1^{r_D}\xi_D g(\xi_D)\Big(u\bar{T}_{D0,ou}-f_1(\xi_D)\Big)I_0(\frac{a}{2}\sqrt{(4c+u)}\xi_D)d\xi_D. \tag{4.369}$$

If we evaluate Eq. 4.369 at $r_D = 1$, we obtain

$$r_D\frac{\partial \bar{T}_{D2,ou}}{\partial r_D}\mid_{r_D=1} = \frac{a}{2}\sqrt{(4c+u)}\frac{H_0(\frac{a}{2}\sqrt{(4c+u)}r_{fD},\frac{a}{2}\sqrt{(4c+u)})}{G_0(\frac{a}{2}\sqrt{(4c+u)},\frac{a}{2}\sqrt{(4c+u)}r_{fD})}\Bigg[\bar{\hat{T}}_{D2,inl}(z_D,u)+\frac{a^2}{4}$$
$$\times\int_1^{r_{fD}}\xi_D g(\xi_D)\Big(u\bar{T}_{D0,ou}-f_1(\xi_D)\Big)G_0(\frac{a}{2}\sqrt{(4c+u)}\xi_D,\frac{a}{2}\sqrt{(4c+u)})d\xi_D\Bigg]$$
$$+\frac{a^3}{8}\sqrt{(4c+u)}K_1(\frac{a}{2}\sqrt{(4c+u)})\int_1^{r_{fD}}\xi_D g(\xi_D)\Big(u\bar{T}_{D0,ou}-f_1(\xi_D)\Big)I_0(\frac{a}{2}\sqrt{(4c+u)}\xi_D)d\xi_D$$
$$+\frac{a^3}{8}\sqrt{(4c+u)}I_1(\frac{a}{2}\sqrt{(4c+u)})\int_1^{r_{fD}}\xi_D g(\xi_D)\Big(u\bar{T}_{D0,ou}-f_1(\xi_D)\Big)K_0(\frac{a}{2}\sqrt{(4c+u)}\xi_D)d\xi_D, \tag{4.370}$$

which becomes

$$r_D\frac{\partial \bar{T}_{D2,ou}}{\partial r_D}\mid_{r_D=1} = \frac{a}{2}\sqrt{(4c+u)}\frac{H_0(\frac{a}{2}\sqrt{(4c+u)}r_{fD},\frac{a}{2}\sqrt{(4c+u)})}{G_0(\frac{a}{2}\sqrt{(4c+u)},\frac{a}{2}\sqrt{(4c+u)}r_{fD})}\Bigg[\bar{\hat{T}}_{D2,inl}(z_D,u)+\frac{a^2}{4}$$
$$\times\int_1^{r_{fD}}\xi_D g(\xi_D)\Big(u\bar{T}_{D0,ou}-f_1(\xi_D)\Big)G_0(\frac{a}{2}\sqrt{(4c+u)}\xi_D,\frac{a}{2}\sqrt{(4c+u)})d\xi_D\Bigg]$$
$$+\frac{a^3}{8}\sqrt{(4c+u)}\int_1^{r_{fD}}\xi_D g(\xi_D)\Big(u\bar{T}_{D0,ou}-f_1(\xi_D)\Big)H_0(\frac{a}{2}\sqrt{(4c+u)}\xi_D,\frac{a}{2}\sqrt{(4c+u)})d\xi_D, \tag{4.371}$$

by using the definition of the function H_0. Introducing the following function,

$$M_4(z_D,u)=\frac{a^2}{4}M_1(u)\int_1^{r_{fD}}\xi_D g(\xi_D)\Big(u\bar{T}_{D0,ou}-f_1(\xi_D)\Big)G_0(\frac{a}{2}\sqrt{(4c+u)}\xi_D,\frac{a}{2}\sqrt{(4c+u)})d\xi_D$$
$$+\frac{a^3}{8}\sqrt{(4c+u)}\int_1^{r_{fD}}\xi_D g(\xi_D)\Big(u\bar{T}_{D0,ou}-f_1(\xi_D)\Big)H_0(\frac{a}{2}\sqrt{(4c+u)}\xi_D,\frac{a}{2}\sqrt{(4c+u)})d\xi_D, \tag{4.372}$$

we can rewrite Eq. 4.371 as

$$r_D\frac{\partial\bar{T}_{D2,ou}}{\partial r_D}\bigg|_{r_D=1}=M_1(u)\bar{\hat{T}}_{D2,inl}(z_D,u)+M_4(z_D,u). \tag{4.373}$$

Wellbore Region Solution $0\le z_D\le 1$

As mentioned previously, the dimensionless temperature in the region $0<z_D<1$ is also given by

$$\bar{\hat{T}}_{D,inl}(z_D,u)=\bar{\hat{T}}_{D0,inl}+\epsilon\bar{\hat{T}}_{D1,inl}+\delta\bar{\hat{T}}_{D2,inl}. \tag{4.374}$$

Substituting Eqs. 4.374 and 4.291 into Eqs. 4.271 and 4.272 gives

$$\frac{\partial^2}{\partial z_D^2}\Big(\bar{\hat{T}}_{D0,inl}+\epsilon\bar{\hat{T}}_{D1,inl}+\delta\bar{\hat{T}}_{D2,inl}\Big)-bu\Big(\bar{\hat{T}}_{D0,inl}+\epsilon\bar{\hat{T}}_{D1,inl}+\delta\bar{\hat{T}}_{D2,inl}\Big)$$
$$+\frac{8}{a^2}\frac{K_{eD}}{K_{wD}}r_D\frac{\partial}{\partial r_D}\Big(\bar{T}_{D0,ou}+\epsilon\bar{T}_{D1,ou}+\delta\bar{T}_{D2,ou}\Big)\bigg|_{r_D=1}=-b, \tag{4.375}$$

and

$$\bar{\hat{T}}_{D0,inl}(z_D=0,u)+\epsilon\bar{\hat{T}}_{D1,inl}(z_D=0,u)+\delta\bar{\hat{T}}_{D2,inl}(z_D=0,u)=0. \tag{4.376}$$

By noting that $K_{eD}(r_D=1)=1$ and rearranging Eq. 4.375, we obtain

$$\frac{\partial^2 \bar{\hat{T}}_{D0,inl}}{\partial z_D^2} - bu\bar{\hat{T}}_{D0,inl} + \frac{8}{a^2 K_{wD}} r_D \frac{\partial \bar{T}_{D0,ou}}{\partial r_D}\bigg|_{r_D=1}$$
$$+ \epsilon\left[\frac{\partial^2 \bar{\hat{T}}_{D1,inl}}{\partial z_D^2} - bu\bar{\hat{T}}_{D1,inl} + \frac{8}{a^2 K_{wD}} r_D \frac{\partial \bar{T}_{D1,ou}}{\partial r_D}\right]_{r_D=1}\Bigg|$$
$$+ \delta\left[\frac{\partial^2 \bar{\hat{T}}_{D2,inl}}{\partial z_D^2} - bu\bar{\hat{T}}_{D2,inl} + \frac{8}{a^2 K_{wD}} r_D \frac{\partial \bar{T}_{D2,ou}}{\partial r_D}\bigg|_{r_D=1}\right] = -b. \quad (4.377)$$

A comparison of both sides of Eqs. 4.377 and 4.376 yields the following three system of equations

The $O(1)$ system:

$$\frac{\partial^2 \bar{\hat{T}}_{D0,inl}}{\partial z_D^2} - bu\bar{\hat{T}}_{D0,inl} + \frac{8}{a^2 K_{wD}} r_D \frac{\partial \bar{T}_{D0,ou}}{\partial r_D}\bigg|_{r_D=1} = -b, \quad (4.378)$$

$$\bar{\hat{T}}_{D0,inl}(z_D = 0, u) = 0. \quad (4.379)$$

The $O(\epsilon)$ system:

$$\frac{\partial^2 \bar{\hat{T}}_{D1,inl}}{\partial z_D^2} - bu\bar{\hat{T}}_{D1,inl} + \frac{8}{a^2 K_{wD}} r_D \frac{\partial \bar{T}_{D1,ou}}{\partial r_D}\bigg|_{r_D=1} = 0, \quad (4.380)$$

$$\bar{\hat{T}}_{D1,inl}(z_D = 0, u) = 0. \quad (4.381)$$

The $O(\delta)$ system:

$$\frac{\partial^2 \bar{\hat{T}}_{D2,inl}}{\partial z_D^2} - bu\bar{\hat{T}}_{D2,inl} + \frac{8}{a^2 K_{wD}} r_D \frac{\partial \bar{T}_{D2,ou}}{\partial r_D}\bigg|_{r_D=1} = 0, \quad (4.382)$$

$$\bar{\hat{T}}_{D2,inl}(z_D = 0, u) = 0. \quad (4.383)$$

We discuss first the solution of the leading system by using the expression that we derived for the term $r_D \frac{\partial \bar{T}_{D0,ou}}{\partial r_D}\Big|_{r_D=1}$ given by Eq. 4.324 in Eq. 4.378 as follows

$$\frac{\partial^2 \bar{\hat{T}}_{D0,inl}}{\partial z_D^2} - bu\bar{\hat{T}}_{D0,inl} + \frac{8}{a^2 K_{wD}}\left(M_1(u)\bar{\hat{T}}_{D0,inl}(z_D,u) + M_2(u)\right) = -b, \tag{4.384}$$

where the functions $M_1(u)$ and $M_2(u)$ are defined respectively by Eqs. 4.322 and 4.323. If we rearrange Eq. 4.384, we obtain

$$\frac{\partial^2 \bar{\hat{T}}_{D0,inl}}{\partial z_D^2} - \left(bu - \frac{8M_1(u)}{a^2 K_{wD}}\right)\bar{\hat{T}}_{D0,inl} + b + \frac{8M_2(u)}{a^2 K_{wD}} = 0. \tag{4.385}$$

Let us introduce a new variable $\bar{U}_{D0,in}$ defined by

$$\bar{U}_{D0,in} = \bar{\hat{T}}_{D0,inl} - \frac{b + \frac{8M_2(u)}{a^2 K_{wD}}}{bu - \frac{8M_1(u)}{a^2 K_{wD}}}. \tag{4.386}$$

If we express the $O(1)$ equation in terms of $\bar{U}_{D0,in}$, we obtain

$$\frac{\partial^2 \bar{U}_{D0,in}}{\partial z_D^2} - \left(bu - \frac{8M_1(u)}{a^2 K_{wD}}\right)\bar{U}_{D0,in} = 0, \tag{4.387}$$

whose solution is a combination of exponential functions as follows:

$$\bar{U}_{D0,in} = A_1 \exp\left[-\sqrt{\left(bu - \frac{8M_1(u)}{a^2 K_{wD}}\right)} z_D\right] + A_2 \exp\left[+\sqrt{\left(bu - \frac{8M_1(u)}{a^2 K_{wD}}\right)} z_D\right], \tag{4.388}$$

where A_1 and A_2 are two constants of integration to be determined. Note here that the term $\left(bu - \frac{8M_1(u)}{a^2 K_{wD}}\right)$ is positive because $M_1(u)$ is negative (Eq. 4.322). In terms of the dimensionless temperature $\bar{\hat{T}}_{D0,inl}$, the solution is obtained by simply replacing Eq. 4.388 into Eq. 4.386. The result is

$$\bar{\hat{T}}_{D0,inl} = \frac{b + \frac{8M_2(u)}{a^2 K_{wD}}}{bu - \frac{8M_1(u)}{a^2 K_{wD}}} + A_1 \exp\left[-\sqrt{\left(bu - \frac{8M_1(u)}{a^2 K_{wD}}\right)} z_D\right] + A_2 \exp\left[+\sqrt{\left(bu - \frac{8M_1(u)}{a^2 K_{wD}}\right)} z_D\right]. \tag{4.389}$$

For $z_D = 0$, we have

$$\bar{\hat{T}}_{D0,inl}(z_D = 0, u) = \frac{b + \frac{8M_2(u)}{a^2 K_{wD}}}{bu - \frac{8M_1(u)}{a^2 K_{wD}}} + A_1 + A_2 = 0. \tag{4.390}$$

Thus,

$$A_1 = -A_2 - \frac{b + \frac{8M_2(u)}{a^2 K_{wD}}}{bu - \frac{8M_1(u)}{a^2 K_{wD}}}, \tag{4.391}$$

and Eq. 4.389 becomes

$$\begin{aligned}\bar{\hat{T}}_{D0,inl} = \frac{b + \frac{8M_2(u)}{a^2 K_{wD}}}{bu - \frac{8M_1(u)}{a^2 K_{wD}}}\left(1 - \exp\left[-\sqrt{\left(bu - \frac{8M_1(u)}{a^2 K_{wD}}\right)} z_D\right]\right) \\ + A_2\left(\exp\left[+\sqrt{\left(bu - \frac{8M_1(u)}{a^2 K_{wD}}\right)} z_D\right] - \exp\left[-\sqrt{\left(bu - \frac{8M_1(u)}{a^2 K_{wD}}\right)} z_D\right]\right),\end{aligned} \tag{4.392}$$

or simply,

$$\begin{aligned}\bar{\hat{T}}_{D0,inl} = \frac{b + \frac{8M_2(u)}{a^2 K_{wD}}}{bu - \frac{8M_1(u)}{a^2 K_{wD}}}\left(1 - \exp\left[-\sqrt{\left(bu - \frac{8M_1(u)}{a^2 K_{wD}}\right)} z_D\right]\right) \\ + 2A_2 \sinh\left[\sqrt{\left(bu - \frac{8M_1(u)}{a^2 K_{wD}}\right)} z_D\right].\end{aligned} \tag{4.393}$$

Recall that the first order system in ϵ is given by Eqs. 4.380 and 4.381. But, because we have an expression for the term $r_D \frac{\partial \bar{T}_{D1,ou}}{\partial r_D}\Big|_{r_D=1}$ provided by Eq. 4.353, we can use it in Eq. 4.380 to obtain

$$\frac{\partial^2 \bar{\hat{T}}_{D1,inl}}{\partial z_D^2} - bu\bar{\hat{T}}_{D1,inl} + \frac{8}{a^2 K_{wD}}\left[M_1(u)\bar{\hat{T}}_{D1,inl}(z_D, u) + M_3(z_D, u)\right] = 0, \tag{4.394}$$

or after rearranging

$$\frac{\partial^2 \bar{\hat{T}}_{D1,inl}}{\partial z_D^2} - \left(bu - \frac{8M_1(u)}{a^2 K_{wD}}\right)\bar{\hat{T}}_{D1,inl} = -\frac{8M_3(z_D,u)}{a^2 K_{wD}}. \tag{4.395}$$

Eq. 4.395 is a non-homogeneous second order differential equation whose solution is the sum of any particular solution denoted by $\bar{\hat{T}}^p_{D1,inl}$ and a corresponding homogeneous solution $\bar{\hat{T}}^h_{D1,inl}$ that we obtain by setting $M_3(z_D,u) = 0$. It is easy to show that the homogeneous solution is a combination of exponential functions that we write as

$$\bar{\hat{T}}^h_{D1,inl} = C_1 \exp\left[-\sqrt{\left(bu - \frac{8M_1(u)}{a^2 K_{wD}}\right)} z_D\right] + C_2 \exp\left[+\sqrt{\left(bu - \frac{8M_1(u)}{a^2 K_{wD}}\right)} z_D\right], \tag{4.396}$$

where C_1 and C_2 are two constants. In order to find a particular solution, we apply the variation of parameters technique which assumes for our case, a particular solution of the form

$$\bar{\hat{T}}^p_{D1,inl} = u_1(z_D,u)\exp\left[-\sqrt{\left(bu - \frac{8M_1(u)}{a^2 K_{wD}}\right)} z_D\right] + u_2(z_D,u)\exp\left[+\sqrt{\left(bu - \frac{8M_1(u)}{a^2 K_{wD}}\right)} z_D\right]. \tag{4.397}$$

The functions u_1 and u_2 are underdetermined so we have the freedom to impose a constraint which simplifies subsequent equations. This constraint is chosen to be

$$u_1'(z_D,u)\exp\left[-\sqrt{\left(bu - \frac{8M_1(u)}{a^2 K_{wD}}\right)} z_D\right] + u_2'(z_D,u)\exp\left[+\sqrt{\left(bu - \frac{8M_1(u)}{a^2 K_{wD}}\right)} z_D\right] = 0, \tag{4.398}$$

where the notation u_1' and u_2' is introduced to refer to the derivative of u_1 and u_2 with respect to the variable z_D. The general solution to the $O(\epsilon)$ system is then given by the following expression

$$\bar{\hat{T}}_{D1,inl} = C_1 \exp\left[-\sqrt{\left(bu - \frac{8M_1(u)}{a^2 K_{wD}}\right)} z_D \right] + C_2 \exp\left[+\sqrt{\left(bu - \frac{8M_1(u)}{a^2 K_{wD}}\right)} z_D \right]$$
$$+ u_1(z_D, u) \exp\left[-\sqrt{\left(bu - \frac{8M_1(u)}{a^2 K_{wD}}\right)} z_D \right] + u_2(z_D, u) \exp\left[+\sqrt{\left(bu - \frac{8M_1(u)}{a^2 K_{wD}}\right)} z_D \right]. \tag{4.399}$$

Next, we differentiate Eq. 4.399 with respect to z_D to obtain

$$\frac{\partial \bar{\hat{T}}_{D1,inl}}{\partial z_D} = \sqrt{\left(bu - \frac{8M_1(u)}{a^2 K_{wD}}\right)} \Bigg(- C_1 \exp\left[-\sqrt{\left(bu - \frac{8M_1(u)}{a^2 K_{wD}}\right)} z_D \right]$$
$$+ C_2 \exp\left[+\sqrt{\left(bu - \frac{8M_1(u)}{a^2 K_{wD}}\right)} z_D \right] - u_1(z_D, u) \exp\left[-\sqrt{\left(bu - \frac{8M_1(u)}{a^2 K_{wD}}\right)} z_D \right]$$
$$+ u_2(z_D, u) \exp\left[+\sqrt{\left(bu - \frac{8M_1(u)}{a^2 K_{wD}}\right)} z_D \right] \Bigg) + u_1'(z_d, u) \exp\left[-\sqrt{\left(bu - \frac{8M_1(u)}{a^2 K_{wD}}\right)} z_D \right]$$
$$+ u_2'(z_D, u) \exp\left[+\sqrt{\left(bu - \frac{8M_1(u)}{a^2 K_{wD}}\right)} z_D \right]. \tag{4.400}$$

Using the constraint defined by Eq. 4.398, Eq. 4.400 simplifies to

$$\frac{\partial \bar{\hat{T}}_{D1,inl}}{\partial z_D} = \sqrt{\left(bu - \frac{8M_1(u)}{a^2 K_{wD}}\right)} \Bigg(- C_1 \exp\left[-\sqrt{\left(bu - \frac{8M_1(u)}{a^2 K_{wD}}\right)} z_D \right]$$
$$+ C_2 \exp\left[+\sqrt{\left(bu - \frac{8M_1(u)}{a^2 K_{wD}}\right)} z_D \right] - u_1(z_D, u) \exp\left[-\sqrt{\left(bu - \frac{8M_1(u)}{a^2 K_{wD}}\right)} z_D \right]$$
$$+ u_2(z_D, u) \exp\left[+\sqrt{\left(bu - \frac{8M_1(u)}{a^2 K_{wD}}\right)} z_D \right] \Bigg). \tag{4.401}$$

Differentiating the above expression yields

$$\frac{\partial^2 \bar{\hat{T}}_{D1,inl}}{\partial z_D^2} = \left(bu - \frac{8M_1(u)}{a^2 K_{wD}}\right)\left(C_1 \exp\left[-\sqrt{\left(bu - \frac{8M_1(u)}{a^2 K_{wD}}\right)} z_D\right]\right.$$
$$+ C_2 \exp\left[+\sqrt{\left(bu - \frac{8M_1(u)}{a^2 K_{wD}}\right)} z_D\right] + u_1(z_D, u) \exp\left[-\sqrt{\left(bu - \frac{8M_1(u)}{a^2 K_{wD}}\right)} z_D\right]$$
$$\left. + u_2(z_D, u) \exp\left[+\sqrt{\left(bu - \frac{8M_1(u)}{a^2 K_{wD}}\right)} z_D\right]\right) - \sqrt{\left(bu - \frac{8M_1(u)}{a^2 K_{wD}}\right)}\left(u_1'(z_D, u)\right.$$
$$\left. \times \exp\left[-\sqrt{\left(bu - \frac{8M_1(u)}{a^2 K_{wD}}\right)} z_D\right] - u_2'(z_D, u) \exp\left[+\sqrt{\left(bu - \frac{8M_1(u)}{a^2 K_{wD}}\right)} z_D\right]\right). \quad (4.402)$$

Replacing the result of Eq. 4.402 and Eq. 4.399 into Eq. 4.395 gives

$$\left(bu - \frac{8M_1(u)}{a^2 K_{wD}}\right)\left(C_1 \exp\left[-\sqrt{\left(bu - \frac{8M_1(u)}{a^2 K_{wD}}\right)} z_D\right]\right.$$
$$+ C_2 \exp\left[+\sqrt{\left(bu - \frac{8M_1(u)}{a^2 K_{wD}}\right)} z_D\right] + u_1(z_D, u) \exp\left[-\sqrt{\left(bu - \frac{8M_1(u)}{a^2 K_{wD}}\right)} z_D\right]$$
$$\left. + u_2(z_D, u) \exp\left[+\sqrt{\left(bu - \frac{8M_1(u)}{a^2 K_{wD}}\right)} z_D\right]\right) - \sqrt{\left(bu - \frac{8M_1(u)}{a^2 K_{wD}}\right)}\left(u_1'(z_D, u)\right.$$
$$\left. \times \exp\left[-\sqrt{\left(bu - \frac{8M_1(u)}{a^2 K_{wD}}\right)} z_D\right] - u_2'(z_D, u) \exp\left[+\sqrt{\left(bu - \frac{8M_1(u)}{a^2 K_{wD}}\right)} z_D\right]\right)$$
$$- \left(bu - \frac{8M_1(u)}{a^2 K_{wD}}\right)\left(C_1 \exp\left[-\sqrt{\left(bu - \frac{8M_1(u)}{a^2 K_{wD}}\right)} z_D\right]\right.$$
$$+ C_2 \exp\left[+\sqrt{\left(bu - \frac{8M_1(u)}{a^2 K_{wD}}\right)} z_D\right] + u_1(z_D, u) \exp\left[-\sqrt{\left(bu - \frac{8M_1(u)}{a^2 K_{wD}}\right)} z_D\right]$$
$$\left. + u_2(z_D, u) \exp\left[+\sqrt{\left(bu - \frac{8M_1(u)}{a^2 K_{wD}}\right)} z_D\right]\right) = -\frac{8M_3(z_D, u)}{a^2 K_{wD}}, \quad (4.403)$$

which simply can be rewritten as

$$u_1'(z_D,u)\exp\left[-\sqrt{\left(bu-\frac{8M_1(u)}{a^2K_{wD}}\right)}z_D\right]-u_2'(z_D,u)\exp\left[+\sqrt{\left(bu-\frac{8M_1(u)}{a^2K_{wD}}\right)}z_D\right]=\frac{8M_3(z_D,u)}{a^2K_{wD}\sqrt{\left(bu-\frac{8M_1(u)}{a^2K_{wD}}\right)}}. \quad (4.404)$$

The solution of the simultaneous equations Eqs. 4.398 and 4.404 for u_1' and u_2' is

$$u_1'(z_D,u)=\frac{1}{W}\begin{pmatrix}\frac{8M_3(z_D,u)}{a^2K_{wD}\sqrt{\left(bu-\frac{8M_1(u)}{a^2K_{wD}}\right)}} & -\exp\left[+\sqrt{\left(bu-\frac{8M_1(u)}{a^2K_{wD}}\right)}z_D\right]\\ 0 & \exp\left[+\sqrt{\left(bu-\frac{8M_1(u)}{a^2K_{wD}}\right)}z_D\right]\end{pmatrix}$$
$$=\frac{1}{W}\frac{8M_3(z_D,u)}{a^2K_{wD}\sqrt{\left(bu-\frac{8M_1(u)}{a^2K_{wD}}\right)}}\exp\left[+\sqrt{\left(bu-\frac{8M_1(u)}{a^2K_{wD}}\right)}z_D\right], \quad (4.405)$$

$$u_2'(z_D,u)=\frac{1}{W}\begin{pmatrix}\exp\left[-\sqrt{\left(bu-\frac{8M_1(u)}{a^2K_{wD}}\right)}z_D\right] & \frac{8M_3(z_D,u)}{a^2K_{wD}\sqrt{\left(bu-\frac{8M_1(u)}{a^2K_{wD}}\right)}}\\ \exp\left[-\sqrt{\left(bu-\frac{8M_1(u)}{a^2K_{wD}}\right)}z_D\right] & 0\end{pmatrix}$$
$$=-\frac{1}{W}\frac{8M_3(z_D,u)}{a^2K_{wD}\sqrt{\left(bu-\frac{8M_1(u)}{a^2K_{wD}}\right)}}\exp\left[-\sqrt{\left(bu-\frac{8M_1(u)}{a^2K_{wD}}\right)}z_D\right], \quad (4.406)$$

where W is the Wronskian defined by

$$W = \begin{pmatrix} \exp\left[-\sqrt{\left(bu - \frac{8M_1(u)}{a^2 K_{wD}} \right)} z_D \right] & -\exp\left[\sqrt{\left(bu - \frac{8M_1(u)}{a^2 K_{wD}} \right)} z_D \right] \\ \exp\left[-\sqrt{\left(bu - \frac{8M_1(u)}{a^2 K_{wD}} \right)} z_D \right] & \exp\left[\sqrt{\left(bu - \frac{8M_1(u)}{a^2 K_{wD}} \right)} z_D \right] \end{pmatrix} = 2. \quad (4.407)$$

Integrating Eq. 4.405 from 0 to z_D gives

$$\int_0^{z_D} u_1'(z_D, u) dz_D = \frac{4}{a^2 K_{wD} \sqrt{\left(bu - \frac{8M_1(u)}{a^2 K_{wD}} \right)}} \int_0^{z_D} M_3(\psi_D, u) \exp\left[+\sqrt{\left(bu - \frac{8M_1(u)}{a^2 K_{wD}} \right)} \psi_D \right] d\psi_D, \quad (4.408)$$

or

$$u_1(z_D, u) = u_1(0, u) + \frac{4}{a^2 K_{wD} \sqrt{\left(bu - \frac{8M_1(u)}{a^2 K_{wD}} \right)}} \times \int_0^{z_D} M_3(\psi_D, u) \exp\left[+ \sqrt{\left(bu - \frac{8M_1(u)}{a^2 K_{wD}} \right)} \psi_D \right] d\psi_D. \quad (4.409)$$

Similarly, if we integrate Eq. 4.406 from z_D to 1, we get

$$\int_{z_D}^1 u_2'(z_D, u) dz_D = -\frac{4}{a^2 K_{wD} \sqrt{\left(bu - \frac{8M_1(u)}{a^2 K_{wD}} \right)}} \int_{z_D}^1 M_3(\psi_D, u) \exp\left[-\sqrt{\left(bu - \frac{8M_1(u)}{a^2 K_{wD}} \right)} \psi_D \right] d\psi_D, \quad (4.410)$$

or

$$u_2(z_D,u) = u_2(1,u) + \frac{4}{a^2 K_{wD}\sqrt{\left(bu - \frac{8M_1(u)}{a^2K_{wD}}\right)}} \times \int_{z_D}^{1} M_3(\psi_D,u)\exp\left[-\sqrt{\left(bu-\frac{8M_1(u)}{a^2K_{wD}}\right)}\psi_D\right]d\psi_D. \quad (4.411)$$

Now, if we replace Eqs. 4.409 and 4.411 into the general solution given by Eq. 4.399, we obtain

$$\begin{aligned}\bar{\hat{T}}_{D1,inl} = {} & C_1\exp\left[-\sqrt{\left(bu-\frac{8M_1(u)}{a^2K_{wD}}\right)}z_D\right] + C_2\exp\left[+\sqrt{\left(bu-\frac{8M_1(u)}{a^2K_{wD}}\right)}z_D\right] \\ & + \exp\left[-\sqrt{\left(bu-\frac{8M_1(u)}{a^2K_{wD}}\right)}z_D\right]\left(u_1(0,u) + \frac{4}{a^2K_{wD}\sqrt{\left(bu-\frac{8M_1(u)}{a^2K_{wD}}\right)}}\right. \\ & \left. \times \int_0^{z_D} M_3(\psi_D,u)\exp\left[+\sqrt{\left(bu-\frac{8M_1(u)}{a^2K_{wD}}\right)}\psi_D\right]d\psi_D\right) \\ & + \exp\left[+\sqrt{\left(bu-\frac{8M_1(u)}{a^2K_{wD}}\right)}z_D\right]\left(u_2(1,u) + \frac{4}{a^2K_{wD}\sqrt{\left(bu-\frac{8M_1(u)}{a^2K_{wD}}\right)}}\right. \\ & \left. \times \int_{z_D}^{1} M_3(\psi_D,u)\exp\left[-\sqrt{\left(bu-\frac{8M_1(u)}{a^2K_{wD}}\right)}\psi_D\right]d\psi_D\right), \quad (4.412)\end{aligned}$$

or after rearranging,

$$\bar{\hat{T}}_{D1,inl} = A_3 \exp\left[-\sqrt{\left(bu - \frac{8M_1(u)}{a^2 K_{wD}}\right)} z_D \right] + A_4 \exp\left[+\sqrt{\left(bu - \frac{8M_1(u)}{a^2 K_{wD}}\right)} z_D \right]$$
$$+ \frac{4}{a^2 K_{wD}\sqrt{\left(bu - \frac{8M_1(u)}{a^2 K_{wD}}\right)}} \int_0^{z_D} M_3(\psi_D, u) \exp\left[+\sqrt{\left(bu - \frac{8M_1(u)}{a^2 K_{wD}}\right)} (\psi_D - z_D) \right] d\psi_D$$
$$+ \frac{4}{a^2 K_{wD}\sqrt{\left(bu - \frac{8M_1(u)}{a^2 K_{wD}}\right)}} \int_{z_D}^1 M_3(\psi_D, u) \exp\left[-\sqrt{\left(bu - \frac{8M_1(u)}{a^2 K_{wD}}\right)} (\psi_D - z_D) \right] d\psi_D, \tag{4.413}$$

where for simplicity, the new constants A_3 and A_4 are introduced and defined respectively by

$$A_3 = C_1 + u_1(0, u), \tag{4.414}$$

and

$$A_4 = C_2 + u_2(1, u). \tag{4.415}$$

Recall that the $O(\epsilon)$ system has an outer boundary condition given by Eq. 4.381. If we replace z_D by 0 in Eq. 4.413 and we set the solution to zero according to the boundary condition, we obtain

$$A_3 + A_4 + \frac{4}{a^2 K_{wD}\sqrt{\left(bu - \frac{8M_1(u)}{a^2 K_{wD}}\right)}} \int_0^1 M_3(\psi_D, u) \exp\left[-\sqrt{\left(bu - \frac{8M_1(u)}{a^2 K_{wD}}\right)} \psi_D \right] d\psi_D = 0, \tag{4.416}$$

or equivalently,

$$A_3 = -A_4 - \frac{4}{a^2 K_{wD}\sqrt{\left(bu - \frac{8M_1(u)}{a^2 K_{wD}}\right)}} \int_0^1 M_3(\psi_D, u) \exp\left[- \sqrt{\left(bu - \frac{8M_1(u)}{a^2 K_{wD}}\right)}\psi_D \right] d\psi_D. \tag{4.417}$$

Finally, replacing Eq. 4.417 into the general solution Eq. 4.413 and rearranging yields

$$\begin{aligned}\bar{\hat{T}}_{D1,inl} = 2A_4 \sinh\left[\sqrt{\left(bu - \frac{8M_1(u)}{a^2 K_{wD}}\right)} z_D\right] + \frac{4}{a^2 K_{wD}\sqrt{\left(bu - \frac{8M_1(u)}{a^2 K_{wD}}\right)}} \times \\ \left(- \int_0^1 M_3(\psi_D, u) \exp\left[- \sqrt{\left(bu - \frac{8M_1(u)}{a^2 K_{wD}}\right)}(\psi_D + z_D)\right] d\psi_D \right. \\ + \int_0^{z_D} M_3(\psi_D, u) \exp\left[+ \sqrt{\left(bu - \frac{8M_1(u)}{a^2 K_{wD}}\right)}(\psi_D - z_D)\right] d\psi_D \\ \left. + \int_{z_D}^1 M_3(\psi_D, u) \exp\left[- \sqrt{\left(bu - \frac{8M_1(u)}{a^2 K_{wD}}\right)}(\psi_D - z_D)\right] d\psi_D \right). \end{aligned} \tag{4.418}$$

The first order system in δ is given by Eqs. 4.382 and 4.383. By substituting the term $r_D \frac{\partial \bar{T}_{D2,ou}}{\partial r_D}\Big|_{r_D=1}$ by its expression provided by Eq. 4.373, Eq. 4.382 becomes

$$\frac{\partial^2 \bar{\hat{T}}_{D2,inl}}{\partial z_D^2} - bu\bar{\hat{T}}_{D2,inl} + \frac{8}{a^2 K_{wD}}\left[M_1(u)\bar{\hat{T}}_{D2,inl}(z_D, u) + M_4(z_D, u)\right] = 0, \tag{4.419}$$

or

$$\frac{\partial^2 \bar{\hat{T}}_{D2,inl}}{\partial z_D^2} - \left(bu - \frac{8M_1(u)}{a^2 K_{wD}}\right)\bar{\hat{T}}_{D2,inl} = -\frac{8M_4(z_D, u)}{a^2 K_{wD}}. \tag{4.420}$$

The system constituted of Eq. 4.420 and its associated boundary condition Eq. 4.383 is similar to the first order system in ϵ with the exception of the right hand side of Eq. 4.395, i.e., $M_3(z_D, u)$ which is replaced by $M_4(z_D, u)$ in Eq. 4.420. Therefore, the $O(\delta)$ system has the same solution as the $O(\epsilon)$ system which is given based on Eq. 4.418 by

$$\bar{\hat{T}}_{D2,inl} = 2A_6 \sinh\left[\sqrt{\left(bu - \frac{8M_1(u)}{a^2 K_{wD}}\right)} z_D\right] + \frac{4}{a^2 K_{wD}\sqrt{\left(bu - \frac{8M_1(u)}{a^2 K_{wD}}\right)}} \times$$
$$\left(- \int_0^1 M_4(\psi_D, u) \exp\left[- \sqrt{\left(bu - \frac{8M_1(u)}{a^2 K_{wD}}\right)} (\psi_D + z_D)\right] d\psi_D \right.$$
$$+ \int_0^{z_D} M_4(\psi_D, u) \exp\left[+ \sqrt{\left(bu - \frac{8M_1(u)}{a^2 K_{wD}}\right)} (\psi_D - z_D)\right] d\psi_D$$
$$\left. + \int_{z_D}^1 M_4(\psi_D, u) \exp\left[- \sqrt{\left(bu - \frac{8M_1(u)}{a^2 K_{wD}}\right)} (\psi_D - z_D)\right] d\psi_D \right), \quad (4.421)$$

where A_6 is a constant. At this point, we have the general solution for the dimensionless temperature evaluated in Laplace space at any point in the wellbore region for $0 \leq z_D \leq 1$. However, this solution is not fully defined as the determination of the three constants of integration A_2, A_4 and A_6 is still required. We will show how to obtain them based on the continuity conditions at the interface $z_D = 1$, but first, we need to evaluate the solution in the wellbore for $1 \leq z_D \leq z_{tD}$.

Wellbore Region Solution $1 \leq z_D \leq z_{tD}$

The dimensionless temperature in the region $1 < z_D < z_{tD}$ is also given by the following perturbation expansion in powers of ϵ and δ

$$\bar{\hat{T}}_{D,inu}(z_D, u) = \bar{\hat{T}}_{D0,inu} + \epsilon \bar{\hat{T}}_{D1,inu} + \delta \bar{\hat{T}}_{D2,inu}. \quad (4.422)$$

Substituting Eq. 4.422 into Eqs. 4.269 and 4.270 gives

$$\frac{\partial^2}{\partial z_D^2}\left(\bar{\hat{T}}_{D0,inu} + \epsilon \bar{\hat{T}}_{D1,inu} + \delta \bar{\hat{T}}_{D2,inu}\right) - bu\left(\bar{\hat{T}}_{D0,inu} + \epsilon \bar{\hat{T}}_{D1,inu} + \delta \bar{\hat{T}}_{D2,inu}\right) = -b, \quad (4.423)$$

and

$$\frac{\partial}{\partial z_D}\left(\bar{\hat{T}}_{D0,inu} + \epsilon \bar{\hat{T}}_{D1,inu} + \delta \bar{\hat{T}}_{D2,inu}\right)\Big|_{z_D = z_{tD}} = 0. \quad (4.424)$$

Rearranging the above equations leads to

$$\frac{\partial^2 \bar{\hat{T}}_{D0,inu}}{\partial z_D^2} - bu\bar{\hat{T}}_{D0,inu} + \epsilon\left[\frac{\partial^2 \bar{\hat{T}}_{D1,inu}}{\partial z_D^2} - bu\bar{\hat{T}}_{D1,inu}\right] + \delta\left[\frac{\partial^2 \bar{\hat{T}}_{D2,inu}}{\partial z_D^2} - bu\bar{\hat{T}}_{D2,inu}\right] = -b, \quad (4.425)$$

and

$$\left.\frac{\partial \bar{\hat{T}}_{D0,inu}}{\partial z_D}\right|_{z_D=z_{tD}} + \epsilon\left.\frac{\partial \bar{\hat{T}}_{D1,inu}}{\partial z_D}\right|_{z_D=z_{tD}} + \delta\left.\frac{\partial \bar{\hat{T}}_{D2,inu}}{\partial z_D}\right|_{z_D=z_{tD}} = 0. \quad (4.426)$$

If we compare both sides of the two equations, we obtain three systems of equations given by

The $O(1)$ system:

$$\frac{\partial^2 \bar{\hat{T}}_{D0,inu}}{\partial z_D^2} - bu\bar{\hat{T}}_{D0,inu} = -b, \quad (4.427)$$

$$\left.\frac{\partial \bar{\hat{T}}_{D0,inu}}{\partial z_D}\right|_{z_D=z_{tD}} = 0. \quad (4.428)$$

The $O(\epsilon)$ system:

$$\frac{\partial^2 \bar{\hat{T}}_{D1,inu}}{\partial z_D^2} - bu\bar{\hat{T}}_{D1,inu} = 0, \quad (4.429)$$

$$\left.\frac{\partial \bar{\hat{T}}_{D1,inu}}{\partial z_D}\right|_{z_D=z_{tD}} = 0. \quad (4.430)$$

The $O(\delta)$ system:

$$\frac{\partial^2 \bar{\hat{T}}_{D2,inu}}{\partial z_D^2} - bu\bar{\hat{T}}_{D2,inu} = 0, \quad (4.431)$$

$$\left.\frac{\partial \bar{\hat{T}}_{D2,inu}}{\partial z_D}\right|_{z_D=z_{tD}} = 0. \quad (4.432)$$

We discuss first the solution of the leading system by introducing a new variable $\bar{V}_{D0,inu}$

defined by

$$\bar{V}_{D0,inu} = \bar{\hat{T}}_{D0,inu} - \frac{1}{u}. \tag{4.433}$$

If we express $O(1)$ system in terms of $\bar{V}_{D0,inu}$, we obtain

$$\frac{\partial^2 \bar{V}_{D0,inu}}{\partial z_D^2} - bu\bar{V}_{D0,inu} = 0, \tag{4.434}$$

and

$$\left.\frac{\partial \bar{V}_{D0,inu}}{\partial z_D}\right|_{z_D=z_{tD}} = 0, \tag{4.435}$$

whose solution is given by

$$\bar{V}_{D0,inu} = D_1 \exp(-\sqrt{bu} z_D) + D_2 \exp(+\sqrt{bu} z_D). \tag{4.436}$$

D_1 and D_2 in the solution represent the constant of integration. Differentiating Eq. 4.436 with respect to z_D and evaluating the resulting expression at $z_D = z_{tD}$ according to Eq. 4.435 yields

$$\sqrt{bu}\Big[- D_1 \exp(-\sqrt{bu} z_{tD}) + D_2 \exp(+\sqrt{bu} z_{tD})\Big] = 0, \tag{4.437}$$

or simply,

$$D_1 = D_2 \exp(2\sqrt{bu} z_{tD}). \tag{4.438}$$

Finally, the dimensionless temperature $\bar{\hat{T}}_{D0,inu}$ is obtained by substituting Eq. 4.438 into Eq. 4.436 and using Eq. 4.433 as follows

$$\bar{\hat{T}}_{D0,inu} = \frac{1}{u} + D_2 \exp(\sqrt{bu} z_D)\left[1 + \exp\left(2\sqrt{bu}(z_{tD} - z_D)\right)\right]. \tag{4.439}$$

The first order systems in ϵ and δ have the same solution also expressed as a linear combination of exponential functions. Therefore, we can write

$$\bar{\hat{T}}_{D1,inu} = D_3 \exp(-\sqrt{bu} z_D) + D_4 \exp(+\sqrt{bu} z_D), \tag{4.440}$$

and

$$\bar{\hat{T}}_{D2,inu} = D_5 \exp(-\sqrt{bu} z_D) + D_6 \exp(+\sqrt{bu} z_D), \tag{4.441}$$

where D_3 to D_6 are also constants of integration. Using the same argument as for the constant D_1, it is easy to show that

$$D_3 = D_4 \exp(2\sqrt{bu} z_{tD}), \tag{4.442}$$

and

$$D_5 = D_6 \exp(2\sqrt{bu} z_{tD}), \tag{4.443}$$

such that the solutions become simply

$$\bar{\hat{T}}_{D1,inu} = D_4 \exp(\sqrt{bu} z_D) \left[1 + \exp\left(2\sqrt{bu}(z_{tD} - z_D) \right) \right], \tag{4.444}$$

and

$$\bar{\hat{T}}_{D2,inu} = D_6 \exp(\sqrt{bu} z_D) \left[1 + \exp\left(2\sqrt{bu}(z_{tD} - z_D) \right) \right]. \tag{4.445}$$

Continuity Equations

These are the two conditions applied at the interface $z_D = 1$ given by Eqs. 4.260 and 4.261 in real time domain or by similar expression in the s domain (see Eqs. 4.273 and 4.274) since they retain their form in this space. The first condition expresses the continuity of the temperature which in our case, using Eqs. 4.374 and 4.422 in Eq. 4.273 translates to

$$\bar{\hat{T}}_{D0,inl}(1,u)+\epsilon\bar{\hat{T}}_{D1,inl}(1,u)+\delta\bar{\hat{T}}_{D2,inl}(1,u)=\bar{\hat{T}}_{D0,inu}(1,u)+\epsilon\bar{\hat{T}}_{D1,inu}(1,u)+\delta\bar{\hat{T}}_{D2,inu}(1,u). \tag{4.446}$$

Comparing both sides of Eq. 4.446 gives the following equations

$$\bar{\hat{T}}_{D0,inl}(1,u)=\bar{\hat{T}}_{D0,inu}(1,u), \tag{4.447}$$

$$\bar{\hat{T}}_{D1,inl}(1,u)=\bar{\hat{T}}_{D1,inu}(1,u), \tag{4.448}$$

and

$$\bar{\hat{T}}_{D2,inl}(1,u)=\bar{\hat{T}}_{D2,inu}(1,u). \tag{4.449}$$

The second condition expresses the continuity of the fluxes at the interface $z_D=1$. Recall that it is given by

$$\left.\frac{\partial\bar{\hat{T}}_{D,inl}}{\partial z_D}\right|_{z_D=1}=\left.\frac{\partial\bar{\hat{T}}_{D,inu}}{\partial z_D}\right|_{z_D=1}. \tag{4.450}$$

Using Eqs. 4.374 and 4.422 for the temperatures in Eq. 4.450 gives

$$\left.\frac{\partial\bar{\hat{T}}_{D0,inl}}{\partial z_D}\right|_{z_D=1}+\epsilon\left.\frac{\partial\bar{\hat{T}}_{D1,inl}}{\partial z_D}\right|_{z_D=1}+\delta\left.\frac{\partial\bar{\hat{T}}_{D2,inl}}{\partial z_D}\right|_{z_D=1}= \left.\frac{\partial\bar{\hat{T}}_{D0,inu}}{\partial z_D}\right|_{z_D=1}+\epsilon\left.\frac{\partial\bar{\hat{T}}_{D1,inu}}{\partial z_D}\right|_{z_D=1}+\delta\left.\frac{\partial\bar{\hat{T}}_{D2,inu}}{\partial z_D}\right|_{z_D=1}. \tag{4.451}$$

Comparing both sides of Eq. 4.451 yields

$$\left.\frac{\partial\bar{\hat{T}}_{D0,inl}}{\partial z_D}\right|_{z_D=1}=\left.\frac{\partial\bar{\hat{T}}_{D0,inu}}{\partial z_D}\right|_{z_D=1}, \tag{4.452}$$

$$\left.\frac{\partial \bar{\hat{T}}_{D1,inl}}{\partial z_D}\right|_{z_D=1} = \left.\frac{\partial \bar{\hat{T}}_{D1,inu}}{\partial z_D}\right|_{z_D=1}, \tag{4.453}$$

and

$$\left.\frac{\partial \bar{\hat{T}}_{D2,inl}}{\partial z_D}\right|_{z_D=1} = \left.\frac{\partial \bar{\hat{T}}_{D2,inu}}{\partial z_D}\right|_{z_D=1}. \tag{4.454}$$

Evaluating Eqs. 4.393 and 4.439 at $z_D = 1$ and equating the resulting expression according to Eq. 4.447 gives

$$\left(\frac{b+\frac{8M_2(u)}{a^2K_{wD}}}{bu-\frac{8M_1(u)}{a^2K_{wD}}}\right)\left(1-\exp\left[-\sqrt{\left(bu-\frac{8M_1(u)}{a^2K_{wD}}\right)}\right]\right)+2A_2\sinh\left[\sqrt{\left(bu-\frac{8M_1(u)}{a^2K_{wD}}\right)}\right]= \frac{1}{u}+D_2\exp(\sqrt{bu})\left[1+\exp\left(2\sqrt{bu}(z_{tD}-1)\right)\right], \tag{4.455}$$

or

$$2A_2\sinh\left[\sqrt{\left(bu-\frac{8M_1(u)}{a^2K_{wD}}\right)}\right]-D_2\exp(\sqrt{bu})\left[1+\exp\left(2\sqrt{bu}(z_{tD}-1)\right)\right]= \frac{1}{u}-\left(\frac{b+\frac{8M_2(u)}{a^2K_{wD}}}{bu-\frac{8M_1(u)}{a^2K_{wD}}}\right)\left(1-\exp\left[-\sqrt{\left(bu-\frac{8M_1(u)}{a^2K_{wD}}\right)}\right]\right). \tag{4.456}$$

From Eq. 4.452, we have

$$\left.\frac{\partial \bar{\hat{T}}_{D0,inl}}{\partial z_D}\right|_{z_D=1} = \left.\frac{\partial \bar{\hat{T}}_{D0,inu}}{\partial z_D}\right|_{z_D=1}. \tag{4.457}$$

It is clear that we need to obtain the first derivatives of the temperature with respect to z_D in both regions in order to apply the above condition. In the lower part of the wellbore region, we have

$$\frac{\partial \bar{\hat{T}}_{D0,inl}}{\partial z_D} = \left(\frac{b+\frac{8M_2(u)}{a^2K_{wD}}}{bu-\frac{8M_1(u)}{a^2K_{wD}}}\right)\sqrt{\left(bu-\frac{8M_1(u)}{a^2K_{wD}}\right)}\exp\left[-\sqrt{\left(bu-\frac{8M_1(u)}{a^2K_{wD}}\right)}z_D\right] + 2A_2\sqrt{\left(bu-\frac{8M_1(u)}{a^2K_{wD}}\right)}\cosh\left[\sqrt{\left(bu-\frac{8M_1(u)}{a^2K_{wD}}\right)}z_D\right], \quad (4.458)$$

or

$$\frac{\partial \bar{\hat{T}}_{D0,inl}}{\partial z_D} = \frac{b+\frac{8M_2(u)}{a^2K_{wD}}}{\sqrt{bu-\frac{8M_1(u)}{a^2K_{wD}}}}\exp\left[-\sqrt{\left(bu-\frac{8M_1(u)}{a^2K_{wD}}\right)}z_D\right] + 2A_2\sqrt{\left(bu-\frac{8M_1(u)}{a^2K_{wD}}\right)}\cosh\left[\sqrt{\left(bu-\frac{8M_1(u)}{a^2K_{wD}}\right)}z_D\right]. \quad (4.459)$$

In the upper part of the wellbore region, differentiating Eq. 4.439 with respect to z_D gives

$$\frac{\partial \bar{\hat{T}}_{D0,inu}}{\partial z_D} = \sqrt{bu}D_2\exp(\sqrt{bu}z_D) - \sqrt{bu}D_2\exp(2\sqrt{bu}z_{tD})\exp(-\sqrt{bu}z_D), \quad (4.460)$$

or

$$\frac{\partial \bar{\hat{T}}_{D0,inu}}{\partial z_D} = \sqrt{bu}D_2\exp(\sqrt{bu}z_D)\left[1-\exp\left(2\sqrt{bu}(z_{tD}-z_D)\right)\right]. \quad (4.461)$$

Now, if we evaluate both Eqs. 4.459 and 4.461 at $z_D = 1$ and replace the resulting expressions in Eq. 4.457, we obtain

$$\frac{b+\frac{8M_2(u)}{a^2K_{wD}}}{\sqrt{bu-\frac{8M_1(u)}{a^2K_{wD}}}}\exp\Big[-\sqrt{\Big(bu-\frac{8M_1(u)}{a^2K_{wD}}\Big)}\Big] + 2A_2\sqrt{\Big(bu-\frac{8M_1(u)}{a^2K_{wD}}\Big)}\cosh\Big[\sqrt{\Big(bu-\frac{8M_1(u)}{a^2K_{wD}}\Big)}\Big] = \sqrt{bu}D_2\exp(\sqrt{bu})\Big[1-\exp\Big(2\sqrt{bu}(z_{tD}-1)\Big)\Big], \quad (4.462)$$

or simply after rearranging,

$$2A_2\cosh\Big[\sqrt{\Big(bu-\frac{8M_1(u)}{a^2K_{wD}}\Big)}\Big]-\sqrt{\frac{bu}{bu-\frac{8M_1(u)}{a^2K_{wD}}}}D_2\exp(\sqrt{bu})\Big[1-\exp\Big(2\sqrt{bu}(z_{tD}-1)\Big)\Big] = -\Big(\frac{b+\frac{8M_2(u)}{a^2K_{wD}}}{bu-\frac{8M_1(u)}{a^2K_{wD}}}\Big)\exp\Big[-\sqrt{\Big(bu-\frac{8M_1(u)}{a^2K_{wD}}\Big)}\Big]. \quad (4.463)$$

The determinant of the system given by Eqs. 4.456 and 4.463 is defined by

$$\Omega=\begin{pmatrix} 2\sinh\Big[\sqrt{\Big(bu-\frac{8M_1(u)}{a^2K_{wD}}\Big)}\Big] & -\exp(\sqrt{bu})\Big[1+\exp\Big(2\sqrt{bu}(z_{tD}-1)\Big)\Big] \\ 2\cosh\Big[\sqrt{\Big(bu-\frac{8M_1(u)}{a^2K_{wD}}\Big)}\Big] & -\sqrt{\frac{bu}{bu-\frac{8M_1(u)}{a^2K_{wD}}}}\exp(\sqrt{bu})\Big[1-\exp\Big(2\sqrt{bu}(z_{tD}-1)\Big)\Big] \end{pmatrix}, \quad (4.464)$$

or

$$\Omega = 2\exp(\sqrt{bu})\times\Big(\cosh\Big[\sqrt{\Big(bu-\frac{8M_1(u)}{a^2K_{wD}}\Big)}\Big]\Big[1+\exp\Big(2\sqrt{bu}(z_{tD}-1)\Big)\Big] - \sqrt{\frac{bu}{bu-\frac{8M_1(u)}{a^2K_{wD}}}}\sinh\Big[\sqrt{\Big(bu-\frac{8M_1(u)}{a^2K_{wD}}\Big)}\Big]\Big[1-\exp\Big(2\sqrt{bu}(z_{tD}-1)\Big)\Big]\Big). \quad (4.465)$$

It follows that the constant A_2 is obtained by evaluating a determinant which is similar to Ω, normalized to Ω with its elements in the first column replaced by the right hand

side terms of Eqs. 4.456 and 4.463 respectively. The result is

$$\Omega A_2 = -\sqrt{\frac{bu}{bu-\frac{8M_1(u)}{a^2K_{wD}}}}\exp(\sqrt{bu})\left[1-\exp\left(2\sqrt{bu}(z_{tD}-1)\right)\right]\left[\frac{1}{u}-\left(\frac{b+\frac{8M_2(u)}{a^2K_{wD}}}{bu-\frac{8M_1(u)}{a^2K_{wD}}}\right)\right.$$
$$\left.\times\left(1-\exp\left[-\sqrt{\left(bu-\frac{8M_1(u)}{a^2K_{wD}}\right)}\right]\right)\right]-\exp(\sqrt{bu})\left(\frac{b+\frac{8M_2(u)}{a^2K_{wD}}}{bu-\frac{8M_1(u)}{a^2K_{wD}}}\right)$$
$$\times\left[1+\exp\left(2\sqrt{bu}(z_{tD}-1)\right)\right]\exp\left[-\sqrt{\left(bu-\frac{8M_1(u)}{a^2K_{wD}}\right)}\right], \quad (4.466)$$

or

$$A_2 = -\frac{1}{\Omega}\left(\frac{b+\frac{8M_2(u)}{a^2K_{wD}}}{bu-\frac{8M_1(u)}{a^2K_{wD}}}\right)\exp(\sqrt{bu})\left(\left[1+\exp\left(2\sqrt{bu}(z_{tD}-1)\right)\right]\exp\left[-\sqrt{\left(bu-\frac{8M_1(u)}{a^2K_{wD}}\right)}\right]\right.$$
$$+\sqrt{\frac{bu}{bu-\frac{8M_1(u)}{a^2K_{wD}}}}\left[\frac{bu-\frac{8M_1(u)}{a^2K_{wD}}}{u\left(b+\frac{8M_2(u)}{a^2K_{wD}}\right)}-\left(1-\exp\left[-\sqrt{\left(bu-\frac{8M_1(u)}{a^2K_{wD}}\right)}\right]\right)\right]$$
$$\left.\times\left[1-\exp\left(2\sqrt{bu}(z_{tD}-1)\right)\right]\right). \quad (4.467)$$

In order to determine the constant D_2, a similar determinant to Ω, normalized to Ω with its elements in the second column replaced by the right hand side terms of Eqs. 4.456 and 4.463 respectively is evaluated. The result that we obtain is

$$\Omega D_2 = -2\left(\frac{b+\frac{8M_2(u)}{a^2K_{wD}}}{bu-\frac{8M_1(u)}{a^2K_{wD}}}\right)\exp\left[-\sqrt{\left(bu-\frac{8M_1(u)}{a^2K_{wD}}\right)}\right]\sinh\left[\sqrt{\left(bu-\frac{8M_1(u)}{a^2K_{wD}}\right)}\right]$$
$$-2\left[\frac{1}{u}-\left(\frac{b+\frac{8M_2(u)}{a^2K_{wD}}}{bu-\frac{8M_1(u)}{a^2K_{wD}}}\right)\left(1-\exp\left[-\sqrt{\left(bu-\frac{8M_1(u)}{a^2K_{wD}}\right)}\right]\right)\right]\cosh\left[\sqrt{\left(bu-\frac{8M_1(u)}{a^2K_{wD}}\right)}\right], \quad (4.468)$$

or

$$D_2 = -\frac{2}{\Omega}\left(\frac{b+\frac{8M_2(u)}{a^2K_{wD}}}{bu-\frac{8M_1(u)}{a^2K_{wD}}}\right)\Bigg(\exp\left[-\sqrt{\left(bu-\frac{8M_1(u)}{a^2K_{wD}}\right)}\right]\sinh\left[\sqrt{\left(bu-\frac{8M_1(u)}{a^2K_{wD}}\right)}\right]$$
$$-\left[\frac{bu-\frac{8M_1(u)}{a^2K_{wD}}}{u\left(b+\frac{8M_2(u)}{a^2K_{wD}}\right)}-\left(1-\exp\left[-\sqrt{\left(bu-\frac{8M_1(u)}{a^2K_{wD}}\right)}\right]\right)\right]\cosh\left[\sqrt{\left(bu-\frac{8M_1(u)}{a^2K_{wD}}\right)}\right]\Bigg). \tag{4.469}$$

For the first order in ϵ, if we evaluate Eqs. 4.418 and 4.444 at the interface $z_D = 1$ and equate the resulting expressions according to Eq. 4.448, we obtain

$$2A_4\sinh\left[\sqrt{\left(bu-\frac{8M_1(u)}{a^2K_{wD}}\right)}\right]+\frac{4}{a^2K_{wD}\sqrt{\left(bu-\frac{8M_1(u)}{a^2K_{wD}}\right)}}\times$$
$$\Bigg(-\int_0^1 M_3(\psi_D,u)\exp\left[-\sqrt{\left(bu-\frac{8M_1(u)}{a^2K_{wD}}\right)}(\psi_D+1)\right]d\psi_D$$
$$+\int_0^1 M_3(\psi_D,u)\exp\left[+\sqrt{\left(bu-\frac{8M_1(u)}{a^2K_{wD}}\right)}(\psi_D-1)\right]d\psi_D\Bigg)=$$
$$D_4\exp(\sqrt{bu})\left[1+\exp\left(2\sqrt{bu}(z_{tD}-1)\right)\right]. \tag{4.470}$$

Rearranging and simplifying Eq. 4.470 gives

$$2A_4\sinh\left[\sqrt{\left(bu-\frac{8M_1(u)}{a^2K_{wD}}\right)}\right]-D_4\exp(\sqrt{bu})\left[1+\exp\left(2\sqrt{bu}(z_{tD}-1)\right)\right]=$$
$$-\frac{8}{a^2K_{wD}\sqrt{\left(bu-\frac{8M_1(u)}{a^2K_{wD}}\right)}}\exp\left[-\sqrt{\left(bu-\frac{8M_1(u)}{a^2K_{wD}}\right)}\right]$$
$$\times\int_0^1 M_3(\psi_D,u)\sinh\left[\sqrt{\left(bu-\frac{8M_1(u)}{a^2K_{wD}}\right)}\psi_D\right]d\psi_D. \tag{4.471}$$

On the other hand, from the continuity of the fluxes Eq. 4.453, we have

$$\left.\frac{\partial \bar{\hat{T}}_{D1,inl}}{\partial z_D}\right|_{z_D=1} = \left.\frac{\partial \bar{\hat{T}}_{D1,inu}}{\partial z_D}\right|_{z_D=1}. \tag{4.472}$$

Differentiating Eqs. 4.418 and 4.444 with respect to z_D gives respectively

$$\begin{aligned}
\frac{\partial \bar{\hat{T}}_{D1,inl}}{\partial z_D} &= 2A_4\sqrt{\left(bu-\frac{8M_1(u)}{a^2K_{wD}}\right)}\cosh\left[\sqrt{\left(bu-\frac{8M_1(u)}{a^2K_{wD}}\right)}z_D\right] \\
&+\frac{4}{a^2K_{wD}}\exp\left[-\sqrt{\left(bu-\frac{8M_1(u)}{a^2K_{wD}}\right)}z_D\right]\int_0^1 M_3(\psi_D,u)\exp\left[-\sqrt{\left(bu-\frac{8M_1(u)}{a^2K_{wD}}\right)}\psi_D\right]d\psi_D \\
&-\frac{4}{a^2K_{wD}}\exp\left[-\sqrt{\left(bu-\frac{8M_1(u)}{a^2K_{wD}}\right)}z_D\right]\int_0^{z_D} M_3(\psi_D,u)\exp\left[+\sqrt{\left(bu-\frac{8M_1(u)}{a^2K_{wD}}\right)}\psi_D\right]d\psi_D \\
&+\frac{4}{a^2K_{wD}}\exp\left[\sqrt{\left(bu-\frac{8M_1(u)}{a^2K_{wD}}\right)}z_D\right]\int_{z_D}^1 M_3(\psi_D,u)\exp\left[-\sqrt{\left(bu-\frac{8M_1(u)}{a^2K_{wD}}\right)}\psi_D\right]d\psi_D\Bigg),
\end{aligned} \tag{4.473}$$

and

$$\frac{\partial \bar{\hat{T}}_{D1,inu}}{\partial z_D} = \sqrt{bu}D_4\exp(\sqrt{bu}z_D) - \sqrt{bu}D_4\exp(2\sqrt{bu}z_{tD})\exp(-\sqrt{bu}z_D). \tag{4.474}$$

Evaluating these equations at $z_D = 1$ and equating the resulting expressions according to Eq. 4.472 gives

$$\begin{aligned}
&2A_4\sqrt{\left(bu-\frac{8M_1(u)}{a^2K_{wD}}\right)}\cosh\left[\sqrt{\left(bu-\frac{8M_1(u)}{a^2K_{wD}}\right)}\right] \\
&+\frac{4}{a^2K_{wD}}\exp\left[-\sqrt{\left(bu-\frac{8M_1(u)}{a^2K_{wD}}\right)}\right]\int_0^1 M_3(\psi_D,u)\exp\left[-\sqrt{\left(bu-\frac{8M_1(u)}{a^2K_{wD}}\right)}\psi_D\right]d\psi_D \\
&-\frac{4}{a^2K_{wD}}\exp\left[-\sqrt{\left(bu-\frac{8M_1(u)}{a^2K_{wD}}\right)}\right]\int_0^1 M_3(\psi_D,u)\exp\left[+\sqrt{\left(bu-\frac{8M_1(u)}{a^2K_{wD}}\right)}\psi_D\right]d\psi_D = \\
&\qquad\qquad \sqrt{bu}D_4\exp(\sqrt{bu})\left(1-\exp\left[2\sqrt{bu}(z_{tD}-1)\right]\right),
\end{aligned} \tag{4.475}$$

or

$$2A_4 \cosh\left[\sqrt{\left(bu - \frac{8M_1(u)}{a^2K_{wD}}\right)}\right] - \sqrt{\frac{bu}{bu - \frac{8M_1(u)}{a^2K_{wD}}}} D_4 \exp(\sqrt{bu})\left(1 - \exp\left[2\sqrt{bu}(z_{tD} - 1)\right]\right) =$$
$$\frac{8}{a^2K_{wD}\sqrt{\left(bu - \frac{8M_1(u)}{a^2K_{wD}}\right)}} \exp\left[-\sqrt{\left(bu - \frac{8M_1(u)}{a^2K_{wD}}\right)}\right]$$
$$\times \int_0^1 M_3(\psi_D, u) \sinh\left[\sqrt{\left(bu - \frac{8M_1(u)}{a^2K_{wD}}\right)}\psi_D\right] d\psi_D. \quad (4.476)$$

It is obvious that Ω is the determinant of the system given by Eqs. 4.471 and 4.476. Thus, the constant A_4 is obtained by evaluating the determinant Ω, with its elements in the first column replaced by the right hand side terms of Eqs. 4.471 and 4.476 respectively. The result is

$$\Omega A_4 = \frac{8}{a^2K_{wD}\sqrt{\left(bu - \frac{8M_1(u)}{a^2K_{wD}}\right)}} \exp\left[-\sqrt{\left(bu - \frac{8M_1(u)}{a^2K_{wD}}\right)}\right]$$
$$\times \int_0^1 M_3(\psi_D, u) \sinh\left[\sqrt{\left(bu - \frac{8M_1(u)}{a^2K_{wD}}\right)}\psi_D\right] d\psi_D$$
$$\times \left(\sqrt{\frac{bu}{bu - \frac{8M_1(u)}{a^2K_{wD}}}} \exp(\sqrt{bu})\left(1 - \exp\left[2\sqrt{bu}(z_{tD} - 1)\right]\right)\right.$$
$$\left. + \exp(\sqrt{bu})\left[1 + \exp\left(2\sqrt{bu}(z_{tD} - 1)\right)\right]\right), \quad (4.477)$$

or

$$A_4 = \frac{8}{a^2 K_{wD}\Omega\sqrt{\left(bu - \frac{8M_1(u)}{a^2K_{wD}}\right)}} \exp(\sqrt{bu}) \exp\left[- \sqrt{\left(bu - \frac{8M_1(u)}{a^2K_{wD}}\right)}\right]$$
$$\times \int_0^1 M_3(\psi_D, u) \sinh\left[\sqrt{\left(bu - \frac{8M_1(u)}{a^2K_{wD}}\right)}\psi_D\right] d\psi_D$$
$$\times \left(\sqrt{\frac{bu}{bu - \frac{8M_1(u)}{a^2K_{wD}}}}\left(1 - \exp\left[2\sqrt{bu}(z_{tD} - 1)\right]\right)\right.$$
$$\left. + \left[1 + \exp\left(2\sqrt{bu}(z_{tD} - 1)\right)\right]\right). \quad (4.478)$$

By replacing the elements of the second column of Ω by the right hand side terms of Eqs. 4.471 and 4.476 and evaluating the resulting determinant, normalized to Ω leads to the constant D_4. Thus, this results in

$$\Omega D_4 = \frac{16}{a^2 K_{wD}\sqrt{\left(bu - \frac{8M_1(u)}{a^2K_{wD}}\right)}} \exp\left[- \sqrt{\left(bu - \frac{8M_1(u)}{a^2K_{wD}}\right)}\right]$$
$$\times \int_0^1 M_3(\psi_D, u) \sinh\left[\sqrt{\left(bu - \frac{8M_1(u)}{a^2K_{wD}}\right)}\psi_D\right] d\psi_D$$
$$\times \left(\sinh\left[\sqrt{\left(bu - \frac{8M_1(u)}{a^2K_{wD}}\right)}\right] + \cosh\left[\sqrt{\left(bu - \frac{8M_1(u)}{a^2K_{wD}}\right)}\right]\right), \quad (4.479)$$

or equivalently,

$$D_4 = \frac{16}{a^2 K_{wD}\Omega\sqrt{\left(bu - \frac{8M_1(u)}{a^2K_{wD}}\right)}} \times \int_0^1 M_3(\psi_D, u) \sinh\left[\sqrt{\left(bu - \frac{8M_1(u)}{a^2K_{wD}}\right)}\psi_D\right] d\psi_D. \quad (4.480)$$

As for the $O(\delta)$ problem, we showed that the corresponding solutions have the same analytical formulation as the ones that are associated with the $O(\epsilon)$ system. Therefore, it

is obvious that the constants A_6 and D_6 are similar to A_4 and D_4 respectively except for the function $M_3(z_D, u)$ which needs to be replaced by $M_4(z_D, u)$. So based on Eqs. 4.478 and 4.480, we obtain

$$A_6 = \frac{8}{a^2 K_{wD}\Omega\sqrt{\left(bu - \frac{8M_1(u)}{a^2K_{wD}}\right)}} \exp(\sqrt{bu}) \exp\left[-\sqrt{\left(bu - \frac{8M_1(u)}{a^2K_{wD}}\right)}\right] \times \int_0^1 M_4(\psi_D, u) \sinh\left[\sqrt{\left(bu - \frac{8M_1(u)}{a^2K_{wD}}\right)}\psi_D\right] d\psi_D \times \left(\sqrt{\frac{bu}{bu - \frac{8M_1(u)}{a^2K_{wD}}}}\left(1 - \exp\left[2\sqrt{bu}(z_{tD} - 1)\right]\right) + \left[1 + \exp\left(2\sqrt{bu}(z_{tD} - 1)\right)\right]\right), \quad (4.481)$$

and

$$D_6 = \frac{16}{a^2 K_{wD}\Omega\sqrt{\left(bu - \frac{8M_1(u)}{a^2K_{wD}}\right)}} \times \int_0^1 M_4(\psi_D, u) \sinh\left[\sqrt{\left(bu - \frac{8M_1(u)}{a^2K_{wD}}\right)}\psi_D\right] d\psi_D. \quad (4.482)$$

Note that the solution for the temperature profiles during falloff is presented in Laplace space. In order to generate a solution in terms of real time, a numerical Laplace inversion algorithm is needed. The Stefhest algorithm will be used for this purpose.

4.3.3 Pressure Falloff Solution

In chapter 3, we showed we could construct approximate analytical solutions for the pressure falloff response using two different approaches. The first one is based on the Thompson-Reynolds steady-state theory combined with rate superposition extended in an ad hoc way to the two-phase problem. The solution, in this method, is written as the sum of the single-phase oil solution and a multiphase component. In the second approach,

perturbation method is used and the solution for the pressure change is presented as a perturbation expansion. Both methods, however, assumed isothermal conditions. In this section, we generalize the steady-state concept to construct a pressure falloff solution under nonisothermal conditions. We start our analysis by writing the equation for the wellbore pressure change during falloff for the case of a homogeneous reservoir of constant thickness. This equation is given by

$$\Delta p_{ws} = p_{ws} - p_i = \frac{\alpha}{h} \int_{r_w}^{\infty} \frac{q_s(r, \Delta t)}{\lambda_t(r, t_p)} \frac{dr}{rk(r)}, \tag{4.483}$$

where t_p denotes the injection time prior to shut-in and p_{ws} is wellbore pressure. $q_s(r, \Delta t)$ represents the total flow rate distribution in the reservoir during the shut-in time Δt. The preceding equation can be rewritten as

$$\Delta p_{ws} = \frac{\alpha}{h} \int_{r_w}^{r_f(t_p)} \frac{q_s(r, \Delta t)}{\lambda_t(r, t_p)} \frac{dr}{rk(r)} + \frac{\alpha}{h} \int_{r_f(t_p)}^{\infty} \frac{q_s(r, \Delta t)}{\lambda_t(r, t_p)} \frac{dr}{rk(r)}, \tag{4.484}$$

where $r_f(t_p)$ is the radius of the flood front at the instant of shut-in. Not only is the total mobility λ_t a function of the water saturation S_w but also a function of the temperature T through the fluid viscosities. By adding and subtracting an integral from r_w to $r_f(t_p)$ to this equation, we get

$$\Delta p_{ws} = \frac{\alpha}{h} \int_{r_w}^{r_f(t_p)} \frac{q_s(r, \Delta t)}{\lambda_t(r, t_p)} \frac{dr}{rk(r)} + \frac{\alpha}{h} \int_{r_f(t_p)}^{\infty} \frac{q_s(r, \Delta t)}{\lambda_t(r, t_p)} \frac{dr}{rk(r)} + \frac{\alpha}{h} \int_{r_w}^{r_f(t_p)} \frac{q_{os}(r, \Delta t)}{\hat{\lambda}_{oh}} \frac{dr}{rk(r)} - \frac{\alpha}{h} \int_{r_w}^{r_f(t_p)} \frac{q_{os}(r, \Delta t)}{\hat{\lambda}_{oh}} \frac{dr}{rk(r)}. \tag{4.485}$$

In Eq. 4.486, $q_{os}(r, \Delta t)$ denotes the oil flow rate distribution in the reservoir during the shut-in time Δt that would be obtained under single-phase flow conditions, i.e., if we injected oil at a rate q_{inj} RB/D at the same reservoir temperature T_{oi}. As previously, we assume that for $r \geq r_f(t_p)$, $q_s(r, \Delta t) = q_{os}(r, \Delta t)$ and $\lambda_t(r, \Delta t) = \hat{\lambda}_{oh}$. In this case, Eq. 4.485 becomes

$$\Delta p_{ws} = \frac{\alpha}{h\hat{\lambda}_{oh}} \int_{r_w}^{\infty} q_{os}(r, \Delta t) \frac{dr}{rk(r)} + \frac{\alpha}{h} \int_{r_w}^{r_f(t_p)} \left(\frac{q_s(r, \Delta t)}{\lambda_t(r, t_p)} - \frac{q_{os}(r, \Delta t)}{\hat{\lambda}_{oh}} \right) \frac{dr}{rk(r)}, \quad (4.486)$$

or simply,

$$\Delta p_{ws} = \Delta p_{os}(T = T_{oi}) + \frac{\alpha}{h\hat{\lambda}_{oh}} \int_{r_w}^{r_f(t_p)} \left(\frac{\hat{\lambda}_{oh}}{\lambda_t(r, t_p)} q_s(r, \Delta t) - q_{os}(r, \Delta t) \right) \frac{dr}{rk(r)}, \quad (4.487)$$

where $\Delta p_{os}(T = T_{oi})$ is the falloff single-phase flow pressure change based on oil properties evaluated at irreducible water saturation assuming oil is injected into a hot oil reservoir of constant temperature T_{oi} at an injection rate equal to q_{inj}.

Since $q_{os}(r, \Delta t)$ is a single-phase flow rate, we can use the rate superposition in terms of rates following Eq. 3.37 to obtain

$$q_{os}(r, \Delta t) = q_{inj} \left[\exp\Big(- \frac{\phi c_{to} r^2}{4\beta k \hat{\lambda}_{oh}(t_p + \Delta t)} \Big) - \exp\Big(- \frac{\phi c_{to} r^2}{4\beta k \hat{\lambda}_{oh} \Delta t} \Big) \right]. \quad (4.488)$$

In oil field units with time in hours, $4\beta = 10.548 \times 10^{-4}$. In order to evaluate the total rate $q_s(r, \Delta t)$ in the two-phase flow region, the total compressibility and the total mobility at irreducible water saturation in Eq. 4.488 are replaced by local values of these properties as follows:

$$q_s(r, \Delta t) = q_{inj} \left[\exp\Big(- \frac{\phi c_t(r, t_p) r^2}{4\beta k \lambda_t(r, t_p)(t_p + \Delta t)} \Big) - \exp\Big(- \frac{\phi c_t(r, t_p) r^2}{4\beta k \lambda_t(r, t_p) \Delta t} \Big) \right]. \quad (4.489)$$

At any position r in the reservoir and any shut-in time Δt, the total compressibility $c_t(r, t_p)$ is evaluated via the water saturation distribution $S_w(r, t_p)$ at the instant of shut-in that we obtain using the nonisothermal Buckley-leverett theory. As for the total mobility $\lambda_t(r, t_p)$, once we solve for the temperature in the reservoir using perturbation method,

the fluid viscosities can be determined (from given tables or functional relationships with the temperature) and the total mobility can be therefore evaluated using the updated viscosities in Eq. 4.47. The falloff pressure change is obtained from Eq. 4.487 once the rates q_s and q_{os} are generated using Eqs. 4.488 and 4.489 respectively.

In the following, we will present the falloff solution in terms of Δp_s defined by

$$\Delta p_s = p_{wf,s} - p_{ws}(\Delta t), \tag{4.490}$$

where $p_{wf,s} = p_{wf}(t_p)$ is the wellbore pressure at the instant of shut-in. Here, this equation is obtained by subtracting $p_{ws}(\Delta t) - p_i$ given by Eq. 4.487 to $p_{wf}(t_p) - p_i$.

At very late shut-in times, the rates $q_s(r, \Delta t)$ and $q_{os}(r, \Delta t)$ predicted by rate superposition are for all practical purposes equal to zero for $r_w \leq r \leq r_f(t_p)$. It follows that the multiphase pressure drop in Eq. 4.487 is equal to zero and Eq. 4.487 reduces to

$$p_{ws}(\Delta t) - p_i = \Delta p_{os}(T = T_{oi}) = \frac{\alpha q_{inj}}{2kh\hat{\lambda}_{oh}} \ln\left(\frac{t_{pD} + \Delta t_D}{\Delta t_D}\right). \tag{4.491}$$

Assuming that the temperature front is beyond the skin zone when the well is shut-in, the injection solution at the instant of shut-in is then given according to Eq. 4.86 by

$$p_{wf,s} - p_i = \Delta p_o(t_p) + \frac{\alpha q_{inj}}{kh\hat{\lambda}_{oh}}\left[\left(\frac{k}{k_s} - 1\right)\int_{r_w}^{r_s}\left(\frac{\hat{\lambda}_{oh}}{\lambda_{th}(r, t_p)} - 1\right)\frac{dr}{r} + \int_{r_w}^{r_f(t_p)}\left(\frac{\hat{\lambda}_{oh}}{\lambda_{th}(r, t_p)} - 1\right)\frac{dr}{r}\right]$$
$$+ \frac{\alpha q_{inj}}{kh}\left[\left(\frac{k}{k_s} - 1\right)\int_{r_w}^{r_s}\left(\frac{1}{\lambda_{tc}(r, t_p)} - \frac{1}{\lambda_{th}(r, t_p)}\right)\frac{dr}{r} + \int_{r_w}^{r_T(t_p)}\left(\frac{1}{\lambda_{tc}(r, t_p)} - \frac{1}{\lambda_{th}(r, t_p)}\right)\frac{dr}{r}\right], \tag{4.492}$$

that we rewrite as

$$p_{wf,s} - p_i = \Delta p_o(t_p) + \frac{\alpha q_{inj}}{kh\hat{\lambda}_{oh}}\left[\left(\frac{k}{k_s} - 1\right)\int_{r_w}^{r_s}\left(\frac{\hat{\lambda}_{oh}}{\lambda_{tc}(r, t_p)} - 1\right)\frac{dr}{r} + \int_{r_w}^{r_f(t_p)}\left(\frac{\hat{\lambda}_{oh}}{\lambda_{th}(r, t_p)} - 1\right)\frac{dr}{r}\right.$$
$$\left. + \int_{r_w}^{r_T(t_p)}\left(\frac{\hat{\lambda}_{oh}}{\lambda_{tc}(r, t_p)} - \frac{\hat{\lambda}_{oh}}{\lambda_{th}(r, t_p)}\right)\frac{dr}{r}\right]. \tag{4.493}$$

The single-phase oil solution at t_p is given by

$$\Delta p_o(t_p) = \frac{\alpha q_{inj}}{2kh\hat{\lambda}_{oh}} \ln\left(\frac{4t_{pD}}{\exp(\gamma)}\right), \tag{4.494}$$

where $\gamma = 0.57722$ is Euler's constant. By subtracting Eq. 4.491 from Eq. 4.493 and using Eq. 4.494, it is easy to show that

$$p_{wf,s} - p_{ws}(\Delta t) = \frac{\alpha}{kh\hat{\lambda}_{oh}}\left[\frac{1}{2}\ln\left(\frac{4t_{eD}}{\exp(\gamma)}\right) + \left(\frac{k}{k_s} - 1\right)\int_{r_w}^{r_s}\left(\frac{\hat{\lambda}_{oh}}{\lambda_{tc}(r,t_p)} - 1\right)\frac{dr}{r} + \int_{r_w}^{r_f(t_p)}\left(\frac{\hat{\lambda}_{oh}}{\lambda_{th}(r,t_p)} - 1\right)\frac{dr}{r} + \int_{r_w}^{r_T(t_p)}\left(\frac{\hat{\lambda}_{oh}}{\lambda_{tc}(r,t_p)} - \frac{\hat{\lambda}_{oh}}{\lambda_{th}(r,t_p)}\right)\frac{dr}{r}\right], \tag{4.495}$$

where t_{eD} represents the dimensionless equivalent time defined by $t_{eD} = \frac{t_{pD}\Delta t_D}{t_{pD}+\Delta t_D}$. By introducing a total skin factor given by

$$s_t = s + s_\lambda, \tag{4.496}$$

we can rewrite Eq. 4.495 as

$$p_{wf,s} - p_{ws}(\Delta t) = \frac{\alpha}{kh\hat{\lambda}_{oh}}\left[\frac{1}{2}\ln\left(\frac{4t_{eD}}{\exp(\gamma)}\right) + s_t\right], \tag{4.497}$$

such that the multiphase component of the total skin factor is

$$s_\lambda = \left(\frac{k}{k_s} - 1\right)\int_{r_w}^{r_s}\left(\frac{\hat{\lambda}_{oh}}{\lambda_{tc}(r,t_p)} - 1\right)\frac{dr}{r} + \int_{r_w}^{r_f(t_p)}\left(\frac{\hat{\lambda}_{oh}}{\lambda_{th}(r,t_p)} - 1\right)\frac{dr}{r} + \int_{r_w}^{r_T(t_p)}\left(\frac{\hat{\lambda}_{oh}}{\lambda_{tc}(r,t_p)} - \frac{\hat{\lambda}_{oh}}{\lambda_{th}(r,t_p)}\right)\frac{dr}{r}. \tag{4.498}$$

In the skin zone, it is reasonable to assume that oil saturation will be reduced to residual oil saturation. In this case, $\lambda_{tc}(r,t_p) = \hat{\lambda}_{wc}$. Using this assumption, Eq. 4.498 becomes

$$s_\lambda = \left(\frac{k}{k_s} - 1\right)\left(\frac{\hat{\lambda}_{oh}}{\hat{\lambda}_{wc}} - 1\right)\ln\left(\frac{r_s}{r_w}\right) + \int_{r_w}^{r_f(t_p)} \left(\frac{\hat{\lambda}_{oh}}{\lambda_{th}(r,t_p)} - 1\right)\frac{dr}{r} + \int_{r_w}^{r_T(t_p)} \left(\frac{\hat{\lambda}_{oh}}{\lambda_{tc}(r,t_p)} - \frac{\hat{\lambda}_{oh}}{\lambda_{th}(r,t_p)}\right)\frac{dr}{r}. \quad (4.499)$$

Using Hawkins' formula in Eq. 4.499, substituting the resulting equation into Eq. 4.496 and simplifying gives

$$s_t = s\frac{\hat{\lambda}_{oh}}{\hat{\lambda}_{wc}} + \int_{r_w}^{r_f(t_p)} \left(\frac{\hat{\lambda}_{oh}}{\lambda_{th}(r,t_p)} - 1\right)\frac{dr}{r} + \int_{r_w}^{r_T(t_p)} \left(\frac{\hat{\lambda}_{oh}}{\lambda_{tc}(r,t_p)} - \frac{\hat{\lambda}_{oh}}{\lambda_{th}(r,t_p)}\right)\frac{dr}{r}. \quad (4.500)$$

Solving for the mechanical skin factor s, we obtain

$$s = \hat{M}_h\frac{\mu_w(T_{oi})}{\mu_w(T_{wi})}\left[s_t - \int_{r_w}^{r_f(t_p)} \left(\frac{\hat{\lambda}_{oh}}{\lambda_{th}(r,t_p)} - 1\right)\frac{dr}{r} - \int_{r_w}^{r_T(t_p)} \left(\frac{\hat{\lambda}_{oh}}{\lambda_{tc}(r,t_p)} - \frac{\hat{\lambda}_{oh}}{\lambda_{th}(r,t_p)}\right)\frac{dr}{r}\right]. \quad (4.501)$$

Recall that $\hat{M}_h$ is the end-point mobility ratio evaluated at the initial temperature of the reservoir. So, by performing a semi-log analysis at late shut-in times, we can estimate the mechanical skin factor from Eq. 4.501 assuming the relative permeability curves and therefore the total mobility profiles known.

4.4 Numerical Results and Validation

In the following, we proceed to construct analytical solutions for the pressure response as well as the temperature and water saturation distributions during an injection/falloff test on water injection wells under nonisothermal conditions. The validation of these solutions is done using the CMG's STARS simulator by Computer Modeling Group Ltd. ([2]). The basic data used for the computations are summarized in Table 4.1 and heat properties for the fluids and the solid matrix are given in Table 4.2. Since the relative permeability curves are assumed to be functions of the water saturation only

(not the temperature), the same ones used in previous chapters (see Fig. 2.6) were also used here. In all the examples considered here, water was injected at the temperature $T_{wi} = 60.7^o$F in an oil reservoir of initial temperature of $T_{oi} = 180\ ^o$F. Water and oil viscosities at the injected temperature are respectively $\mu_w(T_{wi}) = 0.4$ cp and $\mu_o(T_{wi}) = 8$ cp. The end-point mobility ratio evaluated at T_{wi} is $\hat{M}_c = \frac{\hat{\lambda}_{wc}}{\hat{\lambda}_{oc}} = 6.4$. At the initial reservoir temperature, the viscosities are $\mu_w(T_{oi}) = 0.25$ cp and $\mu_o(T_{oi}) = 2$ cp which gives an end-point mobility ratio of $\hat{M}_h = \frac{\hat{\lambda}_{wh}}{\hat{\lambda}_{oh}} = 2.56$. It is clearly an unfavorable mobility case.

4.4.1 Injection Solutions for Radial Flow

For the runs considered in this subsection, the initial reservoir pressure is $p_i = 3922$ psi, the thickness of the reservoir $h = 50$ ft and the reservoir is considered isotropic of permeability $k = 270$ mD. Cold water was injected at a constant rate of $q_{inj} = 3000$ STB/day into a complete penetrating vertical well for $t_p = 1$ day and then the well was shut-in for a falloff test. Here, we focus on the injection period only. In all runs, the mesh consisted of a $400(r)$ by $1(\theta)$ by $1(z)$ cylindrical coordinate system with a variable gridblock size used in the r-direction.

The single-phase case based on oil properties at irreducible water saturation was run using STARS under the isothermal mode (injection of oil at the temperature of the reservoir T_{oi} into oil) and compared to the analytical solution obtained under the same conditions. Not only does this step help ensure of the adequacy of the grid in STARS, but also constitutes an important point in constructing the approximate analytical solution under two-phase flow. In Fig. 4.5, the numerical injection pressure change and its derivative with respect to $\ln(t)$ are shown by solid circles whereas, the analytical solutions for the wellbore pressure change and its derivative are represented by a solid line. As we can see, the two solutions are in excellent agreement.

Next, we proceed to construct graphically the profiles for the water saturation and the temperature during the injection period. On the fractional flow diagram shown by Fig. 4.6, the fractional flow curve represented by the solid triangles corresponds to the cold fractional flow evaluated at the temperature of injected water. The curve plotted in

Property	value
Porosity, ϕ	0.32
Rock compressibility, c_r, psi^{-1}	5.63×10^{-06}
Residual oil saturation, S_{or}	0.28
Irreducible water saturation, S_{iw}	0.25
Oil FVF, B_o	1.000
Oil compressibility, c_o, psi^{-1}	8.0×10^{-06}
Water FVF, B_w	1.000
Water compressibility, c_w, psi^{-1}	2.84×10^{-06}
Initial pressure, p_i, psi	3922
Formation thickness, h, ft	50.
Wellbore radius, r_w, ft	0.35
Injection rate, q_{inj}, STB/day	3,000
Injection temperature, T_{wi}, ^{o}F	60.7
Initial reservoir temperature, T_{oi}, ^{o}F	180

Table 4.1: Reservoir and well data for cold waterflooding problem.

Property	value
Rock specific heat capacity, $\rho_r C_r$, BTU /ft^3/F	42.45
Rock thermal conductivity, K_r, BTU/ft/day/F	33
Overburden thermal conductivity, K_{rt}, BTU/ft/day/F	33
Underburden thermal conductivity, K_{rb}, BTU/ft/day/F	33
Oil specific heat capacity, $\rho_o C_o$, BTU /ft^3/F	23
Oil thermal conductivity, K_o, BTU/ft/day/F	1.8
Water specific heat capacity, $\rho_w C_w$, BTU /ft^3/F	62.40
Water thermal conductivity, K_w, BTU/ft/day/F	8.6

Table 4.2: Rock and fluids thermal properties.

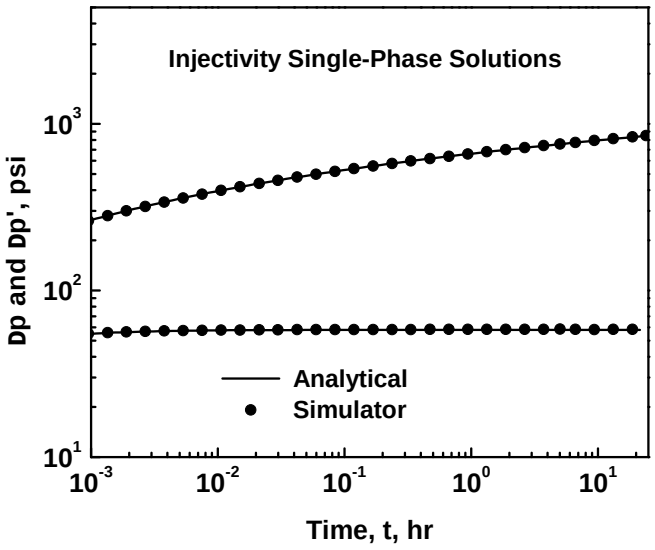

Figure 4.5: Comparison of numerical results to analytical solution for injectivity, single-phase flow under isothermal conditions.

solid circles corresponds to the hot fractional curve evaluated at the initial reservoir temperature. The dashed line and the dotted line, tangent to the hot fractional flow curve, represent the characteristic curves of slope $\frac{df_w}{dS_w}$ and $\frac{f_w+\lambda}{S_w+\tau}$ respectively. Recall that the two tangent points for these characteristic curves and the hot fractional flow curve are the discontinuity points in the profiles to ensure uniqueness of the solution. Our computations indicate that the first discontinuity which represents the flood front saturation is at $S_{wf} = 0.42$, whereas, the second discontinuity which represents the temperature front is at $S_{wT} = 0.652$. In Fig. 4.7, the derivatives (or the slopes) of both fractional flow curves are displayed. These slopes are traced in order to generate the solution for the water saturation profile. Basically, if we start from the boundary condition at $r = r_w$ where the water saturation is $1 - S_{or}$, the derivative of the cold fractional flow curve is followed up to the value of S_w such that $\frac{df_{wc}}{dS_w}(S_w) = \frac{f_w(S_w)+\lambda}{S_w+\tau}$, which occurs at $S_w = 0.684$. This represents the transition point from the cold to the hot curve. Then, the characteristic curve given by $\frac{f_w+\lambda}{S_w+\tau} = constant$ is followed until we reach the hot fractional flow curve at the water saturation S_{wT}. We continue along this curve up to the second discontinuity at S_{wf}. Finally, once we pass that point, all the saturations are moving at the same velocity as the water front leading to the standard Buckley-Leverett type of profile.

Fig. 4.8 illustrates a comparison between water saturation distributions obtained analytically according to the above procedure and numerical profiles simulated using CMG STARS at three different injection times. The numerical solution was generated using the same simulation with convection as the main mechanism to heat transfer; conduction being negligible during the injection test. As we see from this figure, a good agreement is obtained between the two sets of data except for the expected smear around the flood and temperature fronts exhibited by the simulator. We need to keep in mind that this is an unfavorable mobility ratio case. In Fig. 4.9, the temperature profiles obtained from the simulator at the three same injection times when considering only convection are represented by the solid stars. The solid line curves represent the analytical temperature distributions obtained at the same times which indicate a reasonable agreement with the simulator.

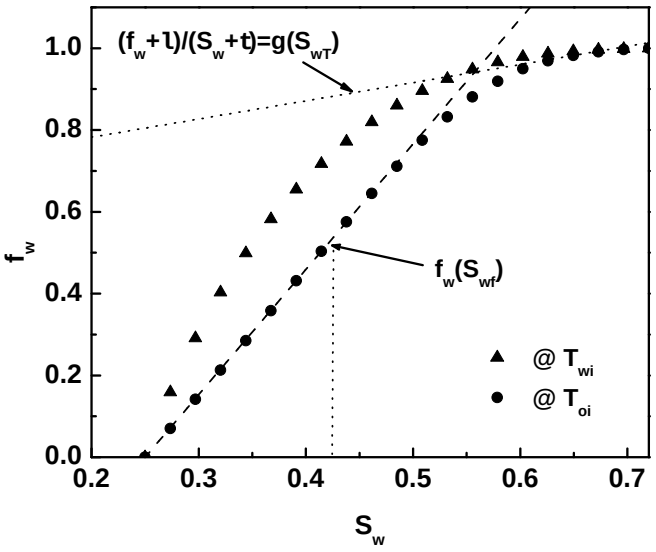

Figure 4.6: Fractional flow diagram.

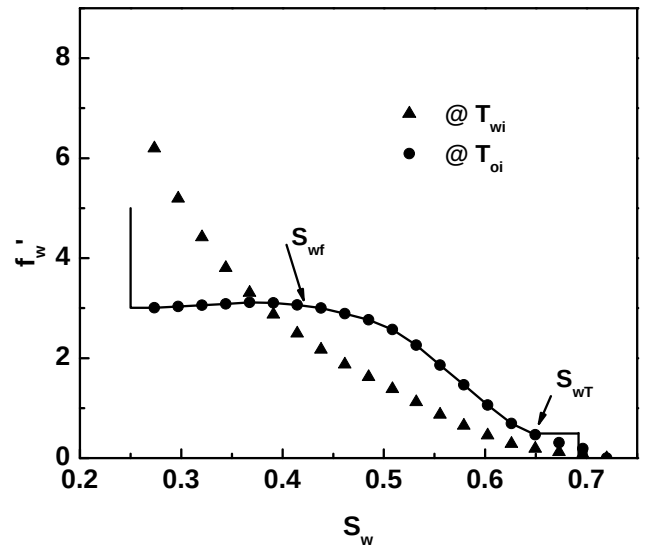

Figure 4.7: Derivative of fractional flow diagram.

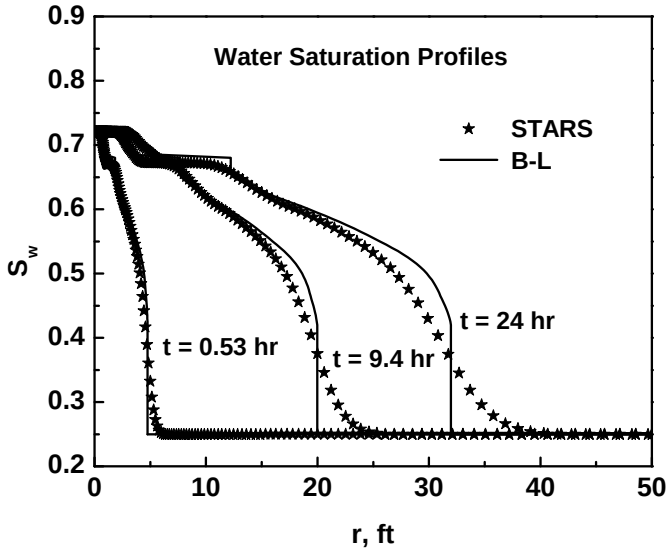

Figure 4.8: Comparison of numerical results to analytical solution for water saturation profiles.

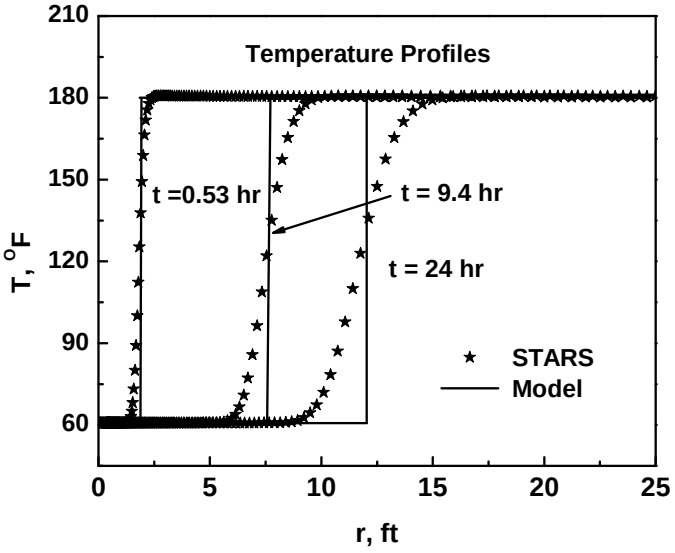

Figure 4.9: Comparison of numerical results to analytical solution for temperature profiles.

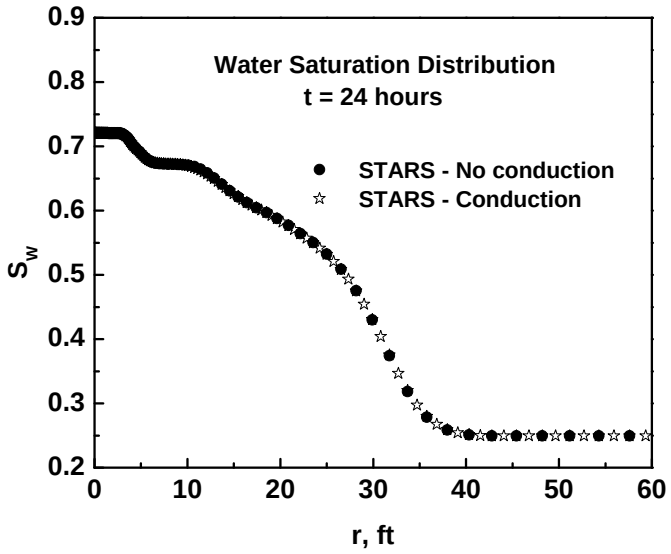

Figure 4.10: Impact of thermal conduction on water saturation profiles during injection.

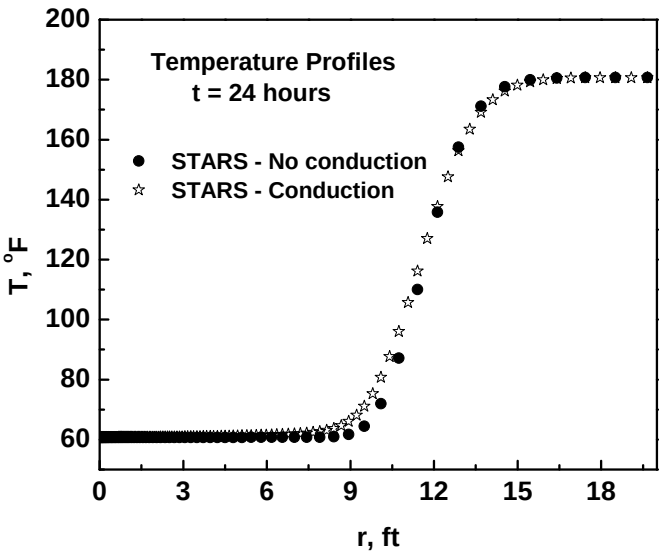

Figure 4.11: Impact of thermal conduction on temperature profiles during injection.

In order to examine the impact of thermal conduction which had to be neglected during the injection process to solve for the problem analytically, the simulator STARS was run where in addition to convection, horizontal and vertical conduction were included through fluids, rock and overburden and underburden thermal conductivities (their values are given in Table 4.2). In Figs. 4.10 and 4.11, the profiles for water saturation and temperature generated from this run at the instant of shut-in ($t_p = 1$ day) are represented by solid stars. In the same figures, numerical profiles obtained without the effects of conduction are also displayed for comparison purposes. Clearly, horizontal and vertical conduction do not have any effect on the distribution of water in the reservoir during injection as the two profiles are identical. However, the case is different for the temperature distributions. Although the location of the temperature front did not change when including conduction, the profile obtained seems to exhibit higher temperature in the cold region confirming therefore the numerical study conducted by Platenkamp [30]. For instance, at the location $r = 10.4$ ft, the simulator predicts a temperature of $T = 87.6^o$F when thermal conduction is included compared to $T = 78.4^o$F obtained with only convection (see Fig. 4.11).

Fig. 4.12 illustrates a log-log plot of the injectivity solution for the wellbore pressure change, $\Delta p = p_{wf}(t) - p_i$, and its derivative with respect to $\ln t$ obtained under nonisothermal conditions (without conduction) and represented by the solid star dots. Also shown in this figure is the injectivity solution for the wellbore pressure drop and its derivative obtained numerically under isothermal conditions, meaning that the temperature of the injected fluid is the same as the temperature of the formation. This solution is represented by the solid circle dots. At very early times, both numerical solutions reflect oil properties at the initial formation temperature through the semi-log slope exhibited by the pressure derivative given by

$$\Delta p' = \frac{\alpha q_{inj}}{2kh\hat{\lambda}_{oh}} = 58.08. \tag{4.502}$$

However, as time goes on, the two solutions diverge and eventually reach different semi-log

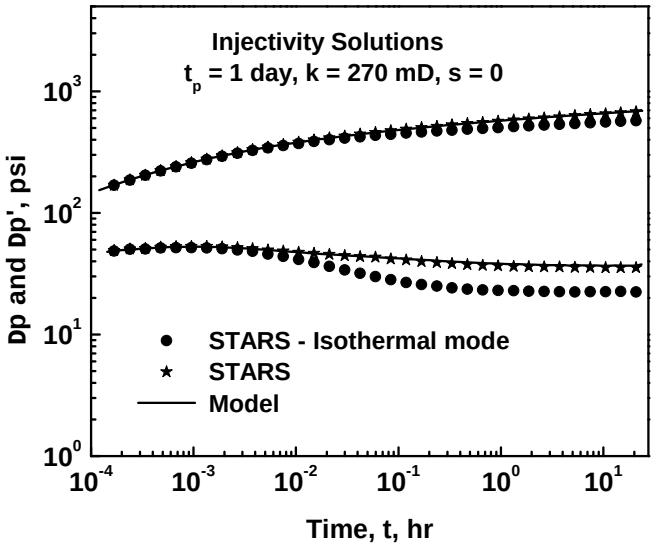

Figure 4.12: Comparison between the results for the injection test from the simulator and the analytical solution from the model.

lines at late times. While the isothermal solution reflects water properties at the initial temperature of the formation according to the following semi-log line

$$\Delta p' = \frac{\alpha q_{inj}}{2kh\hat{\lambda}_{wh}} = 22.68, \tag{4.503}$$

the nonisothermal solution shows water properties but at the injected fluid temperature according to Eq. 4.90 with a much lower mobility and therefore a much higher semi-log slope given by

$$\Delta p' = \frac{\alpha q_{inj}}{2kh\hat{\lambda}_{wc}} = 36.27. \tag{4.504}$$

The analytical solution for the pressure change and its derivative is also shown in Fig. 4.12 as a solid line. This solution was generated by computing the two integrals in Eqs. 4.56 and 4.57 for different values of time upon the determination of the total mobility profile from the nonisothermal Buckley-Leverett equation and adding the result to the single-phase solution based on oil-properties at the initial reservoir temperature. Fig. 4.12 shows a good agreement between the model and the simulator. The wellbore

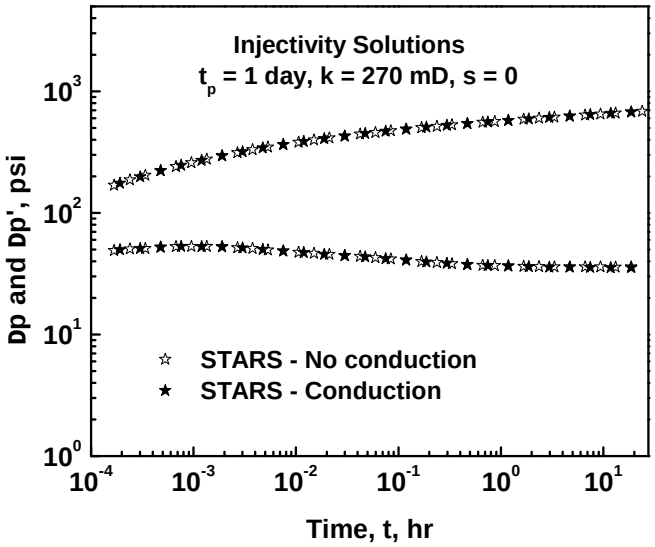

Figure 4.13: Impact of thermal conduction on wellbore pressure change during injection.

pressure change and its derivative with respect to the natural logarithm of time were also obtained numerically from the simulator when both convection and conduction were included. This solution is represented by open stars in Fig. 4.13. In the same figure, the solution obtained numerically with only convection is superposed. This comparison indicates that thermal conduction (vertical and horizontal) has no effect on the pressure response during injection.

The results above pertain to a case with no skin. Next, the same problem was considered but with a positive skin factor $s = 2.45$. To do so, the permeability of a cylindrical region around the wellbore of radius $r_s = 1.48$ ft was set to $k_s = 100$ mD. All other parameters were kept the same. Fig. 4.14 compares the pressure change and its derivative obtained analytically (solid line) to the corresponding data generated from STARS (solid stars). Although the pressure data match very well, the derivative data from the simulator are slightly shifted from the ones obtain from the model for injection times $0.3 < t < 2$ hours. According to computations based on the model, the flood and the temperature fronts reach the location r_s at $t = 0.048$ hours and $t = 0.3$ hours respectively. Thus, the disagreement between the derivative data occur when both the

water front and the temperature front are outside the damaged zone. We also show in this figure analytical and numerical solutions for the wellbore pressure change and their derivative obtained when considering an isothermal injection of water (initial temperature of the reservoir). An interesting point is that unlike the isothermal injection solution, the nonisothermal solution in terms of the pressure derivative does not take negative values at any time during the injection test. Our derivations based on the steady-state theory predict negative values of the derivative when the flood front is still in the damaged zone ($t < 0.048$ hours) if the condition given by Eq. 4.73 rewritten here as

$$\hat{M}_c(1 - \frac{k_s}{k}) > \frac{\hat{\lambda}_{oh}}{\hat{\lambda}_{oc}} = \frac{\mu_{oc}}{\mu_{oh}}. \tag{4.505}$$

is satisfied. While the term $\hat{M}_c(1-\frac{k_s}{k})$ is numerically equal to 4.0, the ratio $\frac{\mu_{oc}}{\mu_{oh}}$ is also equal to 4 such that the above condition does not hold. That is why the pressure derivative starts decreasing during this flow period but never reaches a negative value unlike the isothermal case where a combination of an unfavorable mobility ratio and a positive skin factor guarantees negative values of the pressure derivative during the time period when the flood front is in the damaged zone. Recall that the condition for the isothermal case is $\hat{M}_h(1 - \frac{k_s}{k}) = 1.6 > 1$.

According to Eq. 4.83, the nonisothermal pressure derivative may take negative values during the flow period corresponding to when the water front is propagating beyond the skin zone while the temperature front is still in the damaged zone ($0.048 < t < 0.3$ hours). Recall this equation is given by

$$\lambda_{th}(r_s, t) < \hat{\lambda}_{wc}\left(1 - \frac{k_s}{k}\right). \tag{4.506}$$

Since the term $\hat{\lambda}_{wc}\left(1 - \frac{k_s}{k}\right)$ is numerically equal to 0.27, the derivative data become negative only if for some water saturation values, the total mobility evaluated at r_s at the initial temperature of the reservoir is less than the numerical value of 0.27. In Fig. 4.15, we show the total mobility as function of water saturation evaluated at the initial temperature of the reservoir and represented by solid circle dots whereas the total mobility computed

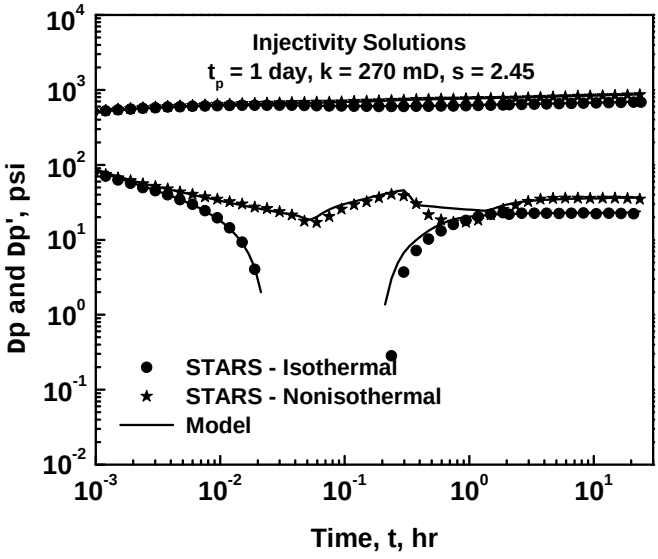

Figure 4.14: Comparison between the results for the injection test from the simulator and the analytical solution from the model, $s = 2.45$.

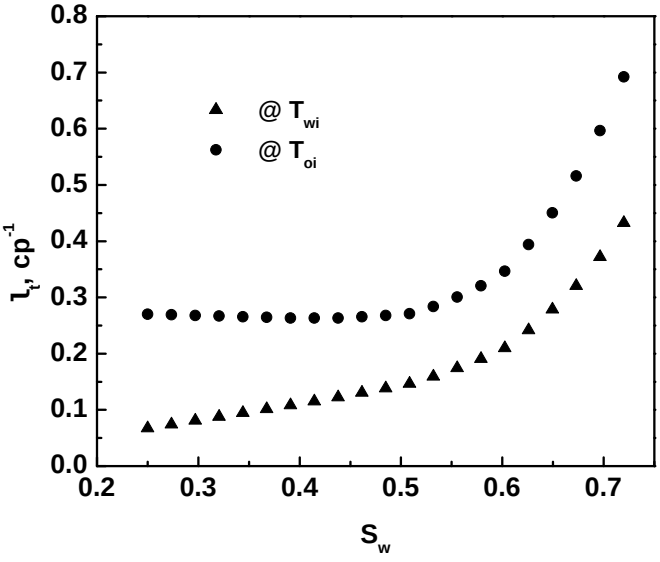

Figure 4.15: Total mobility curves.

at the temperature of injected water is illustrated by solid triangle dots. As you see from this graph, the condition $\lambda_{th} < 0.27$ is satisfied for values of water saturation that are less than the water front saturation S_{wf}. Since these saturations propagate ahead of the flood front, they are hence located at $r > r_s$. This clearly suggests that the condition given by Eq. 4.83 or equivalently Eq. 4.506 cannot be satisfied and that the pressure derivative data are not negative during this time period as illustrated in Fig. 4.14. As time goes on ($t > 0.3$ hours), the total mobility increases first and reaches the value $\hat{\lambda}_{wh}$ during a very short period of time ($1.5 < t < 1.9$ hours) and then decreases (derivative increases) to eventually reach the end-point water mobility $\hat{\lambda}_{wc}$ for times greater than 6 hours.

4.4.2 Falloff Solutions for Radial Flow

In this section, we analyze the numerical falloff data obtained from the injection/falloff test simulated in the previous section. Recall that the test assumed an injection at a constant rate of $q_{inj} = 3000$ STB/day for $t_p = 1$ day through a complete penetration vertical well. The reservoir, initially at $p_i = 3922$ psi, is isotropic with permeability $k = 270$ mD and has a thickness $h = 50$ ft. At the instant of shut-in, the water front is located at $r_f(t_p) = 32.03$ ft whereas the temperature front is at $r_T(t_p) = 12.13$ ft according to the nonisothermal Buckley-Leverett theory. In order to examine the effect of the instant of shut-in, t_p, a shorter test was considered where the injection was carried on for only 5 hours. For this case, $r_f(t_p) = 14.62$ ft and $r_T(t_p) = 5.55$ ft.

To illustrate the fact that the water saturation distribution in the reservoir remains stationary upon shut-in the well and throughout the entire falloff test, we compare in Fig. 4.16 the numerical profiles simulated using STARS at the shut-in times $\Delta t = 51.9$ hours and $\Delta t = 168$ hours. We also superpose the water saturation distribution obtained analytically according to the nonisothermal Buckley-Leverett theory evaluated at the instant of shut-in $t_p = 24$ hours. Clearly, the two numerical profiles are identical which indicates that the change in temperature in the reservoir due to cold waterflloding does not have any effect on how the water saturation is distributed in the reservoir during the shut-in period as long as the system is incompressible. Fig. 4.16 also suggests that it is

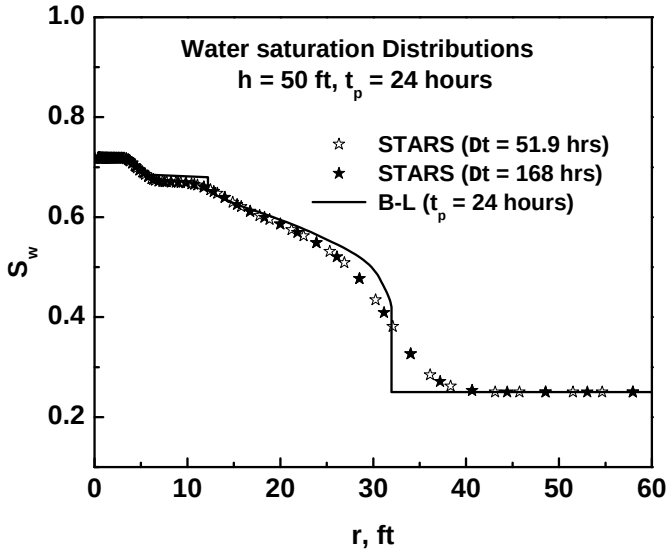

Figure 4.16: Comparison of water saturation distributions obtained during falloff.

a good approximation to consider the analytical profile of water saturation evaluated at the instant of shut-in when carrying on temperature and pressure computations during the falloff period.

In Fig. 4.17, the temperature profiles obtained from the simulator at the shut-in times $\Delta t = 51.9$ hours and $\Delta t = 168$ hours are represented by open stars and solid stars respectively. The solid circles represent the temperature distribution generated from the simulator at the instant of shut-in $t_p = 24$ hours and the solid line curve is the analytical profile also obtained at t_p. As we can see from this figure, the temperature distributions spread out as a consequence of an increase of temperature with Δt behind the temperature front due to conduction heat transfer. Although Fig. 4.17 shows a stationary temperature front for the shut-in times considered in this example which seems to be in accordance with the work of Bratvold and Horne [12], this is not always true as the temperature front will eventually disappear when the system recovers its original reservoir temperature. This will be illustrated by the short injection example.

Fig. 4.18 presents a comparison between predictions from our model and the simulator for the bottom hole temperature as a function of the shut-in time, Δt, for the two

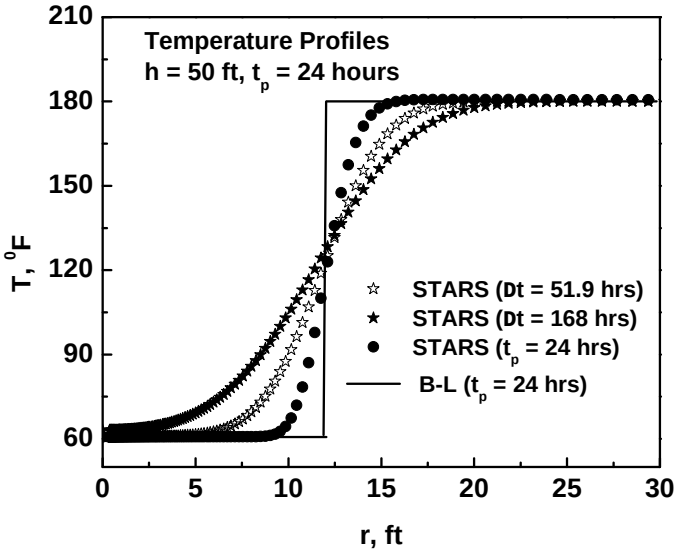

Figure 4.17: Comparison of temperature distributions obtained during falloff.

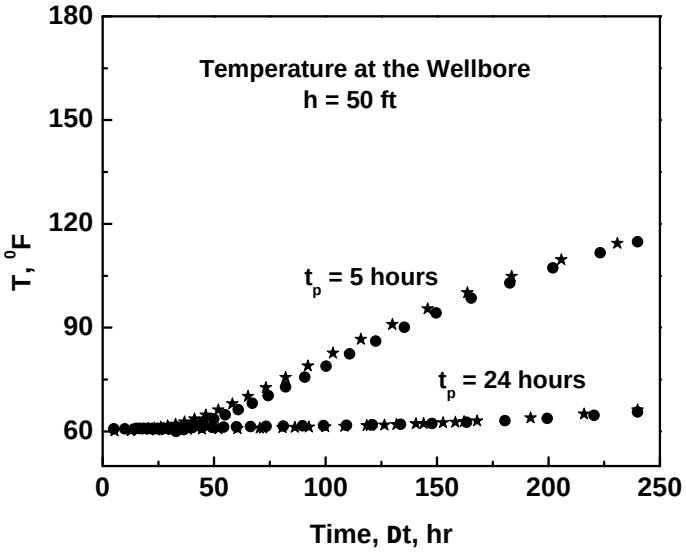

Figure 4.18: Comparison of numerical results to analytical solution for bottom hole temperature during falloff.

values of t_p. Our analytical solution referred to as $\bar{\hat{T}}_{D,inl}$ was evaluated in Laplace space at $z_D = \frac{1}{2}$ or equivalently $z = \frac{h}{2}$ using Eq. 4.374 with the leading order term $\bar{\hat{T}}_{D0,inl}$ and the two first order terms in ϵ and δ denoted by $\bar{\hat{T}}_{D1,inl}$ and $\bar{\hat{T}}_{D2,inl}$ defined by Eqs. 4.393, 4.418 and 4.421 respectively. Stefhest algorithm was used for the numerical inversion. Generally speaking, a good match between the two sets of results is observed for both values of t_p. Another remark is that the wellbore temperatures obtained during the falloff subsequent to a shorter injection period are much higher than the wellbore temperature obtained after a longer injection period. This is an expected result since the volume of water being injected in the first case (short injection case) is smaller leading therefore to a faster recovery to the original temperature of the reservoir once the well is shut-in.

Next, we compare the temperature distribution in the reservoir generated using our model to the one obtained from STARS at three different shut-in times subsequent to an injection during $t_p = 5$ hours. The general equation used for the generation of the temperature $\bar{T}_{D,ou}(r_D, s)$ based on perturbation method is provided by Eq. 4.291 with the terms $\bar{T}_{D0,ou}$, $\bar{T}_{D1,ou}$ and $\bar{T}_{D2,ou}$ evaluated from Eqs. 4.314, 4.345 and 4.368 respectively. This comparison is illustrated in Fig. 4.19. A good match between the model and the simulator is observed. Moreover, this figure shows how the temperature front dissipates for long shut-in times so that the system recovers its original temperature.

In order to study the effect of the thickness of the reservoir on the temperature, two tests were run where cold water was injected at the same rate as previously for a total time of 5 hours. The injection test in each case is followed by a falloff. In the first run, the thickness of the reservoir is reduced to $h = 25$ ft. the second run pertains to a thickness equal to 75 ft. All the other data were kept the same. In each case, the wellbore temperature function of shut-in time Δt curves are generated from the simulator and compared against the ones obtained from the model. Numerical results are shown in Fig. 4.20. In the same plot, both numerical and analytical solutions evaluated for the case $h = 50$ ft are also included for comparison purposes. As seen from this figure, a good match between the simulator and the model is observed for each case. This figure also shows the impact of the thickness of the reservoir on the behavior of the wellbore temperature.

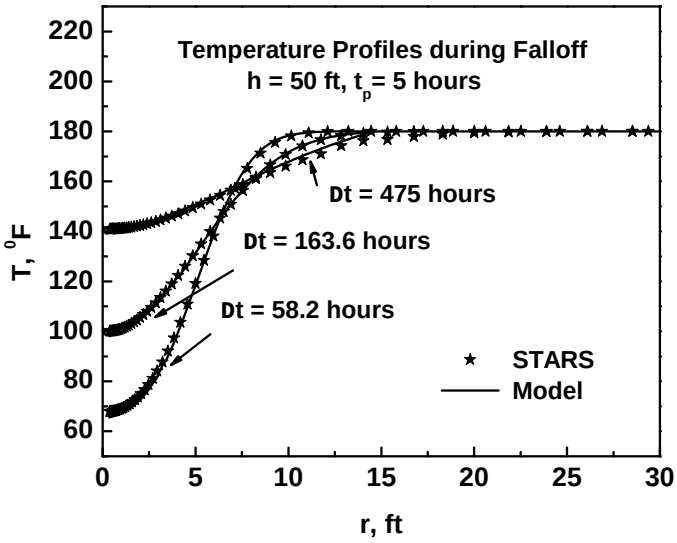

Figure 4.19: Comparison of numerical results to analytical solution for temperature distributions during falloff.

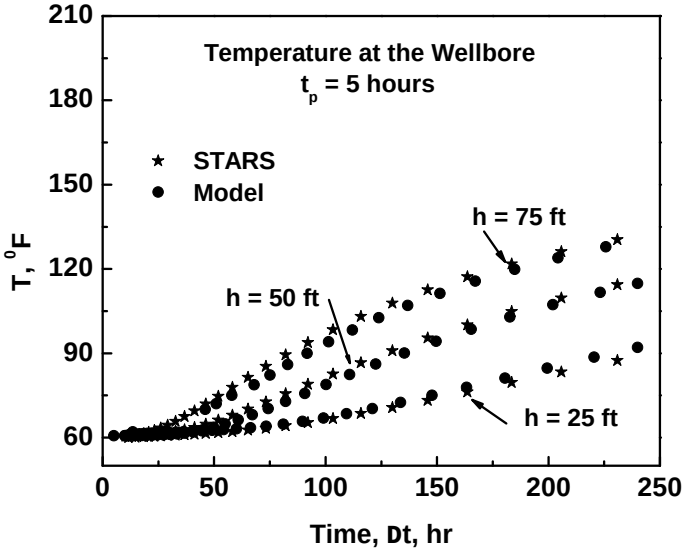

Figure 4.20: Comparison of numerical results to analytical solution for the wellbore temperature during falloff for different values of the reservoir thickness.

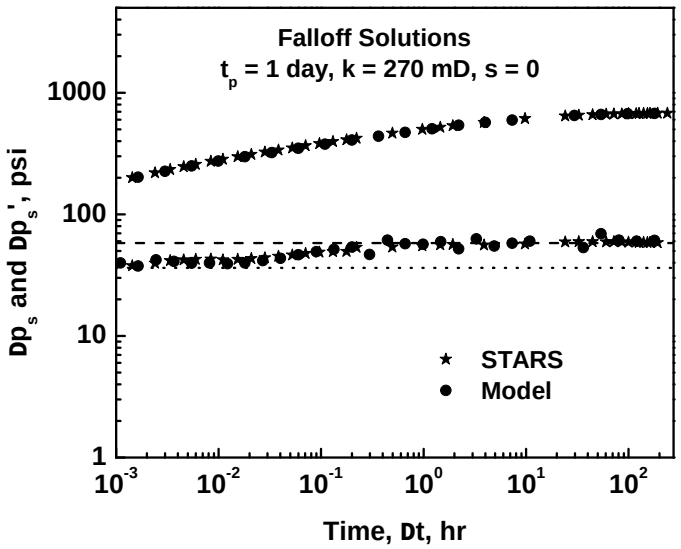

Figure 4.21: Comparison between the results for the falloff test from the simulator and the analytical solution, $s = 0$.

More specifically, both the simulator and our model predict a higher temperature at the same shut-in time if the thickness is increased. As the same volume of water is injected in all cases, this is explained by the fact that an increase in h leads to an increase in the surface area across which heat flows and therefore to a decrease in the temperature change in the system. That is why the temperatures are much higher for large values of h.

Fig. 4.21 compares the multiphase flow results obtained from our proposed model for the pressure change Δp_s and its derivative with respect to the equivalent time $t_e = \frac{tp\Delta t}{t_p+\Delta t}$ against the corresponding data obtained from the simulator. This example pertains to the case where $h = 50$ ft and the mechanical skin factor $s = 0$. Fig. 4.21 shows a good agreement for the falloff pressure change solution. Except for the small oscillations exhibited by the pressure derivative data generated from our analytical solution, the agreement with the simulator is also good. We also observe a semi-log slope exhibited by the pressure derivative for times Δt bigger than 10 hours reflecting, as expected, oil properties at the initial temperature of the reservoir. This semi-log slope, represented by a dashed line, is given by

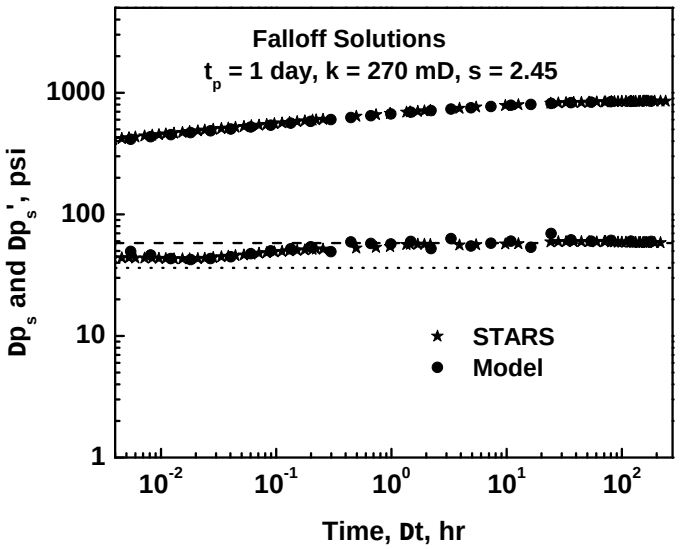

Figure 4.22: Comparison between the results for the falloff test from the simulator and the analytical solution, $s = 2.45$.

$$\Delta p'_s = \frac{\alpha q_{inj}}{2kh\hat{\lambda}_{oh}} = 58.1. \tag{4.507}$$

The dotted line represents the semi-log line based on water properties at the temperature of the injected fluid defined by the following equation

$$\Delta p'_s = \frac{\alpha q_{inj}}{2kh\hat{\lambda}_{wc}} = 36.3, \tag{4.508}$$

and expected to be observed at early times. However, both the simulator and the analytical solution for the derivative reflect a slightly higher value ($\Delta p'_s \approx 39.2$) for times $0.001 < \Delta t < 0.01$ hours.

The case with $s = 2.45$ is shown in Fig. 4.22 where our analytical falloff solution for the pressure drop and its derivative is also compared to the results extracted from the simulator. A good match between the two sets of data is observed.

4.4.3 Horizontal Well Case

Here, we simulate injection of cold water at a constant rate of $q_{inj} = 31,450$

STB/day through a horizontal well of length $L = 1312.4$ ft that penetrates a hot reservoir of constant formation thickness $h = 78.74$ ft and absolute permeability $k = 5600$ mD. All the other basic data used for the computations are the same as the ones used in the vertical well case (see Tables 4.1 and 4.2). This example pertains to a case where the horizontal well is located in the center of the formation. The simulation grid consisted of a 149 (x) by 194 (y) by 1 (z) Cartesian grid plus a local hybrid grid refinement of 50 (r) by 1 (θ) by 1 (z') used in all the well blocks where z'-direction coincides with the y-direction. Other relevant data are the parameters used to generate the saturation profiles. They are: $x_1 = 30.9$ ft and $x_3 = 515.4$ ft. According to the nonisothermal Buckley-Leverett equation, the water front at the instant of shut-in $t_p = 10$ days is located at $x_f(t_p) = 81.5$ ft whereas, the temperature front is still propagating radially in the (x, z) plane ($r_{zx,T}(t_p) = 24.6$ ft). Here, we show only results for the injection period as at the date of this writing, we have been unable to provide a theoretical derivation for the falloff pressure solution which takes into account the temperature changes.

The two-phase flow problem was run using STARS and compared to the numerical solution obtained under isothermal conditions (injection of water at the temperature of the reservoir). This comparison is illustrated in Fig. 4.23 where the results are presented in terms of the wellbore pressure change Δp and its derivative with respect to $\ln(t)$ and represented by solid circle dots for the isothermal solution and solid star dots for the nonisothermal solution. Unlike the vertical well case (see Fig. 4.12) where the two solutions diverge at late times to reflect the properties of water at the two temperature of the system, the two solutions obtained for the horizontal well case are essentially identical. In order to observe such divergence when comparing the isothermal and nonisothermal solutions for a horizontal well, we will need to inject water for a very long period of time.

The analytical solution for the the pressure change was generated by computing Eq. 4.191 for different values of time upon the determination of the total mobility profile from the nonisothermal radial and linear advance Buckley-Leverett equations. Fig. 4.24 illustrates a log-log plot of the injectivity solution for the wellbore pressure change and its derivative obtained analytically using the model and represented by solid lines. Also

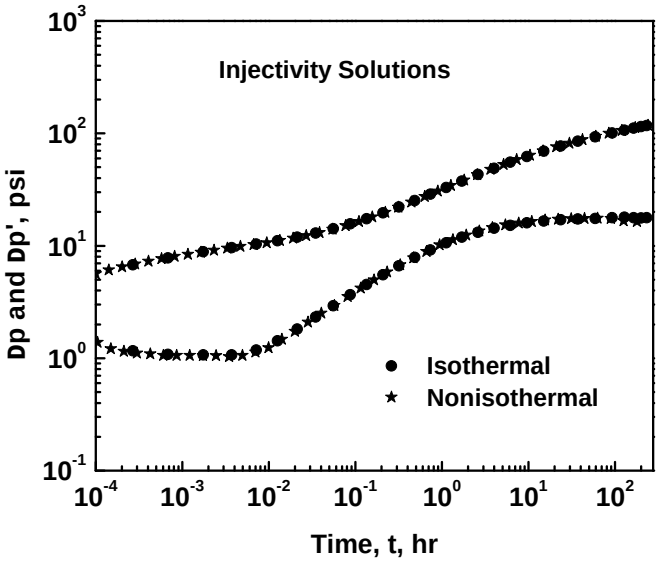

Figure 4.23: Comparison of numerical solution under nonisothermal conditions to numerical isothermal solution during injection, $z_w = 39.37$ ft.

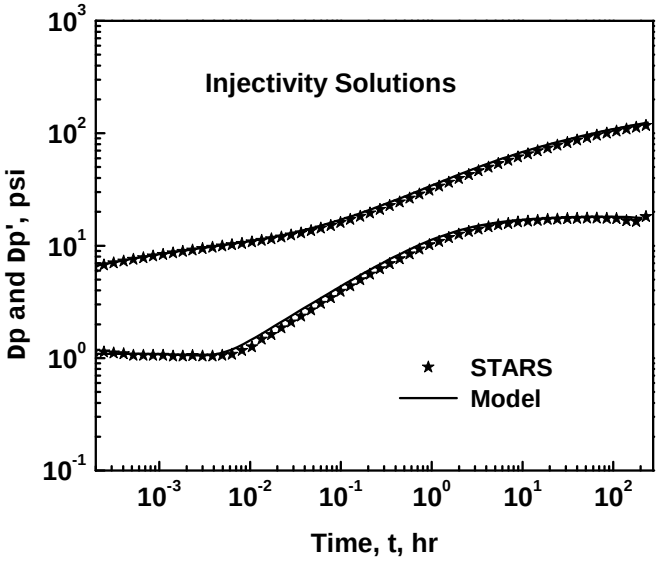

Figure 4.24: Comparison between the results for the injection test from the simulator and the analytical solution from the model, $z_w = 39.37$ ft.

shown in this figure is the injectivity solution for the wellbore pressure change and its derivative obtained numerically under nonisothermal conditions and represented by the solid star dots. This figure shows a good agreement between the model and the simulator.

CHAPTER 5

PRACTICAL ANALYSIS OF INJECTION/FALLOFF DATA

In this chapter, our focus is on the analysis of synthetic injection/falloff pressure data at horizontal wells. A gradient based optimization algorithm is implemented and coupled with our analytical solutions for the injection and falloff pressures as the forward model, for nonlinear parameter estimation. The implementation of such an algorithm requires the computation of the sensitivity of the theoretical model to all model parameters to be considered for the formulation of the Hessian matrix. Because the analysis of well test data usually involves few model parameters, the computation of all sensitivity coefficients is feasible for such problems.

5.1 Generation of Estimates

5.1.1 Model parameters

Throughout, m denotes the N_m-dimensional column vector of model parameters considered for estimation. For the synthetic cases presented in this study, these parameters are reservoir absolute permeability, the length of the horizontal well, the mechanical skin factor and the relative permeabilities. All other reservoir and well properties are assumed to be known input variables. In the nonlinear regression, anisotropy is considered. Thus, the permeabilities in the three directions, that is k_x, k_y and k_z are set to be parameters. When estimating the mechanical skin factor, s, the radius of the skin zone is assumed to be known.

Relative permeabilities are given by power law models normalized so that the relative permeability to oil at irreducible water saturation S_{iw} is equal to unity. With this assumption, the relative permeability curves are defined by

$$k_{rw}(S_{wD}) = a_w S_{wD}^{n_w}, \tag{5.1}$$

and

$$k_{ro}(S_{wD}) = (1 - S_{wD})^{n_o}, \tag{5.2}$$

where S_{wD} is the dimensionless saturation defined by

$$S_{wD} = \frac{S_w - S_{iw}}{1 - S_{or} - S_{iw}}, \tag{5.3}$$

and $a_w = k_{rw}(1 - S_{or})$ is the end-point of the water relative permeability curve. In this work, residual oil saturation, S_{or}, and irreducible water saturation, S_{iw}, are assumed to be known. Therefore, only three parameters are needed for the estimation of the relative permeabilities. These are the two exponents n_w and n_o and the water end-point a_w.

In summary, for an injection/falloff test on a horizontal well in an anisotropic reservoir, $N_m = 8$ and the vector of model parameters is

$$m = [k_x, k_y, k_z, L, s, a_w, n_w, n_o]^T, \tag{5.4}$$

where L denotes the length of the well.

5.1.2 Optimization Algorithm - Levenberg-Marquardt Method

In our inverse problem, we are interested in finding a probability density function among all probability distributions the model describes, that most likely reproduces the observed data. In order to do so, we usually define a likelihood function expressed by

$$f(m|d_{obs}) = \frac{1}{(2\pi)^{N_d/2}\sqrt{\det C_D}} \exp\left(-\frac{1}{2}(d_{pred}(m) - d_{obs})^T C_D^{-1}(d_{pred}(m) - d_{obs})\right). \tag{5.5}$$

In this equation, d_{obs} is an N_d-dimensional vector of observed data and C_D is an $N_d \times N_d$ covariance matrix that describes the correlation between measurement errors in the

observed data. The vector d_{pred} is an N_d-dimensional vector representing the predicted model that depends on the vector of model parameters m. In this work, it is assumed that the bottom hole pressures recorded during injection/falloff tests are the only observed data. In addition, the measurement errors of these data are assumed to be independent random variables with mean zero and a constant variances, $\sigma^2_{d,i}$, with $i = 1, N_d$, so that the data covariance matrix, C_D, is diagonal. These variances are assumed to be identical, i.e., $\sigma^2_{d,i} = \sigma^2_d$ for all $i = 1, N_d$.

The maximum likelihood estimate is the model that maximizes the likelihood function $f(m|d_{obs})$ defined by Eq. 5.5 or equivalently the vector of the model parameters that minimizes the objective function

$$\Theta(m) = \frac{1}{2}(d_{pred}(m) - d_{obs})^T C_D^{-1}(d_{pred}(m) - d_{obs}). \tag{5.6}$$

Since a gradient-based algorithm (Levenberg-Marquardt method) is used to minimize the objective function, it is necessary to evaluate the gradient $\nabla\Theta(m)$ and the Hessian $H(m)$ of the objective function. Taking the first derivative of Eq. 5.6 with respect to the model parameter vector m gives the gradient vector defined by:

$$\nabla\Theta(m) = \begin{pmatrix} \frac{\partial\Theta(m)}{\partial m_1} \\ \frac{\partial\Theta(m)}{\partial m_2} \\ \vdots \\ \frac{\partial\Theta(m)}{\partial m_k} \\ \vdots \\ \frac{\partial\Theta(m)}{\partial m_{N_m}} \end{pmatrix} = \nabla d^T_{pred} C_D^{-1}(d_{pred}(m) - d_{obs}). \tag{5.7}$$

Here, $(\nabla d^T_{pred})^T$, also denoted by G, is an $N_d \times N_m$ matrix which measures the sensitivity of the predicted data, d_{pred}, to the model parameters. The coefficients of this matrix are

$$G(m) = \begin{pmatrix} \frac{\partial d_{pred,1}}{\partial m_1} & \frac{\partial d_{pred,1}}{\partial m_2} & \cdots & \frac{\partial d_{pred,1}}{\partial m_k} & \cdots & \frac{\partial d_{pred,1}}{\partial m_{N_m}} \\ \frac{\partial d_{pred,2}}{\partial m_1} & \frac{\partial d_{pred,2}}{\partial m_2} & \cdots & \frac{\partial d_{pred,2}}{\partial m_k} & \cdots & \frac{\partial d_{pred,2}}{\partial m_{N_m}} \\ \cdots & \cdots & \cdots & \cdots & \cdots & \\ \frac{\partial d_{pred,N_d}}{\partial m_1} & \frac{\partial d_{pred,N_d}}{\partial m_2} & \cdots & \frac{\partial d_{pred,N_d}}{\partial m_k} & \cdots & \frac{\partial d_{pred,N_d}}{\partial m_{N_m}} \end{pmatrix}. \tag{5.8}$$

The second derivative of the objective function is the $N_m \times N_m$ Hessian matrix $H(m)$ given by

$$H(m) = \nabla\Big(\nabla\Theta(m)\Big)^T. \tag{5.9}$$

Using Eq. 5.7 in the preceding equation yields

$$\begin{aligned} H(m) = \nabla\Big(G^T C_D^{-1}(d_{pred}(m) - d_{obs})\Big)^T & \\ = \nabla\Big((d_{pred}(m) - d_{obs})^T C_D^{-1} G\Big) & \\ = G^T C_D^{-1} G + (\nabla G^T) C_D^{-1}(d_{pred}(m) - d_{obs}). & \end{aligned} \tag{5.10}$$

For nonlinear problems, the second term in Eq. 5.10 that involves the gradient of G should be small in the neighborhood of the minimum of the objective function. In the Gauss-Newton method, this term is dropped and the approximation to the Hessian is given by

$$H(m) \approx G^T C_D^{-1} G. \tag{5.11}$$

The Levenberg-Marquardt (LM) method was applied to perform the nonlinear regression upon the construction of the gradient and the Hessian of the objective function from Eqs. 5.7 and 5.11 respectively. One iteration of the algorithm is represented by the following equation:

$$(\lambda I + H(m^n))\delta m^{n+1} = -\nabla\Theta(m^n), \tag{5.12}$$

where λ is a positive scalar called the Levenberg-Marquardt parameter and I is the $N_m \times N_m$ identity matrix. Once the vector δm^{n+1} is determined by solving the system of Eq. 5.12, the model parameter m is then updated by the following equation:

$$m^{n+1} = m^n + \delta m^{n+1}. \tag{5.13}$$

The parameter λ needs to have a positive value to ensure that the Hessian of the objective function is positive definite. At the beginning of the optimization, it is desirable to consider a large value of this parameter to make the Hessian more well-conditioned. In our implementation of the LM method, the starting value of λ is set to

$$\lambda_0 = \frac{1}{10N_d}\Theta(m^0), \tag{5.14}$$

according to Abacioglu et al. [3]. In Eq. 5.14, m^0 represents the initial guess. If Eqs. 5.12 and 5.13 give a vector of model parameters, m^{n+1}, such that $\Theta(m^{n+1}) \geq \Theta(m^n)$, then m^{n+1} is not accepted as the new estimate and λ is increased by a factor of 10 and the iteration is redone. On other hand, if $\Theta(m^{n+1}) < \Theta(m^n)$, then λ is divided by a factor of 10 and Eq. 5.12 is repeated with m^{n+1} as a vector of model parameters at the previous time step until convergence is reached.

In this study, two criteria to determine convergence of the nonlinear regression were applied. The first one is on the change in the objective function and is expressed by

$$\frac{|\Theta(m^{n+1}) - \Theta(m^n)|}{\max\left(|\Theta(m^{n+1})|, 1\right)} < 10^{-3}, \tag{5.15}$$

and the other one is based on the change in the vector of model parameters and given by

$$\max_{1\leq j\leq N_m}\left[\frac{|m_j^{n+1} - m_j^n|}{\max\left(|m_j^{n+1}|, 1\right)}\right] < 10^{-2}. \tag{5.16}$$

Note that both criteria must be satisfied for the optimization problem to converge.

5.1.3 Logarithm Transformation of Model parameters

Due to the ill-conditioning nature of the inverse problem, It is possible for the optimization algorithm to converge to a vector of model parameters which contains non physical values. For such cases, imposing constraints in the history matching process is recommended if one wishes to avoid unreasonable results. Gao and Reynolds [19] introduced a logarithmic transformation which allows each ith entry of the vector m to be constrained between a lower bound $m_{l,i}$ and an upper bound $m_{u,i}$ as follows:

$$s_i(m_i) = \ln\left(\frac{m_i - m_{l,i}}{m_{u,i} - m_i}\right). \tag{5.17}$$

Note that when $m_i \to m_{l,i}$, $s_i \to -\infty$ and when $m_i \to m_{u,i}$, $s_i \to +\infty$. This is an important feature of the transformation because by mapping the lower bound to $-\infty$ and the upper bound to $+\infty$, the boundaries are removed and the constrained optimization problem is transformed to an unconstrained optimization problem. Another feature of the logarithmic transformation is that it has an inverse obtained by expressing the original variable m_i function of s_i, i.e., $m_i = m_i(s_i)$. Using Eq. 5.17, it is easy to show that this relationship is given by

$$m_i(s_i) = \frac{m_{l,i} + m_{u,i}e^{s_i}}{1 + e^{s_i}}, \text{for } s_i < 0, \tag{5.18}$$

and

$$m_i(s_i) = \frac{m_{u,i} + m_{l,i}e^{-s_i}}{1 + e^{-s_i}}, \text{for } s_i > 0. \tag{5.19}$$

In the minimization process, we replaced the vector of model parameters, m, by the new vector of model parameters based on the logarithmic transform, s, as follows:

$$(\lambda I + H(s^n))\delta s^{n+1} = -\nabla\Theta(s^n), \tag{5.20}$$

$$s^{n+1} = s^n + \delta s^{n+1}. \tag{5.21}$$

The Hessian H is given by Eq. 5.11 with the sensitivity matrix G in this case obtained using the following chain rule:

$$G = \left(\nabla_s (d_{pred}(s))^T\right)^T = \left(\nabla_m (d_{pred}(m))^T\right)^T D_s, \tag{5.22}$$

where D_s is an $N_m \times N_m$ diagonal matrix with its entry $d_{s,i}$ equal to

$$d_{s,i} = \frac{\partial m_i}{\partial s_i} = \frac{(m_{u,i} - m_i)(m_i - m_{l,i})}{m_{u,i} - m_{l,i}}. \tag{5.23}$$

5.2 Analysis of Sensitivity of Pressure Data to Model Parameters

As mentioned earlier, the predicted pressure data during injection/falloff tests through horizontal wells are constructed analytically using approximate solutions derived in chapters 2 and 3. Based on our computational results, the analytical injection solution is only accurate for times such that water is moving radially in the (x, z) plane or linearly in the x-direction, assuming the axis of the horizontal well is along the y-axis. Having said that, depending on the location of the well with respect to the top and bottom boundaries of the reservoir and the length of the well, these flow regimes may last hundreds of hours for problems of interests (see Figs. 2.33 and 2.34 for example). Therefore, this limitation does not obviate the utility of our analytical solution.

For the synthetic cases considered in this chapter, water is injected at a constant rate for a total time which does not exceed the time where our model predicts a radial propagation of water in the (x, y) plane. For these cases, the general solutions for the well-bore pressure change during the injection and falloff periods under isothermal conditions are given respectively by

$$\Delta p = p_{wf}(t) - p_i = \overline{\Delta p}_o + \Delta p_\lambda, \tag{5.24}$$

where Δp_λ is defined by

$$\Delta p_\lambda = \frac{\alpha q_{inj}}{\bar{k} L_n \hat{\lambda}_o} \int_{r_{we}}^{\min(z_{wn}, r_{zx,fn}(t))} \left(\frac{\hat{\lambda}_o}{\lambda_t(r_n, t)} - 1 \right) \frac{\bar{k}}{\bar{k}(r_n)} \frac{dr_n}{r_n} + \frac{\pi \alpha q_{inj}}{\bar{k} L_n \hat{\lambda}_o} \int_{x_{n1}}^{b_n} \left(\frac{\hat{\lambda}_o}{\lambda_t(x_n, t)} - 1 \right) \frac{dx_n}{h_n(x_n)}, \quad (5.25)$$

and

$$\Delta p_{ws} = p_{ws}(\Delta t) - p_i = \overline{\Delta p}_{os} + \Delta p_{\lambda s}, \quad (5.26)$$

with

$$\Delta p_{\lambda s} = \frac{\alpha}{L_n \hat{\lambda}_o} \int_{r_{we}}^{\min(z_{wn}, r_{zx,fn}(t_p))} \left[\frac{\hat{\lambda}_o}{\lambda_t(r_n, t_p)} q_s(r_n, \Delta t) - \hat{q}_{os}(r_n, \Delta t) \right] \frac{dr_n}{r_n \bar{k}(r_n)} + \frac{\pi \alpha}{\bar{k} L_n \hat{\lambda}_o} \int_{x_{n1}}^{b_n} \left[\frac{\hat{\lambda}_o}{\lambda_t(x_n, t_p)} q_s(x_n, \Delta t) - \hat{q}_{os}(x_n, \Delta t) \right] \frac{dx_n}{h_n(x_n)}. \quad (5.27)$$

Recall that these equations, expressed in the new coordinate system (x_n, y_n, z_n), were obtained by applying a spatial transformation to convert an anisotropic reservoir to an equivalent isotropic reservoir of permeability $\bar{k}$ given by

$$\bar{k}(r_n) = \begin{cases} \bar{k}_s = \sqrt[3]{k_{xs} k_{ys} k_{zs}} & \text{for } r_{we} < r_n < r_{sn}, \\ \bar{k} = \sqrt[3]{k_x k_y k_z} & \text{for } r_n > r_{sn}. \end{cases} \quad (5.28)$$

Recall also that the effective wellbore radius of the well, r_{we}, is

$$r_{we} = \frac{r_w}{2} \left(\sqrt{\frac{\bar{k}}{k_x}} + \sqrt{\frac{\bar{k}}{k_z}} \right), \quad (5.29)$$

and that the thickness of the reservoir, h_n, the distance from the centerline of the well to the top boundary of the reservoir, z_{wn}, and the length of the horizontal well, L_n, in this system are given respectively by

$$h_n = \sqrt{\frac{\bar{k}}{k_z}} h, \tag{5.30}$$

$$z_{wn} = \sqrt{\frac{\bar{k}}{k_z}} z_w, \tag{5.31}$$

and

$$L_n = \sqrt{\frac{\bar{k}}{k_y}} L. \tag{5.32}$$

In Eqs. 5.24 and 5.26, the positions x_{n1} and x_{n3} are the parameters of the two models for the movement of water in the new system obtained from Deppe's constructions as follows:

$$x_{n1} = \frac{\pi}{4} z_{wn}, \tag{5.33}$$

and

$$x_{n3} = \frac{\pi}{8} L_n, \tag{5.34}$$

and the constant b_n is defined by

$$b_n = \min(\max(x_{n1}, x_{fn}(t)), x_{n3}). \tag{5.35}$$

Based on the fact that for the horizontal well case, model 2 performed better than model 1 (see the numerical section of chapter 2 and 3), it was used to construct the total mobility profiles necessary for the computation of Eqs. 5.24 and 5.26. In this model, recall that water moves over a variable thickness when propagating linearly in the x-direction. This variable thickness is given by

$$h_n(x_n) = \begin{cases} 2z_{wn} & \text{for } 0 \leq x_n \leq x_{n1}, \\ h_n - \frac{(h_n - 2z_{wn})}{(x_{n2} - x_{n1})}(x_{n2} - x_n) & \text{for } x_{n1} \leq x_n \leq x_{n2}, , \\ h_n & \text{for } x_{n2} \leq x_n \leq x_{n3}, \end{cases} \tag{5.36}$$

where the parameter x_{n2}, as seen previously, is computed by applying the steady-state

single-phase theory for convergence pseudo-skin factor computations which yield

$$x_{n2} = \frac{\frac{\pi^2}{8(h_n/2z_{wn}-1)} \ln\left(\frac{h_n}{2z_{wn}}\right) + \ln\left(\frac{h_n}{2\pi z_{wn}\sin(\pi z_{wn}/h_n)}\right)}{\frac{\pi}{h_n}\left[\frac{h_n/2z_{wn}}{(h_n/2z_{wn}-1)} \ln\left(\frac{h_n}{2z_{wn}}\right) - 1\right]}. \tag{5.37}$$

In Eq. 5.26, rate superposition was applied to compute $\hat{q}_{os}(r_n, \Delta t)$ and $q_s(r_n, \Delta t)$ (see Eqs. 3.102 and 3.103) as well as the flow rate distributions $\hat{q}_{os}(x_n, \Delta t)$ and $q_s(x_n, \Delta t)$ (see Eqs. 3.107 and 3.108).

A perturbation method based on finite-difference approximation was applied to compute the sensitivity of predicted data (Eqs. 5.24 and 5.26) to model parameters that we wish to estimate. Again, these are the permeabilities in the three directions, the length of the horizontal well, the mechanical skin factor and the relative permeability parameters. The appropriate size of the perturbation were chosen based on previous experiments (Chen and Reynolds [17], Chen et al. [15] and Chen et al. [16]). They were found to be equal to 0.5 per cent for the permeabilities, 1 per cent for the well length, 0.5 and 5 per cent for the water and oil exponents, respectively, and as much as 10 per cent for the mechanical skin factor and the end-point water relative permeablity.

Since our analytical solutions for both injection and falloff are written as the sum of the single-phase solution based on oil properties at initial water saturation and a two-phase component term which reflects the deviation of the total mobility in the region invaded by injected water from end-point oil mobility, the sensitivity coefficients of each term was determined in order to measure the effect of a small change in the model parameters on the single-phase pressure data and the multiphase component separately. The purpose of this is to give us an insight on the information that can be brought by the multiphase component with respect to the model parameters that we wish to resolve.

5.2.1 Sensitivity of the Single-Phase Pressure Data to Model Parameters

Before showing results for calculated sensitivity coefficients of the single-phase solution to the model parameters k_x, k_y, k_z, s and L, we present a summary of the equations for the flow regimes that a horizontal well may exhibit during the test period.

For detailed derivations of these equations, see references [23], [20] and [25].

First Radial and Semi-Radial Flow Regimes

The first radial flow regime manifests itself at very early times when the pressure at the wellbore is not affected by the boundaries of the reservoir. The corresponding equation for the wellbore pressure is given by

$$p_i - p_{wf} = \frac{\alpha q B_o \mu_o}{\sqrt{k_x k_z} L}\left[\frac{1}{2}\ln\left(\frac{4\beta\sqrt{k_x k_z}t}{e^{\gamma}\phi\mu c_t r_w^2}\right) + s\right]. \tag{5.38}$$

A semi-radial flow regime may occur if the well is not drilled near the center of the formation due to the effect of the nearest boundary on the wellbore pressure. During this flow regime, the pressure behavior is given by

$$p_i - p_{wf} = \frac{\alpha q B_o \mu_o}{\sqrt{k_x k_z} L}\left[\ln\left(\frac{4\beta\sqrt{k_x k_z}t}{e^{\gamma}\phi\mu c_t r_w^2}\right) + s + s'\right], \tag{5.39}$$

where s' is the pseudo-skin factor due to anisotropy and defined according to Kuchuk et al. [23] by

$$s' = -\ln\left[\left(1+\sqrt{\frac{k_x}{k_z}}\right)\frac{z_w}{r_w}\right]. \tag{5.40}$$

First Linear Flow Regime

A linear flow regime may occur when the wellbore pressure is dominated by the top and bottom boundaries and the well length is significantly longer than the formation thickness. During this period, the wellbore pressure response reflects pressure diffusion in the x-direction which is given by the following equation:

$$p_i - p_{wf} = \frac{\alpha q B_o \mu_o}{k_x h}\left[\sqrt{\frac{4\pi\beta k_x t}{\phi\mu c_t L^2}} + \sqrt{\frac{k_x}{k_z}}\frac{h}{L}(s_z + s)\right]. \tag{5.41}$$

In this equation, s_z is a pseudo-skin factor representing an additional dimensionless pressure drop due to the convergence of flow lines from linear to radial near the wellbore. It is defined according to Kuchuk et al. [23] by

$$s_z = \ln\left(\frac{h}{2\pi r'_w \sin(\pi z_w/h)}\right), \tag{5.42}$$

with r'_w given by

$$r'_w = \frac{r_w}{2}\left(1+\sqrt{\frac{k_z}{k_x}}\right). \tag{5.43}$$

Second Radial Flow Regime

This flow regime may develop at later times when both the top and bottom boundaries of the reservoir and the flow beyond the well tips affect the wellbore pressure response. In this case, the solution is governed by

$$\Delta p = p_i - p_{wf} = \frac{\alpha q B_o \mu_o}{\sqrt{k_x k_y}h}\left[\frac{1}{2}\ln\left(\frac{4\beta k_y t}{e^\gamma \phi \mu c_t L^2}\right) + \sqrt{\frac{k_y}{k_z}}\frac{h}{L}(s_z + s'_z + s) + C\right], \tag{5.44}$$

where we previously defined s_z (see Eq. 5.42). The expression for s'_z is given by

$$s'_z = -2\sqrt{\frac{k_y}{k_z}}\frac{h}{L}\left[\frac{1}{3} - \frac{z_w}{h} + \left(\frac{z_w}{h}\right)^2\right]. \tag{5.45}$$

In Eq. 5.44, C is a constant which value depends on how the wellbore boundary condition is represented mathematically. For an infinite conductivity wellbore model, $C = 1.791$, whereas, for a uniform flux wellbore model, $C = 2.094$.

If the lateral boundaries of the reservoir (in the y- and z-directions) affect the pressure behavior at the wellbore, a second linear flow regime in the x-direction occurs. This flow period usually happens at very late times and is, therefore, not of interest for the cases we considered in this work.

Next, we show results for calculated sensitivity of the single-phase pressures to model parameters. The sequence of the test considered here consisted of an injection of oil at a constant rate of 31450 STB/day for a total time of $t_p = 20$ days followed by a shut-in period of equal duration. The reservoir is initially at a pressure $p_i = 3922$ psi. The injectivity and falloff single-phase flow pressures are based on oil properties at irreducible

Property	Value
Porosity, ϕ	0.32
Permeability in the x-direction, k_x, mD	4500
Permeability in the y-direction, k_y, mD	2700
Permeability in the z-direction, k_z, mD	300
Thickness of the formation, h, ft	78.74
Rock compressibility, c_r, psi^{-1}	5.63×10^{-6}
Residual oil saturation, S_{or}	0.28
Irreducible water saturation, S_{iw}	0.25
End-point water relative permeability, a_w	0.5
Water exponent, n_w	2.
Oil exponent, n_o	2.5
Oil FVF, B_o, RB/STB	1.318
Oil compressibility, c_o, psi^{-1}	8.0×10^{-6}
Water viscosity, μ_o, cp	5.1
Water FVF, B_w, RB/STB	1.008
Water compressibility, c_w, psi^{-1}	2.84×10^{-6}
Water viscosity, μ_w, cp	0.516
Wellbore radius, r_w, ft	0.35
Skin zone radius, r_s, ft	1.5
Mechanical skin factor, s,	5.
Length of the well, L, ft	1312.4

Table 5.1: Reservoir and well data.

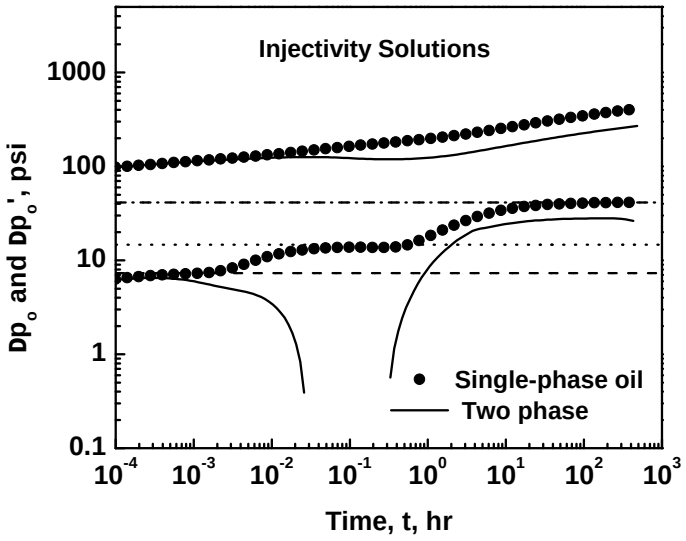

Figure 5.1: Analytical solution for injectivity single-phase flow, $\mu_o = 5.1$ cp, $s = 5$.

water saturation. Only the term c_t in Eqs. 5.38, 5.39, 5.41 and 5.44 was replaced by $\hat{c}_{to} = c_o(1 - S_{iw}) + c_w S_{iw} + c_r$ since the oil relative permeability curve was normalized to 1, i.e., $a_o = k_{ro}(S_{iw}) = 1$. The properties of the reservoir and the well are shown in Table 5.1.

Fig. 5.1 is a log-log plot of the analytical injectivity single-phase solution for the wellbore pressure change $p_{wf} - p_i$ and its derivative with respect to logarithm of time. This plot was generated for the purpose of flow regimes identification.

As can be seen from this figure, the semi-log slope that the pressure derivative exhibits at very early times (up to 0.0016 hours) and represented by a dashed line, is due to the first radial flow regime which is equal to $\Delta p' = \frac{\alpha q_{inj} \mu_o}{2\sqrt{k_x k_z} L} = 7.5$. For times $0.05 < t < 0.4$ hours, the pressure derivative reflects a semi-log slope equal to twice the value observed during the first radial flow regime. This doubling of slope, represented by a dotted line in Fig. 5.1, is the signature of a semi-radial flow period due to the fact that in this case, the well is very close to the top boundary of the reservoir (the distance to the top reservoir boundary is $z_w = 5$ ft). For intermediate times, the pressure derivative shows a half-slope line indicating the occurrence of a linear flow regime. This flow period

is, however, very short as it lasts only few hours ($0.4 < t < 2$ hours). Finally, for times bigger than 20 hours, the pressure derivative exhibits a semi-log slope represented by a dashed-dotted line and equal to $\Delta p' = \frac{\alpha q_{inj} \mu_o}{2\sqrt{k_x k_y} h} = 41.3$. This flow period corresponds to the second radial flow regime.

Fig. 5.2 illustrates the sensitivity of the injectivity single-phase oil solution to the logarithm of the model parameters k_x, k_y, k_z, L and s as a function of time. Note that the sensitivity of the pressure change to the permeability in the y-direction, that is k_y, is zero for times up to 2 hours which is the time corresponding to the end of the first linear flow regime. This result is consistent with Eqs. 5.38, 5.39 and 5.41 as the wellbore pressure response does not depend on k_y. During the last flow regime, however, Eq. 5.44 indicates that a small increase of k_y decreases the value of the wellbore pressure. This is exactly what we observe in Fig. 5.2 except for the negative sign of the sensitivity. Eq. 5.44 is based on a standard drawdown, for which the pressure change considered is given by $p_i - p_{wf}$, whereas, in our computations of the sensitivities, we considered $p_{wf} - p_i$ as the pressure change (injection of oil).

In Fig. 5.2, the sensitivities to k_x and k_z decrease with time for times up to the time corresponding to the end of the first radial flow regime. Moreover, these sensitivities take negative values during the same flow periods. Again, this behavior is consistent with Eqs. 5.38 and 5.39 as an increase in either k_x or k_z causes the wellbore pressure to decrease. While the sensitivity to k_x continues to decrease with time during the first linear and the second radial flow regime according to Eqs. 5.41 and 5.44, the sensitivity of the single-phase wellbore pressure to k_z remains constant during these flow periods. This is due to the fact that k_z appears only in the second term of both Eqs. 5.41 and 5.44, a term which does not depend on time. So, the derivatives of these equations with respect to $\ln(k_z)$ are also independent of time.

As shown in Fig. 5.2, the sensitivity to the mechanical skin factor is positive and constant throughout the entire test. Taking the derivative of Eqs. 5.38, 5.39, 5.41 and 5.44 with respect to $\ln(s)$ gives the same expression defined by

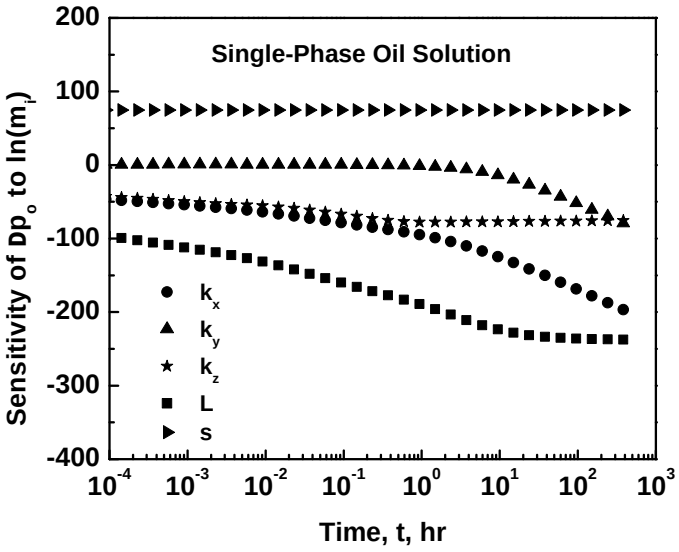

Figure 5.2: Sensitivity of the injectivity single-phase oil solution to model parameters.

$$\frac{\partial(p_i - p_{wf})}{\partial \ln(s)} = s\frac{\partial(p_i - p_{wf})}{\partial s} = s\frac{\alpha q_{inj}\mu_o}{\sqrt{k_x k_z}L} = 74.85, \tag{5.46}$$

or equivalently,

$$\frac{\partial(p_{wf})}{\partial \ln(s)} = -74.85. \tag{5.47}$$

This is the value observed in Fig. 5.2 but with a positive sign due to the same argument discussed above.

Finally, Fig. 5.2 indicates a decreasing sensitivity to the length of the well with respect to time for times up to the time corresponding to the end of the first linear flow regime. This is again consistent with the equations for the first radial and first linear flow regimes which show a decrease in the value of p_{wf} if the length L is increased. However, differentiating Eq. 5.44 with respect to $\ln(L)$ leads to a result which is independent of time. That is why the sensitivity to the length of the well during the second radial flow regime is constant as can be seen in Fig. 5.2.

The falloff results are shown in Fig. 5.3. These results are presented as the sensi-

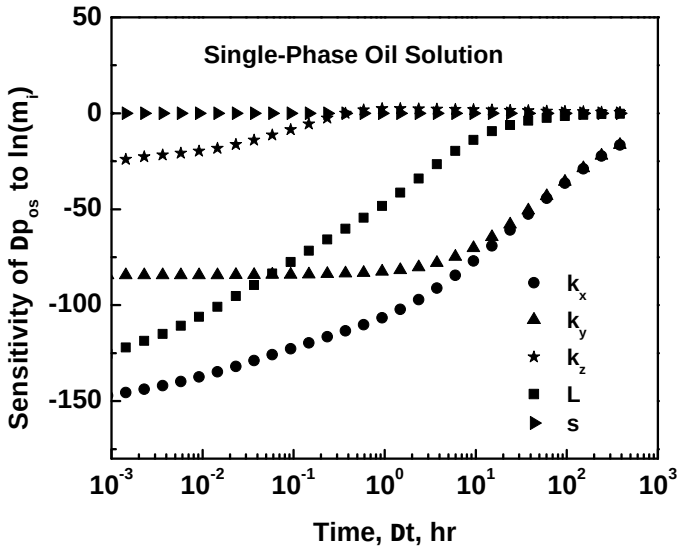

Figure 5.3: Sensitivity of the falloff single-phase oil solution to model parameters.

tivities of the single-phase wellbore pressure change $p_{ws} - p_i$ to the logarithm of the model parameters k_x, k_y, k_z, L and s function of the shut-in time $\Delta t = t - t_p$, where t_p denotes the instant of shut-in. As expected, the sensitivity of $p_{ws} - p_i$ to the mechanical skin factor is zero. Another expected result is that the sensitivities to all the model parameters go to zero towards the end of the falloff test. This is due to the fact that as times Δt increases, the wellbore pressure p_{ws} approaches the initial pressure of the reservoir p_i, so that no information on the model parameters can be obtained from the wellbore pressure.

5.2.2 Sensitivity of the Multiphase Component Data to Model Parameters

Figs. 5.4 and 5.5 show the sensitivities of the multiphase components Δp_λ and $\Delta p_{\lambda s}$ to the logarithm of the entries of the vector of model parameters m given by Eq. 5.4 during injection and falloff period, respectively. Recall that the term Δp_λ is obtained by subtracting $\overline{\Delta p}_o$ from the injection pressure change at the wellbore Δp given by Eq. 5.24, whereas, subtracting the single-phase oil solution during shut-in, $\overline{\Delta p}_{os}$, from the falloff wellbore pressure change Δp_{ws} provided by Eq. 5.26 gives the component $\Delta p_{\lambda s}$.

Note that at early times corresponding to $t < 0.0016$ hours, the sensitivities of Δp_λ

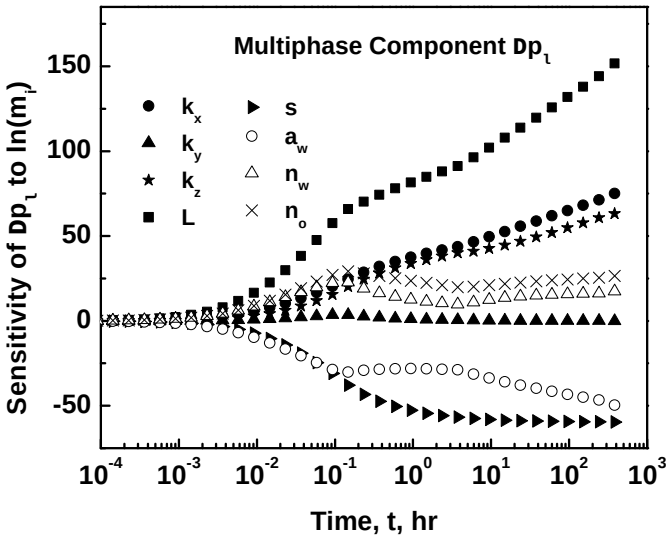

Figure 5.4: Sensitivity of the injectivity multiphase component to model parameters.

to all model parameters are zero. This is due to the fact that during this flow period, the multiphase component does not have any contribution to the injection solution as can be seen in Fig. 5.1.

It is not an obvious task to understand the behavior of the sensitivity coefficients of the multiphase components to the model parameters through their analytical formulations as their dependence to these parameters is via the reservoir and well properties in the transformed coordinate system, namely $\bar{k}(r_n)$, r_{we}, h_n, z_{wn} and L_n given by Eqs. 5.28 to 5.32. However, some of them are consistent with what would be expected. For instance, we expect that an increase of the mechanical skin factor will increase the wellbore pressure change during injection. Since the multiphase component takes negative values for the unfavorable mobility ratio (which is our case as $\hat{M} = 4.942$), for the injection pressure change to increase, the multiphase component has to decrease with an increase of s, behavior that we observe in Figs. 5.4. We would also expect no effect of the skin factor on the wellbore pressure change during falloff. Since the sensitivity of the single-phase solution to this parameter is zero (see Fig. 5.3), the multiphase component has to be also insensitive to s. That is exactly what we observe in Fig. 5.5.

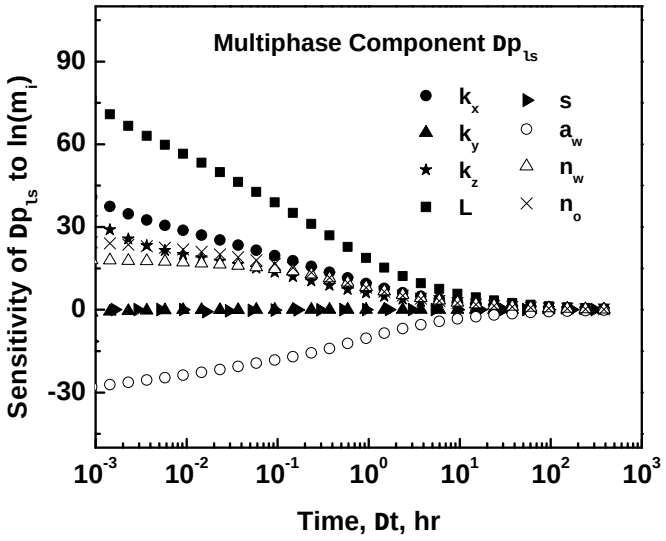

Figure 5.5: Sensitivity of the falloff multiphase component to model parameters.

An interesting remark about Fig. 5.4 is the presence of two fairly sharp changes, one at $t \approx 0.13$ hours exhibited by the sensitivities to L, a_w, n_w, n_o and k_y and the other one at $t \approx 4.4$ hours showed in the sensitivities to all the model parameters except for s. Our computations based on Buckley-Leverett theory indicate that the water front reaches the radius of the damaged zone at the time corresponding to when the first discontinuity occurs, whereas, the time at which the second discontinuity occurs, corresponds to the time when the water front hits the top reservoir boundary and water starts to propagate linearly in the x-direction.

In Fig. 5.5, the sensitivities of $\Delta p_{\lambda s}$ to the logarithm of the model parameters go to zero as times increases. This is explained by the fact that at long times, the falloff solution reflects oil properties at irreducible water saturation which means that the contribution of the multiphase component to the two-phase solution is negligible during this flow period.

5.2.3 Sensitivity of Pressure Data to Model Parameters

For the same injection/falloff test sequence and using the same reservoir and well data, the sensitivities of the wellbore pressure change to the logarithm of the entries of

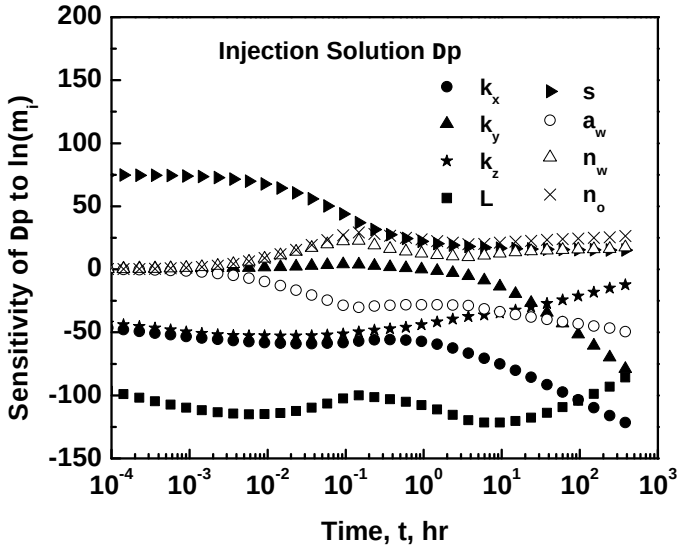

Figure 5.6: Sensitivity of the injectivity solution to model parameters.

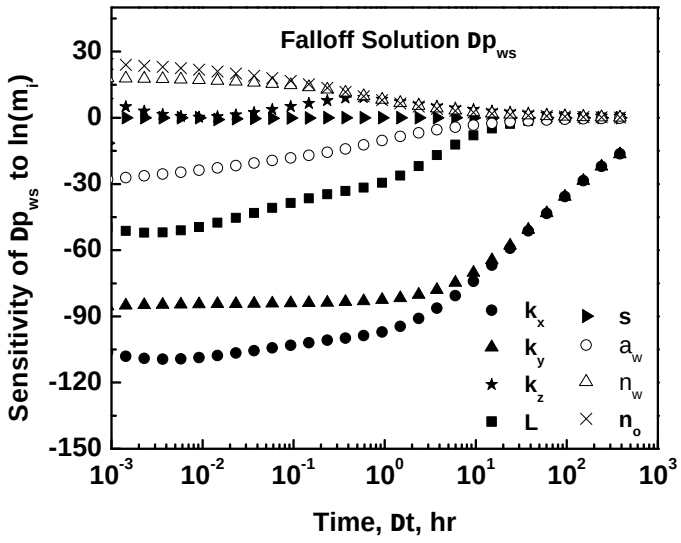

Figure 5.7: Sensitivity of the falloff solution to model parameters.

the vector of model parameters m were generated. They are displayed in Fig. 5.6 for the injectivity pressure change at the wellbore, $\Delta p = p_{wf} - p_i$ and in Fig. 5.7 for the falloff pressure change at the wellbore, $\Delta p_{ws} = p_{ws} - p_i$. Intuitively, these sensitivities suggest that at least for this test, the use of injection and falloff data may resolve the model parameters considered in this study. A very simplistic way to look at this problem is to determine qualitatively how each term in the general solution contributes in resolving the model parameters. By considering only the single-phase solution as observed data, Eqs. 5.38 and 5.39 suggest that $\bar{k}L_n = \sqrt{k_x k_z}L$ can be determined through the semi-log slope. During the linear flow regime, the parameter $\sqrt{\bar{k}}L_n h_n = \sqrt{k_x}hL$ can also be determined (see Eq. 5.41). Therefore, combining these two parameters enables us to resolve not only for the permeability k_z but also for the mechanical skin factor s through Eqs. 5.38 and 5.41. Once the second radial flow regime is established, the only information obtained from the pressure data according to Eq. 5.44 is $\bar{k}h_n = \sqrt{k_x k_y}h$, or equivalently $\sqrt{k_x k_y}$ assuming the thickness of the reservoir, h, known. Although the single-phase solution, if allowed to reach the second radial flow regime, can resolve the parameters $\bar{k}$, L_n and h_n in the new coordinate system, the parameters in the real coordinate system, that is the permeabilities k_x and k_y and the length of the well L, will not be resolved. Later, we will illustrate this fact in a numerical example.

Adding the contribution of the multiphase component by considering injection and falloff solutions as observed data in the nonlinear regression will give at least some information on the permeability k_x when the water moves radially in the (x, z) plane at the beginning of the test. This is illustrated by Eq. 2.174 obtained during the first linear/first radial flow regime. We rewrite this equation for an anisotropic case as

$$\Delta p = \Delta p_o + \frac{\alpha q_{inj}}{2\bar{k}L_n\hat{\lambda}_o}\left[\left(\frac{\bar{k}}{\bar{k}_s}-1\right)\int_{r_{we}^2/4t}^{r_{sn}^2/4t}\left(\frac{\hat{\lambda}_o}{\lambda_t(Z)}-1\right)\frac{dZ}{Z}+\int_{r_{we}^2/4t}^{Z_f}\left(\frac{\hat{\lambda}_o}{\lambda_t(Z)}-1\right)\frac{dZ}{Z}\right]. \quad (5.48)$$

If we assume that the skin zone is completely swept by water, $\lambda_t(Z) \approx \hat{\lambda}_w$ and Eq. 5.48 becomes

$$\Delta p = \Delta p_o + \frac{\alpha q_{inj}}{2\bar{k}L_n\hat{\lambda}_o}\left[2\left(\frac{\bar{k}}{\bar{k}_s}-1\right)\left(\frac{\hat{\lambda}_o}{\hat{\lambda}_w}-1\right)\ln\left(\frac{r_{sn}}{r_{we}}\right)+\int_{r_{we}^2/4t}^{Z_f}\left(\frac{\hat{\lambda}_o}{\lambda_t(Z)}-1\right)\frac{dZ}{Z}\right], \quad (5.49)$$

or simply,

$$\Delta p = \Delta p_o + \frac{\alpha q_{inj}}{2\bar{k}L_n\hat{\lambda}_o}\left[2\left(\frac{\hat{\lambda}_o}{\hat{\lambda}_w}-1\right)s+\int_{r_{we}^2/4t}^{Z_f}\left(\frac{\hat{\lambda}_o}{\lambda_t(Z)}-1\right)\frac{dZ}{Z}\right], \quad (5.50)$$

if Hawkin's formula for mechanical skin factor is used. Taking the derivative of Eq. 5.50 with respect to the natural logarithm of time using Leibnitz's rule gives

$$\Delta p' = \Delta p'_o + \frac{\alpha q_{inj} t}{2\bar{k}L_n\hat{\lambda}_o}\left[-\left(\frac{\hat{\lambda}_o}{\lambda_t(r_{we}^2/4t)}-1\right)\left(\frac{4t}{r_{we}^2}\right)\left(-\frac{r_{we}^2}{4t^2}\right)\right], \quad (5.51)$$

which reduces to

$$\Delta p' = \Delta p'_o + \frac{\alpha q_{inj}}{2\bar{k}L_n\hat{\lambda}_o}\left(\frac{\hat{\lambda}_o}{\lambda_t(r_{we},t)}-1\right). \quad (5.52)$$

The derivative of the single-phase solution with respect to logarithm of time based on oil properties at irreducible water saturation is given by

$$\Delta p'_o = \frac{\alpha q_{inj}}{2\sqrt{k_x}Lh\hat{\lambda}_o}\sqrt{\frac{4\pi\beta\hat{\lambda}_o t}{\phi\hat{c}_{to}}}. \quad (5.53)$$

Then, using Eq. 5.53 in Eq. 5.52 and rearranging gives

$$\Delta p' = \frac{\alpha q_{inj}}{2\sqrt{k_x}Lh\hat{\lambda}_o}\left[\sqrt{\frac{4\pi\beta\hat{\lambda}_o t}{\phi\hat{c}_{to}}}+\frac{h}{\sqrt{k_z}}\left(\frac{\hat{\lambda}_o}{\lambda_t(r_{we},t)}-1\right)\right]. \quad (5.54)$$

This equation clearly indicates that r_{we} through $\lambda_t(r_{we},t)$ is the only unknown since $\sqrt{k_x}L$ and k_z are resolved by the single-phase flow solution. Recall that the effective wellbore radius, r_{we} is defined by

$$r_{we} = \frac{r_w}{2}\left(\sqrt{\frac{\bar{k}}{k_x}}+\sqrt{\frac{\bar{k}}{k_z}}\right). \quad (5.55)$$

	k_x (mD)	k_y (mD)	k_z (mD)	s	L (ft)	a_w	n_w	n_o
Maximum	6000	6000	6000	15.	10000.	0.8	4.	4.
Minimum	1.	1.	1.	$-1.$	50.	0.1	1.	1.

Table 5.2: Maximum and minimum values of model parameters.

Therefore, we believe that k_x is resolved through the effective wellbore radius r_{we}. With k_x determined, the permeability k_y may be resolved from $\sqrt{k_x k_y}$. Finally, given $\bar{k}$ and L_n, the length of the well in the real coordinate system, that is L, can be resolved from Eq. 5.32.

5.3 Synthetic Examples

In all the examples considered in this section, The test consisted of a 24 hour period of injection followed by a 24 hour period of falloff. Both injection and falloff pressure data were used in the nonlinear regression. Random Gaussian noise with a mean of zero and a variance of $\sigma^2 = 0.25^2$ psi^2 was generated and added to synthetic pressure data (referred to as true data) obtained with the input of Table 5.1. The resulting noisy data represent the observed data. The maximum and minimum of model parameters used for the computations are shown in Table 5.2. The prior model parameters, using as starting values (guess) in the optimization algorithm, are given in Table 5.3 along with the true model parameters and the model estimates for each testing scenario considered.

5.3.1 Single-Phase Solution Case

The purpose of this example is to demonstrate the fact that the permeability k_z and the skin factor s are the only parameters that can be resolved using the single-phase flow pressures as observed data in the nonlinear regression.

Fig. 5.8 displays the normalized objective function during the Levenberg-Marquardt iterative process. The normalized objective function is defined as the objective function

	k_x (mD)	k_y (mD)	k_z (mD)	s	L (ft)	a_w	n_w	n_o
True value	4500	2700	300	5.	1312.4	0.5	2.0	2.5
Prior model	2000	2000	100	2.	1000	0.6	1.5	2.0
single-phase flow $z_w = 5$ ft	3664.3	3315.8	299.1	5.01	1455.03	–	–	–
1 day injection/ 1 day falloff $z_w = 5$ ft	4544.1	2678.2	303.41	5.0213	1303.3	0.4999	2.0051	2.5184
1 day injection/ 1 day falloff $z_w = 39.34$ ft	4341.1	2800.8	298.75	4.9845	1335.3	0.4959	1.9561	2.4758
9 days injection/ 9 days falloff $z_w = 39.34$ ft	4530.6	2682.4	300.1	5.0003	1308.1	0.4981	2.0228	2.4786

Table 5.3: Estimations of model parameter based on single and two-phase flow solution.

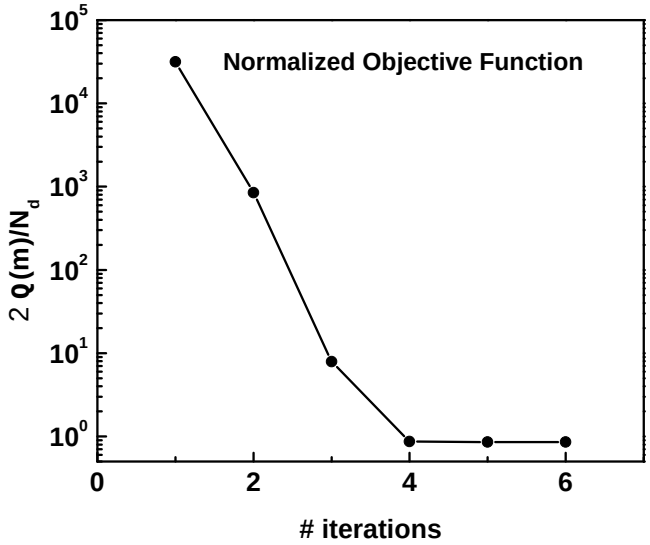

Figure 5.8: Normalized objective function for the single-phase flow case.

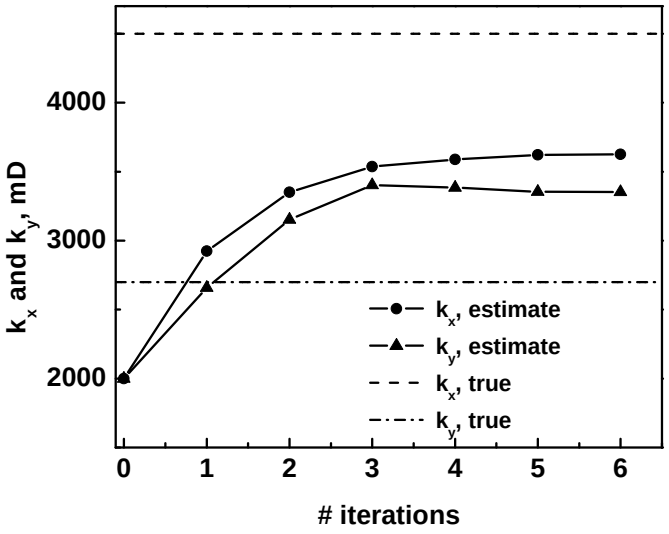

Figure 5.9: Estimates of permeabilities k_x and k_y for the single-phase flow case.

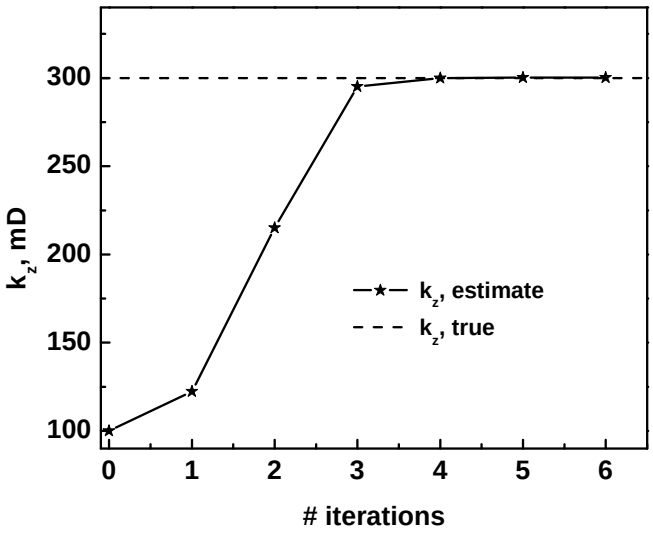

Figure 5.10: Estimates of permeability k_z for the single-phase flow case.

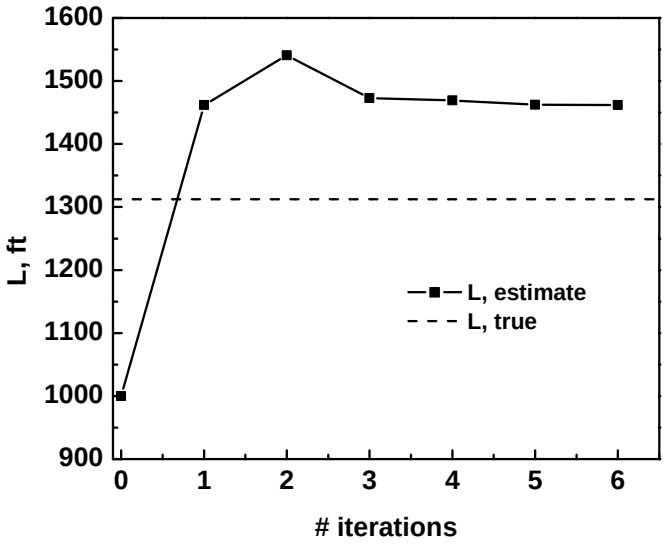

Figure 5.11: Estimates of the well length L for the single-phase flow case.

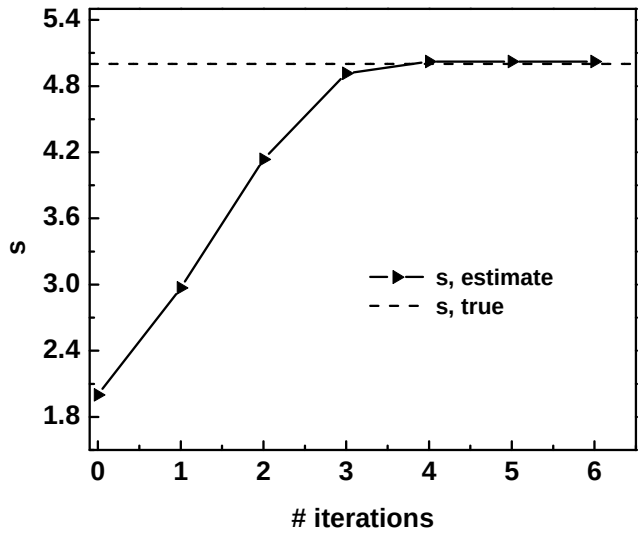

Figure 5.12: Estimates of the mechanical skin factor s for the single-phase flow case.

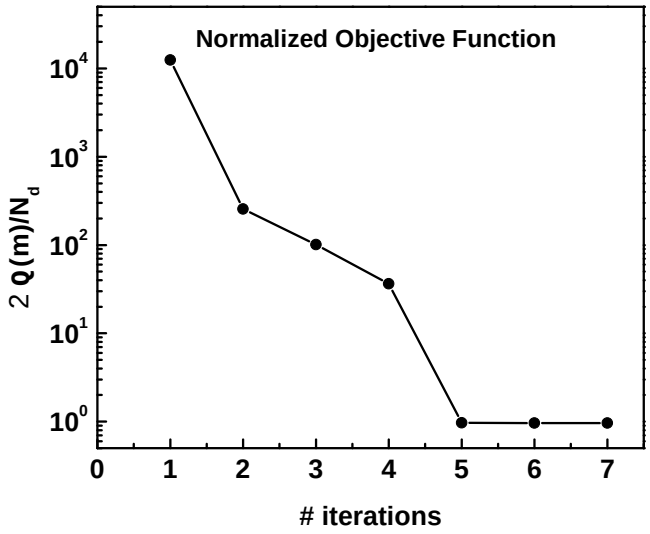

Figure 5.13: Normalized objective function for the two-phase flow case, $z_w = 5$ ft.

given by Eq. 5.6 divided by $N_d/2$, where N_d represents the number of observed data used in the history matching. In general, when convergence is reached, the normalized objective function should reach a value close to 1 assuming there is no modeling error in the system. Fig. 5.8 indicates that the convergence for this case is reached after 6 iterations. The estimates of the model parameters k_x, k_y, k_z, L and s at each iteration are shown in Figs. 5.9- 5.12 where they are represented by curves through data points. In the same figures, the horizontal dashed or dotted lines are the true values and the iteration 0 corresponds to the initial guess. The model parameters obtained at convergence are given in Table 5.2. From Figs. 5.9- 5.12, we see that except for the vertical permeability, k_z, and the skin factor, s, we do not obtain a good estimate of the other parameters. Based on an earlier discussion, this result was expected.

5.3.2 Two-Phase Solution Cases

A case of injection of water through a horizontal well was considered where water was also injected for a period of one day followed by a shut-in of one day. This case pertains to a well located at $z_w = 5$ ft from the top reservoir boundary. Based on our Buckley-Leverett computations, the water front begins to move in the x-direction

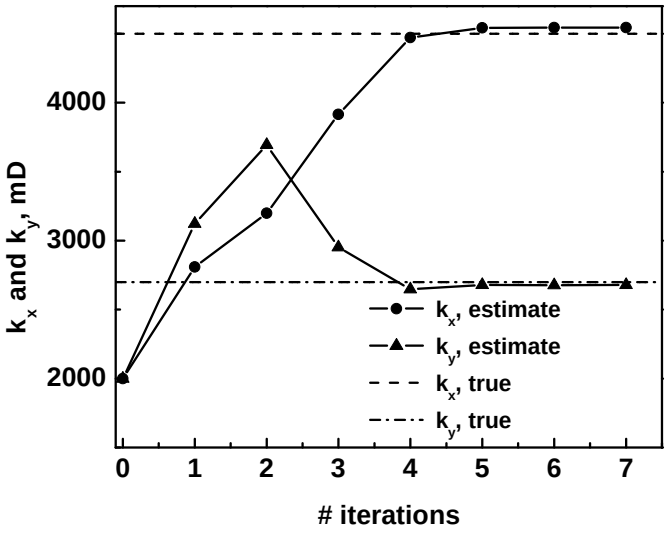

Figure 5.14: Estimates of permeabilities k_x and k_y for the two-phase flow case, $z_w = 5$ ft.

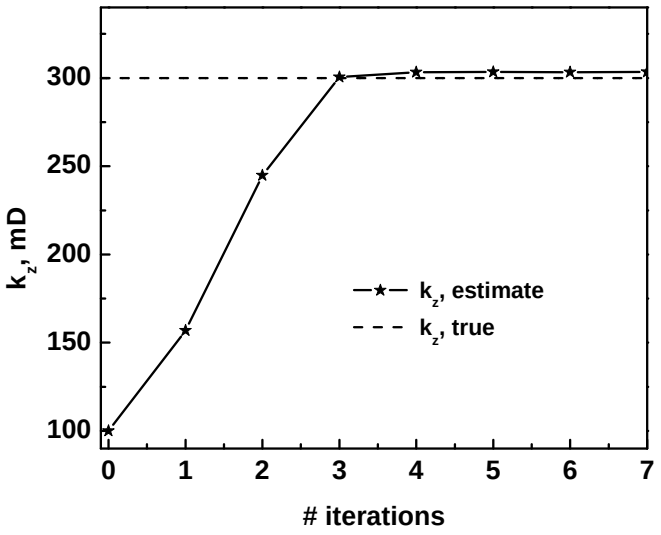

Figure 5.15: Estimates of permeability k_z for the two-phase flow case, $z_w = 5$ ft.

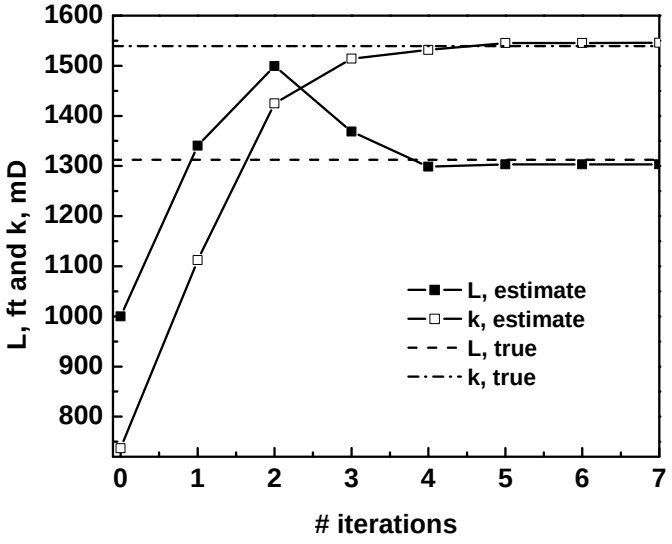

Figure 5.16: Estimates of the well length L and the equivalent isotropic permeability $\bar{k}$ for the two-phase flow case, $z_w = 5$ ft.

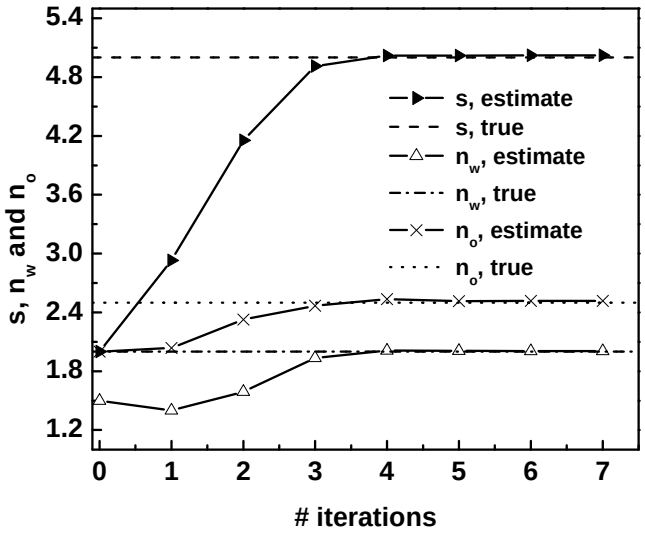

Figure 5.17: Estimates of the mechanical skin factor s and the water and oil exponents n_w and n_o for the two-phase flow case, $z_w = 5$ ft.

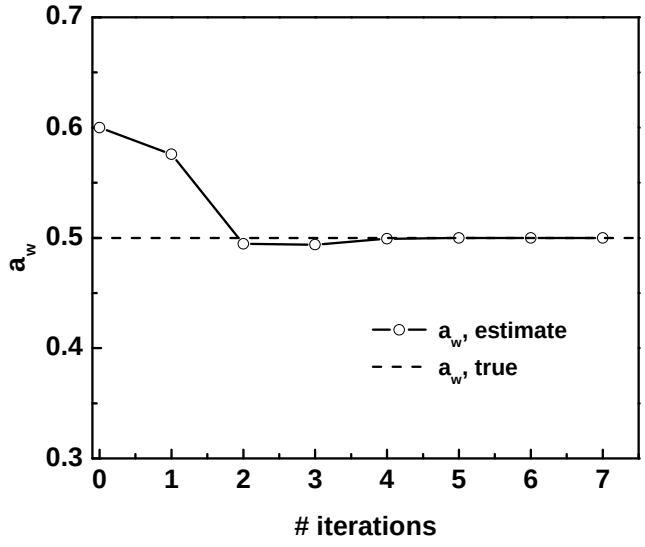

Figure 5.18: Estimates of the end-point water relative permeability a_w for the two-phase flow case, $z_w = 5$ ft.

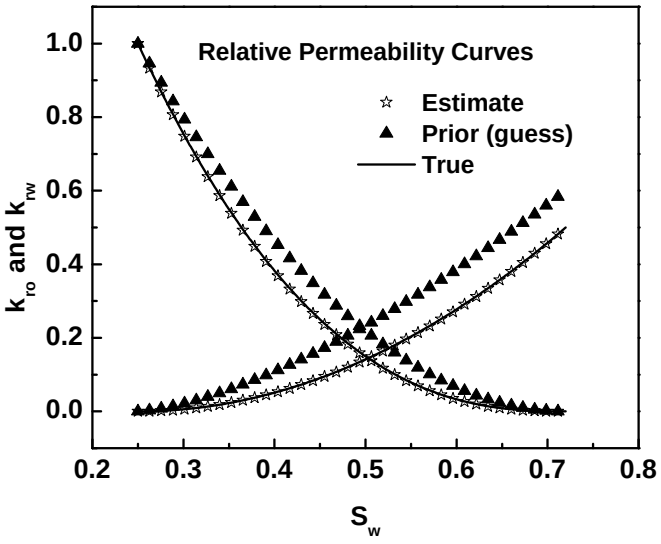

Figure 5.19: Estimate of relative permeability curves from the two-phase flow case, $z_w = 5$ ft.

right before the instant of shut-in. That means that the multiphase component during injection, Δp_λ, or during falloff, $\Delta p_{\lambda s}$, has two contributions: a pressure drop due to the radial movement of water in the (x, z) plane and a second pressure drop due to the linear propagation of water in the x-direction (see Eqs. 5.26 and 5.29). In Fig. 5.13, we show the behavior of the optimization algorithm through the normalized objective function. The convergence was achieved after 7 iterations. We give the values of all the eight model parameters obtained at the last iteration in Table 5.3, whereas, Figs. 5.14 to 5.18 show their estimations, iteration by iteration. Note that the values of $\bar{k}$, the equivalent isotropic permeability, displayed in Fig. 5.16, were not obtained by considering $\bar{k}$ as a model parameter in the nonlinear regression but rather from the estimates of k_x, k_y and k_z through Eq. 5.28. Fig. 5.19 shows the estimated relative permeability curves in open stars compared to the true curves in solid lines and to the initial guess represented by solid triangles. All these figures indicate that unlike the single-phase case, excellent estimates of all model parameters are obtained.

The injectivity solution for the pressure change and its derivative with respect to $\ln(t)$ obtained with the estimated model parameters is represented in Fig. 5.20 by open star dots. Also shown in this figure are the solutions generated with the true model and the initial guess in solid line and solid triangle dots respectively. The solid circle dots are the observed data, i.e., the true data with random noise added to them. Note that in the matching process, we matched only the pressure data, not the pressure derivatives. These were obtained by performing a numerical differentiation on the corresponding pressure change data generated. The results for the falloff period are shown in Fig. 5.21 where the same legend is used. Note that the pressure change considered in this plot are with respect to the wellbore injection pressure at the instant of shut-in, that is $\Delta p_s = p_{wf,s} - p_{ws}$, and that the pressure derivatives are obtained with respect to the logarithm of Agarwal's equivalent time. For both periods, the predicted pressure-pressure derivative data match very well the synthetic data used in the regression.

We believe that the accuracy of the estimation of the model parameters for this particular case resulted from the fact that the duration of the test was long enough for the

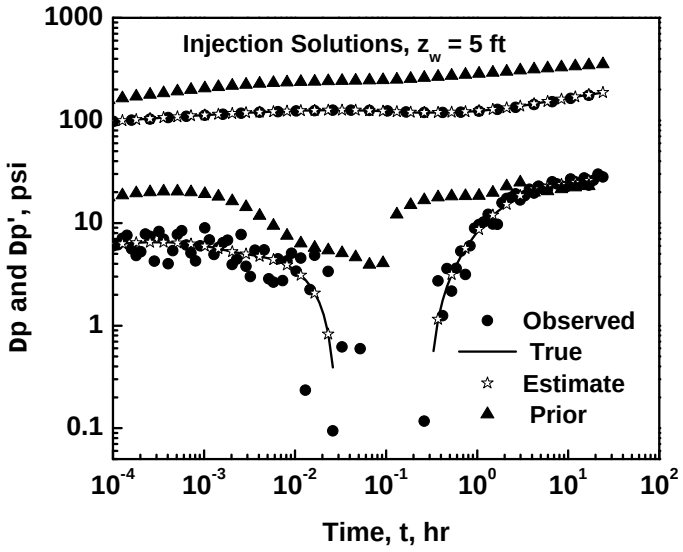

Figure 5.20: Match of injectivity solution for the pressure change and its derivative, $z_w = 5$ ft.

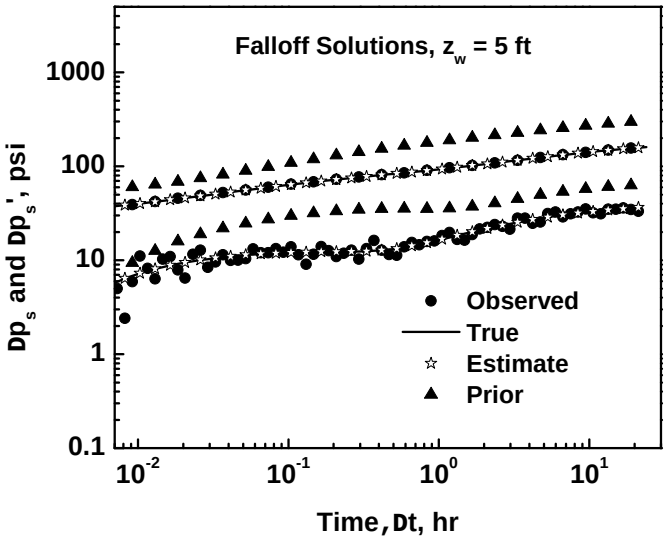

Figure 5.21: Match of falloff solution for the pressure change and its derivative, $z_w = 5$ ft.

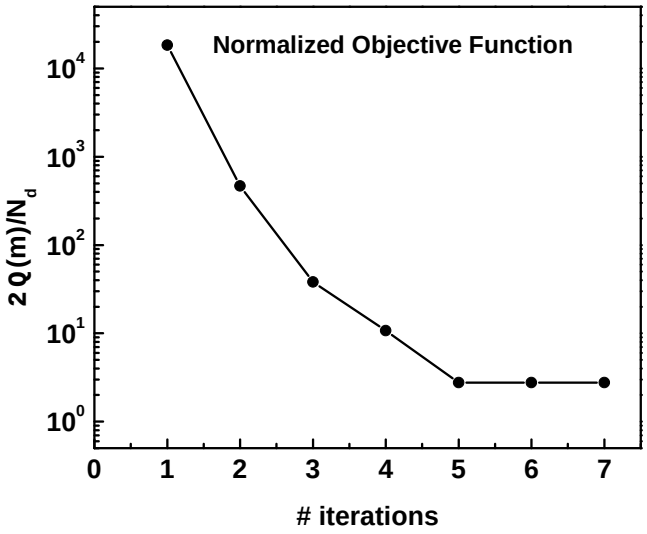

Figure 5.22: Normalized objective function for the two-phase flow case, $z_w = 39.34$ ft.

diffusion to reach the second radial flow regime during which the semi-log slope reflects $\sqrt{k_x k_y}$. With the accurate estimate of k_z obtained from the single-phase part of the solution and k_x obtained from the multiphase component, we can resolve k_y and L.

The next case consisted of a similar test sequence (24 hour injection/24 hour falloff) with a horizontal well located in the center of the formation, i.e., $z_w = 39.34$ ft. Note that at the instant of shut-in, the water front is still moving radially in the (x, z) plane according to Buckley-Leverett equations.

Fig. 5.22 displays the normalized objective function during the iterative process. This figure indicates that unlike the preceding case, the normalized objective function is not as close to 1 when convergence is reached. The estimates of all the eight model parameters during each iteration are shown in Figs. 5.23 to 5.27. The estimates at the last iteration are summarized in Table.5.3. While an accurate estimate of k_z, s and the parameters a_w, n_w and n_o involved in the construction of the relative permeability curves shown in Fig. 5.28 was achieved, we did not obtain good estimates of k_x, k_y and L when considering this test even though the permeability in the new coordinate system, that is $\bar{k}$, was resolved during the nonlinear regression (see Fig. 5.25). The missing information

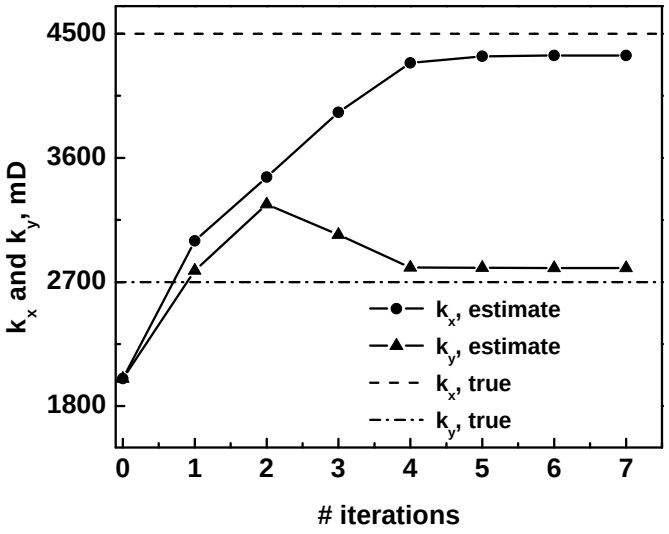

Figure 5.23: Estimates of permeabilities k_x and k_y for the two-phase flow case, $z_w = 39.34$ ft.

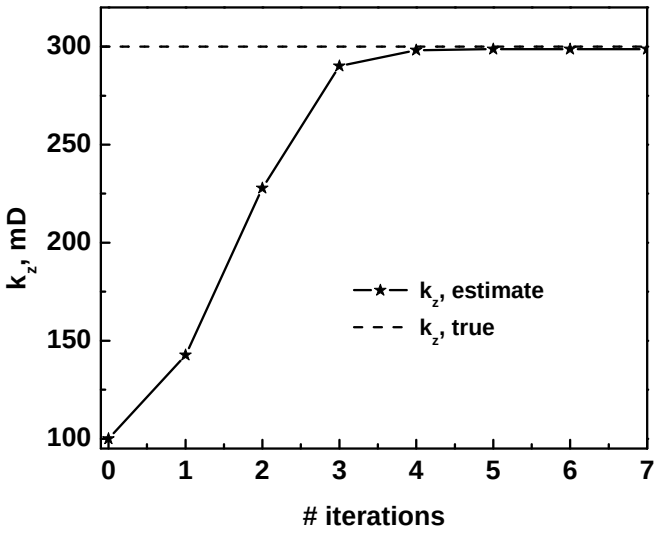

Figure 5.24: Estimates of permeability k_z for the two-phase flow case, $z_w = 39.34$ ft.

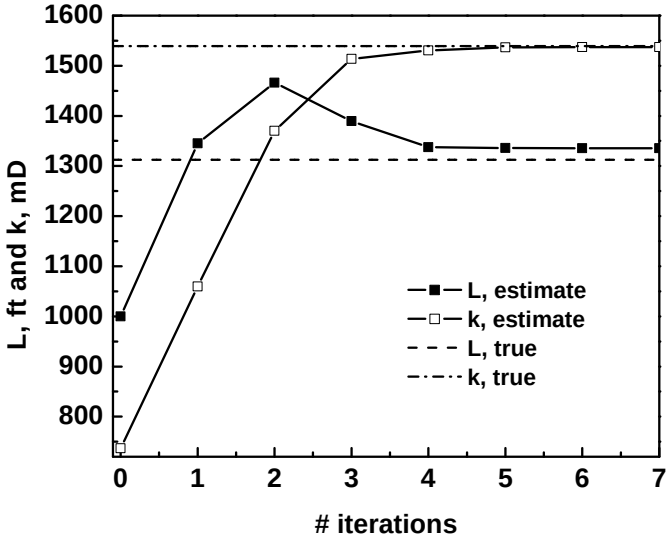

Figure 5.25: Estimates of the well length L and the equivalent isotropic permeability $\bar{k}$ for the two-phase flow case, $z_w = 39.34$ ft.

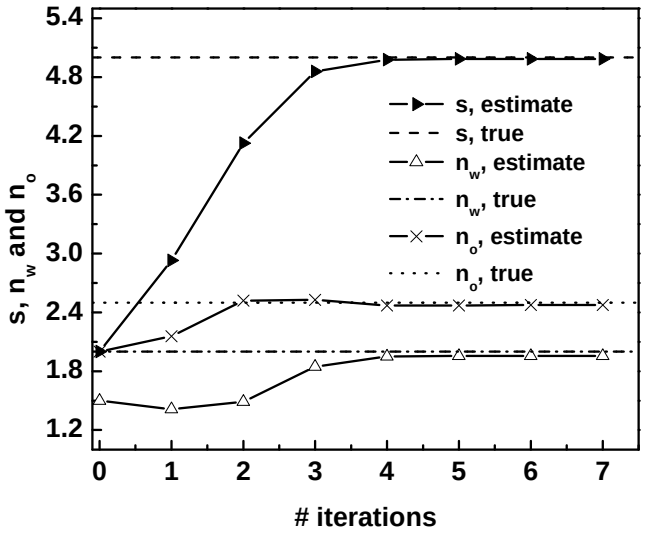

Figure 5.26: Estimates of the mechanical skin factor s and the water and oil exponents n_w and n_o for the two-phase flow case, $z_w = 39.34$ ft.

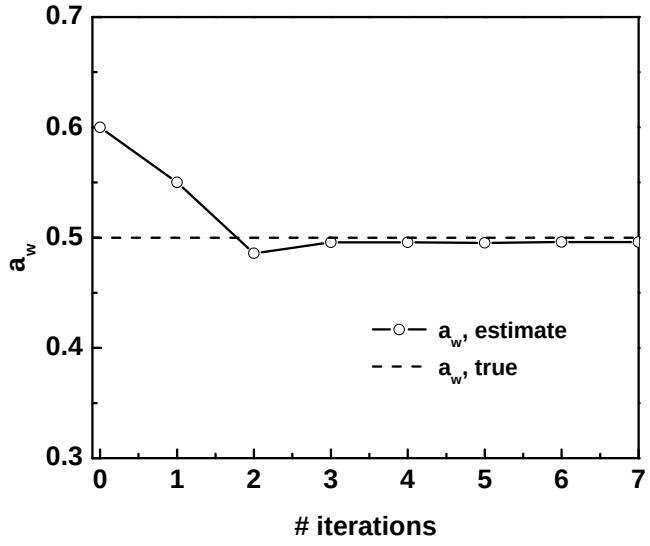

Figure 5.27: Estimates of the end-point water relative permeability a_w for the two-phase flow case, $z_w = 39.34$ ft.

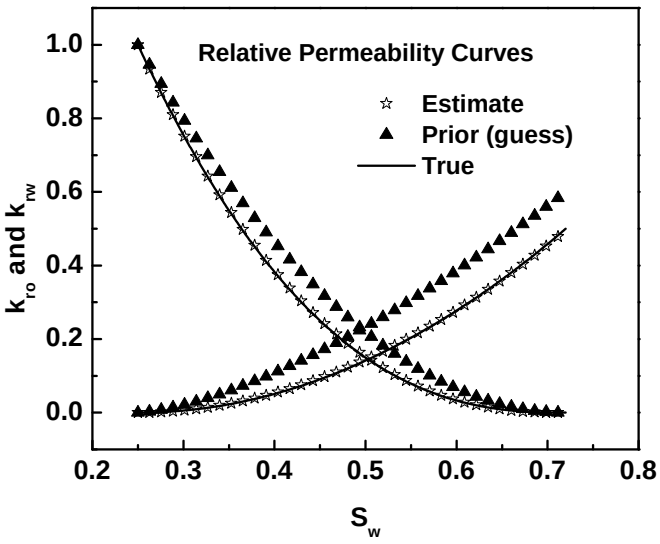

Figure 5.28: Estimate of relative permeability curves from the two-phase flow case, $z_w = 39.34$ ft.

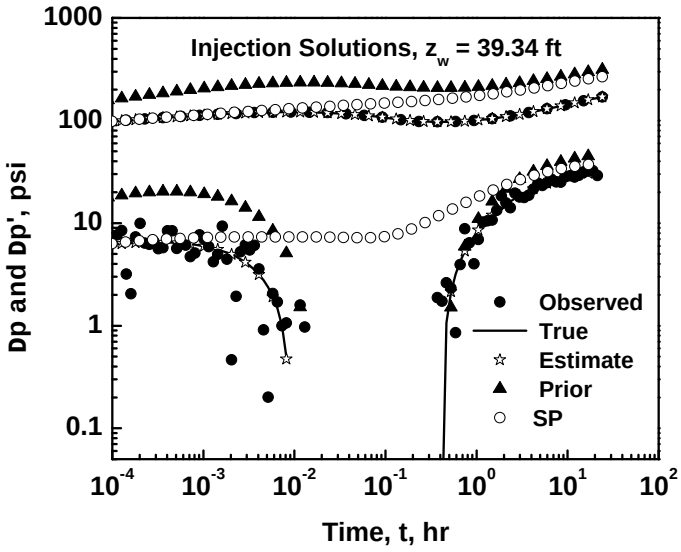

Figure 5.29: Match of injectivity solution for the pressure change and its derivative, $z_w = 39.34$ ft.

for this case, compared to the first case, is the term $\sqrt{k_x k_y}$, usually obtained from the single-phase solution during the second radial flow regime (late times). In Figs. 5.29 and 5.30, the open circle dots represent the single-phase solution obtained with the true model during injection and falloff periods. As can be seen on these diagnostic plots, the second radial flow regime does not occur. This is the reason that estimates of the parameters k_x, k_y and L are not as good as the parameters obtained when the well was close to the top boundary of the reservoir. Having said that, it is clear that this does not affect the injection and falloff solutions generated with the estimated model parameters since the flow is governed by $\bar{k}L_n = \sqrt{k_x k_z}L$, a parameter which is resolved during the regression. Figs. 5.29 and 5.30 show the two-phase injectivity and falloff solutions generated with the estimated model compared to the true and observed data. As expected, the synthetic data are matched very well.

For the same case, we extended the injection period to 9 days to allow the single-phase solution to reach the second radial flow regime. Then, the well was put to shut-in for 9 days. At the instant of shut-in, the water front did not hit the top and bottom reservoir boundaries. According to the radial advance Buckley-Leverett equation, this situation

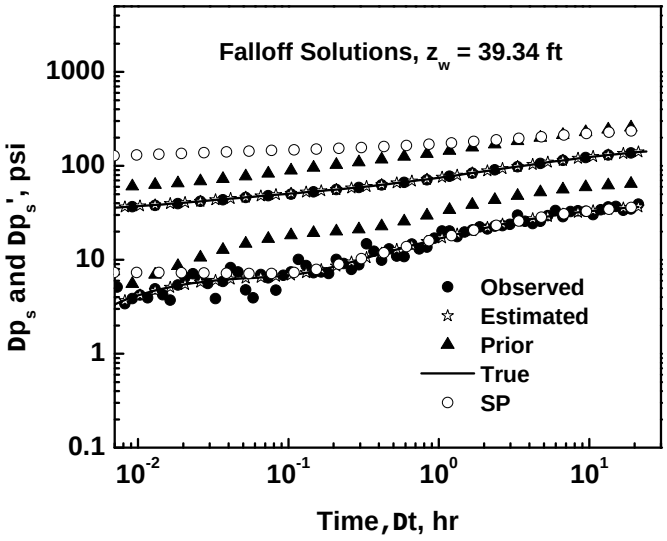

Figure 5.30: Match of falloff solution for the pressure change and its derivative, $z_w = 39.34$ ft.

occurs after 11 days of continuous injection. The last row of Table 5.3 gives the values of all eight model parameters obtained when convergence of the optimization algorithm was reached. As expected, these estimates are excellent. Again, the resolution of all three permeabilities is due to the fact that the late time data which contain information on the semi-log slope that reflects the product $\sqrt{k_x k_y}$ were added into the nonlinear regression. This also means that the location of the flood front at the instant of shut-in does not play a major role in resolving the model parameters as long as the duration of the test is long enough to permit the diffusion to reach the second radial flow regime.

CHAPTER 6

DISCUSSION AND CONCLUSIONS

In this work, we have addressed the issue of the effect of the two-phase flow on well-test data by examining the pressure response at vertical and horizontal water-injection wells. Although the approximate analytical solutions for the pressure response that we constructed are based on simplifying assumptions such as no wellbore storage effects, no gravity and capillary pressure effects, infinite acting reservoir, operating above the bubble point pressure and uniform initial water saturation distribution, these solutions enhanced our understanding of the behavior of injectivity and falloff tests on vertical and horizontal wells. Based on this study, the following comments are made:

Approximate analytical solutions for the injection pressure at vertical and horizontal water injection wells have been developed based on the steady-state theory of Thompson and Reynolds [34]. These solutions are in terms of the single-phase solution based on oil properties at irreducible water saturation plus an additional multiphase component due to the contrast, in the region invaded by injected water, between total mobility and oil mobility at irreducible water saturation. Since single-phase flow analytical solutions for the problems of our interest are readily available, determining the two-phase flow solution is reduced to determining the additional multiphase component. Generation of the multiphase component is done by combining different one-dimensional Buckley-Leverett frontal advance equations. This requires models for the movement of water in order to map the water saturation distributions in the reservoir.

For restricted-entry vertical wells, we have proposed two different models for the movement of water. When used to generate the saturation and mobility profiles necessary for the evaluation of the approximate analytical solution, both models give reasonable results when compared to results generated from the black oil simulator IMEX [1], although

the model where water is allowed to move along a variable thickness in the inner region gives more accurate results.

Our analytical solution provides insight into the behavior of injectivity tests for the restricted-entry vertical well case. We demonstrated that during the flow period which corresponds to when both the single-phase solution and the flood front propagate radially in the region $r < r_c$, the injection data can highly be affected if the well is damaged as a drastic decrease of the pressure change is observed (negative pressure derivative). During this flow period the pressure derivative is given by Eq. 2.90 that we rewrite here as

$$\Delta p' = \frac{\alpha q_{inj}}{2kh_p\hat{\lambda}_w}, \tag{6.1}$$

assuming the skin zone is completely swept with water such that $\lambda_t(r_s, t) = \hat{\lambda}_w$. Even though Eq. 2.90 indicates it is possible to see a semi-log straight line slope inversely proportional to $kh_p\hat{\lambda}_w$ at early times, the data from the synthetic examples considered in this study did not reflect such a line. For this semi-log slope to be apparent, the vertical permeability k_z has to be very small assuming negligible wellbore storage effects which, in practice, is unlikely to occur. Once the diffusion propagates in the region $r > r_c$ while the water front is still moving in the region $r < r_c$, our analytical solution predicts a pressure derivative (see Eq. 2.114) which can take negative values if the following condition holds:

$$\hat{M}(1 - b) > 1. \tag{6.2}$$

This was verified numerically when considering an unfavorable mobility ratio example which shows that the pressure derivatives remained negative throughout most of the injectivity test and never reached the late time semi-log slope inversely proportional to $kh\hat{\lambda}_w$ predicted by our analytical solution.

For horizontal wells, the solution of Peres and Reynolds [28] was generalized to an unequal offset configuration and anisotropic permeability. Similar to the restricted-entry vertical well case, two models for the movement of water have been developed in which water saturation distributions were mapped using a combination of a radial

frontal advance Buckley-Leverett equation in the (x, z) plane at early time, a linear frontal advance equation in the x-direction with a variable thickness during intermediate times and a second radial frontal equation in the (x, y) plane at late times. Our proposed models seem to deliver results that match accurately data obtained synthetically by the mean of the simulator except for the time period corresponding to when the water front starts to move radially in the (x, y) plane. As the first radial and first linear flow regimes may last a few hundreds of hours for problems of interest, this limitation does not obviate the use of the analytical solution in practice.

Similar to the vertical well case, the early time data may be affected if a thick skin region exists. Our analytical solution, confirmed by simulator results, show that the pressure derivative becomes negative for some combinations of the end-point mobility ratio, $\hat{M}$, and the ratio k_s/k. Once the skin zone is swept by water, analytical results, confirmed by numerical results show that, unlike in the vertical well case, there is a correlation between the injectivity solution and the single-phase flow solution based on oil properties at irreducible water saturation throughout most of the injectivity test.

A second objective was to construct solutions for the falloff response subsequent to water injection at a vertical or horizontal well. Two methods were presented in this work. The first one is based on the steady-state theory of Thompson and Reynolds combined with rate superposition. In this method, approximate analytical solutions for wellbore pressure change are also presented as the sum of the single-phase flow solution based on oil properties at irreducible water saturation and a multiphase component due to the contrast between initial total mobility $\hat{\lambda}_o$ and the total mobility in the invaded zone. The evaluation of the multiphase component requires not only the knowledge of the total mobility profiles but also the knowledge of the flow rate distributions in the reservoir during the shut-in period. Using the assumption that the total mobility distribution in the reservoir during falloff is equal to the total mobility profile that exists at the instant of shut-in and extending rate superposition equations for 1D single-phase flow problems in an ad hoc way to generate rate profiles during the shut-in period, we have constructed approximate solutions for the wellbore pressure change for both restricted-entry vertical

wells and horizontal wells which are in reasonable agreement with those generated with the simulator IMEX.

In the second approach, we have applied a first order perturbation in both total mobility and total compressibility in the invaded zone of the reservoir to solve the complete initial-boundary value problem for a radial flow case. Our analytical solutions for the falloff pressure are presented in a power-series expansion with a leading term which contains the important features of the solution while further terms describe the deviation in the solution due to the variation of the water saturation in the system. Although the comparison of our solutions for wellbore pressure change and total rate profiles to corresponding results obtained from the numerical simulator showed quite good agreements, we believe that better results can be achieved using the perturbation method if the numerical inversion is improved.

We need to point out that mechanical skin effect was not included into the analysis when solving for the falloff pressure using perturbation method. In order to include skin, the IBVP which describes the system, needs to be solved with an additional zone, $r_w < r < r_s$, where the absolute permeability k is replaced by the skin permeability k_s. However, this does not constitute a limitation to the use of our analytical solutions for practical purposes. The reason is that during shut-in, the zero rate propagates from the wellbore into the reservoir. This zero rate will pass through the damaged zone in a very short period of time such that there will be no effect of the presence of a skin zone on the wellbore pressure change during shut-in, except at extremely early times.

In deriving approximate injection and falloff solutions, we have assumed that the effect of capillary pressure and gravity on the pressure solutions were not significant. Although incorporating capillary pressure would yield a smearing of the flood front, it has been shown (see [4]), based on a numerical study, that it has a negligible effect on the injection/falloff response. This is reasonable if we consider the multiphase component of the injection or falloff solution (see Eqs . 2.8 and 3.11 for example). In these integrals, the term $1/r$ appears so that the contrast between the single-phase oil terms and the multiphase terms has the greatest effect on the integrals near the wellbore region. Thus,

it is expected that the dispersive effects of capillary pressure on the pressure response would be small.

Gravity could have a significant effect on the pressure response if oil and water phases segregate. The segregation of the phases is expected to occur during the falloff period. Based on a sensitivity analysis that we conducted, we found that the effect of the segregation is not significant and takes a long time to affect the falloff wellbore pressures if injection rates are high, which are typically the rates considered in this work, and the injection time is sufficiently long so that the injected water results in a reasonably uniform saturation distribution with oil saturation close to residual.

We extended the approximate analytical solutions for the injection/falloff pressures at vertical and horizontal water injection wells in an isotropic reservoir to an anisotropic system. The trick here was to apply a spatial transformation to the anisotropic system, as suggested for instance in [9], to obtain an equivalent isotropic system with new properties for which analytical solutions developed for an isotropic permeability field can still be used to obtain the injection/falloff wellbore pressures in an anisotropic reservoir. This transformation was validated by the mean of single-phase flow solutions and our solutions for injection and falloff obtained analytically were checked against the simulator.

We also extended the approximate solutions to include the nonisothermal effects which occur when cold waterflooding a hot reservoir. We showed numerically that convection is the dominant process for heat transfer during an injection test, and similar to the injection solutions under isothermal conditions, the nonisothermal solutions are in terms of the single-phase solution based on oil properties at the initial temperature of the reservoir plus an additional multiphase pressure change term due to the contrast, in the region invaded by water, between total mobility and oil mobility at different temperatures of the system. Evaluation of the multiphase component is done by generating appropriate saturation distributions using nonisothermal Buckley-Leverett theory. Our analytical results, confirmed by numerical results generated using the simulator STARS, show that the pressure derivative data reflect a semi-log straight line slope inversely proportional to $kh\hat{\lambda}_{wc}$ at late times for vertical wells. The situation is somewhat different for horizon-

tal wells, where the nonisothermal injection solution for the wellbore pressure change is virtually identical to the isothermal solution.

To solve the falloff problem, we made the assumption that conduction is the only dominant cause of temperature changes in the system. We also assumed that the flood front remains stationary during shut-in, an assumption that we verified numerically using the simulator. Under these conditions, we were able, based on the conservation of energy equation, to mathematically model the temperature changes in the reservoir and in the wellbore in particular. The temperature equation was solved using a perturbation method and temperature profiles were generated at different shut-in times. These profiles, which match fairly well the profiles obtained from STARS, clearly indicate that the temperature front will eventually dissipate as a consequence of the system recovering its original temperature. Solutions for the falloff pressure response were also constructed using rate superposition extended to the two-phase problem. As predicted by our analytical solution, the pressure derivative data reflect water properties at the temperature of the injected fluid at early times and oil properties at the initial temperature of the formation at late times, results that are in accordance with the simulator. These results pertain to a radial flow case. The falloff solution for the horizontal well case is not shown. As at the date of this writing, we have been unable to provide a theoretical derivation for the falloff pressure solution which takes into account the temperature changes for this case.

Our final objective was to provide a practical analysis procedure for injection/falloff testing of water injection wells. Using non-linear regression based on the Levenberg-Marquardt optimization algorithm, we analyzed injection/falloff data with our analytical solutions used to construct the predicted pressure response. By applying this approach to synthetic data obtained for the case of horizontal wells, we showed we were able to find good estimates of the absolute permeabilities of the reservoir, the mechanical skin factor, the length of the well and the relative permeability curves assuming a power law model as long as the duration of the injection test is long enough to permit the diffusion to reach the second radial flow regime, regardless of the position of the water front at the instant of shut-in.

BIBLIOGRAPHY

[1] *IMEX Version 2000 User's Guide*. Computer Modeling Group, Ltd., Calgary, 2000.

[2] *STARS Version 2006 User's Guide*. Computer Modeling Group, Ltd., Calgary, 2006.

[3] Y. Abacioglu, D. S. Oliver, and A. C. Reynolds. Efficient reservoir history matching using subspace vectors. *Computational Geosciences*, 5(2):151–172, 2001.

[4] M. Abbaszadeh and M. Kamal. Pressure-transient testing of water injection wells. *SPE Reservoir Engineering*, 4(1):115–124, 1989.

[5] R. Banerjee, L. G. Thompson, and A. C. Reynolds. Injection/falloff testing in heterogeneous reservoirs. *SPE Reservoir Evaluation & Engineering*, 1(6):519–527, 1998.

[6] T. Barkve. Nonisothermal effects in water-injection well tests. *SPEFE*, pages 281–286, June 1989.

[7] T. Barkve. The riemann problem for a nonstrictly hyperbolic system modeling nonisothermal, two-phase flow in a porous medium. *SIAM Journal on Applied Mathematics*, 49(3):784–798, June 1989.

[8] J. Bear. *Dynamics of Fluids in Porous Media*. American Elsevier Publishing Company, Inc., New York, 1972.

[9] J. Besson. Performance of slanted and horizontal wells in an anisotropic medium, SPE 20965. pages 219–231, 1990.

[10] R. B. Bird, W. E. Stewart, and E. N. Lightfoot. *Transport Phenomena*. John Wiley and Sons, Inc., 2002.

[11] R. B. Bratvold and R. N. Horne. Analysis of pressure-falloff tests following cold water injection. *SPE Formation Evaluation*, 5(3):293–302, 1990.

[12] Reidar Bratvold. *An Analytical Study of Pressure Response Following Cold Water Injection*. Ph.D. thesis, Stanford University, Stanford, California, 1989.

[13] W. E. Brigham. Discussion of productivity of a horizontal well (SPE 20394). *SPE Reservoir Engineering*, pages 254–255, 1990.

[14] H. S. Carslaw and J.C. Jaeger. *Conduction of Heat in Solids*. Oxford University Press, 1959.

[15] Shi Chen, Gaoming Li, and A. C. Reynolds. An in situ test for the estimation of two phase relative permeability curves. In *TUPREP Research Report 22*. The University of Tulsa, 2005.

[16] Shi Chen, Gaoming Li, and A. C. Reynolds. An in situ test for the estimation of t relative permeabilities: An approximate analytical solution for the wellbore pressure. In *TUPREP Research Report 23*. The University of Tulsa, 2006.

[17] Shi Chen and A. C. Reynolds. Numerical well testing for multiphase flow problems. *TUPREP Research Report 21*, pages 310–355, 2004.

[18] J. C. Deppe. The effect of mobility ratio, area swept and pattern. *Soc. Petrol. Eng. J.*, 1(2):81–91, 1961.

[19] Guohua Gao and A. C. Reynolds. An improved implementation of the LBFGS algorithm for automatic history matching. *SPE Journal*, 11(1):5–17, 2006.

[20] P. A. Goode and R. K. M. Thambynayagam. Pressure drawdown and buildup analysis of horizontal wells in anisotropic media. *SPE Formation Evaluation*, 2(4):683–697, 1987.

[21] M. F. Jr. Hawkins. A note on the skin effect. *Trans. AIME*, 207:356–357, 1956.

[22] D. D. Joseph. *Stability of Fluid Motions II*. Springer-Verlag Berlin Heidelberg New York, 1976.

[23] F. J. Kuchuk, P. A. Goode, D. J. Wilkinson, and R. K. M. Thambynayagam. Pressure-transient behavior of horizontal wells with and without gas cap or aquifer. *SPE Formation Evaluation*, 6:86–94, 1991.

[24] Michael M. Levitan. Application of water injection/falloff tests for reservoir appraisal: New analytical solution method for two-phase variable rate problems, (SPE-77532). In *2002 SPE Annual Technical Conference and Exhibition*, 2002.

[25] A. S. Odeh and D. K. Babu. Transient flow behavior of horizontal wells: Pressure drawdown and buildup analysis. *SPE Formation Evaluation*, 5(1):7–15, 1990.

[26] A. M. M. Peres and A. C. Reynolds. Injectivity and falloff tests on horizontal wells. TUPREP report, The University of Tulsa, 2001.

[27] A. M. M. Peres and A. C. Reynolds. Theory and analysis of injectivity tests on horizontal wells SPE 71582. In *Proceedings of the 2001 SPE Annual Technical Conference and Exhibition*, 2001.

[28] A. M. M. Peres and A. C. Reynolds. Theory and analysis of injectivity tests on horizontal wells. *SPE J.*, 8(2):147–159, 2003.

[29] A. M. M. Peres, A. C. Reynolds, A. Boughrara, and S. Chen. Some theoretical results on injection/falloff testing of vertical and horizontal wells. *TUPREP Research Report 20*, pages 162–230, 2003.

[30] R. J. Platenkamp. Temperature distribution around water injectors: Effects on injection performance (SPE 13746). *SPE J.*, 1985.

[31] R. Raghavan. *Well Test Analysis*. P T R Prentice Hall Inc., New Jersey, 1993.

[32] B. Temple. Global solution of the cauchy problem for a class of 2 by 2 nonstrictly hyperbolic conservation laws. *Advanced in Applied Mathematics*, 3:335–375, 1982.

[33] L. G. Thompson and A. C. Reynolds. Pressure transient analysis for gas condensate reservoirs. *In Situ*, 21(2):101–144, 1997.

[34] L. G. Thompson and A. C. Reynolds. Well testing for radially heterogeneous reservoirs under single and multiphase flow conditions. *SPE Formation Evaluation*, 12(1):57–64, 1997.

[35] E.J. Witterholt and M.P. Tixier. Temperature logging in injection wells (SPE 4022). *SPE*, 1972.

[36] D. K. Woodward and R. K. M. Thambynayagam. Pressure buildup and falloff analysis of water injection wells (SPE-12344). In *Unsolicited Manuscript*, page 44, 1983.

[37] Nai-Shong Yeh and A. C. Reynolds. Computation of the pseudoskin factor for a restricted-entry well completed in a multilayer reservoir. *SPE Formation Evaluation*, 4(2):253–263, 1989.

APPENDIX A

RADIUS OF CONVERGENCE

To obtain an expression for the radius of convergence, r_c, we approximate the convergence of flow lines using two concentric radial regions under single-phase flow regions. In the inner region $r < r_c$ the thickness $h(r)$ is variable and in the outer region $r > r_c$ the thickness is equal to the total reservoir thickness, h. At the interface, r_c, we require continuity of the pressure. We also assume long time behavior meaning that the constant total rate steady-state radius is beyond the radius of convergence.

For single-phase flow, we can compute the pressure drop between two points based on Darcy's law

$$dp = \frac{\alpha q B \mu}{k} \frac{dr}{r h(r)}. \tag{A.1}$$

Specifically, the pressure drop between a radius r, such that $r < r_c$ and the wellbore radius r_w is obtained by integrating Eq. A.1 as follows

$$\int_{p_{wf}}^{p(r)} dp = p(r) - p_{wf} = \frac{\alpha q B \mu}{k} \int_{r_w}^{r} \frac{1}{r h(r)}\, dr, \tag{A.2}$$

where p_{wf} represents the bottom hole flowing pressure and α is a constant which depends on the units system used. In field units, $\alpha = 141.2$. Dimensionless radius and dimensionless pressure for a single-phase flow are defined by

$$r_D = \frac{r}{r_w}, \tag{A.3}$$

and

$$p_D(r_D, t_D) = \frac{kh}{\alpha q B \mu}(p_i - p(r,t)). \tag{A.4}$$

Adding and subtracting to Eq. A.2 the initial reservoir pressure, p_i , and multiplying the resulting equation by $kh/(\alpha q B \mu)$, it follows that

$$p_{wD} - p_D(r_D, t_D) = \int_{r_w}^{r} \frac{h}{rh(r)}\, dr, \tag{A.5}$$

where, here, p_{wD} is the dimensionless wellbore pressure obtained by replacing $p(r)$ in Eq. A.4 by p_{wf}.

At late times, we have pseudo-radial flow and the dimensionless wellbore pressure is given by

$$p_{wD} = \frac{1}{2}\ln\left(\frac{4t_D}{e^{\gamma}}\right) + s_b, \tag{A.6}$$

where γ represents the Euler's constant ($\gamma = 0.57722...$) and s_b is the pseudo-skin factor due to the restricted-entry. The dimensionless time t_D is defined by

$$t_D = \frac{\beta k t}{\phi \mu c_t r_w^2}, \tag{A.7}$$

where β is a constant which depends on the system of units used. If oil field units with time in hours are used, then $\beta = 2.637 \times 10^{-4}$. Using Eq. A.6 in Eq. A.5 and then solving for $p_D(r_D, t_D)$ gives

$$p_D(r_D, t_D) = \frac{1}{2}\ln\left(\frac{4t_D}{e^{\gamma}}\right) + s_b - \int_{r_w}^{r} \frac{h}{rh(r)}\, dr. \tag{A.8}$$

For radial distances greater than the convergence radius, that is for $r > r_c$, the solution for the dimensionless pressure is given by the line source solution which at late times can be approximated by

$$p_D(r_D, t_D) = \frac{1}{2}\ln\left(\frac{4t_D}{e^{\gamma} r_D^2}\right). \tag{A.9}$$

At the interface $r = r_c$, the pressure must be continuous, i.e., Eqs. A.8 and A.9 must give the same value of p_D. Equating these two equations with $r = r_c$ gives

$$\frac{1}{2}\ln\left(\frac{4t_D}{e^\gamma}\right) + s_b - \int_{r_w}^{r_c} \frac{h}{rh(r)}\,dr = \frac{1}{2}\ln\left(\frac{4t_D}{e^\gamma r_{cD}^2}\right), \tag{A.10}$$

or

$$\ln(r_{cD}) = \int_{r_w}^{r_c} \frac{h}{rh(r)}\,dr - s_b, \tag{A.11}$$

where r_{cD} is the dimensionless radius of convergence obtained by replacing r in Eq. A.3 by r_c. For model 1, Eq. A.11 reduces to

$$\ln(r_{cD}) = \int_{r_w}^{r_c} \frac{h}{h_p r}\,dr - s_b = \frac{h}{h_p}\ln\left(\frac{r_c}{r_w}\right) - s_b. \tag{A.12}$$

Introducing the penetration ratio b defined by Eq. 2.38 in Eq. A.12 and simplifying gives

$$r_{cD} = \exp\left(\frac{bs_b}{1-b}\right), \tag{A.13}$$

or in terms of r_c

$$r_c = r_w \exp\left(\frac{bs_b}{1-b}\right). \tag{A.14}$$

The derivation for the radius of the convergence for model 2 is similar, but the algebra is slightly more complicated. For model 2, $h(r)$ is given by Eq. 2.35, repeated here as

$$h(r) = h + (\frac{h-h_p}{r_c-r_w})(r-r_c). \tag{A.15}$$

In this case, integrating Eq. A.11 yields

$$\ln(r_{cD}) = \int_{r_w}^{r_c} \frac{h}{h + (\frac{h-h_p}{r_c-r_w})(r-r_c)}\,\frac{dr}{r} - s_b = (r_c - r_w)\int_{r_w}^{r_c} \frac{1}{(1-b)r + (br_c - r_w)}\,\frac{dr}{r} - s_b. \tag{A.16}$$

or after rearranging,

$$\ln(r_{cD}) = (r_c - r_w)\int_{r_w}^{r_c} \frac{1}{(1-b) + (br_c - r_w)\frac{1}{r}} \frac{dr}{r^2} - s_b. \tag{A.17}$$

By making the following change of variable:

$$u = (1-b) + (br_c - r_w)\frac{1}{r}, \tag{A.18}$$

it is easy to show that Eq. A.17 becomes

$$\ln(r_{cD}) = \frac{(r_c - r_w)}{(r_w - br_c)} \int_{b(\frac{r_c}{r_w}-1)}^{1-\frac{r_w}{r_c}} \frac{du}{u} - s_b, \tag{A.19}$$

which yields

$$\ln(r_{cD}) = \frac{(r_c - r_w)}{(r_w - br_c)} \ln\left(\frac{1-\frac{r_w}{r_c}}{b(\frac{r_c}{r_w}-1)}\right) - s_b. \tag{A.20}$$

If we express Eq. A.20 in terms of r_{cD}, we obtain

$$\ln(r_{cD}) = -\frac{r_{cD}-1}{1-br_{cD}} \ln(br_{cD}) - s_b, \tag{A.21}$$

or equivalently,

$$\frac{(b-1)r_{cD}}{1-br_{cD}} \ln(r_{cD}) = s_b + \left(\frac{r_{cD}-1}{1-br_{cD}}\right) \ln(b). \tag{A.22}$$

Unlike the formula that we have for the convergence radius in model 1 (Eq. A.14), Eq. A.22 is nonlinear and needs to be solved numerically in order to get the dimensionless convergence radius.

Many formulas have been proposed for the pseudo-skin factor due to restricted-entry. We will use the one presented by [37]. For the case of a homogeneous reservoir, this formula is equivalent to

$$s_b = \frac{1-b}{b}\Big(\ln\big(C'(1-b)h_{wD}\big) - C_1\Big), \tag{A.23}$$

where

$$C_1 = 0.481 + 1.01b - 0.838b^2, \tag{A.24}$$

and

$$h_{wD} = \frac{h_p}{r_w}\sqrt{\frac{k}{k_z}}. \tag{A.25}$$

C' in Eq. A.23 is given by the graph shown in Fig. 6 of [37]. $C' = 2$ when the top of the perforated interval of the wellbore coincides with the top of the formation, or the bottom of the perforated interval coincides with the bottom of the formation. When the center of the open interval coincides with the midpoint (vertically) of the formation, $C' = 1$. For the configuration of model 1 and 2, $C' = 2$.

APPENDIX B

PERTURBATION METHOD

In this appendix, we present the complete derivation of the solution of the initial value boundary problem described by Eqs. 3.131 to 3.136 in Laplace space using a procedure based on perturbation method. In this framework, the approximate analytical solution for the falloff pressure is represented in a power-series expansion given by Eq. 3.182. A pressure solution will be derived in the inner region of the reservoir (invaded zone) as well as in the outer region (unevaded zone). These two solutions will be matched at the interface r_{fD} which represents the dimensionless location of the flood front at the instant of shut-in. In the following, we assume that the first three terms in the series of Eq. 3.182 are enough to adequately describe the falloff solution for the pressure. For simplicity, we do not consider skin effect ($\frac{k(r_D)}{k} = 1$ for $1 \leq r_D \leq r_{fD}$). If mechanical skin is considered, we will have to solve the IVBP in the following three regions: the skin zone $1 \leq r_D \leq r_{sD}$ for which the permeability is equal to k_s and the ratio $\frac{k(r_D)}{k} = \frac{k_s}{k}$, the water bank $r_{sD} \leq r_D \leq r_{fD}$ with $k(r_D) = k$ and the oil zone $r_D \geq r_{fD}$ where the permeability is also equal to k.

Inner Region Solution

The dimensionless falloff pressure in the region $r_D \leq r_{fD}$ is given by

$$\bar{p}_{D,in}(r_D, u) = \bar{p}_{D0,in} + \epsilon \bar{p}_{D1,in} + \delta \bar{p}_{D2,in}. \tag{B.1}$$

Substituting Eqs. 3.180 3.181 and B.1 into Eqs. 3.131 and 3.132 gives

$$\frac{1}{r_D}\frac{\partial}{\partial r_D}\left[(1-\epsilon f(r_D))r_D\frac{\partial}{\partial r_D}(\bar{p}_{D0,in}+\epsilon\bar{p}_{D1,in}+\delta\bar{p}_{D2,in})\right]= (1-\delta g(r_D))\left[u(\bar{p}_{D0,in}+\epsilon\bar{p}_{D1,in}+\delta\bar{p}_{D2,in})-f_1(r_D)\right], \quad \text{(B.2)}$$

and

$$r_D\frac{\partial}{\partial r_D}(\bar{p}_{D0,in}+\epsilon\bar{p}_{D1,in}+\delta\bar{p}_{D2,in})\mid_{r_D=1}=0. \quad \text{(B.3)}$$

Expanding Eqs. B.2 and B.3 and dropping higher orders of ϵ and δ gives respectively

$$\frac{1}{r_D}\frac{\partial}{\partial r_D}\left(r_D\frac{\partial\bar{p}_{D0,in}}{\partial r_D}\right)+\epsilon\left[\frac{1}{r_D}\frac{\partial}{\partial r_D}\left(r_D\frac{\partial\bar{p}_{D1,in}}{\partial r_D}\right)-\frac{1}{r_D}\frac{\partial}{\partial r_D}\left(f(r_D)r_D\frac{\partial\bar{p}_{D0,in}}{\partial r_D}\right)\right] + \delta\frac{1}{r_D}\frac{\partial}{\partial r_D}\left(r_D\frac{\partial\bar{p}_{D2,in}}{\partial r_D}\right)= u\bar{p}_{D0,in}-f_1(r_D)+\epsilon u\bar{p}_{D1,in}+\delta\left(u\bar{p}_{D2,in}-ug(r_D)\bar{p}_{D0,in}+g(r_D)f_1(r_D)\right), \quad \text{(B.4)}$$

and

$$r_D\frac{\partial\bar{p}_{D0,in}}{\partial r_D}\bigg|_{r_D=1}+\epsilon r_D\frac{\partial\bar{p}_{D1,in}}{\partial r_D}\bigg|_{r_D=1}+\delta r_D\frac{\partial\bar{p}_{D2,in}}{\partial r_D}\bigg|_{r_D=1}=0. \quad \text{(B.5)}$$

A comparison of both sides of the two preceding equations yields the following three system of equations

The $O(1)$ system:

$$\frac{1}{r_D}\frac{\partial}{\partial r_D}\left(r_D\frac{\partial\bar{p}_{D0,in}}{\partial r_D}\right)-u\bar{p}_{D0,in}=-f_1(r_D), \quad \text{(B.6)}$$

$$r_D\frac{\partial\bar{p}_{D0,in}}{\partial r_D}\bigg|_{r_D=1}=0. \quad \text{(B.7)}$$

The $O(\epsilon)$ system:

$$\frac{1}{r_D}\frac{\partial}{\partial r_D}\left(r_D\frac{\partial \bar{p}_{D1,in}}{\partial r_D}\right) - u\bar{p}_{D1,in} = \frac{1}{r_D}\frac{\partial}{\partial r_D}\left(f(r_D)r_D\frac{\partial \bar{p}_{D0,in}}{\partial r_D}\right), \tag{B.8}$$

$$r_D\frac{\partial \bar{p}_{D1,in}}{\partial r_D}\bigg|_{r_D=1} = 0. \tag{B.9}$$

The $O(\delta)$ system:

$$\frac{1}{r_D}\frac{\partial}{\partial r_D}\left(r_D\frac{\partial \bar{p}_{D2,in}}{\partial r_D}\right) - u\bar{p}_{D2,in} = -g(r_D)\left(u\bar{p}_{D0,in} - f_1(r_D)\right), \tag{B.10}$$

$$r_D\frac{\partial \bar{p}_{D2,in}}{\partial r_D}\bigg|_{r_D=1} = 0. \tag{B.11}$$

First, we discuss the solution of the $O(1)$ system. It is a non-homogeneous second order differential equation whose solution is the sum of any particular solution $\bar{p}^p_{D0,in}$ and a corresponding homogeneous solution $\bar{p}^h_{D0,in}$ obtained by setting $f_1(r_D) = 0$. Thus, we have

$$\bar{p}_{D0,in} = \bar{p}^p_{D0,in} + \bar{p}^h_{D0,in}. \tag{B.12}$$

It is easy to show that the homogeneous solution to the $O(1)$ system is a combination of modified Bessel functions of zero order as follows:

$$\bar{p}^h_{D0,in} = c_1 I_0(\sqrt{u}r_D) + c_2 K_0(\sqrt{u}r_D), \tag{B.13}$$

where c_1 and c_2 are functions of the variable u to be determined later. In order to find a particular solution, we apply the variation of parameters technique which assumes for our case, a particular solution of the form

$$\bar{p}^p_{D0,in} = u_1(r_D,u)I_0(\sqrt{u}r_D) + u_2(r_D,u)K_0(\sqrt{u}r_D). \tag{B.14}$$

The functions u_1 and u_2 are underdetermined so we have the freedom to impose a constraint which simplifies subsequent equations. This constraint is chosen to be

$$u_1'(r_D,u)I_0(\sqrt{u}r_D)+u_2'(r_D,u)K_0(\sqrt{u}r_D)=0, \tag{B.15}$$

where u_1' and u_2' are the derivatives of u_1 and u_2 with respect to r_D. The general solution to the $O(1)$ system is then given by the following expression

$$\bar{p}_{D0,in}=c_1I_0(\sqrt{u}r_D)+c_2K_0(\sqrt{u}r_D)+u_1(r_D,u)I_0(\sqrt{u}r_D)+u_2(r_D,u)K_0(\sqrt{u}r_D). \tag{B.16}$$

Next, we differentiate Eq. B.16 with respect to r_D to obtain

$$\begin{aligned}\frac{\partial\bar{p}_{D0,in}}{\partial r_D}=&c_1\sqrt{u}I_1(\sqrt{u}r_D)-c_2\sqrt{u}K_1(\sqrt{u}r_D)+u_1'(r_D,u)I_0(\sqrt{u}r_D)+\\&u_2'(r_D,u)K_0(\sqrt{u}r_D)+\sqrt{u}u_1(r_D,u)I_1(\sqrt{u}r_D)-\sqrt{u}u_2(r_D,u)K_1(\sqrt{u}r_D).\end{aligned} \tag{B.17}$$

Using the constraint defined by Eq. B.15, Eq. B.17 simplifies to

$$\begin{aligned}\frac{\partial\bar{p}_{D0,in}}{\partial r_D}=&c_1\sqrt{u}I_1(\sqrt{u}r_D)-c_2\sqrt{u}K_1(\sqrt{u}r_D)+\sqrt{u}u_1(r_D,u)I_1(\sqrt{u}r_D)-\\&\sqrt{u}u_2(r_D,u)K_1(\sqrt{u}r_D).\end{aligned} \tag{B.18}$$

Multiplying Eq. B.18 by r_D and differentiating the resulting expression yields

$$\frac{\partial}{\partial r_D}\left(r_D\frac{\partial \bar{p}_{D0,in}}{\partial r_D}\right) = \frac{\partial}{\partial r_D}\Bigg(c_1\sqrt{u}r_D I_1(\sqrt{u}r_D) - c_2\sqrt{u}r_D K_1(\sqrt{u}r_D) +$$
$$\sqrt{u}r_D u_1(r_D,u) I_1(\sqrt{u}r_D) - \sqrt{u}r_D u_2(r_D,u) K_1(\sqrt{u}r_D)\Bigg) =$$
$$c_1\sqrt{u}I_1(\sqrt{u}r_D) - c_2\sqrt{u}K_1(\sqrt{u}r_D) + \sqrt{u}u_1(r_D,u)I_1(\sqrt{u}r_D) -$$
$$\sqrt{u}u_2(r_D,u)K_1(\sqrt{u}r_D) + c_1 u r_D I_0(\sqrt{u}r_D) - c_1\sqrt{u}I_1(\sqrt{u}r_D) +$$
$$c_2 u r_D K_0(\sqrt{u}r_D) + c_2\sqrt{u}K_1(\sqrt{u}r_D) + \sqrt{u}r_D u_1'(r_D,u)I_1(\sqrt{u}r_D) +$$
$$u r_D u_1(r_D,u)I_0(\sqrt{u}r_D) - \sqrt{u}u_1(r_D,u)I_1(\sqrt{u}r_D) - \sqrt{u}r_D u_2'(r_D,u)K_1(\sqrt{u}r_D) +$$
$$u r_D u_2(r_D,u)K_0(\sqrt{u}r_D) + \sqrt{u}r_D u_2(r_D,u)K_1(\sqrt{u}r_D) =$$
$$c_1 u r_D I_0(\sqrt{u}r_D) + c_2 u r_D K_0(\sqrt{u}r_D) + \sqrt{u}r_D u_1'(r_D,u)I_1(\sqrt{u}r_D) + u r_D u_1(r_D,u)I_0(\sqrt{u}r_D) -$$
$$\sqrt{u}r_D u_2'(r_D,u)K_1(\sqrt{u}r_D) + u r_D u_2(r_D,u)K_0(\sqrt{u}r_D). \quad \text{(B.19)}$$

Replacing the result of Eq. B.19 and Eq. B.16 into Eq. B.6 gives

$$c_1 u I_0(\sqrt{u}r_D) + c_2 u K_0(\sqrt{u}r_D) + \sqrt{u}u_1'(r_D,u)I_1(\sqrt{u}r_D) + u u_1(r_D,u)I_0(\sqrt{u}r_D) -$$
$$\sqrt{u}u_2'(r_D,u)K_1(\sqrt{u}r_D) + u u_2(r_D,u)K_0(\sqrt{u}r_D) - u c_1 I_0(\sqrt{u}r_D) - u c_2 K_0(\sqrt{u}r_D) -$$
$$u u_1(r_D,u)I_0(\sqrt{u}r_D) - u u_2(r_D,u)K_0(\sqrt{u}r_D) = -f_1(r_D), \quad \text{(B.20)}$$

which simplifies to

$$\sqrt{u}u_1'(r_D,u)I_1(\sqrt{u}r_D) - \sqrt{u}u_2'(r_D,u)K_1(\sqrt{u}r_D) = -f_1(r_D). \quad \text{(B.21)}$$

The solution of the simultaneous equations given by Eqs. B.15 and B.21 for u_1' and u_2' is

$$u_1'(r_D,u) = \frac{1}{W}\begin{pmatrix} -f_1(r_D) & -\sqrt{u}K_1(\sqrt{u}r_D) \\ 0 & K_0(\sqrt{u}r_D) \end{pmatrix} = -\frac{1}{W}f_1(r_D)K_0(\sqrt{u}r_D), \quad \text{(B.22)}$$

$$u_2'(r_D,u)=\frac{1}{W}\begin{pmatrix}\sqrt{u}I_1(\sqrt{u}r_D) & -f_1(r_D)\\ I_0(\sqrt{u}r_D) & 0\end{pmatrix}=\frac{1}{W}f_1(r_D)I_0(\sqrt{u}r_D), \tag{B.23}$$

where W is the Wronskian defined by

$$W=\begin{pmatrix}\sqrt{u}I_1(\sqrt{u}r_D) & -\sqrt{u}K_1(\sqrt{u}r_D)\\ I_0(\sqrt{u}r_D) & K_0(\sqrt{u}r_D)\end{pmatrix}=$$

$$\sqrt{u}\Big(I_1(\sqrt{u}r_D)K_0(\sqrt{u}r_D)+I_0(\sqrt{u}r_D)K_1(\sqrt{u}r_D)\Big)=$$

$$\sqrt{u}\frac{1}{\sqrt{u}r_D}=\frac{1}{r_D}. \tag{B.24}$$

Integrating Eq. B.22 from r_D to r_{fD} gives

$$\int_{r_D}^{r_{fD}}u_1'(r_D,u)dr_D=-\int_{r_D}^{r_{fD}}\xi_D f_1(\xi_D)K_0(\sqrt{u}\xi_D)d\xi_D, \tag{B.25}$$

or

$$u_1(r_D,u)=u_1(r_{fD},u)+\int_{r_D}^{r_{fD}}\xi_D f_1(\xi_D)K_0(\sqrt{u}\xi_D)d\xi_D. \tag{B.26}$$

Similarly, if we integrate Eq. B.23 from 1 to r_D, we get

$$\int_{1}^{r_D}u_2'(r_D,u)dr_D=\int_{1}^{r_D}\xi_D f_1(\xi_D)I_0(\sqrt{u}\xi_D)d\xi_D, \tag{B.27}$$

or

$$u_2(r_D,u)=u_2(1,u)+\int_{1}^{r_D}\xi_D f_1(\xi_D)I_0(\sqrt{u}\xi_D)d\xi_D. \tag{B.28}$$

Now, if we replace Eqs. B.26 and B.28 into the general solution given by Eq. B.16, we obtain

$$\bar{p}_{D0,in} = c_1 I_0(\sqrt{u} r_D) + c_2 K_0(\sqrt{u} r_D) + \left[u_1(r_{fD}, u) + \int_{r_D}^{r_{fD}} \xi_D f_1(\xi_D) K_0(\sqrt{u}\xi_D) d\xi_D \right] I_0(\sqrt{u} r_D) + \left[u_2(1,u) + \int_1^{r_D} \xi_D f_1(\xi_D) I_0(\sqrt{u}\xi_D) d\xi_D \right] K_0(\sqrt{u} r_D), \quad \text{(B.29)}$$

or after rearranging

$$\bar{p}_{D0,in} = A_1 I_0(\sqrt{u} r_D) + A_2 K_0(\sqrt{u} r_D) + I_0(\sqrt{u} r_D) \int_{r_D}^{r_{fD}} \xi_D f_1(\xi_D) K_0(\sqrt{u}\xi_D) d\xi_D + K_0(\sqrt{u} r_D) \int_1^{r_D} \xi_D f_1(\xi_D) I_0(\sqrt{u}\xi_D) d\xi_D, \quad \text{(B.30)}$$

where for simplicity, the new constants A_1 and A_2 are introduced and defined respectively by

$$A_1 = c_1 + u_1(r_{fD}, u), \quad \text{(B.31)}$$

and

$$A_2 = c_2 + u_2(1, u). \quad \text{(B.32)}$$

Recall that the $O(1)$ system has an inner boundary condition given by Eq. B.7. If we substitute first Eqs. B.26 and B.28 into the expression for the derivative pressure given by Eq. B.18, we obtain

$$\frac{\partial \bar{p}_{D0,in}}{\partial r_D} = c_1 \sqrt{u} I_1(\sqrt{u} r_D) - c_2 \sqrt{u} K_1(\sqrt{u} r_D) + \sqrt{u} I_1(\sqrt{u} r_D) \left[u_1(r_{fD}, u) + \int_{r_D}^{r_{fD}} \xi_D f_1(\xi_D) K_0(\sqrt{u}\xi_D) d\xi_D \right] - \sqrt{u} K_1(\sqrt{u} r_D) \left[u_2(1,u) + \int_1^{r_D} \xi_D f_1(\xi_D) I_0(\sqrt{u}\xi_D) d\xi_D \right]. \quad \text{(B.33)}$$

Using the definitions given by Eqs. B.31 and B.32, Eq. B.33 becomes

$$\frac{\partial \bar{p}_{D0,in}}{\partial r_D} = A_1\sqrt{u}I_1(\sqrt{u}r_D) - A_2\sqrt{u}K_1(\sqrt{u}r_D) + \sqrt{u}I_1(\sqrt{u}r_D)\int_{r_D}^{r_{fD}} \xi_D f_1(\xi_D)K_0(\sqrt{u}\xi_D)d\xi_D - \sqrt{u}K_1(\sqrt{u}r_D)\int_1^{r_D} \xi_D f_1(\xi_D)I_0(\sqrt{u}\xi_D)d\xi_D. \quad \text{(B.34)}$$

At the wellbore,i.e., $r_D = 1$, we have

$$r_D\frac{\partial \bar{p}_{D0,in}}{\partial r_D} = 0, \quad \text{(B.35)}$$

which translates into

$$A_1\sqrt{u}I_1(\sqrt{u}) - A_2\sqrt{u}K_1(\sqrt{u}) + \sqrt{u}I_1(\sqrt{u})\int_1^{r_{fD}} \xi_D f_1(\xi_D)K_0(\sqrt{u}\xi_D)d\xi_D = 0, \quad \text{(B.36)}$$

or simply,

$$A_2 = A_1\frac{I_1(\sqrt{u})}{K_1(\sqrt{u})} + \frac{I_1(\sqrt{u})}{K_1(\sqrt{u})}\int_1^{r_{fD}} \xi_D f_1(\xi_D)K_0(\sqrt{u}\xi_D)d\xi_D. \quad \text{(B.37)}$$

Finally, substituting Eq. B.37 into Eq. B.30 and rearranging yields

$$\bar{p}_{D0,in} = \frac{A_1}{K_1(\sqrt{u})}\Big[K_1(\sqrt{u})I_0(\sqrt{u}r_D) + I_1(\sqrt{u})K_0(\sqrt{u}r_D)\Big] + \frac{I_1(\sqrt{u})}{K_1(\sqrt{u})}K_0(\sqrt{u}r_D)\int_1^{r_{fD}} \xi_D f_1(\xi_D)K_0(\sqrt{u}\xi_D)d\xi_D + K_0(\sqrt{u}r_D)\int_1^{r_D} \xi_D f_1(\xi_D)I_0(\sqrt{u}\xi_D)d\xi_D + I_0(\sqrt{u}r_D)\int_{r_D}^{r_{fD}} \xi_D f_1(\xi_D)K_0(\sqrt{u}\xi_D)d\xi_D. \quad \text{(B.38)}$$

Next, we move to the $O(\epsilon)$ system. Recall from Eqs. B.8 and B.9 that the ODE and the associated boundary condition that describe this system are given respectively by the following equations

$$\frac{1}{r_D}\frac{\partial}{\partial r_D}\left(r_D\frac{\partial \bar{p}_{D1,in}}{\partial r_D}\right) - u\bar{p}_{D1,in} = \frac{1}{r_D}\frac{\partial}{\partial r_D}\left(f(r_D)r_D\frac{\partial \bar{p}_{D0,in}}{\partial r_D}\right), \tag{B.39}$$

$$r_D\frac{\partial \bar{p}_{D1,in}}{\partial r_D}\bigg|_{r_D=1} = 0. \tag{B.40}$$

The right hand side of the above ODE is function of only the dimensionless radial distance r_D. Thus, we set

$$U(r_D) = -\frac{1}{r_D}\frac{\partial}{\partial r_D}\left(f(r_D)r_D\frac{\partial \bar{p}_{D0,in}}{\partial r_D}\right), \tag{B.41}$$

and Eq. B.39 becomes

$$\frac{1}{r_D}\frac{\partial}{\partial r_D}\left(r_D\frac{\partial \bar{p}_{D1,in}}{\partial r_D}\right) - u\bar{p}_{D1,in} = -U(r_D), \tag{B.42}$$

Note that Eq. B.42 is similar to Eq. B.6. Therefore, they have the same solution with $f_1(r_D)$ replaced by the function that we defined as $U(r_D)$. So, by analogy to Eq. B.30, we have

$$\bar{p}_{D1,in} = A_3 I_0(\sqrt{u}r_D) + A_4 K_0(\sqrt{u}r_D) + I_0(\sqrt{u}r_D)\int_{r_D}^{r_{fD}} \xi_D U(\xi_D) K_0(\sqrt{u}\xi_D)d\xi_D + K_0(\sqrt{u}r_D)\int_1^{r_D} \xi_D U(\xi_D) I_0(\sqrt{u}\xi_D)d\xi_D, \tag{B.43}$$

where A_3 and A_4 are the new constants of integration. If we use the expression of $U(r_D)$ given by Eq. B.41, we have

$$\int_1^{r_D} \xi_D U(\xi_D) I_0(\sqrt{u}\xi_D)d\xi_D = -\int_1^{r_D} \frac{\partial}{\partial \xi_D}\left(f(\xi_D)\xi_D\frac{\partial \bar{p}_{D0,in}}{\partial \xi_D}\right) I_0(\sqrt{u}\xi_D)d\xi_D. \tag{B.44}$$

Integrating Eq. B.44 by parts, we obtain

$$\int_1^{r_D} \xi_D U(\xi_D) I_0(\sqrt{u}\xi_D) d\xi_D = -\xi_D f(\xi_D) \frac{\partial \bar{p}_{D0,in}}{\partial \xi_D} I_0(\sqrt{u}\xi_D) \Big]_1^{r_D} + \sqrt{u} \int_1^{r_D} \xi_D f(\xi_D) \frac{\partial \bar{p}_{D0,in}}{\partial \xi_D} I_1(\sqrt{u}\xi_D) d\xi_D, \quad \text{(B.45)}$$

or simplifying using Eq. B.7,

$$\int_1^{r_D} \xi_D U(\xi_D) I_0(\sqrt{u}\xi_D) d\xi_D = -r_D f(r_D) \frac{\partial \bar{p}_{D0,in}}{\partial r_D} I_0(\sqrt{u} r_D) + \sqrt{u} \int_1^{r_D} \xi_D f(\xi_D) \frac{\partial \bar{p}_{D0,in}}{\partial \xi_D} I_1(\sqrt{u}\xi_D) d\xi_D. \quad \text{(B.46)}$$

Similarly, we have

$$\int_{r_D}^{r_{fD}} \xi_D U(\xi_D) K_0(\sqrt{u}\xi_D) d\xi_D = -\int_{r_D}^{r_{fD}} \frac{\partial}{\partial \xi_D} \left(f(\xi_D) \xi_D \frac{\partial \bar{p}_{D0,in}}{\partial \xi_D} \right) K_0(\sqrt{u}\xi_D) d\xi_D. \quad \text{(B.47)}$$

Integrating the above equation by parts yields

$$\int_{r_D}^{r_{fD}} \xi_D U(\xi_D) K_0(\sqrt{u}\xi_D) d\xi_D = -\xi_D f(\xi_D) \frac{\partial \bar{p}_{D0,in}}{\partial \xi_D} K_0(\sqrt{u}\xi_D) \Big]_{r_D}^{r_{fD}} - \sqrt{u} \int_{r_D}^{r_{fD}} \xi_D f(\xi_D) \frac{\partial \bar{p}_{D0,in}}{\partial \xi_D} K_1(\sqrt{u}\xi_D) d\xi_D, \quad \text{(B.48)}$$

or

$$\int_{r_D}^{r_{fD}} \xi_D U(\xi_D) K_0(\sqrt{u}\xi_D) d\xi_D = r_D f(r_D) \frac{\partial \bar{p}_{D0,in}}{\partial r_D} K_0(\sqrt{u} r_D) - r_{fD} f(r_{fD}) \frac{\partial \bar{p}_{D0,in}}{\partial r_D} \Big|_{r_{fD}} K_0(\sqrt{u} r_{fD}) - \sqrt{u} \int_{r_D}^{r_{fD}} \xi_D f(\xi_D) \frac{\partial \bar{p}_{D0,in}}{\partial \xi_D} K_1(\sqrt{u}\xi_D) d\xi_D. \quad \text{(B.49)}$$

Substituting Eqs. B.46 and B.49 into Eq. B.43, then rearranging and simplifying the

resulting equation gives

$$\bar{p}_{D1,in} = A_3 I_0(\sqrt{u}r_D) + A_4 K_0(\sqrt{u}r_D) - r_{fD} f(r_{fD}) \frac{\partial \bar{p}_{D0,in}}{\partial r_D}\bigg|_{r_{fD}} K_0(\sqrt{u}r_{fD}) I_0(\sqrt{u}r_D)$$
$$+ \sqrt{u} K_0(\sqrt{u}r_D) \int_1^{r_D} \xi_D f(\xi_D) \frac{\partial \bar{p}_{D0,in}}{\partial \xi_D} I_1(\sqrt{u}\xi_D) d\xi_D$$
$$- \sqrt{u} I_0(\sqrt{u}r_D) \int_{r_D}^{r_{fD}} \xi_D f(\xi_D) \frac{\partial \bar{p}_{D0,in}}{\partial \xi_D} K_1(\sqrt{u}\xi_D) d\xi_D, \quad \text{(B.50)}$$

which constitutes the general solution to the $O(\epsilon)$ system. The expression above contains two constants. In order to eliminate one constant, A_4 for instance, we need to apply the inner boundary condition given by Eq. B.40. We start by differentiating Eq. B.50 with respect to r_D as follows:

$$\frac{\partial \bar{p}_{D1,in}}{\partial r_D} = A_3 \sqrt{u} I_1(\sqrt{u}r_D) - A_4 \sqrt{u} K_1(\sqrt{u}r_D) - \sqrt{u} r_{fD} f(r_{fD}) \frac{\partial \bar{p}_{D0,in}}{\partial r_D}\bigg|_{r_{fD}} K_0(\sqrt{u}r_{fD}) I_1(\sqrt{u}r_D)$$
$$- u K_1(\sqrt{u}r_D) \int_1^{r_D} \xi_D f(\xi_D) \frac{\partial \bar{p}_{D0,in}}{\partial \xi_D} I_1(\sqrt{u}\xi_D) d\xi_D$$
$$- u I_1(\sqrt{u}r_D) \int_{r_D}^{r_{fD}} \xi_D f(\xi_D) \frac{\partial \bar{p}_{D0,in}}{\partial \xi_D} K_1(\sqrt{u}\xi_D) d\xi_D$$
$$+ \sqrt{u} r_D f(r_D) \frac{\partial \bar{p}_{D0,in}}{\partial r_D} K_0(\sqrt{u}r_D) I_1(\sqrt{u}r_D) + \sqrt{u} r_D f(r_D) \frac{\partial \bar{p}_{D0,in}}{\partial r_D} I_0(\sqrt{u}r_D) K_1(\sqrt{u}r_D). \quad \text{(B.51)}$$

Using the fact that

$$K_0(\sqrt{u}r_D) I_1(\sqrt{u}r_D) + I_0(\sqrt{u}r_D) K_1(\sqrt{u}r_D) = \frac{1}{\sqrt{u}r_D}, \quad \text{(B.52)}$$

Eq. B.51 becomes

$$\frac{\partial \bar{p}_{D1,in}}{\partial r_D} = A_3\sqrt{u}I_1(\sqrt{u}r_D) - A_4\sqrt{u}K_1(\sqrt{u}r_D) - \sqrt{u}r_{fD}f(r_{fD})\frac{\partial \bar{p}_{D0,in}}{\partial r_D}\bigg|_{r_{fD}} K_0(\sqrt{u}r_{fD})I_1(\sqrt{u}r_D)$$
$$- uK_1(\sqrt{u}r_D)\int_1^{r_D} \xi_D f(\xi_D)\frac{\partial \bar{p}_{D0,in}}{\partial \xi_D} I_1(\sqrt{u}\xi_D)d\xi_D$$
$$- uI_1(\sqrt{u}r_D)\int_{r_D}^{r_{fD}} \xi_D f(\xi_D)\frac{\partial \bar{p}_{D0,in}}{\partial \xi_D} K_1(\sqrt{u}\xi_D)d\xi_D + f(r_D)\frac{\partial \bar{p}_{D0,in}}{\partial r_D}. \quad \text{(B.53)}$$

At the wellbore, we have

$$\frac{\partial \bar{p}_{D1,in}}{\partial r_D}\bigg|_{r_D=1} = A_3\sqrt{u}I_1(\sqrt{u}) - A_4\sqrt{u}K_1(\sqrt{u}) - \sqrt{u}r_{fD}f(r_{fD})\frac{\partial \bar{p}_{D0,in}}{\partial r_D}\bigg|_{r_{fD}} K_0(\sqrt{u}r_{fD})I_1(\sqrt{u})$$
$$- uI_1(\sqrt{u})\int_1^{r_{fD}} \xi_D f(\xi_D)\frac{\partial \bar{p}_{D0,in}}{\partial \xi_D} K_1(\sqrt{u}\xi_D)d\xi_D = 0, \quad \text{(B.54)}$$

which yields

$$A_4 = A_3\frac{I_1(\sqrt{u})}{K_1(\sqrt{u})} - \frac{I_1(\sqrt{u})}{K_1(\sqrt{u})}r_{fD}f(r_{fD})\frac{\partial \bar{p}_{D0,in}}{\partial r_D}\bigg|_{r_{fD}} K_0(\sqrt{u}r_{fD})$$
$$- \sqrt{u}\frac{I_1(\sqrt{u})}{K_1(\sqrt{u})}\int_1^{r_{fD}} \xi_D f(\xi_D)\frac{\partial \bar{p}_{D0,in}}{\partial \xi_D} K_1(\sqrt{u}\xi_D)d\xi_D. \quad \text{(B.55)}$$

Finally, if we replace A_4 in Eq. B.50 by its expression provided above and rearrange, we obtain

$$\bar{p}_{D1,in} = \frac{A_3}{K_1(\sqrt{u})}\left[K_1(\sqrt{u})I_0(\sqrt{u}r_D) + I_1(\sqrt{u})K_0(\sqrt{u}r_D)\right]$$
$$- r_{fD}f(r_{fD})\frac{\partial \bar{p}_{D0,in}}{\partial r_D}\bigg|_{r_{fD}} \frac{K_0(\sqrt{u}r_{fD})}{K_1(\sqrt{u})}\left[K_1(\sqrt{u})I_0(\sqrt{u}r_D) + I_1(\sqrt{u})K_0(\sqrt{u}r_D)\right]$$
$$- \sqrt{u}\frac{I_1(\sqrt{u})}{K_1(\sqrt{u})}K_0(\sqrt{u}r_D)\int_1^{r_{fD}} \xi_D f(\xi_D)\frac{\partial \bar{p}_{D0,in}}{\partial \xi_D}K_1(\sqrt{u}\xi_D)d\xi_D$$
$$+ \sqrt{u}K_0(\sqrt{u}r_D)\int_1^{r_D} \xi_D f(\xi_D)\frac{\partial \bar{p}_{D0,in}}{\partial \xi_D}I_1(\sqrt{u}\xi_D)d\xi_D$$
$$- \sqrt{u}I_0(\sqrt{u}r_D)\int_{r_D}^{r_{fD}} \xi_D f(\xi_D)\frac{\partial \bar{p}_{D0,in}}{\partial \xi_D}K_1(\sqrt{u}\xi_D)d\xi_D. \quad \text{(B.56)}$$

Finally, we solve the $O(\delta)$ system. From Eqs. B.10 and B.11, we recall that ODE and the associated boundary condition that describe the system are given respectively by

$$\frac{1}{r_D}\frac{\partial}{\partial r_D}\left(r_D\frac{\partial \bar{p}_{D2,in}}{\partial r_D}\right) - u\bar{p}_{D2,in} = -g(r_D)\left(u\bar{p}_{D0,in} - f_1(r_D)\right), \quad \text{(B.57)}$$

$$r_D\frac{\partial \bar{p}_{D2,in}}{\partial r_D}\bigg|_{r_D=1} = 0. \quad \text{(B.58)}$$

we set

$$V(r_D) = g(r_D)\left(u\bar{p}_{D0,in} - f_1(r_D)\right). \quad \text{(B.59)}$$

Then, Eq. B.57 becomes

$$\frac{1}{r_D}\frac{\partial}{\partial r_D}\left(r_D\frac{\partial \bar{p}_{D2,in}}{\partial r_D}\right) - u\bar{p}_{D2,in} = -V(r_D), \quad \text{(B.60)}$$

which is again similar to Eq. B.6. Based on the previous results for the leading problem, we can write our general solution for the $O(\delta)$ system as

$$\bar{p}_{D2,in} = A_5 I_0(\sqrt{u}r_D) + A_6 K_0(\sqrt{u}r_D) + I_0(\sqrt{u}r_D)\int_{r_D}^{r_{fD}} \xi_D V(\xi_D) K_0(\sqrt{u}\xi_D) d\xi_D + K_0(\sqrt{u}r_D)\int_1^{r_D} \xi_D V(\xi_D) I_0(\sqrt{u}\xi_D) d\xi_D, \quad \text{(B.61)}$$

where A_5 and A_6 are the new constants of integration. Using the expression for $V(r_D)$ given by Eq. B.59, we have

$$\bar{p}_{D2,in} = A_5 I_0(\sqrt{u}r_D) + A_6 K_0(\sqrt{u}r_D) + I_0(\sqrt{u}r_D)\int_{r_D}^{r_{fD}} \xi_D g(\xi_D)\Big(u\bar{p}_{D0,in} - f_1(\xi_D)\Big) K_0(\sqrt{u}\xi_D) d\xi_D + K_0(\sqrt{u}r_D)\int_1^{r_D} \xi_D g(\xi_D)\Big(u\bar{p}_{D0,in} - f_1(\xi_D)\Big) I_0(\sqrt{u}\xi_D) d\xi_D. \quad \text{(B.62)}$$

Here, we also take the derivative of Eq. B.62 with respect to r_D and then apply the condition at the wellbore given by Eq. B.58. The first operation yields

$$\frac{\partial \bar{p}_{D2,in}}{\partial r_D} = A_5\sqrt{u} I_1(\sqrt{u}r_D) - A_6\sqrt{u} K_1(\sqrt{u}r_D) - \sqrt{u}K_1(\sqrt{u}r_D)\int_1^{r_D} \xi_D g(\xi_D)\Big(u\bar{p}_{D0,in} - f_1(\xi_D)\Big) I_0(\sqrt{u}\xi_D) d\xi_D + \sqrt{u}I_1(\sqrt{u}r_D)\int_{r_D}^{r_{fD}} \xi_D g(\xi_D)\Big(u\bar{p}_{D0,in} - f_1(\xi_D)\Big) K_0(\sqrt{u}\xi_D) d\xi_D. \quad \text{(B.63)}$$

The second operation on the other hand gives

$$\left.\frac{\partial \bar{p}_{D2,in}}{\partial r_D}\right|_{r_D=1} = A_5\sqrt{u} I_1(\sqrt{u}) - A_6\sqrt{u} K_1(\sqrt{u}) + \sqrt{u}I_1(\sqrt{u})\int_1^{r_{fD}} \xi_D g(\xi_D)\Big(u\bar{p}_{D0,in} - f_1(\xi_D)\Big) K_0(\sqrt{u}\xi_D) d\xi_D = 0, \quad \text{(B.64)}$$

which yields

$$A_6 = A_5 \frac{I_1(\sqrt{u})}{K_1(\sqrt{u})} + \frac{I_1(\sqrt{u})}{K_1(\sqrt{u})} \int_1^{r_{fD}} \xi_D g(\xi_D) \Big(u\bar{p}_{D0,in} - f_1(\xi_D) \Big) K_0(\sqrt{u}\xi_D) d\xi_D. \quad \text{(B.65)}$$

Using Eq. B.65 in Eq. B.62 gives

$$\begin{aligned}
\bar{p}_{D2,in} = {} & \frac{A_5}{K_1(\sqrt{u})} \Big[K_1(\sqrt{u}) I_0(\sqrt{u} r_D) + I_1(\sqrt{u}) K_0(\sqrt{u} r_D) \Big] + \\
& \frac{I_1(\sqrt{u})}{K_1(\sqrt{u})} K_0(\sqrt{u} r_D) \int_1^{r_{fD}} \xi_D g(\xi_D) \Big(u\bar{p}_{D0,in} - f_1(\xi_D) \Big) K_0(\sqrt{u}\xi_D) d\xi_D + \\
& I_0(\sqrt{u} r_D) \int_{r_D}^{r_{fD}} \xi_D g(\xi_D) \Big(u\bar{p}_{D0,in} - f_1(\xi_D) \Big) K_0(\sqrt{u}\xi_D) d\xi_D + \\
& K_0(\sqrt{u} r_D) \int_1^{r_D} \xi_D g(\xi_D) \Big(u\bar{p}_{D0,in} - f_1(\xi_D) \Big) I_0(\sqrt{u}\xi_D) d\xi_D, \quad \text{(B.66)}
\end{aligned}$$

which represents the dimensionless pressure solution for the $O(\delta)$ system. At this point, we have the general solution for the dimensionless pressure evaluated in Laplace space at any point in the invaded zone of the reservoir. However, this solution is not fully defined as the determination of the three constants of integration A_1, A_3 and A_5 is still required. Later, we will show how to obtain them based on the continuity conditions.

Outer Region Solution

The pressure distribution in the univaded zone is described by the dimensionless differential equation and its associated boundary condition equation given respectively by Eqs. 3.133 and 3.134. Based on the perturbation method, we write our falloff solution in this region as

$$\bar{p}_{D,ou}(r_D, u) = \bar{p}_{D0,ou} + \epsilon \bar{p}_{D1,ou} + \delta \bar{p}_{D2,ou}, \quad \text{(B.67)}$$

where the terms $\bar{p}_{D1,ou}$ and $\bar{p}_{D2,ou}$ are supposed to have small contribution compared to the leading term $\bar{p}_{D0,ou}$. As we did before, we substitute the above expression into Eqs. 3.133 and 3.134 to obtain

$$\frac{1}{r_D}\frac{\partial}{\partial r_D}\left[r_D\frac{\partial \bar{p}_{D0,ou}(r_D,u)}{\partial r_D}+\epsilon r_D\frac{\partial \bar{p}_{D1,ou}(r_D,u)}{\partial r_D}+\delta r_D\frac{\partial \bar{p}_{D2,ou}(r_D,u)}{\partial r_D}\right]= \eta\Big(u\bar{p}_{D0,ou}(r_D,u)-f_2(r_D)+\epsilon u\bar{p}_{D1,ou}(r_D,u)+\delta u\bar{p}_{D2,ou}(r_D,u)\Big), \quad \text{(B.68)}$$

and

$$\lim_{r_D\to\infty}\Big(\bar{p}_{D0,ou}+\epsilon\bar{p}_{D1,ou}+\delta\bar{p}_{D2,ou}\Big)=0. \quad \text{(B.69)}$$

If we compare both sides of Eqs. B.68 and B.69, we obtain the three systems for the perturbation solution,

The $O(1)$ system:

$$\frac{1}{r_D}\frac{\partial}{\partial r_D}\left[r_D\frac{\partial \bar{p}_{D0,ou}}{\partial r_D}\right]-\eta u\bar{p}_{D0,ou}=-\eta f_2(r_D), \quad \text{(B.70)}$$

$$\lim_{r_D\to\infty}(\bar{p}_{D0,ou})=0. \quad \text{(B.71)}$$

The $O(\epsilon)$ system:

$$\frac{1}{r_D}\frac{\partial}{\partial r_D}\left[r_D\frac{\partial \bar{p}_{D1,ou}}{\partial r_D}\right]-\eta u\bar{p}_{D1,ou}=0, \quad \text{(B.72)}$$

$$\lim_{r_D\to\infty}(\bar{p}_{D1,ou})=0. \quad \text{(B.73)}$$

The $O(\delta)$ system:

$$\frac{1}{r_D}\frac{\partial}{\partial r_D}\left[r_D\frac{\partial \bar{p}_{D2,ou}}{\partial r_D}\right]-\eta u\bar{p}_{D2,ou}=0, \quad \text{(B.74)}$$

$$\lim_{r_D\to\infty}(\bar{p}_{D2,ou})=0. \quad \text{(B.75)}$$

Since the leading system is described by a non-homogeneous second order differential equation, it is easy to show that based on the treatment of the $O(1)$ system in the

invaded zone, i.e., the water bank, we can write the general solution of Eq. B.70 as

$$\bar{p}_{D0,ou} = d_1 I_0(\sqrt{\eta u} r_D) + d_2 K_0(\sqrt{\eta u} r_D) + v_1(r_D, u) I_0(\sqrt{\eta u} r_D) + v_2(r_D, u) K_0(\sqrt{\eta u} r_D), \tag{B.76}$$

with d_1 and d_2 constants. By analogy to the functions u_1 and u_2 given respectively by Eqs. B.22 and B.23, we define the functions v_1 and v_2 in Eq. B.76 by

$$v_1'(r_D, u) = -\eta r_D f_2(r_D) K_0(\sqrt{\eta u} r_D), \tag{B.77}$$

and

$$v_2'(r_D, u) = \eta r_D f_2(r_D) I_0(\sqrt{\eta u} r_D). \tag{B.78}$$

Integrating Eq. B.77 from r_D to ∞ gives

$$\int_{r_D}^{\infty} v_1'(r_D, u) dr_D = -\eta \int_{r_D}^{\infty} \xi_D f_2(\xi_D) K_0(\sqrt{\eta u} \xi_D) d\xi_D, \tag{B.79}$$

or

$$v_1(r_D, u) = v_1(\infty) + \eta \int_{r_D}^{\infty} \xi_D f_2(\xi_D) K_0(\sqrt{\eta u} \xi_D) d\xi_D. \tag{B.80}$$

Similarly, if we integrate Eq. B.78 from r_{fD} to r_D, we get

$$\int_{r_{fD}}^{r_D} v_2'(r_D, u) dr_D = \eta \int_{r_{fD}}^{r_D} \xi_D f_2(\xi_D) I_0(\sqrt{\eta u} \xi_D) d\xi_D, \tag{B.81}$$

or

$$v_2(r_D, u) = v_2(r_{fD}, u) + \eta \int_{r_{fD}}^{r_D} \xi_D f_2(\xi_D) I_0(\sqrt{\eta u} \xi_D) d\xi_D. \tag{B.82}$$

Thus, substituting Eqs. B.80 and B.82 into Eq. B.76 yields

$$\bar{p}_{D0,ou} = d_1 I_0(\sqrt{\eta u} r_D) + d_2 K_0(\sqrt{\eta u} r_D) + \left[v_1(\infty) + \eta \int_{r_D}^{\infty} \xi_D f_2(\xi_D) K_0(\sqrt{\eta u}\xi_D) d\xi_D \right] I_0(\sqrt{\eta u} r_D) + \left[v_2(r_{fD}, u) + \eta \int_{r_{fD}}^{r_D} \xi_D f_2(\xi_D) I_0(\sqrt{\eta u}\xi_D) d\xi_D \right] K_0(\sqrt{\eta u} r_D), \quad \text{(B.83)}$$

or after rearranging

$$\bar{p}_{D0,ou} = B_1 I_0(\sqrt{\eta u} r_D) + B_2 K_0(\sqrt{\eta u} r_D) + \eta I_0(\sqrt{\eta u} r_D) \int_{r_D}^{\infty} \xi_D f_2(\xi_D) K_0(\sqrt{\eta u}\xi_D) d\xi_D + \eta K_0(\sqrt{\eta u} r_D) \int_{r_{fD}}^{r_D} \xi_D f_2(\xi_D) I_0(\sqrt{\eta u}\xi_D) d\xi_D, \quad \text{(B.84)}$$

where for simplicity, the new constants B_1 and B_2 are introduced and defined respectively by

$$B_1 = d_1 + v_1(\infty), \quad \text{(B.85)}$$

and

$$B_2 = d_2 + v_2(r_{fD}, u). \quad \text{(B.86)}$$

Using the outer boundary condition Eq. B.71 in Eq. B.84 gives

$$B_1 = 0. \quad \text{(B.87)}$$

Thus, Eq. B.84 becomes

$$\bar{p}_{D0,ou} = B_2 K_0(\sqrt{\eta u} r_D) + \eta I_0(\sqrt{\eta u} r_D) \int_{r_D}^{\infty} \xi_D f_2(\xi_D) K_0(\sqrt{\eta u}\xi_D) d\xi_D + \eta K_0(\sqrt{\eta u} r_D) \int_{r_{fD}}^{r_D} \xi_D f_2(\xi_D) I_0(\sqrt{\eta u}\xi_D) d\xi_D. \quad \text{(B.88)}$$

The first order systems in ϵ and δ have the same solution expressed as a linear

combination of modified Bessel functions of order zero. Therefore, we can write

$$\bar{p}_{D1,ou} = B_3 I_0(\sqrt{\eta u} r_D) + B_4 K_0(\sqrt{\eta u} r_D), \tag{B.89}$$

and

$$\bar{p}_{D2,ou} = B_5 I_0(\sqrt{\eta u} r_D) + B_6 K_0(\sqrt{\eta u} r_D), \tag{B.90}$$

where B_3 to B_6 are constants of integration. By applying the outer boundary conditions given for both systems by Eqs. B.73 and B.75, it is easy to show that

$$B_3 = B_5 = 0, \tag{B.91}$$

and Eqs. B.89 and B.90 become respectively

$$\bar{p}_{D1,ou} = B_4 K_0(\sqrt{\eta u} r_D), \tag{B.92}$$

and

$$\bar{p}_{D2,ou} = B_6 K_0(\sqrt{\eta u} r_D). \tag{B.93}$$

Note that in order to compute the falloff dimensionless pressure at any point in the unevaded zone, the constants B_2, B_4 and B_6 need to be determined. In the following, not only will we show how to evaluate these constants but also the parameters A_1, A_3 and A_5 that appear in the falloff dimensionless pressure in the inner zone by writing and solving a system of six decoupled equations.

Continuity Equations

The two continuity conditions applied at the interface, r_{fD}, are given by Eqs. 3.128 and 3.129 in the time domain or by similar expression in the Laplace domain (see Eqs. 3.135 and 3.136) since they retain their form in this space. The first condition expresses the continuity of the pressure which in our case, using Eqs. B.1 and B.67 in Eq. 3.135 translates to

$$\bar{p}_{D0,in}(r_{fD},u)+\epsilon\bar{p}_{D1,in}(r_{fD},u)+\delta\bar{p}_{D2,in}(r_{fD},u)=\bar{p}_{D0,ou}(r_{fD},u) + \epsilon\bar{p}_{D1,ou}(r_{fD},u)+\delta\bar{p}_{D2,ou}(r_{fD},u). \quad \text{(B.94)}$$

Comparing both sides of Eq. B.94 gives the following equations

$$\bar{p}_{D0,in}(r_{fD},u)=\bar{p}_{D0,ou}(r_{fD},u), \quad \text{(B.95)}$$

$$\bar{p}_{D1,in}(r_{fD},u)=\bar{p}_{D1,ou}(r_{fD},u), \quad \text{(B.96)}$$

$$\bar{p}_{D2,in}(r_{fD},u)=\bar{p}_{D2,ou}(r_{fD},u). \quad \text{(B.97)}$$

The second condition expresses the continuity of the fluxes at the interface. Recall that it is given by

$$\hat{M}\lambda_{tD}(r_D)r_D\frac{\partial\bar{p}_{D,in}}{\partial r_D}\bigg|_{r_D=r_{fD}}=r_D\frac{\partial\bar{p}_{D,ou}}{\partial r_D}\bigg|_{r_D=r_{fD}}. \quad \text{(B.98)}$$

Using Eqs. B.1 and B.67 for the pressures and Eq. 3.180 for the dimensionless total mobility in Eq. B.98 gives

$$\hat{M}(1-\epsilon f(r_D))\left(r_D\frac{\partial\bar{p}_{D0,in}}{\partial r_D}\bigg|_{r_D=r_{fD}}+\epsilon r_D\frac{\partial\bar{p}_{D1,in}}{\partial r_D}\bigg|_{r_D=r_{fD}}+\delta r_D\frac{\partial\bar{p}_{D2,in}}{\partial r_D}\bigg|_{r_D=r_{fD}}\right)= r_D\frac{\partial\bar{p}_{D0,ou}}{\partial r_D}\bigg|_{r_D=r_{fD}}+\epsilon r_D\frac{\partial\bar{p}_{D1,ou}}{\partial r_D}\bigg|_{r_D=r_{fD}}+\delta r_D\frac{\partial\bar{p}_{D2,ou}}{\partial r_D}\bigg|_{r_D=r_{fD}}. \quad \text{(B.99)}$$

Expanding the terms and comparing both sides of Eq. B.99 yields

$$\hat{M}r_D\frac{\partial\bar{p}_{D0,in}}{\partial r_D}\bigg|_{r_D=r_{fD}}=r_D\frac{\partial\bar{p}_{D0,ou}}{\partial r_D}\bigg|_{r_D=r_{fD}}, \quad \text{(B.100)}$$

$$\hat{M}\left(r_D\frac{\partial\bar{p}_{D1,in}}{\partial r_D}\bigg|_{r_D=r_{fD}} - r_D f(r_D)\frac{\partial\bar{p}_{D0,in}}{\partial r_D}\bigg|_{r_D=r_{fD}}\right) = r_D\frac{\partial\bar{p}_{D1,ou}}{\partial r_D}\bigg|_{r_D=r_{fD}}, \tag{B.101}$$

and

$$\hat{M}r_D\frac{\partial\bar{p}_{D2,in}}{\partial r_D}\bigg|_{r_D=r_{fD}} = r_D\frac{\partial\bar{p}_{D2,ou}}{\partial r_D}\bigg|_{r_D=r_{fD}}. \tag{B.102}$$

Evaluating Eqs. B.38 and B.88 at r_{fD} and using the resulting expressions in Eq. B.95 gives

$$\begin{aligned}\frac{A_1}{K_1(\sqrt{u})}\Big[K_1(\sqrt{u})I_0(\sqrt{u}r_{fD}) + I_1(\sqrt{u})K_0(\sqrt{u}r_{fD})\Big] \\ + \frac{I_1(\sqrt{u})}{K_1(\sqrt{u})}K_0(\sqrt{u}r_{fD})\int_1^{r_{fD}}\xi_D f_1(\xi_D)K_0(\sqrt{u}\xi_D)d\xi_D \\ + K_0(\sqrt{u}r_{fD})\int_1^{r_{fD}}\xi_D f_1(\xi_D)I_0(\sqrt{u}\xi_D)d\xi_D = \\ B_2K_0(\sqrt{\eta u}r_{fD}) + \eta I_0(\sqrt{\eta u}r_{fD})\int_{r_{fD}}^{\infty}\xi_D f_2(\xi_D)K_0(\sqrt{\eta u}\xi_D)d\xi_D.\end{aligned} \tag{B.103}$$

If we rearrange Eq. B.103, we obtain

$$\begin{aligned}B_2K_0(\sqrt{\eta u}r_{fD}) = \frac{A_1}{K_1(\sqrt{u})}\Big[K_1(\sqrt{u})I_0(\sqrt{u}r_{fD}) + I_1(\sqrt{u})K_0(\sqrt{u}r_{fD})\Big] \\ + \frac{K_0(\sqrt{u}r_{fD})}{K_1(\sqrt{u})}\int_1^{r_{fD}}\xi_D f_1(\xi_D)\Big[I_1(\sqrt{u})K_0(\sqrt{u}\xi_D) + K_1(\sqrt{u})I_0(\sqrt{u}\xi_D)\Big]d\xi_D \\ - \eta I_0(\sqrt{\eta u}r_{fD})\int_{r_{fD}}^{\infty}\xi_D f_2(\xi_D)K_0(\sqrt{\eta u}\xi_D)d\xi_D.\end{aligned} \tag{B.104}$$

From Eq. B.100, we have

$$\hat{M}\frac{\partial\bar{p}_{D0,in}}{\partial r_D}\bigg|_{r_D=r_{fD}} = \frac{\partial\bar{p}_{D0,ou}}{\partial r_D}\bigg|_{r_D=r_{fD}}. \tag{B.105}$$

It is clear that we need to obtain the first derivatives of the pressure with respect to r_D

in both regions in order to apply the above condition. In the inner zone, substituting Eq. B.37 for A_2 into Eq. B.34 and rearranging gives

$$\frac{\partial \bar{p}_{D0,in}}{\partial r_D} = \frac{A_1\sqrt{u}}{K_1(\sqrt{u})}\Big[K_1(\sqrt{u})I_1(\sqrt{u}r_D) - I_1(\sqrt{u})K_1(\sqrt{u}r_D)\Big] + \sqrt{u}I_1(\sqrt{u}r_D)\int_{r_D}^{r_{fD}} \xi_D f_1(\xi_D)K_0(\sqrt{u}\xi_D)d\xi_D - \sqrt{u}K_1(\sqrt{u}r_D)\int_1^{r_D} \xi_D f_1(\xi_D)I_0(\sqrt{u}\xi_D)d\xi_D - \frac{I_1(\sqrt{u})}{K_1(\sqrt{u})}\sqrt{u}K_1(\sqrt{u}r_D)\int_1^{r_{fD}} \xi_D f_1(\xi_D)K_0(\sqrt{u}\xi_D)d\xi_D. \quad \text{(B.106)}$$

In the outer zone, differentiating Eq. B.88 with respect to r_D gives

$$\frac{\partial \bar{p}_{D0,ou}}{\partial r_D} = -\sqrt{\eta u}B_2K_1(\sqrt{\eta u}r_D) + \eta\sqrt{\eta u}I_1(\sqrt{\eta u}r_D)\int_{r_D}^{\infty} \xi_D f_2(\xi_D)K_0(\sqrt{\eta u}\xi_D)d\xi_D - \eta\sqrt{\eta u}K_1(\sqrt{\eta u}r_D)\int_{r_{fD}}^{r_D} \xi_D f_2(\xi_D)I_0(\sqrt{\eta u}\xi_D)d\xi_D. \quad \text{(B.107)}$$

Now, if we evaluate both Eqs. B.106 and B.107 at r_{fD} and use the resulting expressions in Eq. B.105, we obtain

$$\hat{M}\frac{A_1\sqrt{u}}{K_1(\sqrt{u})}\Big[K_1(\sqrt{u})I_1(\sqrt{u}r_{fD}) - I_1(\sqrt{u})K_1(\sqrt{u}r_{fD})\Big] - \hat{M}\sqrt{u}K_1(\sqrt{u}r_{fD})\int_1^{r_{fD}} \xi_D f_1(\xi_D)I_0(\sqrt{u}\xi_D)d\xi_D - \hat{M}\frac{I_1(\sqrt{u})}{K_1(\sqrt{u})}\sqrt{u}K_1(\sqrt{u}r_{fD})\int_1^{r_{fD}} \xi_D f_1(\xi_D)K_0(\sqrt{u}\xi_D)d\xi_D = -\sqrt{\eta u}B_2K_1(\sqrt{\eta u}r_{fD}) + \eta\sqrt{\eta u}I_1(\sqrt{\eta u}r_{fD})\int_{r_{fD}}^{\infty} \xi_D f_2(\xi_D)K_0(\sqrt{\eta u}\xi_D)d\xi_D, \quad \text{(B.108)}$$

or after rearranging,

$$B_2 K_1(\sqrt{\eta u} r_{fD}) = -\frac{\hat{M}}{\sqrt{\eta}} \frac{A_1}{K_1(\sqrt{u})} \left[K_1(\sqrt{u}) I_1(\sqrt{u} r_{fD}) - I_1(\sqrt{u}) K_1(\sqrt{u} r_{fD}) \right]$$
$$+ \frac{\hat{M}}{\sqrt{\eta}} \frac{K_1(\sqrt{u} r_{fD})}{K_1(\sqrt{u})} \int_1^{r_{fD}} \xi_D f_1(\xi_D) \left[K_1(\sqrt{u}) I_0(\sqrt{u} \xi_D) + I_1(\sqrt{u}) K_0(\sqrt{u} \xi_D) \right] d\xi_D$$
$$+ \eta I_1(\sqrt{\eta u} r_{fD}) \int_{r_{fD}}^{\infty} \xi_D f_2(\xi_D) K_0(\sqrt{\eta u} \xi_D) d\xi_D. \quad \text{(B.109)}$$

For simplification purposes, we introduce new functions defined by the following expressions

$$H_\nu(\alpha x, \alpha y) = K_{\nu+1}(\alpha y) I_\nu(\alpha x) + I_{\nu+1}(\alpha y) K_\nu(\alpha x), \quad \text{(B.110)}$$

and

$$G_\nu(\alpha x, \alpha y) = K_\nu(\alpha y) I_\nu(\alpha x) - I_\nu(\alpha y) K_\nu(\alpha x). \quad \text{(B.111)}$$

Based on these definitions, we can write

$$H_0(\sqrt{u} r_{fD}, \sqrt{u}) = K_1(\sqrt{u}) I_0(\sqrt{u} r_{fD}) + I_1(\sqrt{u}) K_0(\sqrt{u} r_{fD}), \quad \text{(B.112)}$$

and

$$G_1(\sqrt{u} r_{fD}, \sqrt{u}) = K_1(\sqrt{u}) I_1(\sqrt{u} r_{fD}) - I_1(\sqrt{u}) K_1(\sqrt{u} r_{fD}), \quad \text{(B.113)}$$

so that Eqs. B.104 and B.109 simplify respectively to

$$B_2 K_0(\sqrt{\eta u} r_{fD}) = \frac{A_1}{K_1(\sqrt{u})} H_0(\sqrt{u} r_{fD}, \sqrt{u}) + \frac{K_0(\sqrt{u} r_{fD})}{K_1(\sqrt{u})} \int_1^{r_{fD}} \xi_D f_1(\xi_D) H_0(\sqrt{u} \xi_D, \sqrt{u}) d\xi_D$$
$$- \eta I_0(\sqrt{\eta u} r_{fD}) \int_{r_{fD}}^{\infty} \xi_D f_2(\xi_D) K_0(\sqrt{\eta u} \xi_D) d\xi_D, \quad \text{(B.114)}$$

and

$$B_2K_1(\sqrt{\eta u}r_{fD}) = -\frac{\hat{M}}{\sqrt{\eta}}\frac{A_1}{K_1(\sqrt{u})}G_1(\sqrt{u}r_{fD},\sqrt{u}) + \frac{\hat{M}}{\sqrt{\eta}}\frac{K_1(\sqrt{u}r_{fD})}{K_1(\sqrt{u})}\int_1^{r_{fD}}\xi_D f_1(\xi_D)H_0(\sqrt{u}\xi_D,\sqrt{u})d\xi_D + \eta I_1(\sqrt{\eta u}r_{fD})\int_{r_{fD}}^{\infty}\xi_D f_2(\xi_D)K_0(\sqrt{\eta u}\xi_D)d\xi_D. \quad \text{(B.115)}$$

Multiplying Eq. B.114 by $K_1(\sqrt{\eta u}r_{fD})$ and Eq. B.115 by $K_0(\sqrt{\eta u}r_{fD})$ and equating the resulting expressions yields

$$\frac{A_1}{K_1(\sqrt{u})}K_1(\sqrt{\eta u}r_{fD})H_0(\sqrt{u}r_{fD},\sqrt{u}) + \frac{K_0(\sqrt{u}r_{fD})K_1(\sqrt{\eta u}r_{fD})}{K_1(\sqrt{u})}\times \int_1^{r_{fD}}\xi_D f_1(\xi_D)H_0(\sqrt{u}\xi_D,\sqrt{u})d\xi_D - \eta I_0(\sqrt{\eta u}r_{fD})K_1(\sqrt{\eta u}r_{fD})\int_{r_{fD}}^{\infty}\xi_D f_2(\xi_D)K_0(\sqrt{\eta u}\xi_D)d\xi_D = -\frac{\hat{M}}{\sqrt{\eta}}\frac{A_1}{K_1(\sqrt{u})}K_0(\sqrt{\eta u}r_{fD})G_1(\sqrt{u}r_{fD},\sqrt{u}) + \frac{\hat{M}}{\sqrt{\eta}}\frac{K_1(\sqrt{u}r_{fD})K_0(\sqrt{\eta u}r_{fD})}{K_1(\sqrt{u})}\int_1^{r_{fD}}\xi_D f_1(\xi_D)H_0(\sqrt{u}\xi_D,\sqrt{u})d\xi_D + \eta I_1(\sqrt{\eta u}r_{fD})K_0(\sqrt{\eta u}r_{fD})\int_{r_{fD}}^{\infty}\xi_D f_2(\xi_D)K_0(\sqrt{\eta u}\xi_D)d\xi_D. \quad \text{(B.116)}$$

Rearranging the preceding equation gives

$$\frac{A_1}{K_1(\sqrt{u})}\left[K_1(\sqrt{\eta u}r_{fD})H_0(\sqrt{u}r_{fD},\sqrt{u}) + \frac{\hat{M}}{\sqrt{\eta}}K_0(\sqrt{\eta u}r_{fD})G_1(\sqrt{u}r_{fD},\sqrt{u})\right] = -\frac{1}{K_1(\sqrt{u})}\left[K_0(\sqrt{u}r_{fD})K_1(\sqrt{\eta u}r_{fD}) - \frac{\hat{M}}{\sqrt{\eta}}K_1(\sqrt{u}r_{fD})K_0(\sqrt{\eta u}r_{fD})\right]\times \int_1^{r_{fD}}\xi_D f_1(\xi_D)H_0(\sqrt{u}\xi_D,\sqrt{u})d\xi_D + \eta\left[I_0(\sqrt{\eta u}r_{fD})K_1(\sqrt{\eta u}r_{fD}) + I_1(\sqrt{\eta u}r_{fD})K_0(\sqrt{\eta u}r_{fD})\right]\times \int_{r_{fD}}^{\infty}\xi_D f_2(\xi_D)K_0(\sqrt{\eta u}\xi_D)d\xi_D. \quad \text{(B.117)}$$

Using the fact that

$$I_0(\sqrt{\eta u}r_{fD})K_1(\sqrt{\eta u}r_{fD}) + I_1(\sqrt{\eta u}r_{fD})K_0(\sqrt{\eta u}r_{fD}) = \frac{1}{\sqrt{\eta u}r_{fD}}, \tag{B.118}$$

Eq. B.117 becomes

$$\begin{aligned}\frac{A_1}{K_1(\sqrt{u})}\left[K_1(\sqrt{\eta u}r_{fD})H_0(\sqrt{u}r_{fD},\sqrt{u}) + \frac{\hat{M}}{\sqrt{\eta}}K_0(\sqrt{\eta u}r_{fD})G_1(\sqrt{u}r_{fD},\sqrt{u})\right] = \\ -\frac{1}{K_1(\sqrt{u})}\left[K_0(\sqrt{u}r_{fD})K_1(\sqrt{\eta u}r_{fD}) - \frac{\hat{M}}{\sqrt{\eta}}K_1(\sqrt{u}r_{fD})K_0(\sqrt{\eta u}r_{fD})\right]\times \\ \int_1^{r_{fD}} \xi_D f_1(\xi_D)H_0(\sqrt{u}\xi_D,\sqrt{u})d\xi_D + \frac{1}{r_{fD}}\sqrt{\frac{\eta}{u}}\int_{r_{fD}}^{\infty}\xi_D f_2(\xi_D)K_0(\sqrt{\eta u}\xi_D)d\xi_D,\end{aligned} \tag{B.119}$$

or

$$\begin{aligned}A_1 = \frac{1}{\left[K_1(\sqrt{\eta u}r_{fD})H_0(\sqrt{u}r_{fD},\sqrt{u}) + \frac{\hat{M}}{\sqrt{\eta}}K_0(\sqrt{\eta u}r_{fD})G_1(\sqrt{u}r_{fD},\sqrt{u})\right]}\times \\ \left(-\left[K_0(\sqrt{u}r_{fD})K_1(\sqrt{\eta u}r_{fD}) - \frac{\hat{M}}{\sqrt{\eta}}K_1(\sqrt{u}r_{fD})K_0(\sqrt{\eta u}r_{fD})\right]\times\right. \\ \left.\int_1^{r_{fD}} \xi_D f_1(\xi_D)H_0(\sqrt{u}\xi_D,\sqrt{u})d\xi_D + \frac{K_1(\sqrt{u})}{r_{fD}}\sqrt{\frac{\eta}{u}}\int_{r_{fD}}^{\infty}\xi_D f_2(\xi_D)K_0(\sqrt{\eta u}\xi_D)d\xi_D\right).\end{aligned} \tag{B.120}$$

Now that the constant A_1 is determined, B_2 can be evaluated by substituting Eq. B.120 into either Eq. B.114 or Eq. B.115. The result, after manipulation, simplification and rearrangement is given by the following equation

$$B_2 = \frac{1}{\left[K_1(\sqrt{\eta u}r_{fD})H_0(\sqrt{u}r_{fD},\sqrt{u}) + \frac{\hat{M}}{\sqrt{\eta}}K_0(\sqrt{\eta u}r_{fD})G_1(\sqrt{u}r_{fD},\sqrt{u})\right]}\times$$
$$\left(\frac{\hat{M}}{\sqrt{\eta u}r_{fD}}\int_1^{r_{fD}}\xi_D f_1(\xi_D)H_0(\sqrt{u}\xi_D,\sqrt{u})d\xi_D + \frac{1}{r_{fD}}\sqrt{\frac{\eta}{u}}\frac{H_0(\sqrt{u}r_{fD},\sqrt{u})}{K_0(\sqrt{\eta u}r_{fD})}\times\right.$$
$$\left.\int_{r_{fD}}^{\infty}\xi_D f_2(\xi_D)K_0(\sqrt{\eta u}\xi_D)d\xi_D\right) - \eta\frac{I_0(\sqrt{\eta u}r_{fD})}{K_0(\sqrt{\eta u}r_{fD})}\int_{r_{fD}}^{\infty}\xi_D f_2(\xi_D)K_0(\sqrt{\eta u}\xi_D)d\xi_D. \quad \text{(B.121)}$$

For the first order in ϵ, let us evaluate Eqs. B.56 and B.92 at the interface r_{fD} and equating the resulting expressions according to Eq. B.96. We have

$$\frac{A_3}{K_1(\sqrt{u})}\left[K_1(\sqrt{u})I_0(\sqrt{u}r_{fD}) + I_1(\sqrt{u})K_0(\sqrt{u}r_{fD})\right]$$
$$- r_{fD}f(r_{fD})\frac{\partial\bar{p}_{D0,in}}{\partial r_D}\bigg|_{r_{fD}}\frac{K_0(\sqrt{u}r_{fD})}{K_1(\sqrt{u})}\left[K_1(\sqrt{u})I_0(\sqrt{u}r_{fD}) + I_1(\sqrt{u})K_0(\sqrt{u}r_{fD})\right]$$
$$- \sqrt{u}\frac{I_1(\sqrt{u})}{K_1(\sqrt{u})}K_0(\sqrt{u}r_{fD})\int_1^{r_{fD}}\xi_D f(\xi_D)\frac{\partial\bar{p}_{D0,in}}{\partial\xi_D}K_1(\sqrt{u}\xi_D)d\xi_D$$
$$+ \sqrt{u}K_0(\sqrt{u}r_{fD})\int_1^{r_{fD}}\xi_D f(\xi_D)\frac{\partial\bar{p}_{D0,in}}{\partial\xi_D}I_1(\sqrt{u}\xi_D)d\xi_D = B_4K_0(\sqrt{\eta u}r_{fD}). \quad \text{(B.122)}$$

Using the new functions given by Eqs. B.112 and B.113, Eq. B.122 simplifies to

$$B_4K_0(\sqrt{\eta u}r_{fD}) = \frac{A_3}{K_1(\sqrt{u})}H_0(\sqrt{u}r_{fD},\sqrt{u}) - r_{fD}f(r_{fD})\frac{\partial\bar{p}_{D0,in}}{\partial r_D}\bigg|_{r_{fD}}\frac{K_0(\sqrt{u}r_{fD})}{K_1(\sqrt{u})}\times$$
$$H_0(\sqrt{u}r_{fD},\sqrt{u}) + \sqrt{u}\frac{K_0(\sqrt{u}r_{fD})}{K_1(\sqrt{u})}\int_1^{r_{fD}}\xi_D f(\xi_D)\frac{\partial\bar{p}_{D0,in}}{\partial\xi_D}G_1(\sqrt{u}\xi_D,\sqrt{u})d\xi_D. \quad \text{(B.123)}$$

On the other hand, from the continuity of the fluxes Eq. B.101, we have

$$\hat{M}\left(\frac{\partial\bar{p}_{D1,in}}{\partial r_D}\bigg|_{r_D=r_{fD}} - f(r_D)\frac{\partial\bar{p}_{D0,in}}{\partial r_D}\bigg|_{r_D=r_{fD}}\right) = \frac{\partial\bar{p}_{D1,ou}}{\partial r_D}\bigg|_{r_D=r_{fD}}. \quad \text{(B.124)}$$

If we use Eq. B.55 into Eq. B.53, we obtain

$$\frac{\partial \bar{p}_{D1,in}}{\partial r_D} = \frac{A_3\sqrt{u}}{K_1(\sqrt{u})}\left[K_1(\sqrt{u})I_1(\sqrt{u}r_D) - I_1(\sqrt{u})K_1(\sqrt{u}r_D)\right]$$
$$- \sqrt{u}r_{fD}f(r_{fD})\frac{\partial \bar{p}_{D0,in}}{\partial r_D}\bigg|_{r_{fD}} \frac{K_0(\sqrt{u}r_{fD})}{K_1(\sqrt{u})}\left[K_1(\sqrt{u})I_1(\sqrt{u}r_D) - I_1(\sqrt{u})K_1(\sqrt{u}r_D)\right]$$
$$+ u\frac{I_1(\sqrt{u})}{K_1(\sqrt{u})}K_1(\sqrt{u}r_D)\int_1^{r_{fD}} \xi_D f(\xi_D)\frac{\partial \bar{p}_{D0,in}}{\partial \xi_D}K_1(\sqrt{u}\xi_D)d\xi_D$$
$$- uK_1(\sqrt{u}r_D)\int_1^{r_D} \xi_D f(\xi_D)\frac{\partial \bar{p}_{D0,in}}{\partial \xi_D}I_1(\sqrt{u}\xi_D)d\xi_D$$
$$- uI_1(\sqrt{u}r_D)\int_{r_D}^{r_{fD}} \xi_D f(\xi_D)\frac{\partial \bar{p}_{D0,in}}{\partial \xi_D}K_1(\sqrt{u}\xi_D)d\xi_D + f(r_D)\frac{\partial \bar{p}_{D0,in}}{\partial r_D}. \quad \text{(B.125)}$$

After evaluating the preceding equation at $r_D = r_{fD}$ and rearranging, we get

$$\frac{\partial \bar{p}_{D1,in}}{\partial r_D}\bigg|_{r_D=r_{fD}} - f(r_D)\frac{\partial \bar{p}_{D0,in}}{\partial r_D}\bigg|_{r_D=r_{fD}} = \frac{A_3\sqrt{u}}{K_1(\sqrt{u})}G_1(\sqrt{u}r_{fD},\sqrt{u})$$
$$- \sqrt{u}r_{fD}f(r_{fD})\frac{\partial \bar{p}_{D0,in}}{\partial r_D}\bigg|_{r_{fD}} \frac{K_0(\sqrt{u}r_{fD})}{K_1(\sqrt{u})}G_1(\sqrt{u}r_{fD},\sqrt{u})$$
$$+ u\frac{I_1(\sqrt{u})}{K_1(\sqrt{u})}K_1(\sqrt{u}r_{fD})\int_1^{r_{fD}} \xi_D f(\xi_D)\frac{\partial \bar{p}_{D0,in}}{\partial \xi_D}K_1(\sqrt{u}\xi_D)d\xi_D$$
$$- uK_1(\sqrt{u}r_{fD})\int_1^{r_{fD}} \xi_D f(\xi_D)\frac{\partial \bar{p}_{D0,in}}{\partial \xi_D}I_1(\sqrt{u}\xi_D)d\xi_D. \quad \text{(B.126)}$$

Using Eq. B.113, we can combine the two integral terms in Eq. B.126 and thus, rewrite Eq. B.126 as

$$\frac{\partial \bar{p}_{D1,in}}{\partial r_D}\bigg|_{r_D=r_{fD}} - f(r_D)\frac{\partial \bar{p}_{D0,in}}{\partial r_D}\bigg|_{r_D=r_{fD}} = \frac{A_3\sqrt{u}}{K_1(\sqrt{u})}G_1(\sqrt{u}r_{fD},\sqrt{u})$$
$$- \sqrt{u}r_{fD}f(r_{fD})\frac{\partial \bar{p}_{D0,in}}{\partial r_D}\bigg|_{r_{fD}} \frac{K_0(\sqrt{u}r_{fD})}{K_1(\sqrt{u})}G_1(\sqrt{u}r_{fD},\sqrt{u})$$
$$- u\frac{K_1(\sqrt{u}r_{fD})}{K_1(\sqrt{u})}\int_1^{r_{fD}} \xi_D f(\xi_D)\frac{\partial \bar{p}_{D0,in}}{\partial \xi_D}G_1(\sqrt{u}\xi_D,\sqrt{u})d\xi_D. \quad \text{(B.127)}$$

If we differentiate Eq. B.92 with respect to r_D, we obtain

$$\frac{\partial \bar{p}_{D1,ou}}{\partial r_D} = -\sqrt{\eta u} B_4 K_1(\sqrt{\eta u} r_D). \tag{B.128}$$

At the interface r_{fD}, we have

$$\left.\frac{\partial \bar{p}_{D1,ou}}{\partial r_D}\right|_{r_D = r_{fD}} = -\sqrt{\eta u} B_4 K_1(\sqrt{\eta u} r_{fD}). \tag{B.129}$$

using Eqs. B.127 and B.129 in Eq. B.124 gives

$$\begin{aligned}
&\hat{M}\frac{A_3\sqrt{u}}{K_1(\sqrt{u})} G_1(\sqrt{u} r_{fD}, \sqrt{u}) - \hat{M}\sqrt{u} r_{fD} f(r_{fD}) \left.\frac{\partial \bar{p}_{D0,in}}{\partial r_D}\right|_{r_{fD}} \frac{K_0(\sqrt{u} r_{fD})}{K_1(\sqrt{u})} G_1(\sqrt{u} r_{fD}, \sqrt{u}) \\
&- \hat{M} u \frac{K_1(\sqrt{u} r_{fD})}{K_1(\sqrt{u})} \int_1^{r_{fD}} \xi_D f(\xi_D) \frac{\partial \bar{p}_{D0,in}}{\partial \xi_D} G_1(\sqrt{u}\xi_D, \sqrt{u}) d\xi_D = -\sqrt{\eta u} B_4 K_1(\sqrt{\eta u} r_{fD}),
\end{aligned} \tag{B.130}$$

or

$$\begin{aligned}
B_4 K_1(\sqrt{\eta u} r_{fD}) = &-\frac{\hat{M}}{\sqrt{\eta}} \frac{A_3}{K_1(\sqrt{u})} G_1(\sqrt{u} r_{fD}, \sqrt{u}) \\
&+ \frac{\hat{M}}{\sqrt{\eta}} r_{fD} f(r_{fD}) \left.\frac{\partial \bar{p}_{D0,in}}{\partial r_D}\right|_{r_{fD}} \frac{K_0(\sqrt{u} r_{fD})}{K_1(\sqrt{u})} G_1(\sqrt{u} r_{fD}, \sqrt{u}) \\
&+ \hat{M}\sqrt{\frac{u}{\eta}} \frac{K_1(\sqrt{u} r_{fD})}{K_1(\sqrt{u})} \int_1^{r_{fD}} \xi_D f(\xi_D) \frac{\partial \bar{p}_{D0,in}}{\partial \xi_D} G_1(\sqrt{u}\xi_D, \sqrt{u}) d\xi_D.
\end{aligned} \tag{B.131}$$

Multiplying Eq. B.123 by $K_1(\sqrt{\eta u} r_{fD})$ and Eq. B.131 by $K_0(\sqrt{\eta u} r_{fD})$ and equating the resulting expressions yields

$$\frac{A_3}{K_1(\sqrt{u})}K_1(\sqrt{\eta u}r_{fD})H_0(\sqrt{u}r_{fD},\sqrt{u}) - r_{fD}f(r_{fD})\frac{\partial \bar{p}_{D0,in}}{\partial r_D}\bigg|_{r_{fD}} \times$$
$$\frac{K_0(\sqrt{u}r_{fD})}{K_1(\sqrt{u})}K_1(\sqrt{\eta u}r_{fD})H_0(\sqrt{u}r_{fD},\sqrt{u})$$
$$+\sqrt{u}\frac{K_0(\sqrt{u}r_{fD})}{K_1(\sqrt{u})}K_1(\sqrt{\eta u}r_{fD})\int_1^{r_{fD}}\xi_D f(\xi_D)\frac{\partial \bar{p}_{D0,in}}{\partial \xi_D}G_1(\sqrt{u}\xi_D,\sqrt{u})d\xi_D =$$
$$-\frac{\hat{M}}{\sqrt{\eta}}\frac{A_3}{K_1(\sqrt{u})}K_0(\sqrt{\eta u}r_{fD})G_1(\sqrt{u}r_{fD},\sqrt{u})$$
$$+\frac{\hat{M}}{\sqrt{\eta}}r_{fD}f(r_{fD})\frac{\partial \bar{p}_{D0,in}}{\partial r_D}\bigg|_{r_{fD}}\frac{K_0(\sqrt{u}r_{fD})}{K_1(\sqrt{u})}K_0(\sqrt{\eta u}r_{fD})G_1(\sqrt{u}r_{fD},\sqrt{u})$$
$$+\hat{M}\sqrt{\frac{u}{\eta}}\frac{K_1(\sqrt{u}r_{fD})}{K_1(\sqrt{u})}K_0(\sqrt{\eta u}r_{fD})\int_1^{r_{fD}}\xi_D f(\xi_D)\frac{\partial \bar{p}_{D0,in}}{\partial \xi_D}G_1(\sqrt{u}\xi_D,\sqrt{u})d\xi_D, \quad \text{(B.132)}$$

or rearranging and solving for A_3,

$$A_3 = r_{fD}f(r_{fD})\frac{\partial \bar{p}_{D0,in}}{\partial r_D}\bigg|_{r_{fD}}K_0(\sqrt{u}r_{fD})$$
$$-\sqrt{u}\frac{\left[K_0(\sqrt{u}r_{fD})K_1(\sqrt{\eta u}r_{fD}) - \frac{\hat{M}}{\eta}K_1(\sqrt{u}r_{fD})K_0(\sqrt{\eta u}r_{fD})\right]}{\left[K_1(\sqrt{\eta u}r_{fD})H_0(\sqrt{u}r_{fD},\sqrt{u}) + \frac{\hat{M}}{\sqrt{\eta}}K_0(\sqrt{\eta u}r_{fD})G_1(\sqrt{u}r_{fD},\sqrt{u})\right]}\times$$
$$\int_1^{r_{fD}}\xi_D f(\xi_D)\frac{\partial \bar{p}_{D0,in}}{\partial \xi_D}G_1(\sqrt{u}\xi_D,\sqrt{u})d\xi_D. \quad \text{(B.133)}$$

Since the constant A_3 is now determined, B_4 is evaluated by substituting Eq. B.133 into either Eq. B.123 or Eq. B.131. Using Eq. B.123, the result for B_4, after manipulation, simplification and rearrangement is given by the following equation

$$B_4 = \frac{\hat{M}}{r_{fD}\sqrt{\eta}}\frac{1}{\left[K_1(\sqrt{\eta u}r_{fD})H_0(\sqrt{u}r_{fD},\sqrt{u}) + \frac{\hat{M}}{\sqrt{\eta}}K_0(\sqrt{\eta u}r_{fD})G_1(\sqrt{u}r_{fD},\sqrt{u})\right]}\times$$
$$\int_1^{r_{fD}}\xi_D f(\xi_D)\frac{\partial \bar{p}_{D0,in}}{\partial \xi_D}G_1(\sqrt{u}\xi_D,\sqrt{u})d\xi_D. \quad \text{(B.134)}$$

As for the $O(\delta)$ problem, we need to equate the dimensionless pressure obtained for the inner zone (Eq. B.66) with the dimensionless falloff pressure valid in the outer region (Eq. B.93) at the interface, that is for $r_D = r_{fD}$. The result is

$$\begin{aligned}
&\frac{A_5}{K_1(\sqrt{u})}\Big[K_1(\sqrt{u})I_0(\sqrt{u}r_{fD}) + I_1(\sqrt{u})K_0(\sqrt{u}r_{fD})\Big] \\
&\quad + \frac{I_1(\sqrt{u})}{K_1(\sqrt{u})}K_0(\sqrt{u}r_{fD})\int_1^{r_{fD}} \xi_D g(\xi_D)\Big(u\bar{p}_{D0,in} - f_1(\xi_D)\Big)K_0(\sqrt{u}\xi_D)d\xi_D \\
&\quad + K_0(\sqrt{u}r_{fD})\int_1^{r_{fD}} \xi_D g(\xi_D)\Big(u\bar{p}_{D0,in} - f_1(\xi_D)\Big)I_0(\sqrt{u}\xi_D)d\xi_D = B_6 K_0(\sqrt{\eta u}r_{fD}),
\end{aligned} \tag{B.135}$$

or by simplifying the above expression using the definition of the H_0 function,

$$\begin{aligned}
B_6 K_0(\sqrt{\eta u}r_{fD}) &= \frac{A_5}{K_1(\sqrt{u})}H_0(\sqrt{u}r_{fD},\sqrt{u}) \\
&\quad + \frac{K_0(\sqrt{u}r_{fD})}{K_1(\sqrt{u})}\int_1^{r_{fD}} \xi_D g(\xi_D)\Big(u\bar{p}_{D0,in} - f_1(\xi_D)\Big)H_0(\sqrt{u}\xi_D,\sqrt{u})d\xi_D.
\end{aligned} \tag{B.136}$$

We need another equation in order to solve for the constants A_5 and B_6. This condition is provided by the continuity of fluxes Eq. B.102 which is expressed again by

$$\hat{M}r_D\frac{\partial\bar{p}_{D2,in}}{\partial r_D}\bigg|_{r_D=r_{fD}} = r_D\frac{\partial\bar{p}_{D2,ou}}{\partial r_D}\bigg|_{r_D=r_{fD}}, \tag{B.137}$$

or simply,

$$\hat{M}\frac{\partial\bar{p}_{D2,in}}{\partial r_D}\bigg|_{r_D=r_{fD}} = \frac{\partial\bar{p}_{D2,ou}}{\partial r_D}\bigg|_{r_D=r_{fD}}. \tag{B.138}$$

From Eqs. B.65 and B.63, we have

$$\frac{\partial \bar{p}_{D2,in}}{\partial r_D} = \frac{A_5\sqrt{u}}{K_1(\sqrt{u})}\Big[K_1(\sqrt{u})I_1(\sqrt{u}r_D) - I_1(\sqrt{u})K_1(\sqrt{u}r_D)\Big]$$
$$- \sqrt{u}\frac{I_1(\sqrt{u})}{K_1(\sqrt{u})}K_1(\sqrt{u}r_D)\int_1^{r_{fD}} \xi_D g(\xi_D)\Big(u\bar{p}_{D0,in} - f_1(\xi_D)\Big)K_0(\sqrt{u}\xi_D)d\xi_D$$
$$- \sqrt{u}K_1(\sqrt{u}r_D)\int_1^{r_D} \xi_D g(\xi_D)\Big(u\bar{p}_{D0,in} - f_1(\xi_D)\Big)I_0(\sqrt{u}\xi_D)d\xi_D$$
$$+ \sqrt{u}I_1(\sqrt{u}r_D)\int_{r_D}^{r_{fD}} \xi_D g(\xi_D)\Big(u\bar{p}_{D0,in} - f_1(\xi_D)\Big)K_0(\sqrt{u}\xi_D)d\xi_D. \quad \text{(B.139)}$$

At the interface,

$$\left.\frac{\partial \bar{p}_{D2,in}}{\partial r_D}\right|_{r_D=r_{fD}} = \frac{A_5\sqrt{u}}{K_1(\sqrt{u})}\Big[K_1(\sqrt{u})I_1(\sqrt{u}r_{fD}) - I_1(\sqrt{u})K_1(\sqrt{u}r_{fD})\Big]$$
$$- \sqrt{u}\frac{I_1(\sqrt{u})}{K_1(\sqrt{u})}K_1(\sqrt{u}r_{fD})\int_1^{r_{fD}} \xi_D g(\xi_D)\Big(u\bar{p}_{D0,in} - f_1(\xi_D)\Big)K_0(\sqrt{u}\xi_D)d\xi_D$$
$$- \sqrt{u}K_1(\sqrt{u}r_{fD})\int_1^{r_{fD}} \xi_D g(\xi_D)\Big(u\bar{p}_{D0,in} - f_1(\xi_D)\Big)I_0(\sqrt{u}\xi_D)d\xi_D, \quad \text{(B.140)}$$

or

$$\left.\frac{\partial \bar{p}_{D2,in}}{\partial r_D}\right|_{r_D=r_{fD}} = \frac{A_5\sqrt{u}}{K_1(\sqrt{u})}G_1(\sqrt{u}r_{fD},\sqrt{u})$$
$$- \sqrt{u}\frac{K_1(\sqrt{u}r_{fD})}{K_1(\sqrt{u})}\int_1^{r_{fD}} \xi_D g(\xi_D)\Big(u\bar{p}_{D0,in} - f_1(\xi_D)\Big)H_0(\sqrt{u}\xi_D,\sqrt{u})d\xi_D. \quad \text{(B.141)}$$

Differentiating Eq. B.93 with respect to r_D yields for any r_D

$$\frac{\partial \bar{p}_{D2,ou}}{\partial r_D} = -\sqrt{\eta u}B_6 K_1(\sqrt{\eta u}r_D), \quad \text{(B.142)}$$

and for r_{fD}

$$\left.\frac{\partial \bar{p}_{D2,ou}}{\partial r_D}\right|_{r_D=r_{fD}} = -\sqrt{\eta u}B_6 K_1(\sqrt{\eta u}r_{fD}). \quad \text{(B.143)}$$

Finally, using Eqs. B.143 and B.141 in Eq. B.138 gives

$$\hat{M}\frac{A_5\sqrt{u}}{K_1(\sqrt{u})}G_1(\sqrt{u}r_{fD},\sqrt{u})-\hat{M}\sqrt{u}\frac{K_1(\sqrt{u}r_{fD})}{K_1(\sqrt{u})}\times$$
$$\int_1^{r_{fD}}\xi_D g(\xi_D)\Big(u\bar{p}_{D0,in}-f_1(\xi_D)\Big)H_0(\sqrt{u}\xi_D,\sqrt{u})d\xi_D=-\sqrt{\eta u}B_6K_1(\sqrt{\eta u}r_{fD}), \quad \text{(B.144)}$$

or after rearranging,

$$B_6K_1(\sqrt{\eta u}r_{fD})=-\frac{\hat{M}}{\sqrt{\eta}}\frac{A_5}{K_1(\sqrt{u})}G_1(\sqrt{u}r_{fD},\sqrt{u})+\frac{\hat{M}}{\sqrt{\eta}}\frac{K_1(\sqrt{u}r_{fD})}{K_1(\sqrt{u})}\times$$
$$\int_1^{r_{fD}}\xi_D g(\xi_D)\Big(u\bar{p}_{D0,in}-f_1(\xi_D)\Big)H_0(\sqrt{u}\xi_D,\sqrt{u})d\xi_D. \quad \text{(B.145)}$$

One way to find the constant A_5 is to multiply respectively Eq. B.136 by $K_1(\sqrt{\eta u}r_{fD})$ and Eq. B.145 by $K_0(\sqrt{\eta u}r_{fD})$ and equate the results to get rid of the constant B_6. If we do so, we obtain the following

$$\frac{A_5}{K_1(\sqrt{u})}K_1(\sqrt{\eta u}r_{fD})H_0(\sqrt{u}r_{fD},\sqrt{u})$$
$$+\frac{K_0(\sqrt{u}r_{fD})}{K_1(\sqrt{u})}K_1(\sqrt{\eta u}r_{fD})\int_1^{r_{fD}}\xi_D g(\xi_D)\Big(u\bar{p}_{D0,in}-f_1(\xi_D)\Big)H_0(\sqrt{u}\xi_D,\sqrt{u})d\xi_D=$$
$$-\frac{\hat{M}}{\sqrt{\eta}}\frac{A_5}{K_1(\sqrt{u})}K_0(\sqrt{\eta u}r_{fD})G_1(\sqrt{u}r_{fD},\sqrt{u})+\frac{\hat{M}}{\sqrt{\eta}}\frac{K_1(\sqrt{u}r_{fD})}{K_1(\sqrt{u})}K_0(\sqrt{\eta u}r_{fD})\times$$
$$\int_1^{r_{fD}}\xi_D g(\xi_D)\Big(u\bar{p}_{D0,in}-f_1(\xi_D)\Big)H_0(\sqrt{u}\xi_D,\sqrt{u})d\xi_D. \quad \text{(B.146)}$$

If we rearrange the above equation, we can write

$$\frac{A_5}{K_1(\sqrt{u})}\left[K_1(\sqrt{\eta u}r_{fD})H_0(\sqrt{u}r_{fD},\sqrt{u})+\frac{\hat{M}}{\sqrt{\eta}}K_0(\sqrt{\eta u}r_{fD})G_1(\sqrt{u}r_{fD},\sqrt{u})\right]=$$
$$-\frac{1}{K_1(\sqrt{u})}\left[K_0(\sqrt{u}r_{fD})K_1(\sqrt{\eta u}r_{fD})-\frac{\hat{M}}{\sqrt{\eta}}K_1(\sqrt{u}r_{fD})K_0(\sqrt{\eta u}r_{fD})\right]\times$$
$$\int_1^{r_{fD}}\xi_D g(\xi_D)\left(u\bar{p}_{D0,in}-f_1(\xi_D)\right)H_0(\sqrt{u}\xi_D,\sqrt{u})d\xi_D, \quad \text{(B.147)}$$

or simply,

$$A_5=-\frac{\left[K_0(\sqrt{u}r_{fD})K_1(\sqrt{\eta u}r_{fD})-\frac{\hat{M}}{\sqrt{\eta}}K_1(\sqrt{u}r_{fD})K_0(\sqrt{\eta u}r_{fD})\right]}{\left[K_1(\sqrt{\eta u}r_{fD})H_0(\sqrt{u}r_{fD},\sqrt{u})+\frac{\hat{M}}{\sqrt{\eta}}K_0(\sqrt{\eta u}r_{fD})G_1(\sqrt{u}r_{fD},\sqrt{u})\right]}\times$$
$$\int_1^{r_{fD}}\xi_D g(\xi_D)\left(u\bar{p}_{D0,in}-f_1(\xi_D)\right)H_0(\sqrt{u}\xi_D,\sqrt{u})d\xi_D. \quad \text{(B.148)}$$

Finally, the constant B_6 is obtained by substituting Eq. B.148 into Eq. B.136 to obtain

$$B_6=\frac{\hat{M}}{r_{fD}\sqrt{\eta u}}\frac{1}{\left[K_1(\sqrt{\eta u}r_{fD})H_0(\sqrt{u}r_{fD},\sqrt{u})+\frac{\hat{M}}{\sqrt{\eta}}K_0(\sqrt{\eta u}r_{fD})G_1(\sqrt{u}r_{fD},\sqrt{u})\right]}\times$$
$$\int_1^{r_{fD}}\xi_D g(\xi_D)\left(u\bar{p}_{D0,in}-f_1(\xi_D)\right)H_0(\sqrt{u}\xi_D,\sqrt{u})d\xi_D. \quad \text{(B.149)}$$